

Special Issue Reprint

Natural Products Chemistry

Advances in Synthetic, Analytical
and Bioactivity Studies

Edited by
Giovanni Ribaudò

www.mdpi.com/journal/molecules

Natural Products Chemistry: Advances in Synthetic, Analytical and Bioactivity Studies

Natural Products Chemistry: Advances in Synthetic, Analytical and Bioactivity Studies

Editor

Giovanni Ribaudò



Basel • Beijing • Wuhan • Barcelona • Belgrade • Novi Sad • Cluj • Manchester

Editor

Giovanni Ribaudo
University of Brescia
Brescia, Italy

Editorial Office

MDPI
St. Alban-Anlage 66
4052 Basel, Switzerland

This is a reprint of articles from the Special Issue published online in the open access journal *Molecules* (ISSN 1420-3049) (available at: https://www.mdpi.com/journal/molecules/special_issues/Nat_Prod_Chem).

For citation purposes, cite each article independently as indicated on the article page online and as indicated below:

Lastname, A.A.; Lastname, B.B. Article Title. <i>Journal Name</i> Year , <i>Volume Number</i> , Page Range.
--

ISBN 978-3-0365-8484-3 (Hbk)

ISBN 978-3-0365-8485-0 (PDF)

doi.org/10.3390/books978-3-0365-8485-0

Cover image courtesy of Giovanni Ribaudo

© 2023 by the authors. Articles in this book are Open Access and distributed under the Creative Commons Attribution (CC BY) license. The book as a whole is distributed by MDPI under the terms and conditions of the Creative Commons Attribution-NonCommercial-NoDerivs (CC BY-NC-ND) license.

Contents

About the Editor vii

Giovanni Ribaudo

Natural Products Chemistry: Advances in Synthetic, Analytical and Bioactivity Studies
Reprinted from: *Molecules* **2023**, *28*, 5577, doi:10.3390/molecules28145577 1

Akiko Nagata, Kazuto Iijima, Ryota Sakamoto, Yuka Mizumoto, Miho Iwaki, Masaki Takiwaki, et al.

Synthesis of Deuterium-Labeled Vitamin D Metabolites as Internal Standards for LC-MS Analysis
Reprinted from: *Molecules* **2022**, *27*, 2427, doi:10.3390/molecules27082427 3

Lirong Guo, Qing Gao, Jieqiong Zhu, Xiaobao Jin, Hui Yin and Tao Liu

A Docosahexaenoic Acid Derivative (*N*-Benzyl Docosahexaenamide) as a Potential Therapeutic Candidate for Treatment of Ovarian Injury in the Mouse Model
Reprinted from: *Molecules* **2022**, *27*, 2754, doi:10.3390/molecules27092754 11

Siyuan Peng, Xiwen Ling, Wenjing Rui, Xiaobao Jin and Fujiang Chu

LMWP (S3-3) from the Larvae of *Musca domestica* Alleviate D-IBS by Adjusting the Gut Microbiota
Reprinted from: *Molecules* **2022**, *27*, 4517, doi:10.3390/molecules27144517 25

Evan P. Vanable, Laurel G. Habgood and James D. Patrone

Current Progress in the Chemoenzymatic Synthesis of Natural Products
Reprinted from: *Molecules* **2022**, *27*, 6373, doi:10.3390/molecules27196373 51

Xiao Sun, Zhanying Lu, Zhenzhen Liang, Bowen Deng, Yuping Zhu, Jing Shi and Xiaoling Lu

Transcriptomics and Proteomics Characterizing the Anticancer Mechanisms of Natural Rebeccamycin Analog Loonamycin in Breast Cancer Cells
Reprinted from: *Molecules* **2022**, *27*, 6958, doi:10.3390/molecules27206958 67

Lixiang Sun, Huannan Wang, Maocai Yan, Chunmei Sai and Zhen Zhang

Research Advances of Bioactive Sesquiterpenoids Isolated from Marine-Derived *Aspergillus* sp.
Reprinted from: *Molecules* **2022**, *27*, 7376, doi:10.3390/molecules27217376 83

Shijie Ye, Dongjie Yin, Xiaoyan Sun, Qinyi Chen, Ting Min, Hongxun Wang and Limei Wang

Molecular Cloning, Expression, and Functional Analysis of Glycosyltransferase (TbUGGT) Gene from *Trapa bispinosa* Roxb.
Reprinted from: *Molecules* **2022**, *27*, 8374, doi:10.3390/molecules27238374 103

Alexandra Németh-Rieder, Péter Keglevich, Attila Hunyadi, Ahmed Dhahir Latif, István Zupkó and László Hazai

Synthesis and In Vitro Anticancer Evaluation of Flavone—1,2,3-Triazole Hybrids
Reprinted from: *Molecules* **2023**, *28*, 626, doi:10.3390/molecules28020626 119

Wenli Sun and Mohamad Hesam Shahrajabian

Therapeutic Potential of Phenolic Compounds in Medicinal Plants—Natural Health Products for Human Health
Reprinted from: *Molecules* **2023**, *28*, 1845, doi:10.3390/molecules28041845 135

Md. Rezaul Islam, Md. Mominur Rahman, Puja Sutro Dhar, Feana Tasmim Nowrin, Nasrin Sultana, Muniya Akter, et al.	
The Role of Natural and Semi-Synthetic Compounds in Ovarian Cancer: Updates on Mechanisms of Action, Current Trends and Perspectives	
Reprinted from: <i>Molecules</i> 2023 , <i>28</i> , 2070, doi:10.3390/molecules28052070	179
Ying Yin, Dongyang Wang, Dan Wu, Wenwen He, Mingxing Zuo, Weiming Zhu, et al.	
Two New 4-Hydroxy-2-pyridone Alkaloids with Antimicrobial and Cytotoxic Activities from <i>Arthrinium</i> sp. GZWMJZ-606 Endophytic with <i>Houttuynia cordata</i> Thunb	
Reprinted from: <i>Molecules</i> 2023 , <i>28</i> , 2192, doi:10.3390/molecules28052192	207

About the Editor

Giovanni Ribaldo

Dr. Giovanni Ribaldo, PhD, works as a researcher at the Department of Molecular and Translational Medicine of the University of Brescia, Italy. He utilizes the combination of drug discovery tools from organic synthesis, analytical chemistry (HPLC, NMR, mass spectrometry), and computational studies to aid conduct research into his topics of interest, which include the design and screening of small molecules that interact with peculiar DNA arrangements, the development of phosphodiesterase (PDE) inhibitors, and novel applications of natural and semi-synthetic compounds in medicinal chemistry.

Editorial

Natural Products Chemistry: Advances in Synthetic, Analytical and Bioactivity Studies

Giovanni Ribaldo

Department of Molecular and Translational Medicine, University of Brescia, 25123 Brescia, Italy;
giovanni.ribaldo@unibs.it

The chemistry of natural compounds inspired and still guides several branches of modern chemical sciences. In particular, natural compounds paved the way for the development of new therapeutic options, and the history of medicinal chemistry is rich in examples in this direction. Moreover, contemporary drug discovery tools can breathe new life into natural derivatives, as they allow the traditional uses of nature-inspired molecules to be rationalized and translated into modern medicinal chemistry. These traditional uses also allow for the identification of novel potential pathways and mechanisms of action targeted by such compounds.

The chemical diversity of scaffolds, the variety of nature and positioning of substituents, the presence of peculiar functional groups, and chirality represent the main features that enrich the intrinsic value and complexity of natural compounds. At the same time, these characteristics represent the most intriguing and challenging aspects when undertaking the study of such molecules.

The first challenge comprises the extraction process, which must be optimized to efficiently obtain the desired compound. Similarly, synthetic approaches are often very complicated when the total syntheses of natural compounds are involved. In the context of compound characterization and quantification, chemists must take into account the complications related to sample preparation and the effects of matrices. Additionally, the structural characterization of complicated natural molecules often pushes advanced analytical techniques, such as NMR and mass spectrometry, to their technical limits. A further challenge involves compound modification and the production of semi-synthetic derivatives: organic and medicinal chemists put their best efforts into the derivatization of natural molecules to produce optimized analogues, thus unleashing the potential of these semi-synthetic derivatives.

This Special Issue represents an ideal continuation and extension of the one that I previously guest-edited for the sister journal *Molbank*, entitled “Synthesis of Flavonoids and Nature-Inspired Small Molecules” [1]. The current Special Issue was launched in spring 2022 and aimed at collecting original contributions and review articles related to the extraction, structural elucidation, synthesis, analysis, and biological evaluation of natural, semisynthetic derivatives and nature-inspired molecules. Additionally, particular attention was dedicated to drug-discovery-oriented research works. This Special Issue includes contributions from researchers all over the world, testifying once again to the growing interest of the scientific community towards the applications of natural products in modern chemistry. A total of 11 research and review papers were published during this year of activity, and a brief overview of the articles is reported in the following.

More in detail, Nagata et al. described the synthesis of deuterium-labelled vitamin D analogues with applications in the field of analytical chemistry [2]. Guo et al. studied the derivatives of docosahexaenoic acid as candidates for the treatment of ovarian injury in vivo [3]. Peng et al. proposed an extract from *Musca domestica* as a tool for regulating gut microbiota [4]. Vanable et al. overviewed the state of the art of chemoenzymatic synthesis in the field of natural compounds [5]. X. Sun et al. described the application

Citation: Ribaldo, G. Natural Products Chemistry: Advances in Synthetic, Analytical and Bioactivity Studies. *Molecules* **2023**, *28*, 5577. <https://doi.org/10.3390/molecules28145577>

Received: 15 July 2023

Accepted: 20 July 2023

Published: 22 July 2023



Copyright: © 2023 by the author. Licensee MDPI, Basel, Switzerland. This article is an open access article distributed under the terms and conditions of the Creative Commons Attribution (CC BY) license (<https://creativecommons.org/licenses/by/4.0/>).

of transcriptomics and proteomics in the investigation of the anticancer mechanisms of loonamycin, a derivative of rebeccamycin, in breast cancer [6]. In the field of natural compounds of marine origin, L. Sun et al. explored the bioactive sesquiterpenoids isolated from *Aspergillus* sp. [7]. The genetic and functional aspects of glycosyltransferase *Trapa bispinosa* were the focus of the work by Ye et al. [8]. Németh-Rieder et al. proposed flavone-1,2,3-triazole hybrids as potential anticancer agents [9]. Sun and Shahrajabian overviewed the latest findings in the field of phenolic natural compounds from medicinal plants and their therapeutic applications [10]. Yin et al. reported the antimicrobial and cytotoxic activity of two alkaloids from *Arthrinium* sp. [11]. Finally, our research group contributed to this Special Issue with a comprehensive review on the role of natural and semi-synthetic compounds in ovarian cancer, in which a detailed discussion on chemical classes and involved mechanisms is provided [12].

To conclude, as the Guest Editor, I would like to thank all the authors for having chosen to publish their research in our Special Issue, as well as the Reviewers and the Assistant and Academic Editors for their support.

Acknowledgments: The Guest Editor would like to thank Jessica Tecchio for her kind support.

Conflicts of Interest: The author declares no conflict of interest.

References

- Ribaudo, G. Synthesis of Flavonoids or Other Nature-Inspired Small Molecules. *Molbank* **2022**, *2022*, M1313. [[CrossRef](#)]
- Nagata, A.; Iijima, K.; Sakamoto, R.; Mizumoto, Y.; Iwaki, M.; Takiwaki, M.; Kikutani, Y.; Fukuzawa, S.; Odagi, M.; Tera, M.; et al. Synthesis of Deuterium-Labeled Vitamin D Metabolites as Internal Standards for LC-MS Analysis. *Molecules* **2022**, *27*, 2427. [[CrossRef](#)] [[PubMed](#)]
- Guo, L.; Gao, Q.; Zhu, J.; Jin, X.; Yin, H.; Liu, T. A Docosahexaenoic Acid Derivative (N-Benzyl Docosahexaenamide) as a Potential Therapeutic Candidate for Treatment of Ovarian Injury in the Mouse Model. *Molecules* **2022**, *27*, 2754. [[CrossRef](#)] [[PubMed](#)]
- Peng, S.; Ling, X.; Rui, W.; Jin, X.; Chu, F. LMWP (S3-3) from the Larvae of *Musca Domestica* Alleviate D-IBS by Adjusting the Gut Microbiota. *Molecules* **2022**, *27*, 4517. [[CrossRef](#)] [[PubMed](#)]
- Vanable, E.P.; Habgood, L.G.; Patrone, J.D. Current Progress in the Chemoenzymatic Synthesis of Natural Products. *Molecules* **2022**, *27*, 6373. [[CrossRef](#)] [[PubMed](#)]
- Sun, X.; Lu, Z.; Liang, Z.; Deng, B.; Zhu, Y.; Shi, J.; Lu, X. Transcriptomics and Proteomics Characterizing the Anticancer Mechanisms of Natural Rebeccamycin Analog Loonamycin in Breast Cancer Cells. *Molecules* **2022**, *27*, 6958. [[CrossRef](#)] [[PubMed](#)]
- Sun, L.; Wang, H.; Yan, M.; Sai, C.; Zhang, Z. Research Advances of Bioactive Sesquiterpenoids Isolated from Marine-Derived *Aspergillus* sp. *Molecules* **2022**, *27*, 7376. [[CrossRef](#)] [[PubMed](#)]
- Ye, S.; Yin, D.; Sun, X.; Chen, Q.; Min, T.; Wang, H.; Wang, L. Molecular Cloning, Expression, and Functional Analysis of Glycosyltransferase (TbUGGT) Gene from *Trapa Bispinosa* Roxb. *Molecules* **2022**, *27*, 8374. [[CrossRef](#)] [[PubMed](#)]
- Németh-Rieder, A.; Keglevich, P.; Hunyadi, A.; Latif, A.D.; Zupkó, I.; Hazai, L. Synthesis and In Vitro Anticancer Evaluation of Flavone—1,2,3-Triazole Hybrids. *Molecules* **2023**, *28*, 626. [[CrossRef](#)] [[PubMed](#)]
- Sun, W.; Shahrajabian, M.H. Therapeutic Potential of Phenolic Compounds in Medicinal Plants—Natural Health Products for Human Health. *Molecules* **2023**, *28*, 1845. [[CrossRef](#)] [[PubMed](#)]
- Yin, Y.; Wang, D.; Wu, D.; He, W.; Zuo, M.; Zhu, W.; Xu, Y.; Wang, L. Two New 4-Hydroxy-2-Pyridone Alkaloids with Antimicrobial and Cytotoxic Activities from *Arthrinium* Sp. GZWMJZ-606 Endophytic with *Houttuynia Cordata* Thunb. *Molecules* **2023**, *28*, 2192. [[CrossRef](#)] [[PubMed](#)]
- Islam, M.R.; Rahman, M.M.; Dhar, P.S.; Nowrin, F.T.; Sultana, N.; Akter, M.; Rauf, A.; Khalil, A.A.; Gianoncelli, A.; Ribaudo, G. The Role of Natural and Semi-Synthetic Compounds in Ovarian Cancer: Updates on Mechanisms of Action, Current Trends and Perspectives. *Molecules* **2023**, *28*, 2070. [[CrossRef](#)] [[PubMed](#)]

Disclaimer/Publisher's Note: The statements, opinions and data contained in all publications are solely those of the individual author(s) and contributor(s) and not of MDPI and/or the editor(s). MDPI and/or the editor(s) disclaim responsibility for any injury to people or property resulting from any ideas, methods, instructions or products referred to in the content.

Communication

Synthesis of Deuterium-Labeled Vitamin D Metabolites as Internal Standards for LC-MS Analysis

Akiko Nagata ¹, Kazuto Iijima ¹, Ryota Sakamoto ¹, Yuka Mizumoto ¹, Miho Iwaki ¹, Masaki Takiwaki ², Yoshikuni Kikutani ², Seketsu Fukuzawa ², Minami Odagi ¹, Masayuki Tera ¹ and Kazuo Nagasawa ^{1,*}

¹ Department of Biotechnology and Life Science, Tokyo University of Agriculture and Technology, Koganei, Tokyo 184-8588, Japan; s193819x@st.go.tuat.ac.jp (A.N.); s206189q@st.go.tuat.ac.jp (K.I.); s218969x@st.go.tuat.ac.jp (R.S.); s200343y@st.go.tuat.ac.jp (Y.M.); s218363r@st.go.tuat.ac.jp (M.I.); odagi@cc.tuat.ac.jp (M.O.); tera@go.tuat.ac.jp (M.T.)

² Medical Equipment Business Operations, Management Strategy Planning Division, JEOL Ltd., Akishima, Tokyo 196-8558, Japan; mtakiwak@jeol.co.jp (M.T.); ykikutan@jeol.co.jp (Y.K.); sfukuzaw@jeol.co.jp (S.F.)

* Correspondence: knaga@cc.tuat.ac.jp; Tel.: +81-42-388-7295

Abstract: Blood levels of the vitamin D₃ (D₃) metabolites 25-hydroxyvitamin D₃ (25(OH)D₃), 24R,25-dihydroxyvitamin D₃, and 1α,25-dihydroxyvitamin D₃ (1,25(OH)₂D₃) are recognized indicators for the diagnosis of bone metabolism-related diseases, D₃ deficiency-related diseases, and hypercalcemia, and are generally measured by liquid-chromatography tandem mass spectrometry (LC-MS/MS) using an isotope dilution method. However, other D₃ metabolites, such as 20-hydroxyvitamin D₃ and lactone D₃, also show interesting biological activities and stable isotope-labeled derivatives are required for LC-MS/MS analysis of their concentrations in serum. Here, we describe a versatile synthesis of deuterium-labeled D₃ metabolites using A-ring synthons containing three deuterium atoms. Deuterium-labeled 25(OH)D₃ (**2**), 25(OH)D₃-23,26-lactone (**6**), and 1,25(OH)₂D₃-23,26-lactone (**7**) were synthesized, and successfully applied as internal standards for the measurement of these compounds in pooled human serum. This is the first quantification of 1,25(OH)₂D₃-23,26-lactone (**7**) in human serum.

Keywords: vitamin D; deuterium labeling; liquid-chromatography tandem mass spectrometry; measurement of vitamin D metabolites in blood

Citation: Nagata, A.; Iijima, K.; Sakamoto, R.; Mizumoto, Y.; Iwaki, M.; Takiwaki, M.; Kikutani, Y.; Fukuzawa, S.; Odagi, M.; Tera, M.; et al. Synthesis of Deuterium-Labeled Vitamin D Metabolites as Internal Standards for LC-MS Analysis.

Molecules **2022**, *27*, 2427. <https://doi.org/10.3390/molecules27082427>

Academic Editor: Giovanni Ribaudou

Received: 19 March 2022

Accepted: 6 April 2022

Published: 9 April 2022

Publisher's Note: MDPI stays neutral with regard to jurisdictional claims in published maps and institutional affiliations.



Copyright: © 2022 by the authors. Licensee MDPI, Basel, Switzerland. This article is an open access article distributed under the terms and conditions of the Creative Commons Attribution (CC BY) license (<https://creativecommons.org/licenses/by/4.0/>).

1. Introduction

Vitamin D₃ (D₃) (**1**) is metabolized by members of the cytochrome P450 (CYP) family to generate more than 50 compounds in vivo. Among them, 25-hydroxyvitamin D₃ (25(OH)D₃) (**2**) is generated from D₃ (**1**) by CYP2R1 and/or CYP27A1-mediated hydroxylation at C25 in the liver, and the resulting 25(OH)D₃ (**2**) is further metabolized to the active form of D₃, 1α,25-dihydroxyvitamin D₃ (1,25(OH)₂D₃) (**3**), by CYP27B1-mediated oxidation at C1α in the kidneys (Figure 1). 1,25(OH)₂D₃ (**3**) plays a key role in the regulation of bone metabolism in vivo [1]. In normal conditions, production of **3** from **2** is strictly controlled by the concentrations of calcium and parathyroid hormone (PTH) in the blood, and thus the concentration of **3** in the blood is a useful indicator of functional status [2] and is helpful in the diagnosis of diseases such as hypercalcemia, hyperphosphatemia, rickets, and bone metabolism-related diseases [3,4]. The concentration of **2** in the blood is also useful as an indicator for the diagnosis of various vitamin D deficiency-related diseases [3,4]. Recently, various D₃ metabolites, mostly oxidized at the D-ring side chain, have also been found to show biological activities. For example, 20S,25(OH)₂D₃, which is generated by CYP11A1, inhibits the growth of keratinocytes, leukemia cells, and melanoma cells [5–9], while 24R,25(OH)₂D₃ (**4**), produced by CYP24A1, shows inhibitory activity against various cancer cell lines [10,11]. Further, 25(OH)D₃-23,26 lactone (**6**) and 1,25(OH)₂D₃-23,26 lactone (**7**), which are thought to be final metabolites of D₃, show antagonistic activity

towards $1,25(\text{OH})_2\text{D}_3$ [12–14], thereby, inhibiting bone formation and resorption. Recently, compound 7 was reported to inhibit fatty acid oxidation [15]. Thus, there is a need to measure the blood levels of these metabolites.

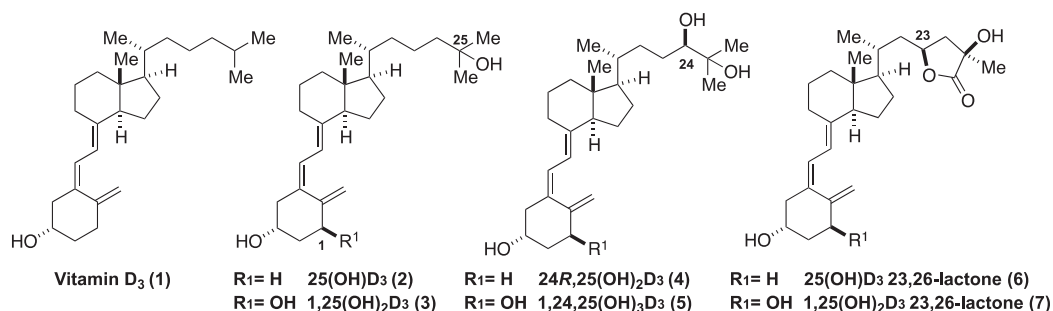


Figure 1. Structures of vitamin D₃ (1) and its metabolites (2)–(7).

The concentrations of metabolites 2 and 3 in blood have been measured for clinical purposes by radioimmunoassay (RIA) or chemiluminescent enzyme immunoassay (CLEIA) [16]. They, however, have disadvantages such as the need to handle radioactive materials, and insufficient discrimination of vitamin D metabolites by antibodies [17]. More recently, a liquid-chromatography tandem mass spectrometry (LC-MS/MS) method has been developed to determine the concentration of multiple vitamin D metabolites simultaneously in blood [18]. However, LC-MS/MS-based measurement also has some problems, such as the low ionization efficiency of vitamin D derivatives and interference by contaminants including multiple D₃ metabolites in the blood. To address these issues, several approaches have been investigated. Cookson-type reagents have been developed to improve the ionization efficiency of D₃ metabolites, affording high sensitivity even at low abundance [19,20]. The isotope dilution method has also been applied to avoid interference from contaminants in the blood. This method requires a stable isotope-labeled compound as an internal standard, and so far, deuterium-labeled $25(\text{OH})_2\text{D}_3$ (2), $1,25(\text{OH})_2\text{D}_3$ (3), and $24R,25(\text{OH})_2\text{D}_3$ (4), in which deuterium is introduced at C26, C27, C6, and C19, have been synthesized (Figure 2) [21–25].

In the synthesis of the deuterium-labeled metabolites 2–4-*d*₆, deuterium was introduced into the side chain at C26 and C27 by reacting esters 8 with deuterated Grignard reagent, CD_3MgBr (Figure 2B) [21,22]. On the other hand, 2–3-*d*₃ were synthesized by reacting SO_2 adducts of cyclic compounds 9 derived from D₃ with deuterium oxide (D_2O) [23–25]. In both strategies, the range of metabolites that can be synthesized is limited due to the restrictions imposed by the use of steroid precursors. Therefore, a more versatile approach is required. Convergent strategies, with coupling between CD-ring and A-ring moieties, have been widely applied for the synthesis of D₃ derivatives [26,27]. Since the CD-ring structures of the metabolites are diverse, whereas the A-ring structures are relatively constant, we considered that deuterium-labeled A-ring synthons would be suitable for the preparation of a variety of deuterium-labeled D₃ metabolites (Figure 2D). In addition, labeling in the A-ring has an advantage in metabolism studies because the side chains of the D₃ are well known to be enzymatically metabolized easily. In this study, we have developed a synthesis of deuterium-labeled A-ring precursors 13-*d*₃ and 16-*d*₃ incorporating three deuterium atoms. These precursors were coupled with CD-ring moieties 17 and 18 to afford deuterium-labeled $25(\text{OH})\text{D}_3$ -*d*₃ (2-*d*₃) and vitamin D lactones $25(\text{OH})\text{D}_3$ -23,26-lactone-*d*₃ (6-*d*₃) and $1,25(\text{OH})_2\text{D}_3$ -23,26-lactone-*d*₃ (7-*d*₃). We also confirmed that the concentrations of 2, 6, and 7 in human serum could be measured by LC-MS/MS using the corresponding deuterium-labeled compounds as the internal standards (IS) (see Supplementary Materials).

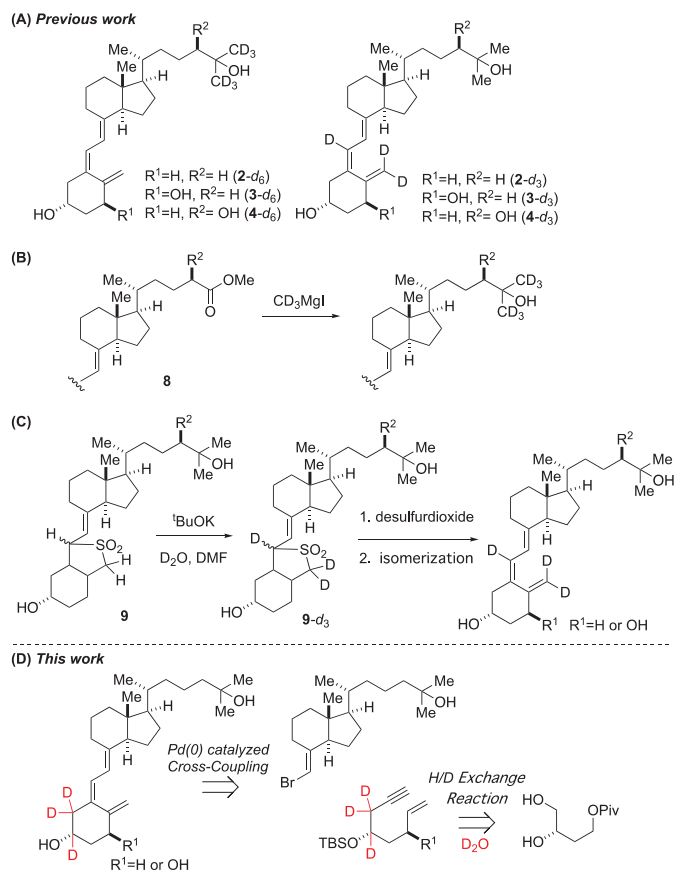
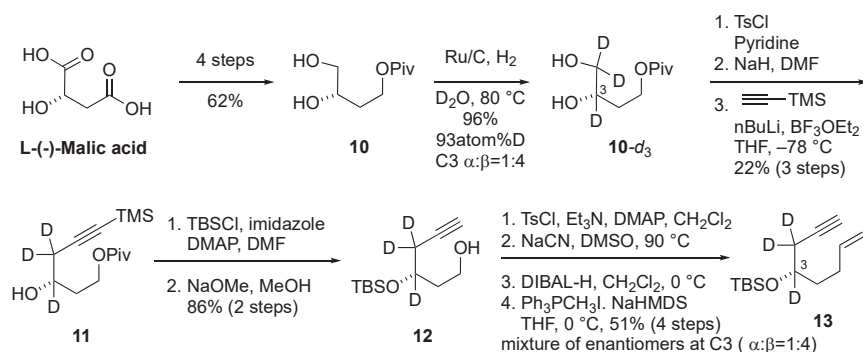


Figure 2. Synthetic strategy of deuterium-labeled D_3 metabolites. (A) Structures of reported deuterium-labeled D_3 metabolites. (B) Previous work on the synthesis of 2–4- d_6 . (C) Previous work on the synthesis of 2–4- d_3 . (D) This work: general synthesis of deuterium-labeled D_3 metabolites.

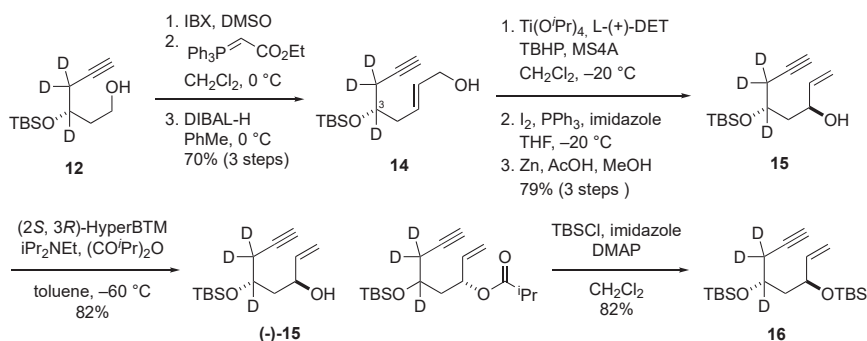
2. Results

We employed a convergent strategy using the palladium-catalyzed coupling reaction of enyne-type deuterium-labeled A-ring precursors **13- d_3** and **16- d_3** with bromoolefins **17** and **18** as the CD-ring moieties. The deuterium atoms in **13- d_3** and **16- d_3** were introduced by the H/D exchange at the α -position of the alcohol, as reported by Sajiki et al. [28]. Our synthesis of deuterium-labeled enyne **13** commenced with the H/D exchange reaction of alcohol **10**, which was obtained from L-($-$)-malic acid in 4 steps (Scheme 1) [29]. The alcohol **10** was subjected to the H/D exchange reaction with a catalytic amount of Ru/C in D_2O at 80 °C under an H_2 atmosphere to afford **10- d_3** deuterium-labeled at C3 and C4 in a 96% yield with over 93% deuteride content [28]. In this reaction, the stereochemistry at C3 was isomerized (4:1 ratio of α -**10a** and β -**10b**). The deuterium-labeled alcohol **10** (enantiomeric mixture) was converted into alkyne **11** by tosylation of the primary alcohol followed by epoxidation with NaH and reaction with TMS-acetylene (22% yield from **10- d_3**). The hydroxyl group in alkyne **11** was protected with TBS ether, followed by deprotection of the TMS and pivaloyl groups with NaOMe in MeOH to give the alcohol **12** in an 86% yield from **11**. Enyne **13** was obtained in a 51% yield from **12** via 4 steps, (i) tosylation of the primary alcohol; (ii) cyanation with NaCN; (iii) reduction of the nitrile group with DIBAL-H to aldehyde; and (iv) a Wittig reaction with Ph_3PCH_3I and NaHMDS. It was confirmed by 1H -NMR that the deuteration rate did not decrease in these reaction steps [30].



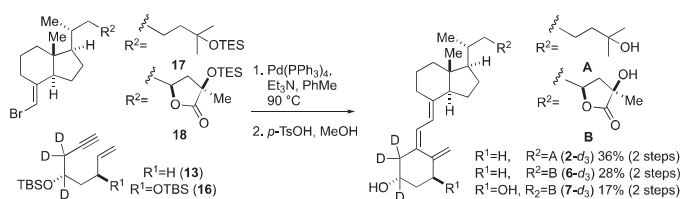
Scheme 1. Synthesis of deuterium-labeled enyne **13-d₃**.

Next, the deuterium-labeled enyne **16** bearing a hydroxyl group at C1α was synthesized (Scheme 2). The alcohol moiety in **12** was oxidized with an IBX and the resulting aldehyde was reacted with a HWE Wittig reagent to give an unsaturated ester, whose ester group was reduced with a DIBAL-H to give allyl alcohol **14** in a 70% yield from **12** [31,32]. The allyl alcohol **14** was subjected to a Sharpless asymmetric epoxidation with a TBHP in the presence of Ti(OiPr)₄ and L-(+)-DET [33], and the resulting epoxy alcohol was subjected to iodination with iodine and triphenylphosphine followed by treatment with zinc to give a secondary alcohol **15** in a 79% yield (3 steps) [31,32]. The diastereomer ratio at C1 in **15** was 10:1, and the undesired C1β diastereomer was removed by kinetic resolution, using acylation with isopropyl acid anhydride in the presence of (2*S*,3*R*)-HyperBTM [34], to give (-)-**15** in an 82% yield as a single diastereomer. The undesired diastereomer at C3 was also removed via silica gel column purification. The deuterium-labeled enyne **16**, in which the secondary alcohol was protected as the TBS ether, was obtained in an 82% yield.



Scheme 2. Synthesis of deuterium-labeled enyne **16-d₃**.

The palladium-catalyzed coupling reaction of **13-d₃** and bromoolefin **17** followed by deprotection of the silyl groups provided 25(OH)D₃-d₃ (**2-d₃**) in a 36% yield [35]. Next, 25(OH)D₃-23,26-lactone-d₃ (**6-d₃**) and 1,25(OH)₂D₃-23,26-lactone-d₃ (**7-d₃**) were similarly synthesized by reacting bromoolefin **18** and enynes **13-d₃** and **16-d₃**, respectively [36]. In the synthesis of **2-d₃** and **6-d₃**, the undesired diastereomers at C3α were separated by an HPLC (Scheme 3).



Scheme 3. Synthesis of vitamin D₃ metabolites-*d*₃ (2-*d*₃, 6-*d*₃, 7-*d*₃).

2.1. Derivatization of 2, 6, 7 for LC-MS/MS, and Preparation of Calibration Curves

With the deuterium-labeled D₃ metabolites of 2-*d*₃, 6-*d*₃, and 7-*d*₃ in hand, we next examined the quantitative analysis of the three D₃ metabolites in pooled human serum by LC-MS/MS. First, we confirmed that our deuterium-labeled D₃ metabolites were suitable as the internal standards for the isotope dilution method in an LC-MS/MS analysis. As described above, D₃ and its metabolites have low ionization efficiency in an LC-MS/MS, and derivatization is necessary to improve the ionization efficiency. Thus, the D₃ metabolites 2, 6, and 7, as well as 2-*d*₃, 6-*d*₃, and 7-*d*₃, were derivatized with a recently developed reagent DAP-PA (4-(4'-dimethylaminophenyl)-1,2,4-triazoline-3,5-dione-phenyl anthracene) [20], and the ion peaks of the DAP adducts were detected by selective reaction monitoring (SRM) under the LC-MS/MS conditions shown in Table 1 (Figure 3).

Table 1. Parameters for the LC/MS/MS analysis.

Compound	SRM Transition (m/z)	Cone Voltage (kv)	CE (eV)
25(OH)D ₃ -DAP (2-DAP)	619.4 > 341.2 [M + H] ⁺ [A] ⁺	48	28
25(OH)D ₃ -23,26-lactone-DAP (6-DAP)	647.4 > 341.2	48	28
1,25(OH) ₂ D ₃ -23,26-lactone-DAP (7-DAP)	663.4 > 357.2	48	28
25(OH)D ₃ - <i>d</i> ₃ -DAP (2- <i>d</i> ₃ -DAP)	622.4 > 344.2	48	28
25(OH)D ₃ -23,26-lactone- <i>d</i> ₃ -DAP (6- <i>d</i> ₃ -DAP)	650.4 > 344.2	48	28
1,25(OH) ₂ D ₃ -23,26-lactone- <i>d</i> ₃ -DAP (7- <i>d</i> ₃ -DAP)	666.4 > 360.2	48	28

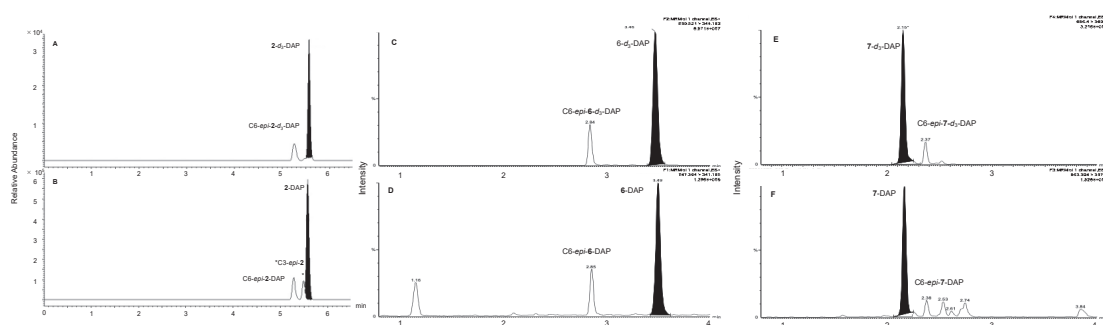


Figure 3. SRM chromatograms for the DAP adducts of D₃ metabolites 2, 6, and 7, as well as 2-*d*₃, 6-*d*₃, and 7-*d*₃.

In the case of the DAP-adducts of 2 and 2-*d*₃ (Figure 3A,B), we observed identical ion peaks at the retention time of 5.60 min (abbreviated as *t*_R: 5.60 min). Similarly, 6 and 6-*d*₃ showed the same *t*_R of 3.50 min, and 7 and 7-*d*₃ showed the same *t*_R of 2.15 min, indicating that the deuterium-labeled compounds are suitable as internal standards for the

isotope dilution method. We also observed small peaks at the retention times of 5.20 min (Figure 3A,B), 2.65 min (Figure 3C,D), and 2.37 min (Figure 3E,F) for 2/2- d_3 , 6/6- d_3 , and 7/7- d_3 , respectively. These peaks are due to the epimers at C6 of the DAP adducts, because DAP-PA reacts from both the α - and β -faces.

Next, the calibration curves were prepared as follows (Figure 4). A total of 100 μL of each one of the calibrator solutions was mixed with 200 μL of the internal standard solution and evaporated to dryness. After derivatization with DAP-PA, an LC-MS/MS analysis of the unlabeled and labeled DAP-adducts was performed, and the calibration curves were prepared by plotting the concentration of unlabeled DAP-adduct against the ion peak area ratio of unlabeled versus labeled DAP-adduct. All of the calibration curves showed good linearity.

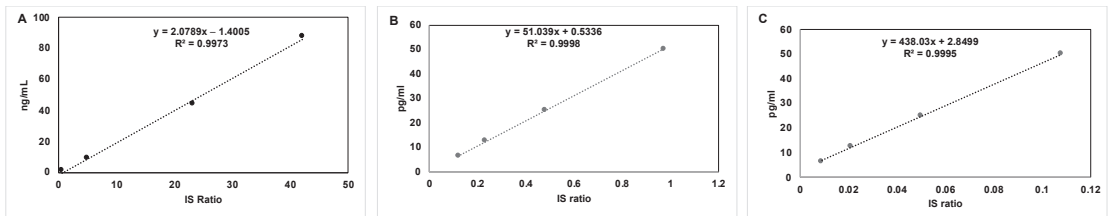


Figure 4. Calibration curve of D_3 metabolites; (A) 25(OH) D_3 (2); (B) 25(OH) D_3 -23,26-lactone (6); and (C) 1,25(OH) $_2D_3$ -23,26-lactone (7).

2.2. Quantification of the D_3 Derivatives in Human Serum

The levels of 2, 6, and 7 in pooled human serum were quantified by the LC-MS/MS using the isotope dilution method with the constructed calibration curves. The serum was pretreated as follows. An aliquot of serum (100 μL) was mixed with the internal standards solution (200 μL). Each sample was loaded onto a supported liquid extraction column (ISOLUTE SLE+ 300 μL sample Volume, Biotage, Uppsala, Sweden) and eluted three times with 600 mL hexane/ethyl acetate (1/1, v/v) using a PRESSURE+48 positive pressure manifold (Biotage, Uppsala, Sweden). The combined eluates were evaporated to dryness in a centrifugal evaporator. The ion peaks of the metabolites matched well with those of the corresponding internal standards in the pretreated samples (Figure 5).

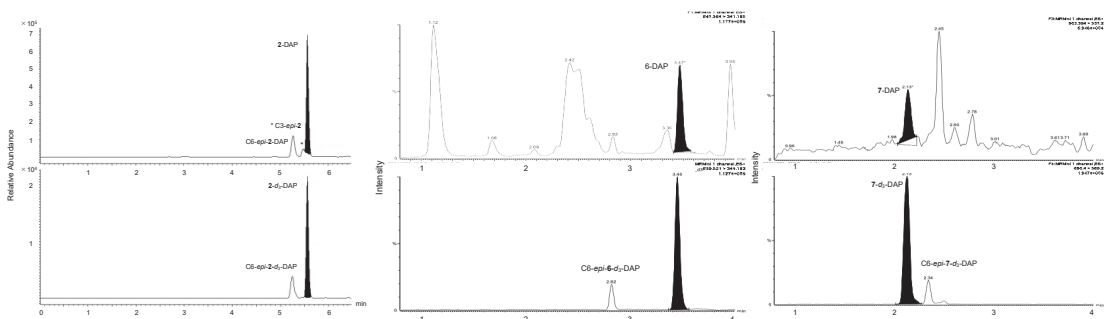


Figure 5. SRM chromatograms for D_3 derivatives 2, 6, and 7 in pooled human serum.

The concentrations of 2, 6, and 7 in human serum were calculated to be 5.1 ng/mL, 38.3 pg/mL, and 8.9 pg/mL, respectively, based on the area ratios of the detected peaks. The concentrations of 2 and 6 were in agreement with previously reported values [37], while this is the first quantification of 1 α -lactone 7 in human serum.

3. Conclusions

We synthesized deuterium-labeled A-ring-*d*₃ synthons **13** and **16** and utilized them for the convergent synthesis of deuterium-labeled D₃ derivatives 25(OH)D₃ (**2**), 25(OH)D₃-23, 26-lactone (**6**), and 1,25(OH)₂D₃-23, 26-lactone (**7**). These deuterium-labeled D₃ metabolites were successfully applied as internal standards for the quantification of the metabolites in pooled human serum by LC-MS/MS using the isotope dilution method. This is the first quantification of 1,25(OH)₂D₃-23, 26-lactone (**7**) in human serum.

Supplementary Materials: The following supporting information can be downloaded at: <https://www.mdpi.com/article/10.3390/molecules27082427/s1>, Experimental procedures for synthesis and characterization of compounds, Experimental procedure for LC-MS/MS analysis using the isotope dilution method, ¹H and ¹³C NMR spectra.

Author Contributions: Conceptualization, A.N., S.F. and K.N.; investigation, A.N., K.I., R.S., Y.M. and M.I.; analysis, M.T. (Masaki Takiwakiand), Y.K. and S.F.; writing—original draft preparation, A.N. and K.N.; resources, M.O., M.T. (Masayuki Tera) and K.N.; funding acquisition, K.N. All authors have read and agreed to the published version of the manuscript.

Funding: This research received no external funding.

Acknowledgments: This work was supported by the Japan Agency for Medical Research and Development (AMED- CREST).

Conflicts of Interest: The authors declare no conflict of interest.

References and Notes

- Fleet, J.C. Regulation of intestinal calcium and phosphate absorption. In *Vitamin D*; Elsevier: Amsterdam, The Netherlands, 2018; pp. 329–342.
- David, V.; Quarles, L.D. FGF23/Klotho new regulators of vitamin D metabolism. In *Vitamin D*; Elsevier: Amsterdam, The Netherlands, 2011; pp. 747–761.
- Lips, P. Relative Value of 25(OH)D and 1,25(OH)₂D measurements. *J. Bone Miner. Res.* **2007**, *22*, 1668–1671. [[CrossRef](#)] [[PubMed](#)]
- Holick, M.F. Vitamin D status: Measurement, interpretation, and clinical application. *Ann. Epidemiol.* **2009**, *19*, 73–78. [[CrossRef](#)] [[PubMed](#)]
- Janjetovic, Z.; Tuckey, R.C.; Nguyen, M.N.; Thorpe, E.M.; Slominski, A.T. 20,23-dihydroxyvitamin D₃, novel P450scc product, stimulates differentiation and inhibits proliferation and NF-κB activity in human keratinocytes. *J. Cell. Physiol.* **2010**, *223*, 36–48. [[PubMed](#)]
- Janjetovic, Z.; Zmijewski, M.A.; Tuckey, R.C.; DeLeon, D.A.; Nguyen, M.N.; Pfeiffer, L.M.; Slominski, A.T. 20-Hydroxycholecalciferol product of vitamin D₃ hydroxylation by P450scc, decreases NF-κB activity by increasing IκBα levels in human keratinocytes. *PLoS ONE* **2009**, *4*, e5988. [[CrossRef](#)]
- Wang, J.; Slominski, A.T.; Tuckey, R.C.; Janjetovic, Z.; Kulkarni, A.; Chen, J.; Postlethwaite, A.E.; Miller, D.; Li, W. 20-Hydroxyvitamin D₃ inhibits proliferation of cancer cells with high efficacy while being non-toxic. *Anticancer Res.* **2012**, *32*, 739–746.
- Li, W.; Chen, J.; Janjetovic, Z.; Kim, T.K.; Sweatman, T.; Lu, Y.; Zjawiony, J.; Tuckey, R.C.; Miller, D.; Slominski, A.T. Chemical synthesis of 20S-hydroxyvitamin D₃, which shows antiproliferative activity. *Steroids* **2010**, *75*, 926–935. [[CrossRef](#)]
- Slominski, A.T.; Janjetovic, Z.; Fuller, B.E.; Zmijewski, M.A.; Tuckey, R.C.; Nguyen, M.N.; Sweatman, T.; Li, W.; Zjawiony, J.; Miller, D.; et al. Products of vitamin D₃ or 7-dehydrocholesterol metabolism by cytochrome P450scc show anti-leukemia effects, having low or absent calcemic activity. *PLoS ONE* **2010**, *5*, e9907. [[CrossRef](#)]
- Verma, A.; Cohen, D.J.; Schwartz, N.; Muktipaty, C.; Koblinski, J.E.; Boyan, B.D.; Schwartz, Z. 24R,25-Dihydroxyvitamin D₃ regulates breast cancer cells in vitro and in vivo. *Biochim. Biophys. Acta BBA—Gen. Subj.* **2019**, *1863*, 1498–1512. [[CrossRef](#)]
- Verma, A.; Cohen, D.J.; Jacobs, T.W.; Boyan, B.D.; Schwartz, Z. The relative expression of ERα Isoforms ERα66 and ERα36 controls the cellular response to 24R,25-Dihydroxyvitamin D₃ in breast cancer. *Mol. Cancer Res.* **2021**, *19*, 99–111. [[CrossRef](#)]
- Kiyoki, M.; Kurihara, N.; Ishizuka, S.; Ishii, S.; Hakea, Y.; Kumegawa, M.; Norman, A.W. The unique action for bone metabolism of 1α,25-(OH)₂D₃-26,23-lactone. *Biochem. Biophys. Res. Commun.* **1985**, *127*, 693–698. [[CrossRef](#)]
- Ishizuka, S.; Miura, D.; Eguchi, H.; Ozono, K.; Chokki, M.; Kamimura, T.; Norman, A.W. Antagonistic action of novel 1α,25-Dihydroxyvitamin D₃-26,23-lactone analogs on 25-hydroxyvitamin-D₃-24-hydroxylase gene expression Induced by 1α,25-dihydroxy-vitamin D₃ in human promyelocytic leukemia (HL-60) cells. *Arch. Biochem. Biophys.* **2000**, *380*, 92–102. [[CrossRef](#)] [[PubMed](#)]
- Ishizuka, S.; Norman, A.W. The difference of biological activity among four diastereoisomers of 1α,25dihydroxycholecalciferol-26,23-lactone. *J. Steroid Biochem.* **1986**, *25*, 505–510. [[PubMed](#)]

15. Mendoza, A.; Takemoto, Y.; Cruzado, K.T.; Masoud, S.S.; Nagata, A.; Tantipanjanorn, A.; Okuda, S.; Kawagoe, F.; Sakamoto, R.; Odagi, M.; et al. Controlled lipid β -oxidation and carnitine biosynthesis by a vitamin D metabolite. *Cell Chem. Biol.* **2021**. [[CrossRef](#)] [[PubMed](#)]
16. Shah, I.; Akhtar, M.K.; Hisaindee, S.; Rauf, M.A.; Sadig, M.; Ashraf, S.S. Clinical diagnostic tools for vitamin D assessment. *J. Steroid Biochem. Mol. Biol.* **2018**, *180*, 105–117. [[CrossRef](#)]
17. It is difficult to develop an antibody that specifically recognizes the structure of the side chain of vitamin D metabolites, see; Kobayashi, N.; Higashi, T.; Saito, K.; Niurayama, T.; Douya, R.; Shimada, K. Specificity of polyclonal antibodies raised against a novel 24,25-dihydroxyvitamin D₃-bovine serum albumin conjugant linked through the C-11 α or C-3 position. *J. Steroid Biochem. Mol. Biol.* **1997**, *62*, 79–87.
18. Müller, M.J.; Volmer, D.A. Mass spectrometric profiling of vitamin D metabolites beyond 25-hydroxyvitamin D. *Clin. Chem.* **2015**, *61*, 1033–1048. [[CrossRef](#)]
19. Higashi, T.; Shimada, K. Application of Cookson-type reagents for biomedical HPLC and LC/MS analyses: A brief overview: Cookson-type reagents for biomedical HPLC and LC/MS analyses. *Biomed. Chromatogr.* **2017**, *31*, e3808. [[CrossRef](#)]
20. Seki, M.; Sato, M.; Takiwaki, M.; Takahashi, K.; Kikutani, Y.; Satoh, M.; Nomura, F.; Kuroda, Y.; Fukuzawa, S. A novel caged Cookson-type reagent toward a practical vitamin D derivatization method for mass spectrometric analyses. *Rapid Commun. Mass Spectrom.* **2020**, *34*, e8648. [[CrossRef](#)]
21. Nicoletti, D.; Mouriño, A.; Torneiro, M.S. Synthesis of 25-hydroxyvitamin D₃ and 26,26,26,27,27,27-hexadeutero-25-hydroxyvitamin D₃ on solid support. *J. Org. Chem.* **2009**, *74*, 4782–4786. [[CrossRef](#)]
22. Perlman, K.; Schnoes, H.K.; Tanaka, Y.; DeLuca, H.F.; Kabayashi, Y.; Taguchi, T. Chemical synthesis of (24R)-24,25-dihydroxy[26,27-³H]vitamin D₃ of high specific activity. *Biochemistry* **1984**, *23*, 5041–5048. [[CrossRef](#)]
23. Ray, R.; Vicchio, D.; Yergey, A.; Holick, M.F. Synthesis of 25-hydroxy-[6,19,19'-²H₃]vitamin D₃ and 1 α ,25-dihydroxy-[6,19'-²H₃]vitamin D₃. *Steroids* **1992**, *57*, 142–146. [[CrossRef](#)]
24. Yamada, S.; Shimizu, M.; Fukushima, K.; Niimura, K.; Maeda, Y. Syntheses of 24R,25-dihydroxy-[6,19,19-³H]vitamin D₃ and 24R,25-dihydroxy-[6,19,19-²H]vitamin D₃. *Steroids* **1989**, *54*, 145–157. [[CrossRef](#)]
25. Yamada, S.; Suzuki, T.; Takayama, H. Novel regioselective C-6 and C-19 alkylation of vitamin D₃ via its sulfur-dioxide adducts. *Tetrahedron Lett.* **1981**, *22*, 3085–3088. [[CrossRef](#)]
26. Zhu, G.D.; Okamura, W.H. Synthesis of vitamin D (Calciferol). *Chem. Rev.* **1995**, *95*, 1877–1952. [[CrossRef](#)]
27. Gu, J.; Rodriguez, K.; Kanda, Y.; Yang, S.; Ociepa, M.; Wilke, H.; Abrishami, A.; Joergensen, L.; Skak-Nielsen, T.; Chen, J.; et al. Convergent total synthesis of (+)-Calcipotriol: A scalable, modular approach to vitamin D analogs. *ChemRxiv* **2021**. [[CrossRef](#)]
28. Maegawa, T.; Fujiwara, Y.; Inagaki, Y.; Monguchi, Y.; Sajiki, H. A convenient and effective method for the regioselective deuteration of alcohols. *Adv. Synth. Catal.* **2008**, *350*, 2215–2218. [[CrossRef](#)]
29. Pattenden, G.; González, M.A.; Little, P.B.; Millan, D.S.; Plowright, A.T.; Tornos, J.A.; Ye, T. Total synthesis of (\pm)-phorboxazole A, a potent cytostatic agent from the sponge *Phorbas* sp. *Org. Biomol. Chem.* **2003**, *1*, 4173–4208. [[CrossRef](#)]
30. The enantiomers at C3 were separated after coupling the CD rings by HPLC purification.
31. Akagi, Y.; Usuda, K.; Tanami, T.; Yasui, K.; Asano, L.; Uesugi, M.; Nagasawa, K. Synthesis of 1 α - and 1 β -amino-25-hydroxyvitamin D₃. *Asian J. Org. Chem.* **2016**, *5*, 1247–1252. [[CrossRef](#)]
32. Venkanna, A.; Sreedhar, E.; Siva, B.; Babu, K.S.; Prasad, K.R.; Rao, J.M. Studies directed towards the total synthesis of koshikalide: Stereoselective synthesis of the macrocyclic core. *Tetrahedron Asymmetry* **2013**, *24*, 1010–1022. [[CrossRef](#)]
33. Gao, Y.; Klunder, J.M.; Hanson, R.M.; Masamune, H.; Ko, S.Y.; Sharpless, K.B. Catalytic asymmetric epoxidation and kinetic resolution: Modified procedures including in situ derivatization. *J. Am. Chem. Soc.* **1987**, *109*, 5765–5780. [[CrossRef](#)]
34. Joannesse, C.; Johnston, C.P.; Concellón, C.; Simal, C.; Philp, D.; Smith, A.D. Isothiourea-catalyzed enantioselective carboxy group transfer. *Angew. Chem. Int. Ed.* **2009**, *48*, 8914–8918. [[CrossRef](#)] [[PubMed](#)]
35. Trost, B.M.; Dumas, J.; Villa, M. New strategies for the synthesis of vitamin D metabolites via palladium-catalyzed reactions. *J. Am. Chem. Soc.* **1992**, *114*, 9836–9845. [[CrossRef](#)]
36. Nagata, A.; Akagi, Y.; Masoud, S.S.; Yamanaka, M.; Kittaka, A.; Uesugi, M.; Odagi, M.; Nagasawa, K. Stereoselective synthesis of four calcitriol lactone diastereomers at C23 and C25. *J. Org. Chem.* **2019**, *84*, 7630–7641. [[CrossRef](#)] [[PubMed](#)]
37. Kaufmann, M.; Schlingmann, K.; Berezin, L.; Molin, A.; Sheftel, J.; Vig, M.; Gallagher, J.C.; Nagata, A.; Masoud, S.S.; Sakamoto, R.; et al. Differential diagnosis of vitamin D-related hypercalcemia using serum vitamin D metabolite profiling. *J. Bone Miner. Res.* **2021**, *36*, 1340–1350. [[CrossRef](#)]

Article

A Docosahexaenoic Acid Derivative (*N*-Benzyl Docosahexaenamide) as a Potential Therapeutic Candidate for Treatment of Ovarian Injury in the Mouse Model

Lirong Guo ^{1,2}, Qing Gao ^{1,2}, Jieqiong Zhu ¹, Xiaobao Jin ¹, Hui Yin ^{1,*} and Tao Liu ^{1,*}

¹ Guangdong Provincial Key Laboratory of Pharmaceutical Bioactive Substances, School of Biosciences and Biopharmaceutics, Guangdong Pharmaceutical University, Guangzhou 510006, China; glr19951215@163.com (L.G.); qinggao0403@foxmail.com (Q.G.); zhujieqiong999@foxmail.com (J.Z.); jinxf2001@163.com (X.J.)

² School of Pharmacy, Guangdong Pharmaceutical University, Guangzhou 510006, China

* Correspondence: huiyin0103@gdpu.edu.cn (H.Y.); tliu@foxmail.com (T.L.)

Abstract: Commonly used clinical chemotherapy drugs, such as cyclophosphamide (CTX), may cause injury to the ovaries. Hormone therapies can reduce the ovarian injury risk; however, they do not achieve the desired effect and have obvious side effects. Therefore, it is necessary to find a potential therapeutic candidate for ovarian injury after chemotherapy. *N*-Benzyl docosahexaenamide (NB-DHA) is a docosahexaenoic acid derivative. It was recently identified as the specific macamide with a high degree of unsaturation in maca (*Lepidium meyenii*). In this study, the purified NB-DHA was administered intragastrically to the mice with CTX-induced ovarian injury at three dose levels. Blood and tissue samples were collected to assess the regulation of NB-DHA on ovarian function. The results indicated that NB-DHA was effective in improving the disorder of estrous cycle, and the CTX+NB-H group can be recovered to normal levels. NB-DHA also significantly increased the number of primordial follicles, especially in the CTX+NB-M and CTX+NB-H groups. Follicle-stimulating hormone and luteinizing hormone levels in all treatment groups and estradiol levels in the CTX+NB-H group returned to normal. mRNA expression of ovarian development-related genes was positive regulated. The proportion of granulosa cell apoptosis decreased significantly, especially in the CTX+NB-H group. The expression of anti-Müllerian hormone and follicle-stimulating hormone receptor significantly increased in ovarian tissues after NB-DHA treatment. NB-DHA may be a promising agent for treating ovarian injury.

Keywords: docosahexaenoic acids; ovary; granulosa cells; cyclophosphamide; macamide

Citation: Guo, L.; Gao, Q.; Zhu, J.; Jin, X.; Yin, H.; Liu, T. A Docosahexaenoic Acid Derivative (*N*-Benzyl Docosahexaenamide) as a Potential Therapeutic Candidate for Treatment of Ovarian Injury in the Mouse Model. *Molecules* **2022**, *27*, 2754. <https://doi.org/10.3390/molecules27092754>

Academic Editor: Giovanni Ribaudò

Received: 31 March 2022

Accepted: 23 April 2022

Published: 25 April 2022

Publisher's Note: MDPI stays neutral with regard to jurisdictional claims in published maps and institutional affiliations.



Copyright: © 2022 by the authors. Licensee MDPI, Basel, Switzerland. This article is an open access article distributed under the terms and conditions of the Creative Commons Attribution (CC BY) license (<https://creativecommons.org/licenses/by/4.0/>).

1. Introduction

Docosahexaenoic acid (DHA) is mainly used in the form of DHA-triglycerides or DHA-ethyl esters (DHA-EE). DHA and its derivatives have attracted considerable attention in various research fields, including those involving cell signaling, photoreceptors, the nervous system, and brain development, and exhibit positive effects on ovarian functions and diseases [1]. Additionally, DHA can migrate from different tissues to the ovary during gonadal development and promote the development of model animal ovaries [2]. The DHA content in the lungs is significantly reduced after removal of the ovaries [3]. The dysregulation of ovarian gene expression induced by a high-fat diet is restored by chronic polyunsaturated fatty acid (PUFA)/DHA supplementation [4]. Considering this progress in DHA research for the prevention and mitigation of ovarian-related diseases and functions, the continued discovery and development of new DHA derivatives for ovarian injury remains imperative.

N-benzyl docosahexaenamide (NB-DHA) is characterized by the presence of benzylamine-conjugated DHA via an amide bond. Benzylated fatty acids are active ingredients exclusive to maca (*Lepidium meyenii*), named macamides. Notably, NB-DHA had the highest

degree of unsaturation among all the identified macamides. Benzylamide is a chemical used to enhance drug activity. For example, *N*-benzyl salinomycin has been reported to exhibit anticancer and antibacterial activities [5]. Deoxynojirimycin derivatives have been studied and can be used as α -glucosidase inhibitors to improve type II diabetes; compound 18, containing an *N*-benzyl amide residue, showed the highest activity [6]. A molecule containing an *N*-benzyl amide residue was screened from a library of compounds, and the results revealed that the synthesized compound is a severe acute respiratory syndrome coronavirus 2 (SARS-CoV-2) replication inhibitor at non-toxic concentrations in vitro and a dual-acting SARS-CoV-2 protease inhibitor against the main protease [7]. Macamides possess various bioactivities, including reproductive health improvement, antioxidation, neuroprotection, anticancer, immunomodulation, and digestive system function-improving activities [8–13]. As a newly identified PUFA, NB-DHA can protect the intestinal epithelial barrier and effectively relieve the symptoms of acute colitis in mice [14], while *N*-benzyl eicosapentaenoamide (NB-EPA) alleviates neurobehavioral disorders in neonatal mice with hypoxic-ischemic brain injury through the p53–PUMA signaling pathway [15].

Chemotherapeutic drugs, such as clinically available cyclophosphamide (CTX), are toxic to dividing and proliferating cells [16,17]. Chemotherapy with CTX can cause ovarian injury, permanent amenorrhea, and increase the risk of premature menopause [18,19]. The maintenance of ovarian reserve function and prevention of infertility have always been considered by physicians as important prognostic factors during chemotherapy [20–22]. Granulosa cells (GCs), as the largest cell group in follicles, play a crucial role in follicle growth and ovarian function regulation. GCs also regulate the development of follicles and are the main functional cells that secrete reproductive hormones [23]. Therefore, it is necessary to find potential therapeutic candidates to relieve and treat ovarian injury, protect GCs, and maintain the growth and development of follicles and ovaries. Although hormone-based treatments for ovarian injury have been adopted in current clinical practice, they do not achieve the desired therapeutic effect, and they also have obvious side effects on the human body [24].

In the present study, NB-DHA were synthesized, purified, and administered intragastrically into mice with CTX-induced ovarian injury to assess the regulation of ovarian function. Frequency of occurrence, the stages of the estrous cycle, follicle numbers after H&E staining, four typical sex hormone levels, mRNA expression of five ovarian development-related genes (FOXL2, GDF9, LIF, OCT4, and SCF), granular cell apoptosis ratios, anti-Müllerian hormone (AMH), and follicle-stimulating hormone receptor (FSHR) expression were obtained and analyzed. Terminal deoxynucleotidyl transferase dUTP nick end labeling (TUNEL) fluorescence staining was performed to explore the ovarian injury repair mechanism.

2. Results

2.1. Preparation of DHA-EE and NB-DHA

Fish oil was hydrolyzed by lipase into free fatty acids, which were used for the synthesis of DHA-EE via the esterification reaction and NB-DHA via the carbodiimide condensation method. The DHA-EE and NB-DHA fractions were collected separately from an HPLC system with elution times of 26.5–30.5 and 26.0–29.0 min, respectively. Both collected fractions were rotary evaporated to dryness and identified by infrared spectroscopy and mass spectrometry (data not shown). Their purities, analyzed by HPLC, were 96.2% (DHA-EE, Figure 1A) and 98.3% (NB-DHA, Figure 1B). The dried samples were used for subsequent animal experiments.

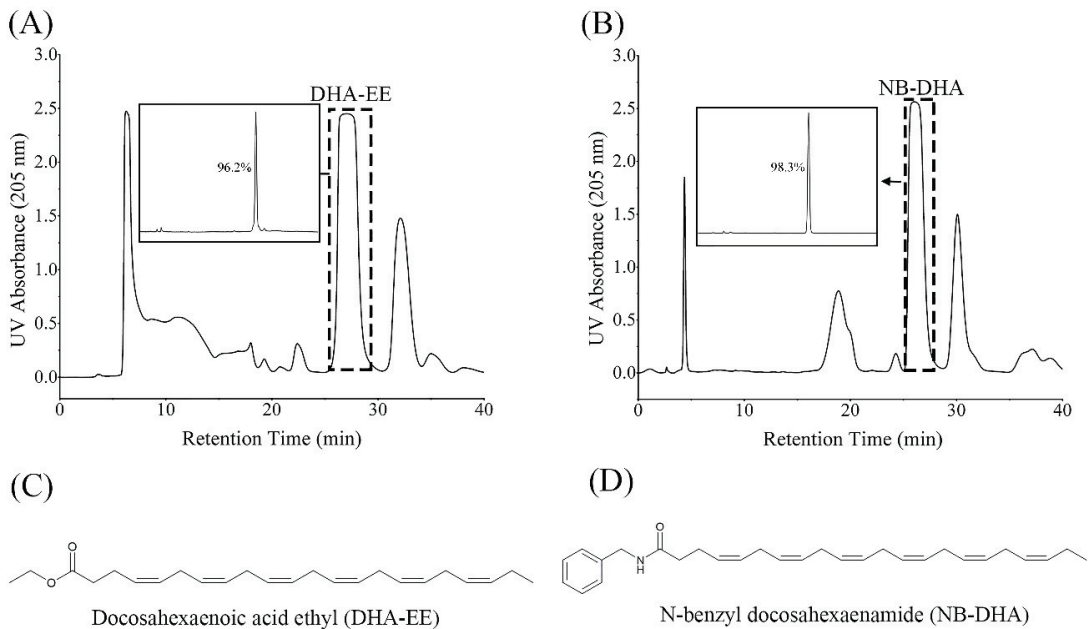


Figure 1. Chromatograms and structural formulas of DHA-EE and NB-DHA. (A) Chromatograms of synthetic DHA-EE material and purified DHA-EE sample collected using a semipreparative HPLC system (26.5–30.5 min). (B) Chromatograms of synthetic NB-DHA material and purified NB-DHA sample collected using a semipreparative HPLC system (26.0–29.0 min). Structural formulas of DHA-EE (C) and NB-DHA (D).

2.2. Body/Ovarian Weight and Estrous Cycle Analysis

As shown in Figure 2A, CTX caused a significant decrease in body weight compared with the control group. The body weight of mice in all DHA-treated groups was significantly higher than that of mice in the CTX group at the end of the 21-day experiment, and body weight recovery was ranked as follows: CTX+NB-H > CTX+NB-M > CTX+DHA-EE > CTX+NB-L. Additionally, compared with the control group, CTX significantly decreased the ovarian weight in the CTX group. After modeling with CTX, ovarian atrophy and ovarian weight decreased significantly. The ovarian weight of mice in the CTX+NB-H, CTX+NB-M, and CTX+DHA-EE groups was higher than that in the CTX group (Figure 2B). CTX is an inducer for the ovarian model that involves prolonging or stagnating the female estrous cycle. The statistical results showed that the time of estrus was shortened, and proestrus, metestrus, and diestrus were prolonged in the CTX group, indicating a disordered estrous cycle in CTX-treated mice (Figure 2C). The 21-day complete estrous cycle of mice was plotted, and the results showed that the average estrous cycle of the control group was 5–6 days. In the CTX group, a complete cycle could not be observed after modeling, but a complete estrous cycle could be observed in each DHA group. DHA-EE and NB-DHA were both effective in alleviating the disorder of the estrous cycle and were ranked as follows: CTX+NB-H > CTX+NB-M > CTX+DHA-EE (Figure 2D).

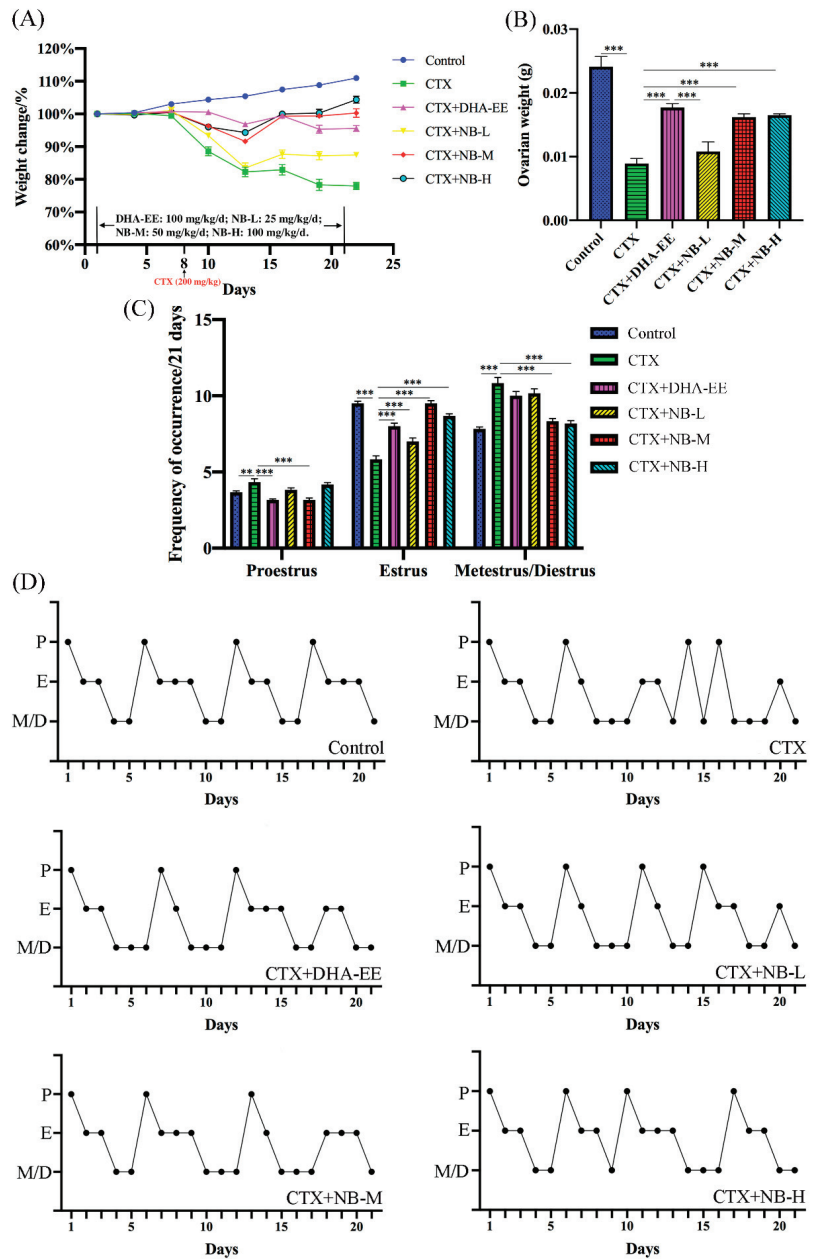


Figure 2. Body weight, ovarian weight, frequency of occurrence, and estrous cycle. Weight Change/% (A) and ovarian weight (B) measured on days 1, 4, 7, 10, 13, 16, 19, and 22 after administration. Initial average weight of mice was set as 100%. Effect of DHA-EE and NB-DHA on estrous cycles. Frequency of occurrence of cycle stages during the 21 days (n = 6) (C) and estrous cycle regularity (D). Values in all figures are expressed as the mean ± SEM (x ± sem, n = 6), ** p < 0.01, *** p < 0.005 (the same below).

2.3. Follicle Counting and Morphological Analysis

The effects of DHA-EE and NB-DHA on follicular development were analyzed by H&E staining of the ovarian sections (Figure 3A). Abundant healthy follicles were observed in the control group, including primordial, primary, secondary, and atretic follicles, while the distribution of the four types of follicles in the other groups was altered (Figure 3B–E). For example, there were fewer primordial, primary, and secondary follicles, but more atretic follicles in the CTX group than in the control group. Compared with the CTX group, both CTX+DHA-EE and CTX+NB-DHA significantly increased the number of primordial follicles, especially in the CTX+NB-M and CTX+NB-H groups. Moreover, there were fewer atretic follicles in all DHA-treated groups than in the CTX group. The groups ranked as follows: CTX+NB-H > CTX+NB-M > CTX+DHA-EE > CTX+NB-L.

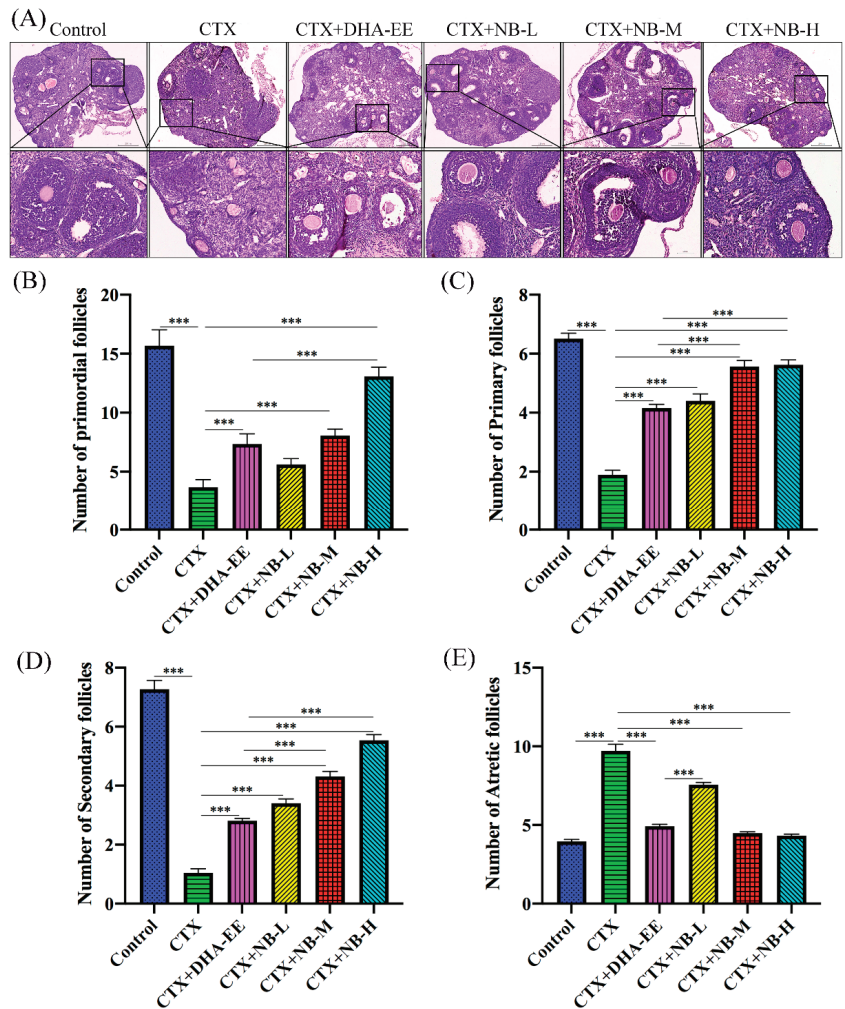


Figure 3. Effect of DHA-EE and NB-DHA on the development of follicles. Follicles after H&E staining (A). Magnification 100 \times and 400 \times . Scale bar: 250 and 50 μ m. Number of different follicles: primordial follicles (B), primary follicles (C), secondary follicles (D), and atretic follicles (E). *** $p < 0.005$.

2.4. Ovarian Hormone Levels in Serum and mRNA Expression Levels in Ovarian Tissue

As shown in Figure 4A–D, serum gonadotropin levels, including E2 and AMH, were significantly lower in the CTX group than in the control group, whereas those of serum FSH and LH were significantly higher. Furthermore, the E2 level was significantly higher in all treatment groups compared with the CTX group. FSH and LH levels in all treatment groups and E2 levels in the CTX+NB-H group returned to normal. Additionally, the mRNA expression of five ovarian development-related genes (FOXL2, GDF9, LIF, OCT4, and SCF) were measured; FOXL2, OCT4, GDF9, and LIF were significantly downregulated (Figure 4E–H), whereas that of SCF was significantly upregulated in the CTX group compared with the control group (Figure 4I). Compared with those in the CTX group, the mRNA expression levels of FOXL2 and LIF in CTX+NB-M, FOXL2, GDF9, LIF, and OCT4 in CTX+NB-H, and FOXL2, LIF, and OCT4 in CTX+DHA-EE were significantly upregulated. SCF in CTX+NB-M, CTX+NB-H, and CTX+DHA-EE was significantly downregulated.

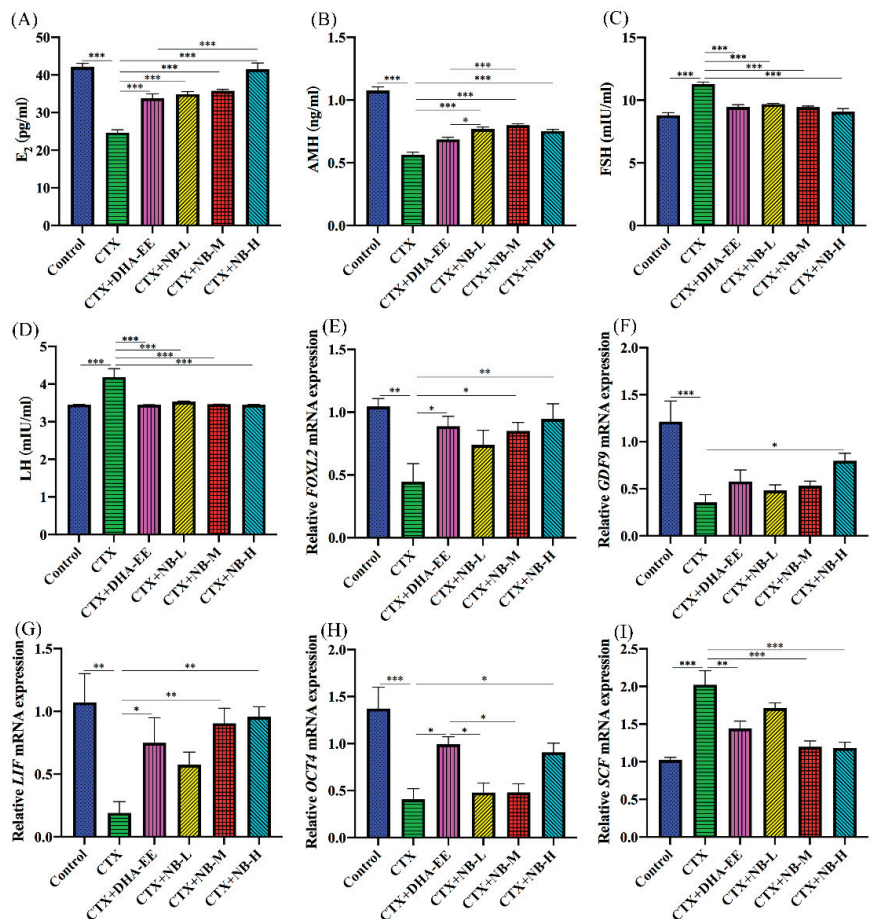


Figure 4. Effect of model and treatment on sex hormone levels and mRNA expression in mice. Sex hormone levels of E2 (A), AMH (B), FSH (C), and LH (D). mRNA expression levels of FOXL2 (E), GDF9 (F), LIF (G), OCT4 (H), and SCF (I) in mouse ovarian tissues, as determined by real-time PCR. * $p < 0.05$, ** $p < 0.01$, *** $p < 0.005$.

2.5. GC Apoptosis

To analyze ovarian cell apoptosis, the fractured DNA of apoptotic GCs in the antral follicles was observed using an in situ TUNEL assay. The number of apoptotic cells in the CTX group was significantly higher than that in the control group. However, after treatment with DHA-EE and NB-DHA, apoptosis of GCs was significantly decreased (Figure 5A). These results showed that apoptosis of GCs plays a crucial role in ovarian function development and growth in ovarian injured mice, and that DHA-EE and NB-DHA can restore ovarian function by inhibiting apoptosis. The proportion of TUNEL-positive cells decreased significantly after the additional administration of different doses of DHA-EE and NB-DHA (Figure 5C), especially in the CTX+NB-H and CTX+DHA-EE groups, in which the TUNEL-positive cell ratio was similar to that of the control group. This result reveals that high-dose NB-DHA can be considered suitable for the alleviation of CTX-induced ovarian cell apoptosis. DHA-EE also reduced GC apoptosis. The groups ranked as follows: CTX+NB-H > CTX+NB-M > CTX+DHA-EE > CTX+NB-L.

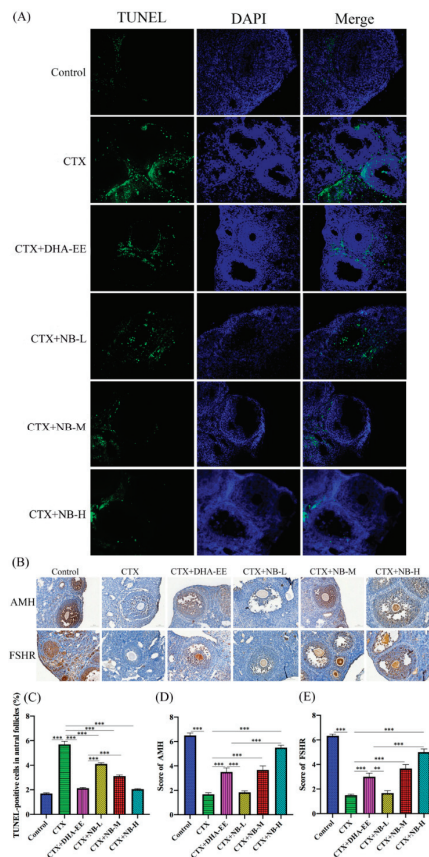


Figure 5. TUNEL and immunohistochemical analysis. Apoptosis of granulosa cells in ovarian tissues was measured via TUNEL assay (A). Green fluorescence: apoptotic cells; blue fluorescence: nucleus; magnification: 400 \times . The expression of AMH and FSHR in ovarian tissues were measured by immunohistochemical analysis (B). Blue: nucleus; brown: cells expressing AMH and FSHR in the cytoplasm; scale bar: 50 μ m; magnification: 400 \times . TUNEL-positive cell ratios in the treatment groups were analyzed according to the number of TUNEL-positive granulosa cells among all granulosa cells in the follicle (C). Scoring of staining results (D,E). ** $p < 0.01$, *** $p < 0.005$.

2.6. AMH and FSHR Expression in Ovaries

FSHR and AMH expression was detected by immunohistochemical analysis. Positive immunohistochemical results were scored. As shown in Figure 5B, the expression of AMH and FSHR in the CTX group was significantly lower than that in the control group. The expression of AMH and FSHR significantly increased after DHA-EE and NB-DHA treatment (Figure 5D,E). Notably, the effect of NB-H was better than that of DHA-EE at the same dosage. The treatments increased the expression of AMH and FSHR in the following order: CTX+NB-H > CTX+NB-M > CTX+DHA-EE > CTX+NB-L.

3. Discussion

Macamide-rich extract has been reported to stimulate the reproductive system, increase the number of mature follicular cells in female mice, and increase the number of sperm produced by male mice [25]. NB-DHA is a DHA derivative that belongs to the macamide family. It is difficult for higher plants to synthesize long-chain PUFAs, causing the content of NB-DHA in maca to be extremely low [14]. Therefore, in this study, DHA-rich fish oil was used as the starting material, and NB-DHA was efficiently synthesized with the carbodiimide condensation method [26]. Commercially available DHA is mainly in the form of ethyl esters or triglycerides. Theoretically, the degradation of the ester and benzylamide groups is different *in vivo*; as DHA-EE and NB-DHA are metabolized and absorbed at different rates and via different mechanisms, they might display different bioactive profiles in the human body [27–29].

After modeling with CTX, the mice lost their appetite and caused weight loss. After the experiment, the ovaries atrophied and the weight of the ovaries decreased, causing ovarian injury. Compared with the CTX group, the body and ovarian weights of the mice increased significantly after the administration of CTX+NB-M and CTX+NB-H, and CTX+DHA-EE treatment has just stabilized their body weight. We speculated that CTX caused changes in the ovarian microenvironment in mice, causing ovarian damage and leading to ovarian atrophy, while DHA-EE and NB-DHA alleviated CTX-induced ovarian injury. Our results indicate that both DHA-EE and NB-DHA reverse ovarian injury by increasing the number of normal follicles and decreasing that of atretic follicles. Ovarian injury clinically manifests as an abnormal estrous cycle and ovarian function, and severe injury may lead to premature ovarian failure and infertility [30–32]. CTX-induced ovarian injury mice in the CTX group exhibited an irregular estrous cycle and changes in ovarian function indicators. The primordial follicles, which act as the initial unit of follicle maturation or generation, undergo a series of developmental stages that form primary, secondary, and mature follicles, which then release the oocytes for reproduction. Most primitive follicles eventually become closed follicles, and only a few reach maturity [33,34]. Therefore, the growth of primordial follicles is related to the development of the entire ovary. Ovarian injury can cause a decrease in AMH and E2 levels and an increase in FSH and LH levels, which are considered four important indices for the evaluation of ovarian injury and abnormal follicular maturation. Our results indicated that the irregular estrous cycles of mice in the CTX+DHA-EE, CTX+NB-M, and CTX+NB-H groups were positively regulated to close the regular cycle of mice in the control group with a prolonged estrus period and shortened late estrus and interval. CTX-induced ovarian injury resulted in enhanced serum FSH and LH levels and decreased serum E2 and AMH levels. Meanwhile, the number of primordial, primary, and secondary follicles was reduced, and the number of atresia follicles increased. However, the administration of DHA-EE and different doses of NB-DHA to alleviate this injury increased the number of primordial, primary, and secondary follicles, reduced the number of atretic follicles, increased serum AMH and E2 levels, and reduced FSH and LH levels. These results reveal the regulatory function of both DHA-EE and NB-DHA on the estrous cycle of mice with ovarian injury caused by CTX.

The formation, maturation, and growth of follicles are regulated by many intra- and extra-ovarian factors. FOXL2 is involved in multiple dysfunctional states in the ovary and is essential for GC differentiation and maintenance of ovarian function, and is expressed in

GCs with low differentiation in small- and medium-sized follicles [35]. GDF9 encodes a protein secreted into the follicle by oocytes [36] and plays a pivotal role in optimizing the oocyte microenvironment and growth, development, atresia, ovulation, fertilization, and normal reproduction of the follicle [37]. It also has a role in promoting the proliferation and apoptosis of GCs while stimulating the expression of Kit ligands on GCs. LIF is expressed in the ovaries and promotes follicle growth. LIF has also been shown to coordinate follicular growth and ovulation sequences and can locally regulate follicular growth [38]. Oct4 has the potential to recruit mature oocytes. Overexpression in ovarian stem/stromal cells enhances oocyte-like differentiation *in vitro* and follicle formation *in vivo* [39]. SCF is essential for the early follicular development. It stimulates stromal cell function and promotes follicular growth through the Erk1/2 pathway, and can be used as a crucial regulator of embryo and ovarian growth to exert its biological effects [40,41]. CTX can cause ovarian injury and disorders in the expression levels of these mRNA [40]. Our results also revealed that the mRNA levels of FOXL2, GDF9, LIF, and OCT4 were decreased, while those of SCF were increased in the CTX group. After high-dose NB-DHA treatment, the levels of FOXL2, GDF9, LIF, and OCT4 increased, whereas those of SCF decreased. The mechanism of action of NB-DHA might be to promote the growth and maturation of follicles via the regulation of the mRNA expression levels of these five genes, thereby reversing ovarian injury caused by CTX and protecting the ovaries. At the same dose, the effect of NB-H was better than that of DHA-EE.

According to previous reports, follicular atresia occurs when more than 10% of GCs undergo apoptosis. Follicular atresia can cause a decline in ovarian function [42,43]. Our results indicated that apoptotic GCs and atretic follicles were significantly increased in the CTX group and reduced after both DHA-EE and NB-DHA treatment, whereas that of other types of follicles increased, suggesting that NB-DHA acts on AMH expression through cytokines secreted by granulocytes. AMH is produced by GCs of early ovarian developing follicles and is expressed at high levels throughout follicle formation. When ovarian GCs undergo apoptosis, DNA is fragmented and 3'-OH is combined with TdT to generate fluorescence. Our results analyzed the ratio of fluorescent cells and showed that CTX induced apoptosis of ovarian cells, which was reversed by DHA-EE and NB-DHA administration. In this case, we infer that DHA-EE and NB-DHA can reduce the apoptosis of ovarian granulosa cells, thereby achieving the effect of protecting the ovary. However, the anti-apoptotic activity of NB-DHA remains to be explored. The serum AMH level may represent the quantity and quality of the follicular pool, which is related to ovarian aging and failure, and reflects the state of the ovaries. Follicles are surrounded by GCs instead of membranous cells, oocytes, and ovarian stromal cells [44,45]. In addition, there is no expression of AMH when the follicle is atresia [43]. FSHR is expressed specifically in the GCs of the ovary and plays a key role in follicular function by interacting with its ligand FSH in the ovaries. When the follicle is atresia, FSHR expression is downregulated [46]. The immunohistochemical analysis results showed that both AMH and FSHR were expressed in secondary follicles, and the serum levels of AMH and FSHR were consistent with those in the ovary. The expression of AMH and FSHR in the CTX group was significantly lower than that in the other groups. The levels of both recovered after NB-DHA treatment, indicating that NB-DHA facilitates the growth of GCs and the expression of AMH and FSHR, thereby promoting follicle growth. The decreased primary follicles in the mouse model of ovarian injury, potentially owing to decreased serum AMH levels, lead to premature depletion of the original follicular pool. After treatment with NB-DHA, the levels of AMH and FSHR increased, indicating that NB-DHA increased the number of primordial follicles, reduced the failure of the primordial follicle pool caused by CTX, restored GC growth, and restored ovarian function. However, DHA-EE at the same dose as high-dose NB-DHA had no significant effect on AMH and FSHR expression in the follicles.

4. Materials and Methods

4.1. Materials

Fish oil (DHA content > 80%) was obtained from Shanxi Taike Biotech Co., Ltd. (20200712-002, Xi'an, China). Rhizomucor miehei lipase (L8621) was obtained from Solarbio (Beijing, China). Ethyl dimethylaminopropyl carbodiimide (EDC), benzylamine, dichloromethane, HOBT ·H₂O, and triethylamine were obtained from Aladdin Co., Ltd. (Shanghai, China). The 3,3-diaminobenzidine kit (20×) (CW0125) was obtained from Cwbio Co., Ltd. (Beijing, China). Proteinase K (BL104A) and anti-fluorescence quenching mounting fluid (BL701A) were obtained from Biosharp Co., Ltd. (Hefei, China). Anti-FSHR (#40941) and anti-Müllerian-inhibiting factor (#42063) polyclonal antibodies were obtained from SAB Co., Ltd. (Baltimore, MD, USA).

Enzyme-linked immunosorbent assay (ELISA) kits for luteinizing hormone (LH; CSB-E12770m), follicle-stimulating hormone (FSH; CSB-E06871m), estradiol (E2; CSB-E05109m), and anti-Müllerian hormone (AMH; CSB-E13156m) were obtained from Cusabio Biotech Co., Ltd. (Wuhan, China). Evo M-MLV RT Mix Kit with gDNA Clean for qPCR (AG11728) and SYBR Green Pro Taq HS premixed qPCR kits (AG11701) were obtained from AgBio Co., Ltd. (Changsha, China). A TUNEL kit (in situ cell death detection; C1086) and DAPI (4',6-diamidino-2-phenylindole; C1005) were obtained from Beyotime Biotech Co., Ltd. (Shanghai, China).

4.2. Synthesis and Purification of DHA-EE and NB-DHA

Twenty milliliters of fish oil were added to 20 mL of 10% (*w/v*) lipase solution, mixed homogeneously, and hydrolyzed at 45 °C for 24 h. The oil layer was collected, washed alternately with distilled water (40 mL) and n-hexane (40 mL), and the aqueous layer was discarded. The supernatant was concentrated using a rotating vacuum evaporator at 45 °C for 30 min. The fatty-acid-rich residues were stored frozen for subsequent synthesis experiments. DHA-EE was synthesized using a transesterification method. In brief, free fatty acids (700 µL) were mixed with 500 µL of NaOH-ethanol solution at 70 °C for 30 min, washed twice with saturated NaCl solution, and centrifuged at 5000× *g* for 10 min to collect the oil layer containing DHA-EE. NB-DHA was synthesized using the carbodiimide condensation method. Briefly, 100 mL of dichloromethane, 700 µL of free fatty acids, 528.6 µL of triethylamine, 0.206 g of HOBT H₂O, and 0.292 g of EDC were mixed and agitated at 25 °C for 20 h, and 166 µL of benzylamine was added and stirred at 25 °C for 4 h. Subsequently, 200 mL of 10% HCl was added to the residue after drying, and 200 mL n-hexane was added, mixed homogeneously, and rested for 10 min. The upper layer was collected and washed alternately with 10% HCl and 10% NaOH to remove macroscopic impurities. Finally, DHA-EE and NB-DHA were purified according to our previous method, and their purities were analyzed by HPLC [14].

4.3. Animals and Treatment

Healthy female mice (20 ± 2 g, 7–8 weeks old, C57BL/6) were obtained from the Guangdong Medical Laboratory Animal Center (Guangzhou, China). The mice were kept under pathogen-free conditions in a temperature (23 ± 2 °C) and humidity (55% ± 15%) control system, and all animal facilities were kept in a 12 h light–dark cycle. Food and water were provided free access for one week prior to the experiment. A preliminary experiment was carried out to determine the effective dose range of DHA-EE and NB-DHA. The mice were randomly divided into six independent groups (*n* = 6): control, ovarian injury model caused by CTX, CTX+DHA-EE (100 mg/kg/day), CTX+low-dose NB-DHA (CTX+NB-L, 25 mg/kg/day), CTX+medium-dose NB-DHA (CTX+NB-M, 50 mg/kg/day), and CTX+high-dose NB-DHA (CTX+NB-H, 100 mg/kg/day) groups. All drugs were administered to the mice after dissolving in Tween 80 solution at a concentration of 1%. Mice in the DHA-EE and NB-DHA groups were gavaged once a day from day 1 to day 21. The CTX, CTX+NB-DHA, and CTX+DHA-EE groups were injected intraperitoneally with CTX (200 mg/kg) on the eighth day after adaptive feeding. The control group was fed

normally without any drugs until the end of the experiment. All treatments were started at the same time and were sustained for 21 days. The survival rate of the mice was 100% during the experiments.

4.4. Ovarian Index and Estrous Cycle Examination

The mice were weighed prior to euthanasia. The isolated ovaries were repeatedly rinsed with precooled sterile saline, blotted dry with filter paper, and weighed. Nucleated cells, keratinized epithelial cells, and leukocytes in vaginal smears were observed under a light microscope, and the stages of the estrous cycle, including proestrus, estrus, metestrus, and diestrus phases, were determined based on the identification and proportions of cells. The estrous cycle was monitored continuously for 21 d.

4.5. Morphological Analysis and Follicle Counting

The ovaries were fixed with paraformaldehyde solution (4%) for 12 h and then washed with running water for 12 h. Subsequently, ovaries were dehydrated, embedded in paraffin, and stored at -20°C . The tissues were sliced serially (4 μm thick), and one every five sheets was selected for hematoxylin and eosin (H&E) staining. Filming was performed using a slide scanning system (SQS-40P, Teksqray, Shenzhen, China). The viewing angle was determined under a microscope at low magnification, while primordial, primary, secondary, and atretic follicles were counted at high magnification. Six ovarian samples were randomly selected from each group, and sections were observed in 3 views under $400\times$ to count follicles at all stages.

4.6. ELISA

The mice were fasted for 8 h after the final administration. Blood samples were collected from the eye veins, placed in anticoagulation tubes, and centrifuged at $4000\times g$ for 15 min. The levels of serum FSH, LH, E2, and AMH were measured using an ELISA kit.

4.7. RNA Extraction and Reverse-Transcription qPCR

Total RNA was extracted from ovarian tissues using an RNA extraction kit. The RNA concentration was 500–1000 ng/ μL . Then, 1 μg of RNA was reverse transcribed into cDNA, as required by the reverse transcription kit. The qPCR kit was used to measure the expression levels of GAPDH, FOXL2, GDF9, LIF, OCT4, and SCF. The primer sequences were as follows:

GAPDH-forward primer: 5'-TGTGTCCGTCGTGGATCTGA-3',
 GAPDH-reverse primer: 5'-TTGCTGTTGAAGTCGCAGGAG-3';
 FOXL2-forward primer: 5'-CACCTCCAGGCCAGGTCTTTA-3',
 FOXL2-reverse primer: 5'-TTTAGCAAACCTCCAAGGCCATTAC-3';
 GDF9-forward primer: 5'-GTTCCCAAACCCAGCAGAAGTC-3',
 GDF9-reverse primer: 5'-GTCCAGGTAAACAGCAGGTCCA-3';
 LIF-forward primer: 5'-TTGATCCCGACTCAAGCAACC-3',
 LIF-reverse primer: 5'-CTGAAGCCGCTACCATGCAA-3';
 OCT4-forward primer: 5'-CAGACCACCATCTGTCGTTCC-3',
 OCT4-reverse primer: 5'-AGACTCCACCTCACACGGTTCTC-3';
 SCF-forward primer: 5'-AGATCTGCGGGAATCCTGTGA-3',
 SCF-reverse primer: 5'-CATCCCGGCGACATAGTTGA-3'.

4.8. In Situ Cell Death Detection

For the in situ TUNEL paraffin staining, a part of each ovarian sample slice was randomly selected ($n = 6$). The sections were covered with protease K solution (20 mg/mL) and incubated in a wet chamber at 37°C for 30 min. The sections were washed five times with PBS and then covered with Triton X-100 (1%) at 4°C for 10 min. An in situ cell death assay kit was used for the TUNEL assay. The sections were incubated in TUNEL reaction mixture (TdT enzyme and fluorescent-labeled buffer) for 60 min at 37°C under

dark and humid conditions to capture the fragmented DNA of apoptotic cells. The sections were then incubated with DAPI at 24 °C for 5 min, washed with PBS, dried around the tissues, mounted with an anti-fluorescence quencher, and observed under a fluorescence microscope (BX53, Olympus, Tokyo, Japan). Whether the section was intact was established at 100× magnification, and the apoptosis of atretic follicles was carefully observed at 400× magnification. ImageJ 1.53a software was used to analyze the proportion of TUNEL-positive cells in the antral follicles.

4.9. Immunohistochemistry

Paraffin-embedded tissue sections were dewaxed in a microwave oven for antigen repair. Immunohistochemical staining was performed using an SP immunohistochemistry kit. Rabbit anti-AMH (1:100) and anti-FSHR (1:150) antibodies were incubated with the tissue at 4 °C for 12 h. Six areas on each slide were randomly selected for inspection and filmed using the SQS-40P slide scanning system. The German immune response scoring standard (IRS) was used to score the staining results [47].

4.10. Data Analysis

All data were analyzed using GraphPad Prism 8 software, and the results are shown as the mean ± standard error of the mean (SEM). One-way analysis of variance was used to evaluate statistical significance among the experimental groups. All data were considered statistically significant at * $p < 0.05$, ** $p < 0.01$, and *** $p < 0.005$.

5. Conclusions

In summary, these data demonstrate that NB-DHA alleviates ovarian injury in mice. NB-DHA reverses the high levels of gonadotropins and low levels of estrogen in the serum of mice with ovarian injury, promotes follicular development, inhibits follicular atresia and GC apoptosis via the upregulation of AMH and FSHR expression in GCs, and regulates the mRNA expression levels of ovarian-related genes to increase the ovarian reserve capacity. Natural DHA can be used as a beneficial dietary supplement to improve ovarian function, and NB-DHA is a promising compound for the clinical treatment of patients with ovarian injury.

Author Contributions: L.G.: Methodology and Writing—Original Draft; Q.G. and J.Z.: Investigation; X.J.: Data Curation; T.L. and H.Y.: Conceptualization, Writing—Review and Editing. All authors have read and agreed to the published version of the manuscript.

Funding: This research was funded by the National Natural Science Foundation of China (81770527 and 82171700) and Shenzhen Longgang District medical and health science and technology plan project (LGKCYLWS2021000022).

Institutional Review Board Statement: The animal study protocol was approved by the Ethics Committee of Guangdong Pharmaceutical University (protocol code: gdpulac2020124, 3 April 2020).

Data Availability Statement: Not available.

Conflicts of Interest: The authors declare no conflict of interest.

Sample Availability: Samples of the compounds *N*-Benzyl Docosahexaenamide are available from the authors.

References

1. West, L.; Yin, Y.; Pierce, S.R.; Fang, Z.; Fan, Y.; Sun, W.; Tucker, K.; Staley, A.; Zhou, C.; Bae-Jump, V. Docosahexaenoic acid (DHA), an omega-3 fatty acid, inhibits tumor growth and metastatic potential of ovarian cancer. *Am. J. Cancer Res.* **2020**, *10*, 4450–4463. [PubMed]
2. Zhu, Y.; Tan, Q.; Zhang, L.; Yao, J.; Zhou, H.; Hu, P.; Liang, X.; Liu, H. The migration of docosahexaenoic acid (DHA) to the developing ovary of female zebrafish (*Danio rerio*). *Comp. Biochem. Physiol. A Mol. Integr. Physiol.* **2019**, *233*, 97–105. [CrossRef]

3. Yaeger, M.J.; Reece, S.W.; Kilburg-Basnyat, B.; Hodge, M.X.; Pal, A.; Dunigan-Russell, K.; Luo, B. Sex Differences in Pulmonary Eicosanoids and Specialized Pro-Resolving Mediators in Response to Ozone Exposure. *Toxicol. Sci.* **2021**, *183*, 170–183. [[CrossRef](#)] [[PubMed](#)]
4. Taghizadeh, M.; Asemi, Z.; Keshavarz, S.A.; Jafarnejad, S. The Effect of Omega-3 Fatty Acids, EPA, and/or DHA on Male Infertility: A Systematic Review and Meta-analysis. *J. Diet Suppl.* **2019**, *16*, 245–256.
5. Antoszczak, M.; Maj, E.; Napiórkowska, A.; Stefańska, J.; Augustynowicz-Kopeć, E.; Wietrzyk, J.; Janczak, J.; Brzezinski, B.; Huczynski, A. Synthesis, anticancer and antibacterial activity of salinomycin N-benzyl amides. *Molecules* **2014**, *19*, 19435–19459. [[CrossRef](#)] [[PubMed](#)]
6. Zeng, F.; Yin, Z.; Chen, J.; Nie, X.; Lin, P.; Lu, T.; Wang, M.; Peng, D. Design, Synthesis, and Activity Evaluation of Novel N-benzyl Deoxynojirimycin Derivatives for Use as α -Glucosidase Inhibitors. *Molecules* **2019**, *24*, 3309. [[CrossRef](#)]
7. Di Sarno, V.; Lauro, G.; Musella, S.; Ciaglia, T.; Vestuto, V.; Sala, M.; Scala, M.C.; Smaldone, G.; Di Matteo, F.; Novi, S.; et al. Identification of a dual acting SARS-CoV-2 proteases inhibitor through in silico design and step-by-step biological characterization. *Eur. J. Med. Chem.* **2021**, *226*, 113863. [[CrossRef](#)] [[PubMed](#)]
8. Cheng, C.; Shen, F.; Ding, G.; Liu, A.; Chu, S.; Ma, Y.; Hou, X.; Hao, E.; Wang, X.; Hou, Y. Lepidilina A Improves the Balance of Endogenous Sex Hormones and Increases Fecundity by Targeting HSD17B1. *Mol. Nutr. Food Res.* **2020**, *64*, e1900706. [[CrossRef](#)] [[PubMed](#)]
9. Tang, W.; Jin, L.; Xie, L.; Huang, J.; Wang, N.; Chu, B.; Dai, X.; Liu, Y.; Wang, R. Structural Characterization and Antifatigue Effect In Vivo of Maca (*Lepidium meyenii* Walp) Polysaccharide. *J. Food Sci.* **2017**, *82*, 757–764. [[CrossRef](#)] [[PubMed](#)]
10. Patel, S.S.; Raghuvanshi, R.; Masood, M.; Acharya, A.; Jain, S.K. Medicinal plants with acetylcholinesterase inhibitory activity. *Rev. Neurosci.* **2018**, *29*, 491–529. [[CrossRef](#)] [[PubMed](#)]
11. Fu, L.; Wei, J.; Gao, Y.; Chen, R. Antioxidant and antitumoral activities of isolated macamide and macaene fractions from *Lepidium meyenii* (Maca). *Talanta* **2021**, *221*, 121635. [[CrossRef](#)]
12. da Silva Leitão Peres, N.; Cabrera Parra Bortoluzzi, L.; Medeiros Marques, L.L.; Formigoni, M.; Fuchs, R.H.B.; Droval, A.A.; Reitz Cardoso, F.A. Medicinal effects of Peruvian maca (*Lepidium meyenii*): A review. *Food Funct.* **2020**, *11*, 83–92. [[CrossRef](#)]
13. Jin, W.; Chen, X.; Huo, Q.; Cui, Y.; Yu, Z.; Yu, L. Aerial parts of maca (*Lepidium meyenii* Walp.) as functional vegetables with gastrointestinal prokinetic efficacy in vivo. *Food Funct.* **2018**, *9*, 3456–3465. [[CrossRef](#)] [[PubMed](#)]
14. Zha, R.; Ge, E.; Guo, L.; Gao, Q.; Lin, Q.; Zhou, W.; Jin, X.; Xie, W.; Yin, H.; Liu, T. A newly identified polyunsaturated macamide alleviates dextran sulfate sodium-induced colitis in mice. *Fitoterapia* **2021**, *152*, 104916. [[CrossRef](#)]
15. Jiao, M.; Dong, Q.; Zhang, Y.; Lin, M.; Zhou, W.; Liu, T.; Yuan, B.; Yin, H. Neuroprotection of N-benzyl Eicosapentaenamide in Neonatal Mice Following Hypoxic-Ischemic Brain Injury. *Molecules* **2021**, *26*, 3108. [[CrossRef](#)]
16. Meirrow, D.; Biederman, H.; Anderson, R.A.; Wallace, W.H. Toxicity of chemotherapy and radiation on female reproduction. *Clin. Obstet. Gynecol.* **2010**, *53*, 727–739. [[CrossRef](#)] [[PubMed](#)]
17. Slater, C.A.; Liang, M.H.; McCune, J.W.; Christman, G.M.; Laufer, M.R. Preserving ovarian function in patients receiving cyclophosphamide. *Lupus* **1999**, *8*, 3–10. [[CrossRef](#)]
18. D’Avila, Á.M.; Biolchi, V.; Capp, E.; Corleta, H.V. Age, anti-müllerian hormone, antral follicles count to predict amenorrhea or oligomenorrhea after chemotherapy with cyclophosphamide. *J. Ovarian Res.* **2015**, *8*, 82. [[CrossRef](#)] [[PubMed](#)]
19. Meirrow, D.; Lewis, H.; Nugent, D.; Epstein, M. Subclinical depletion of primordial follicular reserve in mice treated with cyclophosphamide: Clinical importance and proposed accurate investigative tool. *Hum. Reprod.* **1999**, *14*, 1903–1907. [[CrossRef](#)]
20. Anderson, R.A.; Themmen, A.P.; Al-Qahtani, A.; Groome, N.P.; Cameron, D.A. The effects of chemotherapy and long-term gonadotrophin suppression on the ovarian reserve in premenopausal women with breast cancer. *Hum. Reprod.* **2006**, *21*, 2583–2592. [[CrossRef](#)]
21. de Pedro, M.; Otero, B.; Martín, B. Fertility preservation and breast cancer: A review. *Ecancermedicalscience* **2015**, *9*, 503. [[CrossRef](#)] [[PubMed](#)]
22. Letourneau, J.M.; Ebbel, E.E.; Katz, P.P.; Oktay, K.H.; McCulloch, C.E.; Ai, W.Z.; Chien, A.J.; Melisko, M.E.; Cedars, M.I.; Rosen, M.P. Acute ovarian failure underestimates age-specific reproductive impairment for young women undergoing chemotherapy for cancer. *Cancer* **2012**, *118*, 1933–1939. [[CrossRef](#)]
23. Massin, N.; Méduri, G.; Bachelot, A.; Misrahi, M.; Touraine, P. Evaluation of different markers of the ovarian reserve in patients presenting with Premature Ovarian Failure. *Mol. Cell. Endocrinol.* **2008**, *282*, 95–100. [[CrossRef](#)]
24. Gleicher, N.; Kim, A.; Weghofer, A.; Kushnir, V.A.; Shohat-Tal, A.; Lazzaroni, E.; Lee, H.J.; Barad, D.H. Hypoandrogenism in association with diminished functional ovarian reserve. *Hum. Reprod.* **2013**, *28*, 1084–1091. [[CrossRef](#)] [[PubMed](#)]
25. Wang, S.; Zhu, F. Chemical composition and health effects of maca (*Lepidium meyenii*). *Food Chem.* **2019**, *288*, 422–443. [[CrossRef](#)] [[PubMed](#)]
26. Jaradat Da’san, M.M. Thirteen decades of peptide synthesis: Key developments in solid phase peptide synthesis and amide bond formation utilized in peptide ligation. *Amino Acids* **2018**, *50*, 39–68. [[CrossRef](#)]
27. Scarsi, C.; Levesque, A.; Lisi, L.; Navarra, P. The free fractions of circulating docosahexaenoic acid and eicosapentaenoic acid as optimal end-point of measure in bioavailability studies on n-3 fatty acids. *Prostaglandins Leukot. Essent. Fat. Acids* **2015**, *96*, 11–16. [[CrossRef](#)] [[PubMed](#)]

28. Browning, L.M.; Walker, C.G.; Mander, A.P.; West, A.L.; Madden, J.; Gambell, J.M.; Young, S.; Wang, L.; Jebb, S.A.; Calder, P.C. Incorporation of eicosapentaenoic and docosahexaenoic acids into lipid pools when given as supplements providing doses equivalent to typical intakes of oily fish. *Am. J. Clin. Nutr.* **2012**, *96*, 748–758. [[CrossRef](#)] [[PubMed](#)]
29. Li LXia, Y.; Zhao, S.; Ding, L.; Ji, S. LC-APCI-MS/MS assay for quantitation of ethyl esters of eicosapentaenoic acid and docosahexaenoic acid in human plasma and its application in a pharmacokinetic study. *Biomed. Chromatogr.* **2020**, *34*, e4905.
30. Rafique, S.; Sterling, E.W.; Nelson, L.M. A new approach to primary ovarian insufficiency. *Obstet. Gynecol. Clin. N Am.* **2012**, *39*, 567–586. [[CrossRef](#)]
31. Yan, Z.; Dai, Y.; Fu, H.; Zheng, Y.; Bao, D.; Yin, Y.; Chen, Q.; Nie, X.; Hao, Q.; Hou, D.; et al. Curcumin exerts a protective effect against premature ovarian failure in mice. *J. Mol. Endocrinol.* **2018**, *60*, 261–271. [[CrossRef](#)] [[PubMed](#)]
32. He, L.; Ling, L.; Wei, T.; Wang, Y.; Xiong, Z. Ginsenoside Rg1 improves fertility and reduces ovarian pathological damages in premature ovarian failure model of mice. *Exp. Biol. Med. Maywood* **2017**, *242*, 683–691. [[CrossRef](#)] [[PubMed](#)]
33. Skinner, M.K. Regulation of primordial follicle assembly and development. *Hum. Reprod Update* **2005**, *11*, 461–471. [[CrossRef](#)]
34. Li, Y.; Qiu, W.; Zhang, Z.; Han, X.; Bu, G.; Meng, F.; Kong, F.; Cao, X.; Huang, A.; Feng, Z.; et al. Oral oyster polypeptides protect ovary against d-galactose-induced premature ovarian failure in C57BL/6 mice. *J. Sci. Food Agric.* **2020**, *100*, 92–101. [[CrossRef](#)] [[PubMed](#)]
35. Schmidt, D.; Ovitt, C.E.; Anlag, K.; Fehsenfeld, S.; Gredsted, L.; Treier, A.C.; Treier, M. The murine winged-helix transcription factor Foxl2 is required for granulosa cell differentiation and ovary maintenance. *Development* **2004**, *131*, 933–942. [[CrossRef](#)]
36. Paulini, F.; Melo, E.O. The role of oocyte-secreted factors GDF9 and BMP15 in follicular development and oogenesis. *Reprod. Domest. Anim.* **2011**, *46*, 354–361. [[CrossRef](#)] [[PubMed](#)]
37. Orisaka, M.; Jiang, J.Y.; Orisaka, S.; Kotsuji, F.; Tsang, B.K. Growth differentiation factor 9 promotes rat preantral follicle growth by up-regulating follicular androgen biosynthesis. *Endocrinology* **2009**, *150*, 2740–2748. [[CrossRef](#)]
38. Komatsu, K.; Koya, T.; Wang, J.; Yamashita, M.; Kikkawa, F.; Iwase, A. Analysis of the Effect of Leukemia Inhibitory Factor on Follicular Growth in Cultured Murine Ovarian Tissue. *Biol. Reprod.* **2015**, *93*, 18. [[CrossRef](#)]
39. Lee, Y.M.; Kim, T.H.; Lee, J.H.; Lee, W.J.; Jeon, R.H.; Jang, S.J.; Ock, S.A.; Lee, S.L.; Park, B.W.; Rho, G.J. Overexpression of Oct4 in porcine ovarian stem/stromal cells enhances differentiation of oocyte-like cells in vitro and ovarian follicular formation in vivo. *J. Ovarian Res.* **2016**, *9*, 24. [[CrossRef](#)]
40. Liu, R.; Zhang, X.; Fan, Z.; Wang, Y.; Yao, G.; Wan, X.; Liu, Z.; Yang, B.; Yu, L. Human amniotic mesenchymal stem cells improve the follicular microenvironment to recover ovarian function in premature ovarian failure mice. *Stem Cell Res. Ther.* **2019**, *10*, 299. [[CrossRef](#)]
41. Jin, X.; Han, C.S.; Zhang, X.S.; Yuan, J.X.; Hu, Z.Y.; Liu, Y.X. Signal transduction of stem cell factor in promoting early follicle development. *Mol. Cell Endocrinol.* **2005**, *229*, 3–10. [[CrossRef](#)] [[PubMed](#)]
42. Fu, X.; He, Y.; Xie, C.; Liu, W. Bone marrow mesenchymal stem cell transplantation improves ovarian function and structure in rats with chemotherapy-induced ovarian damage. *Cytotherapy* **2008**, *10*, 353–363. [[CrossRef](#)] [[PubMed](#)]
43. Zhang, H.; Luo, Q.; Lu, X.; Yin, N.; Zhou, D.; Zhang, L.; Zhao, W.; Wang, D.; Du, P.; Hou, Y.; et al. Effects of hPMSCs on granulosa cell apoptosis and AMH expression and their role in the restoration of ovary function in premature ovarian failure mice. *Stem Cell Res. Ther.* **2018**, *9*, 20. [[CrossRef](#)]
44. Pellatt, L.; Rice, S.; Dilaver, N.; Heshri, A.; Galea, R.; Brincat, M.; Brown, K.; Simpson, E.R.; Mason, H.D. Anti-Müllerian hormone reduces follicle sensitivity to follicle-stimulating hormone in human granulosa cells. *Fertil. Steril.* **2011**, *96*, 1246–1251. [[CrossRef](#)] [[PubMed](#)]
45. La Marca, A. Anti-Müllerian hormone (AMH) in female reproduction: Is measurement of circulating AMH a useful tool? *Clin. Endocrinol.* **2006**, *64*, 603–610. [[CrossRef](#)]
46. Du, X.; Zhang, L.; Li, X.; Pan, Z.; Liu, H.; Li, Q. TGF- β signaling controls FSHR signaling-reduced ovarian granulosa cell apoptosis through the SMAD4/miR-143 axis. *Cell Death Dis.* **2016**, *7*, e2476. [[CrossRef](#)] [[PubMed](#)]
47. Remmele, W.; Stegner, H.E. Recommendation for uniform definition of an immunoreactive score (IRS) for immunohistochemical estrogen receptor detection (ER-ICA) in breast cancer tissue. *Pathologe* **1987**, *8*, 138–140.

Article

LMWP (S3-3) from the Larvae of *Musca domestica* Alleviate D-IBS by Adjusting the Gut Microbiota

Siyan Peng ^{1,†}, Xiwen Ling ^{2,†}, Wenjing Rui ², Xiaobao Jin ² and Fujiang Chu ^{2,*}

¹ Department of Clinical Laboratory, Third Affiliated Hospital of Guangzhou Medical University, No. 63 Duobao Road, Liwan District, Guangzhou 510150, China; 2022683061@gzhu.edu.cn

² Guangdong Provincial Key Laboratory of Pharmaceutical Bioactive Substances, Guangdong Pharmaceutical University, Guangzhou 510006, China; 18122415951@163.com (X.L.); ruiwenjin2019@163.com (W.R.); jin1960gdpu@163.com (X.J.)

* Correspondence: chufujiang8868@163.com; Tel.: +86-020-39352552

† These authors contributed equally to this work.

Abstract: Diarrhea-based Irritable Bowel Syndrome (D-IBS) and diarrhea are both associated with ecological imbalance of the gut microbiota. Low Molecular Weight Peptides (LMWP) from the larvae of *Musca domestica* have been shown to be effective in the treatment of diarrhea and regulation of gut microbiota. Meanwhile, the single polypeptide S3-3 was successfully isolated and identified from LMWP in our previous studies. It remains unclear exactly whether and how LMWP (S3-3) alleviate D-IBS through regulating gut microbiota. We evaluated the gut microbiota and pharmacology to determine the regulation of gut microbiota structure and the alleviating effect on D-IBS through LMWP (S3-3). The rates of loose stools, abdominal withdrawal reflex (AWR) and intestinal tract motility results revealed that LMWP (S3-3) from the larvae of *Musca domestica* had a regulating effect against diarrhea, visceral hypersensitivity and gastrointestinal (GI) dysfunction in D-IBS model mice. Additionally, 16S rRNA gene sequencing was utilized to examine the gut microbiota, which suggests that LMWP induce structural changes in the gut microbiota and alter the levels of the following gut microbiota: *Bacteroidetes*, *Proteobacteria* and *Verrucomicrobia*. LMWP putatively functioned through regulating 5-HT, SERT, 5-HT2AR, 5-HT3AR and 5-HT4R according to the results of ELISA, qRT-PCR and IHC. The findings of this study will contribute to further understanding how LMWP (S3-3) attenuate the effects of D-IBS on diarrhea, visceral hypersensitivity and GI dysfunction.

Keywords: larvae of *Musca domestica*; D-IBS; GI dysfunction; 5-HT; gut microbiota

Citation: Peng, S.; Ling, X.; Rui, W.; Jin, X.; Chu, F. LMWP (S3-3) from the Larvae of *Musca domestica* Alleviate D-IBS by Adjusting the Gut Microbiota. *Molecules* **2022**, *27*, 4517. <https://doi.org/10.3390/molecules27144517>

Academic Editors: Masahide Hamaguchi and Giovanni Ribaudo

Received: 9 May 2022

Accepted: 11 July 2022

Published: 15 July 2022

Publisher's Note: MDPI stays neutral with regard to jurisdictional claims in published maps and institutional affiliations.



Copyright: © 2022 by the authors. Licensee MDPI, Basel, Switzerland. This article is an open access article distributed under the terms and conditions of the Creative Commons Attribution (CC BY) license (<https://creativecommons.org/licenses/by/4.0/>).

1. Introduction

Irritable Bowel Syndrome (IBS) is a functional disorder of the GI tract that is characterized by stomach ache, bloating and altered bowel behavior. Notably, the global prevalence of IBS was estimated to be around 7–30% [1]. The latest epidemiological study shows that the global prevalence of IBS is 11.2%, which also showed that D-IBS, C-IBS, M-IBS and U-IBS subtypes accounted for 23.4%, 22.0%, 24.0% and 22.2% of patients with IBS, respectively [2]. Although IBS is not a life-threatening disease, it seriously affects the normal life of patients and also creates economic burden. Among the four types of IBS, D-IBS is the most common. Young and middle-aged groups (18–59 years old) are the main patients who have the disease [3]. Stress in life comes from various sources, which act as predisposing risk factors for the development of irritable bowel syndrome (IBS). Physical stressors can affect visceral events. Additionally, IBS patients are at a greater risk of comorbidities, incur higher overall medical costs and have a reduced quality of life. Existing evidence suggests that the pathogenesis of IBS is multifaceted, including immunological, genetic and environmental influences [1]. Nonetheless, the etiology of IBS remains unclear, although accumulating evidence suggests that visceral hypersensitivity, impaired gastrointestinal motility, disturbance of microbial equilibrium, inflammation and/or intestinal infection may all be biological

abnormalities associated with the condition [4–6]. Additionally, IBS can be classified into four groups based on clinical symptoms: Diarrhea-based Irritable Bowel Syndrome (D-IBS), Constipation-based Irritable Bowel Syndrome (C-IBS), Mixed Irritable Bowel Syndrome (M-IBS) and Undefined Irritable Bowel Syndrome (U-IBS) [7], with D-IBS being the most common. Notably, antispasmodic drugs, anticholinergics, antidiarrheal agents, visceral analgesics and antipsychotics are currently used to treat D-IBS [8]. Furthermore, treatment of D-IBS is primarily symptomatic relief medication, although it is associated with adverse effects that may have severe psychiatric consequences for patients [9]. Having similar efficacy, natural drugs have safer and less adverse effects as compared to synthetic chemical drugs. Therefore, it is critical to identify new therapeutic approaches capable of changing the composition of gut microbiota, enhancing the metabolism of neuroendocrine transmitters, decreasing visceral vulnerability and having a comprehensive regulatory effect on gut microbiota.

Currently, *Musca domestica* (housefly, Diptera: Muscidae) larvae are regarded as excellent sources of high-quality protein, polyunsaturated fats, saccharides, vitamins, minerals and other nutrients, for both human consumption and animal feed. In China, Li Shizhen demonstrated the role of these larvae in alleviating malnutrition in infants (stool induration or diarrhea) [10].

These peptides from natural sources were identified and had an alleviative effect on disease. A recent study showed that a spider-venom peptide with multi-target activity on sodium and calcium channels alleviates chronic visceral pain in IBS [11]. Bioactive fish collagen peptides weaken intestinal inflammation by orienting colonic macrophages phenotype through mannose receptor activation [12]. *Musca domestica* cecropin, a novel antimicrobial peptide, possessed potential antibacterial, anti-inflammatory, immunological functions and had a protective effect on colonic mucosal barrier injury caused by *Salmonella typhimurium*, which were reported by our laboratory [13].

Moreover, our previous studies reported that LMWP from the larvae of *Musca domestica* had antidiarrheal effects via regulation of the gut microecology and LMWP (S3-3) that were successfully isolated and identified [14]. Notably, the gut microbiota consists of more than 100 trillion microbes residing within the GI tract. Furthermore, extensive research has demonstrated that gut microbiota play a vital role in maintaining human health [15–17]. Additionally, disturbance of microbial equilibrium or dysbiosis has been shown to be closely related to multiple disorders including D-IBS, obesity, hyperlipidemia, atherosclerosis and numerous types of cancer. Therefore, the present study hypothesized that LMWP (S3-3) from the larvae of *Musca domestica* would be effective in alleviating diarrhea and D-IBS.

Therefore, this study aimed to determine the in vivo effect of LMWP (S3-3) from larvae of *Musca domestica* in alleviating D-IBS and gut microbiota imbalance. The psychosocial stress (restraint) model better simulates the pathogenesis of human IBS and gastrointestinal dysfunction [18,19]. Similar studies also verified the high efficacy and sustainability of the model, allowing for a better understanding of the pathological process as well as the vulnerability and triggering factors in D-IBS [20–22].

2. Materials and Methods

2.1. Preparation of LMWP (S3-3) from the Larvae of *Musca domestica*

LMWP (S3-3) from the larvae of *Musca domestica* (purity 94.70%, molecular weight: 1069.4391 Da; the 10 amino acid sequences of S3-3 were Val-Tyr-Arg-Asp-Asn-Val-Leu-Phe-Gln-Ala) were prepared as described in our previous study [14].

The laboratory strain of *Musca domestica* was obtained as a kind gift from the Guangdong Provincial Center for Disease Control and Prevention CDC, China. The larvae of *Musca domestica* were then dried using conventional drying systems. Briefly, third-instar larvae of *Musca domestica* were collected, washed for 3 h with running tap water, frozen for 2 h at $-20\text{ }^{\circ}\text{C}$ and sun dried for 6 h.

Following that, 1000 g of dried larvae were fried until they turned light yellow and then sifted using 40-mesh sieves. The larvae was fried to modulate the therapeutic properties of

treated herbal medicines, i.e., enhancing efficacy, reducing toxicity or side effects, which is a kind of processing of Chinese medicine [23–25]. Following that, the dried powder of larvae of *Musca domestica* (10.0 g) was immersed in deionized water (250 mL) in a beaker for 30 min [14]. The samples were then simmered for 10 min before removing the supernatant and centrifuging at 12,000 r/min for 10 min. In addition, an equal volume of deionized water was added, and the same procedure was repeated. Following that, both supernatants with a molecular weight of <30 kD were collected by ultrafiltration technology (ultrafiltration membrane with a molecular weight cut-off of 30 kD) and lyophilized [15]. Finally, the supernatants were freeze-dried and LMWP were collected from larvae of *Musca domestica*.

A suitable amount (800 mg) of the LMWP powder was accurately weighed and dissolved in 2.0 mL of ultra-pure water, and the mixture was filtered on a 0.22 µm filter. Then, the LMWP powder was fractionated according to their molecular masses by using gel-filtration chromatography (GFC) on a column packed with Superdex™ 30 and eluted with deionized water at a flow rate of 0.6 mL/min. Each eluate (3 mL) was collected and monitored at 280 nm, and the fractions (1 mL) were collected at a flow of 0.25 mL/min. Based on gel-filtration chromatography, the components of LMWP (S3-3) ($t = 3.0$ min) were further separated by RP-HPLC. YMC-Pack C4-HG columns (4.6 mm × 250 mm, 10 µm) were separately used for S3-3 separation. The fractions were automatically collected at a flow rate of 1 mL/min and dried by centrifugation under vacuum. The identification of the LMWP (S3-3) from the larvae of *Musca domestica* was performed in our previous study [9]. The purity of the fractions was determined by HPLC, the molecular weight was identified by MALDI-TOF spectrometer and the N-terminal sequences were determined using Edman degradation (Supplementary Figures S1–S3, Supplementary Table S1).

2.2. Animals and Experimental Design

A total of 32 male SPF C57BL/6J mice were provided by Medical Laboratory Animal Center, Guangdong Province (Guangzhou, China approval number SCXK (Yue) 2013-0002). The 6-week-old male mice were then housed in a specific-pathogen-free facility (room temperature 22 ± 2 °C and 12/12 h light/dark cycle) for 7 days (eating and drinking ad libitum). This was conducted in accordance with the guidelines by Care and Use of Experimental Animals. Additionally, the use of animals was approved by the Guangdong Pharmaceutical University and the Guangdong Pharmaceutical University Animal Care and Use Committee, China. Animal grouping design is shown in Figure 1. The 32 C57/BL6J mice (20 ± 2 g) were randomly assigned to four groups ($n = 8$) as shown in Figure 1: the Control, D-IBS, LMWP and LMWP + ampicillin groups. Among these groups, the LMWP + ampicillin group was established to identify the role of gut microbiota in D-IBS. After confirming the successful establishment of the D-IBS model, mice in the Control and D-IBS groups were given 10 mL/kg of Control saline, the LMWP group was intragastrically treated with 0.2 g/kg of LMWP (S3-3) from the larvae of *Musca domestica* (10 mL/kg) and those in the LMWP + ampicillin group received 500 mg/kg of ampicillin (10 mL/kg) and 0.2 g/kg of the LMWP (S3-3) from the larvae of *Musca domestica* (10 mL/kg), through the intragastric route, and all the mice were treated for 7 days. Thereafter, at the end of the therapy cycle, five fecal samples were randomly collected from each group for 16S rDNA gene sequencing.

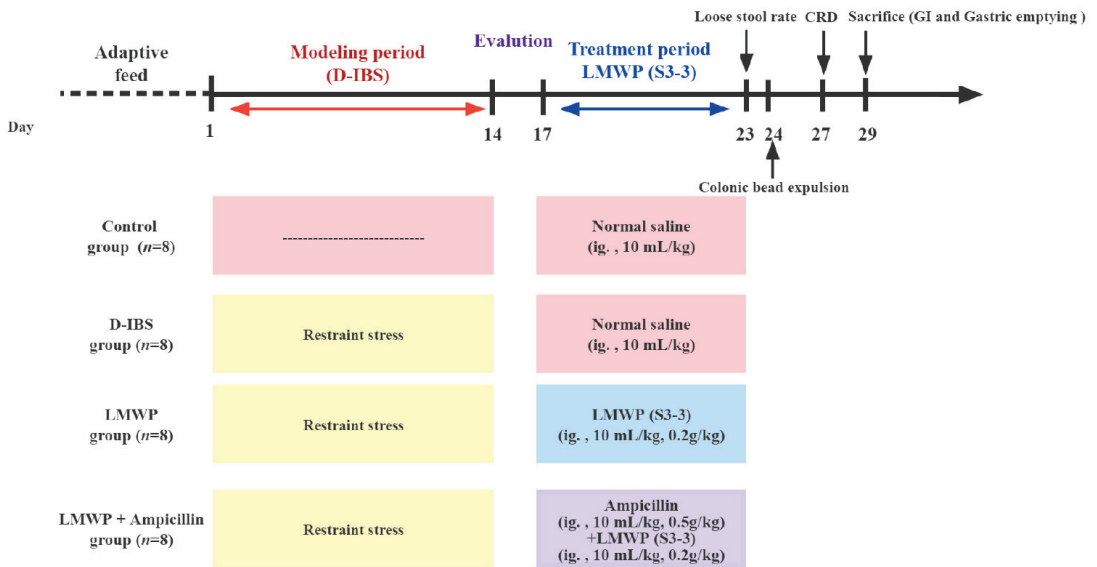


Figure 1. Timeline of experimental procedures.

2.3. Introduction of D-IBS in Mice

The D-IBS model was then established by chronic restraint stress (24 mice were immobilized using a plastic restrainer for a duration of 1 h daily) for 14 days [18,19], in D-IBS, LMWP and LMWP + ampicillin groups. An abdominal withdrawal reflex (AWR) score ≥ 2 points and a loose stool rate ≥ 0.5 revealed that the D-IBS mice model was successfully established. Physical stressors can affect visceral events. Animals subjected to stress result in abnormal intestinal motility and visceral hypersensitivity. Stress-induced IBS models, e.g., restraint stress, could largely mimic IBS symptoms from intestinal motility to visceral sensitivity [20–22].

2.4. Determination of the Rate of Loose Stool

The total number of stools and loose stools was determined using the filter paper imprinting method [26,27]. The mice were placed in individual cages and the cage floor was covered with filter paper. The number and morphology of the stools were recorded for 6 h. The loose stools were classified into five grades based on the diameters of stain formed by loose stools on the filter paper: Grade 1 (0 < 1 cm), Grade 2 (1~2 cm), Grade 3 (2~3 cm), Grade 4 (3~4 cm) and Grade 5 (4~5 cm). Therefore, the rate of loose stool (%) = number of loose stools/total number of stools \times 100%. Loose stool grade was defined as the calculated mean of the diameters of stain formed by loose stools on the filter paper. Loose stool index was determined as follows: loose stool index = rate of loose stool \times loose stool grade.

2.5. The Abdominal Retraction Reflex (AWR) Score

The mice were subjected to a 24 h fast before inserting the 6F catheter, after paraffin oil lubrication, through the anus. A double-lumen balloon was then placed about 2.0 cm from the anus. Then, mice were placed inside a restraint device. After adapting to the new environment, the mice were gradually injected with water to dilate the balloon. The dilation capacity was 0.25 mL, 0.35 mL and 0.50 mL and each rectal dilation lasted for 30 s. The procedure was repeated thrice and the mean value was calculated. Finally, the AWR scores were determined using the following scale: 0, no behavioral response to Colorectal Distension (CRD); 1, brief head movement followed by immobility; 2, contraction of abdominal

muscles; 3, lifting of the abdomen; 4, body arching and lifting of pelvic structures. These methodologies were performed and modified according to those previously described [28].

2.6. Colonic Bead Expulsion Test

Under anesthesia, glass beads (2 mm in diameter) were inserted into the rectum (about 3 cm from the anus). The mice were then placed in a cage (1 mouse/cage) with no access to food or water. After the mice were fully awake (the standard was that the mice could turn over freely and climb up), the study began by observing the time to bead ejection. These methodologies were performed and modified as previously described [29,30].

2.7. Upper GI Transit

The mice in each group were fasted for 24 h and then orally administered with 0.2 mL of a suspension of the charcoal meal (10% charcoal in 5% gum arabic). The mice were sacrificed 20 min after receiving the charcoal meal. The small intestine was removed en bloc and the length of the small bowel and the distance traveled by the charcoal meal were then measured for each mouse. The ratio of the distance traveled by the charcoal meal to the total length of the small bowel was then used as the upper GI transit. These methodologies were performed and modified according to those previously described [31,32].

2.8. Gastric Emptying

The mice in each group received 0.2 mL of a suspension of the charcoal meal (10% charcoal in 5% gum arabic) and were sacrificed after 20 min. This was followed by abdominal dissection and ligation of the gastric cardia and pylorus. The stomach was then dried using a filter paper and the full weight was obtained. Following that, the stomach was cut along its bend before washing off the stomach contents and drying with filter paper. Gastric emptying (%) was calculated using the following formula: Gastric emptying (%) = (full weight of stomach – dry weight of stomach/weight of suspension of charcoal meal) × 100%. These methodologies were performed and modified according to those previously described [32,33].

2.9. Histological Analysis

The colonic tissues from 8 mice were examined in each group. Colon sections were excised to assess histological changes in the colon and were gently irrigated with normal saline to dislodge the intestinal contents. They were then fixed immediately at 4 °C overnight in 4% paraformaldehyde solution. Following three washes in tap water, they were dehydrated with serial ethanol concentrations. They were rinsed with xylene, paraffin-embedded, sliced into 4 µm sections and stained with Hematoxylin and Eosin (H&E). They were then examined under a light microscope and photomicrographs of the sections were taken using a digital camera (DFC495 Digital camera Leica, Leica Microsystems, Wetzlar, Germany).

2.10. Enzyme-Linked Immunoassay (ELISA)

Blood samples were centrifuged at 3000 rpm for 10 min at 4 °C. Following that, serum was collected and immediately frozen in liquid nitrogen before being stored at –80 °C for further analysis. Additionally, the distal colon was homogenized in cold PBS. Following this, the frozen colonic tissues were homogenized and lysed in the tissue lysis buffer, followed by centrifugation at 12,000 rpm for 10 min at 4 °C. The supernatant was then collected. 5-HT, a critical signaling molecule in the gut, activated both intrinsic and extrinsic primary afferent neurons to initiate peristaltic and secretory reflexes. The levels of 5-HT in serum and colonic tissues were determined using an ELISA kit (Shanghai MLBIO Biotechnology Co., Ltd., Shanghai, China), and the operation steps of the kit were performed following the manufacturer's instructions.

2.11. Real-Time Quantitative PCR Detection

RNA from the distal colon was extracted. Total RNA isolation and cDNA synthesis were accomplished using the Trizol reagent (Accurate Biology Co., Ltd., Changsha, China) and the PrimeScriptTM RT reagent Kit with a gDNA Eraser (Accurate Biology Co., Ltd., Changsha, China), respectively. The mRNA levels of particular genes were then determined by real-time PCR using SYBR Green Pro Taq HS Premix (Accurate Biology Co., Ltd., Changsha, China) in the CFX Connect fluorescence quantitative PCR detection system (BIO-RAD, Hercules, CA, USA). Notably, the 20 μ L PCR reaction mixture comprised 10 μ L 2 \times SYBR Green Pro Taq HS Premix, 0.4 μ L Forward Primer (10 μ M), 0.4 μ L Reverse Primer (10 μ M), 2 μ L reaction solution (cDNA) and 7.2 μ L RNase-free water. Additionally, the following protocol was used for the Shuttle PCR: Stage 1 was the initial denaturation of one cycle at 95 $^{\circ}$ C for 30 s; Stage 2 was the PCR reaction of 40 cycles at 95 $^{\circ}$ C for 5 s, and 60 $^{\circ}$ C for 30 s; Stage 3 was the dissociation step. The data were analyzed using the comparative threshold cycle (Cq) method and normalized to an endogenous reference, Glyceraldehyde-3-phosphate Dehydrogenase (GAPDH). 5-HT2AR, 5-HT3AR and 5-HT4R were 5-HT receptors, and SERT was a 5-HT reuptake transporter, which was involved in the reuptake and inactivity of 5-HT. The relative expression levels of genes associated with gastrointestinal movement (5-HT2AR, 5-HT3AR, 5-HT4R, SERT) were then determined in colon tissues and calculated using the $2^{-\Delta\Delta CT}$ method. The primers used in this experiment are listed in Table 1.

Table 1. The primers used in this experiment.

Gene Name	Primer Sequence (from 5' End to 3' End)	Product Size (bp)
5-HT2AR-F	ACCGCTTTGGCAGTTTT	140
5-HT2AR-R	GCGTTGAGGTGGCTTATT	
5-HT3AR-F	GCAACCCCAGTCTCTTTGT	143
5-HT3AR-R	GCTTGACGCCCTGATAAGT	
5-HT4R-F	CATGCCCAGCAGATACAG	147
5-HT4R-R	GAAACAGAAGCAGCCCAT	
SERT-F	CTCCTCCCCTCTAAGCCA	185
SERT-R	CCTCCTTCCTCTCCTCACA	
GAPDH-F	GATGGACACATTGGGGTT	148
GAPDH-R	AAAGCTGTGGCGTGATG	

2.12. Immunohistochemistry (IHC)

Mice were sacrificed at the end of the experiments. Colon tissues were then isolated, embedded on paraffinized blocks and cut into 4 μ m-thick sections, individually, using a microtome (Leica, Wetlar, Germany). Next, the sections were incubated with anti-5-HT1AR rabbit polyclonal antibody, anti-5-HT2AR rabbit polyclonal antibody, anti-SERT polyclonal antibody (1:50) (Sangon Biotech, Shanghai, China) and anti-5-HT4AR rabbit polyclonal antibody (1:100) (Bioss, Beijing, China) overnight at 4 $^{\circ}$ C in a dilution ratio of 1:100 using the BondTM Primary Antibody Diluent (Servicebio, Wuhan, China). On the next day, the sections were incubated for 1 h with horseradish peroxidase 4-layered goat anti-rabbit secondary antibodies at 37 $^{\circ}$ C (Sangon Biotech) according to the manufacturer's instructions. Finally, the sections were treated with diaminobenzidine (DAB) solution (Servicebio, Wuhan, China) and visualized under a microscope (NIKON, Eclipse, Ci, Tokyo, Japan). We measured the integrated optical density (IOD) from at least three fields of each slice using the Image pro-plus 6.0 software (Media Cybernetics, Bethesda, MD, USA), which could accurately reflect the complete expression of the proteins in immunohistochemical staining.

2.13. Gut Microbiota Analysis

The fresh stool was collected from the colons of mice after being sacrificed and immediately frozen at $-80\text{ }^{\circ}\text{C}$. Additionally, bacterial genomic DNA was extracted from frozen stool samples using the Qiagen QIAamp DNA stool Mini Kit (Hilden, Germany) according to the manufacturer's instructions. Following that, the 16S rRNA in the V3-V4 region (341F-805R, F: GATCCTACGGGAGGCAGCA; R: GCTTACCGCGGCTGCTGGC) was amplified via thermal cycling consisting of initial denaturation step at $98\text{ }^{\circ}\text{C}$ for 1 min, followed by 30 cycles of denaturation at $98\text{ }^{\circ}\text{C}$ for 10 s, annealing at $50\text{ }^{\circ}\text{C}$ for 30 s and elongation at $72\text{ }^{\circ}\text{C}$ for 60 s and a final hold at $72\text{ }^{\circ}\text{C}$ for 5 min. Purification was subsequently performed using the MinElute Gel Extraction Kit (Qiagen, Shanghai, China) and samples with 400–450 bps were chosen for further experiments. Sequencing libraries were generated using the NEB Next Ultra DNA Library Prep Kit for Illumina (NEB, Ipswich, MA, USA), following the manufacturer's instructions, and index codes were added. The PCR results were then subjected to high-throughput sequencing on an Illumina HiSeq2500 platform (Biomarker Technologies Co., Ltd., Beijing, China). Additionally, in the GreenGenes database (13.5 version) (Lawrence Berkeley National Laboratory, Berkeley, CA, USA), USEARCH software (10.0 version) (Robert Edgar, Tiburon, CA, USA) was used to select OTUs and the RDP classifier (2.2 version) was used to annotate taxonomic information for each representative sequence. The alpha diversity indices among groups were compared after the sequences were rarefied to control for depth. The QIIME software package was also used to perform UniFrac distance-based Principal Component Analysis (PCA). Permutational Multivariate Analysis of Variance (PERMANOVA) was also performed. The Z score, the value corresponding to the heatmap, was obtained after the relative abundance of each row of species had been standardized in the heatmap of the gut microbiota at the genus level. Finally, Linear discriminant analysis Effect Size (LEfSe) analysis was performed using Metastats software to identify the biomarker species, Linear Discriminant Analysis (LDA) highlighting significant biomarker species among each group's microbiota, LDA threshold of >4 . The relative abundance of significant biomarker species, obtained in gut microbiota from the LEfSe results, was compared in each group.

2.14. Statistical Analysis

SPSS Statistics 17.0 software (IBM, Armonk, NY, USA) was used to perform statistical analyses. All data were presented as mean \pm SD and multiple comparisons were performed using one-way Analysis of Variance (ANOVA). p values less than 0.05 were considered statistically significant. Spearman's correlation was measured to demonstrate the relationships between parameters, the correlation coefficient was always in the range of +1 to -1 . The correlations between gut microbial biomarkers and the phenotype were corrected by False Discovery Rate (FDR), which was calculated through the Benjamini–Hochberg (BH) method.

3. Results

3.1. Effects of LMWP (S3-3) from Larvae of *Musca domestica* on Physiological Conditions and the Frequency of Loose Stools in D-IBS Mice

After 14 days of D-IBS induction, D-IBS mice had significantly lower body weight and food intakes than the Control group. On day 1 of treatment, there were no statistically significant differences in initial body weight and food intake between the D-IBS, LMWP and LMWP + ampicillin groups. After 7 days of administration of LMWP (S3-3) from larvae of *Musca domestica*, the body weight and food intake in the LMWP group were significantly greater than in the D-IBS group. After seven days of treatment, the body weight and food intake in the LMWP + ampicillin group were significantly lower than in the LMWP group (Figure 2A,B). The D-IBS group had a higher loose stool rate, loose stool grade and loose stool index than the Control group. Additionally, when compared to the D-IBS group, the LMWP group demonstrated significant improvement in loose stool rate, loose stool grade and loose stool index. Additionally, as demonstrated in Figure 2C–E, the

LMWP + ampicillin group had increased loose stools rate, loose stool grade and loose stool index compared to the LMWP group.

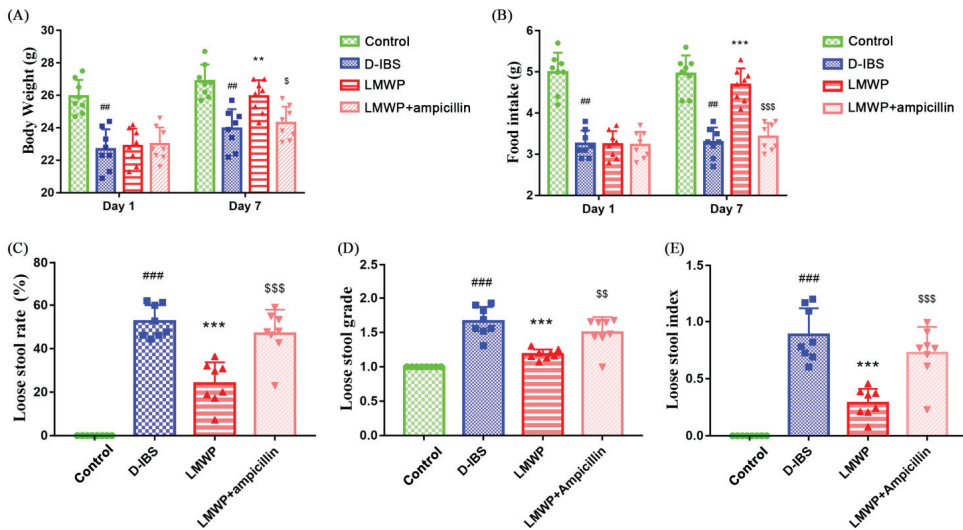


Figure 2. LMWP (S3-3) from the larvae of *Musca domestica* affects body weight, food intake and diarrhea in D-IBS mice. (A) Body weight on day 1 and day 7 in the treatment period. (B) Food intake on day 1 and day 7 in the treatment period. (C–E) Loose stool rate, loose stool grade and loose stool index. Values are presented as means \pm SD ($n = 8$). # $p < 0.01$ and ### $p < 0.001$ compared with Control, ** $p < 0.01$ and *** $p < 0.001$ compared with D-IBS, \$ $p < 0.05$, \$\$ $p < 0.01$ and \$\$\$ $p < 0.001$ compared with LMWP (S3-3) from the larvae of *Musca domestica*.

3.2. Effects of LMWP (S3-3) from Larvae of *Musca domestica* on Gastrointestinal Motility and Visceral Sensitivity in Mice

Intestinal transit in mice was evaluated using the time to bead expulsion, upper GI transit and degree of gastric emptying. There was an increase in upper GI transit and a significant decrease in the efflux time of glass beads as well as in the degree of gastric emptying in mice in the D-IBS group compared to those in the Control group during the modeling process (Figure 3A–C). This indicated that the frequency of GI transport increased significantly after the modeling process. Additionally, mice in the LMWP group exhibited a slower upper GI transit and an increased efflux time for the glass beads, as well as a greater degree of gastric emptying, compared to those in the D-IBS group. However, there were significant differences in upper GI transit, efflux time of glass beads and degree of gastric emptying between the LMWP + ampicillin and LMWP groups. LMWP + ampicillin group had increased upper GI transit and decreased efflux time of glass beads, as well as a greater degree of gastric emptying than the LMWP group.

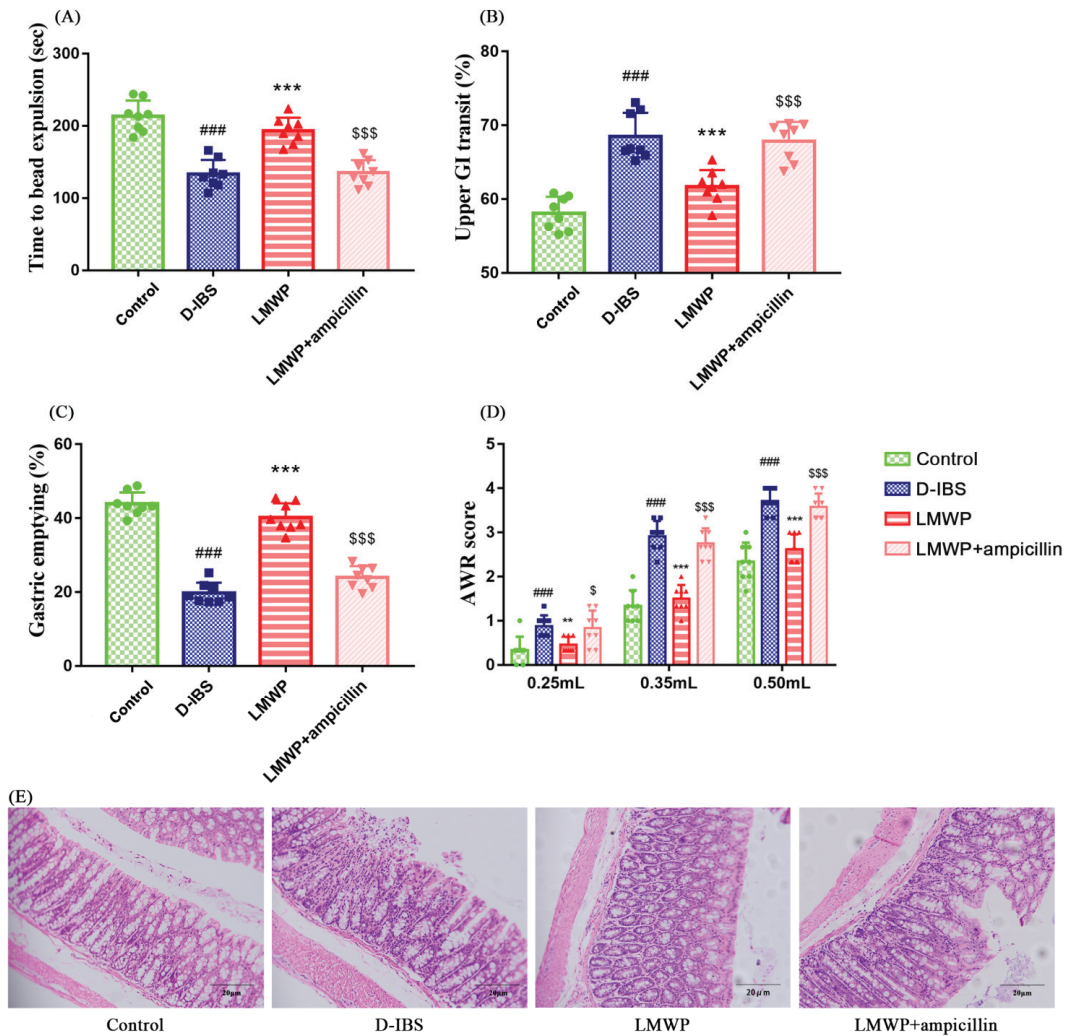


Figure 3. LMWP (S3-3) from the larvae of *Musca domestica* affect intestinal tract motility, visceral hypersensitivity and colonic histology in D-IBS mice. (A) Time to bead expulsion. (B) Upper gut transit. (C) Gastric emptying. (D) AWR scores. (E) Morphology found in the colon. Values are presented as means \pm SD ($n = 8$). ### $p < 0.001$ compared with Control, ** $p < 0.01$ and *** $p < 0.001$ compared with D-IBS, \$ $p < 0.05$ and \$\$\$ $p < 0.001$ compared with LMWP (S3-3) from the larvae of *Musca domestica*.

Additionally, visceral sensitivity was assessed using the abdominal uplift and back arch volume thresholds. Compared to the Control group, there was a significant increase in the AWR scores of the D-IBS group, demonstrating increased visceral sensitivity following the modeling process. However, as compared to the D-IBS group, the AWR scores decreased significantly following treatment with LMWP (S3-3) from larvae of *Musca domestica* (Figure 3D), suggesting meliorative visceral sensitivity following treatment with LMWP (S3-3) from larvae of *Musca domestica*. In comparison to the LMWP group, the LMWP + ampicillin group showed significantly higher AWR scores.

3.3. Effect of LMWP (S3-3) from Larvae of *Musca domestica* on Colonic Histological Assessment

Figure 3E showed that the colon tissues of the Control, D-IBS, LMWP and LMWP + ampicillin groups were normal. The mucosa was normal and complete, and neatly arranged villi were observed; the muscle layer was even and moderate, and colonic epithelial cells were arranged regularly in each group. Moreover, no significant pathological changes were observed in any group.

3.4. Effect of LMWP (S3-3) from Larvae of *Musca domestica* on the Expression of Genes and Proteins Involved in 5-HT-Related Pathways

The levels of 5-HT in the serum and colon of mice were examined to investigate the effect of LMWP (S3-3) from the larvae of *Musca domestica* by ELISA. The 5-HT concentrations in the serum and colon of mice are shown in Figure 4A,B. Notably, the serum and colon 5-HT concentrations were significantly decreased following treatment with LMWP (S3-3) from the larvae of *Musca domestica*. Additionally, the study used qPCR to examine the expression of the 5-HT2AR, 5-HT3AR, 5-HT4R and SERT genes. The results showed that 5-HT2AR and 5-HT3AR expression in the colon was higher, whereas 5-HT4R and SERT expression was lower in the D-IBS group compared to the Control group (Figure 4C–F). However, LMWP (S3-3) from larvae of *Musca domestica* resulted in a decrease in the expression of both 5-HT2AR and 5-HT3AR (Figure 4C,D). The treatment of larvae of *Musca domestica* with LMWP (S3-3) increased the expression of both 5-HT4R and SERT (Figure 4E,F). However, the LMWP + ampicillin groups increased the 5-HT concentrations in serum and colon tissue, increased 5-HT2AR and 5-HT3AR expression and decreased 5-HT4R and SERT expression (Figure 4). Next, the immunohistological changes in the protein levels of 5-HT2AR, 5-HT3AR, 5-HT4R and SERT were examined in the colon. The results suggested that stress caused an increase in the levels of 5-HT2AR and 5-HT3AR on the membrane surface of the intestinal tissues, which decreased substantially after LMWP (S3-3) treatment (Figure 5A,B). Furthermore, potential immunohistological changes in the protein expressions of SERT in the colon were evaluated. The results showed a significant increase in 5-HT4R and SERT-positive protein expression in the colon in the LMWP (S3-3) group relative to the IBS group (Figure 6A,B). Furthermore, results showed a significant increase in 5-HT2AR, 5-HT3AR protein and a remarkable decrease in 5-HT4R, SERT protein in the colon tissues obtained from mouse in the LMWP (S3-3) + ampicillin group as compared to those in the LMWP (S3-3) group (Figures 5 and 6).

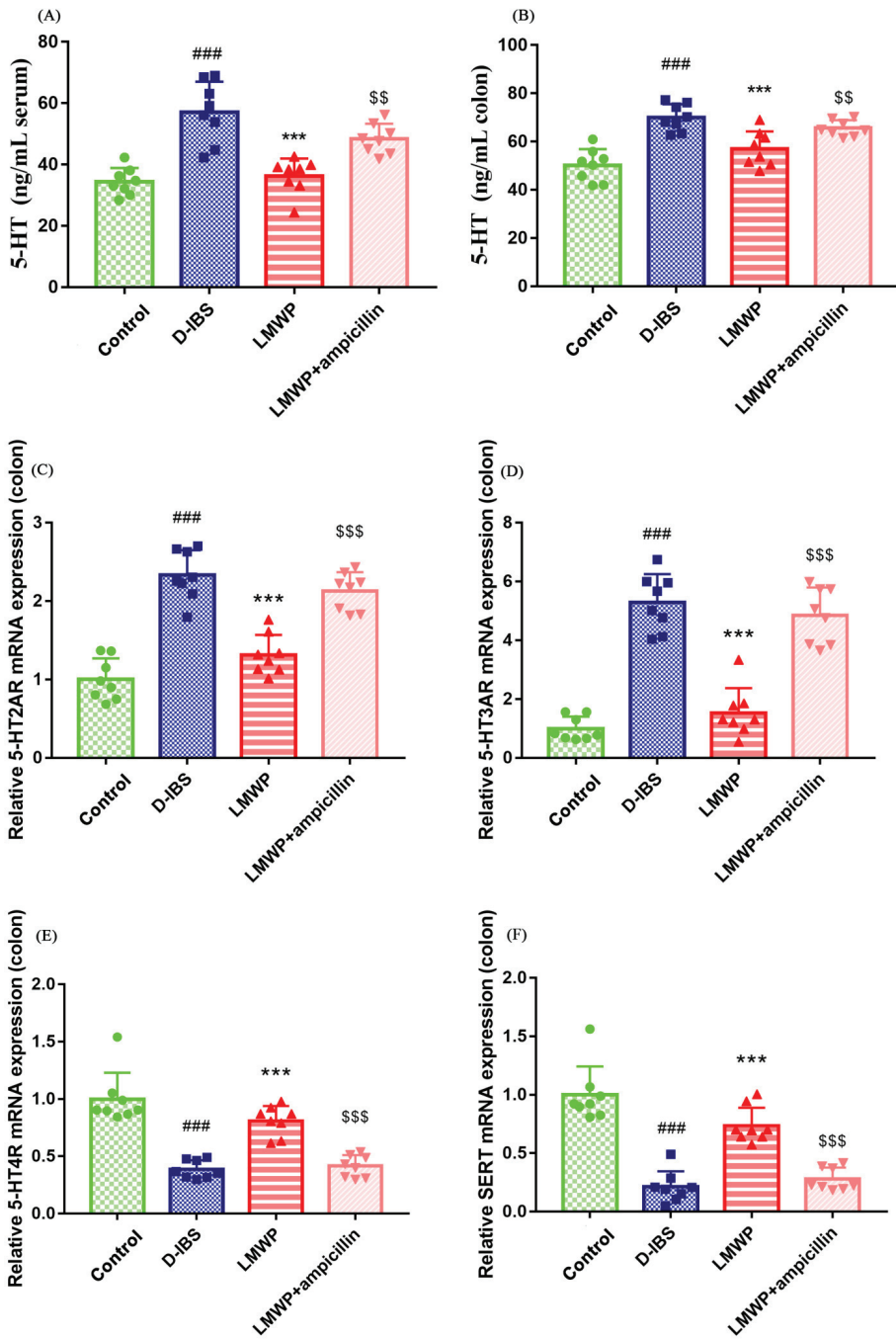


Figure 4. LMWP (S3-3) from the larvae of *Musca domestica* affect 5-HT, 5-HT_{2A}R, 5-HT_{3A}R, 5-HT₄R and SERT in D-IBS mice. (A,B) 5-HT levels in serum and colon. (C–F) The relative expression of 5-HT_{2A}R, 5-HT_{3A}R, 5-HT₄R and SERT mRNA in the colon. Values are presented as means \pm SD ($n = 8$). ### $p < 0.001$ compared with Control, *** $p < 0.001$ compared with D-IBS, \$\$\$ $p < 0.001$ and \$\$ $p < 0.01$ compared with LMWP (S3-3) from the larvae of *Musca domestica*.

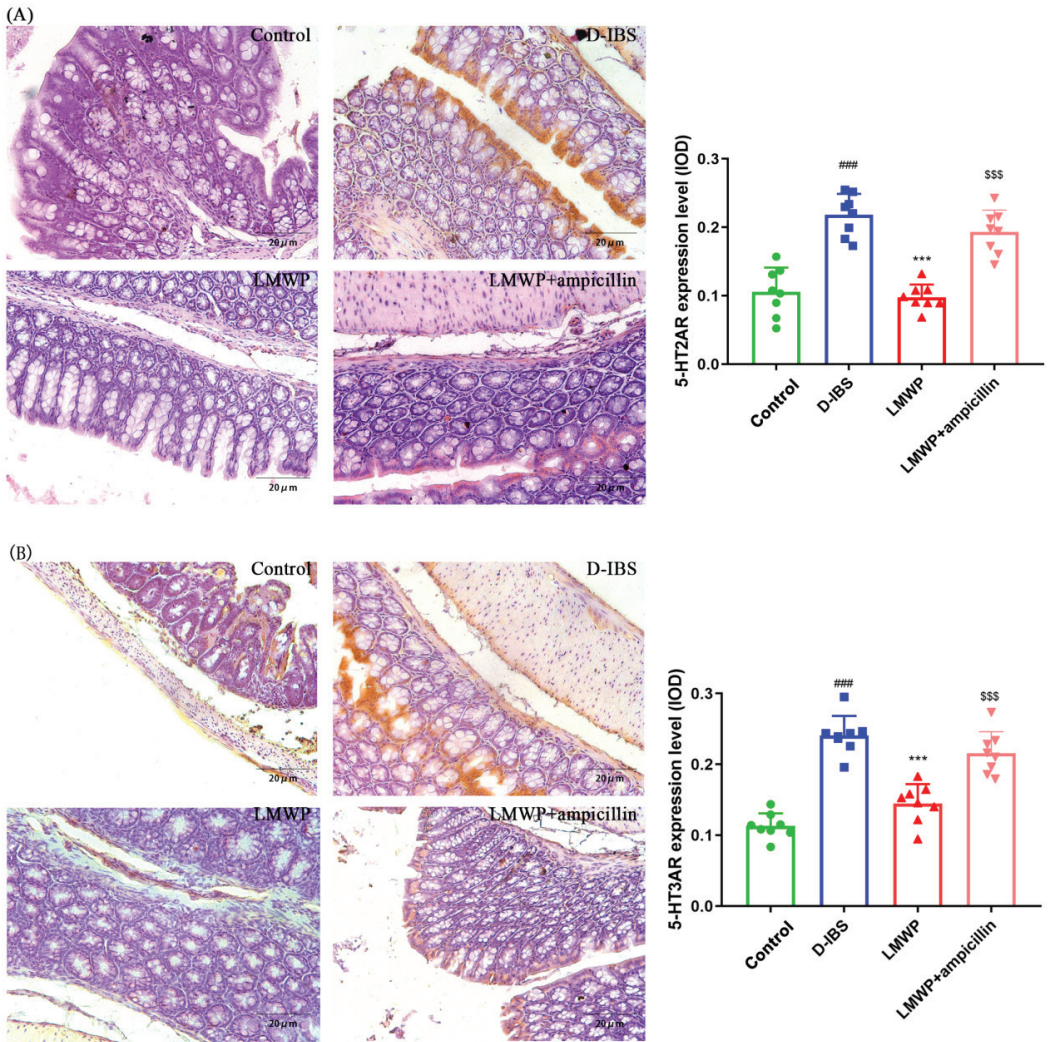


Figure 5. Immunohistochemical staining in the colon. (A,B) 5-HT2AR and 5-HT3AR. Values are presented as the means \pm SD ($n = 8$). ### $p < 0.001$ compared to Control, *** $p < 0.001$ compared to D-IBS and \$\$\$ $p < 0.001$ compared to LMWP (S3-3) from the larvae of *Musca domestica*.

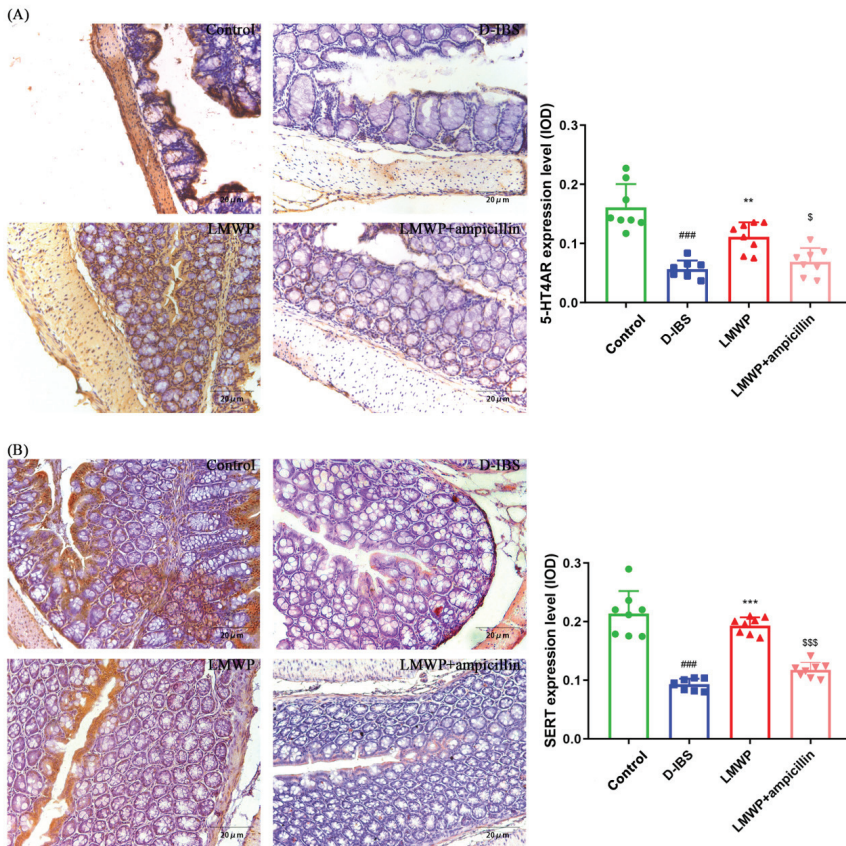


Figure 6. Immunohistochemical staining in the colon. (A,B) 5-HT4R and SERT. Values are presented as the means \pm SD ($n = 8$). ### $p < 0.001$ compared to Control, ** $p < 0.01$ compared to D-IBS, *** $p < 0.001$ compared to D-IBS, \$ $p < 0.05$ compared to LMWP (S3-3) from the larvae of *Musca domestica* and \$\$\$ $p < 0.001$ compared to LMWP (S3-3) from the larvae of *Musca domestica*.

3.5. Effects of LMWP (S3-3) from Larvae of *Musca domestica* on Gut Microbiota in D-IBS Mice

In this study, 16S rDNA sequencing was conducted to determine whether LMWP (S3-3) from larvae of *Musca domestica* influenced the gut microbiota and to define the changes in the composition of gut microbiota. It is noteworthy that the interaction between LMWP (S3-3) from larvae of *Musca domestica* feeding and the gut microbiota has been linked to D-IBS-related metabolic disorder. Therefore, the present study examined the effects of LMWP (S3-3) from the larvae of *Musca domestica* on the composition of gut microbiota by sequencing the V3 + V4 region of bacterial 16S rRNA. The samples were analyzed using high-throughput sequencing, which produced 1,600,995 pairs of raw reads. However, pair-end read alignment and filtering resulted in 1,551,510 clean tags which were subjected to subsequent analysis. All of the effective reads were then clustered into Operational Taxonomic Units (OTUs) based on a 97% similarity level. The dilution curve showed an inflection point at about 1000 and then leveled off, indicating that the sequencing amount of this study was enough to cover almost all bacterial species, indicating that the sample sequence was sufficient. The graded abundance curve indicates that the abundance and evenness of this study are both high, which supports the following data analysis (Supplementary Figures S4 and S5). The functional role of LMWP (S3-3) from the Larvae of *Musca domestica* in improving species richness and diversity of gut microbiota was further supported by increased numbers of OTUs

(Figure 7A), ACE (Figure 7B), Shannon (Figure 7D), Chao1 (Figure 7E) index and a lower Simpson index (Figure 7C). However, the LMWP + ampicillin group showed a decrease in species richness and diversity compared to the LMWP group.

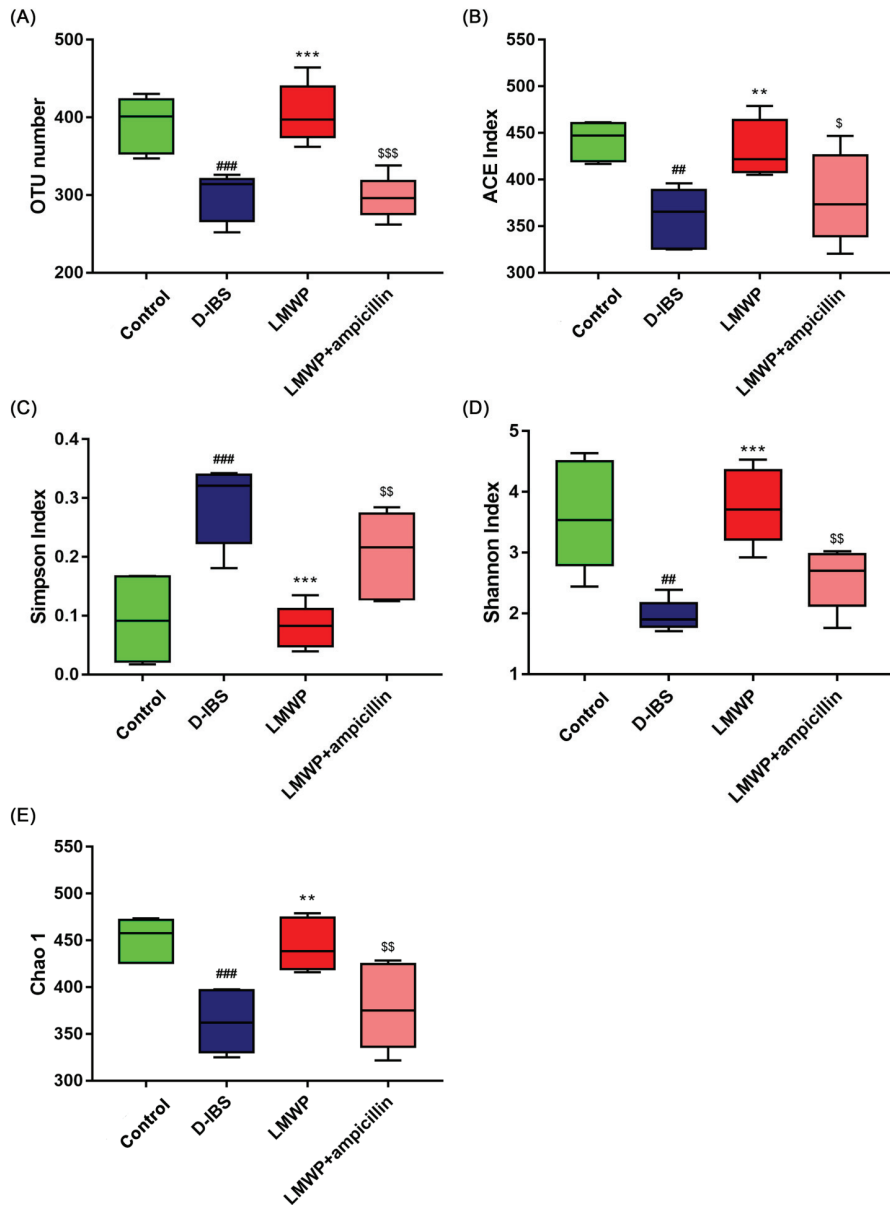


Figure 7. The diversity, richness and structure of the gut microbiota in response to LMWP (S3-3) from the larvae of *Musca domestica* in D-IBS mice. **(A)** The number of OTUs in the gut microbiota. **(B–E)** The ACE index, Simpson index, Shannon index and Chao1 index. Values are presented as means \pm SD ($n = 5$). # $p < 0.01$ and ### $p < 0.001$ compared with Control, * $p < 0.05$ and ** $p < 0.01$ and *** $p < 0.001$ compared with D-IBS, \$ $p < 0.05$, \$\$ $p < 0.01$ and \$\$\$ $p < 0.001$ compared with LMWP (S3-3) from the larvae of *Musca domestica*.

A deeper examination of the microbial community revealed that LMWP (S3-3) from larvae of *Musca domestica* had a significant positive effect on the phylum and genus levels. According to the findings, the phylum level, the 10 most abundant bacteria in the level of phylum could be found and compared in all samples, and the most abundant phyla in all samples were *Firmicutes*, *Bacteroidetes*, *Proteobacteria* and *Verrucomicrobia* (Figure 8A). At the genus level (Figure 8B), the 10 most abundant bacteria were found and listed in all samples. Additionally, unsupervised multivariate statistical methods such as Principal Component Analysis (PCA) were used to assess structural changes in the gut microbiota. All four groups presented distinct clustering of microbiota composition, and the LMWP group had a similar structure to that of the Control group (Figure 8C). The results of PCA were confirmed through PERMANOVA test, detecting significant differences between groups (Supplementary Figure S7).

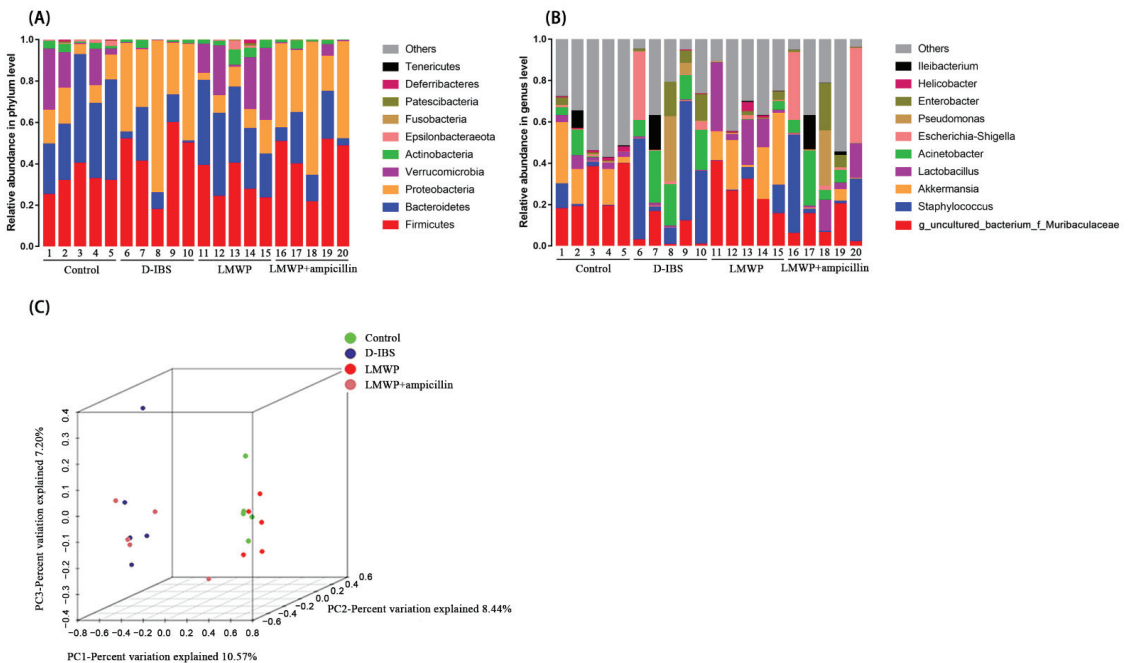


Figure 8. Gut microbiota diversity at the phylum and genus level. (A,B) Relative abundances of the gut microbiota at the phylum and genus levels. (C) Weighted UniFrac-based PCA.

Additionally, an overview of the heatmap (Figure 9) suggested a significant effect of LMWP (S3-3) from the larvae of *Musca domestica* on the profile of the gut microbiota. As seen in Figure 9, the abundance increased with the color changing from blue to red; genus-level species clustering analysis was performed according to the distance between each genus-level species. The clustering indicated the similarity of the abundance of different species between samples. The closer the distance between two species was, the shorter the branch length was, indicating that the abundance of these two species was more similar between samples. The clustering revealed the similarity of community composition at each classification level. Therefore, all effective sequences were evaluated using the LEfSe approach to determine the major phenotypes that were significantly altered in response to LMWP (S3-3) of larvae from *Musca domestica* treatment. The findings of the LEfSe analysis revealed the presence of high-dimensional biomarkers in the gut microbiota in each group (Supplementary Figure S8).

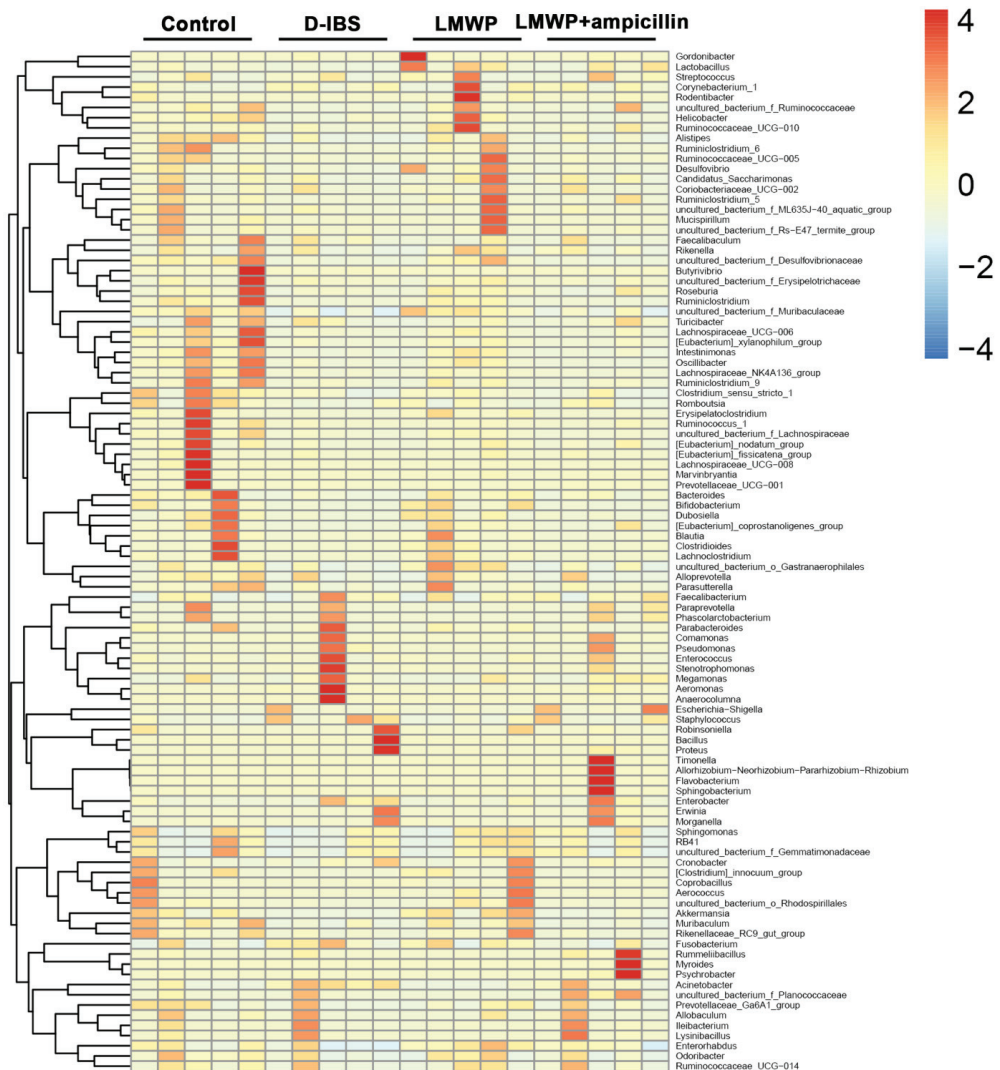


Figure 9. Heatmap of the gut microbiota at the genus level.

Collectively, these findings indicated that treatment with LMWP (S3-3) from larvae of *Musca domestica* reversed D-IBS-induced dysbiosis of the gut microbiota. In comparison to the LMWP group, the LMWP + ampicillin group induced a decrease in *Bacteroidetes* and *Verrucomicrobia* but increased *Proteobacteria* at the phylum level (Figure 10A–C). The LMWP + ampicillin group induced a decrease in *g_uncultured_bacterium_f_Muribaculaceae*, *Akkermansia*, *Lachnospiraceae_NK4A136_group* and *Lachnoclostridium* but an increase in *Acinetobacter* at the genus level in comparison to the LMWP group (Figure 11A–F).

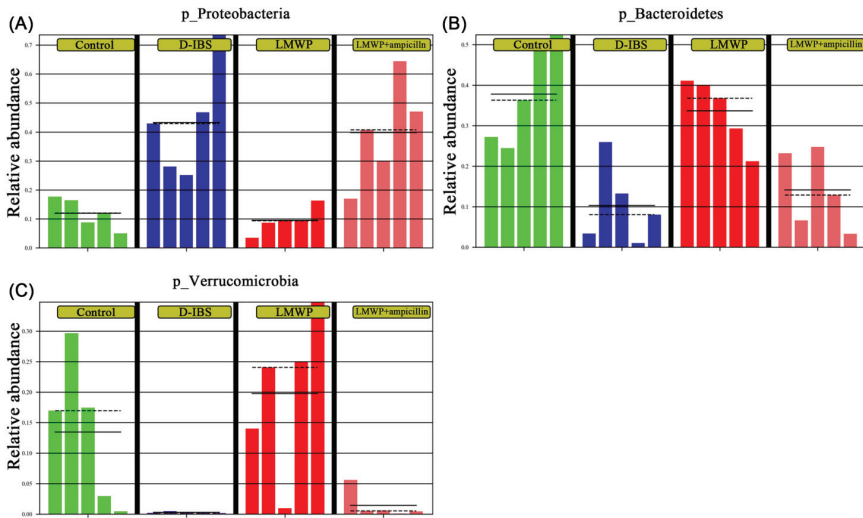


Figure 10. Relative abundances of the gut microbiota at the phylum level. (A–C) Relative abundances of *Proteobacteria*, *Bacteroidetes* and *Verrucomicrobia*.

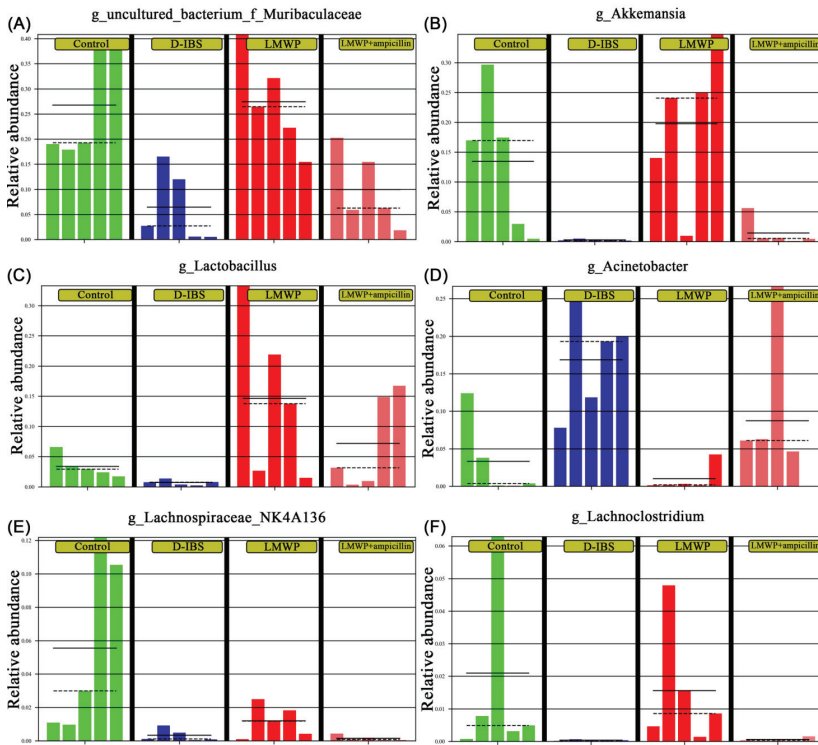


Figure 11. Relative abundances of the gut microbiota at the genus level. (A–F) Relative abundances of *Uncultured_bacterium_f_Muribaculaceae*, *Akkermansia*, *Lactobacillus*, *Acinetobacter*, *Lachnospiraceae_NK4A136_group* and *Lachnoclostridium* at the genus level.

3.6. Potential Correlations among Phenotypes, Molecular Biology Indicators and Gut Microbiota

To further investigate the potential role of the gut microbiota in D-IBS, correlation analyses were performed between diarrhea, gastrointestinal motility, visceral sensitivity, 5-HT, 5-HT2AR, 5-HT3AR, 5-HT4R, SERT and changes in the microbiota (Figure 12). 5-HT, 5-HT2AR and 5-HT3AR were positively correlated with the genus *Acinetobacter*. Negative correlations between 5-HT4R and SERT with *Acinetobacter* were also observed. Additionally, 5-HT, 5-HT2AR and 5-HT3AR were negatively correlated with *Akkermansia* and *Lachnoclostridium*, while 5-HT4R and SERT were positively correlated. *Lactobacillus* was also negatively correlated with 5-HT2AR and 5-HT3AR. *g_uncultured_bacterium_f_Muribaculaceae* and *Lactobacillus* were positively correlated with 5-HT4R and SERT, respectively.

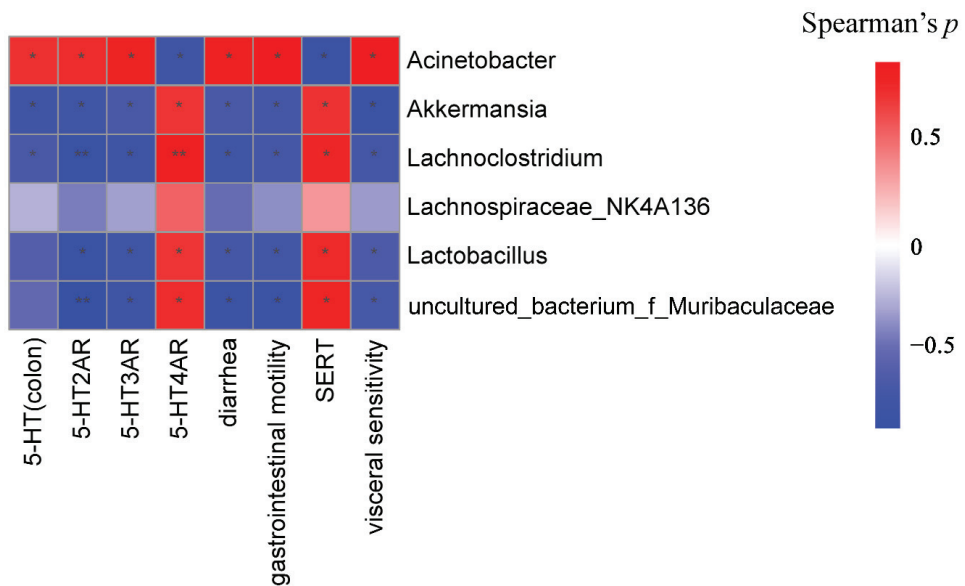


Figure 12. Association map for three-tiered analyses integrating the gut microbiome, D-IBS phenotypes and molecular biology indicator. Scale indicates the level of positive (red) or negative (blue) correlation, * $p < 0.05$ and ** $p < 0.01$.

4. Discussion

IBS is a chronic relapsing functional gastrointestinal disorder that is characterized by diarrhea and abdominal pain, both of which significantly decrease patients' quality of life. Currently, available management options mainly focus on symptom alleviation and control of the disease course.

Moreover, our previous study proved intestinal microbiological regulation might be one of the potential antidiarrheal mechanisms of LMWP from the larvae of *Musca domestica* and LMWP (S3-3) successfully isolated and identified from LMWP from the larvae of *Musca domestica* [14]. Therefore, this study focused on determining whether LMWP (S3-3) alleviated D-IBS through regulating gut microbiota. The results suggested that LMWP (S3-3) could alleviate D-IBS by impacting the gut microbiota.

Therefore, the present study established a restraint stress model of D-IBS in mice. After 4 weeks, mice in the D-IBS group had a lower body weight and a higher diarrheal index, indicating that they were experiencing diarrhea. Interestingly, LMWP (S3-3) from the larvae of *Musca domestica* decreased diarrhea caused by D-IBS, indicating that LMWP (S3-3) from the larvae of *Musca domestica* was capable of relieving diarrhea in these mice. Additionally, LMWP (S3-3) from the larvae of *Musca domestica* reduced the AWR scores in D-IBS mice, implying that it might be able to alleviate intestinal visceral hypersensitivity in

the animals. LMWP (S3-3) from the larvae of *Musca domestica* also inhibited colonic motility and prolonged gastrointestinal transit in mice. These results demonstrated that LMWP (S3-3) from the larvae of *Musca domestica* were beneficial for gastrointestinal motility and possessed antinociceptive properties. Nonetheless, cotreatment with antibiotics (ampicillin + LMWP (S3-3) from the larvae of *Musca domestica*) significantly reduced the beneficial effects of LMWP (S3-3) from larvae of *Musca domestica* against D-IBS. Metabolic products from gastrointestinal microbiota fermentation, such as SCFAs, or peptides can act on the ENS and affect gut transit [34]. The neuroendocrine system of the gut has also been shown to interact with microbiota [35] via 5-HT [36]. 5-HT is produced in both the ENS and CNS and is a key neurotransmitter that plays a pivotal role in mediating motor and secretory responses in the ENS [37]. 5-HT stimulates local enteric nervous reflexes to initiate secretion and propulsive motility and acts on vagal afferents to modulate contractile activities [37].

IBS is a complex disorder characterized by changes in sensation, secretion and gastrointestinal motility. 5-HT is a critical signaling molecule in the gut that targets enterocytes, smooth muscles and enteric neurons, activating both intrinsic and extrinsic primary afferent neurons to initiate peristaltic and secretory reflexes, as well as transmitting information to the central nervous system. Therefore, the serum and colon 5-HT concentrations were determined in this study by ELISA. Additionally, the data revealed that LMWP (S3-3) from the larvae of *Musca domestica* were capable of lowering 5-HT levels in the serum and colon. 5-HT has been shown to play an important role in regulating intestinal motility [38]. However, excessive 5-HT production induces high visceral sensitivity, and this is an important mechanism of D-IBS [38,39]. 5-HT has a remarkable range of effects that are attributable to the existence of multiple receptor subtypes on enteric neurons, enterochromaffin cells (EC cells), GI smooth muscle and probably enterocytes and immune tissue. 5-HT receptors are now classified into seven families and subtypes, with 5-HT₂AR, 5-HT₃AR and 5-HT₄AR known to affect gut motor functions. Additionally, 5-HT is inactivated by the SERT-mediated uptake into enterocytes or neurons. Therefore, the genes and proteins of the 5-HT-related pathway were detected by qPCR and IHC in this study. The present study demonstrated that LMWP (S3-3) from the larvae of *Musca domestica* could decrease the levels of 5-HT in the colon of D-IBS model mice by down-regulating the expression of 5-HT₂AR, 5-HT₃AR and up-regulating the expression of 5-HT₄AR and SERT. Furthermore, the binding of 5-HT and 5-HT₂AR was reported to block voltage-gated K⁺ channels and increase visceral sensitivity by generating enteric neuron excitation [40]. Moreover, 5-HT₃AR are found in a variety of locations, including peripheral primary sensory nerve endings, autonomic preganglionic and postganglionic neurons, the central nervous system and the lower brainstem, among other areas. Notably, activation of the 5-HT₃AR, which has excitatory effects, mediates the rapid activation of sensory afferents, hence enhancing nerve-mediated gastrointestinal motility and secretion. Additionally, it generates visceral pain stimuli, which results in abdominal pain [41]. Furthermore, 5-HT₄AR is positively associated with adenylate cyclase, which is located on the mesenteric plexus neurons [42]. 5-HT₄AR has also been identified in the intestinal primary afferent neurons [43] and was shown to be involved in the peristaltic reflex [38,39]. On the other hand, Serotonin Reuptake Transporter (SERT) is a highly regulated protein, located on the membrane of intestinal epithelial cells and is involved in the reuptake of 5-HT [44]. Moreover, excess 5-HT is often transported into epithelial cells via SERT and inactivated there. Therefore, inhibiting the expression of SERT can induce the sensitivity of primary neurons to 5-HT, and this can, in turn, enhance visceral sensitivity [44,45].

The findings indicated that the levels of 5-HT in the serum and colon were elevated in D-IBS mice and that LMWP (S3-3) from the larvae of *Musca domestica* could decrease the levels of 5-HT in the serum and colon of D-IBS mice. 5-HT, which is primarily produced in the gut, regulates intrinsic reflexes (e.g., stimulates motility, secretion and vasodilation) and may contribute to the development of diarrhea by promoting inflammation [46,47]. The EC cells are mucosal sensory cells that release mediators (5-HT, among others) in response to chemical or mechanical stimulation [48]. It is hypothesized that excessive release of 5-HT

from EC cells may contribute to diarrhea in IBS patients [48]. Rapid intake of 5-HT occurs via a selective SERT transporter that regulates 5-HT in the gut [48]. The enteric nervous system (ENS) is also involved in intestinal absorption and secretion, and diarrhea has been associated with decreased absorption of ions and/or solutes and water [49]. Numerous studies indicate that 5-HT and the ENS may play an important role in the pathophysiology of IBS and perhaps in diarrhea [48]. The findings also demonstrated that the SERT levels in the colon of D-IBS mice were decreased and LMWP (S3-3) from the larvae of *Musca domestica* could enhance the levels of SERT in the colon of D-IBS mice. SERT decrease can affect motility and thus contribute to diarrhea [48,50]. Therefore, LMWP (S3-3) from the larvae of *Musca domestica* may be used to treat diarrhea in D-IBS mice by regulating 5-HT and SERT levels.

In our view, LMWP (S3-3) supplemented intestinal nutrition and produced prebiotics, then regulated gut microbiota through prebiotics, and then regulated SCFAs, which affect release of 5-HT, through gut microbiota [51–53]. In this study, changes in the composition of the microbiota were examined using high-throughput sequencing. The results demonstrated that the alpha diversity of the gut microbiota was reduced in the D-IBS group, which had a lower Shannon index, ACE index and Chao1 index and a higher Simpson index than the Control group. Nevertheless, treatment with LMWP (S3-3) from the larvae of *Musca domestica* was able to restore diversity. Additionally, PCoA indicated significant distances between each group, indicating that the beta diversity of gut microbiota was different in D-IBS model mice and LMWP (S3-3)-treated mice. According to the findings, the relative abundance of *Lactobacillus* was decreased in D-IBS model mice compared to Control mice. Moreover, treatment with LMWP (S3-3) from the larvae of *Musca domestica* increased the relative abundance of *Lactobacillus*, which has previously been shown to have positive therapeutic benefits on IBS [54,55]. Short-chain Fatty Acids (SCFAs) are the primary metabolites of the gut microbiota and can boost the growth of *Lactobacillus*. They are also critical signaling molecules that affect intestinal function, and abnormal changes in SCFA levels have been associated with IBS. Additionally, it was demonstrated that intestinal microbiota imbalances in IBS patients have a direct effect on the normal signaling interactions between intestinal microbiota, SCFAs and intestinal epithelial cells, resulting in a low inflammatory response, increased permeability of the intestinal epithelial barrier and hypermotility [56]. We also found that LMWP (S3-3) increased related SCFA concentration, such as propionate and butyrate (Supplementary Figure S6, Supplementary Methods). On the contrary, the current study found a significant increase in the abundance of *Akkermansia* after treatment with LMWP (S3-3) from the larvae of *Musca domestica*. *Akkermansia* is a probiotic belonging to the *Verrucomicrobia* phylum and is involved in nutrition metabolism. Recent studies also indicate that *Akkermansia* improves metabolic health and protects against obesity, diabetes and inflammation in the intestinal tract of rodents by interacting with intestinal epithelial cells [56,57]. Additionally, *Akkermansia muciniphila* is the type species of the genus *Akkermansia*, which was first proposed in 2004 as a mucin-degrading, anaerobic Gram-negative bacterium that resides in the mucus layer [58]. Notably, the mucus layer lining the intestinal tract serves as a lubricant and physiological barrier between the luminal contents and mucosal surface. Furthermore, the presence of *A. muciniphila* in IBS mice may play an important role in preserving the integrity of the mucin layer. However, it is unclear whether LMWP (S3-3) from the larvae of *Musca domestica* increases the abundance of *A. muciniphila* by providing the primary source of energy for this bacterium, thereby favoring its growth. Additionally, it is unknown if an increase in *A. muciniphila* increases mucus production and degradation. However, it was discovered that treatment with LMWP (S3-3) from the larvae of *Musca domestica* inhibited the proliferation of *Acinetobacter*, which are mostly opportunistic microbes whose population increased significantly in mice with diarrhea [59]. According to the findings, the relative abundance of *g_uncultured_bacterium_f_Muribaculaceae* was decreased in D-IBS model mice compared to Control mice, which belong to *Muribaculaceae*. LMWP (S3-3) also increased the relative abundance of *g_uncultured_bacterium_f_Muribaculaceae*. Schmidt et al. also found that the

abundance of *Muribaculaceae* was strongly correlated with the concentration of propionate belonging to SCFAs [60].

The findings also showed that gut microbiota play a key role in D-IBS by enhancing the function of LMWP (S3-3) from the larvae of *Musca domestica*. This is because when LMWP (S3-3) from larvae of *Musca domestica* were combined with an antibiotic, the regulatory effect on physiological conditions, diarrhea, gastrointestinal motility, visceral sensitivity, colon histology, levels of 5-HT, expression of associated pathway genes and proteins, and gut microbiota were significantly reduced. Ampicillin is a β -lactam antibiotic that has the potential to disrupt gut microbiota and cause diarrhea [61,62]. The mechanism of ampicillin-induced diarrhea may be related to disruption to the normal composition and functional attributes of the gut microbiota [63], where 5-HT was related to diarrhea [64]. Compared with the LMWP group, for LMWP (S3-3) from larvae of *Musca domestica* that were combined with ampicillin, the regulatory effect on physiological conditions, diarrhea, gastrointestinal motility, visceral sensitivity, colon histology, levels of 5-HT, expression of associated pathway genes and proteins, and gut microbiota were significantly reduced, which suggested that the changes in gut microbiota composition might alter colonic motility. Gut microbiota regulated SCFAs, which affect release of 5-HT [51,52]. 5-HT has been shown to play an important role in regulating GI motility [38]. Additionally, several studies have revealed that the germ-free condition is characterized by increased plasma 5-HT concentrations. Plasma 5-HT levels are thought to be mostly derived from intestinal EC cells of the gut [65,66].

In this study, these data suggested that LMWP (S3-3) from the larvae of *Musca domestica* had an obvious protective effect on D-IBS through regulating 5-HT-pathway-related genes and proteins and adjusting gut microbiota.

5. Conclusions

According to the current study's findings, treatment with LMWP (S3-3) from the larvae of *Musca domestica* regulates gut microbiota by increasing the relative abundance of *Akkermansia* and *Lactobacillus*. Additionally, LMWP (S3-3) treatment decreases *Acinetobacter* levels, resulting in favorable benefits against diarrhea, increased visceral sensitivity and excessive gastrointestinal motility. This also regulates the 5-HT levels in serum and colon as well as the expression of 5-HT-pathway-related genes and proteins (Figure 13). The data of this study suggested that LMWP (S3-3) from larvae of *Musca domestica* had an obvious protective effect on D-IBS, potentially by adjusting gut microbiota, down-regulating 5-HT, 5-HT_{2A}R and 5-HT_{3A}R, up-regulating 5-HT₄R and SERT, relieving diarrhea, decelerating the gastrointestinal motility and alleviating intestinal visceral hypersensitivity. These findings could enhance our understanding of the effect and mechanism of LMWP (S3-3) from larvae of *Musca domestica* on D-IBS and contribute to developing effective therapies in the future.

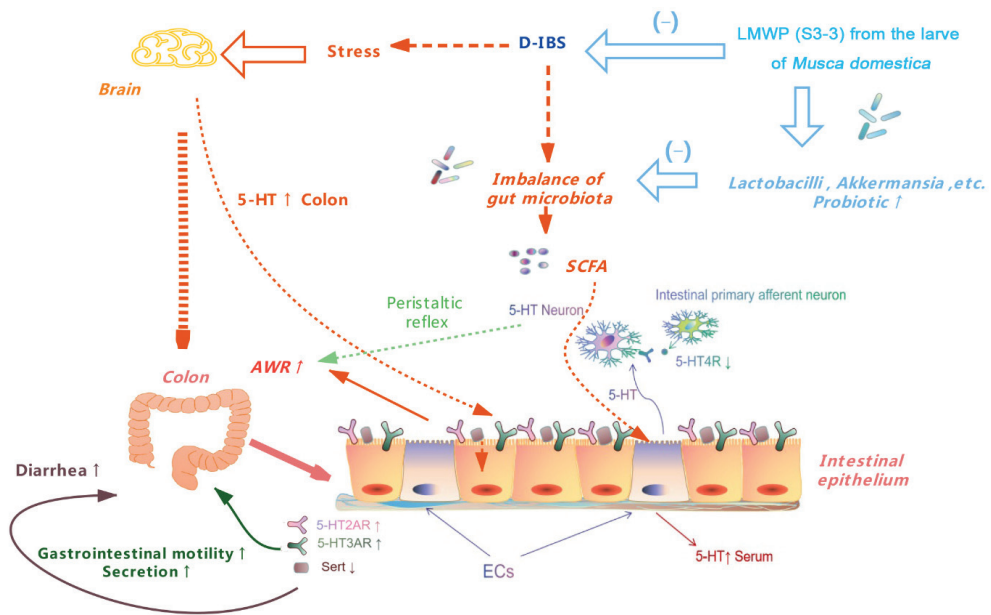


Figure 13. A schematic presentation of the therapeutic effect of LMWP (S3-3) from the larvae of *Musca domestica* on D-IBS.

Supplementary Materials: The following supporting information can be downloaded at: <https://www.mdpi.com/article/10.3390/molecules27144517/s1>, Figure S1: The retention time in the RP-HPLC; Figure S2: The molecular weight of LMWP(S3-3) was detected by MALDI-TOF spectromete; Figure S3: N-terminal sequence of LMWP(S3-3) were determined by Edman degradation; Figure S4: OTU Rarefaction Curve; Figure S5: Rank Abundance Curve; Figure S6: SCFA variations; Figure S7: Permanova test; Figure S8: LefSe analysis results; Table S1: LMWP(S3-3) HPLC peak area integral results. Table S2: Association map data.

Author Contributions: F.C. and S.P. conceived and designed the research; S.P., X.L. and W.R. performed the experiments; S.P. analyzed the data; S.P. interpreted the results of the experiments; S.P. prepared the figures; S.P. and X.L. drafted the manuscript; F.C. and X.J. edited and revised the manuscript; S.P., X.L., W.R., X.J. and F.C. approved the final version of the manuscript. All authors have read and agreed to the published version of the manuscript.

Funding: This work was supported by the National Natural Science Foundation of China (Grant No. 81373960 and 81573600); Science and Technology Planning Project of Guangdong Province, China (Grant No. 2014A020212416); and Guangzhou Municipal Science and Technology Project, China (Grant No. 201707010132).

Institutional Review Board Statement: The animal study was reviewed and approved by the Medical Ethics Committee of Guangdong Pharmaceutical University (approval code: gdpulacspf2017134, 11 June 2019).

Informed Consent Statement: Not applicable.

Data Availability Statement: The original contributions presented in the study are publicly available. These data can be found here: <https://www.ncbi.nlm.nih.gov/bioproject/900466> (accessed on 23 February 2022), BioProject ID is PRJNA900466.

Conflicts of Interest: The authors declare that they have no conflict of interest.

Sample Availability: Samples of the compounds LMWP(S3-3) are available from the authors.

References

- Lee, S.H.; Kim, K.N.; Kim, K.M.; Joo, N.S. Irritable Bowel Syndrome May Be Associated with Elevated Alanine Aminotransferase and Metabolic Syndrome. *Yonsei Med. J.* **2016**, *57*, 146–152. [[CrossRef](#)] [[PubMed](#)]
- Lovell, R.M.; Ford, A.C. Global prevalence of and risk factors for irritable bowel syndrome: A meta-analysis. *Clin. Gastroenterol. Hepatol. Off. Clin. Pract. J. Am. Gastroenterol. Assoc.* **2012**, *10*, 712–721.e714. [[CrossRef](#)] [[PubMed](#)]
- Choi, M.G.; Jung, H.K. Health related quality of life in functional gastrointestinal disorders in Asia. *J. Neurogastroenterol. Motil.* **2011**, *17*, 245–251. [[CrossRef](#)]
- Gao, X.; Qin, Q.; Yu, X.; Liu, K.; Li, L.; Qiao, H.; Zhu, B. Acupuncture at heterotopic acupoints facilitates distal colonic motility via activating M3 receptors and somatic afferent C-fibers in normal, constipated, or diarrhoeic rats. *Neurogastroenterol. Motil. Off. J. Eur. Gastrointest. Motil. Soc.* **2015**, *27*, 1817–1830. [[CrossRef](#)] [[PubMed](#)]
- Samarajeewa, A.D.; Hammad, A.; Masson, L.; Khan, I.U.; Scroggins, R.; Beaudette, L.A. Comparative assessment of next-generation sequencing, denaturing gradient gel electrophoresis, clonal restriction fragment length polymorphism and cloning-sequencing as methods for characterizing commercial microbial consortia. *J. Microbiol. Methods* **2015**, *108*, 103–111. [[CrossRef](#)]
- Yano, J.M.; Yu, K.; Donaldson, G.P.; Shastri, G.G.; Ann, P.; Ma, L.; Nagler, C.R.; Ismagilov, R.F.; Mazmanian, S.K.; Hsiao, E.Y. Indigenous bacteria from the gut microbiota regulate host serotonin biosynthesis. *Cell* **2015**, *161*, 264–276. [[CrossRef](#)]
- Canavan, C.; West, J.; Card, T. Review article: The economic impact of the irritable bowel syndrome. *Aliment. Pharmacol. Ther.* **2014**, *40*, 1023–1034. [[CrossRef](#)]
- Adriani, A.; Ribaldone, D.G.; Astegiano, M.; Durazzo, M.; Saracco, G.M.; Pellicano, R. Irritable bowel syndrome: The clinical approach. *Panminerva Med.* **2018**, *60*, 213–222. [[CrossRef](#)]
- Wilson, A.; Longstreth, G.F.; Knight, K.; Wong, J.; Wade, S.; Chiou, C.F.; Barghout, V.; Frech, F.; Ofman, J.J. Quality of life in managed care patients with irritable bowel syndrome. *Manag. Care Interface* **2004**, *17*, 24–28, 34.
- Ai, H.; Wang, F.; Xia, Y.; Chen, X.; Lei, C. Antioxidant, antifungal and antiviral activities of chitosan from the larvae of housefly, *Musca domestica* L. *Food Chem.* **2012**, *132*, 493–498. [[CrossRef](#)]
- Cardoso, F.C.; Castro, J.; Grundy, L.; Schober, G.; Garcia-Caraballo, S.; Zhao, T.; Herzig, V.; King, G.F.; Brierley, S.M.; Lewis, R.J. A spider-venom peptide with multitarget activity on sodium and calcium channels alleviates chronic visceral pain in a model of irritable bowel syndrome. *Pain* **2021**, *162*, 569–581. [[CrossRef](#)] [[PubMed](#)]
- Rahabi, M.; Salon, M.; Bruno-Bonnet, C.; Prat, M.; Jacquemin, G.; Benmoussa, K.; Alaeddine, M.; Parny, M.; Bernad, J.; Bertrand, B.; et al. Bioactive fish collagen peptides weaken intestinal inflammation by orienting colonic macrophages phenotype through mannose receptor activation. *Eur. J. Nutr.* **2022**, *61*, 2051–2066. [[CrossRef](#)] [[PubMed](#)]
- Zhang, L.; Gui, S.; Liang, Z.; Liu, A.; Chen, Z.; Tang, Y.; Xiao, M.; Chu, F.; Liu, W.; Jin, X.; et al. *Musca domestica* Cecropin (Mdc) Alleviates Salmonella typhimurium-Induced Colonic Mucosal Barrier Impairment: Associating With Inflammatory and Oxidative Stress Response, Tight Junction as Well as Intestinal Flora. *Front. Microbiol.* **2019**, *10*, 522. [[CrossRef](#)]
- Chu, F.; Jin, X.; Ma, H. Anti-diarrhea effects and identification of *Musca domestica* larvae low molecular weight peptides (LMWP). *J. Pharm. Biomed. Anal.* **2019**, *173*, 162–168. [[CrossRef](#)] [[PubMed](#)]
- Chang, S.H.; Lin, H.T.; Wu, G.J.; Tsai, G.J. pH Effects on solubility, zeta potential, and correlation between antibacterial activity and molecular weight of chitosan. *Carbohydr. Polym.* **2015**, *134*, 74–81. [[CrossRef](#)]
- Hall, H.N.; Masey O'Neill, H.V.; Scholey, D.; Burton, E.; Dickinson, M.; Fitches, E.C. Amino acid digestibility of larval meal (*Musca domestica*) for broiler chickens. *Poult. Sci.* **2018**, *97*, 1290–1297. [[CrossRef](#)]
- Pei, Z.; Sun, X.; Tang, Y.; Wang, K.; Gao, Y.; Ma, H. Cloning, expression, and purification of a new antimicrobial peptide gene from *Musca domestica* larva. *Gene* **2014**, *549*, 41–45. [[CrossRef](#)]
- Li, L.; Cui, H.; Li, T.; Qi, J.; Chen, H.; Gao, F.; Tian, X.; Mu, Y.; He, R.; Lv, S.; et al. Synergistic Effect of Berberine-Based Chinese Medicine Assembled Nanostructures on Diarrhea-Predominant Irritable Bowel Syndrome In Vivo. *Front. Pharmacol.* **2020**, *11*, 1210. [[CrossRef](#)]
- Zhu, H.M.; Li, L.; Li, S.Y.; Yan, Q.; Li, F. Effect of water extract from Berberis heteropoda Schrenk roots on diarrhea-predominant irritable bowel syndrome by adjusting intestinal flora. *J. Ethnopharmacol.* **2019**, *237*, 182–191. [[CrossRef](#)]
- Lu, Y.; Huang, J.; Zhang, Y.; Huang, Z.; Yan, W.; Zhou, T.; Wang, Z.; Liao, L.; Cao, H.; Tan, B. Therapeutic Effects of Berberine Hydrochloride on Stress-Induced Diarrhea-Predominant Irritable Bowel Syndrome Rats by Inhibiting Neurotransmission in Colonic Smooth Muscle. *Front. Pharmacol.* **2021**, *12*, 596686. [[CrossRef](#)]
- Bülbül, M.; Sinen, O.; Bayramoğlu, O.; Akkoyunlu, G. Enteric apelin enhances the stress-induced stimulation of colonic motor functions. *Stress (Amst. Neth.)* **2020**, *23*, 201–212. [[CrossRef](#)] [[PubMed](#)]
- Agostini, S.; Gubern, M.; Tondereau, V.; Salvador-Cartier, C.; Bezirard, V.; Lévêque, M.; Keränen, H.; Theodorou, V.; Bourdu-Naturel, S.; Goupil-Feuillerat, N.; et al. A marketed fermented dairy product containing Bifidobacterium lactis CNCM I-2494 suppresses gut hypersensitivity and colonic barrier disruption induced by acute stress in rats. *Neurogastroenterol. Motil. Off. J. Eur. Gastrointest. Motil. Soc.* **2012**, *24*, 376–e172. [[CrossRef](#)]
- Wu, X.; Wang, S.; Lu, J.; Jing, Y.; Li, M.; Cao, J.; Bian, B.; Hu, C. Seeing the unseen of Chinese herbal medicine processing (Paozhi): Advances in new perspectives. *Chin. Med.* **2018**, *13*, 4. [[CrossRef](#)] [[PubMed](#)]
- Li, R.L.; Zhang, Q.; Liu, J.; He, L.Y.; Huang, Q.W.; Peng, W.; Wu, C.J. Processing methods and mechanisms for alkaloid-rich Chinese herbal medicines: A review. *J. Integr. Med.* **2021**, *19*, 89–103. [[CrossRef](#)] [[PubMed](#)]

25. Zhou, L.; Xu, J.D.; Zhou, S.S.; Shen, H.; Mao, Q.; Kong, M.; Zou, Y.T.; Xu, Y.Y.; Xu, J.; Li, S.L. Chemomics-based marker compounds mining and mimetic processing for exploring chemical mechanisms in traditional processing of herbal medicines, a continuous study on *Rehmanniae Radix*. *J. Chromatogr. A* **2017**, *1530*, 232–240. [\[CrossRef\]](#)
26. Li, Z.; Li, J.; Zhang, F.; Zhu, N.; Sha, Z.; Li, D.; Tu, Y.; Hou, J. Antidiarrheal Effect of Sechang-Zhixie-San on Acute Diarrhea Mice and Network Pharmacology Deciphering Its Characteristics and Potential Mechanisms. *Evid.-Based Complement. Altern. Med. Ecam* **2020**, *2020*, 8880298. [\[CrossRef\]](#)
27. Mo, L.; Zeng, Z.; Li, Y.; Li, D.; Yan, C.Y.; Xiao, S.; Huang, Y.H. Animal study of the anti-diarrhea effect and microbial diversity of dark tea produced by the Yao population of Guangxi. *Food Funct.* **2019**, *10*, 1999–2009. [\[CrossRef\]](#)
28. Xu, Z.; Zhang, M.; Dou, D.; Kang, T.; Li, F. Effects of Deoxyschisandrins on Visceral Sensitivity of Mice with Inflammatory Bowel Disease. *Evid.-Based Complement. Altern. Med. Ecam* **2019**, *2019*, 2986097. [\[CrossRef\]](#)
29. Jiang, J.; Jin, W.; Peng, Y.; He, Z.; Wei, L.; Li, S.; Wang, X.; Chang, M.; Wang, R. In vivo and vitro characterization of the effects of kisspeptin-13, endogenous ligands for GPR54, on mouse gastrointestinal motility. *Eur. J. Pharmacol.* **2017**, *794*, 216–223. [\[CrossRef\]](#)
30. Wang, D.; Gao, N.; Zhou, T.; Zhang, Q.; Wang, J.; Li, A. Effect of Neurologin1 and Neurexin1 on the Colonic Motility in a Mouse Model of Neuronal Intestinal Dysplasia. *Gastroenterol. Res. Pract.* **2020**, *2020*, 9818652. [\[CrossRef\]](#)
31. Hayeeawaema, F.; Wichienchot, S.; Khuituan, P. Amelioration of gut dysbiosis and gastrointestinal motility by konjac oligo-glucomannan on loperamide-induced constipation in mice. *Nutr. (Burbank Los Angeles Cty. Calif.)* **2020**, *73*, 110715. [\[CrossRef\]](#) [\[PubMed\]](#)
32. Lu, J.; Mao, D.; Li, X.; Ma, Y.; Luan, Y.; Cao, Y.; Luan, Y. Changes of intestinal microflora diversity in diarrhea model of KM mice and effects of *Psidium guajava* L. as the treatment agent for diarrhea. *J. Infect. Public Health* **2020**, *13*, 16–26. [\[CrossRef\]](#) [\[PubMed\]](#)
33. Szymaszkiwicz, A.; Włodarczyk, J.; Mazur, M.; Olczak, J.; Fichna, J.; Zielińska, M. Cyclic derivatives of morphiceptin possess anti-transit effect in the gastrointestinal tract and alleviate abdominal pain in mice. *Pharmacol. Rep. PR* **2020**, *72*, 314–321. [\[CrossRef\]](#)
34. Barbara, G.; Stanghellini, V.; Brandi, G.; Cremon, C.; Di Nardo, G.; De Giorgio, R.; Corinaldesi, R. Interactions between commensal bacteria and gut sensorimotor function in health and disease. *Am. J. Gastroenterol.* **2005**, *100*, 2560–2568. [\[CrossRef\]](#) [\[PubMed\]](#)
35. Lyte, M. Microbial endocrinology and infectious disease in the 21st century. *Trends Microbiol.* **2004**, *12*, 14–20. [\[CrossRef\]](#)
36. Uribe, A.; Alam, M.; Johansson, O.; Midtvedt, T.; Theodorsson, E. Microflora modulates endocrine cells in the gastrointestinal mucosa of the rat. *Gastroenterology* **1994**, *107*, 1259–1269. [\[CrossRef\]](#)
37. Spiller, R. Recent advances in understanding the role of serotonin in gastrointestinal motility in functional bowel disorders: Alterations in 5-HT signalling and metabolism in human disease. *Neurogastroenterol. Motil. Off. J. Eur. Gastrointest. Motil. Soc.* **2007**, *19* (Suppl. 2), 25–31. [\[CrossRef\]](#)
38. Gershon, M.D.; Liu, M.T. Serotonin and neuroprotection in functional bowel disorders. *Neurogastroenterol. Motil. Off. J. Eur. Gastrointest. Motil. Soc.* **2007**, *19* (Suppl. 2), 19–24. [\[CrossRef\]](#)
39. Gershon, M.D.; Tack, J. The serotonin signaling system: From basic understanding to drug development for functional GI disorders. *Gastroenterology* **2007**, *132*, 397–414. [\[CrossRef\]](#)
40. Stasi, C.; Bellini, M.; Bassotti, G.; Blandizzi, C.; Milani, S. Serotonin receptors and their role in the pathophysiology and therapy of irritable bowel syndrome. *Tech. Coloproctol.* **2014**, *18*, 613–621. [\[CrossRef\]](#)
41. Zhang, Z.W.; Arseneault, D. Gain modulation by serotonin in pyramidal neurones of the rat prefrontal cortex. *J. Physiol.* **2005**, *566*, 379–394. [\[CrossRef\]](#) [\[PubMed\]](#)
42. Fayyaz, M.; Lackner, J.M. Serotonin receptor modulators in the treatment of irritable bowel syndrome. *Ther. Clin. Risk Manag.* **2008**, *4*, 41–48. [\[CrossRef\]](#) [\[PubMed\]](#)
43. Gershon, M.D. Review article: Roles played by 5-hydroxytryptamine in the physiology of the bowel. *Aliment. Pharmacol. Ther.* **1999**, *13* (Suppl. 2), 15–30. [\[CrossRef\]](#)
44. Chumpitazi, B.P.; Shulman, R.J. Underlying molecular and cellular mechanisms in childhood irritable bowel syndrome. *Mol. Cell. Pediatr.* **2016**, *3*, 11. [\[CrossRef\]](#) [\[PubMed\]](#)
45. Gwee, K.A.; Lu, C.L.; Ghoshal, U.C. Epidemiology of irritable bowel syndrome in Asia: Something old, something new, something borrowed. *J. Gastroenterol. Hepatol.* **2009**, *24*, 1601–1607. [\[CrossRef\]](#)
46. Camilleri, M. Physiological underpinnings of irritable bowel syndrome: Neurohormonal mechanisms. *J. Physiol.* **2014**, *592*, 2967–2980. [\[CrossRef\]](#)
47. Furness, J.B.; Kunze, W.A.; Clerc, N. Nutrient tasting and signaling mechanisms in the gut. II. The intestine as a sensory organ: Neural, endocrine, and immune responses. *Am. J. Physiol.* **1999**, *277*, G922–G928. [\[CrossRef\]](#)
48. Surawicz, C.M. Mechanisms of diarrhea. *Curr. Gastroenterol. Rep.* **2010**, *12*, 236–241. [\[CrossRef\]](#)
49. Michelangeli, F.; Ruiz, M.C. I, 2. Physiology and pathophysiology of the gut in relation to viral diarrhea. *Perspect. Med. Virol.* **2003**, *9*, 23–50. [\[CrossRef\]](#)
50. Guilarte, M.; Santos, J.; de Torres, I.; Alonso, C.; Vicario, M.; Ramos, L.; Martínez, C.; Casellas, F.; Saperas, E.; Malagelada, J.R. Diarrhoea-predominant IBS patients show mast cell activation and hyperplasia in the jejunum. *Gut* **2007**, *56*, 203–209. [\[CrossRef\]](#)
51. Fukumoto, S.; Tatewaki, M.; Yamada, T.; Fujimiyama, M.; Mantyh, C.; Voss, M.; Eubanks, S.; Harris, M.; Pappas, T.N.; Takahashi, T. Short-chain fatty acids stimulate colonic transit via intraluminal 5-HT release in rats. *Am. J. Physiol. Regul. Integr. Comp. Physiol.* **2003**, *284*, R1269–R1276. [\[CrossRef\]](#) [\[PubMed\]](#)

52. Li, Y.; Zhang, Y.; Wei, K.; He, J.; Ding, N.; Hua, J.; Zhou, T.; Niu, F.; Zhou, G.; Shi, T.; et al. Review: Effect of Gut Microbiota and Its Metabolite SCFAs on Radiation-Induced Intestinal Injury. *Front. Cell. Infect. Microbiol.* **2021**, *11*, 577236. [[CrossRef](#)] [[PubMed](#)]
53. Liu, X.; Cao, S.; Zhang, X. Modulation of Gut Microbiota-Brain Axis by Probiotics, Prebiotics, and Diet. *J. Agric. Food Chem.* **2015**, *63*, 7885–7895. [[CrossRef](#)] [[PubMed](#)]
54. Fan, Y.J.; Chen, S.J.; Yu, Y.C.; Si, J.M.; Liu, B. A probiotic treatment containing *Lactobacillus*, *Bifidobacterium* and *Enterococcus* improves IBS symptoms in an open label trial. *J. Zhejiang Univ. Sci. B* **2006**, *7*, 987–991. [[CrossRef](#)] [[PubMed](#)]
55. Sinn, D.H.; Song, J.H.; Kim, H.J.; Lee, J.H.; Son, H.J.; Chang, D.K.; Kim, Y.H.; Kim, J.J.; Rhee, J.C.; Rhee, P.L. Therapeutic effect of *Lactobacillus acidophilus*-SDC 2012, 2013 in patients with irritable bowel syndrome. *Dig. Dis. Sci.* **2008**, *53*, 2714–2718. [[CrossRef](#)]
56. Derrien, M.; Collado, M.C.; Ben-Amor, K.; Salminen, S.; de Vos, W.M. The Mucin degrader *Akkermansia muciniphila* is an abundant resident of the human intestinal tract. *Appl. Environ. Microbiol.* **2008**, *74*, 1646–1648. [[CrossRef](#)]
57. Everard, A.; Belzer, C.; Geurts, L.; Ouwerkerk, J.P.; Druart, C.; Bindels, L.B.; Guiot, Y.; Derrien, M.; Muccioli, G.G.; Delzenne, N.M.; et al. Cross-talk between *Akkermansia muciniphila* and intestinal epithelium controls diet-induced obesity. *Proc. Natl. Acad. Sci. USA* **2013**, *110*, 9066–9071. [[CrossRef](#)]
58. Derrien, M.; Vaughan, E.E.; Plugge, C.M.; de Vos, W.M. *Akkermansia muciniphila* gen. nov., sp. nov., a human intestinal mucin-degrading bacterium. *Int. J. Syst. Evol. Microbiol.* **2004**, *54*, 1469–1476. [[CrossRef](#)]
59. Visca, P.; Seifert, H.; Towner, K.J. *Acinetobacter* infection—an emerging threat to human health. *IUBMB Life* **2011**, *63*, 1048–1054. [[CrossRef](#)]
60. Smith, B.J.; Miller, R.A.; Ericsson, A.C.; Harrison, D.C.; Strong, R.; Schmidt, T.M. Changes in the gut microbiome and fermentation products concurrent with enhanced longevity in acarbose-treated mice. *BMC Microbiol.* **2019**, *19*, 130. [[CrossRef](#)]
61. Bartlett, J.G. Clinical practice. Antibiotic-associated diarrhea. *N. Engl. J. Med.* **2002**, *346*, 334–339. [[CrossRef](#)] [[PubMed](#)]
62. Ferrer, M.; Méndez-García, C.; Rojo, D.; Barbas, C.; Moya, A. Antibiotic use and microbiome function. *Biochem. Pharmacol.* **2017**, *134*, 114–126. [[CrossRef](#)] [[PubMed](#)]
63. Silverman, M.A.; Konnikova, L.; Gerber, J.S. Impact of Antibiotics on Necrotizing Enterocolitis and Antibiotic-Associated Diarrhea. *Gastroenterol. Clin. North Am.* **2017**, *46*, 61–76. [[CrossRef](#)]
64. Camilleri, M.; Sellin, J.H.; Barrett, K.E. Pathophysiology, Evaluation, and Management of Chronic Watery Diarrhea. *Gastroenterology* **2017**, *152*, 515–532.e512. [[CrossRef](#)] [[PubMed](#)]
65. O'Mahony, S.M.; Clarke, G.; Borre, Y.E.; Dinan, T.G.; Cryan, J.F. Serotonin, tryptophan metabolism and the brain-gut-microbiome axis. *Behav. Brain Res.* **2015**, *277*, 32–48. [[CrossRef](#)]
66. Wikoff, W.R.; Anfora, A.T.; Liu, J.; Schultz, P.G.; Lesley, S.A.; Peters, E.C.; Siuzdak, G. Metabolomics analysis reveals large effects of gut microflora on mammalian blood metabolites. *Proc. Natl. Acad. Sci. USA* **2009**, *106*, 3698–3703. [[CrossRef](#)]

Review

Current Progress in the Chemoenzymatic Synthesis of Natural Products

Evan P. Venable¹, Laurel G. Habgood² and James D. Patrone^{2,*}¹ Department of Chemistry and Biochemistry, Elmhurst University, Elmhurst, IL 60126, USA² Department of Chemistry, Rollins College, Winter Park, FL 32789, USA

* Correspondence: jpatrone@rollins.edu

Abstract: Natural products, with their array of structural complexity, diversity, and biological activity, have inspired generations of chemists and driven the advancement of techniques in their total syntheses. The field of natural product synthesis continuously evolves through the development of methodologies to improve stereoselectivity, yield, scalability, substrate scope, late-stage functionalization, and/or enable novel reactions. One of the more interesting and unique techniques to emerge in the last thirty years is the use of chemoenzymatic reactions in the synthesis of natural products. This review highlights some of the recent examples and progress in the chemoenzymatic synthesis of natural products from 2019–2022.

Keywords: chemoenzymatic; natural product synthesis; biocatalysis

Citation: Venable, E.P.; Habgood, L.G.; Patrone, J.D. Current Progress in the Chemoenzymatic Synthesis of Natural Products. *Molecules* **2022**, *27*, 6373. <https://doi.org/10.3390/molecules27196373>

Academic Editor: Giovanni Ribaudò

Received: 9 September 2022

Accepted: 23 September 2022

Published: 27 September 2022

Publisher's Note: MDPI stays neutral with regard to jurisdictional claims in published maps and institutional affiliations.



Copyright: © 2022 by the authors. Licensee MDPI, Basel, Switzerland. This article is an open access article distributed under the terms and conditions of the Creative Commons Attribution (CC BY) license (<https://creativecommons.org/licenses/by/4.0/>).

1. Introduction

The biodiversity of organisms from plants to microbes to mammals on Earth has led to a vast wealth of natural products. Throughout history from ancient civilizations to our contemporary one, these natural products have been an invaluable source of bioactive molecules capable of improving their quality of life. Natural products and their derivatives found success in modern drug discovery for a wide range of disease states ranging from diabetes and cardiovascular disease to viral infections and inflammatory diseases with notably high success as antibiotic and anticancer agents [1]. Despite the continued success of natural products in the clinical setting, the pharmaceutical industry divested resources from their discovery in the 1990s due to challenges associated with the rediscovery of known chemical entities, target deconvolution, and resources being allocated to alternative methods of drug discovery [2,3]. More recently there has been a resurgence in natural product discovery, structure elucidation, and progression of natural products to the clinic as a consequence of increased resources and advances in methodologies.

The field of natural product synthesis dates back to 1828, fascinating and inspiring generations of chemists [2,4]. Natural products are often characterized for their high structural complexity stemming from an enriched number of stereocenters, sp³ carbons, oxygen atoms, and rigid carbon skeletons as compared to synthetically designed molecules [1]. The combination of the rich, diverse, and structurally complex structures of natural products and the drive, creativity, and talent within the synthetic community makes the synthesis of natural products one of if not the most important fields for both training chemists and developing novel synthetic methods [4]. The pursuit of these diverse targets has seen the field of organic chemistry expand its capabilities in leaps and bounds in areas such as but not limited to retrosynthetic analysis, stereoselective and regiospecific C-C bond formations, cascade reactions, orthogonal protecting groups, protecting group free synthesis, organometallic catalysis, convergent synthesis, atom efficiency, and green chemistry [4]. To this point, many modern organic techniques have been applied to natural product synthesis. For example, organometallic mediated C-H activation bond activation chemistry (directed and non-directed) such as in the synthesis of (–)-epicoccin G and artemisinin [5]. The

boundaries and application of electrochemical reactions such as decarboxylative couplings have been extended into the synthesis of *R*-(*Z*)- nerolidol [6]. Photochemical reactions such as cycloadditions, arene couplings, and C-N bond formations are an emerging methodology in the synthesis of natural products such as (–)-pavidolide B, (+)-flavisiamine F, and (+)-iosocorynantheol [7].

Over the past twenty years, chemists have been going back to nature and its biosynthetic pathways to develop new advantageous bond forming methodologies through chemoenzymatic syntheses [8–14]. These pioneering scientists have enriched our synthetic landscape across numerous reaction types such as chiral resolutions (many of the first applications of chemoenzymatic processes), saponifications, hemiacetal formations, oxidations and reductions, and C–C bond forming reactions as well as classes of molecules including glycans, peptides or derivatized amino acids, polyketides, and terpenoids. The benign nature, stereospecificity, and potential of chemoenzymatic processes has led researchers to invest heavily in their development.

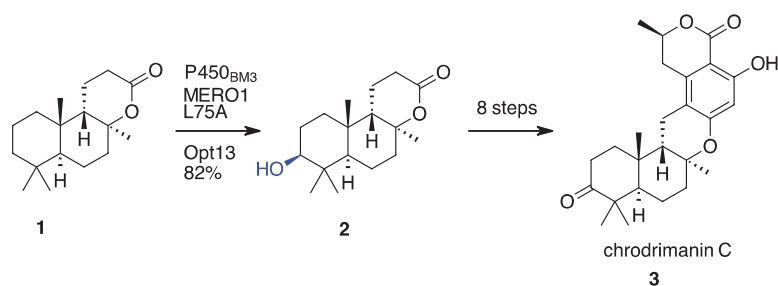
As chemoenzymatic methods became more widely available and applicable, their benefits to the synthetic communities are greater than just expanded methodologies. Enzyme-catalyzed reactions incorporate the majority of the twelve principles of green chemistry that seek to reduce our impact on human health and the environment [15]. Enzymes are inherently non-toxic and natural (less hazardous chemical synthesis and use of renewable feedstocks). Their catalytic nature affords reactions that can be run at ambient to slightly elevated temperatures in biphasic or completely aqueous media (catalysis, design for energy efficiency, safer solvents and auxiliaries) and impart regio- and stereoselectivity (atom economy, waste prevention) [16]. Since chemoenzymatic methods combine high regioselectivity and stereoselectivity with environmental and cost benefits, they are attractive method for large scale synthesis and as such have been adopted for the synthesis of several high value pharmaceutical agents such as sitagliptin, simvastatin, and darunavir [16,17].

The continued application and success of chemoenzymatic syntheses in these settings has continued to fuel the diversity and pace of research into biocatalytic approaches. This research has produced advances in the variety and number of chemoenzymatic processes and increased their capabilities through scalability, multiple enzyme cascades, and flow processes. The importance of the chemoenzymatic synthesis of natural products can be seen in the explosion of recent syntheses and review articles highlighting their accomplishments [11,18–30]. This report is organized by classification of molecule and aims to highlight the diversity and power of this field through selected chemoenzymatic syntheses of natural products from 2019–2022.

2. Selected Natural Product Syntheses Incorporating Chemoenzymatic Methods

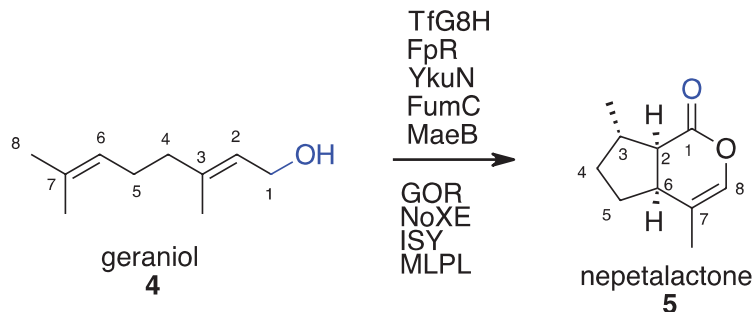
2.1. Terpenoids

One of the principal scientists featured throughout this review, Hans Renata, pushes the boundaries of the utility and elegance of chemoenzymatic synthesis across multiple complex classes of molecules. The work of the Renata group is often impressive in its nuanced design which is integrated within traditional synthetic sequences [20,22,23,31–33]. In a recent paper they disclosed the synthesis of chrodrimanin C (**3**), verruculide A, and polysin using multiple chemoenzymatic steps (**Scheme 1**) [33]. A key step featured in these syntheses is an enzymatic hydroxylation of a 6,6,5 or 6,6,6, steroid core, intermediate **1** in the case of chrodrimanin C (**3**). These reactions were performed on gram scale, 67 & 83% yields, depending on starting material, selectivity for oxidation of a single methylene despite the presence of 6 or 7 other oxidizable methylene groups, and with enantioselectivity of course. This scale is an impressive feature for chemoenzymatic methods, considering the importance of this feature for transformations in total synthesis.



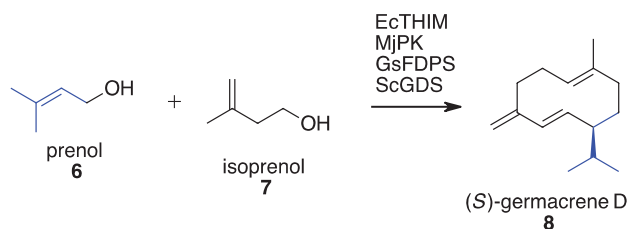
Scheme 1. Selective chemoenzymatic hydroxylation towards the synthesis of chrodrimanin C (**3**) [32].

Tang and co-workers' synthesis of the bicyclic terpenoid nepetalactone, the active molecule in catnip and a natural insect repellent, features a one-pot multienzyme (OPME) system that is stereoselective setting three contiguous stereocenters while utilizing geraniol (**4**) as a precursor (**Scheme 2**). [34]. This synthesis features a ten-enzyme cascade, half of which are necessary to perform the requisite biosynthetic steps, and half of which are required for auxiliary needs or cofactor regeneration. The chemical steps performed by the enzymes are allylic hydroxylation, alcohol oxidation, aldehyde reduction, cyclization, and a hemiacetal oxidation. One of the more elegant aspects of this system is the ability to perform oxidative and reductive steps in the same pot, with the same NAD/NADH system. Although the experiments were run on a small scale, the yields are excellent (93%) with potential to produce approximately 1 g nepetalactone per liter of solution at a reasonable cost (<\$120/g).



Scheme 2. One-pot multienzyme cascade synthesis of nepetalactone (**5**) from geraniol (**4**) [34].

A novel method using an OPME cascade of enzymatic reactions to synthesize triterpenes of highly varied structures, including cyclized variants was recently reported by Allemann and coworkers [35]. Noteworthy is that the scope of starting material, enzymatic variance, and enzymatic combinations, as many as four enzymes total, all within an OPME framework to generate simple but highly varied triterpenoids. The enzymatic transformations utilized include monophosphorylation by *Ec*THIM, diphosphorylation by *Mj*IPK, synthesis of natural and unnatural farnesyl diphosphates by *Gs*FDPS, and cyclization and/or bicyclization using a variety of enzymes. Pyruvate kinase (PK) acts as a supplementary enzyme to replenish the ATP substrate pool throughout the phosphorylation reactions. Seven sesquiterpenoid compounds, many first reported in this study, and the antibacterial/antifungal (*S*)-germacrene D (**8**) are synthesized. Prenol (**6**) and isoprenol (**7**) were mixed in a 1:2 ratio with *Ec*THIM, *Mj*IPK, PK, *Gs*FDPS, and *Sc*GDS to yield germacrene D (**Scheme 3**). Advantages of their methodology include using less expensive 4- or 5-carbon starting materials and producing both natural and unnatural products in a modular fashion on a milligram scale.

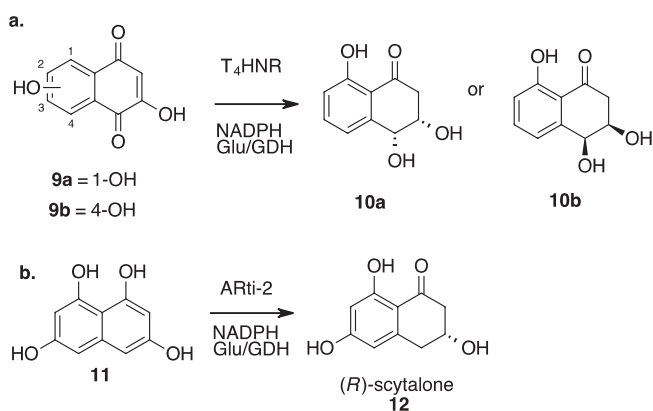


Scheme 3. OPME system utilized in the activation, condensation, and cyclization of prenol (6) and isoprenol (7) for the synthesis of (S)-germacrene D (8) [35].

2.2. Polyketides

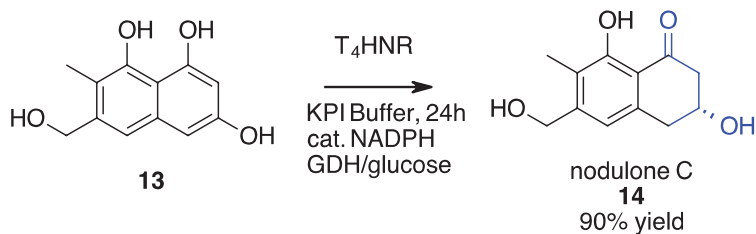
The area of chemoenzymatic synthesis to produce polyketide natural product targets is so critical that it can be said that it is the driver of advancements in the field as a whole. Alison Narayan and David Sherman have been and will continue to build on their pioneering work [14,18,26,28,36–40]. The importance of these two scientists to the field is evidenced by the previous coverage in the literature, including other reviews. Therefore, this work will not include it but allow for interested readers to explore it within these references.

Stereoselective reductions of simple organic moieties are an easy way to introduce stereocenters: if it can be done. To afford the desired diol products selectively, Husain et al. have applied the use of T₄HNR to reduce ketones and enols selectively in naphthol systems (**Scheme 4a**) [41]. Intriguingly this process reacts very differently with 2-hydroxy and 3-hydroxyjuglone starting materials. The phenol orients the molecule within the enzyme active site to provide the selectivity for the adjacent ketone to be reduced. While exhibiting a high level of selectivity, the reduction of 3-hydroxyjuglone affords an 82:18 d.r. for **10a** and **10b** which is comparatively modest for an enzymatic transformation. Building off this initial strategy, the Husain group recently reported the small-scale synthesis (*R*)-scytalone (**12**) from simple accessible starting materials using the anthrole reductase ARTi-2 and a NADPH cofactor (**Scheme 4b**) [42]. Notable about this chemoenzymatic transformation is that scytalone, generated by the desymmetrization of a perfectly flat tetrahydroxynaphthalene in a stereoselective fashion, also includes another phenol, which is oxidized to a ketone. Despite a small scale and modest yield (23%), the selectivity was >99% for the observed stereoisomer is exceptional.



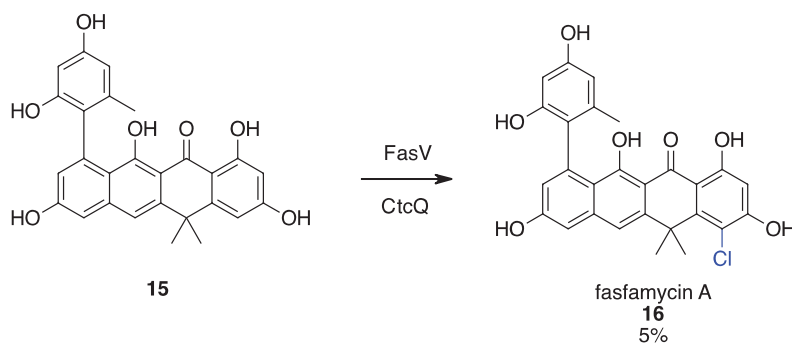
Scheme 4. (a) Stereoselective chemoenzymatic reductions using T₄HNR to form polyketide metabolites **10a**, **10b**. (b) Stereoselective chemoenzymatic reductions using Arti-2 to synthesize (*R*)-scytalone (**12**) [41,42].

Husain and coworkers continued studies utilizing a system of T₄HNR, NADPH, and glucose with GDH to synthesize polyketide natural products in the nodulone family (Scheme 5) [43]. The synthesis of both nodulone C (14) and an unnatural diastereomer of nodulone D are featured. In the case of nodulone D, two stereocenters were set with near perfect d.r. Their ability to doubly hydrogenate the hydroxynaphthoquinone selectively, while leaving a benzylic ketone untouched, would be difficult to duplicate using traditional synthetic organic techniques as overreduction would be facile. In nodulone C they once more selectively reduced a hydroxynaphthalene to a phenol, enacting a single enol reduction in a naphthalene with three hydroxy groups selectively in an excellent 90% yield.



Scheme 5. High yielding stereoselective reduction in the synthesis of nodulone C (14) [43].

A recent synthesis of fasamycin A (6) from the precursor naphthacemycin B1, utilizing a highly unusual enzymatic halogenation, was recently reported by the Renata group (Scheme 6) [33]. The report involved a convergent synthesis that culminated with a halogenation via a chemoenzymatic system that contained a flavin-dependent halogenase, CtcQ as a reductase, Opt13 to regenerate NADH, and NADH/NADPH. The success of the synthesis hinges on a single halogenation of a polyphenol (15), at a specific site, with regioselectivity to afford the product in 5% yield. There are 4 rings in precursor (15) which could be halogenated, two of which are almost identical electronically and sterically making the regioselectivity achieved even more impressive. The author notes that low yield has been previously reported with halogenases and that enzyme engineering may assist with the issue. Progress in the area of halogenases as a whole will allow this methodology to be used by the broader synthetic community.

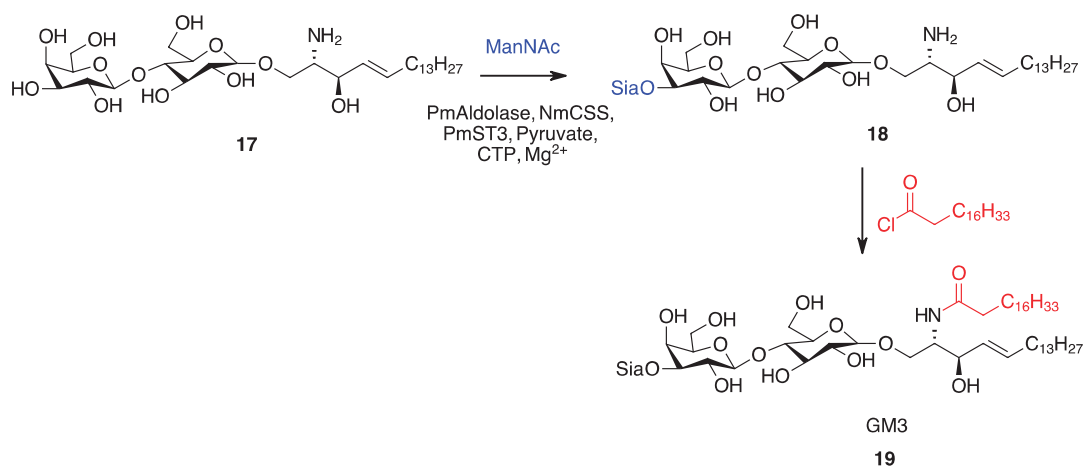


Scheme 6. Regioselective halogenation for the synthesis of fasamycin A (16) [33].

2.3. Glycans

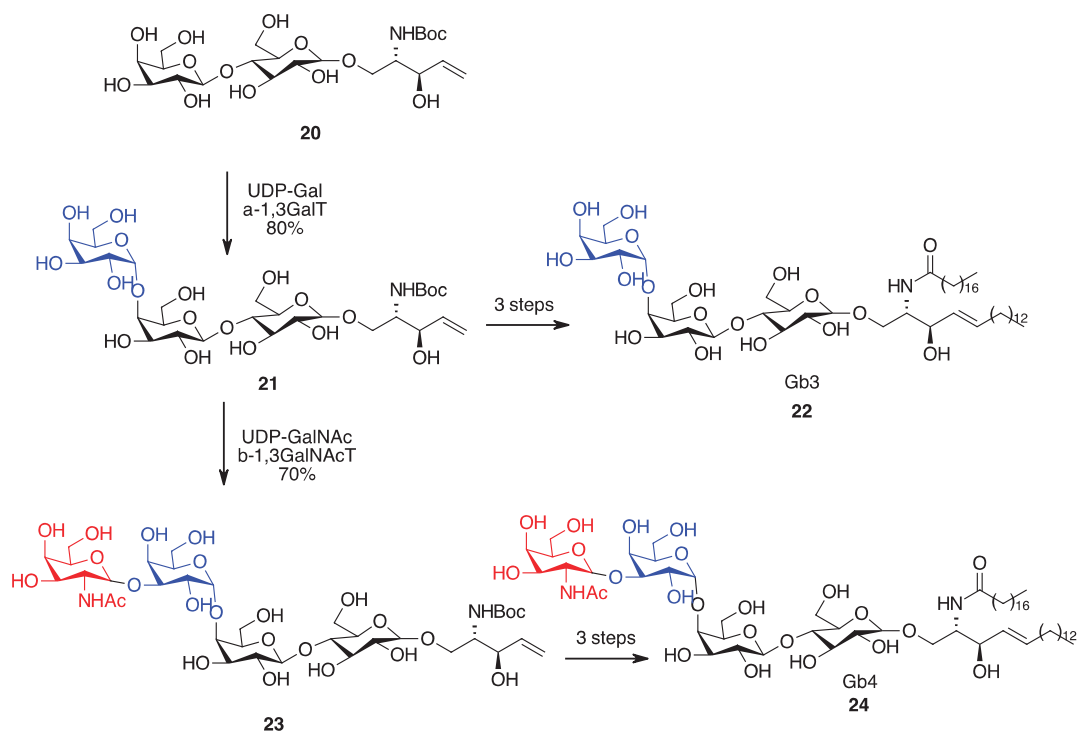
Glycans are a diverse set of natural products whose size and purpose vary greatly. The range in size from small monosaccharides to enormous polysaccharides possessing hundreds of glycan units correlates with their variety of biological targets and purposes of sugars. Given their versatility, they are used in multiple fields such as food chemistry, medicinal chemistry, and investigations of fundamental biological processes [44–53].

The Chen group has continued their focused efforts to improve synthetic routes to create structurally diverse libraries of gangliosides, specifically GM3 (**19**) [54]. Comprised of glycan and lipid moieties, GM3 has been implicated as a risk factor in metabolic diseases as well as placed on a prioritized cancer antigen list. An OPME strategy was employed to install sialic acid variants on lactosyl sphingosine (LacbSph) followed by subsequent acylation of a fatty acyl chain to form multiple GM3bSph gangliosides (**Scheme 7**). The six sialic acid variants (ManNAc) were attached to LacbSph forming the GM3 sphingosines in high yields (85–95%) utilizing a OPME approach containing three enzymes, including PmNanA (*P. multocida* sialic acid aldolase), NmCSS (*N. meningitidis* CMP-sialic acid synthetase), and PmST3 (*P. multocida* a2-3 sialyltransferase). Subsequent acylation with stearoyl chloride (98–100%) or alternate fatty acyl chains (98–100%) produced ten GM3 gangliosides. Advantages of the synthetic strategy include gram-scale production of LacbSph from an L-serine derivative with minimal purification and efficient mg scale (average 25 mg) production of diverse GM3 gangliosides with fluorine, azide, and diazirine sialic acid derivatives.



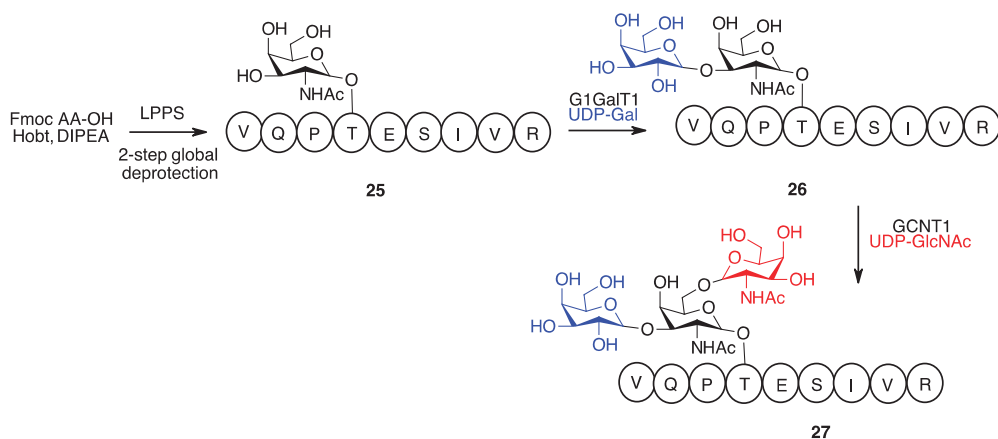
Scheme 7. Chemoenzymatic installation of sialic acid in the synthesis of GM3 (**19**) [54].

Glycosphingolipids (GSLs) comprised of a glycan and ceramide component are a major component of the cell membrane and are notable signaling molecules essential to numerous biological processes and diseases. Future studies related to mechanisms of these processes, diseases, and applications are contingent on the ready availability of pure and structurally characterized GSLs. To meet this need, the Guo group envisioned a diversity-oriented strategy involving chemoenzymatic glycan synthesis in conjunction with the chemoselective modification of the sphingolipid chain [55]. A series of eight natural and non-natural GSLs were synthesized including Gb3 (**22**), Gb4 (**24**), GM3, and GD3, all of which are known cancer biomarkers. The synthesis of Gb 3 starts with the core intermediate of the strategy being diversified enzymatically by adding Gal using an α -1,4-galactosyltransferase to form the trisaccharide (**21**). The trisaccharide is the chemically modified via a Grubbs-Hoveyda-II catalyzed cross metathesis, Boc removal, and amide formation via an acyl chloride to cleanly yield the fully elaborated GSL Gb3 (**Scheme 8**). The strength of this strategy is its readily amenable to other targets with the same core intermediate and route/steps being utilized with an extra enzymatic step to further diversify the glycan with GalNAc to a tetrasaccharide (**23**) before the chemoselective transformations to yield Gb4 (**24**).



Scheme 8. Variable chemoenzymatic glycosylation strategy for the synthesis of Gb3 (23) and Gb4 (24) [55].

Glycopeptides are another class of glycan-based molecules that have implications in normal cellular signaling and disease progression. Again, a major issue with conducting proper studies to understand the biological underpinnings of these molecules is the difficulty of obtain sufficient quantities of pure homogeneous samples. The Li group devised a robust streamlined chemoenzymatic approach to the synthesis of 16 well-defined SARS-CoV-2 O-glycopeptides, 4 complex MUC1 glycopeptides, and a 31-mer glycosylated glucagon-like peptide-1 [56]. Using the SARS-CoV-2 O-glycopeptides as an example, the authors utilized a combination of liquid-phase peptide synthesis (LPPS) and chemoenzymatic glycan synthesis (**Scheme 9**). First the authors used LPPS to build the core 9mer peptide on a 105 mg scale. This was an efficient process using only 1.2 equivalents of amino acid and coupling reagents and leveraging a hydrophobic tag for quick purification by centrifugation and removal of supernatant liquid. Once the 9mer was constructed with the first glycan unit (GalNAc) attached to the T residue a 2-step global deprotection of all sugar, amino acid protecting groups, and the hydrophobic tag yielded the clean core glycosylated peptide. Enzymatic diversification of the GalNAc moiety through the use of varying combinations and orders of glycosyltransferases including C1GalT1, ST6GalNAc1, ST6Gal1, Pd2, 6ST, ST3Gal1, ST3Gal4, GCNT1, B4GalT1 allowed for the formation a and b glycosidic bonds at varying positions with varying substrates to quickly form highly complex glycans highlights the power of this technique.

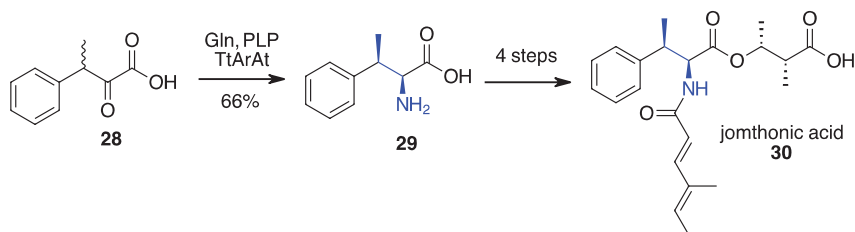


Scheme 9. Enzymatic diversification of core peptide for the synthesis of SARS-CoV-2 O-glycopeptides 26 and 27 [56].

2.4. Peptides and Amino Acids

Peptide and amino acid-based natural products have been some of the most versatile and important natural products used in the clinical setting including molecules such as Vancomycin and Insulin [57]. As such, there is a rich library of literature involving their syntheses and specifically their chemoenzymatic syntheses [58].

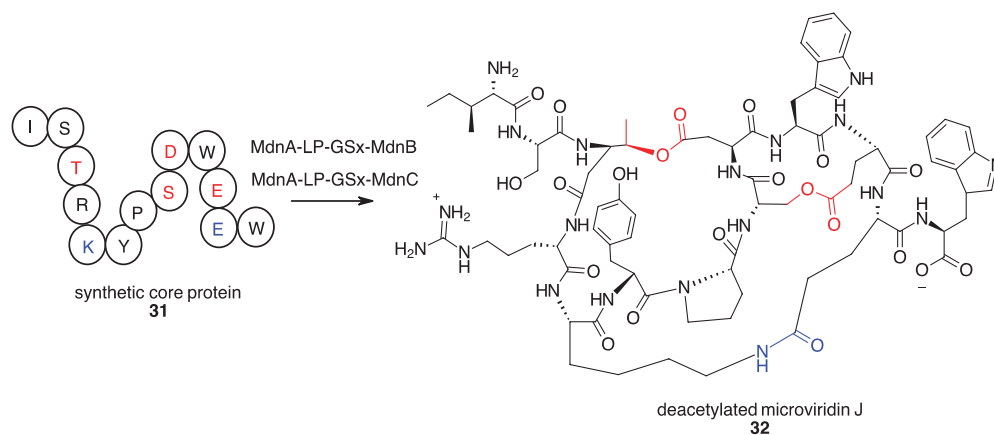
An area which has been developing recently in chemoenzymatic synthesis is the use of enzymes to create stereocenters in small molecules which can be used as a new “chiral pool” to work from towards natural product synthesis. Commonly this is done by dynamic kinetic resolution (DYKAT) or by enzymatic reductions to make enantiomerically enriched alcohols. A recent Renata publication in this area showcases this trend by performing a DYKAT, completed by an enantioselective reductive amination to set two stereocenters: one which was epimerized, one which was generated by the reduction [31]. This reductive amination is actually a transamination from sacrificial glutamine. The scope of this DYKAT was shown through 25 molecules with varying aryl substitutions, one of which was elaborated over four steps to complete the first synthesis of jomthonic acid (**Scheme 10**) (30). Significantly, a scaleup to a half gram with >20:1 d.r. was shown by the authors.



Scheme 10. Biocatalyzed DYKAT within the synthesis of jomthonic acid (30) [31].

Bruner and coworkers disclosed a recent strategy to synthesize deacetylated microviridin J (32) and explore the activity of engineered enzymes MdnB and MdnC, which perform the tricyclization of the 13mer MdnA core peptide sequence (**Scheme 11**) [59]. Fusion expression constructs were engineered with the MdnA leader peptides crosslinked to both MdnB and MdnC, using varying lengths of glycine/serine linkers (GS_n , $n = 5, 10 \text{ \& } 15$). This strategy allows for cyclizing just the synthetically produced core 13mer MdnA since the 36 AA leader sequence is already in place on MdnB and C rendering them

constitutively active. Upon incubation of these various engineered enzymes with the core peptide, it was found that GS_n *n* = 10 & 15 provided the necessary length and flexibility for efficient tricyclization to deacetylated microviridin J. This strategy is an excellent example of engineering and expressing the necessary enzymes for complex macrocyclizations that allowed for a much simpler synthesis of the 13mer core protein versus the endogenously expressed 39 AA leader and core peptide.



Scheme 11. Chemoenzymatic lactonization and lactamization for the synthesis of deacetylated microviridin J (32) [59].

In planta syntheses of moroidin (33, previously unsynthesized), and celogentin C (34, previously synthesized in 23 steps) were recently reported by the Weng group (Figure 1) [60]. Intriguingly, they did this by cloning a gene from *K. japonica*, the predicted precursor gene for Moroidin, and then expressing it in tobacco. They were able to then grow the tobacco with this newly inserted gene, and modified versions thereof, to produce different extractable natural products on the ~10 mg scale. The only synthetic organic chemistry performed during this synthesis was by the plant itself—enforced by the cloned gene.

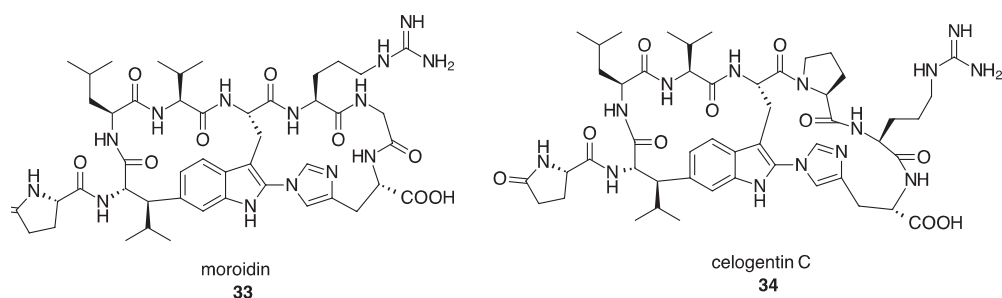
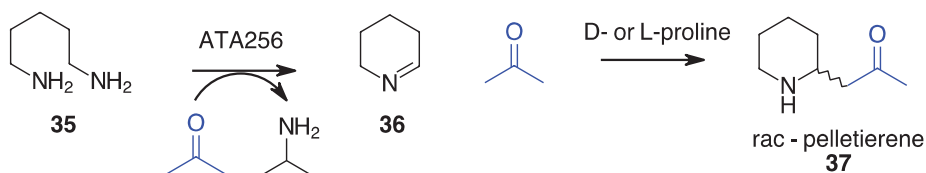


Figure 1. Structures of the peptide-based moroidin (33) and celogentin C (34) synthesized *in planta* [60].

2.5. Alkaloids

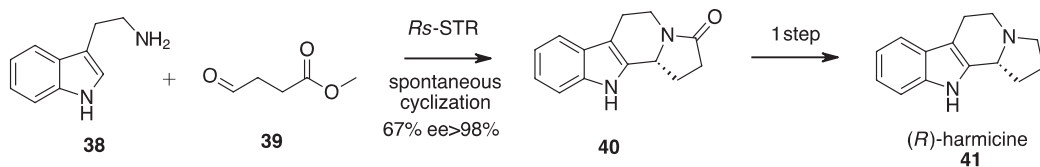
Alkaloid natural products have a rich history as both biologically active molecules and synthetic targets. This class of molecules has also proven to be a remarkable boon for chemoenzymatic syntheses [61,62]. Several syntheses are highlighted here to give exemplars of the diversity of molecule structure and enzymatic reaction. However, as there is not enough space in this report for a thorough coverage of the breadth of the syntheses, an alkaloid specific review can be found in by Cigan et al. [27].

Taday et al. published a hybrid bio-organocatalytic approach to the synthesis of the small piperidine-based natural product pelletierene (**Scheme 12**) (**37**) [63]. This work built upon a previously reported elegant one-pot 2-biocatalytic step approach to norsedaminone that utilized cadaverine, a transaminase, CalB, and a decarboxylative Mannich reaction to synthesize 14 different alkaloids but was unable to synthesize pelletierene [64]. The authors developed a system where transaminase ATA256 generated the reactive imine intermediate (**36**) with acetone playing the dual role as the nitrogen acceptor in this biocatalytic step as well as the nucleophile in the subsequent organocatalyzed Mannich reaction to yield the desired pelletierene. This system was optimized to produce pelletierene in 60% yield with 85 mg isolated. The only weakness of the system is the natural product was isolated as the racemate despite using D- or L-proline in the system. Based upon the lack of difference in ee for the proline isomers, the authors conclude this was most likely due the piperidine racemizing after the reaction [65]. The authors have established a sound system and now are looking to expand the scope of hybrid bio-organocatalytic approaches and further optimize their system to an in vivo model.



Scheme 12. ATA256 biocatalyzed transamination reaction for the synthesis of pelletierene (**37**) [63].

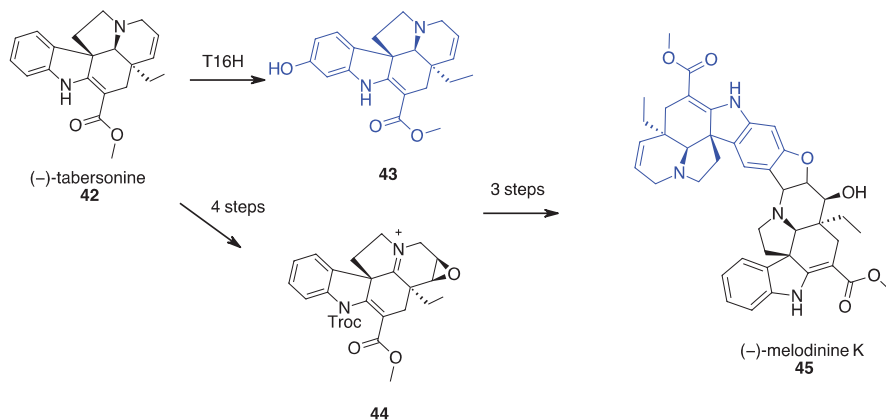
Indole containing alkaloids are abundant throughout nature and often serve as biologically relevant scaffolds. As such there has been an exciting recent push into the utilization of Pictet-Spenglerases for the synthesis of natural products. The Kroutil group published a concise 2-step chemoenzymatic synthesis of (*R*)-harmicine (**Scheme 13**) (**41**) [66]. The authors were exploring the substrate scope for non-natural substrates for strictosidinesynthases (STRs), an important class of Pictet-Spenglerases that could be leveraged for natural product synthesis. Four STRs from different organisms were cloned and expressed in *E. coli*. The best result was obtained by deleting the signal peptide and adding an N-terminal His-tag. Utilizing the STR from *Rauvolfia serpentina*, tryptamine (**38**) and methyl-4-oxobutanoate (**39**) were enzymatically condensed with concomitant cyclization to form product (**40**) in 67% yield with >98% ee on 75 mg scale. Smooth reduction of the carbonyl yielded the desired (*R*)-harmicine in a total yield of 62% with >98% ee. This report highlights the power of the enzyme via the concise high yielding synthesis as well the potential for a broad applicability for the future of other targets.



Scheme 13. Synthesis of (*R*)-harmicine (**41**) via chemoenzymatic Pictet-Spengler reaction [66].

A 2020 report from the Andrade lab details the first synthesis of the complex bis-indole (–)-melodinine K (**45**) via a convergent chemoenzymatic synthesis (**Scheme 12**) [67]. The authors were cognizant of both the efficiency and sustainability of this synthesis and thoughtfully devised their scheme based on the isolation of 1.6 g complex biosynthetic precursor (–)-tabersonine (**42**) from *V. africana* seeds (**Scheme 14**). Beyond the isolation of the carbon skeleton, a critical biotransformation of (–)-tabersonine (**42**) was employed

utilizing the cytochrome P450 monooxygenase tabersonine 16-hydroxylase (T16H) [68,69]. A modified yeast strain, *Saccharomyces cerevisiae* (WAT11 strain) was engineered, and the reaction conditions optimized to allow the site-selective oxidation of (–)-tabersonine (**42**) to (–)-16-hydroxytabersonine (**43**) in 64% yield on the gram scale. (–)-Tabersonine (**42**) is converted to activated epoxide (**44**) in four steps, followed by dimerization with a modified (–)-16-hydroxytabersonine intermediate, which underwent two more synthetic steps to obtain the final product (–)-melodinine K. This synthesis highlights both the power and efficiency of isolating a complex precursor and the selective and efficient site selective chemistry of chemoenzymatic syntheses.



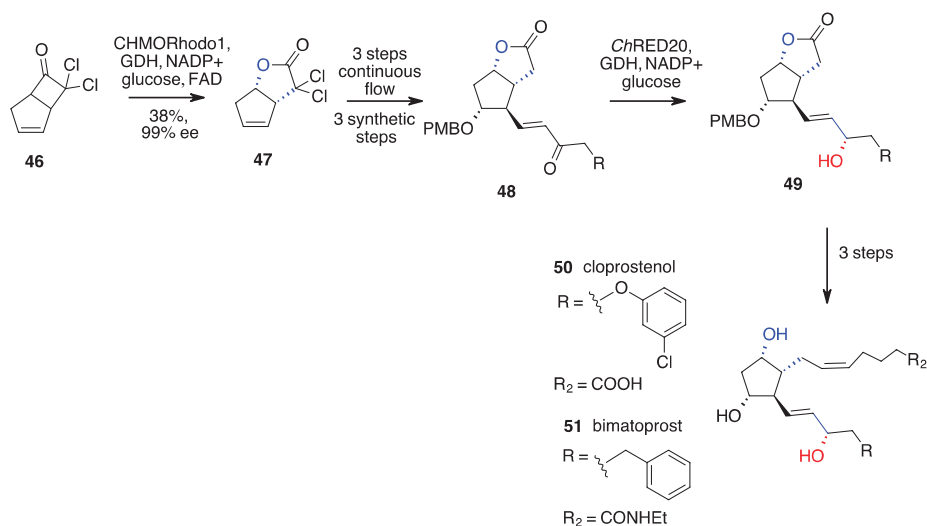
Scheme 14. Convergent synthesis of (–)-melodinine K (**45**) featuring chemoenzymatic oxidation of isolated biosynthetic precursor, (–)-tabersonine (**42**) [67].

2.6. Miscellaneous

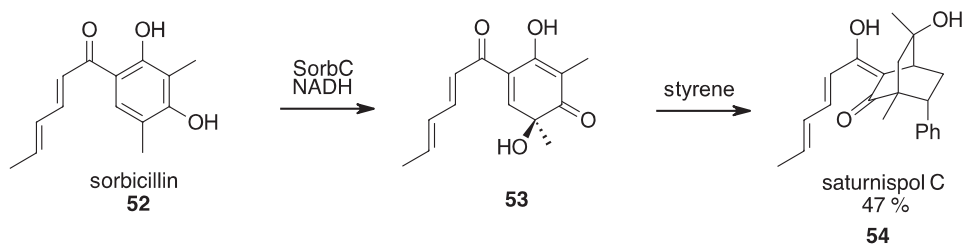
As chemoenzymatic synthesis has expanded, there are many interesting natural products and syntheses that fall into molecule classes outside of those listed above that are noteworthy and deserve highlighted in this report.

Prostaglandins (PGs) are lipid-based hormone-like signaling molecules that play multiple functions in humans and several such as cloprostenol (**50**) and bimatoprost (**51**) are marketed drugs for veterinary purposes and antiglaucoma treatment, respectively. The Chen lab devised a divergent flow-based chemoenzymatic synthesis capable of producing both cloprostenol and bimatoprost and three other PGs [70]. This synthesis is a powerful combination of synthesis, biocatalysis and flow chemistry that utilizes 11–12 steps from a common starting material to synthesize five high value PGs (**Scheme 15**). The strategy is highlighted chemoenzymatically by a novel stereoselective oxidation to lactone **47** in 99% ee by a Baeyer-Villager monooxygenase (BVMO) and a diastereoselective reduction in 87:13 to 99:1 d.r. by a ketoreductase (KRED) to alcohol **49**. From here three synthetic transformations yield the desired prostaglandins. The authors have demonstrated two unique biotransformations that are responsible for setting stereocenters with high ee and d.r., respectively.

The synthesis of sorbicillins requires a dearomatization to afford a sensitive, cyclohexadienone diol. This challenging transformation has been implemented by Gulder and coworkers, using a SorbC monooxygenase enzyme, in order to afford sorbicillinoids which could then be elaborated to natural products including Saturnispol C (**54**), D, and Trichosorbicillin A (**Scheme 16**) [71]. Interestingly enough, the only requisite reaction to afford these three natural products was a Diels-Alder reaction, which was facile using the electron rich cyclic diene afforded by the dearomative hydroxylation of the enzyme under atmospheric conditions. One limitation of this report is potential scalability; reactions were below 0.15 mmol scale, though it is not clear whether this due to cost or a true limitation.



Scheme 15. Synthesis of cloprostenol (50) and bimatoprost (51) via a combination of synthetic chemistry, flow chemistry, and two stereochemical chemoenzymatic steps [70].

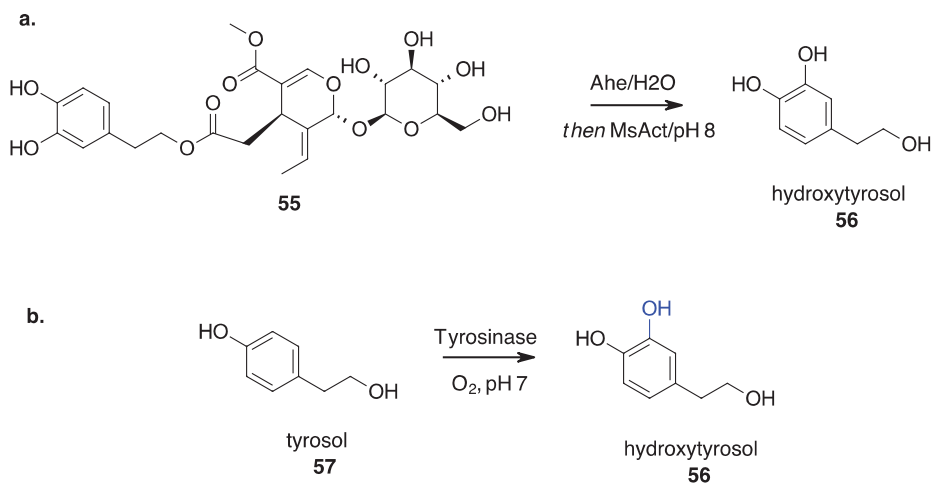


Scheme 16. Stereoselective chemoenzymatic oxidation towards the synthesis of saturnispol C (54) [71].

The conversion of abundant natural compounds to other high-value natural products is a valuable path towards synthesizing them. Hydroxytyrosol (56) is a sought-after antioxidant with a high scale of demand and a deceptively simple chemical structure. Recently several patents and papers have been published for the synthesis of this compound among others, many of which are chemoenzymatic syntheses [72–74]. One such report by Pinto et al. leverages 10–20% of the mass of dry olive leaves isolated as intermediate 55 to form hydroxytyrosol (56), a potentially useful antioxidant compound (Scheme 17a) [75]. This is performed by sequential enzymatic hydrolysis of a hemiacetal moiety and an ester moiety using a glucosidase and an acyl transferase acting as an esterase.

As an alternative strategy, Pinto et al. published a constant-flow chemoenzymatic synthesis of hydroxytyrosol. Their method was to oxidize tyrosol (57) aerobically in the presence of a tyrosinase from *Agaricus bisporus*, in an ascorbic acid/phosphate buffer (Scheme 17b) [76]. Although unable to obtain complete conversions, they were able to design a facile flow-based separation method to afford pure hydroxytyrosol. The authors also demonstrated a flow-based chemoenzymatic acylation of tyrosol and hydroxytyrosol using sacrificial ethyl acetate, catalyzed by an immobilized acyl transferase MsAcT. A current limitation of this is scale: the maximum 0.25 mL/min flow rates were limited the yields obtainable in a 24 h period. This marriage of two frontier tactics in organic synthesis,

flow and chemoenzymatic synthesis, is impressive. It is also an elegant solution to one of the classic issues of chemoenzymatic syntheses: low concentrations are common, which means it is difficult to make large amounts of material. Automated flow syntheses mostly sidestep this issue as the product is made without human involvement, and generally at a rate exceeding that of simply scaling batches.



Scheme 17. (a) Two-step chemoenzymatic hydrolysis in the synthesis of high demand antioxidant hydroxytyrosol (56). (b) One-step chemoenzymatic oxidation to yield hydroxytyrosol (56). [75,76].

3. Conclusions

Natural products continue to fascinate and inspire isolation, synthetic, and bioorganic chemists with their rich library of molecular complexity and biological applications. Pushing the boundaries of synthetic chemistry and biochemistry by using chemoenzymatic syntheses to create these molecules has become a field on to itself. As is the case in reaction methodology-based fields of synthetic chemistry, progress is achieved in incremental steps through the pioneering work of many scientists. Often the first efforts are accomplishments that have limitation in yield, scale, or substrate scope, but the ingenuity and persistence of researchers continues to advance the field. The discovery of new enzymes/reactions, improvement of yields and stereospecificity, and engineering of systems that utilize multiple enzymes, flow chemistry, and other emerging technologies is a testament to the talented scientists working in the field of chemoenzymatic synthesis of natural products. The molecular diversity and breadth of molecule classes to which chemoenzymatic synthesis is applied, as highlighted in this report, is truly remarkable and we look forward to the evolution and expansion of work in this area in the coming years.

Author Contributions: All authors shared equally in the data gathering, analysis, writing, and editing of the manuscript. All authors have read and agreed to the published version of the manuscript.

Funding: The APC was funded by the School of Science, Technology & Mathematics at Elmhurst University and the DJ & JM Cram Endowed Chair at Rollins College.

Institutional Review Board Statement: Not applicable.

Informed Consent Statement: Not applicable.

Conflicts of Interest: The authors declare no conflict of interest.

References

1. Atanasov, A.G.; Zotchev, S.B.; Dirsch, V.M.; Orhan, I.E.; Banach, M.; Rollinger, J.M.; Barreca, D.; Weckwerth, W.; Bauer, R.; Bayer, E.A.; et al. Natural Products in Drug Discovery: Advances and Opportunities. *Nat. Rev. Drug Discov.* **2021**, *20*, 200–216. [[CrossRef](#)] [[PubMed](#)]
2. Truax, N.J.; Romo, D. Bridging the Gap between Natural Product Synthesis and Drug Discovery. *Nat. Prod. Rep.* **2020**, *37*, 1436–1453. [[CrossRef](#)] [[PubMed](#)]
3. Olaizola, M. Commercial Development of Microalgal Biotechnology: From the Test Tube to the Marketplace. *Biomol. Eng.* **2003**, *20*, 459–466. [[CrossRef](#)]
4. Baran, P.S. Natural Product Total Synthesis: As Exciting as Ever and Here to Stay. *J. Am. Chem. Soc.* **2018**, *140*, 4751–4755. [[CrossRef](#)] [[PubMed](#)]
5. Karimov, R.R.; Hartwig, J.F. Transition-Metal-Catalyzed Selective Functionalization of C(Sp³)–H Bonds in Natural Products. *Angew. Chem. Int. Ed.* **2018**, *57*, 4234–4241. [[CrossRef](#)]
6. Harwood, S.J.; Palkowitz, M.D.; Gannett, C.N.; Perez, P.; Yao, Z.; Sun, L.; Abruña, H.D.; Anderson, S.L.; Baran, P.S. Modular Terpene Synthesis Enabled by Mild Electrochemical Couplings. *Science* **2022**, *375*, 745–752. [[CrossRef](#)]
7. Pitre, S.P.; Overman, L.E. Strategic Use of Visible-Light Photoredox Catalysis in Natural Product Synthesis. *Chem. Rev.* **2022**, *122*, 1717–1751. [[CrossRef](#)] [[PubMed](#)]
8. Reed, J.W.; Hudlicky, T. The Quest for a Practical Synthesis of Morphine Alkaloids and Their Derivatives by Chemoenzymatic Methods. *Acc. Chem. Res.* **2015**, *48*, 674–687. [[CrossRef](#)]
9. de Miranda, A.S.; Miranda, L.S.M.; de Souza, R.O.M.A. Lipases: Valuable Catalysts for Dynamic Kinetic Resolutions. *Biotechnol. Adv.* **2015**, *33*, 372–393. [[CrossRef](#)]
10. Langvik, O.; Saloranta, T.; Murzin, D.Y.; Leino, R. Heterogeneous Chemoenzymatic Catalyst Combinations for One-Pot Dynamic Kinetic Resolution Applications. *ChemCatChem* **2015**, *7*, 4004–4015. [[CrossRef](#)]
11. Muthana, S.; Cao, H.; Chen, X. Recent Progress in Chemical and Chemoenzymatic Synthesis of Carbohydrates. *Curr. Opin. Chem. Biol.* **2009**, *13*, 573–581. [[CrossRef](#)]
12. Stöckigt, J.; Chen, Z.; Ruppert, M. Enzymatic and Chemo-Enzymatic Approaches towards Natural and Non-Natural Alkaloids: Indoles, Isoquinolines, and Others. In *BT—Natural Products via Enzymatic Reactions*; Piel, J., Ed.; Springer: Berlin/Heidelberg, Germany, 2010; pp. 67–103. ISBN 978-3-642-16427-9.
13. Azerad, R.; Buisson, D. Dynamic Resolution and Stereoinversion of Secondary Alcohols by Chemo-Enzymatic Processes. *Curr. Opin. Biotechnol.* **2000**, *11*, 565–571. [[CrossRef](#)]
14. Mortison, J.D.; Sherman, D.H. Frontiers and Opportunities in Chemoenzymatic Synthesis. *J. Org. Chem.* **2010**, *75*, 7041–7051. [[CrossRef](#)]
15. Anastas, P.T.; Warner, J.C. *Green Chemistry: Theory and Practice*; Oxford University Press: Oxford, UK, 1998.
16. Abdelraheem, E.M.M.; Busch, H.; Hanefeld, U.; Tonin, F. Biocatalysis Explained: From Pharmaceutical to Bulk Chemical Production. *React. Chem. Eng.* **2019**, *4*, 1878–1894. [[CrossRef](#)]
17. Riehl, P.S.; Lim, J.; Finnigan, J.D.; Charnock, S.J.; Hyster, T.K. An Efficient Synthesis of the Bicyclic Darunavir Side Chain Using Chemoenzymatic Catalysis. *Org. Process Res. Dev.* **2022**, *26*, 2096–2101. [[CrossRef](#)]
18. Chakrabarty, S.; Romero, E.O.; Pyser, J.B.; Yazarians, J.A.; Narayan, A.R.H. Chemoenzymatic Total Synthesis of Natural Products. *Acc. Chem. Res.* **2021**, *54*, 1374–1384. [[CrossRef](#)]
19. Roddan, R.; Carter, E.M.; Thair, B.; Hailes, H.C. Chemoenzymatic Approaches to Plant Natural Product Inspired Compounds. *Nat. Prod. Rep.* **2022**, *39*, 1375–1382. [[CrossRef](#)]
20. Li, J.; Amatuni, A.; Renata, H. Recent Advances in the Chemoenzymatic Synthesis of Bioactive Natural Products. *Curr. Opin. Chem. Biol.* **2020**, *55*, 111–118. [[CrossRef](#)]
21. Murray, L.A.M.; Mckinnie, S.M.K.; Moore, B.S.; George, J.H.; Cruz, S.; States, U.; Jolla, L.; States, U.; Jolla, L.; States, U. Meroterpenoid natural products from *Streptomyces* bacteria—The Evolution of Chemoenzymatic Syntheses. *Nat. Prod. Rep.* **2021**, *37*, 1334–1366. [[CrossRef](#)]
22. Stout, C.N.; Renata, H. Reinventing the Chiral Pool: Chemoenzymatic Approaches to Complex Peptides and Terpenoids. *Acc. Chem. Res.* **2021**, *54*, 1143–1156. [[CrossRef](#)]
23. King-Smith, E.; Zwick, C.R.; Renata, H. Applications of Oxygenases in the Chemoenzymatic Total Synthesis of Complex Natural Products. *Biochemistry* **2018**, *57*, 403–412. [[CrossRef](#)] [[PubMed](#)]
24. Deng, Y.; Zhou, Q.; Wu, Y.; Chen, X.; Zhong, F. Properties and Mechanisms of Flavin-Dependent Monooxygenases and Their Applications in Natural Product Synthesis. *Int. J. Mol. Sci.* **2022**, *23*, 2622. [[CrossRef](#)] [[PubMed](#)]
25. Malico, A.A.; Calzini, M.A.; Gayen, A.K.; Williams, G.J. Synthetic Biology, Combinatorial Biosynthesis, and Chemo-enzymatic Synthesis of Isoprenoids. *J. Ind. Microbiol. Biotechnol.* **2020**, *47*, 675–702. [[CrossRef](#)]
26. Zetsche, L.E.; Chakrabarty, S.; Narayan, A.R.H. The Transformative Power of Biocatalysis in Convergent Synthesis. *J. Am. Chem. Soc.* **2022**, *144*, 5214–5225. [[CrossRef](#)]
27. Cigan, E.; Eggbauer, B.; Schrittwieser, J.H.; Kroutil, W. The Role of Biocatalysis in the Asymmetric Synthesis of Alkaloids—An Update. *RSC Adv.* **2021**, *11*, 28223–28270. [[CrossRef](#)]
28. Pyser, J.B.; Chakrabarty, S.; Romero, E.O.; Narayan, A.R.H. State-of-the-Art Biocatalysis. *ACS Cent. Sci.* **2021**, *7*, 1105–1116. [[CrossRef](#)]

29. Zhao, F.; Masci, D.; Tomarelli, E.; Castagnolo, D. Biocatalytic and Chemo-Enzymatic Approaches for the Synthesis of Heterocycles. *Synthesis* **2020**, *52*, 2948–2961.
30. Kaspar, F.; Schallmeyer, A. Chemo-Enzymatic Synthesis of Natural Products and Their Analogs. *Curr. Opin. Biotechnol.* **2022**, *77*, 102759. [[CrossRef](#)]
31. Li, F.; Yang, L.C.; Zhang, J.; Chen, J.S.; Renata, H. Stereoselective Synthesis of β -Branched Aromatic α -Amino Acids by Biocatalytic Dynamic Kinetic Resolution**. *Angew. Chem. Int. Ed.* **2021**, *60*, 17680–17685. [[CrossRef](#)]
32. Li, F.; Renata, H. A Chiral-Pool-Based Strategy to Access Trans-Syn-Fused Drimane Meroterpenoids: Chemoenzymatic Total Syntheses of Polysin, N-Acetyl-Polyveoline and the Chrodrimanins. *J. Am. Chem. Soc.* **2021**, *143*, 18280–18286. [[CrossRef](#)]
33. Li, J.; Renata, H. Concise Chemoenzymatic Synthesis of Fasamycin A. *J. Org. Chem.* **2021**, *86*, 11206–11211. [[CrossRef](#)] [[PubMed](#)]
34. Bat-Erdene, U.; Billingsley, J.M.; Turner, W.C.; Lichman, B.R.; Ippoliti, F.M.; Garg, N.K.; O'Connor, S.E.; Tang, Y. Cell-Free Total Biosynthesis of Plant Terpene Natural Products Using an Orthogonal Cofactor Regeneration System. *ACS Catal.* **2021**, *11*, 9898–9903. [[CrossRef](#)] [[PubMed](#)]
35. Johnson, L.A.; Dunbabin, A.; Benton, J.C.R.; Mart, R.J.; Allemann, R.K. Modular Chemoenzymatic Synthesis of Terpenes and Their Analogues. *Angew. Chem. Int. Ed.* **2020**, *59*, 8486–8490. [[CrossRef](#)] [[PubMed](#)]
36. Shinde, P.B.; Oh, H.-S.; Choi, H.; Rathwell, K.; Ban, Y.H.; Kim, E.J.; Yang, I.; Lee, D.G.; Sherman, D.H.; Kang, H.-W.; et al. Chemoenzymatic Synthesis of Glycosylated Macrolactam Analogues of the Macrolide Antibiotic YC-17. *Adv. Synth. Catal.* **2015**, *357*, 2697–2711. [[CrossRef](#)]
37. Schmidt, J.J.; Khatri, Y.; Brody, S.I.; Zhu, C.; Pietraszkiewicz, H.; Valeriote, F.A.; Sherman, D.H. A Versatile Chemoenzymatic Synthesis for the Discovery of Potent Cryptophycin Analogs. *ACS Chem. Biol.* **2020**, *15*, 524–532. [[CrossRef](#)]
38. Ding, Y.; Rath, C.M.; Bolduc, K.L.; Håkansson, K.; Sherman, D.H. Chemoenzymatic Synthesis of Cryptophycin Anticancer Agents by an Ester Bond-Forming Non-Ribosomal Peptide Synthetase Module. *J. Am. Chem. Soc.* **2011**, *133*, 14492–14495. [[CrossRef](#)]
39. Lowell, A.N.; DeMars, M.D., 2nd; Slocum, S.T.; Yu, F.; Anand, K.; Chemler, J.A.; Korakavi, N.; Priessnitz, J.K.; Park, S.R.; Koch, A.A.; et al. Chemoenzymatic Total Synthesis and Structural Diversification of Tylactone-Based Macrolide Antibiotics through Late-Stage Polyketide Assembly, Tailoring, and C—H Functionalization. *J. Am. Chem. Soc.* **2017**, *139*, 7913–7920. [[CrossRef](#)]
40. Rittner, A.; Joppe, M.; Schmidt, J.J.; Mayer, L.M.; Reiners, S.; Heid, E.; Herzberg, D.; Sherman, D.H.; Grninger, M. Chemoenzymatic Synthesis of Fluorinated Polyketides. *Nat. Chem.* **2022**, *14*, 1000–1006. [[CrossRef](#)]
41. Saha, N.; Müller, M.; Husain, S.M. Asymmetric Synthesis of Natural Cis-Dihydroarenediols Using Tetrahydroxynaphthalene Reductase and Its Biosynthetic Implications. *Org. Lett.* **2019**, *21*, 2204–2208. [[CrossRef](#)]
42. Singh, S.K.; Rajput, A.; De, A.; Chakraborti, T.; Husain, S.M. Promiscuity of an Unrelated Anthrol Reductase of *Talaromyces islandicus* WF-38-12. *Catal. Sci. Technol.* **2021**, *11*, 474–478. [[CrossRef](#)]
43. Manna, T.; Rajput, A.; Saha, N.; Mondal, A.; Debnath, S.C.; Husain, S.M. Chemoenzymatic Total Synthesis of Nodulones C and D Using a Naphthol Reductase of *Magnaporthe grisea*. *Org. Biomol. Chem.* **2022**, *20*, 3737–3741. [[CrossRef](#)] [[PubMed](#)]
44. Na, L.; Li, R.; Chen, X. Recent Progress in Synthesis of Carbohydrates with Sugar Nucleotide-Dependent Glycosyltransferases. *Curr. Opin. Chem. Biol.* **2021**, *61*, 81–95. [[CrossRef](#)] [[PubMed](#)]
45. Vaccariu, C.M.; Tanner, M.E. Recent Advances in the Synthesis and Biological Applications of Peptidoglycan Fragments. *Chem. A Eur. J.* **2022**, *28*, e202200788. [[CrossRef](#)] [[PubMed](#)]
46. Zheng, J.; Xu, H.; Fang, J.; Zhang, X. Enzymatic and Chemoenzymatic Synthesis of Human Milk Oligosaccharides and Derivatives. *Carbohydr. Polym.* **2022**, *291*, 119564. [[CrossRef](#)]
47. Li, B.-H.; Ye, X.-S. Recent Advances in Glycan Synthesis. *Curr. Opin. Chem. Biol.* **2020**, *58*, 20–27. [[CrossRef](#)]
48. Desmons, S.; Grayson-Steel, K.; Nuñez-Dallos, N.; Vendier, L.; Hurtado, J.; Clapés, P.; Fauré, R.; Dumon, C.; Bontemps, S. Enantioselective Reductive Oligomerization of Carbon Dioxide into L-Erythrose via a Chemoenzymatic Catalysis. *J. Am. Chem. Soc.* **2021**, *143*, 16274–16283. [[CrossRef](#)]
49. Srivastava, A.D.; Unione, L.; Bunyatov, M.; Gagarinov, I.A.; Delgado, S.; Abrescia, N.G.A.; Ardá, A.; Boons, G.J. Chemoenzymatic Synthesis of Complex N-Glycans of the Parasite *S. mansoni* to Examine the Importance of Epitope Presentation on DC-SIGN Recognition. *Angew. Chem. Int. Ed.* **2021**, *60*, 19287–19296. [[CrossRef](#)]
50. Hu, Z.; Benkoulouche, M.; Barel, L.A.; le Heiget, G.; ben Imeddoug, A.; le Guen, Y.; Monties, N.; Guerreiro, C.; Remaud-Siméon, M.; Moulis, C.; et al. Convergent Chemoenzymatic Strategy to Deliver a Diversity of *Shigella flexneri* Serotype-Specific O-Antigen Segments from a Unique Lightly Protected Tetrasaccharide Core. *J. Org. Chem.* **2021**, *86*, 2058–2075. [[CrossRef](#)]
51. Rath, P.; Rapp, J.; Brilisaue, K.; Braun, M.; Kolukisaoglu, Ü.; Forchhammer, K.; Grond, S. Hybrid Chemoenzymatic Synthesis of C 7-Sugars for Molecular Evidence of in Vivo Shikimate Pathway Inhibition. *ChemBioChem* **2022**, *23*, 202200241. [[CrossRef](#)]
52. Dussouy, C.; Téletchéa, S.; Lambert, A.; Charlier, C.; Botez, I.; de Ceuninck, F.; Grandjean, C. Access to Galectin-3 Inhibitors from Chemoenzymatic Synthons. *J. Org. Chem.* **2020**, *85*, 16099–16114. [[CrossRef](#)]
53. Li, R.; Kooner, A.S.; Muthana, S.M.; Yuan, Y.; Yu, H.; Chen, X. A Chemoenzymatic Synthons Strategy for Synthesizing N-Acetyl Analogues of O-Acetylated N. Meningitidis W Capsular Polysaccharide Oligosaccharides. *J. Org. Chem.* **2020**, *85*, 16157–16165. [[CrossRef](#)]
54. Yu, H.; Gadi, M.R.; Bai, Y.; Zhang, L.; Li, L.; Yin, J.; Wang, P.G.; Chen, X. Chemoenzymatic Total Synthesis of GM3 Gangliosides Containing Different Sialic Acid Forms and Various Fatty Acyl Chains. *J. Org. Chem.* **2021**, *86*, 8672–8682. [[CrossRef](#)]

55. Li, Q.; Jaiswal, M.; Rohokale, R.S.; Guo, Z. A Diversity-Oriented Strategy for Chemoenzymatic Synthesis of Glycosphingolipids and Related Derivatives. *Org. Lett.* **2020**, *22*, 8245–8249. [[CrossRef](#)] [[PubMed](#)]
56. Ma, W.; Deng, Y.; Xu, Z.; Liu, X.; Chapla, D.G.; Moremen, K.W.; Wen, L.; Li, T. Integrated Chemoenzymatic Approach to Streamline the Assembly of Complex Glycopeptides in the Liquid Phase. *J. Am. Chem. Soc.* **2022**, *144*, 9057–9065. [[CrossRef](#)]
57. Forneris, C.C.; Nguy, A.K.L.; Seyedsayamdost, M.R. Mapping and Exploiting the Promiscuity of OxyB toward the Biocatalytic Production of Vancomycin Aglycone Variants. *ACS Catal.* **2020**, *10*, 9287–9298. [[CrossRef](#)]
58. Mohanty, I.; Nguyen, N.A.; Moore, S.G.; Biggs, J.S.; Gaul, D.A.; Garg, N.; Agarwal, V. Enzymatic Synthesis Assisted Discovery of Proline-Rich Macrocyclic Peptides in Marine Sponges. *ChemBioChem* **2021**, *22*, 2614–2618. [[CrossRef](#)]
59. Patel, K.P.; Silsby, L.M.; Li, G.; Bruner, S.D. Structure-Based Engineering of Peptide Macrocyclases for the Chemoenzymatic Synthesis of Microviridins. *J. Org. Chem.* **2021**, *86*, 11212–11219. [[CrossRef](#)] [[PubMed](#)]
60. Kersten, R.D.; Mydy, L.S.; Fallon, T.R.; de Waal, F.; Shafiq, K.; Wotring, J.W.; Sexton, J.Z.; Weng, J.-K. Gene-Guided Discovery and Ribosomal Biosynthesis of Moroidin Peptides. *J. Am. Chem. Soc.* **2022**, *144*, 7686–7692. [[CrossRef](#)]
61. Zheng, X.; Li, Y.; Guan, M.; Wang, L.; Wei, S.; Li, Y.-C.; Chang, C.-Y.; Xu, Z. Biomimetic Total Synthesis of the Spiroindimicin Family of Natural Products. *Angew. Chem. Int. Ed.* **2022**, *61*, e202208802. [[CrossRef](#)] [[PubMed](#)]
62. Borowiecki, P.; Zdun, B.; Dranka, M. Chemoenzymatic Enantioselective and Stereo-Convergent Syntheses of Lisofylline Enantiomers via Lipase-Catalyzed Kinetic Resolution and Optical Inversion Approach. *Mol. Catal.* **2021**, *504*, 111451. [[CrossRef](#)]
63. Taday, F.; Cairns, R.; O’Connell, A.; O’Reilly, E. Combining Bio- and Organocatalysis for the Synthesis of Piperidine Alkaloids. *Chem. Commun.* **2022**, *58*, 1697–1700. [[CrossRef](#)] [[PubMed](#)]
64. Galman, J.L.; Slabu, I.; Parmeggiani, F.; Turner, N.J. Biomimetic Synthesis of 2-Substituted N-Heterocycle Alkaloids by One-Pot Hydrolysis, Transamination and Decarboxylative Mannich Reaction. *Chem. Commun.* **2018**, *54*, 11316–11319. [[CrossRef](#)] [[PubMed](#)]
65. Simon, R.C.; Grischek, B.; Zepeck, F.; Steinreiber, A.; Belaj, F.; Kroutil, W. Regio- and Stereoselective Monoamination of Diketones without Protecting Groups. *Angew. Chem. Int. Ed.* **2012**, *51*, 6713–6716. [[CrossRef](#)] [[PubMed](#)]
66. Eger, E.; Schrittwieser, J.H.; Wetzl, D.; Iding, H.; Kuhn, B.; Kroutil, W. Asymmetric Biocatalytic Synthesis of 1-Aryltetrahydro- β -Carbolines Enabled by “Substrate Walking”. *Chem. A Eur. J.* **2020**, *26*, 16281–16285. [[CrossRef](#)]
67. Walia, M.; Tejaro, C.N.; Gardner, A.; Tran, T.; Kang, J.; Zhao, S.; O’Connor, S.E.; Courdavault, V.; Andrade, R.B. Synthesis of (-)-Melodinine K: A Case Study of Efficiency in Natural Product Synthesis. *J. Nat. Prod.* **2020**, *83*, 2425–2433. [[CrossRef](#)]
68. St-Pierre, B.; de Luca, V. A Cytochrome P-450 Monooxygenase Catalyzes the First Step in the Conversion of Tabersonine to Vindoline in *Catharanthus roseus*. *Plant Physiol.* **1995**, *109*, 131–139. [[CrossRef](#)]
69. Besseau, S.; Kellner, F.; Lanoue, A.; Thamm, A.M.K.; Salim, V.; Schneider, B.; Geu-Flores, F.; Höfer, R.; Guirimand, G.; Guihur, A.; et al. A Pair of Tabersonine 16-Hydroxylases Initiates the Synthesis of Vindoline in an Organ-Dependent Manner in *Catharanthus roseus*. *Plant Physiol.* **2013**, *163*, 1792–1803. [[CrossRef](#)] [[PubMed](#)]
70. Zhu, K.; Jiang, M.; Ye, B.; Zhang, G.T.; Li, W.; Tang, P.; Huang, Z.; Chen, F. A Unified Strategy to Prostaglandins: Chemoenzymatic Total Synthesis of Cloprostenol, Bimatoprost, PGF 2α , Fluprostenol, and Travoprost Guided by Biocatalytic Retrosynthesis. *Chem. Sci.* **2021**, *12*, 10362–10370. [[CrossRef](#)]
71. Milzarek, T.M.; Schuler, S.; Matura, A.; Gulder, T.A.M. Evaluation of the Substrate Promiscuity of SorbC for the Chemo-Enzymatic Total Synthesis of Structurally Diverse Sorbicillinoids. *ACS Catal.* **2022**, *12*, 1898–1904. [[CrossRef](#)]
72. Oelschlägel, M.; Stuhr, A.; Pollender, A.; Ganz, D.; Schlömann, M. Process for the Biotechnological Production of 2-Phenylethanols from Plant Sources. PCT/EP2021/084999, 16 June 2022.
73. Guillamón Navarro, J.M.; Muñoz Calvo, S.; Bisquert Alcaraz, R. Recombinant *Saccharomyces cerevisiae* for the Production of Hydroxytyrosol. PCT/ES2021/070769, 2 June 2022.
74. A Kind of Efficient Synthesis of Hydroxytyrosol by *Bacillus licheniformis*, Construction Method and Application. CN114891820A, 14 January 2020.
75. Catinella, G.; Donzella, S.; Boronovo, G.; Dallavalle, S.; Contente, M.L.; Pinto, A. Efficient 2-Step Enzymatic Cascade for the Bioconversion of Oleuropein into Hydroxytyrosol. *Antioxidants* **2022**, *11*, 260. [[CrossRef](#)] [[PubMed](#)]
76. Annunziata, F.; Contente, M.L.; Pinna, C.; Tamborini, L.; Pinto, A. Biocatalyzed Flow Oxidation of Tyrosol to Hydroxytyrosol and Efficient Production of Their Acetate Esters. *Antioxidants* **2021**, *10*, 1142. [[CrossRef](#)]

Article

Transcriptomics and Proteomics Characterizing the Anticancer Mechanisms of Natural Rebeccamycin Analog Loonamycin in Breast Cancer Cells

Xiao Sun ^{1,†}, Zhanying Lu ^{1,†}, Zhenzhen Liang ², Bowen Deng ², Yuping Zhu ¹, Jing Shi ³ and Xiaoling Lu ^{2,*}

¹ Experimental Training Center of Basic Medical Science, College of Basic Medical Sciences, Naval Medical University, Shanghai 200433, China

² Department of Biochemistry and Molecular Biology, College of Basic Medical Sciences, Naval Medical University, Shanghai 200433, China

³ State Key Laboratory of Pharmaceutical Biotechnology, Chemistry and Biomedicine Innovation Center (ChemBIC), School of Life Sciences, Nanjing University, Nanjing 210023, China

* Correspondence: luxiaoling80@126.com; Tel.: +86-21-81870975

† These authors contributed equally to this work.

Abstract: The present study is to explore the anticancer effect of loonamycin (LM) in vitro and in vivo, and investigate the underlying mechanism with combined multi-omics. LM exhibited anticancer activity in human triple negative breast cancer cells by promoting cell apoptosis. LM administration inhibited the growth of MDA-MB-468 tumors in a murine xenograft model of breast cancer. Mechanistic studies suggested that LM could inhibit the topoisomerase I in a dose-dependent manner in vitro experiments. Combined with the transcriptomics and proteomic analysis, LM has a significant effect on O-glycan, p53-related signal pathway and EGFR/PI3K/AKT/mTOR signal pathway in enrichment of the KEGG pathway. The GSEA data also suggests that the TNBC cells treated with LM may be regulated by p53, O-glycan and EGFR/PI3K/AKT/mTOR signaling pathway. Taken together, our findings predicted that LM may target p53 and EGFR/PI3K/AKT/mTOR signaling pathway, inhibiting topoisomerase to exhibit its anticancer effect.

Keywords: loonamycin; triple negative breast cancer; p53; PI3K/AKT/mTOR; O-glycan

Citation: Sun, X.; Lu, Z.; Liang, Z.; Deng, B.; Zhu, Y.; Shi, J.; Lu, X. Transcriptomics and Proteomics Characterizing the Anticancer Mechanisms of Natural Rebeccamycin Analog Loonamycin in Breast Cancer Cells. *Molecules* **2022**, *27*, 6958. <https://doi.org/10.3390/molecules27206958>

Academic Editor: Giovanni Ribaudò

Received: 31 July 2022

Accepted: 12 October 2022

Published: 17 October 2022

Publisher's Note: MDPI stays neutral with regard to jurisdictional claims in published maps and institutional affiliations.



Copyright: © 2022 by the authors. Licensee MDPI, Basel, Switzerland. This article is an open access article distributed under the terms and conditions of the Creative Commons Attribution (CC BY) license (<https://creativecommons.org/licenses/by/4.0/>).

1. Introduction

Triple negative breast cancer (TNBC) is a special subtype of breast cancer, accounting for about 12.7% of breast cancer [1], which is characterized by negative estrogen receptor (ER), progesterone receptor (PR) and human epidermal growth factor receptor-2 (HER2) with high recurrence rate, strong invasiveness, and poor prognosis characteristics. Due to the lack of corresponding targets and high heterogeneity, the treatment of TNBC is mainly limited to chemotherapy [2]. It is valuable to develop novel chemotherapeutics that can broadly target TNBCs to render this highly deadly disease subtype curable.

Marine natural products provide an important source of lead compounds for new drug research and development because of their unique structure and diversity biological activity. At present, more than 35,000 marine natural compounds have been discovered in the world, most of which possess unique structures and present diverse biological activity. Loonamycin (LM) is an indole carbazole compound rebeccamycin analog produced from *Nocardioopsis flavescens* NA01583 isolated from marine sediment in Yongxing Island, South China Sea [3] (Figure 1A). To the best of our knowledge, rebeccamycin is a cytotoxicity compound that binds to topoisomerase I to inhibit the reconnection at the DNA strand incision [4], leading to the break of DNA single strand and double strand. This compound showed an impressive cytotoxicity in vitro but could not be further developed because of poor water solubility. Some rebeccamycin analogues (e.g., becatecarin [5] and edotecacin [6]) have entered clinical research. LM has a rare sugar group and hydroxyl group

compared with rebecamycin [3], which could increase its water solubility, and improve its pharmaceutical potential.

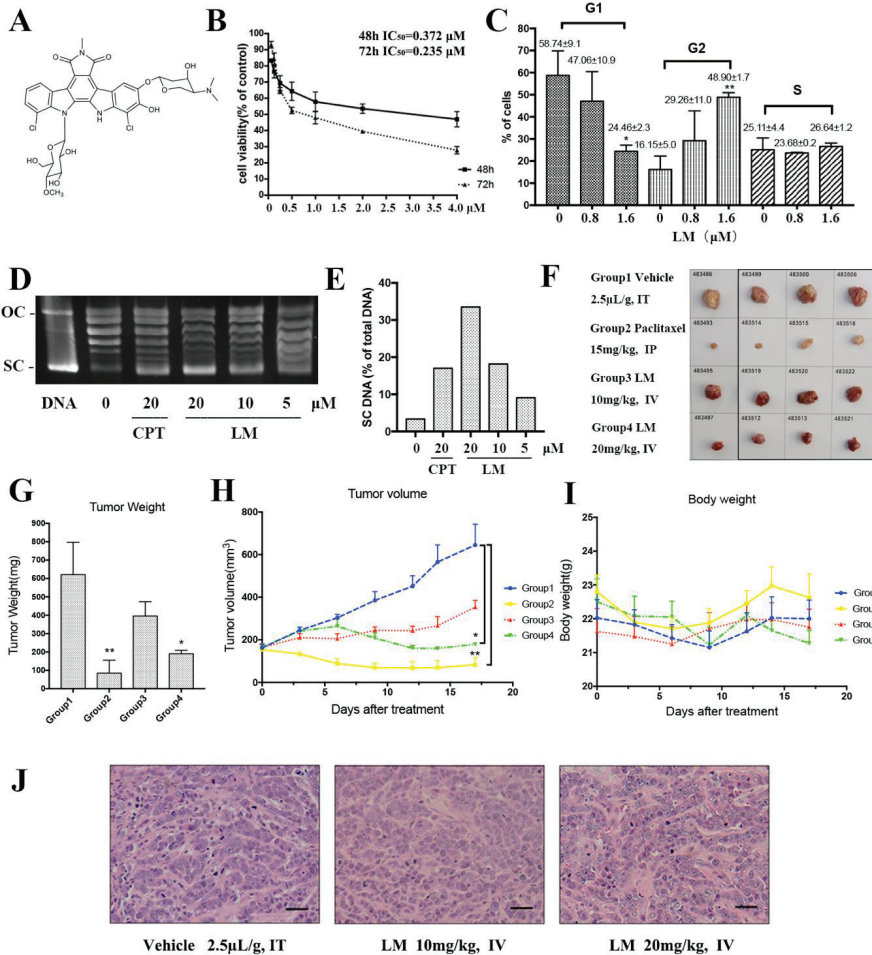


Figure 1. LM targets TNBC in vitro and in vivo. (A) The structure of LM; (B) the cell viability experiment of LM on human TNBC cell line MDA-MB-468. The MDA-MB-468 cells were treated with 0, 0.0625, 0.125, 0.25, 0.5, 1, 2, 4 μM LM for 48 and 72 h, and the cell viability was detected by the CCK8 assay; (C) effects of LM at 0.8 μM and 1.6 μM on MDA-MB-468 cell cycle arrest after 48 h of incubation. Cells were stained with Annexin V and analyzed by flow cytometry. The vertical bars represent the standard deviation of means (SD) ($n = 3$ experiments); * $p < 0.05$ and ** $p < 0.01$, vs. negative control. The G1, G2 and S represent the phase of the cell cycle. (D) The inhibitory effect of LM on topoisomerase I activity. The plasmid was treated with 5, 10, 20 μM LM and the 20 μM camptothecin (CPT) was used as positive control. (E) The quantification of electrophoretic band. The Y axis is SC DNA/total DNA. (F) The images of tumors from each group. Tumor-bearing mice were administered the vehicle (negative control), 15 mg/kg Paclitaxel (positive control), LM (10 or 20 mg/kg per day). (G) The average tumor weight in each group. Data are presented as the mean \pm S.D. $n = 4$, * $p < 0.05$ and ** $p < 0.01$, vs. negative control. (H) The average tumor volume in each group recorded during the treatments. Data are presented as the mean \pm S.D., $n = 4$, * $p < 0.05$ and ** $p < 0.01$, vs. negative control. (I) The average body weight in each group. (J) The HE staining on stripped tumor tissue.

Our previous studies showed that LM had strong cytotoxic activities against various tumor cell lines, especially to the human TNBC cell line MDA-MB-468. In this article, we used RNA-seq and TMT quantitative proteomics technology to uncover the mechanism of LM in TNBC cells.

2. Results

2.1. LM Targets TNBC In Vitro and In Vivo

First, LM was investigated for its inhibitory effects on several breast cancer cell lines (Table 1). LM displayed a preferential anticancer activity against the cell lines with IC₅₀ values of 0.517 μM, 0.197 μM and 0.372 μM in the MCF-7 cell line, MDA-MB-231 cell line and MDA-MB-468 cell line. The IC₅₀ of LM for LO2 was 1.022 μM. The LO2 was used as a control cell line and the result suggested that LM was less toxic to LO2 than the cancer cell line. Then, we further investigated the inhibitory effects of LM on TNBC MDA-MB-468 cells. As exhibited in Figure 1B, LM displayed a good anticancer activity against MDA-MB-468 in a dose-dependent manner with IC₅₀ values of 0.372 μM and 0.235 μM after 48 h and 72 h.

Table 1. IC₅₀ value of LM on multiple tumor cell lines in 48 h.

Cells	IC ₅₀ (μM)	Cells	IC ₅₀ (μM)
L-02	1.022 ± 0.084	L-02	1.02 ± 0.084
MDA-MB-468	0.372 ± 0.201	PANC-1	0.591 ± 0.091
MDA-MB-231	0.197 ± 0.043	SMMC-7721	0.623 ± 0.044
A549	0.578 ± 0.096	HeLa	0.609 ± 0.037
SH-SY5Y	0.629 ± 0.028	NCI-H446	0.664 ± 0.062
PC-3	0.689 ± 0.102	U251	0.935 ± 0.205
MCF-7	0.517 ± 0.146	SW1990	1.30 ± 0.022

Second, we examined the effect of LM on cell cycle in MDA-MB-468 cells. In MDA-MB-468 cells, after 48 h of incubation, LM induced cell cycle arrest in the G2 phase in a dose-dependent manner (Figure 1C). At 1.6 μM LM, the value of G1-phase declined to 24.46%, while G2-phase increased to 48.90%. The values of the S phase showed a slight change. Growing lines of evidence indicate that eukaryotic topoisomerase activity is monitored and regulated throughout the cell cycle [7]. As rebeccamycin is a cytotoxicity compound which is bound to the topoisomerase I, we detected the inhibitory effect of LM on topoisomerase I activity (Figure 1D,E). Topoisomerase I (Topo I) relaxes the super helix structure of DNA by cutting its single strands [8]. The normal plasmid DNA is a closed double stranded DNA. In the process of electrophoresis, the plasmid may have three configurations: the superhelical DNA (SC DNA), the open circular DNA (OC DNA) and the linear DNA (L DNA). The SC DNA is at the front of gel, OC DNA is at the back, and L DNA is between SC DNA and OC DNA. After the cleavage of topoisomerase I, the structure of SC DNA will be destroyed. The experiment showed that LM could inhibit topoisomerase I activity in a dose-dependent manner.

Next, the effects of LM on the growth and formation of subcutaneous xenograft nodes derived from the inoculated MDA-MB-468 cells in vivo in BALB/c nude mice were investigated. Both the volumes and weights of the formed MDA-MB-468 cells tumor nodes were reduced by LM administration every 2 days for a total of 17 days at a concentration of 10 mg/kg or 20 mg/kg LM by i.v., compared to 15 mg/kg for paclitaxel as a positive control [9] by i.p. and 2% DMSO as vehicle by i.v. The low-dose group was of no statistical significance compared with the negative control group. The volumes and weights of tumors in high-dose group reduced significantly (Figure 1F–I). The frozen section and HE staining on the stripped tumor tissue was performed, and obvious tumor-like tissues were observed under the microscope, such as large cell volume, big nucleus and deformity loose arrangement of tumor cells (Figure 1J). There were no detectable toxic or necrotic effects on the heart, liver, spleen, lung or kidney tissues after LM treatment and no significant weight loss. Taken together, these data suggest that LM exhibits good therapeutic activity.

2.2. Functional Annotation Enrichment of LM-Regulated Genes

To uncover the LM regulatory mechanism in TNBC MDA-MB-468 cells, we performed RNA-seq analysis to profile the transcriptomes of MDA-MB-468 cells when treated with 1.6 μ M LM. Differentially abundant genes (DAGs) were those meeting the qualified data (fold change ≥ 1.2 and $p < 0.05$) under comparison of LM vs. the control group. A total of 1764 DAGs were shown in the volcano map, of which 737 genes were upregulated and 1027 genes were down-regulated (Figure 2A). GO (Gene ontology) is a comprehensive database that describes gene functions. GO enrichment analysis basing on the DAGs including up-regulated genes and down-regulated genes, were mapped the differential genes to the entries in the three aspects of cell components (CC), molecular functions (MF), and biological processes (BP) (Figure 2B). Through GO enrichment analysis, we can roughly understand which biological functions, signal pathways, or cell locations are enriched of the DAGs. In terms of the CC, the up-regulated genes were mainly enriched in the extracellular matrix, anchored component of membrane, collagen trimer and MHC protein complex. The down-regulated genes were mainly enriched in postsynapse, synaptic membrane, receptor complex, ion channel complex. In terms of the MF, the up-regulated genes were mainly enriched in the receptor ligand activity, receptor regulator activity, cytokine receptor binding, extracellular matrix structural constituent. The down-regulated genes were mainly enriched in actin binding, ion gated channel activity, Ras GTPase binding, passive transmembrane transporter activity. In terms of the BP, the up-regulated genes were mainly enriched in the regulation of signaling receptor activity, regulation of endothelial cell proliferation, endothelial cell proliferation, positive regulation of locomotion and wound healing. The down-regulated genes were mainly enriched in trans-synaptic signaling, chemical synaptic transmission, anterograde trans-synaptic signaling, regulation of membrane potential and neurotransmitter levels.

KEGG (Kyoto Encyclopedia of Genes and Genomes) is a comprehensive database integrating genome, chemistry and system function information. It stores information on gene pathways of different species. KEGG pathway enrichment analysis was conducted to describe the significant changes in signal pathways of DAGs (Figure 2C). The results showed that the up-regulated differential genes were mainly centered on the pathways in cancer, hippo signaling pathway, p53 signaling pathway, etc. The down-regulated proteins were mainly concentrated on the glucagon signaling pathway, calcium signaling pathway, phosphatidylinositol signaling system, propanoate metabolism, inositol phosphate metabolism, pyruvate metabolism, other types of O-glycan biosynthesis and so on.

GSEA enrichment analysis was conducted to explore the changes of gene expression in the pathway and find the upstream factors leading to these changes (Figure 2D). In our studies, the curated gene sets as the exploration set showed that p53 and downstream signal pathway were up-regulated, and O-glycan and PI3K-AKT-mTOR signaling pathway were down-regulated in LM treatment group.

2.3. Proteomic Expression Profiling of LM-Treated TNBC Cells

To further elucidate cellular mechanism and molecular function, we performed TMT quantitative proteomics analysis to assess the protein expression profiles in MDA-MB-468 cells treated with 1.6 μ M LM. Differentially abundant proteins (DAPs) were those meeting the qualified data (fold change ≥ 1.2 and $p < 0.05$) under comparison of LM vs. control group. A total of 1314 DAPs were shown in the volcano map, of which 778 proteins were upregulated and 536 proteins were down-regulated (Figure 3A). Wolf PSORT software was used for localization analysis of differential proteins, which show that the DAPs were mainly distributed in cytoplasm, nucleus, mitochondria, and plasma membrane (Figure 3B). In total, 119 GO terms were obtained based on the DAPs including up-regulated proteins and down-regulated proteins (Figure 3C). GO enrichment analysis showed that in terms of the cell components (CC), the up-regulated proteins were mainly enriched in the cytosol (GO:0005829), ficolin-1-rich granule lumen (GO:1904813) and nucleus (GO:0005634). The down-regulated proteins were mainly enriched in the mito-

chondrial matrix (GO:0005759), integral component of plasma membrane, (GO:0005887) and nBAF complex (GO:0071565). In terms of biological process (BP), the up-regulated proteins were mainly enriched in the processes related to gluconeogenesis (GO:0006094), negative regulation of ryanodine-sensitive calcium-release channel activity (GO:0060315) and proteasomal ubiquitin-independent protein catabolic process (GO:0010499). The down-regulated proteins were mainly enriched in the processes related to isoleucine catabolic process (GO:0006550), O-glycan processing (GO:0016266) and leucine catabolic process (GO:0006552). In terms of molecular function (MF), the up-regulated proteins were mainly enriched in S100 protein binding (GO:0044548), RAGE receptor binding (GO:0050786) and threonine-type endopeptidase activity (GO:0004298). The down-regulated proteins were mainly enriched in polypeptide N-acetylgalactosaminyl transferase activity (GO:0004653), biotin binding (GO:0009374) and signaling receptor activity (GO:0038023).

KEGG pathway enrichment analysis was conducted to describe the significant changes in pathways of DAPs (Figure 3D). The results showed that the DAPs including up-regulated proteins and down-regulated proteins were classified into 34 terms. The up-regulated differential proteins were mainly centered on the changes of metabolic pathway, like amino acid biosynthesis, glucose metabolism, nucleotide metabolism, glutathione metabolism, and p53 pathway, etc. The down-regulated proteins were mainly concentrated on the pathway of amino acid degradation, mTOR signaling pathway, PI3K-Akt signaling pathway, O-glycan biosynthesis, etc. Among these DAPs, the expressions of classical tumor related signaling pathway p53 were up-regulated and the EGFR/mTOR pathway were down-regulated.

GSEA enrichment analysis was conducted to explore the changes of gene expression in the pathway and find the upstream factors leading to these changes (Figure 3E). In our studies, the curated gene sets as the exploration set showed that p53 and downstream signal pathway were up-regulated, and the EGFR and mTOR related pathway, and O-glycan were down-regulated in LM treatment group.

2.4. Validation of Transcriptomic and Proteomic Results

According to the combined analysis of RNA-seq and TMT-based quantitative proteomic, it is suggested that LM may have a significant effect on O-glycan, p53-related signal pathway and EGFR/PI3K/AKT/mTOR signal pathway in enrichment of the KEGG pathway. The GSEA data also suggests that the TNBC cells treated with LM may be regulated by p53 and EGFR/PI3K/AKT/mTOR signaling pathway.

The Cys124 located in the loop1/sheet3 (L1/S3) pocket of the p53 protein plays a key role in maintaining p53 stable conformation (Figure 4A). The covalently binding model between LM and p53 (L1/S3) was investigated by molecular docking. The binding energy was -26.8 kJ/mol. The main combination modes were the hydrogen bonds, as shown in Figure 4D. The ether bond of LM formed hydrogen bond with Thr102 of p53. The methoxy group on the rare sugar group of LM formed hydrogen bond with Phe113 of p53. The hydroxyl group of LM formed one hydrogen bond with Leu114, His115, Cys124 and His 233 separately. The hydroxyl and ether group of LM formed three hydrogen bonds with Thr123. The above results suggested that LM can target the pockets of wild-type p53 L1/S3, improving the stability of p53 and activating p53 related pathways.

To verify the combined analysis of transcriptomic and proteomic results, the western blot of key proteins was performed. It is determined that expression of p53 was increased after treated with LM for 48 h on MDA-MB-468 (Figure 4B,C), but there was no statistical significance. The expressions of EGFR, PI3K, mTOR and BCL-2 were significantly down-regulated (Figure 4B,D). The expression of p-p53 was significantly up-regulated (Figure 4B,C), and the expression of p-EGFR, p-PI3K and p-mTOR were significantly down-regulated (Figure 4B,D). It was shown that LM could activate p53 and inhibit the expression of EGFR, PI3K, mTOR and BCL-2.

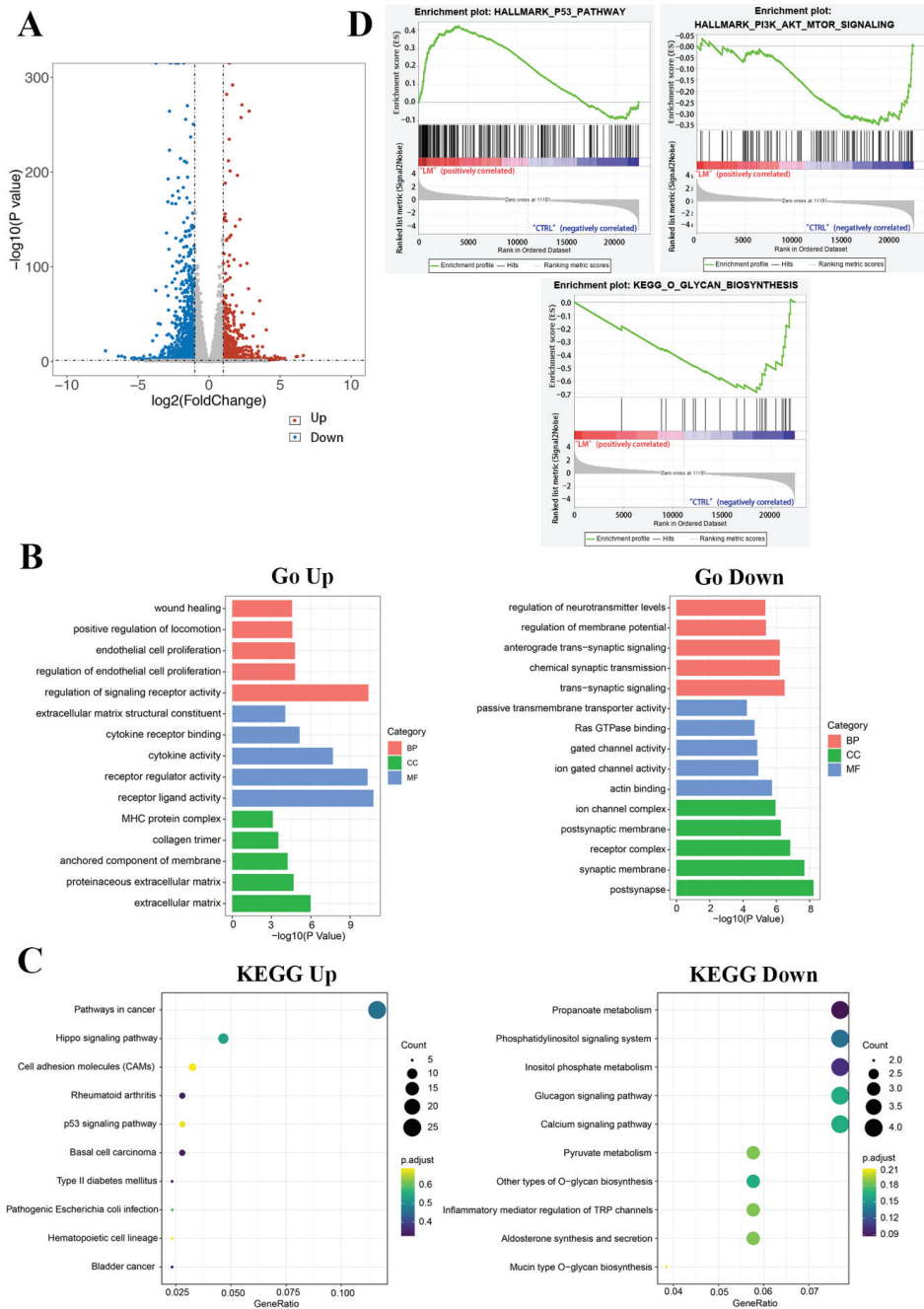


Figure 2. Functional analysis of differential genes. (A) Scatter plots of differentially expressed genes. There were 737 up-regulated genes and 1027 down-regulated genes in the LM group. Abscissa is the difference multiple (logarithmic transformation based on 2); (B) The gene ontology annotation analysis between DAGs and classification of BP, MF, and CC; (C) The KEGG pathway analysis of related DAGs; (D) The GSEA results of differentially abundant genes.

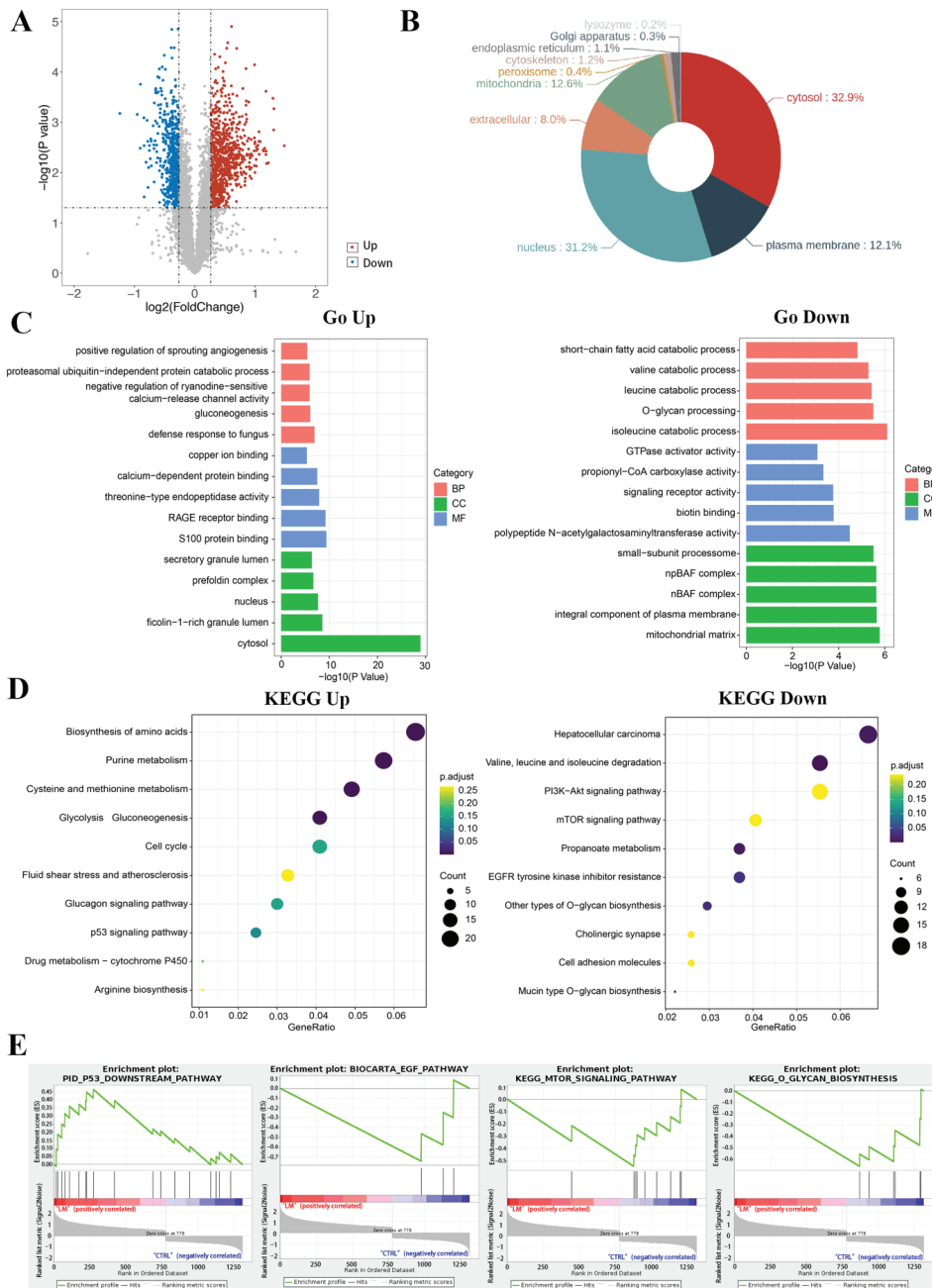


Figure 3. Functional analysis of differentially proteins. (A) Scatter plots of differentially expressed proteins. There were 778 up-regulated proteins and 536 down-regulated proteins in the LM group. Abscissa is the difference multiple (logarithmic transformation based on 2); (B) localization analysis of differentially expressed proteins; (C) the gene ontology annotation analysis between DAPs and classification of BP, MF, and CC; (D) the KEGG pathway analysis of related DAPs; (E) the GSEA results of differentially abundant proteins.

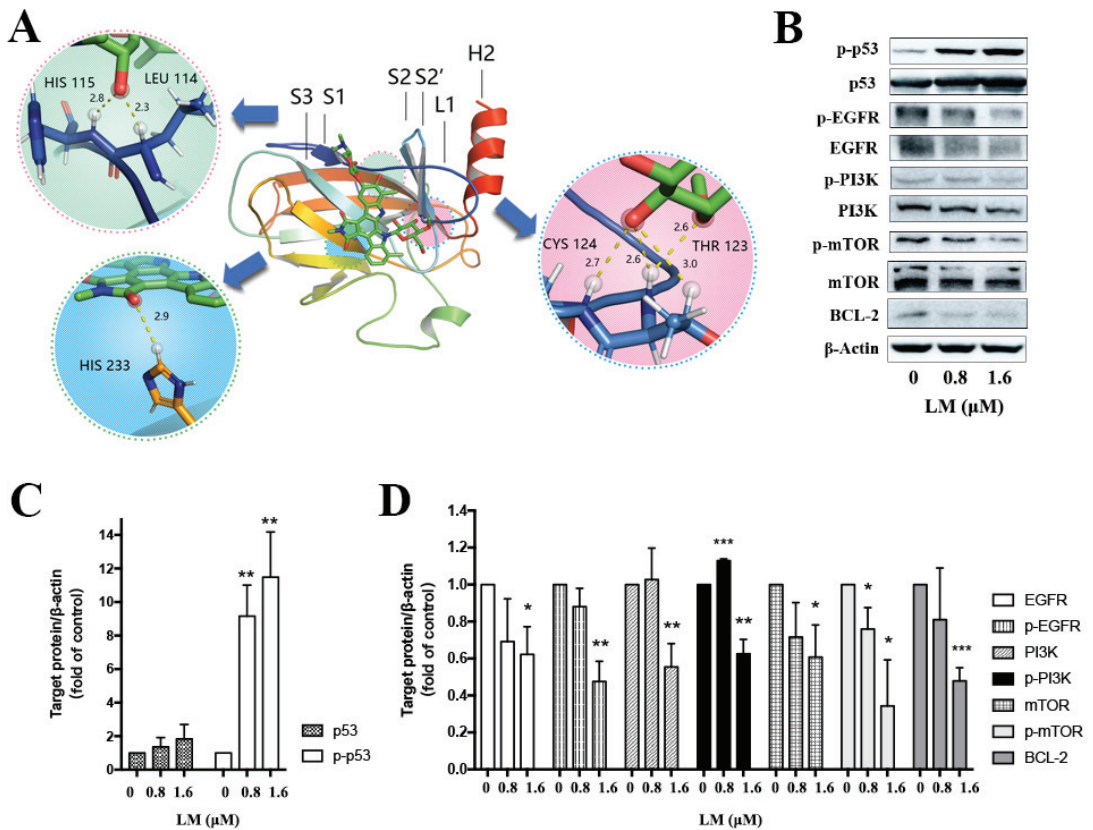


Figure 4. Validation of key proteins based on combined transcriptomic and proteomic results. (A) The docking picture of LM and p53 (L1/S3). (B) Western blot of key differentially abundant proteins. The MDA-MB-468 cells were treated with LM by 0, 0.8 and 1.6 μM . (C,D) Fold change in protein levels (LM treatment group/control group) from Western blot analysis. Significance: * $p < 0.05$, ** $p < 0.01$, *** $p < 0.001$ versus the control, p value based on t -test.

3. Discussion

In this study, we evaluated the anticancer activity of LM, an indole carbazole rebeccamycin analog from *Nocardiopsis flavescens* NA01583. Our data showed that LM could inhibit tumor cell growth both in vitro and in vivo. The inhibitory effect of LM in cancer cells demonstrated that it could inhibit the topoisomerase I in a dose-dependent manner in vitro experiments like other rebeccamycin analogs [10]. Topo I cut one strand of DNA to form single-strand breaks, allowing supercoiled DNA to relax, otherwise it can hinder DNA replication and transcription, and thus block cell growth [11–13]. For rapid cell division, cancer cells need high Topo I activity to finish the DNA metabolic processes. Topoisomerase I inhibitors can block the reconnection of DNA strands, lead to the accumulation of Topo I-breaking complexes, inhibit replication and transcription, and cause DNA damage, thus activating DNA damage checkpoints and inhibiting the progress of cell cycle [14]. Topoisomerase were recognized as promising targets in cancer, and various DNA Topos inhibitors have been on the market [15]. Some rebeccamycin analogues like becatecarin and edotecacin have entered clinical research. Becatecarin intercalates into DNA and inhibits the catalytic activity of topoisomerases I/II [16]. Edotecarin is a potent inhibitor of topoisomerase I and also has an effect on protein kinase C [17].

Next, the RNA-Seq and TMT were conducted to investigate the changes in transcriptomic and proteomic profile of MDA-MB-468 cells treated with LM (LM). The combined transcriptome and proteome analyses revealed that LM may activate p53 and inhibit the O-glycans, inhibiting EGFR/PI3K/mTOR signaling pathway to exhibit its cytotoxicity activity. The tumor suppressor p53 functions mainly as a transcription factor. A mutation of the TP53 gene that encodes p53 protein is the main way of inactivating p53. p53 is a key tumor suppressor in the process of preventing tumorigenesis. The dysfunction of p53 often leads to cancer. When cells suffer from DNA damage, excessive proliferation, hypoxia, lack of nutrition, telomere loss, or in the environment of oxidative stress, lack of nucleotides or replication pressure, p53 will be activated to induce cell cycle arrest, apoptosis, aging or autophagy, preventing cells from growing and dividing and killing cells before they become cancerous [18]. p53 removes cells with high mutation risk in this way, inhibiting tumor formation. In normal cells, p53 remains at a low level and dormant state under non-stress conditions to prevent its adverse effects on cell growth. Its low expression is mainly by its interaction with ubiquitin E3 ligase MDM2 [19]. A stress response can prevent MDM2 mediated p53 degradation by various mechanisms, promoting the stability and activation of p53. About 50% of cancers still express wild-type p53, but these p53 proteins usually lose its function, because of the over activation of MDM2 and MDMX. The stability and transcriptional activity of p53 depend on its phosphorylation [20]. According to research, the phosphorylation of p53 protein Ser15, Ser20, Ser33 and Ser37 could enhance its binding to P300, thereby activating the transcriptional activity of p53. The phosphorylation of Thr18 can not only enhance p53-p300 binding, but also interfere with p53-MDM2 binding [21]. Reactivating p53 and restoring its function is a feasible and promising tumor treatment strategy. Moreover, p53 is the most common mutant gene in human cancer, of which p53 mutations are found in more than 50% of tumors. For example, approximately 80% of TNBCs express an inactive, mutant form of the p53 tumor suppressor protein (mtp53), resulting in rapid tumor growth and metastasis [22]. Many mutations occur in the DNA binding domain of p53 gene and the altered mutant p53 protein (mtp53) is subsequently not degraded, in which high levels of mtp53 protein accumulate within the cell, leading to the development of tumors. Therefore, converting the mtp53 protein back into its functional wild-type conformation is also a promising means to prevent or reverse tumor development. Restoring the function of wild-type p53 and developing drug candidates for mutant p53 to restore the normal function of p53 can activate p53 to inhibit tumor. At present, many anti-cancer drugs targeting p53 have been developed. For example, the arsenic trioxide, which is used for acute primary myeloid leukemia, can restore the transcriptional activity of p53 mutants by arsenic ions binding to three cysteine residues in the DNA-binding domain [23]. HDAC6 (Histone deacetylase 6) can promote the combination of HSP90 (heat shock protein 90) and mutant p53 protein by catalyzing HSP90 deacetylation and thus make mutant p53 molecule more stable. So, some HDAC6 inhibitors (e.g., statin) or HSP90 inhibitors (e.g., Ganetespiib) have been found to induce mutant p53 degradation [24,25]. Small molecule compounds like RG7112 and some nucleic acid drugs can activate p53 by promoting the expression of TP53 gene or inhibiting the expression of MDM2 [26–28].

In 2002, PRIMA-1 was discovered as a mutant p53 reactivator based on the tumor cells screening of the mutated p53 [29]. The specific mechanism was not studied that it directly bound to the Cys124 of mutant p53 protein until 2009 [30]. Cys124 locating in loop1/sheet3 (L1/S3) pocket of p53 protein, plays a key role in maintaining stable conformation. Loop1 can directly interact with helix2 in the p53 DNA binding domain, suggesting that the stability of p53 can be improved by small molecules compounds to stabilize loop1. The compounds targeting wild-type p53 L1/S3 pockets could improve the stability of p53. L1/S3 pocket was a target for pharmaceutical reactivation of p53 mutants [31]. We constructed the computer virtual screening system with wild-type p53 as the target. In the computer docking experiment, LM could bind with L1/S3 pockets of p53 protein well, forming one hydrogen bond with Cys124. Subsequent WB experiments showed that LM could activate p53 signal pathway. Although, the molecular docking

did not provide direct proof that LM interacts with p53, but explored a potential route to influence the p53 pathways.

The epidermal growth factor receptor (EGFR) is a receptor tyrosine kinase that belongs to the ErbB family and is involved in angiogenesis, cell proliferation, metastases as well as inhibition of apoptosis. It was demonstrated that EGFR is overexpressed in TNBC cells [32]. Its expression was an independent poor prognostic factor associated with worse DFS and OS [33,34]. In light of the high expression level of EGFR and its strong effect on cell proliferation and motility, EGFR has been considered as an attractive therapeutic target for TNBC [35]. EGFR is on the upstream of PI3K and activates PI3K/AKT/mTOR pathway. The PI3K/AKT/mTOR pathway is associated with cell metabolism, proliferation, differentiation, and survival. PI3Ks are heterodimers composed of regulatory (p85) and catalytic (p110) subunits and exist in four isoforms (α , β , δ , and γ) [36]. The signaling pathway is activated by stimulation of receptor tyrosine kinases, which in turn trigger PI3K activation, followed by phosphorylation of AKT and mTOR complex 1 (mTORC1). It is speculated that on one hand, LM could restore the function of wild-type p53 to activate p53, on the other hand, LM may inhibit the classical EGFR/PI3K/AKT/mTOR pathway to inhibit the growth of the cells; the specific mechanism needs to be further explored.

Glycosylation is one of the most important post-translational modifications of the protein, including N-glycosylation and O-glycosylation. O-linked glycosylation is considered more complicated than N-linked for its unknown initiation [37]. O-glycosylation added single monosaccharides one by one through enzymatic reaction. The linking monosaccharide GalNAc is added directly to Ser/Thr/Tyr residues in glycoproteins within the Golgi apparatus from the nucleotide sugar donor uridine diphospho-GalNAc (UDP-GalNAc). This linking sugar is commonly modified in all cells by the addition of galactose (Gal) from the donor UDP-Gal to create the disaccharide Gal β 1-3GalNAc α 1-O-Ser/Thr, known as core 1. Such O-glycans can be further modified and extended within the Golgi apparatus to generate an incredible diversity of many tens of thousands of different glycan structures. Meanwhile, the changes in the core structure of several types of O-glycans are related to multiple cancers, which abnormal O-linked glycosylation has been widely proved to act biological functions to directly result in cancer growth and progression. The T antigen and sialyl-Tn antigen (STn), tumor-associated carbohydrate antigens (TACAs), are truncated O-glycans commonly expressed by carcinomas on multiple glycoproteins which serve as potential biomarkers for tumor presence and stage both in immunohistochemistry and in serum diagnostics [38]. CA199 and CA125 are used as circulating tumor biomarkers. In 90% of breast cancers, altered O-glycosylation has been observed to have a correlation with cancer progression, worse prognosis, and metastatic potential; like the number of O-GalNAc glycans in glycoproteins changes, the core structure of O-GalNAc glycosylation changes, and breast cancer cells with shorter O-glycans (abnormal glycosyltransferase activity, premature sialylation of poly-lactosamine chain blocking the addition of more glycans or truncation of O-glycans at core 1 level). These abnormalities lead to the expression of TACA, such as Tn antigen, St antigen and STn antigen [39]. The polypeptide-N-acetylgalactosaminyl transferase (GT) is a key enzyme of O-linked glycosylation. In our validation experiment, LM down-regulated the GalNAc-T2 with no statistical difference. It is speculated that some other members of GTs should be validated in the future.

In general, the study showed that LM was a potential antitumor compound *in vitro* and *in vivo*. LM may target p53 and EGFR/PI3K/AKT/mTOR signaling pathway, inhibiting topoisomerase to exhibit its anticancer activity according to the combined transcriptome and proteome analyses. Our study provided important information for the specific cytotoxicity mechanism of LM and explanation of the anticancer activity of rebeccamycin analog.

4. Materials and Methods

4.1. Reagents

LM was isolated from *Nocardiosis flavescens* NA01583 from marine sediment and provided by research group of Prof. Ge Huiming, Nanjing University. It was dissolved

in dimethyl sulphoxide and stored at $-20\text{ }^{\circ}\text{C}$ until use. The Cell Cycle Analysis Kit, penicillin/streptomycin were acquired from Beyotime. The fetal bovine serum (FBS), phosphate-buffered saline (PBS), Dulbecco's modified Eagle medium (DMEM) and Leibovitz's L-15 medium (L-15) were obtained from Gibco (Thermo Fisher Scientific, Waltham, MA, USA). The cell counting kit-8 (CCK8) was purchased from Dojindo Molecular Technology. Specific primary antibodies against β -actin, mTOR, P-mTOR, PI3K, P-PI3K, EGFR, p-EGFR, AKT, P-AKT, BCL-2, p53, p-p53 were acquired from CST (Cell Signaling Technology, Danvers, MA, USA); 0.25% trypsin and 0.2% EDTA were purchased from Gibco (Thermo Fisher Scientific, Waltham, MA, USA).

4.2. Cell Culture

TNBC cell line MDA-MB-468 (Cat.TCHu136) were cultured in 90% L-15 medium supplemented with 10% fetal bovine serum and 100 mg/L streptomycin–100 U/mL penicillin mixture. Cells were cultured at $37\text{ }^{\circ}\text{C}$ in an incubator with controlled humidified atmosphere. The cell dispersed liquid was prepared by 0.25% trypsin plus 0.2% EDTA for subculturing and then spun down by centrifugation at 800 rpm for 5 min, after which the supernatant was removed and precipitated cells was resuspended in culture medium.

4.3. Growth Curve Measured by CCK-8 Method

The MDA-MB-468 cells were seeded in 96-well E-plates with the density of 5000 cells/well. After 24 h, the cells were treated with LM or 0.06% DMSO as control for 48 h or 72 h. LM treatment concentrations were 0.0625 μM , 0.125 μM , 0.25 μM , 0.5 μM , 1 μM , 2 μM and 4 μM , and each group was performed in triplicate; 10 μL CCK-8 reagent was added for 1 h after treatment and the optical density value (OD_{450}) was measured at the wavelength of 450 nm. The IC_{50} of LM was calculated by the cell growth curves drawn with Prism-GraphPad.

4.4. Topoisomerase I-Mediated DNA Relaxation and Cleavage Assays

The different concentrations of LM (5 μM , 10 μM , 20 μM) and camptothecin (CPT, 20 M) were incubated with supercoiled pUC19 plasmid DNA in relaxation buffer (50 mM Tris-HCl (pH7.5), 100 mM KCl, 0.5 mM EDTA and 30 $\mu\text{g}/\text{mL}$ BSA) for 15 min at $37\text{ }^{\circ}\text{C}$ to ensure binding equilibrium. Then, the recombinant topoisomerase I enzyme (from calf thymus, Beytime, China) was added for a further 30 min of incubation at $37\text{ }^{\circ}\text{C}$. The mixture of sodium dodecyl sulfate (SDS) and protease K (the final concentration was 0.25% and 250 g/mL , respectively) was added for a 30 min incubation at $50\text{ }^{\circ}\text{C}$ to terminate the reaction. To obtain single stranded DNA, samples were loaded onto a 1% agarose gel lacking ethidium bromide at room temperature for 2 h at 120 V in TBE buffer. Gels were stained after migration using Gelred and then washed and finally photographed under UV light.

4.5. RNA-seq Analysis

Total RNA was extracted from cells using TRIzol[®] reagent, and genomic DNA was removed using DNase I. RNA integrity was detected by Agilent 2100 BioAnalyzer. The library was built by the NEB method. AMPure XP Beads were used to screen cDNA, conduct PCR amplification, and purify PCR products. NEBNext[®] Ultra[™] RNA Library Prep Kit for Illumina[®] was used for Library construction. The library was initially quantified by Qubit2.0 Fluorometer and was diluted to 1.5 $\text{ng}/\mu\text{L}$. The insert size of the library was detected using Agilent 2100 BioAnalyzer. qRT-PCR was used to quantify the effective concentration of the library to ensure the quality of the library. Then, the Illumina sequencing was conducted. The basic principle is sequencing by synthesis.

The raw data was filtered by the removal of reads with adapter, the removal of reads with N (N indicates that the base information cannot be determined), and the removal of low-quality reads. At the same time, the Q20, Q30 and GC contents of clean data were calculated. All subsequent analyses were based on clean data. Hisat2v2.0.5 was used to compare clean reads of paired terminal with genomic species: human genes (GrCH38.p12).

String Tie (1.3.3b) (Mihaela-Pertea et al., 2015) was used for new gene prediction. Feature Counts (1.5.0-P3) were used to calculate recounts mapped to each gene. The FPKM of each gene was calculated based on the length of the gene and the readout mapped to the gene was calculated to obtain the expression value matrix.

Gene expression analysis of the different groups was performed by The DESeq2 software (V1.16.1) ($n = 3$). The p -value was adjusted using Benjamini and Hochberg's method. Genes with an adjusted p -value (FDR) < 0.05 were defined as differentially expressed genes (DEGs). Gene Ontology analysis (GO) and KEGG pathway enrichment analysis of DEGs were implemented by clusterProfiler (3.4.4). GSEA enrichment analysis was performed using GSEA (V4.1.0).

4.6. TMT Labeling and LC-MS/MS Analysis

The MDA-MB-468 cells were treated with 1.6 μM LM or 0.06% DMSO control medium for 48 h. SDT buffer was added to the sample. The lysate was sonicated and then boiled for 15 min. After centrifuged at $14,000 \times g$ for 40 min, the supernatant was quantified with the BCA Protein Assay Kit (P0012, Beyotime, Shanghai, China). The protein was digested by Filter aided proteome preparation (FASP) method, and 100 μg peptide mixture of each sample was labeled using TMT reagent according to the manufacturer's instructions (Thermo Fisher Scientific, USA). TMT labeled peptides were fractionated by RP chromatography using the Agilent 1260 infinity II HPLC. The collected fractions were combined into 10 fractions and dried down via vacuum centrifugation at 45 $^{\circ}\text{C}$.

Each fraction was injected for nano LC-MS/MS analysis. The peptide mixture was loaded onto the C18-reversed phase analytical column (Thermo Fisher Scientific, Acclaim PepMap RSLC 50 $\mu\text{m} \times 15 \text{ cm}$, nano viper, P/N164943) in buffer A (0.1% Formic acid) and separated with a linear gradient of buffer B (80% acetonitrile and 0.1% Formic acid) at a flow rate of 300 nL/min. The linear gradient was as follows: 6% buffer B for 3 min, 6–28% buffer B for 42 min, 28–38% buffer B for 5 min, 38–100% buffer B for 5 min, hold in 100% buffer B for 5 min.

LC-MS/MS analysis was performed on a Q Exactive HF mass spectrometer (Thermo Fisher Scientific, Waltham, MA, USA) that was coupled to Easy nLC (Thermo Fisher Scientific, Waltham, MA, USA) for 60 min. The mass spectrometer was operated in positive ion mode. MS data was acquired using a data-dependent top 10 method dynamically choosing the most abundant precursor ions from the survey scan (350–1800 m/z) for HCD fragmentation. Survey scans were acquired at a resolution of 60,000 at m/z 200 with an AGC target of 3×10^6 and a maxIT of 50 ms. MS2 scans were acquired at a resolution of 15,000 for HCD spectra at m/z 200 with an AGC target of 2×10^5 and a maxIT of 45 ms, and the isolation width was 2 m/z . Only ions with a charge state between 2 and 6 and a minimum intensity of 2×10^3 were selected for fragmentation. Dynamic exclusion for selected ions was 30 s. Normalized collision energy was 30 eV.

MS/MS raw files were processed using MASCOT engine (Matrix Science, London, UK; version 2.6) embedded into Proteome Discoverer 2.2. The protein database was Uniprot_HomoSapiens_20367_20200226. The search parameters included trypsin as the enzyme used to generate peptides with a maximum of 2 missed cleavages permitted. A precursor mass tolerance of 10 ppm was specified and 0.05 Da tolerance for MS2 fragments. Except for TMT labels, carbamidomethyl (C) was set as a fixed modification. Variable modifications were Oxidation(M) and Acetyl (Protein N-term). A peptide and protein false discovery rate of 1% was enforced using a reverse database search strategy. Proteins with fold change > 1.2 and p value (Student's t -test) < 0.05 were considered to be differentially expressed proteins. Wolf PSORT software was used for localization analysis of differential proteins. Gene Ontology analysis (GO) and KEGG pathway enrichment analysis of DEGs were implemented by clusterProfiler (3.4.4). GSEA enrichment analysis was performed using GSEA (V4.1.0).

4.7. Molecular Docking

Molecular docking was performed using the Schrodinger software (Schrödinger, Inc., New York, NY, USA). The 3D structure of p53 were retrieved from the protein data bank (PDB ID: 1TSR). In LM-p53 covalent docking, the protein p53 was prepared by Protein Preparation Tool in Schrodinger including optimized hydrogen bond network at pH 7.0 with PROKA tool. The ligand LM was prepared by Avogadro Tool to obtain the structural optimization.

4.8. Western Blot Analysis

The MDA-MB-468 cells were treated with 1.6 μM LM or 0.06% DMSO control medium for 48 h. Cells were harvested with trypsin/EDTA and then total proteins were extracted by using RIPA lysis buffer (RIPA lysis buffer (Beyotime, Shanghai, China)), 100 $\mu\text{g}/\text{mL}$ PMSF (Beyotime, Shanghai, China), and 1 \times protease inhibitor (Sigma, St. Louis, MO, USA). The protein was quantified by BCA methods according to the instructions (Beyotime, Shanghai, China). The proteins extracted from cells were separated by SDS-PAGE electrophoresis and transferred to nitrocellulose membrane. The membrane was incubated with primary antibodies and anti-rabbit IgG (HRP-linked). The bands were detected by ECL Western blot system (Kodak, Rochester, NY, USA). Western blotting bands from three independent measurements were quantified with ImageJ.

4.9. Xenograft Model

Twenty-five female BALB/c nude mice aged 6–8 weeks were kept at constant temperature and humidity. The body weight was 20–24 g. Animals were supplied by Laboratory Animal Business Department of Shanghai Family Planning (certificate of quality: 20210715Abzz0619000729). Each mouse was inoculated subcutaneously at the right flank with MDA-MB-468 tumor cells (1×10^7) in 0.2 mL of PBS with Matrigel (1:1) for tumor development. Treatments were started on day 27 after tumor inoculation when the average tumor size reached 160 mm^3 . The animals were assigned into groups randomly based upon tumor volumes. Each group consisted of 4 tumor-bearing mice. The vehicle was 2%DMSO + 15% Solutol + 83%Saline. The mice in control group were injected 2.5 mL/kg vehicle by i.v. The mice in the positive control group were injected 15 mL/kg Paclitaxel by i.p. The mice in the low-dose group were injected 10 mL/kg LM by i.v. The mice in the high dose group were injected 20 mL/kg LM by i.v. The animals were checked daily for any effects of tumor growth and treatments on normal behavior, and body weights were measured every 3 days. Tumor size was measured every 3 days by a caliper using the formula: $V = 0.5a \times b^2$ where a and b are the long and short diameters of the tumor, respectively.

4.10. Statistical Analysis

One-way ANOVA analysis was used for comparison between groups, and Student's t-test was used for pair-wise comparison within groups. All statistical analyses were processed with GraphPad Prism 7.0 software (GraphPad Software, San Diego, CA, USA). $p < 0.05$ was considered statistically significant.

Author Contributions: Conceptualization, X.L.; Cell culture and cell experiment, X.S. and Z.L. (Zhenzhen Liang); CCK-8 Method, X.S. and Z.L. (Zhenzhen Liang); Topoisomerase I-Mediated DNA Relaxation and Cleavage Assays, X.S.; RNA-seq Analysis, X.S.; TMT quantitative proteomics analysis, X.S.; Molecular Docking, B.D.; Western Blot Analysis, Z.L. (Zhanying Lu); Xenograft Model, X.S. and Z.L. (Zhanying Lu); Statistical Analysis, X.S.; Data curation, Y.Z. and X.S.; writing—original draft preparation, X.S.; writing—review and editing, X.S. and X.L.; Resources, J.S. All authors have read and agreed to the published version of the manuscript.

Funding: This research was funded by the National Key Research and Development Project (2019YFC0312504).

Institutional Review Board Statement: The animal study was reviewed and approved by Naval Medical University Institutional Animal Care and Use Committee.

Informed Consent Statement: Not applicable.

Data Availability Statement: The original contributions presented in the study are included in the article, further inquiries can be directed to the corresponding author.

Conflicts of Interest: The authors declare no conflict of interest.

References

1. Fernández, A.G.; Chabrera, C.; Font, M.G.; Fraile, M.; Lain, J.M.; González, S.; Barco, I.; Torres, J.; Piqueras, M.; Cirera, L.; et al. Differential patterns of recurrence and specific survival between luminal A and luminal B breast cancer according to recent changes in the 2013 St Gallen immunohistochemical classification. *Clin. Transl. Oncol.* **2015**, *17*, 238–246. [[CrossRef](#)] [[PubMed](#)]
2. Schmid, P.; Adams, S.; Rugo, H.S.; Schneeweiss, A.; Barrios, C.H.; Iwata, H.; Diéras, V.; Hegg, R.; Im, S.-A.; Shaw Wright, G.; et al. Atezolizumab and Nab-Paclitaxel in Advanced Triple-Negative Breast Cancer. *N. Engl. J. Med.* **2018**, *379*, 2108–2121. [[CrossRef](#)] [[PubMed](#)]
3. Yang, C.L.; Zhang, B.; Xue, W.W.; Li, W.; Xu, Z.F.; Shi, J.; Shen, Y.; Jiao, R.H.; Tan, R.X.; Ge, H.M. Discovery, Biosynthesis, and Heterologous Production of Loonamycin, a Potent Anticancer Indolocarbazole Alkaloid. *Org. Lett.* **2020**, *22*, 4665–4669. [[CrossRef](#)]
4. Bailly, C.; Colson, P.; Houssier, C.; Rodrigues-Pereira, E.; Prudhomme, M.; Waring, M.J. Recognition of Specific Sequences in DNA by a Topoisomerase I Inhibitor Derived from the Antitumor Drug Rebeccamycin. *Mol. Pharmacol.* **1998**, *53*, 77–87. [[CrossRef](#)] [[PubMed](#)]
5. Schwandt, A.; Mekhail, T.; Halmos, B.; O'Brien, T.; Ma, P.C.; Fu, P.; Ivy, P.; Dowlati, A. Phase-II Trial of Rebeccamycin Analog, a Dual Topoisomerase-I and -II Inhibitor, in Relapsed “Sensitive” Small Cell Lung Cancer. *J. Thorac. Oncol.* **2012**, *7*, 751–754. [[CrossRef](#)] [[PubMed](#)]
6. Saif, M.W.; Sellers, S.; Diasio, R.B.; Douillard, J.-Y. A phase I dose-escalation study of edotecarin (J-107088) combined with infusional 5-fluorouracil and leucovorin in patients with advanced/metastatic solid tumors. *Anti-Cancer Drugs* **2010**, *21*, 716–723. [[CrossRef](#)] [[PubMed](#)]
7. Lee, J.H.; Berger, J.M. Cell Cycle-Dependent Control and Roles of DNA Topoisomerase II. *Genes* **2019**, *10*, 859. [[CrossRef](#)] [[PubMed](#)]
8. Beretta, G.L.; Perego, P.; Zunino, F. Targeting topoisomerase I: Molecular mechanisms and cellular determinants of response to topoisomerase I inhibitors. *Expert Opin. Ther. Targets* **2008**, *12*, 1243–1256. [[CrossRef](#)] [[PubMed](#)]
9. Hu, Y.; Manasrah, B.K.; McGregor, S.M.; Lera, R.F.; Norman, R.X.; Tucker, J.B.; Scribano, C.M.; Yan, R.E.; Humayun, M.; Wisinski, K.B.; et al. Paclitaxel Induces Micronucleation and Activates Pro-Inflammatory cGAS–STING Signaling in Triple-Negative Breast Cancer. *Mol. Cancer Ther.* **2021**, *20*, 2553–2567. [[CrossRef](#)] [[PubMed](#)]
10. Bailly, C. Topoisomerase I Poisons and Suppressors as Anticancer Drugs. *Curr. Med. Chem.* **2000**, *7*, 39–58. [[CrossRef](#)]
11. Nitiss, J.L. Investigating the biological functions of DNA topoisomerases in eukaryotic cells. *Biochim. Et Biophys. Acta Gene Struct. Expr.* **1998**, *1400*, 63–81. [[CrossRef](#)]
12. Wang, J.C. DNA TOPOISOMERASES. *Annu. Rev. Biochem.* **1996**, *65*, 635–692. [[CrossRef](#)]
13. Leppard, J.B.; Champoux, J.J. Human DNA topoisomerase I: Relaxation, roles, and damage control. *Chromosoma* **2005**, *114*, 75–85. [[CrossRef](#)]
14. Baglini, E.; Salerno, S.; Barresi, E.; Robello, M.; Da Settimo, F.; Taliani, S.; Marini, A.M. Multiple Topoisomerase I (TopoI), Topoisomerase II (TopoII) and Tyrosyl-DNA Phosphodiesterase (TDP) inhibitors in the development of anticancer drugs. *Eur. J. Pharm. Sci.* **2021**, *156*, 105594. [[CrossRef](#)]
15. Liu, J.; Geng, G.; Liang, G.; Wang, L.; Luo, K.; Yuan, J.; Zhao, S. A novel topoisomerase I inhibitor DIA-001 induces DNA damage mediated cell cycle arrest and apoptosis in cancer cell. *Ann. Transl. Med.* **2020**, *8*, 89. [[CrossRef](#)]
16. Robey, R.W.; Obrzut, T.; Shukla, S.; Polgar, O.; Macalou, S.; Bahr, J.C.; Di Pietro, A.; Ambudkar, S.V.; Bates, S.E. Becatecarin (rebeccamycin analog, NSC 655649) is a transport substrate and induces expression of the ATP-binding cassette transporter, ABCG2, in lung carcinoma cells. *Cancer Chemother. Pharmacol.* **2009**, *64*, 575–583. [[CrossRef](#)]
17. Saif, M.W.; Diasio, R.B. Edotecarin: A Novel Topoisomerase I Inhibitor. *Clin. Color. Cancer* **2005**, *5*, 27–36. [[CrossRef](#)] [[PubMed](#)]
18. Willenbrink, T.J.; Ruiz, E.S.; Cornejo, C.M.; Schmultz, C.D.; Arron, S.T.; Jambusaria-Pahlajani, A. Field cancerization: Definition, epidemiology, risk factors, and outcomes. *J. Am. Acad. Dermatol.* **2020**, *83*, 709–717. [[CrossRef](#)] [[PubMed](#)]
19. Munisamy, M.; Mukherjee, N.; Thomas, L.; Pham, A.T.; Shakeri, A.; Zhao, Y.; Kolesar, J.; Rao, P.P.N.; Rangnekar, V.M.; Rao, M. Therapeutic opportunities in cancer therapy: Targeting the p53-MDM2/MDMX interactions. *Am. J. Cancer Res.* **2021**, *11*, 5762–5781.
20. Yogosawa, S.; Yoshida, K. Tumor suppressive role for kinases phosphorylating p53 in DNA damage-induced apoptosis. *Cancer Sci.* **2018**, *109*, 3376–3382. [[CrossRef](#)] [[PubMed](#)]
21. Teufel, D.P.; Bycroft, M.; Fersht, A.R. Regulation by phosphorylation of the relative affinities of the N-terminal transactivation domains of p53 for p300 domains and Mdm2. *Oncogene* **2009**, *28*, 2112–2118. [[CrossRef](#)]
22. Berke, T.P.; Slight, S.H.; Hyder, S.M. Role of Reactivating Mutant p53 Protein in Suppressing Growth and Metastasis of Triple-Negative Breast Cancer. *Oncotargets Ther.* **2022**, *15*, 23–30. [[CrossRef](#)]
23. Chen, S.; Wu, J.-L.; Liang, Y.; Tang, Y.-G.; Song, H.-X.; Wu, L.-L.; Xing, Y.-F.; Yan, N.; Li, Y.-T.; Wang, Z.-Y.; et al. Arsenic Trioxide Rescues Structural p53 Mutations through a Cryptic Allosteric Site. *Cancer Cell* **2021**, *39*, 225–239.e8. [[CrossRef](#)]

24. Klemke, L.; Fehrlau, C.F.; Winkler, N.; Toboll, F.; Singh, S.K.; Moll, U.M.; Schulz-Heddergott, R. The Gain-of-Function p53 R248W Mutant Promotes Migration by STAT3 Deregulation in Human Pancreatic Cancer Cells. *Front. Oncol.* **2021**, *11*, 642603. [[CrossRef](#)]
25. Tutuska, K.; Parrilla-Monge, L.; Di Cesare, E.; Nemaierova, A.; Moll, U.M. Statin as anti-cancer therapy in autochthonous T-lymphomas expressing stabilized gain-of-function mutant p53 proteins. *Cell Death Dis.* **2020**, *11*, 274. [[CrossRef](#)]
26. Sargolzaei, J.; Etemadi, T.; Alyasin, A. The P53/microRNA network: A potential tumor suppressor with a role in anticancer therapy. *Pharmacol. Res.* **2020**, *160*, 105179. [[CrossRef](#)]
27. Vu, B.; Wovkulich, P.; Pizzolato, G.; Lovey, A.; Ding, Q.; Jiang, N.; Liu, J.-J.; Zhao, C.; Glenn, K.; Wen, Y.; et al. Discovery of RG7112: A Small-Molecule MDM2 Inhibitor in Clinical Development. *ACS Med. Chem. Lett.* **2013**, *4*, 466–469. [[CrossRef](#)]
28. Tovar, C.; Graves, B.; Packman, K.; Filipovic, Z.; Xia, B.H.M.; Tardell, C.; Garrido, R.; Lee, E.; Kolinsky, K.; To, K.-H.; et al. MDM2 Small-Molecule Antagonist RG7112 Activates p53 Signaling and Regresses Human Tumors in Preclinical Cancer Models. *Cancer Res.* **2013**, *73*, 2587–2597. [[CrossRef](#)]
29. Bykov, V.N.; Issaeva, N.; Shilov, A.; Hultcrantz, M.; Pugacheva, E.; Chumakov, P.; Bergman, J.; Wiman, K.; Selivanova, G. Restoration of the tumor suppressor function to mutant p53 by a low-molecular-weight compound. *Nat. Med.* **2002**, *8*, 282–288. [[CrossRef](#)]
30. Lambert, J.M.; Gorzov, P.; Veprintsev, D.B.; Söderqvist, M.; Segerbäck, D.; Bergman, J.; Fersht, A.R.; Hainaut, P.; Wiman, K.G.; Bykov, V.J. PRIMA-1 Reactivates Mutant p53 by Covalent Binding to the Core Domain. *Cancer Cell* **2009**, *15*, 376–388. [[CrossRef](#)] [[PubMed](#)]
31. Wassman, C.D.; Baronio, R.; Demir, Ö.; Wallentine, B.D.; Chen, C.K.; Hall, L.V.; Salehi, F.; Lin, D.W.; Chung, B.P.; Hatfield, G.W.; et al. Computational identification of a transiently open L1/S3 pocket for reactivation of mutant p53. *Nat. Commun.* **2013**, *4*, 1407. [[CrossRef](#)] [[PubMed](#)]
32. Park, H.S.; Jang, M.H.; Kim, E.J.; Kim, H.J.; Lee, H.J.; Kim, Y.J.; Kim, J.H.; Kang, E.; Kim, S.-W.; Kim, I.A.; et al. High EGFR gene copy number predicts poor outcome in triple-negative breast cancer. *Mod. Pathol.* **2014**, *27*, 1212–1222. [[CrossRef](#)] [[PubMed](#)]
33. Gonzalez-Conchas, G.A.; Rodriguez-Romo, L.; Hernandez-Barajas, D.; Gonzalez-Guerrero, J.F.; Rodriguez-Fernandez, I.A.; Verdines-Perez, A.; Templeton, A.J.; Ocana, A.; Seruga, B.; Tannock, I.F.; et al. Epidermal growth factor receptor overexpression and outcomes in early breast cancer: A systematic review and a meta-analysis. *Cancer Treat. Rev.* **2018**, *62*, 1–8. [[CrossRef](#)] [[PubMed](#)]
34. Abdelrahman, A.E.; Rashed, H.E.; Abdelgawad, M.; Abdelhamid, M.I. Prognostic impact of EGFR and cytokeratin 5/6 immunohistochemical expression in triple-negative breast cancer. *Ann. Diagn. Pathol.* **2017**, *28*, 43–53. [[CrossRef](#)]
35. Lev, S. Targeted therapy and drug resistance in triple-negative breast cancer: The EGFR axis. *Biochem. Soc. Trans.* **2020**, *48*, 657–665. [[CrossRef](#)] [[PubMed](#)]
36. Ellis, H.; Ma, C.X. PI3K Inhibitors in Breast Cancer Therapy. *Curr. Oncol. Rep.* **2019**, *21*, 110. [[CrossRef](#)]
37. Kaur, S.; Kumar, S.; Momi, N.; Sasson, A.R.; Batra, S.K. Mucins in pancreatic cancer and its microenvironment. *Nat. Rev. Gastroenterol. Hepatol.* **2013**, *10*, 607–620. [[CrossRef](#)] [[PubMed](#)]
38. Gupta, R.; Leon, F.; Rauth, S.; Batra, S.K.; Ponnusamy, M.P. A Systematic Review on the Implications of O-linked Glycan Branching and Truncating Enzymes on Cancer Progression and Metastasis. *Cells* **2020**, *9*, 446. [[CrossRef](#)]
39. Cervoni, G.E.; Cheng, J.J.; Stackhouse, K.A.; Heimburg-Molinero, J.; Cummings, R.D. O-glycan recognition and function in mice and human cancers. *Biochem. J.* **2020**, *477*, 1541–1564. [[CrossRef](#)] [[PubMed](#)]

Review

Research Advances of Bioactive Sesquiterpenoids Isolated from Marine-Derived *Aspergillus* sp.

Lixiang Sun ^{1,2,†}, Huannan Wang ^{2,†}, Maocai Yan ², Chunmei Sai ² and Zhen Zhang ^{2,*}¹ School of Pharmacy, Binzhou Medical University, 346 Guanhai Road, Yantai 264003, China² School of Pharmacy, Jining Medical University, 669 Xueyuan Road, Rizhao 276800, China

* Correspondence: zhangz@mail.jnmc.edu.cn; Tel.: +86-633-2983683

† These authors contributed equally to this work.

Abstract: Marine fungi *Aspergillus* sp. is an important source of natural active lead compounds with biological and chemical diversity, of which sesquiterpenoids are an extremely important class of bioactive secondary metabolites. In this paper, we review the sources, chemical structures, bioactivity, biosynthesis, and druggability evaluation of sesquiterpenoids discovered from marine fungi *Aspergillus* sp. since 2008. The *Aspergillus* species involved include mainly *Aspergillus fumigatus*, *Aspergillus versicolor*, *Aspergillus flavus*, *Aspergillus ustus*, *Aspergillus sydowii*, and so on, which originate from sponges, marine sediments, algae, mangroves, and corals. In recent years, 268 sesquiterpenoids were isolated from secondary metabolites of marine *Aspergillus* sp., 131 of which displayed bioactivities such as antitumor, antimicrobial, anti-inflammatory, and enzyme inhibitory activity. Furthermore, the main types of active sesquiterpenoids are bisabolanes, followed by drimanes, nitrobenzoyl, etc. Therefore, these novel sesquiterpenoids will provide a large number of potential lead compounds for the development of marine drugs.

Keywords: marine fungi; sesquiterpenoids; *Aspergillus*; bioactivity

Citation: Sun, L.; Wang, H.; Yan, M.; Sai, C.; Zhang, Z. Research Advances of Bioactive Sesquiterpenoids Isolated from Marine-Derived *Aspergillus* sp. *Molecules* **2022**, *27*, 7376. <https://doi.org/10.3390/molecules27217376>

Academic Editor: Giovanni Ribaudò

Received: 8 October 2022

Accepted: 28 October 2022

Published: 30 October 2022

Publisher's Note: MDPI stays neutral with regard to jurisdictional claims in published maps and institutional affiliations.



Copyright: © 2022 by the authors. Licensee MDPI, Basel, Switzerland. This article is an open access article distributed under the terms and conditions of the Creative Commons Attribution (CC BY) license (<https://creativecommons.org/licenses/by/4.0/>).

1. Introduction

More than 70% area of the earth is covered by oceans, which is the largest known habitat for life. The marine environment is characterized by high salinity, high pressure, low oxygen, low temperature, darkness, scarce nutrients, etc. To adapt to the special environment and obtain advantages in the competition of limited resources, marine microorganisms could produce novel secondary metabolites with unique structures and potent biological activities during evolution [1,2]. Rich marine microorganisms, mainly derived from marine actinomycetes and marine fungi, are ubiquitous in the natural environment [3]. Diverse active natural products exist in endophytic fungi from the marine environment, which can be the resources for new lead compounds [4,5].

Aspergillus is a typical filamentous fungus, which is divided mainly into *Aspergillus fumigatus*, *Aspergillus versicolor*, *Aspergillus flavus*, *Aspergillus ustus*, *Aspergillus sydowii*, and so on [6]. Fumiquinazolines were isolated by Numata from marine *Aspergillus* sp. for the first time in 1992, which opened the door to the study of the metabolites of marine *Aspergillus* [7]. Recent studies have found that many organic compounds with unique structures, which showed a lot of physiological activities, were found in marine *Aspergillus* sp., including terpenoids, alkaloids, and polyketones [8]. Sesquiterpenoids, the most abundant among all the terpenoids skeletons, exhibit excellent biological activities, such as cytotoxicity, antibacterial, antifungal, antiviral, anti-inflammatory, and enzyme inhibitory activity, and have aroused widespread interest of many scholars [9,10]. This paper attempts to review the sources, bioactivities, biosynthesis, and other studies of sesquiterpenoids discovered from marine fungi *Aspergillus* sp. in the last 15 years.

2. Characteristics of Sesquiterpenoids from Marine *Aspergillus* sp.

Secondary metabolites of marine fungi have become one of the most active subfields of natural pharmaceutical discovery [11]. Sesquiterpenoids are an extremely important class of secondary metabolites and have been associated with a wide variety biological activities [12]. Approximately 268 sesquiterpenoids isolated from 56 strains of marine fungi are reviewed in this work. Furthermore, research has found that 37.5% of the sesquiterpenoid compounds came from marine animals (sponges, 21.4% and corals, 8.9%), 28.6% from marine plants (algae, 16.1% and mangroves, 12.5%), and the remaining compounds from the marine environment (21.4% from marine sediments and 1.8% from seawater), and 8.9% from unknown sources (see Figure 1).

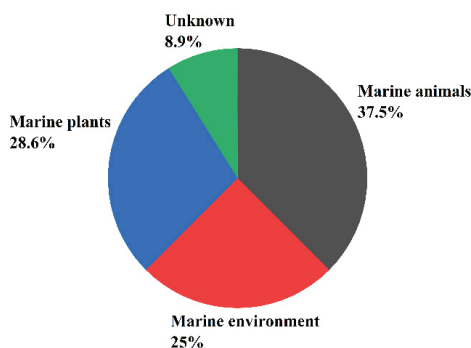


Figure 1. The main sources of the sesquiterpene-rich marine fungi.

Marine fungus *Aspergillus* is a huge community that occupies a great proportion in the fungus family, which is widely distributed in marine plants, marine organisms, marine sediments, and other environments. According to incomplete statistics, there were more than 180 species of fungus *Aspergillus*, such as *Aspergillus fumigatus*, *Aspergillus flavus*, *Aspergillus terreus*, and *Aspergillus versicolor* [13]. The proportions of the 56 species (Table 1) reviewed in this paper are as follows: *Aspergillus versicolor* (14.3%), *Aspergillus sydowii* (12.5%), *Aspergillus ustus* (10.7%), *Aspergillus fumigatus* (5.4%), *Aspergillus insulicola* (3.6%), *Aspergillus ochraceus* (3.6%), *Aspergillus carneus* (3.6%), *Aspergillus terreus* (3.6%), *Aspergillus flavus* (3.6%), *Aspergillus flavipes* (3.6%), and *Aspergillus* unknown (26.8%) (see Figure 2).

Table 1. List of sesquiterpenoids isolated from marine fungi *Aspergillus* sp. with potential biological activity.

Compound Name/Chemical Class	Marine Source	Type of Strains	Activity (MIC)	Reference
Compounds 1,3 and 5 Compound 2 Compound 4	Marine-sponge-derived fungus <i>Aspergillus</i>	not reported <i>S. albus</i> , <i>M. tetragenus</i> <i>S. albus</i> , <i>B. subtilis</i>	not reported 1.25–5 μ M 2.5–5 μ M	[14] 2012
Compound 6 Compound 7 Compound 8	Marine-sponge-derived fungus <i>Aspergillus sydowii</i> ZSDS1-F6	<i>A. hydrophila</i> and <i>K. pneumonia</i> <i>K. pneumonia</i> <i>E. faecalis</i>	4.3 and 21.4 μ M 10.7 μ M 18.8 μ M	[15] 2014
Flavilane A(9) Compound 10	Fresh-seawater-derived fungus <i>Aspergillus flavipes</i> 297	Pathogenic bacteria Pathogenic bacteria and Pathogenic fungus <i>V. mari</i>	2–64 μ M	[16] 2021
Compounds 11,12 Compound 13	Deep sea sediment fungus <i>Aspergillus versicolor</i> SD-330	<i>A. hydrophilia</i> , <i>E. coli</i> , <i>E. tarda</i> , and <i>V. harveyi</i> <i>E. coli</i>	2–8 μ M 1 μ M	[17] 2021

Table 1. Cont.

Compound Name/Chemical Class	Marine Source	Type of Strains	Activity (MIC)	Reference
Compound 14	Seawater-derived fungus <i>Aspergillus sydowii</i> SW9	<i>E. coli</i> and <i>S. pneumonise</i>	2–4 μ M	[18] 2019
Compounds 15,16	Deep sea sediment fungus <i>Aspergillus versicolor</i> SD-330	<i>E. coli</i> , <i>E. trada</i> , <i>V. harveyi</i> , and <i>V. parahaemolyticus</i>	8 μ M	[19] 2019
Compound 17		<i>E. coli</i> , <i>Aeromonas hydrophilia</i> , <i>E. tarda</i> , <i>V. anguillarum</i> , and <i>V. harveyi</i>	1–4 μ M	
Compound 18		not reported	not reported	
Compounds 19–21	Marine-gorgonian-derived fungus <i>Aspergillus</i>	<i>S. aureus</i>	Inhibition zones were 5–11 mm at 100 μ g/mL	[20] 2010
Compounds 22–28	Mangrove endophytic fungus <i>Aspergillus xy02</i>	<i>S. aureus</i>	31.5–41.9 μ M	[21] 2018
Asperchondols A, B(29, 30)	Marine-sponge-derived fungus <i>Aspergillus</i>	<i>S. aureus</i>	25–50 μ M	[22] 2016
Albican-11,14-diol (31)	Marine-alga-derived fungus <i>Aspergillus versicolor</i>	<i>E. coli</i> and <i>S. aureus</i>	Inhibition zones were 7–10.3 mm at 30 μ g/disk	[23] 2012
Compounds 32–35	Marine-alga-derived fungus <i>Aspergillus</i> RR-YLW-12	<i>V. harveyi</i> , <i>V. splendidus</i> , <i>V. parahaemolyticus</i> , and <i>V. anguillarum</i>	not reported	[24] 2021
Compounds 36–38	Marine-coral-derived fungus <i>Aspergillus versicolor</i> ZJ-2008015	<i>S. aureus</i> and <i>S. albus</i>	2.6–6.4 μ M	[25] 2012
Compounds 39,40	Marine-sponge-derived fungus <i>Aspergillus insuetus</i> OY-207	<i>N. crassa</i>	140–242 μ M	[26] 2011
Compound Name/Chemical Class	Marine Source	Cell lines	Activity (IC ₅₀ /EC ₅₀ /ED ₅₀ /inhibition rate)	Reference
Asperolactone (41) Echinolactone D (42)	Marine sediment fungus <i>Aspergillus oryzae</i>	A549, HepG2, and MCF-7	<100 μ M not reported	[27] 2021
Asperienes A-D (43–46)	Marine fungus <i>Aspergillus flavus</i> CF13–11	A549, HeLa, MGC-803, and MCF-7	1.4–8.3 μ M	[28] 2019
Compounds 47,48	Marine sediment fungus <i>Aspergillus flocculosus</i>	Neuro-2a and 22Rv1	3–31.5 μ M	[29] 2019
Compounds 49,50	Marine fungus <i>Aspergillus ochraceus</i> Jcma1F17	H1975, U937, K562, BGC-823, MOLT-4, MCF-7 A549, HeLa, HL60, and Huh-7	1.95–6.35 μ M	[30] 2014
Insulicolide A (51)	Marine-sponge-derived fungus <i>Aspergillus insulicola</i> MD10-2	H-460	6.9 μ M	[31] 2016
Compounds 52, 53 Compound 54	Marine fungus <i>Aspergillus ochraceus</i> Jcma1F17	786-O, ACHN, and OS-RC-2	2.3–11 μ M 0.89–1.5 μ M	[32] 2018
Compounds 57, 58	Marine-sponge-derived fungus <i>Aspergillus insulicola</i>	AsPC-1 and PANC-1	2.3–4.6 μ M	[33] 2022
Compounds 59, 61 Compound 60	Marine-sponge-derived fungus <i>Aspergillus ustus</i>	L5178Y L5178Y, PC12, and HeLa	0.6–5.3 μ M 0.6–7.2 μ M	[34] 2009
Compound 62	Mangrove endophytic fungus <i>Aspergillus ustus</i>	P388	8.7 μ M	[35] 2011
Compounds 63, 65 Compound 64	Marine-sponge-derived fungus <i>Aspergillus</i>	HePG-2 and Caski	2.91–12.4 μ M not reported	[36] 2012
β -D-glucopyranosylaspergillusene A (66)	Marine-sponge-derived fungus <i>Aspergillus sydowii</i> J05B7F-4	HePG-2, HCT116, and KB	50–70 μ M	[37] 2017

Table 1. Cont.

Compound Name/Chemical Class	Marine Source	Type of Strains	Activity (MIC)	Reference
Compound 67 Compound 68 Compound 70	Mangrove endophytic fungus <i>Aspergillus terreus</i> GX3-3B	MCF-7, HL-60 MCF-7 HL-60	3.43–4.49 μ M 2.79 μ M 0.6 μ M	[38] 2013
Aspergiketone (71)	Coastal saline soil fungus <i>Aspergillus fumigatus</i>	HL-60 and A549	12.4–22.1 μ M	[39] 2016
Oxalicine B (72)	Sea-urchin-derived fungus <i>Aspergillus fumigatus</i>	P388	55.9 μ M	[40] 2012
Compound 73 Compounds 74, 75	Marine fungus <i>Aspergillus ustus</i> 094102	HL-60 and A549	20.6–30 μ M 9–10.5 μ M	[41] 2009
Compound 76	Marine-sponge-derived fungus <i>Aspergillus ustus</i>	L5178Y	1.9 μ M	[42] 2008
Compound 77	Marine sediment fungus <i>Aspergillus fumigatus</i> YK-7	U937	84.9 μ M	[43] 2015
Asperflavonoid A (78)	Marine fungus <i>Aspergillus flavipes</i> 297	HepG2 and MKN-45	26.8–38.5 μ M	[44] 2021
Compound Name/Chemical Class	Marine Source	Target Enzyme	Activity (IC ₅₀ /inhibitory rate)	Reference
7-Deoxy-7,14-didehydrodydonol (79)	Mangrove endophytic fungus <i>Aspergillus versicolor</i> SYSU-SKS025	inhibit NO production in RAW 264.7 macrophages	12.5 μ M	[45] 2018
Compounds 80–82 Compound 83	Marine-algal-derived fungus <i>Aspergillus</i> ZLO-1B14	inhibit LPS-stimulated RAW264.7 macrophages inhibit LPS-stimulated RAW264.7 macrophages and exhibited an inhibitory effect against IL-6 production	not reported 69% at 40 μ M	[46] 2015
Compound 84,85	Marine fungus <i>Aspergillus terreus</i>	inhibitory activity of NO production	37.3% and 47.7% at 40 μ M	[47] 2018
Compound 86,87,89	Marine sediment fungus <i>Aspergillus sydowii</i>	not reported inhibition against fMLP/CB-induced superoxide anion generation by human neutrophils and inhibitory activity against the release of elastase induced by fMLP/CB	not reported	[48] 2013
Compounds 88,90			5.23–16.39 μ M	
Compound 91–94	Marine sediment fungus <i>Aspergillus</i> SCSIOW2	inhibitory activity of NO production	not reported	[49] 2016
Compounds 95–99	Mangrove endophytic fungus <i>Aspergillus</i> GXNU-MA1	inhibitory activity of NO production	16.15–27.08 μ M	[50] 2022
Compounds 100,102–107 Compound 101	Marine sediment fungus <i>Aspergillus sydowii</i> MCCC3A00324	against NO secretion in LPS-activated BV-2 microglia cells against NO secretion in LPS-activated BV-2 microglia cells and anti-inflammatory effect inhibiting NF- κ B activation pathway	32.6%–45.4% at 10 μ M 45% at 10 μ M not reported	[51] 2020
Compound 108	Marine fungus <i>Aspergillus ochraceus</i>	suppressed the RANKL-induced osteoclasts formation and bone resorption by targeting NF- κ B	not reported	[52] 2020

Table 1. Cont.

Compound Name/Chemical Class	Marine Source	Type of Strains	Activity (MIC)	Reference
Compound Name/Chemical Class	Marine Source	Target Enzyme	Activity / (IC ₅₀)	Reference
7-Deoxy-7,14-didehydroxydonol (79)	Mangrove endophytic fungus <i>Aspergillus versicolor</i> SYSU-SKS025	inhibitory effect on α -glucosidase	7.5 μ M	[45] 2018
Compounds 109–112	Mangrove endophytic fungus <i>Aspergillus flavus</i> QQSG-3	inhibitory effect on α -glucosidase	1.5–4.5 μ M	[53] 2018
Compound 113 2-deoxy-2 β -hydroxysubergorgic (114)	Marine-coral-derived fungus <i>Aspergillus</i> EGF15-0-3	inhibit ChE	not reported	[54] 2020
Compounds 115–118	Marine-ascidian-derived fungus <i>Aspergillus ustus</i> TK-5	inhibitory activity against neuraminidase	28.4–37.3 μ M	[55] 2018

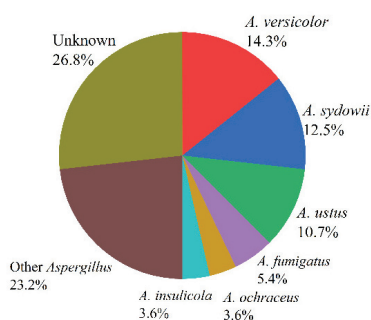
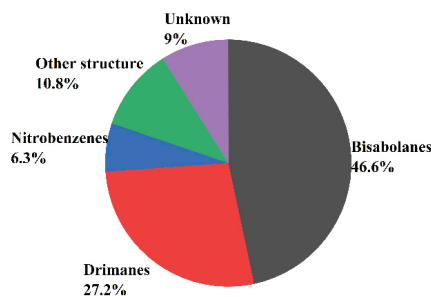


Figure 2. The proportions of marine fungi reviewed in this paper.

In recent years, more and more sesquiterpenoids were found in marine fungi *Aspergillus*, which consisted of the molecular skeleton structure with three isoprene units and contains 15 carbon atoms [56]. In addition, the number and skeleton types of sesquiterpenoids are the most abundant among all the terpenoids. According to the number of carbon rings, sesquiterpenoids can be divided into acyclic sesquiterpenes, monocyclic sesquiterpenoids, bicyclic sesquiterpenoids, tricyclic sesquiterpenoids, tetracyclic sesquiterpenoids, etc., [57]. Acyclic sesquiterpenes are also known as chain sesquiterpenes but rarely reported in fungi. The monocyclic sesquiterpenes referred mainly to bisabolanes, humaranes, and cybrodins, while the bicyclic sesquiterpenes consist mainly of drimanes, lacticinanes, and eudesmanes. This paper finds that the main types of sesquiterpenoids isolated from marine fungi *Aspergillus* were bisabolanes (46.6%), drimanes (27.2%), nitrobenzenes (6.3%), and unknown structure (9%) (see Figure 3).

Figure 3. The main types of sesquiterpenoids isolated from *Aspergillus* sp.

Recent studies have indicated that the metabolic pathway of marine fungi—that results in the production of a number of secondary metabolites with various chemical structures and specific physiological activities—is very different from that of terrestrial fungi [37]. This article concludes that 131 of the 268 sesquiterpenoids isolated from marine fungi *Aspergillus* have significant biological activities. Moreover, the structure types of inactive sesquiterpenoids are mostly bisabolanes and drimanes [58–62]. The relatively large number of sesquiterpenoids shows a variety of biological activities such as antitumor, antibacterial, anti-inflammatory, enzyme inhibitory, antioxidant, antiviral, and other activities. Overall, 30.5% of sesquiterpenoids exhibited antibacterial activity, followed by antitumor activity (29%), anti-inflammatory activity (22.9%), enzyme inhibitory activity (8.4%), and other activities (10.7%) (see Figure 4).

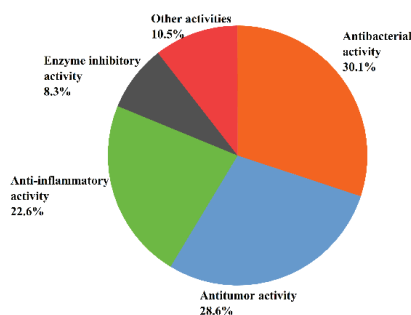


Figure 4. The bioactivity of sesquiterpenoids from *Aspergillus* sp.

3. Bioactivity of Sesquiterpenoids from *Aspergillus* sp.

3.1. Antibacterial Activity

In recent years, inappropriate and irrational use of antibiotics provides favorable conditions for resistant microorganisms to emerge and spread, which has become a global public health problem [63]. Therefore, it is urgent to develop new antibiotics with new structures and significant biological activities. To that end, the secondary metabolites of microorganisms in the marine environment are a great source for new antibacterial agents screening and much attention has been attracted to the relevant studies. This section covers 40 bioactive sesquiterpenoids (Figure 5) with antibacterial activity described to date from marine-derived *Aspergillus* sp.

Li et al. [14] isolated four new and one known bisabolane-type sesquiterpenoid from secondary metabolites of *Aspergillus* sp. from sponge. Compounds 1–5 showed different antibacterial activity against six pathogenic bacteria and two marine bacteria, and compounds 2 and 4 showed selective antibacterial activity. Compound 2 had strong inhibitory effects on *Staphylococcus albus* and *Micrococcus tetragenus*, with minimum inhibiting concentrations (MIC) values of 5.00 and 1.25 μM , respectively. The MIC values of compound 4 with *S. albus* and *Bacillus subtilis* were 5.00 μM and 2.50 μM , respectively. Notably, compound 1 represents the rare example of a bisabolane-type sesquiterpenoid with a 1, 4-disubstituted benzene ring isolated from marine organisms. Compounds 2 and 3 were the enantiomers of (+)-sydonol and (+)-sydonic acid, respectively. This fact suggests that fungi isolated from different marine organisms may produce different stereochemistry compounds. Furthermore, there were three sesquiterpenoids, 6–8, from the sponge-associated fungus *Aspergillus sydowii* ZSDS1-F6, which has certain antibacterial activities; among them, compound 6 and 7 displayed antibacterial activities against *Klebsiella pneumonia*, with MIC values of 21.4 and 10.7 μM , respectively [15]. In addition, compound 6 showed moderate antibacterial activity against *Aeromonas hydrophila* (MIC, 4.3 μM), while compound 8 showed moderate antibacterial activity against *Enterococcus faecalis* (MIC, 18.8 μM). Chen et al. [16] isolated two phenolic bisabolane sesquiterpenoids (PBS) compounds (9–10) from *Aspergillus flavipes* 297, including a pair of new enantiomers (\pm)-flavilane A (9). However, compounds 9 and

10 represent the rare PBS-containing methylsulfinyl group and showed selective antibacterial activities against several pathogenic bacteria; their MIC values were 2–64 $\mu\text{g/mL}$. Furthermore, compound 10 exhibited mild antifungal activity against plant pathogenic fungus *Valsa mари*.

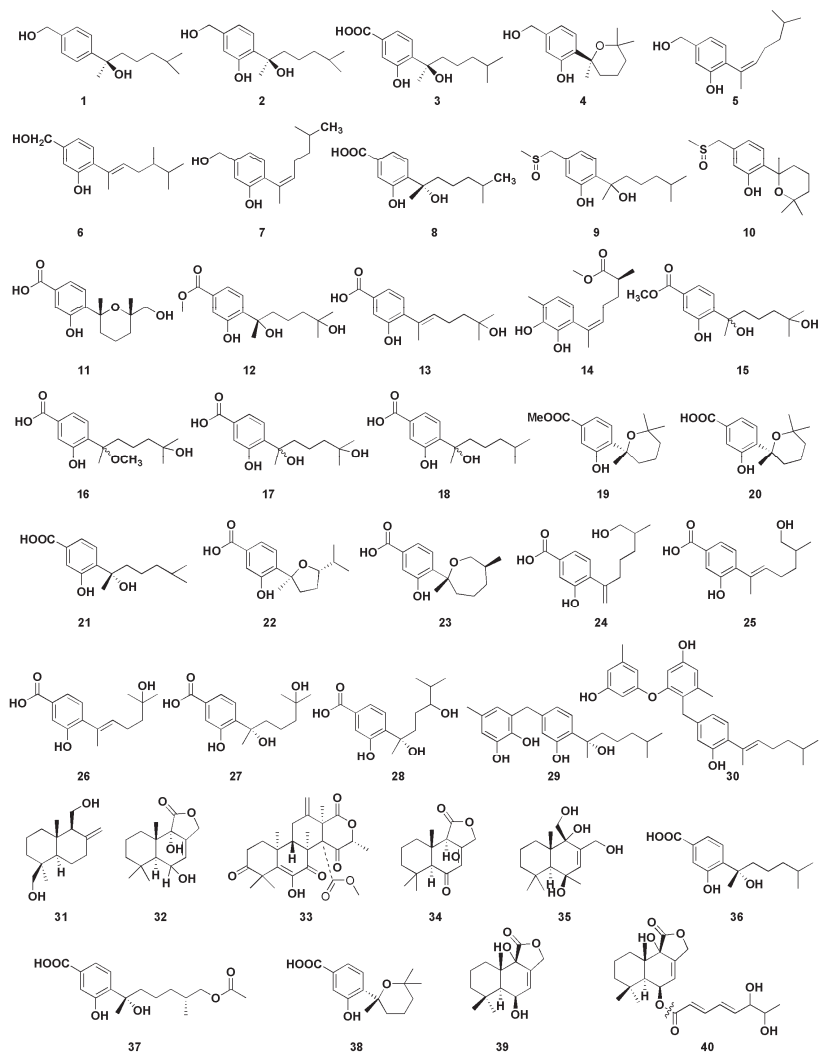


Figure 5. Chemical structures of antimicrobial compounds (1–40).

Aromatic bisabolene-type sesquiterpenoids 11–13 were isolated from the marine fungus *Aspergillus versicolor* SD-330 in the deep-sea sediments [17]. Compounds 11 and 12 had significant inhibitory activities against *A. hydrophilia*, *Escherichia coli*, *Edwardsiella tarda*, and *Vibrio harveyi*, with MIC values ranging from 2.0 to 8.0 $\mu\text{g/mL}$. Moreover, compound 13 had significant inhibitory activity against *E. coli* (MIC value was 1.0 $\mu\text{g/mL}$), which was better than the positive control chloramphenicol (MIC value was 2.0 $\mu\text{g/mL}$). A new aromatic bisabolene-type sesquiterpenoid (14) was discovered in *Aspergillus sydowii* SW9, whose absolute configuration is (S). Compound 14 had significant inhibitory effect on *E. coli*, and its MIC value was 2.0 $\mu\text{g/mL}$, which was similar to that of positive control chloramphenicol (MIC 2.0 $\mu\text{g/mL}$). Compound 14 also exhibited potent activity against *S. pneumoniae*,

with an MIC value of 4.0 µg/mL [18]. Wang et al. [19] obtained four sesquiterpenoids 15–18 with antibacterial activity from marine *Aspergillus versicolor* SD-330. Compounds 15 and 16 showed significant antibacterial activity against *E. coli*, *E. trada*, *V. harveyi*, and *Vibrio parahaemolyticus*, and the MIC values were less than or equal to 8.0 µg/mL. However, compound 17 exhibited significant antibacterial effect on *E. coli* with MIC value of 1.0 µg/mL, which was more potent than that of positive control chloramphenicol (MIC 2.0 µg/mL). Moreover, compound 17 showed strong inhibitory activity against *A. hydrophilia*, *E. tarda*, *Vibrio anguillarum*, and *V. harveyi*, each with MIC value of 4.0 µg/mL. Compound 17 showed a stronger antibacterial activity than compounds 15 and 16, suggesting that C-15 carboxyl group methyl ester or the methylated C-7 hydroxyl group could reduce their antibacterial activity.

Wei et al. isolated three phenolic bisabolane-type sesquiterpenoids compounds 19–21 from *Aspergillus* sp., which is the first report of natural metabolites from marine fungus *Aspergillus* from gorgonian *Dichotella gemmacea* [20]. All of them exhibited weak antibacterial activity against *Staphylococcus aureus*, with the diameters of inhibition zones of 11, 7, and 5 mm at 100 µg/mL, respectively. Seven phenolic bisabolane sesquiterpenoids 22–28 were obtained from the endophytic fungus *Aspergillus* sp. xy02 from a Thai mangrove *Xylocarpus moluccensis* [21] and displayed moderate inhibitory activities against *S. aureus*, with IC₅₀ values ranging from 31.5 to 41.9 µM. Two new phenolic bisabolane sesquiterpenes, asperchondols A (29) and asperchondols B (30), were obtained from the sponge-derived fungus *Aspergillus* sp. and showed antibacterial activity against *S. aureus*, with the MICs of 50 and 25 µM, respectively [22]. Furthermore, structure–activity relationship found that the coexistence of phenolic bisabolane sesquiterpene and diphenyl ether moieties seems to be very important since the hybrid 30 was more active than phenolic bisabolane sesquiterpenoid 29 and phenyl esters.

A series of phenolic bisabolane-type sesquiterpenoids have been discovered from different marine invertebrates such as sponges [64] and gorgonians [65] in the last century. In addition, such compounds were also found in bacterium CNH-741 and fungus CNC-979 isolated from marine sediments [66]. These results indicate that the real producers of these compounds from marine invertebrates, sponges, and corals may be constituents of microorganisms. Albican-11,14-diol (31) is a sesquiterpene compound isolated from the cultures of the endophytic fungus *Aspergillus versicolor*, which is isolated from marine green alga *Codium fragile* [23]. The diameters of inhibition zones of compound 31 against *E. coli* and *S. aureus* were 7 and 10.3 mm, respectively, at the concentration of 30 µg/disk. Fang et al. isolated a drimane-type sesquiterpenoid (32) and three unknown-type sesquiterpenoids (33–35) from the algicolous fungus *Aspergillus* sp. RR-YLW-12, which exhibited little inhibitory activity against four marine-derived pathogenic bacteria, *V. anguillarum*, *V. harveyi*, *V. parahaemolyticus*, and *Vibrio splendidus* [24]. Zheng et al. isolated and purified three bisabolane sesquiterpenes 36–38 from the fermentation products of *Aspergillus versicolor* ZJ-2008015, which were obtained from a soft coral *Sarcophyton* sp. [25]. The results showed that compounds 36–38 exhibited potent antibacterial activity with MICs of 5.3, 6.4, and 5.4 µM against *S. albus* and 2.6, 6.4, and 5.4 µM against *S. aureus*, respectively. Cohen et al. [26] isolated two drimane sesquiterpenes (39–40) from the sponge-derived fungus *Aspergillus insuetus* (OY-207), which exhibited anti-fungal activity against *Neurospora crassa*, with the MICs of 140 and 242 µM, respectively.

3.2. Antitumor Activity

The marine environment represents a unique resource that encloses a massive chemical and biological diversity, which leads to an important source of potential antitumor drugs [67]. Among antitumor compounds, sesquiterpenes (including bisabolane, drimane, illudalane, etc.) are obtained mainly from marine fungi, including *Aspergillus* sp. [68,69]. Therefore, more and more researchers pay close attention to looking for effective antitumor drugs from marine *Aspergillus*. In recent years, there were about 38 bioactive sesquiterpenoids (Figure 6) with antitumor activity isolated from marine-derived *Aspergillus* sp.

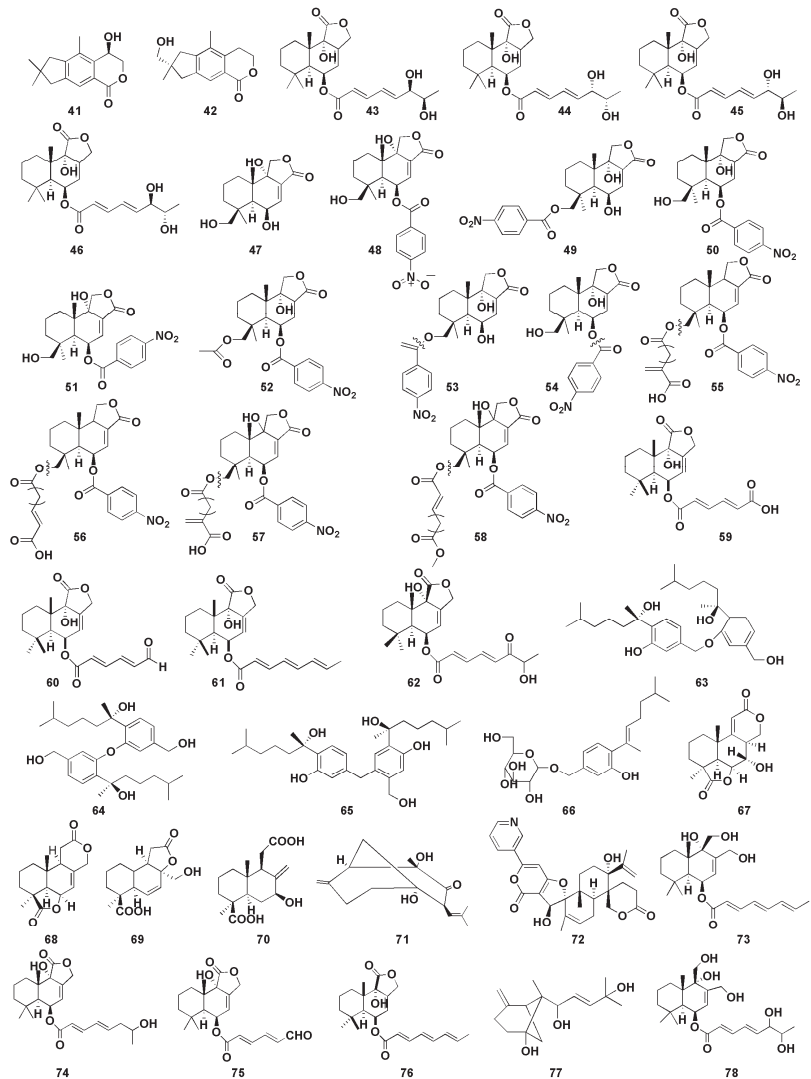


Figure 6. Chemical structures of antitumor compounds (41–78).

Orfali et al. [27] first discovered two illudalane sesquiterpenes, asperorlactone (41) and echinolactone D (42), from marine sediment ascomycete *Aspergillus oryzae*, in which compound 41 has an absolute configuration of (5R). Compounds 41 and 42 showed antiproliferative activity against human lung cancer (A549), liver cancer (HepG2), and breast cancer (MCF-7) cell lines, with half maximal inhibitory concentration (IC₅₀) values of asperorlactone (41) <100 μM. Furthermore, compounds 9 and 10 isolated from *Aspergillus flavipes* 297 exhibited promising cytotoxic effects on MKN-45 and HepG2 cells, respectively, indicating that the methylsulfinyl substituent enhanced the cytotoxicity, to a certain degree [16]. Gao et al. [28] isolated four drimane sesquiterpene esters asperienes A–D (43–46) from marine-derived fungal *Aspergillus flavus* CF13-11, which was the first successful isolation of two pairs of C-6' /C-7' isoforms. Moreover, compounds 43–46 showed significant activity against four tumor cell lines (HeLa, MCF-7, MGC-803, and A549), with IC₅₀ values of 1.4–8.3 μM. Notably, compounds 43 and 46 showed lower toxicity to normal GES-1 cells

than did **44** and **45**, suggesting their great potential for the development of an antitumor agent. Yurchenko et al. [29] isolated two drimane sesquiterpenes (**47–48**) from marine-sediment-derived fungus *Aspergillus flocculosus*, which exhibited potent cytotoxic effect toward mouse neuroblastoma neuro-2A and human prostate cancer 22Rv1 cells, with the IC₅₀ values were 24.1, 4.9 μM and 31.5, 3.0 μM, respectively. It is well known that human prostate cancer 22Rv1 cells are resistant to hormone therapy because of the expression of the androgen receptor splice variants AR-V7 [70]. Therefore, the results indicated that compounds **47** and **48** could be used in the treatment of human drug-resistant prostate cancer. Fang et al. [30] isolated two nitrobenzoyl sesquiterpenoids (**49–50**) from the marine-derived fungus *Aspergillus ochraceus* Jcma1F17, which was the first time nitrobenzoyl sesquiterpenoids obtained from this fungal were reported. Both compounds displayed significant cytotoxic effects on 10 human cancer cell lines (H1975, U937, K562, BGC-823, MOLT-4, McF-7, A549, Hela, HL60, and Huh-7), with IC₅₀ values ranging from 1.95 to 6.35 μM.

Insulicolide A (Nitrobenzoyl substituted sesquiterpene, **51**) was isolated from the marine-sponge-associated endozoic fungus *Aspergillus insulicola* MD10-2 [31]. Compound **51** showed cytotoxic effects against human lung cancer cell line H-460, with an IC₅₀ value of 6.9 μM. However, the cytotoxic activity of the acetylated derivatives of compound **51** decreased markedly, indicating that the double at C-7 might be involved in the cytotoxic activity. Tan et al. isolated three nitrobenzoyl sesquiterpenoids (**52–54**) from the marine fungus *Aspergillus ochraceus* Jcma 1F17 [32]. Compound **54** displayed potent cytotoxicities against three renal carcinoma ACHN, OS-RC-2, and 786-O cells lines (IC₅₀ of 0.89–1.5 μM). The cytotoxic effects of compounds **52** and **53** on 786-O cells (IC₅₀ of 2.3 and 4.3 μM, respectively) were exhibited more strongly than those of OS-RC-2 (IC₅₀ 5.3 and 8.2 μM) and ACHN (IC₅₀ of 4.1 and 11 μM, respectively), suggesting that the C-9 hydroxy group may contribute more to the cytotoxic activities against renal carcinoma cells. Additionally, compound **52** showed stronger inhibitory activity at low concentration levels, compared with the positive control sorafenib, a drug approved for the treatment of primary kidney cancer (advanced renal cell carcinoma). Further investigation revealed that the cell cycle was arrested at G₀/G₁ phase after being treated with compound **52** at 1 μM, whereas after being treated at 2 μM for 72 h, the late apoptosis of 786-O cells were induced. Four nitrobenzoyl sesquiterpenoids (**55–58**) were isolated from an Antarctica-sponge-derived *Aspergillus insulicola* by Sun et al. [33], in which compounds **57** and **58** showed selective inhibitory activity against human pancreatic ductal adenocarcinoma (PDAC) cell lines, whereas compounds **55** and **56** were inactive, indicating that hydroxyl groups at C-9 is essential for cytotoxicity. Furthermore, the IC₅₀ values of compounds **57** and **58** against PDAC cell lines AsPC-1 and PANC-1 were 2.7, 4.6 μM and 2.3, 4.2 μM, respectively. Numerous studies have shown that most of nitrobenzoyl sesquiterpenes were obtained from the marine-derived fungus *Aspergillus ochraceus*, suggesting that *Aspergillus ochraceus* may be a good resource for the production of these compounds.

Liu et al. [34] found three drimane sesquiterpenoids (**59–61**) from marine sponge-derived fungus *Aspergillus ustus*, which showed cytotoxic activities against mouse lymphoma cell line L5178Y, with half maximal effective concentration (EC₅₀) values between 0.6 and 5.3 μM. In addition, the EC₅₀ value of compound **60** against PC12 and HeLa cells were 7.2 μM and 5.9 μM, respectively. Zhou et al. [35] isolated drimane sesquiterpenoid (**62**) from mangrove-derived fungus *Aspergillus ustus* and exhibited moderate cytotoxic effects against the mice lymphocytic leukemia P388 cell line with IC₅₀ value of 8.7 μM. Sun et al. [36] isolated three bisabolane sesquiterpenoid dimers (**63–65**) from the sponge-derived fungus *Aspergillus* sp., and the cytotoxic activity against HePG-2 human hepatoma cell line and Caski human cervical cell line were determined in vitro. Significantly, compounds **63** and **65** with (7S) and (7'S) configuration displayed better potent cytotoxicity toward the tumor cell lines than did compound **64**. The IC₅₀ values of compound **63** and **65** were 9.31, 12.40 μM and 2.91, 10.20 μM, respectively. These results suggest that the cytotoxic activity of the compound may be weakened due to the mesomeric effect since the activity of the compounds is stereoselective. β-D-glucopyranosyl aspergillusene A (**66**) from the

sponge-derived fungus *Aspergillus sydowii* J05B-7F-4 exhibited mild cytotoxicity against KB (human nasopharyngeal carcinoma cells), HepG2 (human liver cancer cells), and HCT 116 (human colon cancer cells), with IC₅₀ values between 50 and 70 µM [37].

Deng et al. [38] found four sesquiterpenoids containing 16 carbon atoms (67–70) from the mangrove endophytic fungus *Aspergillus terreus* GX3-3B, of which compound 67 showed inhibitory activity against human breast cancer cells (MCF-7) and human promyelocytic leukemia cells (HL-60), with the IC₅₀ values were 4.49 and 3.43 µM, respectively. In addition, compound 68 exhibited promising inhibitory effect on MCF-7 cells, with an IC₅₀ value of 2.79 µM, whereas compound 70 showed potent inhibitory effect on HL-60 cells, with an IC₅₀ value of 0.6 µM. The structure–activity relationship indicated that the presence of C or D lactone ring may be helpful for the inhibitory against the human breast cancer cell line MCF-7. Compounds 67 and 70 showed stronger activities than did compounds 68 and 69, indicating that hydroxyl group at the C-7 position could improve the cytotoxicity toward HL-60 cell.

Aspergiketone (71) is the first sesquiterpenoid derivative isolated from *Aspergillus fumigatus*, which exhibited obvious cytotoxicity against HL-60 and A-549 cells, with IC₅₀ values of 12.4 and 22.1 µM, respectively [39]. Oxalicine B (72), a unique pyridino- α -pyrone sesquiterpenoid, was obtained from the sea-urchin-derived fungus *Aspergillus fumigatus* and exhibits moderate cytotoxicity to murine P388 leukemia cells, with IC₅₀ of 55.9 µM [40]. Three drimane sesquiterpenes (73–75) were isolated from marine *Aspergillus ustus* 094102 [41], of which compounds 74 and 75 showed moderate cytotoxicity against A549 and HL-60 cells, with IC₅₀ values of 10.5 and 9.0 µM, respectively. Moreover, compound 73 exhibited weak cytotoxic effect to A549 and HL-60 cells, with IC₅₀ values of 20.6 and 30.0 µM, respectively. Proksch et al. found a drimane sesquiterpene (76) from marine-sponge-derived fungus *Aspergillus ustus*, which exhibited selective inhibition on lymphoma cell line L5178Y cells (median effective dose (ED₅₀), 1.9 µM) [42]. Wang et al. found a β -bergamotane sesquiterpenoids (77) from marine-sediment-derived fungus *Aspergillus fumigatus* YK-7, which exhibited weak inhibitory activities against U937 cells, with an IC₅₀ value of 84.9 µM [43]. Asperflavinoid A (78), a drimane-type sesquiterpenoids, was isolated from *Aspergillus flavipes* 297 and exerted toxic effect on HepG2 and MKN-45 cells, with the IC₅₀ values of 38.5 and 26.8 µM, respectively [44].

3.3. Anti-Inflammatory Activity

Inflammation is a comprehensive array of physiological response to a foreign organism, which has been considered as a major factor for the progression of various chronic diseases/disorders [71]. Therefore, development of effective and economical anti-inflammatory drugs (NSAIDs) is an area of importance in drug discovery while natural anti-inflammatory supplements are becoming more popular and have been the focus of many scientific investigations. This section covers 30 sesquiterpenoids (Figure 7) with anti-inflammatory activity which isolated from marine-derived *Aspergillus* sp.

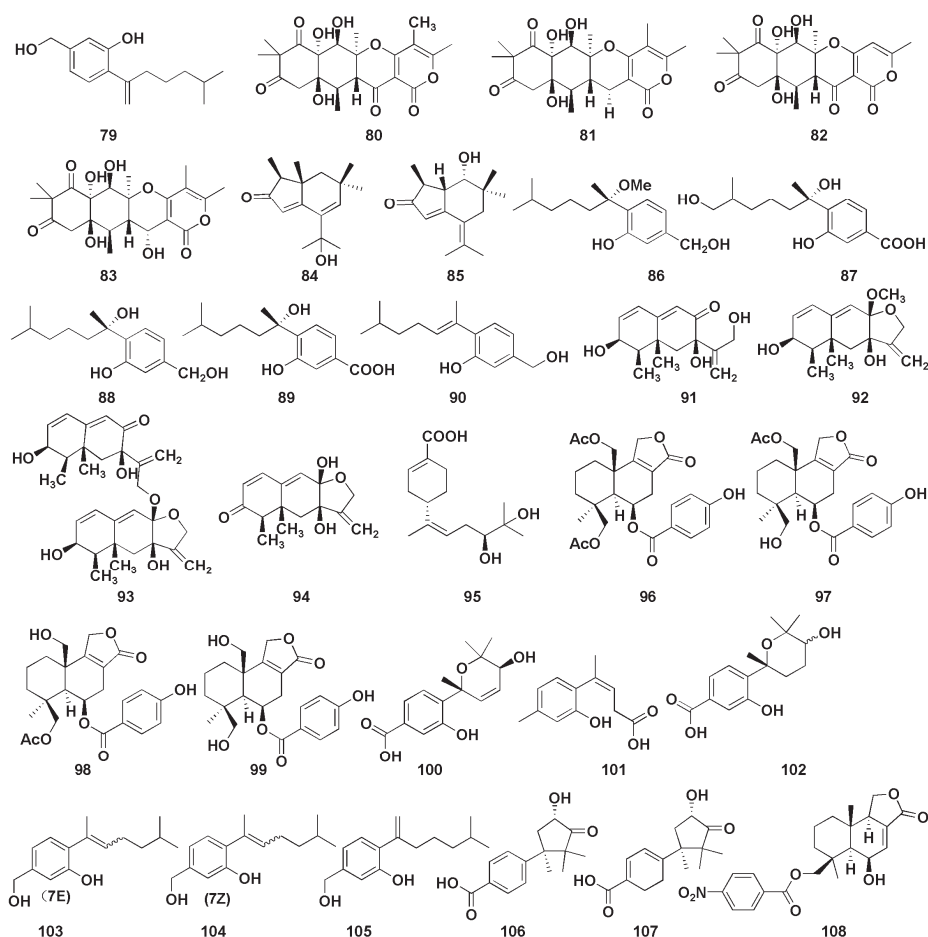


Figure 7. Chemical structures of anti-inflammatory compounds (79–108).

Cui et al. [45] isolated a sesquiterpene derivative (79) from the mangrove endophytic fungus *Aspergillus versicolor* SYSU-SKS025, which was found to inhibit nitric oxide (NO) production RAW 264.7 macrophages, with an IC_{50} value of 12.5 μ M (positive control, indomethacin, IC_{50} = 37.5 μ M). Wang et al. [46] found four triketide-sesquiterpenoids A–D (80–83) from the marine-algal-associated fungus *Aspergillus* sp. ZL0-1B14, which exhibited anti-inflammatory activity in LPS-stimulated RAW264.7 macrophages. In addition, compound 83 inhibited the production of IL-6 with an inhibition rate of 69% at 40 μ M. Wu et al. [47] firstly discovered two brasilane sesquiterpenoids (84–85) with α and β unsaturated ketones from marine-derived fungus *Aspergillus terreus*, both of which showed moderate inhibitory effects; the inhibitory rates of nitric oxide were 47.7% and 37.3%, respectively, at 40 μ M. Chung et al. [48] isolated five sesquiterpenoids (86–90) with anti-inflammatory activity from *Aspergillus sydowii* in marine sediments. Among them, compounds 88 and 90 displayed selective inhibition against fMLP/CB-induced superoxide anion generation by human neutrophils, with IC_{50} values of 5.23 and 6.11 μ M, respectively. At the same time, they also exhibited the most potent inhibitory activity against the release of elastase induced by fMLP/CB, with the IC_{50} values of 16.39 and 8.80 μ M, respectively. Interestingly, the anti-inflammatory activity of compound 88 was better than that of compound 86 indicating the important role of hydroxy group on C-7. Moreover, compounds containing

methylene alcohol on C-3 (**86**, **88**, and **90**) showed more potent anti-inflammatory activity compared with the derivatives with carboxylic acid functional groups (**87** and **89**). Four Eremophilane sesquiterpenoids (**91–94**) were isolated from deep-marine-sediment-derived fungus *Aspergillus* sp. SCS10W2, and all showed inhibitory activity of NO production in a dose-dependent manner [49]. Additionally, five sesquiterpenoids (**95–99**) were isolated from the mangrove endophytic fungus *Aspergillus* sp. GXNU-MA1 by Zhou et al., which exhibited moderate inhibitory activities against NO production, with IC_{50} values ranging from 16.15 to 27.08 μ M [50]. Niu et al. isolated six phenolic bisabolane (**100–105**) and two cuparene sesquiterpenoids (**106–107**) from *Aspergillus sydowii* MCCC3A00324 derived from deep sea sediments [51]. Compounds **100**, **101**, and **103–105** showed anti-inflammatory activity against NO secretion in LPS-activated BV-2 microglia cells, with the inhibition rates of more than 45% at 10 μ M, while those of compounds **102**, **106**, and **107** were 32.8%, 32.6% and 45.4%, respectively. Furthermore, compound **101** exerted an anti-inflammatory effect by inhibiting NF- κ B activation pathway in a dose-dependent manner. Tan et al. isolated a new nitrobenzoyl sesquiterpenoid (**108**) from *Aspergillus ochraceus*, which could suppress the RANKL-induced osteoclasts formation and bone resorption by targeting NF- κ B [52]. Additionally, compound **108** attenuated inflammatory bone loss in vivo.

3.4. Enzymatic Inhibitory Activity

Enzyme inhibitors are of value in treating many diseases in clinical use, and have become a very attractive target for drug development and discovery. In recent years, the prominence of various enzyme inhibitors has been discussed extensively by many researchers in comprehensive systematic reviews [72]. In this section, the inhibitory activities of sesquiterpenoids (Figure 8) from marine *Aspergillus* sp. against three enzymes (α -glucosidase, cholinesterase, and neuraminidase) are briefly reviewed.

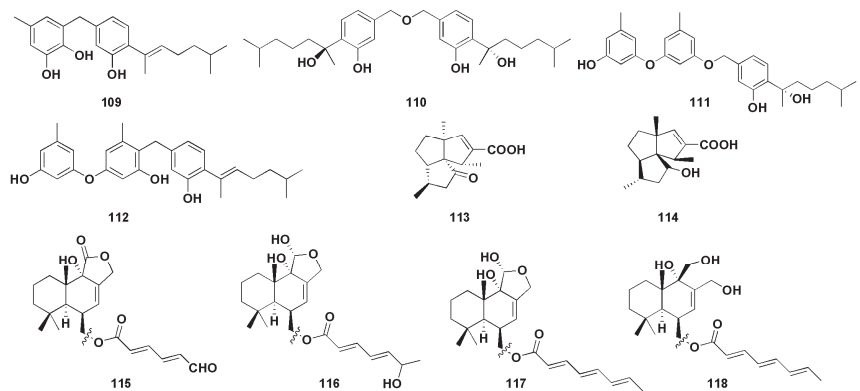


Figure 8. Chemical structures of enzymatic inhibitory compounds (109–118).

α -Glucosidase is a membrane-bound enzyme present in the small intestinal epithelium [73], whose role is to promote the absorption of glucose in the small intestine by catalyzing the hydrolysis of oligosaccharides into absorbable glucose. α -Glucosidase inhibitors are the most widely used drugs in the clinical treatment of diabetes in China. By inhibiting the activity of α -glucosidase, the formation and absorption of glucose can be reduced to achieve the goal of lowering blood glucose. At the same time, it can also reduce the stimulation of blood glucose on the pancreas, effectively preventing and relieving diabetic complications [74]. 7-Deoxy-7,14-didehydroxydonol (**79**) was found from the mangrove endophytic fungus *Aspergillus versicolor* and possessed a significant inhibitory effect on α -glucosidase, with an IC_{50} value of 7.5 μ M (acarbose as 350 μ M), and the terminal ethylene group at C-7 may play a key role in α -glucosidase inhibition activity [45]. Wu et al. [53] isolated four phenolic bisabolane sesquiterpenoids (**109–112**) from the mangrove endophytic

fungus *Aspergillus flavus* QQSG-3. The inhibitory activity studies of α -glucosidase showed that the compounds (**109–112**) had strong inhibitory effects, with IC_{50} values of 4.5, 3.1, 1.5, and 2.3 μ M, respectively (all lower than the positive control drug acarbose).

Alzheimer's Disease (AD) is a degenerative disease with unknown causes, mainly involving cerebral cortical neurons, which is the major cause of dementia [75]. The currently accepted pathogenesis is the cholinergic deficiency hypothesis [76]. Cholinesterase inhibitors (ChEI) are a class of drugs that can bind to cholinesterase (ChE) and inhibit ChE activity; they are also approved as first-line drugs for the treatment of mild-to-moderate AD [77]. Feng et al. firstly isolated the potential reversible cholinesterase inhibitor cyclopentapentalane sesquiterpenoid subergoric (**113**) and its analogues 2-deoxy-2 β -hydroxysubergoric (**114**) from the soft-coral-derived fungus *Aspergillus* sp. EGF15-0-3 [54].

Neuraminidase (NA) is the most critical enzyme for influenza virus replication and diffusion in host cells and has become an important target for anti-influenza virus drug design [78]. Li et al. [55] isolated four drimane sesquiterpenoids (**115–118**) from the ascidian endophytic fungus *Aspergillus ustus* TK-5, which showed significant inhibitory activity against neuraminidase, with IC_{50} values of 31.8, 37.3, 28.4, and 36.8 μ M, respectively. Further results showed that the degree of unsaturation of 11-OH and C-6 linked side chains, which can improve their neuraminidase inhibitory activity.

3.5. Other Activities

Hu et al. isolated an aromatic bisabolane sesquiterpenoid (7S,8S)-8-hydroxysydonic acid (**119**, Figure 9) from the marine red algae endophytic fungus *Aspergillus sydowii* EN-434, which exhibited DPPH free radical scavenging activity, with an IC_{50} value of 113.5 μ M [79]. An et al. found two sesquiterpenoids (**120–121**, Figure 9) with weak DPPH radical scavenging activity, with IC_{50} values of 1.8 mM and 0.6 mM, respectively (V_C as 0.04 mM) [80]. Zhong et al. isolated three sesquiterpenoids (**122–124**, Figure 9) from the marine-offshore-mud-derived fungus *Aspergillus pseudoglaucus* [81]. Among them, compounds **122** and **123** showed strong DPPH radical scavenging activity, with IC_{50} values of 2.42 and 1.86 μ g/mL (V_C was 3.25 μ g/mL), respectively, while compound **124** exhibited moderate antioxidant activity (IC_{50} was 10.89 μ g/mL).

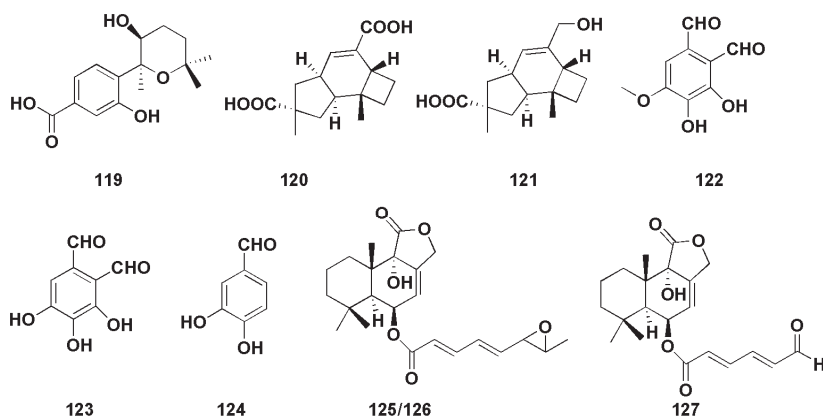


Figure 9. Chemical structures of other biological compounds (**119–127**).

Two bisabolane-type sesquiterpenoids (**4–5**) were derived from sponge-derived fungus *Aspergillus* sp., among which compound **4** completely inhibited larval settlement at 25.0 μ g/mL, while compound **5** displayed an obvious toxic effect on larvae at the same concentration [14]. Compound **7** also showed weak anti- H_3N_2 activity, with IC_{50} values of 57.4 μ M [15]. (–)-(7S)-10-hydroxysydonic acid (**28**) was found to have a mild DPPH radical scavenging activity, with an IC_{50} value of 72.1 μ M [21]. Nitrobenzoyl sesquiterpenoids (**49**) also showed moderate antiviral activities against H_3N_2 and EV71, with IC_{50} values of

17.0 and 9.4 μM , respectively [30]. Liu et al. [82] isolated three drimane sesquiterpenoids (125–127, Figure 9) from the marine-green-alga-derived fungus *Aspergillus ustus*. In the brine shrimp (*Artemia salina*) toxicity assay, there was more than 75% lethality at the concentration of 100 $\mu\text{g}/\text{mL}$, and the LC_{50} values were 41.8, 62.2 and 48.9 $\mu\text{g}/\text{mL}$, respectively.

4. Chemical Synthesis and Biosynthesis of Sesquiterpenoids from Marine *Aspergillus* sp.

4.1. Chemically Induced Synthesis

Aspergillus sp. is the important source for the discovery of natural active products with novel and diverse structures. However, in recent years, the continual study of secondary metabolites of marine fungi has led to a high frequency of repeated discovery of known compounds [83]. This encourages us to develop new strategies to obtain new natural products. Studies have found that a large number of secondary metabolite biosynthesis gene clusters exist in the genome of *Aspergillus* fungi. Furthermore, the genome can be segmented into active and silent clusters, while the silent clusters are inactive under normal environmental conditions [84–86]. In order to obtain more active metabolites, researchers have applied a variety of methods to activate silenced biological genetic gene clusters, such as transcription factor regulation, targeted genome mining, heterologous expression of gene clusters, and chemical epigenetic regulation [87–89]. Because of its simplicity and effectiveness, chemical epigenetic regulation has been widely used in marine fungi to activate silenced gene clusters, which could lead to the production of new secondary metabolites or known components with a higher concentration. Wang et al. [90] cultivated the gorgonian-derived fungus *Aspergillus* sp. SC-20090066 with a DNA methyltransferase inhibitor 5-azacytidine (5-AZA) in the culture medium and led to the isolation of six new bisabolane-type sesquiterpenoids (Figure 10). Among them, compounds (128–130) exhibited broad spectrum activities against *S. aureus*, *Bacillus cereus*, *Rhizophila*, *Pseudomonas putida*, and *Pseudomonas aeruginosa*, with MICs of less than 25 μM . In particular, compound 130 exhibited significant antibacterial activity against *S. aureus*, with MIC value of 3.13 μM , which was close to the positive control ciprofloxacin (MIC value was 2.5 μM). In order to trigger the chemical diversity of marine-derived fungus *Aspergillus versicolor* XS-2009006, epigenetic agents (histone deacetylase inhibitor SAHA and DNA methyltransferase inhibitor 5-AZA) were added to the culture medium by Wu et al. [91] Interestingly, the secondary metabolites was significantly increased and a new bisabolane sesquiterpene aspergillusene E (131, Figure 10) was isolated, which showed anti-larval attachment activity against bryozoan *B. neritina*, with the EC_{50} and (lethal concentration 50%) LC_{50} values of 6.25 $\mu\text{g}/\text{mL}$ and 25 $\mu\text{g}/\text{mL}$, respectively. In addition, compound 131 showed certain antibacterial activities against *Staphylococcus epidermidis* and *S. aureus*, with MIC values ranging from 8 to 16 μM . By adding DNA methyltransferase inhibitors to the medium of *Aspergillus sydowii*, the composition of secondary metabolites was further changed and new bisabolane sesquiterpenoids (86–87) were isolated [48]. In addition, Wang et al. [49] applied chemical epigenetic manipulation to *Aspergillus* sp. SCS10W2 and obtained four eremophilane sesquiterpenes with anti-inflammatory activity (91–94).

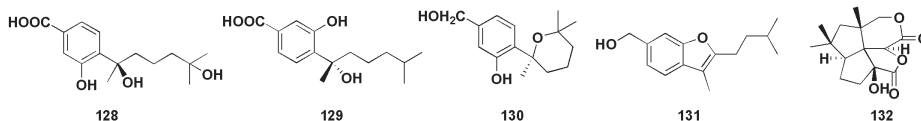


Figure 10. Structures of sesquiterpenoids obtained from chemical synthesis and biosynthesis from the *Aspergillus* sp. (128–132).

4.2. Biosynthetic Pathways

The skeleton structures of sesquiterpenoids were derived from farnesyl diphosphate (FPP) and underwent a series of reaction steps, including intramolecular rearrangement, cyclisation, and other biosynthetic transformations, leading to their structural diversity [92].

Ingavat et al. [93] studied the proposed biosynthesis of sesquiterpene compound **132** in *Aspergillus aculeatus*, which starts from a double-bond migration (C1/C2 to C2/C3) of silphineneene intermediate **2**, and then the double bond of C2/C3 undergoes oxidative cleavage to generate intermediate **3**, which, in turn, undergoes a series of oxidation and lactonizations to finally give **132** (Figure 10).

Wang et al. [46] proposed a biogenetic pathway for the synthesis of aspertetranones A-D (**80–83**). Common drimane-type merosesquiterpene were obtained by cyclization of farnesylated pyrone, followed by oxidation and retro-aldo/aldo rearrangement to produce the unique terpenoid part of aspertetranones. After nucleophilic attack and dehydration, the leaborate preaspertetranone was obtained. Illudalanes derive biosynthetically from a humulene precursor after cyclization, producing a protoilludanes, which is eventually rearranged to form the irudane derivative [94]. According to this report, Orfali et al. speculated a biosynthetic pathway of asperolactone (**41**), in which illudol was a key intermediate. The iluane-type sesquiterpene asperolactone can be synthesized by dehydration, oxidation, and four-membered ring opening [27].

5. Potency of Sesquiterpenoids from Marine *Aspergillus* sp.

Secondary metabolites of microorganisms in the marine environment, mainly derived from marine fungi, are a great source for new drug screening. Currently, the marine drug library includes 15 approved drugs (primarily for cancer treatment), 7 phase I compounds, 12 phase II compounds, and 5 compounds in phase III clinical trials, the latter including a recently recommended drug for symptomatic treatment of COVID-19 (Plitidepsin) [95,96]. Compound **13** displayed significant inhibitory activity against *E. coli* (MIC 1.0 µg/mL), and its antibacterial effect was more potent than that of the positive control chloramphenicol (MIC 2.0 µg/mL), which was expected to be a lead compound for antibiotics [17]. The sesquiterpene compound (**79**) isolated from *Aspergillus versicolor* exhibited better inhibitory effect on α -glucosidase than acarbose, while its anti-inflammatory effect was also stronger than that of indomethacin [45]. Compound **88** derived from marine sediments, showed a significant anti-inflammatory effect and hypoglycemic effect. In addition, compound **88** could also inhibit fat accumulation in adipocytes [48]. These results indicated compound **79** and **88** has the potential to be a lead compound targeting the vicious diabetes-inflammation cycle. Feng et al. found that sesquiterpene compound **113**, the reversible cholinesterase inhibitor, is a promising new drug candidate for the treatment of Alzheimer's Disease and a preclinical trial is already under way [54].

6. Conclusions and Perspective

In this paper, the biosources, bioactivities, structural types, biosynthetic, and pharmacogenic potential of sesquiterpenoids found from marine fungi *Aspergillus* sp. were reviewed. A total of 268 sesquiterpenes were isolated, including 131 bioactive sesquiterpenes, most of which were bisabolanes, followed by drimanes and nitrobenzoyl, etc. Most *Aspergillus* species derived from sponges, marine sediments, algae, mangroves, corals, etc. The main *Aspergillus* species involved are as follows: *Aspergillus fumigatus*, *Aspergillus versicolor*, *Aspergillus flavus*, *Aspergillus ustus*, *Aspergillus sydowii*, and so on. These sesquiterpenes exhibited excellent pharmacological activities such as antibacterial, antitumor, anti-inflammatory, and enzyme inhibitory activities. Additionally, the biosynthesis and total synthesis of sesquiterpenes derived from marine *Aspergillus* sp. have also promoted the in-depth understanding of these sesquiterpenes. Because of the chemical and biological activity of these sesquiterpenoids, it is worthwhile to find promising lead compounds for the development of marine drugs in further studies from marine fungi.

Author Contributions: Conception and design of the manuscript: Z.Z.; conducting literature search and analysis of the information: L.S.; draft and revision of the manuscript: L.S. and H.W.; editing the manuscript: M.Y. and C.S.; finalization and approval of the revised manuscript for submission: Z.Z. and H.W. All authors have read and agreed to the published version of the manuscript.

Funding: This research was funded by the Projects of Medical and Health Technology Development Program in Shandong Province (grant No 2019WS358, 202013050864), Research Fund for Lin He's Academician Workstation of New Medicine and Clinical Translation in Jining Medical University (grant No JYHL2021MS17).

Conflicts of Interest: The authors declare no potential conflict of interest.

References

1. Wang, Y.N.; Meng, L.H.; Wang, B.G. Progress in research on bioactive secondary metabolites from deep-sea derived microorganisms. *Mar. Drugs* **2020**, *18*, 614. [[CrossRef](#)] [[PubMed](#)]
2. Chen, S.H.; Cai, R.L.; Liu, Z.M.; Cui, H.; She, Z.G. Secondary metabolites from mangrove-associated fungi: Source, chemistry and bioactivities. *Nat. Prod. Rep.* **2022**, *39*, 560–595. [[CrossRef](#)]
3. Spitteller, P. Chemical ecology of fungi. *Nat. Prod. Rep.* **2015**, *32*, 971–993. [[CrossRef](#)] [[PubMed](#)]
4. Rateb, M.E.; Ebel, R. Secondary metabolites of fungi from marine habitats. *Nat. Prod. Rep.* **2011**, *28*, 290–344. [[CrossRef](#)]
5. Debbab, A.; Aly, A.H.; Proksch, P. Bioactive secondary metabolites from endophytes and associated marine derived fungi. *Fungal Divers.* **2011**, *49*, 1–12. [[CrossRef](#)]
6. Liu, B.; Tang, Z.J.; Chen, N.; Xu, Y.; Ji, Y.B. Research progress of butyrolactones isolated from marine-derived *Aspergillus* sp. *Chin. J. Mar. Drugs* **2021**, *40*, 59–70.
7. Numata, A.; Takahashi, C.; Matsushita, T.; Miyamoto, T.; Kawai, K.; Usami, Y.; Matsumura, E.; Inoue, M.; Ohishi, H. Fumiquinolines, novel metabolites of a fungus isolated from a saltfish. *Tetrahedron Lett.* **1992**, *33*, 1621–1624. [[CrossRef](#)]
8. Zhao, C.Y.; Liu, H.S.; Zhu, W.M. New natural products from the marine-derived *Aspergillus* fungi—a review. *Acta Microbiol. Sin.* **2016**, *56*, 331–362.
9. Ebel, R. Terpenes from marine-derived fungi. *Mar. Drugs* **2010**, *8*, 2340–2368. [[CrossRef](#)]
10. Elissawy, A.M.; El-Shazly, M.; Ebada, S.S.; Singab, A.B.; Proksch, P. Bioactive terpenes from marine-derived fungi. *Mar. Drugs* **2015**, *13*, 1966–1992. [[CrossRef](#)]
11. Shin, H.J. Natural products from marine fungi. *Mar. Drugs* **2020**, *18*, 230. [[CrossRef](#)]
12. Fraga, B.M. Natural sesquiterpenoids. *Nat. Prod. Rep.* **2012**, *29*, 1334–1366. [[CrossRef](#)]
13. Zhao, W.Y.; Yi, J.; Chang, Y.B.; Sun, C.P.; Ma, X.C. Recent studies on terpenoids in *Aspergillus* fungi: Chemical diversity, biosynthesis, and bioactivity. *Phytochemistry* **2022**, *193*, 113011. [[CrossRef](#)]
14. Li, D.; Xu, Y.; Shao, C.L.; Yang, R.Y.; Zheng, C.J.; Chen, Y.Y.; Fu, X.M.; Qian, P.Y.; She, Z.G.; de Voogd, N.J.; et al. Antibacterial bisabolane-type sesquiterpenoids from the sponge-derived fungus *Aspergillus* sp. *Mar. Drugs* **2012**, *10*, 234–241. [[CrossRef](#)]
15. Wang, J.F.; Lin, X.P.; Qin, C.; Liao, S.; Wan, J.T.; Zhang, T.Y.; Liu, J.; Fredimoses, M.; Chen, H.; Yang, B.; et al. Antimicrobial and antiviral sesquiterpenoids from sponge-associated fungus, *Aspergillus sydowii* ZSDS1-F6. *J. Antibiot.* **2014**, *67*, 581–583. [[CrossRef](#)]
16. Chen, Y.; Zhu, H.Y.; Xu, L.C.; Wang, S.P.; Liu, S.; Liu, G.D.; Luo, W.H.; Cao, G.Y.; Zhang, Z.X. Antimicrobial and cytotoxic phenolic bisabolane sesquiterpenoids from the fungus *Aspergillus flavipes* 297. *Fitoterapia* **2021**, *155*, 105038. [[CrossRef](#)]
17. Li, X.D.; Li, X.; Li, X.M.; Yin, X.L.; Wang, B.G. Antimicrobial bisabolane-type sesquiterpenoids from the deep-sea sediment-derived fungus *Aspergillus versicolor* SD-330. *Nat. Prod. Res.* **2021**, *35*, 4265–4271. [[CrossRef](#)]
18. Liu, Y.J.; Zhang, J.L.; Li, C.; Mu, X.G.; Liu, X.L.; Wang, L.; Zhao, Y.C.; Zhang, P.; Li, X.D.; Zhang, X.X. Antimicrobial secondary metabolites from the seawater-derived fungus *Aspergillus sydowii* SW9. *Molecules* **2019**, *24*, 4596. [[CrossRef](#)]
19. Li, X.D.; Li, X.M.; Yin, X.L.; Li, X.; Wang, B.G. Antimicrobial sesquiterpenoid derivatives and monoterpenoids from the deep-sea sediment-derived fungus *Aspergillus versicolor* SD-330. *Mar. Drugs* **2019**, *17*, 563. [[CrossRef](#)]
20. Wei, M.Y.; Wang, C.Y.; Liu, Q.A.; Shao, C.L.; She, Z.G.; Lin, Y.C. Five sesquiterpenoids from a marine-derived fungus *Aspergillus* sp. isolated from a gorgonian *Dichotella gemmacea*. *Mar. Drugs* **2010**, *8*, 941–949. [[CrossRef](#)]
21. Wang, P.; Yu, J.H.; Zhu, K.K.; Wang, Y.Y.; Cheng, Z.Q.; Jiang, C.S.; Dai, J.G.; Wu, J.; Zhang, H. Phenolic bisabolane sesquiterpenoids from a Thai mangrove endophytic fungus, *Aspergillus* sp. xy02. *Fitoterapia* **2018**, *27*, 322–327. [[CrossRef](#)]
22. Liu, S.; Dai, H.; Konuklugil, B.; Orfali, R.S.; Lin, W.H.; Kalscheuer, R.; Liu, Z.; Proksch, P. Phenolic bisabolanes from the sponge-derived fungus *Aspergillus* sp. *Phytochem Lett.* **2016**, *18*, 187–191. [[CrossRef](#)]
23. Liu, X.H.; Miao, F.P.; Li, X.D.; Yin, X.L.; Ji, N.Y. A new sesquiterpene from an endophytic *Aspergillus versicolor* strain. *Nat. Prod. Commun.* **2012**, *7*, 819–820. [[CrossRef](#)]
24. Fang, S.T.; Liu, X.H.; Yan, B.F.; Miao, F.P.; Yin, X.L.; Li, W.Z.; Ji, N.Y. Terpenoids from the marine-derived fungus *Aspergillus* sp. RR-YLW-12, associated with the Red alga *Rhodomela confervoides*. *J. Nat. Prod.* **2021**, *84*, 1763–1771. [[CrossRef](#)]
25. Zheng, C.J.; Shao, C.L.; Wang, K.L.; Zhao, D.L.; Wang, Y.N. Secondary metabolites and their bioactivities of a soft coral-derived fungus *Aspergillus versicolor*(ZJ-2008015). *Chin. J. Mar. Drugs* **2012**, *31*, 7–13.

26. Cohen, E.; Koch, L.; Thu, K.M.; Rahamim, Y.; Aluma, Y.; Ilan, M.; Yarden, O.; Carmeli, S. Novel terpenoids of the fungus *Aspergillus insuetus* isolated from the Mediterranean sponge *Psammodinia* sp. collected along the coast of Israel. *Bioorg. Med. Chem.* **2011**, *19*, 6587–6593. [\[CrossRef\]](#)
27. Orfali, R.; Perveen, S.; Khan, M.F.; Ahmed, A.F.; Wadaan, M.A.; Al-Taweel, A.M.; Alqahtani, A.S.; Nasr, F.A.; Tabassum, S.; Luciano, P.; et al. Antiproliferative illudalane sesquiterpenes from the marine sediment ascomycete *Aspergillus oryzae*. *Mar. Drugs* **2021**, *19*, 333. [\[CrossRef\]](#)
28. Liu, Y.F.; Yue, Y.F.; Feng, L.X.; Zhu, H.J.; Cao, F. Asperienes A-D, bioactive sesquiterpenes from the marine-derived fungus *Aspergillus flavus*. *Mar. Drugs* **2019**, *17*, 550. [\[CrossRef\]](#)
29. Yurchenko, A.N.; Trinh, P.T.H.; Girich, E.V.; Smetanina, O.F.; Rasin, A.B.; Popov, R.S.; Dyshlovoy, S.A.; von Amsberg, G.; Menchinskaya, E.S.; Van, T.T.T.; et al. Biologically active metabolites from the marine sediment-derived fungus *Aspergillus flocculosus*. *Mar. Drugs* **2019**, *17*, 579. [\[CrossRef\]](#)
30. Fang, W.; Lin, X.P.; Zhou, X.F.; Wan, J.T.; Lu, X.; Yang, B.; Ai, W.; Lin, J.; Zhang, T.Y.; Tu, Z.C.; et al. Cytotoxic and antiviral nitrobenzoyl sesquiterpenoids from the marine-derived fungus *Aspergillus ochraceus* Jcma1F17. *Med. Chem. Comm.* **2014**, *5*, 701–705. [\[CrossRef\]](#)
31. Zhao, H.Y.; Anbuezhian, R.; Sun, W.; Shao, C.L.; Zhang, F.L.; Yin, Y.; Yu, Z.S.; Li, Z.Y.; Wang, C.Y. Cytotoxic nitrobenzoyloxy-substituted sesquiterpenes from sponge derived endozoic fungus *Aspergillus insulicola* MD10-2. *Curr. Pharm. Biotechnol.* **2016**, *17*, 271–274. [\[CrossRef\]](#)
32. Tan, Y.H.; Yang, B.; Lin, X.P.; Luo, X.W.; Pang, X.Y.; Tang, L.; Liu, Y.H.; Li, X.J.; Zhou, X.F. Nitrobenzoyl sesquiterpenoids with cytotoxic activities from a marine-derived *Aspergillus ochraceus* fungus. *J. Nat. Prod.* **2018**, *81*, 92–97. [\[CrossRef\]](#)
33. Sun, C.X.; Liu, X.Y.; Sun, N.; Zhang, X.M.; Shah, M.; Zhang, G.J.; Che, Q.; Zhu, T.J.; Li, J.; Li, D.H. Cytotoxic nitrobenzoyl sesquiterpenoids from an antarctica sponge-derived *Aspergillus insulicola*. *J. Nat. Prod.* **2022**, *85*, 987–996. [\[CrossRef\]](#)
34. Liu, H.B.; Edrada-Ebel, R.; Ebel, R.; Wang, Y.; Schulz, B.; Draeger, S.; Muller, W.E.G.; Wray, V.; Lin, W.H.; Proksch, P. Drimane sesquiterpenoids from the fungus *Aspergillus ustus* isolated from the marine sponge *Suberites domuncula*. *J. Nat. Prod.* **2009**, *72*, 1585–1588. [\[CrossRef\]](#)
35. Zhou, H.N.; Zhu, T.J.; Cai, S.X.; Gu, Q.Q.; Li, D.H. Drimane sesquiterpenoids from the mangrove-derived fungus *Aspergillus ustus*. *Chem. Pharm. Bull.* **2011**, *59*, 762–766. [\[CrossRef\]](#)
36. Sun, L.L.; Shao, C.L.; Chen, J.F.; Guo, Z.Y.; Fu, X.M.; Chen, M.; Chen, Y.Y.; Li, R.; de Voogd, N.J.; She, Z.G.; et al. New bisabolane sesquiterpenoids from a marine-derived fungus *Aspergillus* sp. isolated from the sponge *Xestospongia testudinaria*. *Bioorg. Med. Chem. Lett.* **2012**, *22*, 1326–1329. [\[CrossRef\]](#)
37. Liu, S.; Wang, H.; Su, M.; Hwang, G.J.; Hong, J.; Jung, J.H. New metabolites from the sponge-derived fungus *Aspergillus sydowii* J05B-7F-4. *Nat. Prod. Res.* **2017**, *31*, 1682–1686. [\[CrossRef\]](#)
38. Deng, C.M.; Huang, C.H.; Wu, Q.L.; Pang, J.Y.; Lin, Y.C. A new sesquiterpene from the mangrove endophytic fungus *Aspergillus terreus* (No. GX7-3B). *Nat. Prod. Res.* **2013**, *27*, 1882–1887. [\[CrossRef\]](#)
39. Liu, D.S.; Huang, Y.L.; Li, C.M.; Ma, L.Y.; Pan, X.H.; Ferreira, D.; Liu, W.Z. A new sesquiterpenoid derivative from the coastal saline soil fungus *Aspergillus fumigatus*. *Rec. Nat. Prod.* **2016**, *10*, 708–713.
40. Kitano, M.; Yamada, T.; Amagata, T.; Minoura, K.; Tanaka, R.; Numata, A. Novel pyridino- α -pyrone sesquiterpene type pileotin produced by a sea urchin-derived *Aspergillus* sp. *Tetrahedron Lett.* **2012**, *53*, 4192–4194. [\[CrossRef\]](#)
41. Lu, Z.Y.; Wang, Y.; Miao, C.D.; Liu, P.P.; Hong, K.; Zhu, W.M. Sesquiterpenoids and benzofuranoids from the marine-derived fungus *Aspergillus ustus* 094102. *J. Nat. Prod.* **2009**, *72*, 1761–1767. [\[CrossRef\]](#)
42. Proksch, P.; Ebel, R.; Edrada, R.; Riebe, F.; Liu, H.; Diesel, A.; Bayer, M.; Li, X.; Lin, W.H.; Grebenyuk, V.; et al. Sponge-associated fungi and their bioactive compounds: The *Suberites* case. *Bot. Mar.* **2008**, *51*, 209–218. [\[CrossRef\]](#)
43. Wang, Y.; Li, D.H.; Li, Z.L.; Sun, Y.J.; Hua, H.M.; Liu, T.; Bai, J. Terpenoids from the marine-derived fungus *Aspergillus fumigatus* YK-7. *Molecules* **2015**, *21*, 31. [\[CrossRef\]](#)
44. Xu, L.C.; Liu, G.D.; Chen, Y.; Liu, S.; Luo, W.H.; Hu, P.F.; Huang, C.M.; Ji, X.; Wang, S.P.; Cao, G.Y. Cytotoxic drimane-type sesquiterpenoids from the fungus *Aspergillus flavipes* 297. *Rec. Nat. Prod.* **2021**, *16*, 488–492. [\[CrossRef\]](#)
45. Cui, H.; Liu, Y.N.; Li, T.M.; Zhang, Z.R.; Ding, M.; Long, Y.H.; She, Z.G. 3-Arylisoidolinone and sesquiterpene derivatives from the mangrove endophytic fungi *Aspergillus versicolor* SYSU-SKS025. *Fitoterapia* **2018**, *124*, 177–181. [\[CrossRef\]](#)
46. Wang, Y.Z.; Qi, S.; Zhan, Y.; Zhang, N.W.; Wu, A.A.; Gui, F.; Guo, K.; Yang, Y.R.; Cao, S.G.; Hu, Z.Y.; et al. Aspertetranones A-D, putative meroterpenoids from the marine algal-associated fungus *Aspergillus* sp. ZL0-1b14. *J. Nat. Prod.* **2015**, *78*, 2405–2410. [\[CrossRef\]](#)
47. Wu, Z.D.; Li, D.Y.; Zeng, F.R.; Tong, Q.Y.; Zheng, Y.Y.; Liu, J.J.; Zhou, Q.; Li, X.N.; Chen, C.M.; Lai, Y.J.; et al. Brasilane sesquiterpenoids and dihydrobenzofuran derivatives from *Aspergillus terreus* [CFCC 81836]. *Phytochemistry* **2018**, *156*, 159–166. [\[CrossRef\]](#)
48. Chung, Y.M.; Wei, C.K.; Chuang, D.W.; El-Shazly, M.; Hsieh, C.T.; Asai, T.; Oshima, Y.; Hsieh, T.J.; Hwang, T.L.; Wu, Y.C.; et al. An epigenetic modifier enhances the production of anti-diabetic and anti-inflammatory sesquiterpenoids from *Aspergillus sydowii*. *Bioorgan. Med. Chem.* **2013**, *21*, 3866–3872. [\[CrossRef\]](#)
49. Wang, L.Y.; Li, M.J.; Tang, J.Q.; Li, X.F. Eremophilane sesquiterpenes from a deep marine-derived fungus, *Aspergillus* sp. SCSIO2, cultivated in the presence of epigenetic modifying agents. *Molecules* **2016**, *21*, 473. [\[CrossRef\]](#)

50. Zhou, D.X.; Zhang, W.X.; Hao, L.L.; Qin, X.Y.; Yang, R.Y.; Li, J.; Huang, X.S. A new sesquiterpene from mangrove endophytic fungus *Aspergillus* sp. GXNU-MA1. *Nat. Prod. Res.* **2022**, *36*, 1857–1863. [[CrossRef](#)]
51. Niu, S.W.; Yang, L.H.; Zhang, G.Y.; Chen, T.T.; Hong, B.H.; Pei, S.X.; Shao, Z.Z. Phenolic bisabolane and cuparene sesquiterpenoids with anti-inflammatory activities from the deep-sea-derived *Aspergillus sydowii* MCCC 3A00324 fungus. *Bioorg. Chem.* **2020**, *105*, 104420. [[CrossRef](#)] [[PubMed](#)]
52. Tan, Y.H.; Deng, W.D.; Zhang, Y.Y.; Ke, M.H.; Zou, B.H.; Luo, X.W.; Su, J.B.; Wang, Y.Y.; Xu, J.L.; Nandakumar, K.S.; et al. A marine fungus-derived nitrobenzoyl sesquiterpenoid suppresses receptor activator of NF- κ B ligand-induced osteoclastogenesis and inflammatory bone destruction. *Br. J. Pharmacol.* **2020**, *177*, 4242–4260. [[CrossRef](#)] [[PubMed](#)]
53. Wu, Y.N.; Chen, Y.; Huang, X.S.; Pan, Y.H.; Liu, Z.M.; Yan, T.; Cao, W.H.; She, Z.G. α -Glucosidase inhibitors: Diphenyl ethers and phenolic bisabolane sesquiterpenoids from the mangrove endophytic fungus *Aspergillus flavus* QSG-3. *Mar. Drugs* **2018**, *16*, 307. [[CrossRef](#)]
54. Feng, C.; Wei, X.; Hu, J.S.; Wang, S.Y.; Liu, B.X.; Xie, Z.Y.; Rong, L.; Li, X.H.; Zhang, C.X. Researches on the subergane-type sesquiterpenes from the soft coral-derived fungus *Aspergillus* sp. EGF15-0-3. *Chin. J. Org. Chem.* **2020**, *40*, 1275–1280. [[CrossRef](#)]
55. Li, L.; Li, X.M.; Li, H.L.; Belma, K.; Li, X.; Wang, B.G. Chemical constituents of *Aspergillus ustus* TK-5, an endophytic fungus derived from the ascidian *Herdmania momus*. *Mar. Sci.* **2018**, *42*, 130–137.
56. Dai, Q.; Zhang, F.L.; Feng, T. Sesquiterpenoids specially produced by fungi: Structures, biological activities, chemical and biosynthesis (2015–2020). *J. Fungi* **2021**, *7*, 1026. [[CrossRef](#)]
57. Fu, J.; Li, F.H.; Li, C.K.; Li, B.M.; Chen, R.Y.; Kang, J. Reviews on natural monocyclic sesquiterpenoids and their bioactivities. *China J. Chin. Mater. Med.* **2019**, *44*, 3672–3683.
58. Zhang, Y.H.; Xu, Y.; Wang, C.Y.; Cao, F. Alkaloids and sesquiterpenoids from the marine-derived fungus *Aspergillus versicolor*. *Chem. Nat. Compd.* **2020**, *56*, 971–973. [[CrossRef](#)]
59. Liu, N.Z.; Peng, S.; Yang, J.; Cong, Z.W.; Lin, X.P.; Liao, S.R.; Yang, B.; Zhou, X.F.; Zhou, X.J.; Liu, Y.H.; et al. Structurally diverse sesquiterpenoids and polyketides from a sponge-associated fungus *Aspergillus sydowii* SCSIO41301. *Fitoterapia* **2019**, *135*, 27–32. [[CrossRef](#)]
60. Pang, X.Y.; Lin, X.P.; Zhou, X.F.; Yang, B.; Tian, X.P.; Wang, J.F.; Xu, S.H.; Liu, Y.H. New quinoline alkaloid and bisabolane-type sesquiterpenoid derivatives from the deep-sea-derived fungus *Aspergillus* sp. SCSIO06786. *Fitoterapia* **2020**, *140*, 104406. [[CrossRef](#)]
61. Trisuwan, K.; Rukachaisirikul, V.; Kaewpet, M.; Phongpaichit, S.; Hutadilok-Towatana, N.; Preedanon, S.; Sakayaroj, J. Sesquiterpene and xanthone derivatives from the sea fan-derived fungus *Aspergillus sydowii* PSU-F154. *J. Nat. Prod.* **2011**, *74*, 1663–1667. [[CrossRef](#)]
62. Zhuravleva, O.I.; Afiyatullo, S.S.; Denisenko, V.A.; Ermakova, S.P.; Slinkina, N.N.; Dmitrenko, P.S.; Kim, N.Y. Secondary metabolites from a marine-derived fungus *Aspergillus carneus* Blochwitz. *Phytochemistry* **2012**, *80*, 123–131. [[CrossRef](#)] [[PubMed](#)]
63. Weigel, L.M.; Donlan, R.M.; Shin, D.H.; Jensen, B.; Clark, N.C.; McDougal, L.K.; Zhu, W.M.; Musser, K.A.; Thompson, J.; Kohlerschindt, D.; et al. High-level vancomycin-resistant *Staphylococcus aureus* isolates associated with a polymicrobial biofilm. *Antimicrob. Agents Chemother.* **2007**, *51*, 231–238. [[CrossRef](#)]
64. Chen, C.Y.; Shen, Y.C.; Chen, Y.J.; Sheu, J.H.; Duh, C.Y. Bioactive sesquiterpenes from a Taiwanese marine sponge *Parahigginsia* sp. *J. Nat. Prod.* **1999**, *62*, 573–576. [[CrossRef](#)] [[PubMed](#)]
65. Mcenroe, F.J.; Fenical, W. Structures and synthesis of some new antibacterial sesquiterpenoids from the gorgonian coral *Pseudopterogorgia rigida*. *Tetrahedron* **1978**, *34*, 1661–1664. [[CrossRef](#)]
66. Mulhaupt, T.; Kaspar, H.; Otto, S.; Reichert, M.; Bringmann, G.; Lindel, T. Isolation, structural elucidation, and synthesis of curcutetraol. *Eur. J. Org. Chem.* **2005**, *2005*, 334–341. [[CrossRef](#)]
67. Montaser, R.; Luesch, H. Marine natural products: A new wave of drugs? *Future Med. Chem.* **2011**, *3*, 1475–1489. [[CrossRef](#)] [[PubMed](#)]
68. Temraz, A. Novel illudalane sesquiterpenes from *Encephalartos villosus* Lehm. antimicrobial activity. *Nat. Prod. Res.* **2016**, *30*, 2791–2797. [[CrossRef](#)]
69. Kwon, J.; Lee, H.; Seo, Y.H.; Yun, J.; Lee, J.; Kwon, H.C.; Guo, Y.Q.; Kang, J.S.; Kim, J.J.; Lee, D. Cytotoxic drimane sesquiterpenoids isolated from *Perenniporia maackiae*. *J. Nat. Prod.* **2018**, *81*, 1444–1450. [[CrossRef](#)]
70. Liu, C.; Lou, W.; Zhu, Y.; Nadiminty, N.; Schwartz, C.T.; Evans, C.P. Niclosamide inhibits androgen receptor variants expression and overcomes enzalutamide resistance in castration-resistant prostate cancer. *Clin. Cancer Res.* **2014**, *20*, 3198–3210. [[CrossRef](#)]
71. Arulseelan, P.; Fard, M.T.; Tan, W.S.; Gothai, S.; Fakurazi, S.; Norhaizan, M.E.; Kumar, S.S. Role of antioxidants and natural products in inflammation. *Oxid. Med. Cell Longev.* **2016**, *2016*, 5276130. [[CrossRef](#)] [[PubMed](#)]
72. Orhan, I.E. Enzyme inhibitors as the attractive targets for the treatment of various diseases. *Curr. Med. Chem.* **2019**, *26*, 3206–3207. [[CrossRef](#)] [[PubMed](#)]
73. Amin, S.; Ullah, B.; Ali, M.; Rauf, A.; Khan, H.; Uriarte, E.; Sobarzo-Sanchez, E. Potent in vitro α -glucosidase inhibition of secondary metabolites derived from dryopteris cycadina. *Molecules* **2019**, *24*, 427. [[CrossRef](#)] [[PubMed](#)]
74. Liu, Z.; Ma, S. Recent advances in synthetic α -glucosidase inhibitors. *Chem. Chem.* **2017**, *12*, 819–829. [[CrossRef](#)] [[PubMed](#)]
75. Khan, S.; Barve, K.H.; Kumar, M.S. Recent advancements in pathogenesis, diagnostics and treatment of Alzheimer’s disease. *Curr. Neuropharmacol.* **2020**, *18*, 1106–1125. [[CrossRef](#)] [[PubMed](#)]
76. Francis, P.T. The interplay of neurotransmitters in Alzheimer’s disease. *CNS Spectr.* **2005**, *10*, 6–9. [[CrossRef](#)]

77. Bono, G.F.; Simao-Silva, D.P.; Batistela, M.S.; Josviak, N.D.; Dias, P.F.R.; Nascimento, G.A.; Souza, R.L.R.; Piovezan, M.R.; Souza, R.K.M.; Furtado-Alle, L. Butyrylcholinesterase: K variant, plasma activity, molecular forms and rivastigmine treatment in Alzheimer's disease in a Southern Brazilian population. *Neurochem. Int.* **2015**, *81*, 57–62. [[CrossRef](#)]
78. Air, G.M. Influenza neuraminidase. *Influenza Other Resp.* **2012**, *6*, 245–256. [[CrossRef](#)]
79. Hu, X.Y.; Li, X.M.; Meng, L.H.; Wang, B.G. Antioxidant bisabolane-type sesquiterpenoids from algal-derived fungus *Aspergillus sydowii* EN-434. *J. Oceanol. Limnol.* **2020**, *38*, 1532–1536. [[CrossRef](#)]
80. An, C.L.; Kong, F.D.; Ma, Q.Y.; Xie, Q.Y.; Yuan, J.Z.; Zhou, L.M.; Dai, H.F.; Yu, Z.F.; Zhao, Y.X. Chemical constituents of the marine-derived fungus *Aspergillus* sp. SCS-KFD66. *Mar. Drugs* **2018**, *16*, 468. [[CrossRef](#)]
81. Zhong, M.J.; Kang, H.H.; Ma, L.Y.; Liu, D.S.; Liu, W.Z. Study on the secondary metabolites from *Aspergillus pseudoglaucus* derived from offshore mud in Dandong. *Chin. J. Mar. Drugs* **2021**, *40*, 16–22.
82. Liu, X.H.; Miao, F.P.; Qiao, M.F.; Cichewicz, R.H.; Ji, N.Y. Terretinin, ophiobolin, and drimane terpenes with absolute configurations from an algicolous *Aspergillus ustus*. *RSC Adv.* **2013**, *3*, 588–595. [[CrossRef](#)]
83. Penesyan, A.; Kjelleberg, S.; Egan, S. Development of novel drugs from marine surface associated microorganisms. *Mar. Drugs* **2010**, *8*, 438–459. [[CrossRef](#)] [[PubMed](#)]
84. Keller, N.P. Fungal secondary metabolism: Regulation, function and drug discovery. *Nat. Rev. Microbiol.* **2019**, *17*, 167–180. [[CrossRef](#)]
85. Slot, J.C. Fungal gene cluster diversity and evolution. *Adv. Genet.* **2017**, *100*, 141–178.
86. Lind, A.L.; Wisecaver, J.H.; Lameiras, C.; Wiemann, P.; Palmer, J.M.; Keller, N.P.; Rodrigues, F.; Goldman, G.H.; Rokas, A. Drivers of genetic diversity in secondary metabolic gene clusters within a fungal species. *PLoS Biol.* **2017**, *15*, e2003583. [[CrossRef](#)]
87. Rutledge, P.J.; Challis, G.L. Discovery of microbial natural products by activation of silent biosynthetic gene clusters. *Nat. Rev. Microbiol.* **2015**, *13*, 509–523. [[CrossRef](#)]
88. Li, X.Y.; Awakawa, T.; Mori, T.; Ling, M.Q.; Hu, D.; Wu, B.; Abe, I. Heterodimeric non-heme iron enzymes in fungal meroterpenoid biosynthesis. *J. Am. Chem. Soc.* **2021**, *143*, 21425–21432. [[CrossRef](#)]
89. Guo, Z.; Zou, Z.M. Discovery of new secondary metabolites by epigenetic regulation and NMR comparison from the plant endophytic fungus monosporascus eutypoides. *Molecules* **2020**, *25*, 4192. [[CrossRef](#)]
90. Wang, C.Y.; Liu, Y.F.; Cao, F.; Wang, C.Y. Bisabolane-type sesquiterpenoids from a gorgonian-derived *Aspergillus* sp fungus induced by DNA methyltransferase inhibitor. *Chem. Nat. Compd.* **2016**, *52*, 1129–1132. [[CrossRef](#)]
91. Wu, J.S.; Yao, G.S.; Shi, X.H.; Rehman, S.U.; Xu, Y.; Fu, X.M.; Zhang, X.L.; Liu, Y.; Wang, C.Y. Epigenetic agents trigger the production of bioactive nucleoside derivatives and bisabolane sesquiterpenes from the marine-derived fungus *Aspergillus versicolor*. *Front. Microbiol.* **2020**, *11*, 85. [[CrossRef](#)] [[PubMed](#)]
92. Adekenov, S.M. Sesquiterpene lactones with unusual structure. Their biogenesis and biological activity. *Fitoterapia* **2017**, *121*, 16–30. [[CrossRef](#)] [[PubMed](#)]
93. Ingavat, N.; Mahidol, C.; Ruchirawat, S.; Kittakoop, P. Asperaculin A, a sesquiterpenoid from a marine-derived fungus, *Aspergillus aculeatus*. *J. Nat. Prod.* **2011**, *74*, 1650–1652. [[CrossRef](#)] [[PubMed](#)]
94. Morisaki, N.; Furukawa, J.; Kobayashi, H.; Iwasaki, S.; Nozoe, S. Cyclobutyl cation rearrangements of 6-protoilluden-8 α -ol, 7-protoilluden-6-ol and related compounds. *Chem. Pharm. Bull.* **1987**, *35*, 2678–2685. [[CrossRef](#)]
95. White, K.M.; Rosales, R.; Yildiz, S.; Kehrer, T.; Miorin, L.; Moreno, E.; Jangra, S.; Uccellini, M.B.; Rathnasinghe, R.; Coughlan, L.; et al. Plitidepsin has potent preclinical efficacy against SARS-CoV-2 by targeting the host protein eEF1A. *Science* **2021**, *371*, 926–931. [[CrossRef](#)]
96. Tagliatalata-Scafati, O. New hopes for drugs against COVID-19 come from the sea. *Mar. Drugs* **2021**, *19*, 104. [[CrossRef](#)]

Article

Molecular Cloning, Expression, and Functional Analysis of Glycosyltransferase (TbUGGT) Gene from *Trapa bispinosa* Roxb.

Shijie Ye ¹, Dongjie Yin ¹, Xiaoyan Sun ¹, Qinyi Chen ¹, Ting Min ², Hongxun Wang ¹ and Limei Wang ^{1,*}¹ College of Life Science and Technology, Wuhan Polytechnic University, Wuhan 430023, China² College of Food Science and Engineering, Wuhan Polytechnic University, Wuhan 430023, China

* Correspondence: wanglimeix@whpu.edu.cn; Tel.: +86-27-8395-6793

Abstract: *Trapa bispinosa* Roxb. is an economical crop for medicine and food. Its roots, stems, leaves, and pulp have medicinal applications, and its shell is rich in active ingredients and is considered to have a high medicinal value. One of the main functional components of the *Trapa bispinosa* Roxb. shell is 1-galloyl-beta-D-glucose (β G), which can be used in medical treatment and is also an essential substrate for synthesizing the anticancer drug beta-penta-o-Galloyl-glucosin (PGG). Furthermore, gallate 1-beta-glucosyltransferase (EC 2.4.1.136) has been found to catalyze gallic acid (GA) and uridine diphosphate glucose (UDPG) to synthesize β G. In our previous study, significant differences in β G content were observed in different tissues of *Trapa bispinosa* Roxb. In this study, *Trapa bispinosa* Roxb. was used to clone 1500 bp of the UGGT gene, which was named TbUGGT, to encode 499 amino acids. According to the specificity of the endogenous expression of foreign genes in *Escherichia coli*, the adaptation codon of the cloned original genes was optimized for improved expression. Bioinformatic and phylogenetic tree analyses revealed the high homology of TbUGGT with squalene synthases from other plants. The TbUGGT gene was constructed into a PET-28a expression vector and then transferred into *Escherichia coli* Transsetta (DE3) for expression. The recombinant protein had a molecular weight of 55 kDa and was detected using SDS-PAGE. The proteins were purified using multiple fermentation cultures to simulate the intracellular environment, and a substrate was added for *in vitro* reaction. After the enzymatic reaction, the levels of β G in the product were analyzed using HPLC and LC-MS, indicating the catalytic activity of TbUGGT. The cloning and functional analysis of TbUGGT may lay the foundation for further study on the complete synthesis of β G in *E. coli*.

Citation: Ye, S.; Yin, D.; Sun, X.; Chen, Q.; Min, T.; Wang, H.; Wang, L. Molecular Cloning, Expression, and Functional Analysis of Glycosyltransferase (TbUGGT) Gene from *Trapa bispinosa* Roxb. *Molecules* **2022**, *27*, 8374. <https://doi.org/10.3390/molecules27238374>

Academic Editors: Giovanni Ribauda and Lucia Panzella

Received: 13 October 2022

Accepted: 22 November 2022

Published: 30 November 2022

Publisher's Note: MDPI stays neutral with regard to jurisdictional claims in published maps and institutional affiliations.



Copyright: © 2022 by the authors. Licensee MDPI, Basel, Switzerland. This article is an open access article distributed under the terms and conditions of the Creative Commons Attribution (CC BY) license (<https://creativecommons.org/licenses/by/4.0/>).

Keywords: *Trapa bispinosa* Roxb.; TbUGGT; molecular cloning; expression analysis

1. Introduction

Trapa bispinosa Roxb. is an annual herbaceous floating plant belonging to Myrtle's *Trapa bispinosa* family and is mainly distributed in tropical and temperate regions [1,2]. Ripe *Trapa bispinosa* Roxb. has a hard deep red shell and creamy white flesh with a sweet taste. It can be used to treat common diseases, such as gastric ulcers, esophageal cancer, and dysentery [3]. The fruit hulls are rich in phenols and flavonoids and have been extensively studied. The extracts from *Trapa bispinosa* Roxb. shell contain many phenolic compounds, such as gallic acid, caffeic acid, naringin, and 1,2,3,4,6-pentagalacyl- β -D-glucose [4–6]. These phenolic compounds have specific physiological antioxidant, anti-inflammatory, and anticancer properties [7–10]. *Trapa bispinosa* Roxb. chestnut is native to Europe and Asia but is only cultivated in China and India [11]. The plant exists in most water bodies in China but is considered one of the aquatic specialties of the Hubei Province and has high economic value.

The compound 1-galloyl-beta-D-glucose (β G) exists in plants such as oak leaves, *Trapa bispinosa* Roxb., and pomegranate and possesses a variety of pharmacological activi-

ties. Studies have shown that β G is a noncytotoxic and selective AKR1B1 inhibitor of aldose reductase, which can protect against oxidative stress and treat secondary complications of diabetes [12]. In a previous study, the protective properties of β G and its mitochondrial antioxidative mechanism reduced the effects of oxidative stress in glaucoma [13]. In Raw 267.4 macrophages, β G prevented LPS-induced activation of JNK and p38 and lowered ROS levels [14]. APRE-19 cells pretreated with β G demonstrated decreased apoptosis induced by retinal microglia [15]. Furthermore, β G inhibited the activation of the NLRP3 and TLR4/NF- κ B pathways and decreased the expression of pro-inflammatory cytokines, protecting against LPS-induced sepsis in mice and reducing organ toxicity [16]. The substance has a wide range of applications in clinical practice, but β G is primarily produced via plant extraction, which does not yield high quantities. Therefore, chemical synthesis methods are also being developed but are in opposition to the green concept of modern production. At the same time, biosynthesis has become a popular method for material acquisition. In this study, we aim to develop a β G production method using biosynthesis to meet the medical application demand.

Glycosyltransferase (EC 2.4.x.y) is an enzyme that can transfer activated glycol groups to other small-molecule compounds to complete glycosylation reactions [17]. UGT is a soluble enzyme in plants, with UDPG being the leading sugar donor [18]. According to the different substrate small molecules, the UGT family can be divided into UGGT with gallic acid as the substrate and UDP-glucose with flavonoids as the substrate, such as flavonoid 3-glucosyltransferase (UFGT) [19], etc. UGGT plays an essential role in catalyzing the formation of β G in plant tannin biosynthesis.

U-glutamyl transpeptidase (UGGT) catalyzes the synthesis of β G from gallic acid (GA) and uridine diphosphate glucose (UDPG) [20]. In some higher plants, GA is synthesized via the shikimic acid pathway and converts 3-dehydroshikimic acid to 3,5-dehydroshikimic acid through aroDE enzymes. In addition, 3,5-dehydroshikimic acid can be spontaneously converted to GA via enolization [21–23]. Figure 1 displays the chemical reaction scheme for β G synthesis.

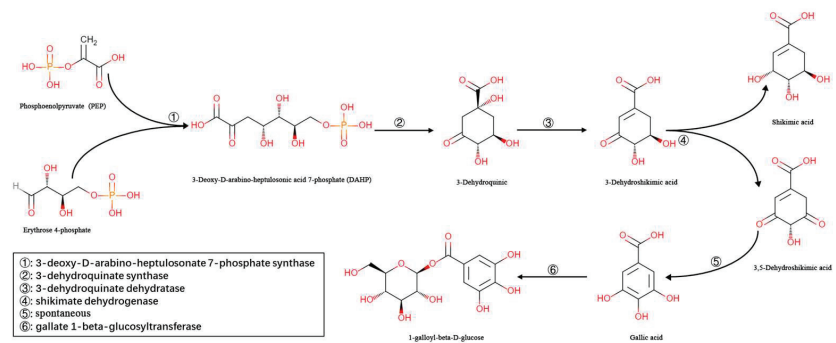


Figure 1. Biosynthesis of β G in some higher plants.

Our previous research study identified this substance in *Trapa bispinosa* Roxb., with varying amounts in different tissues [24]. So far, most of the studies on *Trapa bispinosa* Roxb. have focused on the separation and pharmacological effects of active monomer compounds. However, the specific biosynthetic mechanism of the active components of *Trapa bispinosa* Roxb. has rarely been explored. Currently, the secondary metabolites identified in *Trapa bispinosa* Roxb. contain multiple types of galacyl glucose, using the biosynthetic β G of galacyl glucose as the substrate. However, the gene for its synthesis has not been reported.

The TbUGGT gene sequence was obtained with gene annotation and screening using transcriptomics technology. After codon optimization, the recombinant expression vector was constructed and expressed in *Escherichia coli*, and the enzyme activity was determined. This study lays the foundation for future research on the complete synthesis of β G in *Escherichia coli*.

2. Results

2.1. *TbUGGT* Gene Cloning and Sequence Analysis

The β G biosynthesis pathway starts from phosphoenolpyruvate and D-erythrose 4-phosphate (Figure 2a). Combined with the transcriptome data of *Trapa bispinosa* Roxb., the Unigene expression belonging to this pathway detected using RNA-Seq was analyzed and displayed with a heat map (Figure 2b). A total of 44 Unigenes belonging to this pathway were identified using the transcriptome, which was involved in four genes of the pathway, namely, 3-deoxy-D-Arabino-Heptulosonate 7-phosphate synthase (EC 2.5.1.54), 3-dehydroquininate synthase (EC4.2.3.4), 3-Dehydroquininate dehydratase/Shikimate dehydrogenase (EC 4.2.1.10/EC 1.1.1.25), and gallate 1-beta-glucosyltransferase (EC 2.4.1.136). The primary glycosyltransferase gene *TbUGGT* (CL7060.4) was obtained.

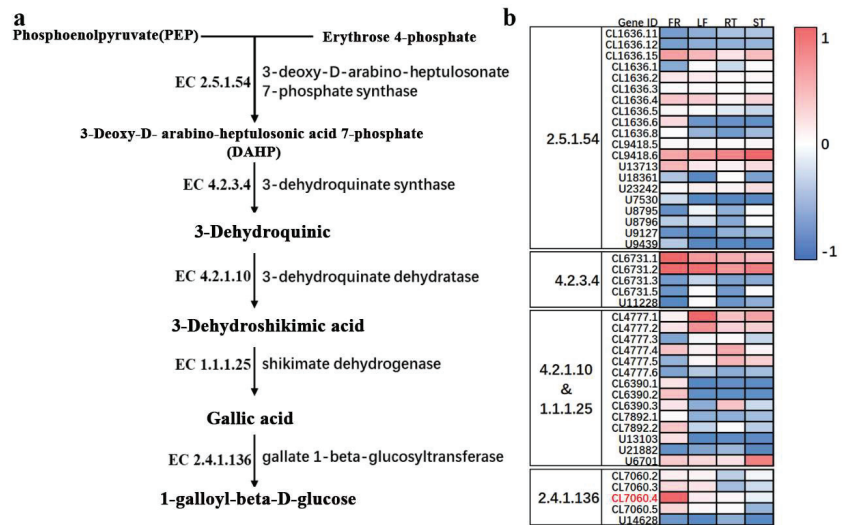


Figure 2. β G biosynthesis pathway (a) and the expression of related genes (b).

The *Trapa bispinosa* Roxb. transferase gene *TbUGGT* was amplified with PCR using specific primers and the preferred codon optimization of *Escherichia coli*. The gene had a total length of 1500 bp, encoding 499 amino acids. The molecular weight of the protein sequence predicted using ProtParam was about 55.8 kDa and was an unstable hydrophilic protein.

qRT-PCR was used to detect the expression pattern of *TbUGGT* and identify the expression of the *TbUGGT* gene in different tissues of *Trapa bispinosa* Roxb., namely, shell (FR), leaf (LR), stem (ST), and root (RT) (Figure 3). Apparent differences in transcription levels were observed in different parts, the highest being shell (FR) expression, and the root (RT) expression being the second. In contrast, the stem (ST) and leaf (LR) yielded relatively low expressions.

According to the conservative structural domain analysis (Figure S1 Supplementary Material), CD Search predicted that the *TbUGGT* protein belonged to the glycosyltransferase_GTB-Type (PLN02555) superfamily with a domain range of 1aa–473aa (Figure S1a). ScanProsite predicted that the protein belonged to the UDP Glycosyltransferases superfamily with a domain range of 343aa–386aa (Figure S1b), while Pfam predicted that the protein belonged to the UDPGT family. The domain range was 238aa–423aa (Figure S1c). ProtScale indicated that the *TbUGGT* protein was hydrophilic (Figure S2). The signal peptide prediction showed no signal peptides in this protein, and the probability of amino acids in each point appearing outside the membrane was close to 1, demonstrating a low probability to appear in the transmembrane region. Therefore, this protein was not a membrane or secreted protein (Figure S3).

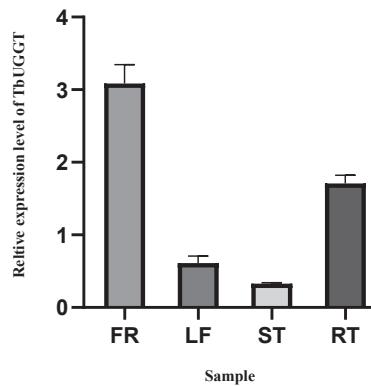


Figure 3. Differential expression of TbUGGT:TbUGGT in different growth sites, including shell (FR), leaf (LR), stem (ST), and root (RT).

2.2. Structure and Phylogenetic Analyses

SOPMA showed that the secondary structure of the TbUGGT protein sequence contained α helices (blue), extended chains (red), β rotations (green), and random curls (purple), accounting for 40.48%, 14.23%, 4.21%, and 41.08%, respectively (Figure S4). The protein structure of TbUGGT was predicted using AlphaFold2, in which the model pLDDT was as high as 91.8. (Figure 4a). pLDDT \geq 90 means that the residue has very high model confidence, which the model can use for later molecular docking analyses. The homology modeling structure was analyzed using PyMOL software (Figure 4b). The docking results between the protein model and the substrate GA molecule showed a binding energy of -6.3 . A smaller binding energy indicated a tighter binding between the receptor and the ligand. Visualization revealed that the binding sites were mainly concentrated in Glu at position 139, in Ile at position 143, in Cys at position 145, and in Lys at position 218.

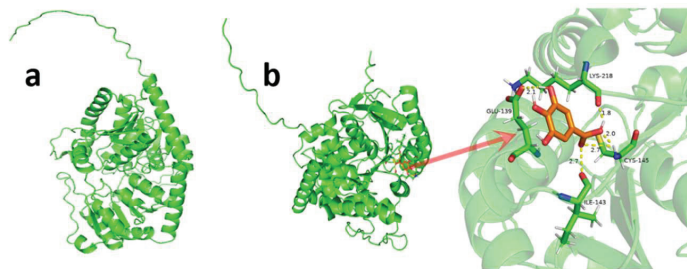


Figure 4. AlphaFold2 predicted TbUGGT protein structure model (a) and PyMOL software molecular docking results (b).

In the homology analysis of the TbUGGT protein sequence, the compared species included *Punica granatum*, *Syzygium oleosum*, *Eucalyptus Grandis*, *Corymbia Citriodora* subsp. *Variegata*, *Eucalyptus Camaldulensis*, *Rhodamnia argentea*, *Juglans regia*, *Carya illinoensis*, and *Vitis Vinifera*. The results showed a similarity of 87.60% between the protein and the compared sequence (Figure 5). About 44 amino acid residues in the blue underlined part of Figure 5 correspond to the conservative domain PSPG of glycosyltransferase [25], which is the binding region of glycosyl donors, suggesting that the cloned gene was the UDP glycosyltransferase gene.

KAF8013769.1 [<i>Corymbia citriodora</i> subsp.ubsp. variegata]	MGSDAESIIVHDIISFFOGHVNLLRLGKRLASKGLLVTFEFSIGKMRKASNIIDDEEPIFGCGIRFEFFFDGWDDBEQRDLDLQ	90
XP 010028410.1 [<i>Eucalyptustus grandis</i>]	MGSDAESIIVHDIISFFOGHVNLLRLGKRLASKGLLVTFEFSIGKMRKASNIIDDEEPIFGCGIRFEFFFDGWDDBEQRDLDLQ	90
XP 030523235.1 [<i>Rhodamnia argentea</i>]	MGSDAESIIVHDIISFFOGHVNLLRLGKRLASKGLLVTFEFSIGKMRKASNIIDDEEPIFGCGIRFEFFFDGWDDBEQRDLDLQ	90
XP 030445800.1 [<i>Syzygium oleosum</i>]	MGSESILVHVHDIISFFOGHVNLLRLGKRLASKGLLVTFEFSIGKMRKASNIIDDEEPIFGCGIRFEFFFDGWDDBEQRDLDLQ	89
XP 031382117.1 [<i>Punicaica granatum</i>]	MGSESILVHVHDIISFFOGHVNLLRLGKRLASKGLLVTFEFSIGKMRKASNIIDDEEPIFGCGIRFEFFFDGWDDBEQRDLDLQ	89
UGGT [<i>Trapa bispinosa</i> Roxb.]	MGSESILVHVHDIISFFOGHVNLLRLGKRLASKGLLVTFEFSIGKMRKASNIIDDEEPIFGCGIRFEFFFDGWDDBEQRDLDLQ	89
BBB21213.1 [<i>Eucalyptus camaldulensis</i>]	MGSEAIVHVHDIISFFOGHVNLLRLGKRLASKGLLVTFEFSIGKMRKASNIIDDEEPIFGCGIRFEFFFDGWDDBEQRDLDLQ	88
XP 002285379.1 [<i>Vitis vinifera</i>]	MGSESILVHVHDIISFFOGHVNLLRLGKRLASKGLLVTFEFSIGKMRKASNIIDDEEPIFGCGIRFEFFFDGWDDBEQRDLDLQ	88
KAG7977068.1 [<i>Caryaya illinoensis</i>]	MGSEAIVHVHDIISFFOGHVNLLRLGKRLASKGLLVTFEFSIGKMRKASNIIDDEEPIFGCGIRFEFFFDGWDDBEQRDLDLQ	88
XP 018827666.1 [<i>Juglans regia</i>]	MGSEAIVHVHDIISFFOGHVNLLRLGKRLASKGLLVTFEFSIGKMRKASNIIDDEEPIFGCGIRFEFFFDGWDDBEQRDLDLQ	88
Consensus	m vhv l sfp qghvnllrlgkrlaskglvtf tp sigk mrkasni iddee pfgc girfeff fdgwd bde qrdldlq	
KAF8013769.1 [<i>Corymbia citriodora</i> subsp.ubsp. variegata]	YLPOLEKRVKLVLEEMIRRRABQRGRSCLINNFPIFWSVDVAGSLGLPSAMLVQSCACAAIYYVYHVLVFFPFSAMEIDQLPFW	180
XP 010028410.1 [<i>Eucalyptustus grandis</i>]	YLPOLEKRVKLVLEEMIRRRABQRGRSCLINNFPIFWSVDVAGSLGLPSAMLVQSCACAAIYYVYHVLVFFPFSAMEIDQLPFW	180
XP 030523235.1 [<i>Rhodamnia argentea</i>]	YLPOLEKRVKLVLEEMIRRRABQRGRSCLINNFPIFWSVDVAGSLGLPSAMLVQSCACAAIYYVYHVLVFFPFSAMEIDQLPFW	180
XP 030445800.1 [<i>Syzygium oleosum</i>]	YLPOLEKRVKLVLEEMIRRRABQRGRSCLINNFPIFWSVDVAGSLGLPSAMLVQSCACAAIYYVYHVLVFFPFSAMEIDQLPFW	180
XP 031382117.1 [<i>Punicaica granatum</i>]	YLPOLEKRVKLVLEEMIRRRABQRGRSCLINNFPIFWSVDVAGSLGLPSAMLVQSCACAAIYYVYHVLVFFPFSAMEIDQLPFW	179
UGGT [<i>Trapa bispinosa</i> Roxb.]	YLPOLEKRVKLVLEEMIRRRABQRGRSCLINNFPIFWSVDVAGSLGLPSAMLVQSCACAAIYYVYHVLVFFPFSAMEIDQLPFW	179
BBB21213.1 [<i>Eucalyptus camaldulensis</i>]	YLPOLEKRVKLVLEEMIRRRABQRGRSCLINNFPIFWSVDVAGSLGLPSAMLVQSCACAAIYYVYHVLVFFPFSAMEIDQLPFW	178
XP 002285379.1 [<i>Vitis vinifera</i>]	YLPOLEKRVKLVLEEMIRRRABQRGRSCLINNFPIFWSVDVAGSLGLPSAMLVQSCACAAIYYVYHVLVFFPFSAMEIDQLPFW	179
KAG7977068.1 [<i>Caryaya illinoensis</i>]	YLPOLEKRVKLVLEEMIRRRABQRGRSCLINNFPIFWSVDVAGSLGLPSAMLVQSCACAAIYYVYHVLVFFPFSAMEIDQLPFW	178
XP 018827666.1 [<i>Juglans regia</i>]	YLPOLEKRVKLVLEEMIRRRABQRGRSCLINNFPIFWSVDVAGSLGLPSAMLVQSCACAAIYYVYHVLVFFPFSAMEIDQLPFW	178
Consensus	ylpplk rkv l v l e e m i r r r a b q r g r s c l i n n f p i f w s v d v a g s l g l p s a m l v q s c a c a a i y y h v l v f f p f s a m e i d q l p f w	
KAF8013769.1 [<i>Corymbia citriodora</i> subsp.ubsp. variegata]	LLKLDVFSFLYPTPYFFLIRRAIGQVNLDRPFCCILDTPQLEDEIIEVSKRPIKRVGPELKNRFRANRNGDGRKADDCIWM	269
XP 010028410.1 [<i>Eucalyptustus grandis</i>]	LLKLDVFSFLYPTPYFFLIRRAIGQVNLDRPFCCILDTPQLEDEIIEVSKRPIKRVGPELKNRFRANRNGDGRKADDCIWM	269
XP 030523235.1 [<i>Rhodamnia argentea</i>]	LLKLDVFSFLYPTPYFFLIRRAIGQVNLDRPFCCILDTPQLEDEIIEVSKRPIKRVGPELKNRFRANRNGDGRKADDCIWM	269
XP 030445800.1 [<i>Syzygium oleosum</i>]	LLKLDVFSFLYPTPYFFLIRRAIGQVNLDRPFCCILDTPQLEDEIIEVSKRPIKRVGPELKNRFRANRNGDGRKADDCIWM	269
XP 031382117.1 [<i>Punicaica granatum</i>]	LLKLDVFSFLYPTPYFFLIRRAIGQVNLDRPFCCILDTPQLEDEIIEVSKRPIKRVGPELKNRFRANRNGDGRKADDCIWM	269
UGGT [<i>Trapa bispinosa</i> Roxb.]	LLKLDVFSFLYPTPYFFLIRRAIGQVNLDRPFCCILDTPQLEDEIIEVSKRPIKRVGPELKNRFRANRNGDGRKADDCIWM	269
BBB21213.1 [<i>Eucalyptus camaldulensis</i>]	LLKLDVFSFLYPTPYFFLIRRAIGQVNLDRPFCCILDTPQLEDEIIEVSKRPIKRVGPELKNRFRANRNGDGRKADDCIWM	267
XP 002285379.1 [<i>Vitis vinifera</i>]	LLKLDVFSFLYPTPYFFLIRRAIGQVNLDRPFCCILDTPQLEDEIIEVSKRPIKRVGPELKNRFRANRNGDGRKADDCIWM	268
KAG7977068.1 [<i>Caryaya illinoensis</i>]	LLKLDVFSFLYPTPYFFLIRRAIGQVNLDRPFCCILDTPQLEDEIIEVSKRPIKRVGPELKNRFRANRNGDGRKADDCIWM	267
XP 018827666.1 [<i>Juglans regia</i>]	LLKLDVFSFLYPTPYFFLIRRAIGQVNLDRPFCCILDTPQLEDEIIEVSKRPIKRVGPELKNRFRANRNGDGRKADDCIWM	267
Consensus	llk ld v f s f l y p t p y f f l i r r a i g q v n l d r p f c c i l d t p q l e d e i e v s k r p i k r v g p e l k n r f r a n r n g d g r k a d d c i w m	
KAF8013769.1 [<i>Corymbia citriodora</i> subsp.ubsp. variegata]	LSKRPASVIVSFGSVYVLRGQDDEIAGLINSQELVWVWKPPHKGGCTVILPEGGEKAGDGRKVVWSFGQVLAHSAVAFV	359
XP 010028410.1 [<i>Eucalyptustus grandis</i>]	LSKRPASVIVSFGSVYVLRGQDDEIAGLINSQELVWVWKPPHKGGCTVILPEGGEKAGDGRKVVWSFGQVLAHSAVAFV	359
XP 030523235.1 [<i>Rhodamnia argentea</i>]	LSKRPASVIVSFGSVYVLRGQDDEIAGLINSQELVWVWKPPHKGGCTVILPEGGEKAGDGRKVVWSFGQVLAHSAVAFV	359
XP 030445800.1 [<i>Syzygium oleosum</i>]	LSKRPASVIVSFGSVYVLRGQDDEIAGLINSQELVWVWKPPHKGGCTVILPEGGEKAGDGRKVVWSFGQVLAHSAVAFV	359
XP 031382117.1 [<i>Punicaica granatum</i>]	LSKRPASVIVSFGSVYVLRGQDDEIAGLINSQELVWVWKPPHKGGCTVILPEGGEKAGDGRKVVWSFGQVLAHSAVAFV	358
UGGT [<i>Trapa bispinosa</i> Roxb.]	LSKRPASVIVSFGSVYVLRGQDDEIAGLINSQELVWVWKPPHKGGCTVILPEGGEKAGDGRKVVWSFGQVLAHSAVAFV	359
BBB21213.1 [<i>Eucalyptus camaldulensis</i>]	LSKRPASVIVSFGSVYVLRGQDDEIAGLINSQELVWVWKPPHKGGCTVILPEGGEKAGDGRKVVWSFGQVLAHSAVAFV	357
XP 002285379.1 [<i>Vitis vinifera</i>]	LSKRPASVIVSFGSVYVLRGQDDEIAGLINSQELVWVWKPPHKGGCTVILPEGGEKAGDGRKVVWSFGQVLAHSAVAFV	358
KAG7977068.1 [<i>Caryaya illinoensis</i>]	LSKRPASVIVSFGSVYVLRGQDDEIAGLINSQELVWVWKPPHKGGCTVILPEGGEKAGDGRKVVWSFGQVLAHSAVAFV	357
XP 018827666.1 [<i>Juglans regia</i>]	LSKRPASVIVSFGSVYVLRGQDDEIAGLINSQELVWVWKPPHKGGCTVILPEGGEKAGDGRKVVWSFGQVLAHSAVAFV	357
Consensus	l s k r p a s v i v s f g s v y l v r g q d d e i a g l i n s q e l v w v w k p p h k g g c t v i l p e g g e k a g d g r k v v w s f g q v l a h s a v a f v	
KAF8013769.1 [<i>Corymbia citriodora</i> subsp.ubsp. variegata]	THCGWNSBEIDASGMPVAFPPQWGDQVTDAYLVLEFKRCMRGCEABNTITRQVHCILREATGSKABEERANALRGAABAAV	449
XP 010028410.1 [<i>Eucalyptustus grandis</i>]	THCGWNSBEIDASGMPVAFPPQWGDQVTDAYLVLEFKRCMRGCEABNTITRQVHCILREATGSKABEERANALRGAABAAV	449
XP 030523235.1 [<i>Rhodamnia argentea</i>]	THCGWNSBEIDASGMPVAFPPQWGDQVTDAYLVLEFKRCMRGCEABNTITRQVHCILREATGSKABEERANALRGAABAAV	449
XP 030445800.1 [<i>Syzygium oleosum</i>]	THCGWNSBEIDASGMPVAFPPQWGDQVTDAYLVLEFKRCMRGCEABNTITRQVHCILREATGSKABEERANALRGAABAAV	449
XP 031382117.1 [<i>Punicaica granatum</i>]	THCGWNSBEIDASGMPVAFPPQWGDQVTDAYLVLEFKRCMRGCEABNTITRQVHCILREATGSKABEERANALRGAABAAV	448
UGGT [<i>Trapa bispinosa</i> Roxb.]	THCGWNSBEIDASGMPVAFPPQWGDQVTDAYLVLEFKRCMRGCEABNTITRQVHCILREATGSKABEERANALRGAABAAV	449
BBB21213.1 [<i>Eucalyptus camaldulensis</i>]	THCGWNSBEIDASGMPVAFPPQWGDQVTDAYLVLEFKRCMRGCEABNTITRQVHCILREATGSKABEERANALRGAABAAV	448
XP 002285379.1 [<i>Vitis vinifera</i>]	THCGWNSBEIDASGMPVAFPPQWGDQVTDAYLVLEFKRCMRGCEABNTITRQVHCILREATGSKABEERANALRGAABAAV	448
KAG7977068.1 [<i>Caryaya illinoensis</i>]	THCGWNSBEIDASGMPVAFPPQWGDQVTDAYLVLEFKRCMRGCEABNTITRQVHCILREATGSKABEERANALRGAABAAV	447
XP 018827666.1 [<i>Juglans regia</i>]	THCGWNSBEIDASGMPVAFPPQWGDQVTDAYLVLEFKRCMRGCEABNTITRQVHCILREATGSKABEERANALRGAABAAV	447
Consensus	thcgwns b e i d a s g m p v a f p p q w g d q v t d a y l v l e f k r c m r g c e a b n t i t r q v h c i l r e a t g s k a b e e r a n a l r g a a b a a v	
KAF8013769.1 [<i>Corymbia citriodora</i> subsp.ubsp. variegata]	AEGSSDRNCRIDEVRRSFEVALAKSGK.STVWEAP.....EVVKEAATD..KRVESVS.	504
XP 010028410.1 [<i>Eucalyptustus grandis</i>]	AEGSSDRNCRIDEVRRSFEVALAKSGK.STVWEAP.....AVVKEAATN..KRVELDS.	505
XP 030523235.1 [<i>Rhodamnia argentea</i>]	AEGSSDRNCRIDEVRRSFEVALAKSGK.STVWEAP.....EAVRGAATN..KRVELSS.	505
XP 030445800.1 [<i>Syzygium oleosum</i>]	VEGSSDRNCRIDEVRRSFEVALAKSAAAVVVEAP.....EAVRGAATN..KRVELSS.	506
XP 031382117.1 [<i>Punicaica granatum</i>]	VEGSSDRNCRIDEVRRSFEITAKSFAVKAAPNGVVA.....AEVSVETKAN..KRVELAA.	508
UGGT [<i>Trapa bispinosa</i> Roxb.]	VEGSSDRNCRIDEVRRSFEVLAASFAAAAEPTAA.....DANGVEVFN.....	499
BBB21213.1 [<i>Eucalyptus camaldulensis</i>]	AEGSSDRNCRIDEVRRSFEVLAASGKSTAN.....DANLGEVFN..KRVELWS.	499
XP 002285379.1 [<i>Vitis vinifera</i>]	AEGSSDRNCRIDEVRRSFEVLCVSKKLI.....	479
KAG7977068.1 [<i>Caryaya illinoensis</i>]	AEGSSDRNCRIDEVRRSFEALTRSTNGVEDFANKSATN...GLADLVELRKNDWNLVVS	510
XP 018827666.1 [<i>Juglans regia</i>]	AEGSSDRNCRIDEVRRSFEALTRSTNGVEDFANKSATN...GLADLVELRKNDWNLVVS	510
Consensus	eggssdrn i dev s	

Figure 5. Comparison of TbUGGT amino acid sequences obtained from GenBank. The species, protein names, and GenBank accession number of the aligned sequences are as follows: *Corymbia Citriodora* subsp. variegata (KAF8013769.1); *Eucalyptustus grandis* (XP 01 0028410.1); *Rhodamnia argentea* (XP 030523235.1); *Syzygium oleosum* (XP 030445800.1); *Punicaica granatum* (XP 031382117.1); *Eucalyptus Camaldulensis* (BBB21213.1); *Vitis Vinifera* (XP 002285379.1); *Caryaya illinoensis* (KAG7977068.1); *Juglans regia* (XP 018827666.1).

MEGA was used to discuss the phylogenetic relationship between TbUGGT protein sequences and the corresponding proteins in different species. The UGT amino acid sequences of 20 plants were downloaded from the GenBank database for a cluster analysis (Figure 6). Higher scores indicated a closer relationship (the maximum score was 100). The closest relationship occurred between *Trapa bispinosa* Roxb. and pomegranate.

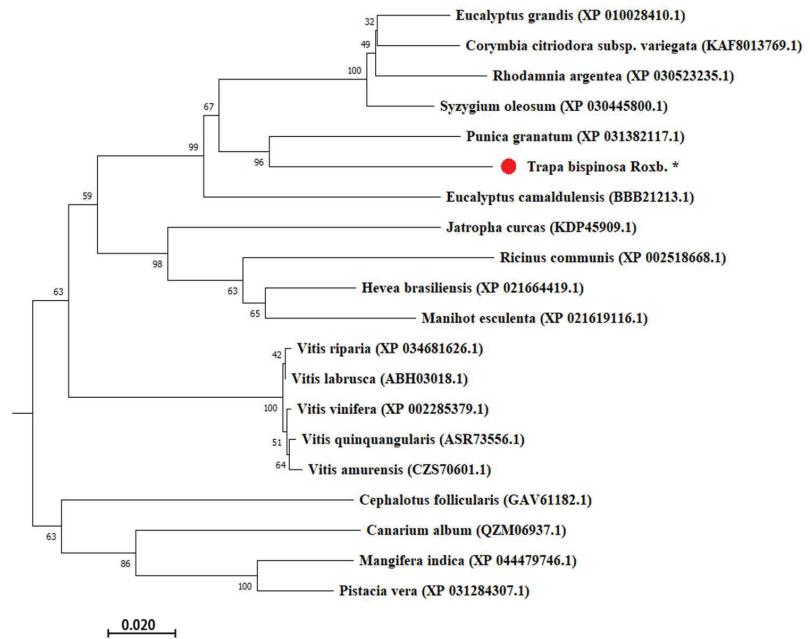


Figure 6. Phylogenetic tree of TbUGGT from various species. ● *Trapa bispinosa* Roxb.*: The target gene TbUGGT in this study. The species, protein names, and GenBank accession number are *Eucalyptus Grandis* (XP010028410.1), *Corymbia Citriodora* subsp. *Variegata* (KAF8013769.1), *Vitis amurensis* (CZS70601.1), *Syzygium oleosum* (XP030445800.1), *Punica granatum* (XP031382117.1), *Eucalyptus Camaldulensis* (BBB21213.1), *Jatropha curcas* (KDP45909.1), *Ricinus communis* (XP002518668.1), *Hevea brasiliensis* (XP021664419.1), *Manihot esculenta* (XP 021619116.1), *Vitis Riparia* (XP 034681626.1), *Vitis labrusca* (ABH03018.1), *Vitis Vinifera* (XP002285379.1), *Vitis quinquangularis* (ASR73556.1), *Rhodamnia argentea* (XP030523235.1), *Cephalotus follicularis* (GAV61182.1), *Canarium album* (QZM06937.1), *Mangifera indica* (XP044479746.1), and *Pistacia vera* (XP031284307.1).

2.3. Prokaryotic Expression of TbUGGT

To obtain the recombinant expression strain, the recombinant plasmid PET-28a-Tbuggt was transformed into the *Escherichia coli* BL21(DE3) expression strain after colony PCR identification. IPTG was used as the inducer to induce fusion protein expression, and the bands were verified using SDS-PAGE electrophoresis (Figure 7a). Compared with the blank control group, specific protein bands of about 55 kDa (theoretically predicted value of 59.6 kDa) appeared in the experimental group, as indicated by the arrow in the figure.

Furthermore, the recombinant protein was purified with mass culture to eliminate the interference of other proteins, and the bacteria and the bacterial liquid were detected using SDS-PAGE (Figure 7b). The target protein band appeared in the bacterial lane at around 55 kDa, while the protein band did not appear in the bacterial liquid lane, indicating that the protein was expressed in *Escherichia coli*. However, the expressed proteins were mainly concentrated in the bacterial solution, and most of them existed in the form of inclusion bodies, which were broken to release the proteins. SDS-PAGE was used to detect the protein before and after purification (Figure 7b), and the target protein bands appeared at about 55 kDa, indicating that the protein was successfully expressed and purified in *Escherichia coli*.

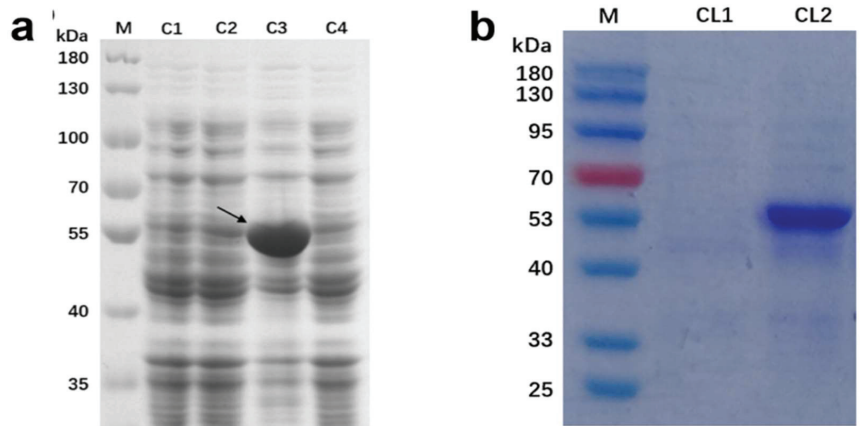


Figure 7. SDS-PAGE results of whole bacterial protein of recombinant strain containing pET-28a-TbUGGT (a) and SDS-PAGE results of purified protein (b). (a) Lane M, protein marker; Lane C1, non-induced whole bacterial protein containing recombinant plasmid; Lane C2, non-induced whole bacterial protein containing empty vector; Lane C3, whole bacterial protein containing recombinant plasmid after induction; Lane C4, whole bacterial protein containing empty carrier after induction. (b) Lane M, protein marker; Lane CL1, supernatant before bacterial fragmentation; Lane CL2, purified protein concentrate.

2.4. Determination of Enzyme Activity of TbUGGT Protein In Vitro

The standard substances of β G, GA, and UDPG were detected under unified-liquid-phase conditions. The liquid-phase detection results (Figure 8) showed that the retention times of the three reference substances were 2.487 min for GA, 7.662 min for UDPG, and 6.662 min for β G. The experimental group showed a signal peak at 6.700, with a retention time similar to that of standard β G, indicating the successful production of β G. In order to confirm that the produced substance was indeed β G, LC-MS was used to verify the material composition of the sample and the blank control (Figure 9). The results showed contrast peaks at 7.28 min~7.90 min. There were β G characteristic ion fragments in the mass spectrum at 7.52 min $m/z = 331.06760$. The molecular formula was $C_{13}H_{15}O_{10}$, and the molecular formula of β G is $C_{13}H_{15}O_{10}$, which aligned with the negative ion scanning situation.

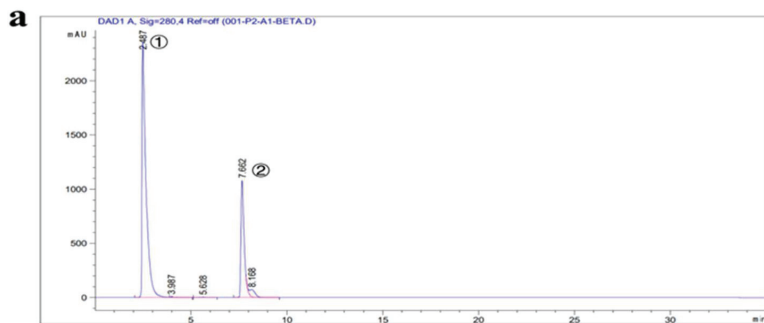


Figure 8. Cont.

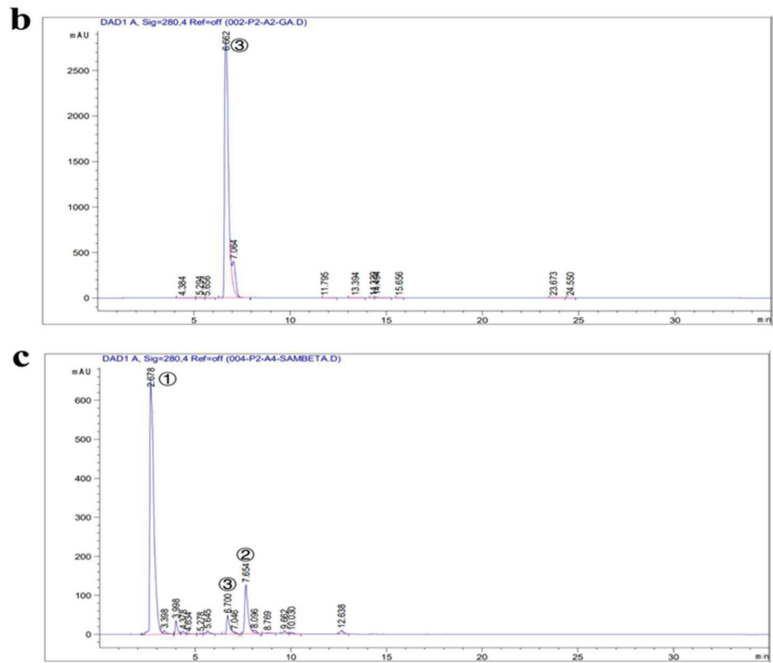


Figure 8. Determination of recombinant TbUGGT enzyme activity using HPLC. (a) UDPG(①) and GA(②) standard; (b) β G(③) standard; (c) experimental group.

Therefore, it is speculated that the recombinant TbUGGT protein has some enzymatic activity and can catalyze the reaction between GA and UDPG to generate β G. However, the product peak area was small, and the conversion rate was low. Subsequent experiments may consider expanding the culture or increasing the amount of enzyme reaction to increase the yield.

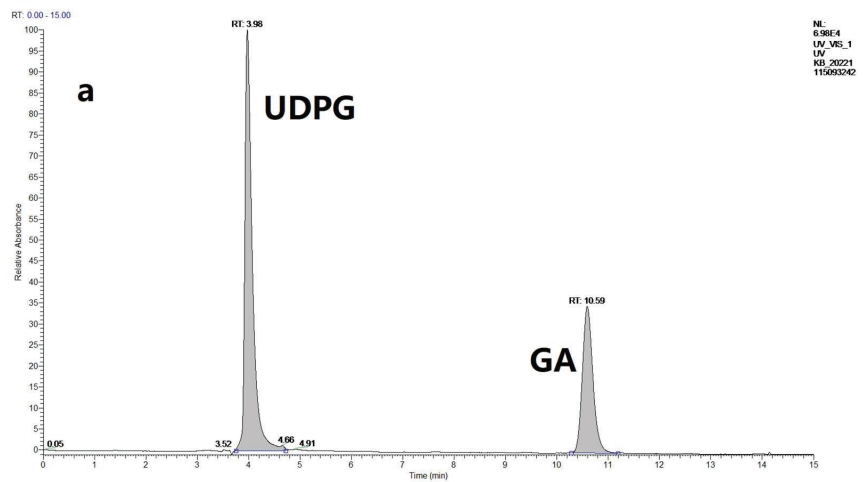


Figure 9. Cont.

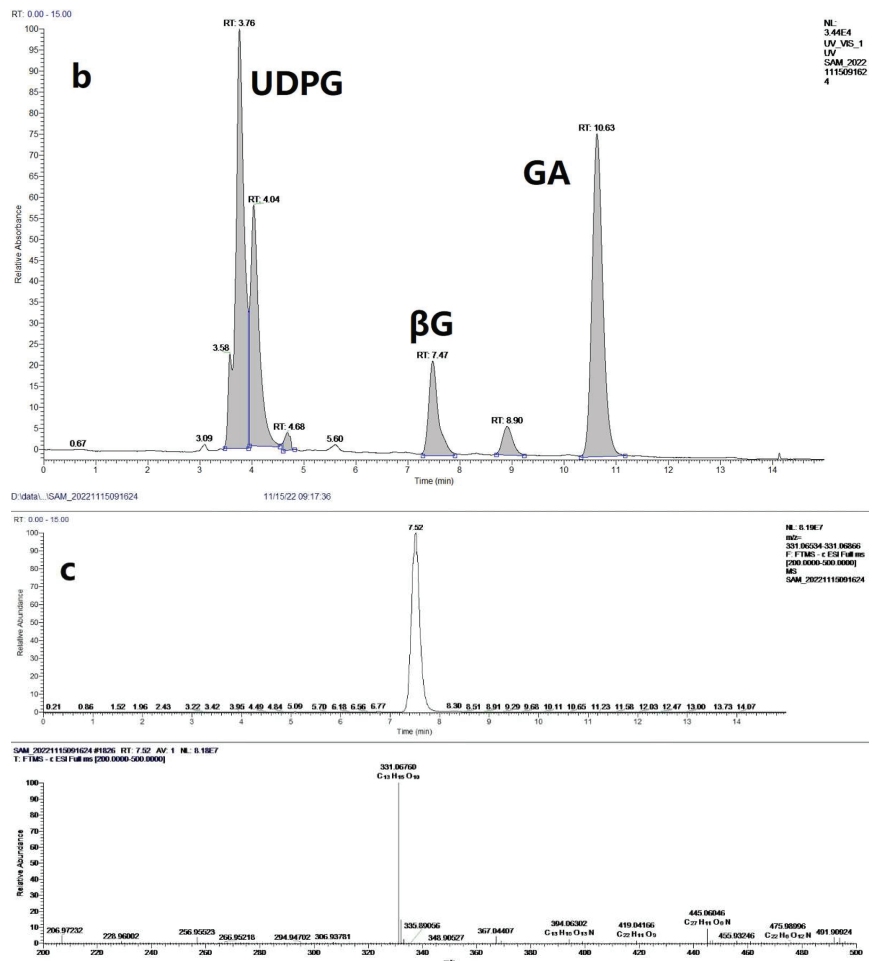


Figure 9. Determination of recombinant TbUGGT enzyme activity using LC-MS. (a) blank control group; (b) sample experiment group (c) β G mass spectrometry results.

3. Discussion

As an alien species, *Trapa bispinosa* Roxb. has been domesticated and cultivated in China [26]. Wuhan, China, is one of the cultivation bases of *Trapa bispinosa*, as the climate and environment are suitable for the growth and development of the plant [27]. Presently, research on *Trapa bispinosa* Roxb. focuses on the extraction of active ingredients [28,29], starch materials [30–32], pharmacological activity [33,34], etc. β G is one of the main active components of riboflavin and has significant medicinal value. Moreover, β G is the primary substrate of PGG, which has anti-cancer properties and has been extensively studied. However, the synthesis mechanism of *Trapa bispinosa* Roxb. remains unelucidated. Therefore, a series of experiments on β G biosynthesis were performed.

Many biochemical reactions are associated with glycosylation, and glycosyltransferase (GA) plays an essential role in plant growth and development, hormone balance, and toxic substance removal through glycosylation [35,36]. Meanwhile, a variety of glycosylation donors are involved in the glycosylation reaction. As a UDP-glycosylation donor-dependent enzyme, UGTs can selectively catalyze the site-directed glycosylation modification of natural and non-natural compounds. These are widely used in research

and discovery of new drugs [37,38]. Here, the full-length gene of TbUGGT was amplified using a high-fidelity enzyme, and its amino acid sequence was compared with the glycosyltransferase of other species. The UGT family is highly conserved in different plant species [39]. The conserved functional domain allows the genes to maintain a certain similarity in catalytic potency. Currently, the UGT crystal structure has been obtained mainly in plants, such as cassava [40], Saffron [41], *Arabidopsis thaliana* [42,43], etc. These UGTs only recognize UDPG as a sugar donor [44]. In subsequent experiments in this study, TbUGGT selectively catalyzed UDPG and GA as substrates to generate β G, confirming the results of the functional analysis.

In this study, during the purification and expression of the TbUGGT protein, most proteins existed in the form of inclusion bodies, as predicted with ProtScale and signal peptide. The protein was a non-membrane and non-secretory protein. As reported in the literature, inclusion body proteins could not be inactivated after ultrasound [45]. Here, the TbUGGT protein was extracted and purified by referring to the particular extraction method of the *Escherichia coli* inclusion body [46]. *Escherichia coli* was used as host bacteria for heterologous expression, producing inclusion bodies and inhibiting protein expression, but its activity remained unaffected. The low content of late catalytic might have been related to the particular processing mode of proteins in *Escherichia coli*, resulting in the protein not being wholly purified [47,48]. The specific reasons need to be investigated in further studies.

The qRT-PCR results demonstrated that the expression levels in the shell and root were higher than those in the other two parts, which may have been related to the influence of phenolic tannins on plant growth. The higher shell expression may have been attributed to the accumulation of plant secondary metabolites in fruits. Studies have shown that the presence of binary phenol or polyphenol may inhibit the activity of indole acetate oxidase, reduce the degree of auxin oxidation, and promote plant growth [49]. Specific concentrations of plant endogenous phenols can enhance their rooting ability. As *Trapa bispinosa* Roxb. is a floating aquatic plant with many roots, the generation of polyphenols is essential to meet its rooting needs. Nevertheless, further research is required to elucidate the specific promoting mechanism.

4. Materials and Methods

4.1. Plant Materials

In this study, the plant materials of *Trapa bispinosa* Roxb. were collected in Jiangxia District, Wuhan City, Hubei Province (114.10° E, 30.27° N). After cleaning, the samples were treated with liquid nitrogen and immediately stored at -80°C .

4.2. RNA Extraction and TbUGGT Enzyme Gene Cloning

RNA was extracted using The Plant Total RNA Isolation Kit (ENOVA BIO, Wuhan, China) The purity and concentration of RNA were determined using an ultra-micro spectrophotometer (MD2000D) and agarose gel electrophoresis (0.8% agarose). Single-strand cDNA was synthesized with PrimeScript IV 1st Strand cDNA Synthesis Mix (Takara Bio, Beijing, China). Specific primers were based on the TbUGGT sequence information obtained from *Trapa bispinosa* Roxb. transcriptome sequencing and designed using PremierX [24], as shown in Table 1. The TbUGGT enzyme gene was amplified using PCR with PrimeSTAR Max DNA Polymerase (Takara Bio, Beijing, China), and an OMEGA PCR purification kit was used to purify the amplified product. The size and quality of PCR products were determined with agarose gel electrophoresis (0.8% agarose).

Table 1. Primer sequences.

Primer Name	Sequence (5'-3')
TbUGGT_F	CGGAATTCATGGGTTCGAGTCTCCG
TbUGGT_R	TAAAGCGGCCGCTCACGGGACCGGCTCTACC
TbUGGT_F	ggatccGAATTCATGGGAAGTGAATC
TbUGGT_R	ataagaatGCGGCCGCTTAGG
T7 F	TAATACGACTCACTATAGGG
T7 R	GCTAGTTATTGCTCAGCGG
q-TbUGGT_F	GTTTCAGATGGGAACGGCACTAGG
q-TbUGGT_R	TCTGCGATGCTGTGGGTTCAAAG
C1168.2 F	GCTTGAAGATATTGTCGCCCTCATCCC
C1168.2 R	AGTCATCCTTTGTGCTGCCATTCTC

4.3. TbUGGT Sequence Analysis and Phylogenetic Prediction

The physicochemical properties of the protein encoded by the TbUGGT gene were analyzed using ProtParam. Subsequently, conserved protein domains, their families, and functional sites were analyzed with CD Search, ScanProsite, and Pfam. Furthermore, ProtScale was used to analyze protein hydrophilicity, while TMHMM was used to predict the protein transmembrane helical region, and the protein signal peptide was predicted with SignalP. SOPMA was used to predict the protein's secondary structure, and AlphaFold2 was used to construct the protein's three-dimensional structure model [50]. The PDB file of the 3D structural model of the protein was downloaded, and the ligand molecules were downloaded from PubChem. Pymol-2.3.4 and AutoDockTools software applications were used to process the ligands and protein molecules, and Vina software was used for molecular docking. For visualization, the docking file was uploaded to Plip after PyMOL processing. The amino acid sequences of the encoded protein were compared using BLAST, and the homology was analyzed using DNAMAN. Mega-x was used to build the phylogenetic tree. Online website addresses are displayed in Table 2.

Table 2. Bioinformatic analysis tools.

Tool Name	Tool Web Site	Access Date
ProtParam	https://web.expasy.org/protparam/	12 February 2022
CD Search	https://www.ncbi.nlm.nih.gov/Structure/cdd/wrpsb.cgi?	12 February 2022
ScanProsite	https://prosite.expasy.org/scanprosite/	12 February 2022
Pfam	http://pfam.xfam.org/	12 February 2022
ProtScale	https://web.expasy.org/protscale/	12 February 2022
TMHMM	https://services.healthtech.dtu.dk/service.php?TMHMM	20 February 2022
SignalP	https://services.healthtech.dtu.dk/service.php?SignalP-6.0	20 February 2022
SOPMA	https://npsa-prabi.ibcp.fr/cgi-bin/npsa_automat.pl?page=npsa_sopma.html	30 July 2022
AlphaFold2	https://github.com/lucidrains/alphafold2	5 November 2022

4.4. TbUGGT Prokaryotic Expression

(1) Vector construction and small-scale expression

The base sequence of the TbUGGT gene was optimized (GenScript Biotech Corp, Nanjing, China) according to the codon preference of *Escherichia coli*. Specific primers were designed, and restriction sites (EcoRI and NotI) were added, as shown in Table 1. The target gene was constructed in the PET-28a vector and transferred to DH5 α . The plasmid was then extracted and sent for nucleic acid sequencing (Sangon Biotech (Shanghai) Co., Ltd., Shanghai, China). The corresponding colonies on the plate were carefully selected and inoculated into a kanamycin medium. The colonies were cultured overnight, and the plasmids were extracted and stored in glycerobacteria. The PET-28a recombinant vector was transformed into *Escherichia coli* BL21 (DE3), and colony PCR verification was performed using T7 primers, as shown in Table 2. BL21 was cultured in Luria-Bertani (LB) with kanamycin until the OD600 value reached about 0.6, and isopropyl- β -d-thiogalactoside

(IPTG) was added at the final concentration of 0.5 mM to induce TbUGGT protein expression. Finally, 10% sodium dodecyl sulfate-polyacrylamide gel electrophoresis (SDS-PAGE) was performed to detect fusion protein expression.

(2) Expression and purification of large amounts of protein

Single colonies containing recombinant plasmids were selected and inoculated into a 10 mL LB liquid medium with corresponding resistance. After overnight culture in a 37 °C shaker, the colonies were transferred to 1 L of LB liquid medium and cultured until OD₆₀₀ reached about 0.6 (duration of 2–3 h). The bacterial control solution was collected, and IPTG was added at a final concentration of 0.5 mM. After shaking the culture at 28 °C for 5 h, bacterial precipitates were collected using centrifugation (6000 RPM, 4 °C, 10 min), and the precipitates were cleaned twice with PBS to remove the residual medium. The bacterial precipitates were then collected and stored at –20 °C for future use.

The fusion protein was purified according to the instructions of the His-Tag Protein Purification Kit (Beyotime Biotechnology, Haimen, China). Subsequently, four milliliters of non-denatured lysate was added per gram of bacterial precipitate and complete suspension. The bacteria supernatant was collected using centrifugation. The BeyoGold™ His-tag packaging column was prepared, and the upper cleaning column was loaded and washed 5 times with 1 mL of washing liquid; then, 0.5 mL of eluent was used ten times. The eluate of each tube was detected using SDS-PAGE electrophoresis, and the eluate that met the requirements was combined. The eluent was concentrated using an ultrafiltration tube, and SDS-PAGE was performed to detect 10 µL of the concentrated protein. The remaining concentrated solution was stored at –80 °C.

4.5. Enzyme Activity Detection of TbUGGT Protein

The total enzymatic reaction system was 100 µL, and 0.5 mM 3,4,5-trihydroxy benzoic acid (GA) and 2.5 mM uridine diphosphate glucose (UDPG) were added. Furthermore, 100 mM MES buffer containing 0.1% β-mercaptoethanol was used to provide a buffer environment. Next, the purified enzyme solution was added to the experimental group, while the enzyme solution was not added to the control group. After 3 h of reaction at 30 °C, methanol was added to terminate the reaction, and HPLC and LC-MS were used for detection. The liquid-phase conditions and methods are described below.

HPLC: chromatographic column, Agilent C18 column; mobile phase, 1% acetic acid water (A) and acetonitrile (B); injection volume, 20 µL; flow rate, 1.0 mL/min; column temperature, 35 °C; detection wavelength, 280 nm. Liquid-phase method: 0–10 min, 3–5% B; 10–15 min, 5–50% B; 15–25 min, 50–5% B; 25–30 min, 5–3% B; 30–35 min, 3% B. The liquid-phase diagram of standard βG was compared with the experimental results to confirm product formation.

LC-MS: chromatographic column, Waters ACQUITY C18 column (50 mm × 2.1 mm, 1.7 µm); mobile phase, 0.2% formic acid aqueous solution (A) and acetonitrile (B). Gradient elution: 0–1.5 min, 93% A; 1.5–8 min, 93%~80% A; 8–15 min, 80%~75% A. Volume flow rate, 0.4 mL/min; injection volume, 4 µL; column temperature, 35 °C.

Mass spectrometry conditions: negative ion scanning mode (ESI; m/z 100~1400); capillary voltage, 2.64 Kv; collision voltage, 45 V; drying gas temperature, 350 °C; source temperature, 150 °C; desolvent gas, N₂, 800 L/Hr.

4.6. TbUGGT Expression Pattern

Four samples, including shell (FR), leaf (LR), stem (ST), and root (FR), were selected from the samples frozen at –80 °C, and the total RNA of the four samples was extracted using the Kit method. An ultra-micro spectrophotometer (MD2000D) and agarose gel electrophoresis (0.8% agarose) were used to evaluate the purity and concentration of RNA. Reverse transcription into cDNA was performed using the PrimeScript™ RT Reagent Kit with gDNA Eraser (Takara Bio, Beijing, China) as the template for qRT-PCR. Table 1 displays the primer sequences (q-TbUGGT-F and q-TbUGGT-R) and reference gene EIF5A (C1168.2-F and C1168.2-R). The reaction systems were prepared according to TB Green®

Premix Ex Taq™ II (Takara Bio, Beijing, China). The data were detected using CFX96™ real-time System (Bio-Rad, Wuhan, China) and analyzed using the 2- $\Delta\Delta$ Ct method [51].

5. Conclusions

In this study, the gene TbUGGT was successfully cloned from *Trapa bispinosa* Roxb. After gene optimization, the nucleic acid and protein sequences were analyzed using bioinformatics and the phylogenetic tree and hosted into *Escherichia coli*. The gene was purified and successfully expressed in *Escherichia coli* BL12 (DE3). The HPLC results showed that TbUGGT could catalyze GA and UDPG to produce β G. This study found the catalytic role of TbUGGT in β G biosynthesis, laying the foundation for subsequent related studies on β G biosynthesis in *Escherichia coli*.

Supplementary Materials: The following supporting information can be downloaded at: <https://www.mdpi.com/article/10.3390/molecules27238374/s1>, Figure S1: Domain prediction of TbUGGT protein (a–c), Figure S2: Hydrophilicity analysis of TbUGGT (a), Figure S3: Signal peptide prediction (a) and transmembrane prediction (b) of TbUGGT, Figure S4: Secondary structure prediction of TbUGGT.

Author Contributions: Conceptualization, S.Y. and D.Y.; methodology, D.Y.; validation, S.Y. and D.Y.; formal analysis, X.S.; investigation, Q.C.; resources, T.M.; data curation, T.M.; writing—original draft preparation, S.Y.; writing—review and editing, T.M.; visualization, L.W.; supervision, L.W.; project administration, H.W. and L.W. All authors have read and agreed to the published version of the manuscript.

Funding: This research was supported by Nature Science Foundation of Hubei Province in China (2022CFB429) and Primary Research & Development Plan of Hubei Province (2022BBA0023).

Institutional Review Board Statement: Not applicable.

Informed Consent Statement: Not applicable.

Data Availability Statement: Not applicable.

Conflicts of Interest: The authors declare no conflict of interest.

Sample Availability: Samples of *Trapa bispinosa* Roxb., vectors and strains carrying the TbUGGT gene, fermentation products of TbUGGT protein purification are available from the authors.

References

- Lim, B.K. *Edible Medicinal and Non-Medicinal Plants*; Springer: Dordrecht, The Netherlands, 2012.
- Nayik, G.A.; Gull, A. *Antioxidants in Vegetables and Nuts—Properties and Health Benefits*; Springer: Singapore, 2020.
- Khare, C.P. *Indian Medicinal Plants: An Illustrated Dictionary*; Springer: New York, NY, USA, 2008.
- Huang, H.C.; Chao, C.L.; Liaw, C.C.; Hwang, S.Y.; Kuo, Y.H.; Chang, T.C.; Chao, C.H.; Chen, C.J.; Kuo, Y.H. Hypoglycemic Constituents Isolated from *Trapa natans* L. Pericarps. *J. Agric. Food Chem.* **2016**, *64*, 3794–3803. [[CrossRef](#)] [[PubMed](#)]
- Kinoshita, S.; Sugawa, H.; Nanri, T.; Ohno, R.-I.; Shirakawa, J.-I.; Sato, H.; Katsuta, N.; Sakake, S.; Nagai, R. *Trapa bispinosa* Roxb. and lutein ameliorate cataract in type 1 diabetic rats. *J. Clin. Biochem. Nutr.* **2020**, *66*, 8–14. [[CrossRef](#)] [[PubMed](#)]
- Stoicescu, I.; Popescu, A.; Sirbu, R.; Bala, C. Simultaneous Determination of Phenolic Acids in Water Caltrop by HPLC-DAD. *Anal. Lett.* **2012**, *45*, 2519–2529. [[CrossRef](#)]
- Claudia, D.P.; Mario, C.H.; Arturo, N.O.; Noel, M.C.O.; Antonio, N.C.; Teresa, R.A.; Gerardo, L.-T.Z.; Margarita, D.M.; Alejandra, L.I.M.; Rosalina, C.M.Y. Phenolic Compounds in Organic and Aqueous Extracts from *Acacia farnesiana* Pods Analyzed by ULPS-ESI-Q-oe/TOF-MS. In Vitro Antioxidant Activity and Anti-Inflammatory Response in CD-1 Mice. *Molecules* **2018**, *23*, 2386. [[CrossRef](#)] [[PubMed](#)]
- Sobeh, M.; Rezaq, S.; Sabry, O.M.; Abdelfattah, M.; Raey, M.E.; El-Kashak, W.A.; El-Shazly, A.M.; Mahmoud, M.F.; Wink, M. *Albizia anthelmintica*: HPLC-MS/MS profiling and in vivo anti-inflammatory, pain killing and antipyretic activities of its leaf extract. *Biomed. Pharmacother.* **2019**, *115*, 108882. [[CrossRef](#)] [[PubMed](#)]
- Vanholme, R.; Morreel, K.; Darrach, C.; Oyarce, P.; Grabber, J.H.; Ralph, J.; Boerjan, W. Metabolic engineering of novel lignin in biomass crops. *New Phytol.* **2012**, *196*, 978–1000. [[CrossRef](#)]
- Xian-Hong, O.U.; Deng, J.G.; Xin, Y.U.; Yuan, Y.F.; University, S.M. Study on the Anti-Inflammatory Active Constituents of *Mangifera indica* L.Seed Kernel. *Chin. Pharm. J.* **2015**, *19*, 1673–1677.
- Gupta, A.; Sahu, T.R.; Sahu, B.K. Cultivation of Trapa crop based on indigenous knowledge. *J. Trop. For.* **2010**, *26*, 50–52.

12. Li, L.; Chang, K.-C.; Zhou, Y.; Shieh, B.; Ponder, J.; Abraham, A.D.; Ali, H.; Snow, A.; Petrash, J.M.; LaBarbera, D.V. Design of an Amide N-Glycoside Derivative of β -Glucogallin: A Stable, Potent, and Specific Inhibitor of Aldose Reductase. *J. Med. Chem.* **2013**, *57*, 71–77. [[CrossRef](#)]
13. Cao, T.; Wang, J.; Wu, Y.; Wang, L.; Zhang, H. Antiglaucoma Potential of beta-Glucogallin Is Mediated by Modulating Mitochondrial Responses in Experimentally Induced Glaucoma. *Neuroimmunomodulation* **2020**, *27*, 142–151. [[CrossRef](#)]
14. Chang, K.C.; Laffin, B.; Ponder, J.; Enzsoly, A.; Nemeth, J.; LaBarbera, D.V.; Petrash, J.M. Beta-glucogallin reduces the expression of lipopolysaccharide-induced inflammatory markers by inhibition of aldose reductase in murine macrophages and ocular tissues. *Chem. Biol. Interact.* **2013**, *202*, 283–287. [[CrossRef](#)] [[PubMed](#)]
15. Chang, K.C.; Snow, A.; LaBarbera, D.V.; Petrash, J.M. Aldose reductase inhibition alleviates hyperglycemic effects on human retinal pigment epithelial cells. *Chem. Biol. Interact.* **2015**, *234*, 254–260. [[CrossRef](#)] [[PubMed](#)]
16. Singh, R.; Chandel, S.; Ghosh, A.; Matta, T.; Gautam, A.; Bhattacharya, A.; Babu, S.S.; Sukla, S.; Nag, D.; Ravichandiran, V.; et al. Glucogallin Attenuates the LPS-Induced Signaling in Macrophages and Protects Mice against Sepsis. *Int. J. Mol. Sci.* **2022**, *23*, 11254. [[CrossRef](#)]
17. Mackenzie, P.I.; Owens, I.S.; Burchell, B.; Bock, K.W.; Bairoch, A.; Belanger, A.; Gigleux, S.F.; Green, M.; Hum, D.W.; Iyanagi, T.; et al. The UDP glycosyltransferase gene superfamily: Recommended nomenclature update based on evolutionary divergence. *Pharm. Genom.* **1997**, *7*, 255–269. [[CrossRef](#)]
18. Kleczkowski, L.; Kunz, S.; Wilczynska, M. Mechanisms of UDP-Glucose Synthesis in Plants. *Crit. Rev. Plant Sci.* **2010**, *29*, 191–203. [[CrossRef](#)]
19. Chen, Y.; Gao, A.; Fu, C.H.; Gui, B.H.; Zhi, C.Z. Functional analysis of the UDP glucose: Flavonoid-3-O-glucosyltransferase (UFGT) promoter from litchi (*Litchi chinesis* Sonn.) and transient expression in onions (*Allium cepa* Linn.). *Afr. J. Plant Sci.* **2015**, *9*, 244–249. [[CrossRef](#)]
20. Ossipov, V.; Salminen, J.P.; Ossipova, S.; Haukioja, E.; Pihlaja, K. Gallic acid and hydrolysable tannins are formed in birch leaves from an intermediate compound of the shikimate pathway. *Biochem. Syst. Ecol.* **2003**, *31*, 3–16. [[CrossRef](#)]
21. Muir, R.M.; Ibáñez, A.; Uratsu, S.L.; Ingham, E.S.; Leslie, C.A.; Mcgranahan, G.H.; Batra, N.; Goyal, S.; Joseph, J.; Jemmis, E.D. Mechanism of gallic acid biosynthesis in bacteria (*Escherichia coli*) and walnut (*Juglans regia*). *Plant Mol. Biol.* **2011**, *75*, 555–565. [[CrossRef](#)]
22. Tahara, K.; Nishiguchi, M.; Funke, E.; Miyazawa, S.I.; Miyama, T.; Milkowski, C. Dehydroquinase dehydratase/shikimate dehydrogenases involved in gallate biosynthesis of the aluminum-tolerant tree species *Eucalyptus camaldulensis*. *Planta* **2021**, *253*, 3. [[CrossRef](#)]
23. Werner, R.A.; Rossmann, A.; Schwarz, C.; Bacher, A.; Schmidt, H.L.; Eisenreich, W. Biosynthesis of gallic acid in *Rhus typhina*: Discrimination between alternative pathways from natural oxygen isotope abundance. *Phytochemistry* **2004**, *65*, 2809–2813. [[CrossRef](#)]
24. Yin, D.J.; Ye, S.J.; Sun, X.Y.; Chen, Q.Y.; Min, T.; Wang, H.X.; Wang, L.M. Integrative Analysis of the Transcriptome and Metabolome Reveals Genes Involved in Phenylpropanoid and Flavonoid Biosynthesis in the *Trapa bispinosa* Roxb. *Front. Plant Sci.* **2022**, *13*, 913265. [[CrossRef](#)] [[PubMed](#)]
25. Xin, S.; Xiang, G.; Man, A.; Qinmei, W.; Dan, Y.; Meng, W.; Yang, F.; Li, W. cDNA cloning and characterization of UDP-glucose: Anthocyanidin 3-O-glucosyltransferase in *Freesia hybrida*. *Plant Cell Rep.* **2011**, *30*, 1209–1218.
26. Dodd, L.L.; Harms, N.E.; Schad, A.N. Reciprocal competitive effects of congeneric invaders, *Trapa natans* L. and *Trapa bispinosa* Roxb. var. *tinumai* Nakano, in established freshwater plant cultures. *Aquat. Bot.* **2021**, *174*, 103419. [[CrossRef](#)]
27. Aiwen, Z.; Xin, S.; Jing, Z.; Liang, H.E.; Chunlong, Y.I.; Leyi, N.I.; Te, C.; Garden, L.B.; Amp, J.P. Diversity and Distribution of Aquatic Plants in Lake Donghu in Wuhan in 2014. *Res. Environ. Sci.* **2017**, *30*, 398–405.
28. Adhikari, B.; Shrestha, O.K. Effect of Processing Variables on Anthocyanin and Total Polyphenol Extraction from Water Chestnut (*Trapa bispinosa*) Hull. *Himal. J. Sci. Technol.* **2018**, *2*, 76–83. [[CrossRef](#)]
29. Mazumder, A.; Majee, C.; Mazumder, R. Determination of total phenolic content and total antioxidant activity of various parts of *Trapa bispinosa*. *Int. J. Pharm. Sci. Res.* **2020**, *11*, 3625–3627.
30. Dularia, C.; Sinhmar, A.; Thory, R.; Pathera, A.K.; Nain, V. Development of starch nanoparticles based composite films from non-conventional source—Water chestnut (*Trapa bispinosa*). *Int. J. Biol. Macromol.* **2019**, *136*, 1161–1168. [[CrossRef](#)]
31. Lutfi, Z. Freeze-thaw stabilization of water chestnut (*Trapa bispinosa*) starch in the presence of gums and salts. *Trakia J. Sci.* **2013**, *11*, 163–169.
32. Wang, J.; Liu, T.; Bia, X.; Hua, Z.; Wu, X. Structural characterization and physicochemical properties of starch from four aquatic vegetable varieties in China. *Int. J. Biol. Macromol.* **2021**, *172*, 542–549. [[CrossRef](#)]
33. Thakkar, A.B.; Kurtkoti, S.K.; Sastry, N.V. Phytochemical screening, antibacterial and free radical scavenging activity of the fruit and peel extracts of *Trapa bispinosa* (water chestnut). *Int. J. Pharma Bio Sci.* **2018**, *9*, 4. [[CrossRef](#)]
34. Adkar, P.P.; Dongare, A.; Ambavade, S.D.; Bhaskar, V.H. Research journal of pharmaceutical, biological and chemical sciences: Effect of *Trapa bispinosa* on HDAC level in animal tissues for its anti-arthritis activity. *Res. J. Pharm. Biol. Chem. Sci.* **2014**, *5*, 1404–1415.
35. Bowles, D.; Isayenkova, J.; Lim, E.K.; Poppenberger, B. Glycosyltransferases: Managers of small molecules—ScienceDirect. *Curr. Opin. Plant Biol.* **2005**, *8*, 254–263. [[CrossRef](#)] [[PubMed](#)]

36. Su, Z.H.; Xu, Z.S.; Peng, R.H.; Tian, Y.S.; Zhao, W.; Han, H.J.; Yao, Q.H.; Wu, A.Z. Phytoremediation of Trichlorophenol by Phase II Metabolism in Transgenic *Arabidopsis* Overexpressing a *Populus* Glucosyltransferase. *Environ. Sci. Technol.* **2012**, *46*, 4016–4024. [[CrossRef](#)] [[PubMed](#)]
37. Liang, H.; Hu, Z.; Zhang, T.; Gong, T.; Chen, J.; Zhu, P.; Li, Y.; Yang, J. Production of a bioactive unnatural ginsenoside by metabolically engineered yeasts based on a new UDP-glycosyltransferase from *Bacillus subtilis*. *Metab. Eng.* **2017**, *44*, 60–69. [[CrossRef](#)] [[PubMed](#)]
38. Chu, L.L.; Pandey, R.P.; Shin, J.Y.; Jung, H.J.; Sohng, J.K. Synthetic analog of anticancer drug daunorubicin from daunorubicinone using one-pot enzymatic UDP-recycling glycosylation. *J. Mol. Catal. B Enzym.* **2016**, *124*, 1–10. [[CrossRef](#)]
39. Li, Y.; Baldauf, S.; Lim, E.-K.; Bowles, D.J. Phylogenetic Analysis of the UDP-glycosyltransferase Multigene Family of *Arabidopsis thaliana* *210. *J. Biol. Chem.* **2001**, *276*, 4338–4343. [[CrossRef](#)]
40. Cwab, C.; Jing, D.; Zcb, C.; Wtbc, E.; Yan, Y.; Hai, Y.D.; Jian, Z.A.; Wei, H. Comprehensive analysis and expression profiles of cassava UDP-glycosyltransferases (UGT) family reveal their involvement in development and stress responses in cassava. *Genomics* **2021**, *113*, 3415–3429.
41. López-Jimenez, A.; Frusciant, S.; Niza, E.; Ahrazem, O.; Rubio-Moraga, N.; Diretto, G.; Gómez-Gómez, L. A New Glycosyltransferase Enzyme from Family 91, UGT91P3, Is Responsible for the Final Glucosylation Step of Crocins in Saffron (*Crocus sativus* L.). *Int. J. Mol. Sci.* **2021**, *22*, 8815. [[CrossRef](#)]
42. Hou, B.; Lim, E.K.; Higgins, G.S.; Bowles, D.J. N-glucosylation of cytokinins by glycosyltransferases of *Arabidopsis thaliana*. *J. Biol. Chem.* **2004**, *279*, 47822–47832. [[CrossRef](#)]
43. Poppenberger, B.; Fujioka, S.; Soeno, K.; George, G.L.; Vaistij, F.E.; Hiranuma, S.; Seto, H.; Takatsuto, S.; Adam, G.; Yoshida, S. The UGT73C5 of *Arabidopsis thaliana* glucosylates brassinosteroids. *Proc. Natl. Acad. Sci. USA* **2005**, *102*, 15253–15258. [[CrossRef](#)]
44. Wang, X. Structure, mechanism and engineering of plant natural product glycosyltransferases. *Febs Lett.* **2009**, *583*, 3303–3309. [[CrossRef](#)] [[PubMed](#)]
45. Wingfield, P.T.; Palmer, I.; Liang, S. Folding and Purification of Insoluble (Inclusion Body) Proteins from *Escherichia coli*. *Curr. Protoc. Protein Sci.* **2014**, *78*, 6.5.1–6.5.30.
46. Palmer, I.; Wingfield, P.T. Preparation and Extraction of Insoluble (Inclusion-Body) Proteins from *Escherichia coli*. *Curr. Protoc. Protein Sci.* **2012**, *70*, 6.3.1–6.3.20. [[CrossRef](#)] [[PubMed](#)]
47. Chew, F.N.; Abidin, N.; Yusof, N.; Rafi, N.M.; Chua, G.K. Recovery of inclusion body protein in *Escherichia coli*: Effects of solubilization methods and process condition. *IOP Conf. Ser. Mater. Sci. Eng.* **2020**, *736*, 022120. [[CrossRef](#)]
48. Jong, W.; Hagen-Jongman, C.; Vikström, D.; Dontje, W.; Luirink, J. Mutagenesis-Based Characterization and Improvement of a Novel Inclusion Body Tag. *Front. Bioeng. Biotechnol.* **2020**, *7*, 442. [[CrossRef](#)]
49. Jones, O.P.; Hatfield, S.G.S. Root Initiation in Apple Shoots Cultured In Vitro with Auxins and Phenolic Compounds. *J. Hortic. Sci.* **1976**, *51*, 495–499. [[CrossRef](#)]
50. Jumper, J.; Evans, R.; Pritzel, A.; Green, T.; Figurnov, M.; Ronneberger, O.; Tunyasuvunakool, K.; Bates, R.; Žídek, A.; Potapenko, A.; et al. Highly accurate protein structure prediction with AlphaFold. *Nature* **2021**, *596*, 583–586. [[CrossRef](#)]
51. Rotenberg, D.; Thompson, T.S.; German, T.L.; Willis, D.K. Methods for effective real-time RT-PCR analysis of virus-induced gene silencing. *J. Virol. Methods* **2006**, *138*, 49–59. [[CrossRef](#)]

Article

Synthesis and In Vitro Anticancer Evaluation of Flavone—1,2,3-Triazole Hybrids

Alexandra Németh-Rieder¹, Péter Keglevich^{1,*}, Attila Hunyadi², Ahmed Dhahir Latif^{3,4}, István Zupkó³ and László Hazai¹

¹ Department of Organic Chemistry and Technology, Faculty of Chemical Technology and Biotechnology, Budapest University of Technology and Economics, Műegyetem rkp. 3., H-1111 Budapest, Hungary

² Institute of Pharmacognosy, University of Szeged, Eötvös u. 6., H-6720 Szeged, Hungary

³ Department of Pharmacodynamics and Biopharmacy, University of Szeged, Eötvös Str. 6, H-6720 Szeged, Hungary

⁴ Department of Pharmacology and Toxicology, Faculty of Medicine, Wasit University, Wasit 52001, Iraq

* Correspondence: keglevich.peter@vbk.bme.hu

Abstract: Hybrid compounds of flavones, namely chrysin and kaempferol, and substituted 1,2,3-triazole derivatives, were synthesized by click reaction of the intermediate *O*-propargyl derivatives. 4-Fluoro- and 4-nitrobenzyl-1,2,3-triazole-containing hybrid molecules were prepared. The mono- and bis-coupled hybrids were investigated on 60 cell lines of 9 common cancer types (NCI60) in vitro as antitumor agents. Some of them proved to have a significant antiproliferative effect.

Keywords: flavones; chrysin; kaempferol; hybrids; 1,2,3-triazole; anticancer activity

1. Introduction

Cancer treatment is one of the most important medical challenges. Permanent research is in progress to produce more effective and less toxic derivatives. One of the exciting and promising directions of this research is the synthesis of antitumor hybrid molecules [1,2]. The concept of molecular hybridization is to incorporate two or more pharmacophores into one molecule with covalent bonds, increasing the chance of effectiveness and improving the drug kinetic properties of the resulting hybrid compared to the corresponding fixed-dose drug combination. It should be noted that rigid distance imposed by the structure of the compound between potentially active parts of the hybrid may prevent biological efficiency.

During our previous work, numerous new molecules exerting a significant antiproliferative effect have been developed in this field. Various hybrids of *Vinca* alkaloids [3] were synthesized, coupling with amino acid esters [4,5], steroids [6], flavones (e.g., 3, chrysin) [7], phosphorus derivatives [8], amines [5], and compounds containing the known pharmacophore 1,2,3-triazole (2) [5]. Recently our work was extended to the synthesis of new aminochrysin derivatives coupled with different aromatics [9].

Several flavonoids with antitumor activity are known in the literature [10,11]. Flavones containing a 2-phenylchromen-4-one (1) backbone, and 1,2,3-triazole derivatives keep attracting much research interest, and many 1,2,3-triazole-containing hybrids are known as effective anticancer agents [12–15]. During the last decade, numerous biologically active flavone—1,2,3-triazole hybrids have been synthesized [16–18], for example, 5 apigenin-7-methyl ether derivative, which showed promising activity against ovarian cancer ($IC_{50} = 10, 15$ and $20 \mu\text{M}$ for SKOV3, OVCAR-3 and Caov-3 cancer cell lines) (Figure 1) [19].

In this study, the above outlined results inspired us to develop synthetic possibilities for the preparation of flavone—1,2,3-triazole hybrids.

Citation: Németh-Rieder, A.; Keglevich, P.; Hunyadi, A.; Latif, A.D.; Zupkó, I.; Hazai, L. Synthesis and In Vitro Anticancer Evaluation of Flavone—1,2,3-Triazole Hybrids. *Molecules* **2023**, *28*, 626. <https://doi.org/10.3390/molecules28020626>

Academic Editor: Giovanni Ribaudò

Received: 15 December 2022

Revised: 4 January 2023

Accepted: 4 January 2023

Published: 7 January 2023



Copyright: © 2023 by the authors. Licensee MDPI, Basel, Switzerland. This article is an open access article distributed under the terms and conditions of the Creative Commons Attribution (CC BY) license (<https://creativecommons.org/licenses/by/4.0/>).

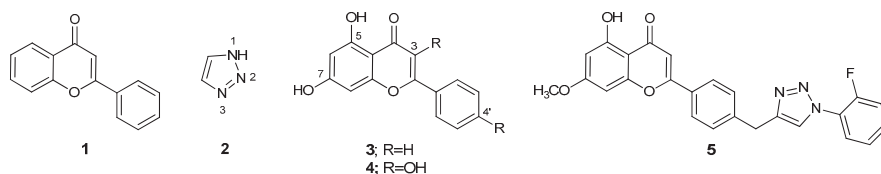


Figure 1. The structure of 2-phenylchromen-4-one (1), 1,2,3-triazole (2), chrysin (3), kaempferol (4), and an anticancer flavone—1,2,3-triazole hybrid (5).

2. Results and Discussion

In the course of elaborating the synthetic design, chrysin (5,7-dihydroxyflavone) (3) and kaempferol (3,4',5,7-tetrahydroxyflavone) (4) were chosen (Figure 1) to couple with 1,2,3-triazole derivatives. Some chrysin—1,2,3-triazole hybrids prepared by a different way, were previously reported as antibacterial agents [20].

2.1. Coupling Components

Chrysin (3) is among the best-known flavones. It is abundant in nature and present in many edible plants and honey [21]. It has an anticancer effect through inducing apoptosis and autophagy [21,22]. Chrysin (3) seems to be suitable for use alone and/or in combination with other chemotherapeutic agents [21]. Kaempferol (4) and its derivatives are also found in many plants. They can prevent coronary heart disease and inflammatory problems, and they also show antiproliferative effects and may induce apoptosis [23].

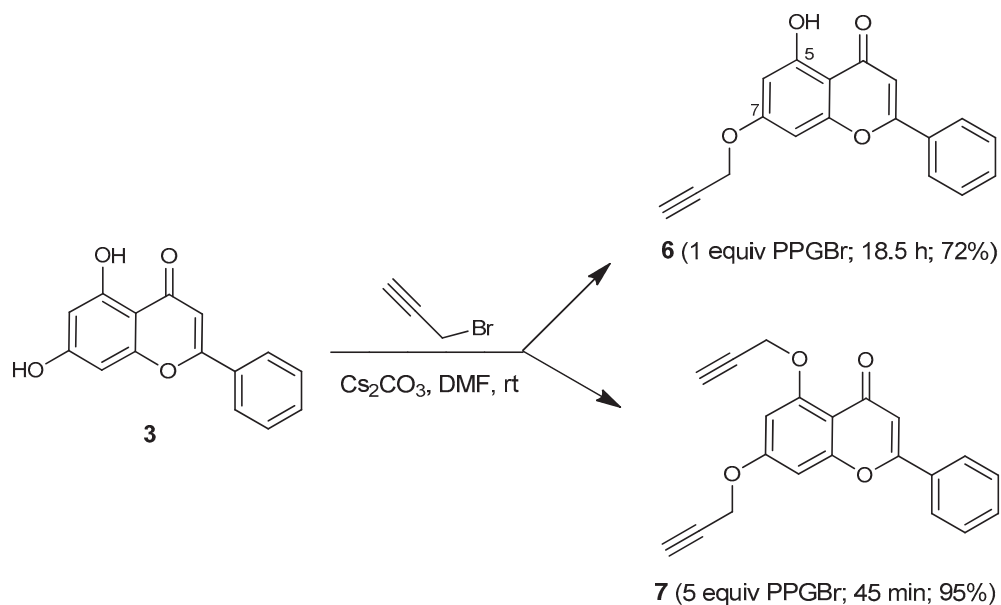
It is known that 1,2,3-Triazole derivatives have been widely used as a pharmacophore in hybrids. In addition to the advantageous physico-chemical properties of this moiety, it is also known to exert various biological effects [24,25]. 1,2,3-Triazole derivatives are characterized by stability, the ability to form hydrogen bonds (increasing their water solubility), and weak basicity (they are not protonated at physiological pH). Moreover, 1,2,3-triazole derivatives have fungicidal, antibacterial, antituberculosis, and anticancer effects [26,27]. The well-known click reaction is used for the preparation of 1,2,3-triazole derivatives, as one of the tools of modern organic synthetic methods based on structure-activity relationships, preferably the N^1 -(4-fluoro- and 4-nitrobenzyl)-1,2,3-triazole derivatives [24,28].

2.2. Chemistry

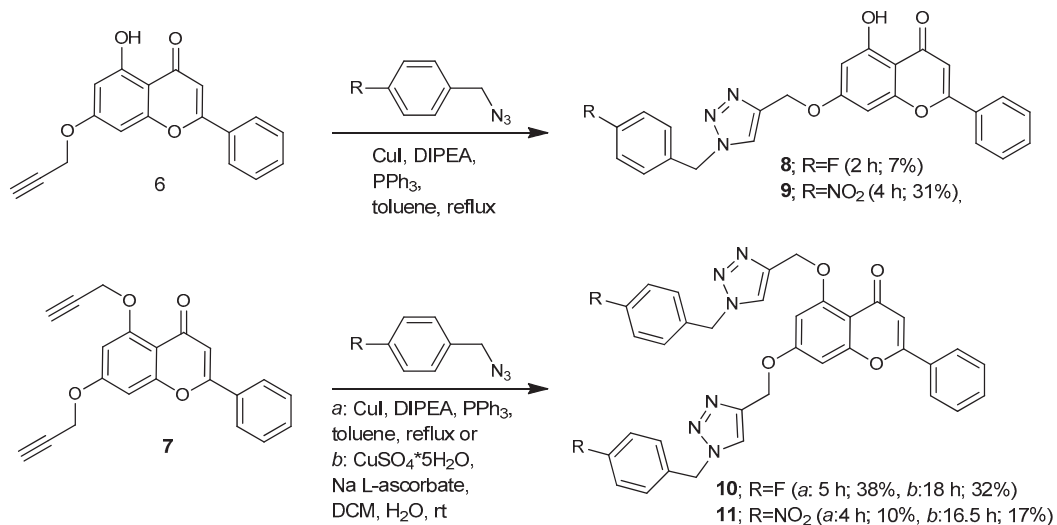
Chrysin (3) reacted with an equimolar quantity of propargyl bromide (PPGBr) in dimethylformamide in the presence of cesium carbonate at room temperature (Scheme 1), resulting in the 7-substituted product (6) (known as an intermediate of antibacterial derivative prepared by a method different from ours [20]). The reason for the regioselectivity is that the proton of the 5-hydroxyl group forms an intramolecular H-bond with the neighboring oxo group. Certainly, with an excess of propargyl bromide (5 equivalent), exclusively the 5,7-disubstituted derivative (7) proved to be the product, as expected. Others also synthesized this compound using gold(I) complexes without reporting any preparative and characterization details [29].

The next reaction step was the click reaction (Scheme 2) using 4-fluoro- and 4-nitrobenzyl azide prepared in situ from the corresponding benzyl bromides with sodium azide in DMF at room temperature [30].

The reaction was carried out in the presence of copper(I) iodide, triphenylphosphine, and *N,N*-diisopropylethylamine, and resulted in known hybrids 8 and 9, respectively. These two hybrids were prepared previously with another method, however, only their antibacterial effect has been investigated [20]. Bis(propargyl) derivative 7 was also treated with the same reaction conditions and gave the bis-hybrids 10 and 11. Avoiding the difficult isolation from the triphenylphosphine oxide formed, the latter click reaction was successfully achieved also with further reagents, namely with copper sulfate pentahydrate and sodium L-ascorbate in a two-phase mixture.

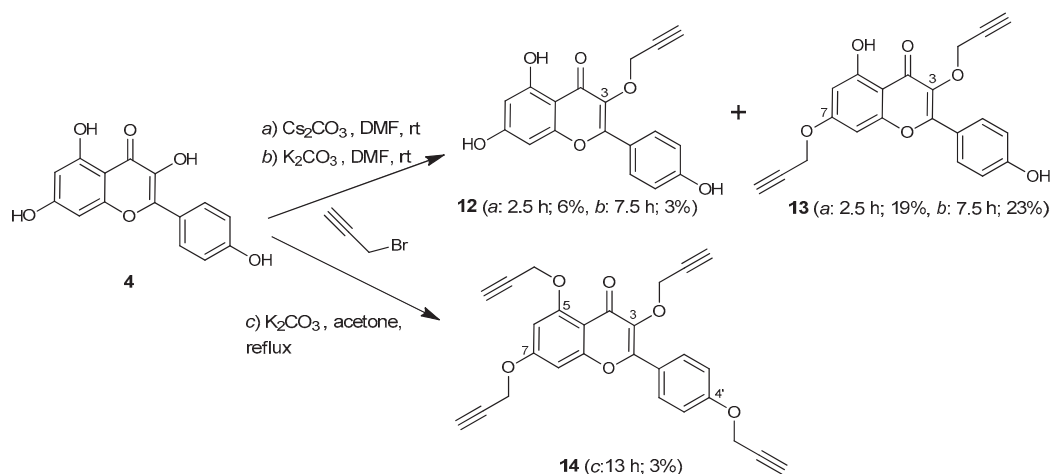


Scheme 1. The reaction between chrysin (3) and propargyl bromide (PPGBr).



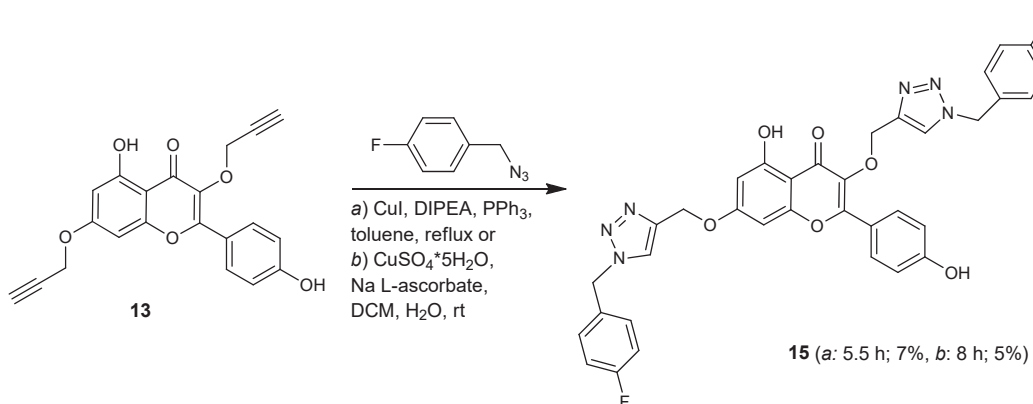
Scheme 2. The synthesis of chrysin hybrids (8–11) containing one or two 1,2,3-triazole units.

The second flavone building block, selected for the synthesis of hybrids, was kaempferol (4). The alkylation with propargyl bromide was investigated with different bases and in different solvents (Scheme 3). Using cesium carbonate or potassium carbonate as a base in dimethylformamide compounds 12 and 13 were isolated. However, in acetone solution compound 14 was obtained.



Scheme 3. The reaction between kaempferol (4) and propargyl bromide.

Derivative **13** was the compound isolated in the relatively largest quantity and was chosen for the click reaction (Scheme 4). Investigating both the reaction conditions resulted in the isolation of the bis-hybrid **15**.



Scheme 4. The synthesis of a kaempferol hybrid (**15**) containing two 1,2,3-triazole units.

2.3. Biological Evaluation

The *in vitro* antiproliferative activities of chrysin (**3**) and the synthesized compounds (**8–11**, **15**) were examined against 60 human tumor cell lines according to the given protocols of NCI (USA) [31–35]. The results are summarized in Table 1. The percentages of growth show the amount of living cancer cells compared to a reference. The negative numbers indicate a significant decrease in the cell number. Since derivatives **8** and **10** had shown remarkable antiproliferative activity on several cancer cell lines during the one-dose test, they were subjected to a five-dose screening. The GI_{50} (50% growth inhibition) values are also given in Table 1.

Table 1. Antiproliferative activities of chrysin (3), hybrids 8–11 and 15 against 60 human cancer cell lines in vitro. In connection with GPR values, the negative numbers causing cell death are highlighted in bold. Values where $GI_{50} < 10 \mu\text{M}$ are highlighted in bold, too.

Type	Growth Percent Rates (GPR) at 10 μM (%), GI_{50} (μM)							
	3	8	9	10	11	15		
	GPR	GPR	GI_{50}	GPR	GPR	GI_{50}	GPR	GPR
Leukemia								
CCRF-CEM	102.24	108.83	>100	112.13	77.52	>100	104.65	60.89
HL-60(TB)	116.20	103.89	>100	114.55	98.05	>100	111.80	105.09
K-562	96.80	109.01	>100	103.64	45.49	>100	97.39	46.23
MOLT-4	105.93	95.46	>100	105.64	83.24	>100	96.99	79.61
RPMI-8226	101.04	93.67	>100	99.31	45.61	-	116.61	72.72
SR	77.87	96.85	-	-	32.75	-	-	64.31
Non-small cell lung cancer								
A549/ATCC	98.46	81.15	19.6	89.08	23.19	-	96.90	65.31
EKVX	89.35	60.13	63.8	90.34	57.19	-	102.98	87.06
HOP-62	113.09	-28.49	3.76	93.12	12.36	2.33	91.16	84.75
HOP-92	77.93	-3.35	4.43	94.82	-17.95	1.89	84.25	44.25
NCI-H226	86.84	60.93	3.51	75.07	-	2.07	-	42.31
NCI-H23	92.57	45.78	7.70	87.18	29.16	3.70	88.96	49.35
NCI-H322M	98.30	86.09	>100	93.16	43.54	-	95.03	70.85
NCI-H460	98.34	71.35	-	98.72	2.98	-	104.21	49.75
NCI-H522	88.95	15.11	6.60	87.56	17.59	3.66	73.12	48.28
Colon cancer								
COLO 205	104.94	102.72	>100	102.46	68.37	-	118.35	108.22
HCC-2998	102.88	100.11	>100	88.27	74.13	>100	100.57	95.35
HCT-116	82.69	48.53	5.91	86.67	18.21	3.52	88.21	41.04
HCT-15	90.99	94.40	-	87.80	73.48	-	96.46	77.80
HT29	102.89	100.18	>100	99.75	35.13	-	113.48	100.61
KM12	92.93	99.40	>100	100.75	43.34	-	100.81	83.69
SW-620	101.60	102.02	>100	99.67	60.30	-	95.28	79.33
CNS cancer								
SF-268	101.55	14.38	4.32	98.12	21.78	3.52	89.15	63.29
SF-295	99.86	10.37	10.2	96.99	38.91	2.32	99.59	65.43
SF-539	92.17	1.10	5.17	84.22	-10.54	2.21	88.21	38.91
SNB-19	86.04	-32.68	4.51	86.51	12.08	4.55	76.47	54.14
SNB-75	88.98	-65.88	3.74	85.58	6.29	1.69	81.23	53.82
U251	80.67	-16.90	13.9	93.22	10.45	2.80	106.25	71.92
Melanoma								
LOX IMVI	85.08	78.50	>100	95.50	34.84	-	99.64	58.11
MALME-3M	101.76	6.44	5.06	83.74	15.21	2.03	88.16	53.41
M14	106.78	65.94	>100	94.81	56.84	-	89.13	55.83

Table 1. Cont.

Type	Growth Percent Rates (GPR) at 10 μ M (%), GI ₅₀ (μ M)							
	3	8	9	10	11	15		
	GPR	GPR	GI ₅₀	GPR	GPR	GI ₅₀	GPR	GPR
MDA-MB-435	99.53	98.22	-	95.76	40.86	-	100.25	67.94
SK-MEL-2	109.90	-39.78	6.80	99.46	48.82	4.49	85.75	83.61
SK-ML-28	101.70	93.61	-	92.25	29.89	-	100.20	39.71
SK-MEL-5	92.85	84.47	>100	93.58	17.09	-	89.29	54.58
UACC-257	118.94	86.27	>100	95.41	46.37	-	94.84	83.76
UACC-62	82.24	53.15	-	76.28	29.96	-	88.18	42.06
Ovarian cancer								
IGROV1	95.22	31.22	17.6	78.98	43.47	4.45	94.68	53.46
OVCAR-3	97.60	61.68	-	112.53	21.16	-	105.28	53.34
OVCAR-4	112.07	-	-	97.37	-9.56	-	100.27	66.63
OVCAR-5	99.07	83.70	>100	95.94	55.10	-	93.98	81.04
OVCAR-8	95.19	20.41	3.76	91.53	12.68	-	91.22	56.95
NCI/ADR-RES	92.84	43.17	5.57	78.12	70.43	>100	99.23	88.99
SK-OV-3	128.15	20.59	6.57	91.10	16.22	-	109.51	87.44
Renal cancer								
786-0	99.20	2.24	9.26	101.61	1.13	1.96	100.98	74.81
A498	86.62	63.12	42.0	88.60	30.81	-	95.12	71.72
ACHN	85.03	5.21	6.23	89.78	7.30	-	85.97	53.80
CAKI-1	83.56	58.70	5.76	96.44	54.63	-	83.45	67.48
RXF 393	91.19	9.11	3.58	-	-8.05	1.78	85.59	37.74
SN12C	85.77	58.08	>100	98.25	38.67	-	85.22	56.19
TK-10	107.21	0.59	10.4	102.72	37.10	3.01	106.68	90.47
UO-31	89.42	67.00	-	74.94	3.64	-	81.08	79.66
Prostate cancer								
PC-3	93.17	75.99	-	92.51	35.99	-	107.77	77.08
DU-145	92.00	65.83	>100	107.16	40.01	-	101.38	67.54
Breast cancer								
MCF7	103.05	65.73	-	87.76	53.27	-	88.82	59.60
MDA-MB-231/ATCC	82.64	12.02	16.6	82.84	9.10	2.34	73.21	57.07
HS 578T	92.51	9.08	6.26	85.62	20.89	3.28	78.08	45.96
BT-549	91.01	16.31	7.98	83.18	18.75	-	78.58	49.15
T-47D	101.44	44.20	-	85.48	40.62	-	96.27	52.68
MDA-MB-468	91.09	53.94	20.0	80.62	38.69	1.97	74.09	54.70

It can be seen from Table 1 that no antiproliferative effect was shown by chrysin (3) and compounds 9 and 11. Hybrids 8 and 10 cause cell death on several cell lines of different types of cancer and show inhibition effect also on some cases. Despite the relatively limited structural diversity of our compounds, the above results revealed some interesting structure-activity relationships. We found that (i) the bis-hybrid compounds

also exert considerable antiproliferative effect and (ii) replacement of the fluorine atom by a nitro group reduces the bioactivity. The kaempferol-triazole hybrid (15) gave rather modest results.

The two promising compounds (8 and 10) were tested for their antiproliferative activity on further two human cervical cancer cell lines HeLa and SiHa (Table 2). Interestingly, the monohybrid derivative 8 was active only against HeLa cells, and SiHa cells were relatively resistant to it. The bis-hybrid derivative 10 was more potent and similarly active against both cell lines, with a sub-micromolar IC_{50} value against HeLa. Both derivatives exhibited higher activity than the reference agent cisplatin against HeLa cells.

Table 2. In vitro antiproliferative activity of compounds 8 and 10 against human cervical cancer cell lines. Compounds were tested in the concentration range of 0.1–30 μ M in 2 biological replicates, 5 parallel measurements each. IC_{50} values and their 95% confidence intervals (C.I.) are presented. Value where $IC_{50} < 1 \mu$ M is highlighted in bold. Cisplatin was included as a reference agent.

Hybrid/Cell Line	IC_{50} [95% Confidence Interval](μ M)	
	HeLa	SiHa
8	1.909 [1.543–2.361]	>30
10	0.7331 [0.5771–0.9312]	1.352 [1.148–1.592]
Cisplatin	12.26 [10.36–14.49]	5.305 [4.650–6.053]

The results obtained in this paper are encouraging for the future optimization of the derivatives. We want to emphasize that this study may be the starting point for more detailed synthetic and anticancer research.

3. Materials and Methods

3.1. General Materials and Methods

All chemicals were purchased from Sigma-Aldrich (Budapest, Hungary) and were used as received. Melting points were measured on a VEB Analytik Dresden PHMK-77/1328 apparatus (Dresden, Germany) and are uncorrected. IR spectra were recorded on Zeiss IR 75 and 80 instruments (Thornwood, NY, USA). NMR measurements were performed on a Bruker Avance III HDX 500 MHz NMR spectrometer equipped with a $^1\text{H}/^{13}\text{C}/^{15}\text{N}$ 5 mm TCI CryoProbe (Bruker Corporation, Billerica, MA, USA). ^1H and ^{13}C chemical shifts are given on the delta scale as parts per million (ppm) relative to tetramethyl silane. One-dimensional ^1H , and ^{13}C spectra and two-dimensional ^1H - ^1H COSY, ^1H - ^1H NOESY, ^1H - ^{13}C HSQC, and ^1H - ^{13}C HMBC spectra were acquired using pulse sequences included in the standard spectrometer software package (Bruker TopSpin 3.5, Bruker Corporation). ESI-HRMS and MS-MS analyses were performed on a Thermo Velos Pro Orbitrap Elite (Thermo Fisher Scientific, Bremen, Germany) system. The ionization method was ESI, operated in positive ion mode. The protonated molecular ion peaks were fragmented by CID (collision-induced dissociation) at a normalized collision energy of 35–65%. For the CID experiment, helium was used as the collision gas. The samples were dissolved in methanol. EI-HRMS analyses were performed on a Thermo Q Exactive GC Orbitrap (Thermo Fisher Scientific, Bremen, Germany) system. The ionization method was EI and operated in positive ion mode. Electron energy was 70 eV and the source temperature was set at 250 °C. Data acquisition and analysis were accomplished with Xcalibur software version 4.0 (Thermo Fisher Scientific). TLC was carried out using DC-Alufolien Kieselgel 60 F₂₅₄ (Merck, Budapest, Hungary) plates. Preparative TLC analyses were performed on silica gel 60 PF₂₅₄₊₃₆₆ (Merck) glass plates.

3.2. Chemistry

3.2.1. 7-(*O*-Propargyl)chrysin (6)

Chrysin (3) (330 mg, 1.3 mmol) and cesium carbonate (426 g, 1.3 mmol) were dissolved in DMF (15 mL), the solution was stirred at 10 min, then propargyl bromide (0.142 mL, 1.3 mmol) was added in 80% toluene solution. After stirring at room temperature for 18.5 hrs, the reaction mixture was evaporated to dryness, and the residue was dissolved in dichloromethane (60 mL). Next, water (60 mL) was added, and the pH was adjusted to 1 with 2M hydrochloric acid solution. The water phase was extracted with dichloromethane (2 × 30 mL), then the combined organic phase was washed with water (60 mL) and saturated sodium chloride solution (60 mL). The organic phase after drying with magnesium sulfate was evaporated to dryness, and the crude product was purified with preparative TLC (dichloromethane-methanol = 40:1) to give 274 mg (72%) of compound 6 as a yellow solid. M.p.: 180–182 °C. TLC (dichloromethane-methanol = 30:1); R_f = 0.83. IR (KBr) 3284, 1663, 1624, 1540, 1331, 1155, 767 cm^{-1} . ^1H NMR (499.9 MHz; DMSO- d_6) δ (ppm) 3.69 (t; J = 2.4 Hz; 1H; C(7)-OCH₂C≡CH); 4.97 (d; J = 2.4 Hz; 2H; C(7)-OCH₂); 6.48 (d; J = 2.3 Hz; 1H; H-6); 6.88 (d; J = 2.3 Hz; 1H; H-8); 7.07 (s; 1H; H-3); 7.58–7.62 (m; 2H; H-3', H-5'); 7.62–7.66 (m; 1H; H-4'); 8.09–8.13 (m; 2H; H-2', H-6'); 12.84 (s; 1H; C(5)-OH). ^{13}C NMR (125.7 MHz; DMSO- d_6) δ (ppm) 56.2 (C(7)-OCH₂); 78.3 (C(7)-OCH₂C≡CH); 79.0 (C(7)-OCH₂C≡CH); 93.7 (C-8); 98.6 (C-6); 105.2 (C-10); 105.4 (C-3); 126.4 (C-2', C-6'); 129.1 (C-3', C-5'); 130.5 (C-1'); 132.1 (C-4'); 157.1 (C-9); 161.1 (C-5); 163.1 (C-7); 163.5 (C-2). 182.1 (C-4). ESI-HRMS: M + H = 293.08086 (delta = 0.08 ppm; C₁₈H₁₃O₄). HR-ESI-MS-MS (CID = 55%; rel. int. %): 269(5); 265(100); 251(56); 247(4); 239(6); 223(10).

3.2.2. 5,7-Bis(*O*-propargyl)chrysin (7)

Chrysin (3) (500 mg, 1.97 mmol) and cesium carbonate (3.2 g, 9.84 mmol) were dissolved in dimethylformamide (20 mL), the solution was stirred at 10 min, then propargyl bromide (1.1 mL, 9.84 mmol) was added in 80% toluene solution. After stirring at room temperature for 45 min, the reaction mixture was evaporated to dryness, and the residue was dissolved in dichloromethane (40 mL). Next, water (40 mL) was added, and the pH was adjusted to 1 with 2M hydrochloric acid solution. The water phase was extracted with dichloromethane (3 × 20 mL), then the combined organic phase was washed with water (2 × 20 mL) and saturated sodium chloride solution (20 mL). The organic phase after drying with magnesium sulfate was evaporated to dryness and 620 mg (95%) pure product (7) was obtained. M.p.: 204–206 °C. TLC (dichloromethane-methanol = 30:1); R_f = 0.33. IR (KBr) 3214, 1635, 1597, 1450, 1343, 1164, 833 cm^{-1} . ^1H NMR (499.9 MHz; DMSO- d_6) δ (ppm) 3.63 (t; J = 2.4 Hz; 1H; C(5)-OCH₂C≡CH); 3.70 (t; J = 2.4 Hz; 1H; C(7)-OCH₂C≡CH); 4.93 (d; J = 2.4 Hz; 2H; C(5)-OCH₂); 4.98 (d; J = 2.4 Hz; 2H; C(7)-OCH₂); 6.67 (d; J = 2.3 Hz; 1H; H-6); 6.82 (s; 1H; H-3); 7.00 (d; J = 2.3 Hz; 1H; H-8); 7.54–7.62 (m; 3H; H-3', H-4', H-5'); 8.01–8.09 (m; 2H; H-2', H-6'). ^{13}C NMR (125.7 MHz; DMSO- d_6) δ (ppm) 56.2 (C(7)-OCH₂); 56.4 (C(5)-OCH₂); 78.3 (C(7)-OCH₂C≡CH); 78.6 (C(5)-OCH₂C≡CH); 78.8 (C(5)-OCH₂C≡CH); 79.0 (C(7)-OCH₂C≡CH); 95.0 (C-8); 98.8 (C-6); 108.2 (C-3); 109.1 (C-10); 125.9 (C-2', C-6'); 129.0 (C-3', C-5'); 130.7 (C-1'); 131.4 (C-4'); 157.8 (C-5); 158.8 (C-9); 159.7 (C-2); 161.2 (C-7); 175.4 (C-4). ESI-HRMS: M + H = 331.09618 (delta = −0.9 ppm; C₂₁H₁₅O₄). HR-ESI-MS-MS (CID = 35%; rel. int. %): 313(6); 303(89); 292(47); 289(16); 275(13); 265(13); 251(100); 185(36); 157(10).

3.2.3. Click Reaction of 7-(*O*-Propargyl)chrysin (6) with 4-Fluorobenzyl Azide; Preparation of 8

To 7-*O*-propargyl chrysin (6) (48 mg, 0.164 mmol) was added 4-fluorobenzyl azide (25 mg, 0.164 mmol) in toluene solution (4 mL) prepared in situ [30], triphenylphosphine (9 mg, 0.0328 mmol), copper(I) iodide (4 mg, 0.0164 mmol) and 0.09 mL (0.492 mmol) diisopropylethylamine. After reflux for 2 h, the reaction mixture was diluted with toluene (25 mL), then the mixture was washed with water (30 mL). After washing the water phase with toluene (10 mL), the combined organic phase after drying with magnesium

sulfate was evaporated to dryness. The preparative TLC (dichloromethane-methanol = 40:1) of the crude product resulted in 5 mg (7%) pure product (8). M.p.: 163–165 °C. M.p. *lit.*: 190–191 °C [20]. TLC (dichloromethane-methanol = 40:1); R_f = 0.34. IR (KBr) 3424, 1660, 1614, 1558, 1161, 766, 541 cm^{-1} . ^1H NMR (499.9 MHz; DMSO- d_6) δ (ppm) 5.29 (s; 2H; H₂-1'); 5.62 (s; 2H; H₂-7'); 6.50 (d; J = 2.2 Hz; 1H; H-6); 6.96 (d; J = 2.2 Hz; 1H; H-8); 7.06 (s; 1H; H-3); 7.19–7.24 (m; 2H; H-10', H-12'); 7.39–7.44 (m; 2H; H-9', H-13'); 7.58–7.66 (m; 3H; C(2)-Ph: 2x H_{meta}, H_{para}); 8.09–8.12 (m; 2H; C(2)-Ph: 2x H_{ortho}); 8.35 (s; 1H; H-6'); 12.8 (br; 1H; C(5)-OH). ^{13}C NMR (125.7 MHz; DMSO- d_6) δ (ppm) 52.0 (C-7'); 61.7 (C-1'); 93.5 (C-8); 98.6 (C-6); 105.0 (C-10); 105.3 (C-3); 115.5 (d; $^2J_{\text{CF}}$ = 21.6 Hz; C-10'; C-12'); 124.9 (C-6'); 126.4 (C(2)-Ph: C_{ortho}); 129.1 (C(2)-Ph: C_{meta}); 130.3 (d; $^3J_{\text{CF}}$ = 8.5 Hz; C-9', C-13'); 130.5 (C(2)-Ph: C_{ipso}); 132.0–132.1 (m; C-8', C(2)-Ph: C_{para}); 142.0 (C-2'); 157.2 (C-9); 161.1 (C-5); 161.8 (d; $^1J_{\text{CF}}$ = 244.2 Hz; C-11'); 163.5 (C-2); 163.9 (C-7); 182.0 (C-4). ESI-HRMS: M+H = 444.13547 (δ = 0.13 ppm; C₂₅H₁₉O₄N₃F). HR-ESI-MS-MS (CID = 45%; rel. int. %): 416(100); 363(32); 307(24); 293(12); 291(60); 267(26); 255(47).

3.2.4. Click Reaction of 7-(*O*-Propargyl)chrysin (6) with 4-Nitrobenzyl Azide; Preparation of 9

To 7-*O*-propargyl chrysin (6) (48 mg, 0.164 mmol) was added 4-nitrobenzyl azide (29 mg, 0.164 mmol) in toluene solution (4 mL) prepared in situ [30], triphenylphosphine (9 mg, 0.0328 mmol), copper(I) iodide (4 mg, 0.0164 mmol) and 0.09 mL (0.492 mmol) diisopropylethylamine. After reflux for 4 h, the reaction mixture was diluted with toluene (25 mL), then the mixture was washed with water (30 mL). After washing the water phase with toluene (10 mL), the combined organic phase after drying with magnesium sulfate was evaporated to dryness. The residue was dissolved in dichloromethane and after filtration, the filtrate was evaporated to dryness, then 24 mg (31%) product (9) was obtained. M.p.: 219–221 °C. M.p. *lit.*: 187–188 °C [20]. TLC (dichloromethane-methanol = 40:1); R_f = 0.45. IR (KBr) 809; 1155; 1349; 1524; 1617; 1656; 3083 cm^{-1} . ^1H NMR (499.9 MHz; DMSO- d_6) δ (ppm) 5.32 (s; 2H; H₂-1'); 5.83 (s; 2H; H₂-7'); 6.51 (d; J = 2.1 Hz; 1H; H-6); 6.97 (d; J = 2.1 Hz; 1H; H-8); 7.07 (s; 1H; H-3); 7.53–7.58 (m; 2H; H-9', H-13'); 7.58–7.67 (m; 3H; C(2)-Ph: 2x H_{meta}, H_{para}); 8.07–8.13 (m; 2H; C(2)-Ph: 2x H_{ortho}); 8.22–8.27 (m; 2H; H-10', H-12'); 8.43 (s; 1H; H-6'); 12.83 (s; 1H; C(5)-OH). ^{13}C NMR (125.7 MHz; DMSO- d_6) δ (ppm) 51.9 (C-7'); 61.7 (C-1'); 93.6 (C-8); 98.7 (C-6); 105.1 (C-10); 105.4 (C-3); 123.9 (C-10', C-12'); 125.4 (C-6'); 126.4 (C(2)-Ph: C_{ortho}); 129.0 (C-9', C-13'); 129.1 (C(2)-Ph: C_{meta}); 130.5 (C(2)-Ph: C_{ipso}); 132.1 (C(2)-Ph: C_{para}); 142.2 (C-2'); 143.2 (C-8'); 147.2 (C-11'); 157.2 (C-9); 161.1 (C-5); 163.5 (C-2); 163.9 (C-7); 182.0 (C-4). ESI-HRMS: M+H = 471.12976 (δ = -0.3 ppm; C₂₅H₁₉O₆N₄). HR-ESI-MS-MS (CID = 35%; rel. int. %): 443(25); 425(12); 307(18); 291(26); 255(100); 189(2).

3.2.5. Click Reaction of 5,7-Bis(*O*-propargyl)chrysin (7) with 4-Fluorobenzyl Azide; Preparation of 10

(a) To 5,7-bis(*O*-propargyl) chrysin (7) (44 mg, 0.133 mmol) was added 4-fluorobenzyl azide (40 mg, 0.265 mmol) in toluene solution (6 mL) prepared in situ [30], triphenylphosphine (14 mg, 0.0532 mmol), copper(I) iodide (5 mg, 0.0265 mmol) and 0.14 mL (0.798 mmol) diisopropylethylamine. After reflux for 5 hrs, the reaction mixture was diluted with toluene (25 mL), and the mixture was washed with water (30 mL), then the water phase was washed with toluene (10 mL). The combined organic phase was dried with magnesium sulfate and the precipitated product (10) (32 mg, 38%) could be separated with filtration.

(b) To 5,7-bis(*O*-propargyl) chrysin (7) (44 mg, 0.133 mmol) was added 4-fluorobenzyl azide (40 mg, 0.266 mmol) in dichloromethane solution (4.5 mL) prepared in situ [30], copper(II) sulfate pentahydrate (56 mg, 0.222 mmol), sodium L-ascorbate (88 mg, 0.443 mmol) and water (4.5 mL). After 18 hrs of intensive stirring at room temperature, the reaction mixture was diluted with water (18 mL) and extracted with dichloromethane (2 × 20 mL). The combined organic phase was washed with saturated sodium chloride solution (50 mL), and after drying with magnesium sulfate the solution was evaporated.

The residue was separated with preparative TLC (dichloromethane-methanol = 15:1) and 27 mg (32%) product (**10**) was obtained (Figure 2). Mp.: 229–231 °C. TLC (dichloromethane-methanol = 20:1); R_f = 0.30. IR (KBr) 1642, 1605, 1511, 1352, 1225, 1159 cm^{-1} . ^1H NMR (499.9 MHz; DMSO- d_6) δ (ppm) 5.23 (s; 2H; H₂-1''); 5.31 (s; 2H; H₂-1'); 5.63 (s; 2H; H₂-7'); 5.64 (s; 2H; H₂-7''); 6.76 (s; 1H; H-3); 6.80 (d; J = 2.2 Hz; 1H; H-6); 7.07 (d; J = 2.2 Hz; 1H; H-8); 7.18–7.24 (m; 4H; H-10', H-12', H-10'', H-12''); 7.38–7.42 (m; 2H; H-9'', H-13''); 7.40–7.45 (m; 2H; H-9', H-13'); 7.54–7.61 (m; 3H; C(2)-Ph: 2x H_{meta}, H_{para}); 8.02–8.06 (m; 2H; C(2)-Ph: 2x H_{ortho}); 8.31 (s; 1H; H-6''); 8.37 (s; 1H; H-6'). ^{13}C NMR (125.7 MHz; DMSO- d_6) δ (ppm) 51.9 (C-7''); 52.0 (C-7'); 61.6 (C-1'); 62.6 (C-1''); 94.8 (C-6); 98.4 (C-6); 108.2 (C-3); 108.8 (C-10); 115.4–115.6 (m; C-10', C-12', C-10'', C-12''); 124.5 (C-6''); 124.9 (C-6'); 125.8 (C(2)-Ph: C_{ortho}); 129.0 (C(2)-Ph: C_{meta}); 130.2 (d; $^3J_{\text{CF}}$ = 8.5 Hz; C-9'', C-13''); 130.3 (d; $^3J_{\text{CF}}$ = 8.5 Hz; C-9', C-13'); 130.7 (C(2)-Ph: C_{ipso}); 131.4 (C(2)-Ph: C_{para}); 132.1–132.2 (m; C-8', C-8''); 142.1 (C-2'); 142.9 (C-2''); 158.7 (C-5); 159.0 (C-9); 159.6 (C-2); 161.78 (d; $^1J_{\text{CF}}$ = 244 Hz), 161.81 (d; $^1J_{\text{CF}}$ = 244 Hz): C-11', C-11''); 162.2 (C-7); 175.4 (C-4). ESI-HRMS: M + H = 633.20636 (δ = 1.14 ppm; C₃₅H₂₇O₄N₆F₂). HR-ESI-MS-MS (CID = 35%; rel. int. %): 605(43); 588(5); 577(6); 552(8); 498(8); 496(8); 456(5); 452(26); 444(48); 424(5); 399(6).

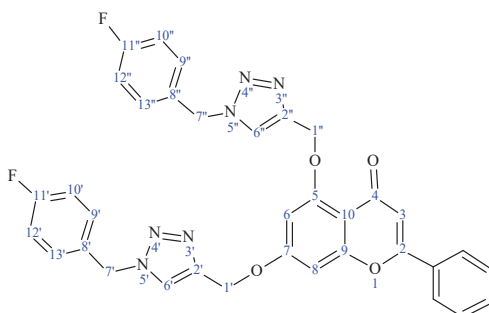


Figure 2. The skeleton numbering of compound **10** used for NMR assignment.

3.2.6. Click Reaction of 5,7-Bis(O-propargyl)chrysin (**7**) with 4-Nitrobenzyl Azide; Preparation of **11**

(a) To 5,7-bis(propargyl) chrysin (**7**) (44 mg, 0.133 mmol) was added 4-nitrobenzyl azide (47 mg, 0.266 mmol) in toluene solution (6 mL) prepared in situ [30], triphenylphosphine (14 mg, 0.0532 mmol), copper(I) iodide (5 mg, 0.0265 mmol) and 0.14 mL (0.798 mmol) diisopropylethylamine. After reflux for 4 hrs, the reaction mixture was diluted with toluene (25 mL), and the mixture was washed with water (30 mL), then the water phase was washed with toluene (10 mL). The combined organic phase was dried with magnesium sulfate, and the precipitated crude product could be separated with filtration. After preparative TLC (dichloromethane-methanol = 15:1) of the crude product, 9 mg (10%) pure product (**11**) was obtained.

(b) To 5,7-bis(O-propargyl) chrysin (**7**) (176 mg, 0.532 mmol) was added 4-nitrobenzyl azide (190 mg, 1.064 mmol) in dichloromethane solution (18 mL) prepared in situ [30], copper(II) sulfate pentahydrate (224 mg, 0.888 mmol), sodium L-ascorbate (352 mg, 1.772 mmol) and water (18 mL). After 16.5 h of intensive stirring at room temperature, the reaction mixture was diluted with water (72 mL) and extracted with dichloromethane (3 × 80 mL). The combined organic phase was washed with saturated sodium chloride solution (200 mL), and after drying with magnesium sulfate the solution was evaporated. The residue was separated with preparative TLC (dichloromethane-methanol = 15:1) and 30 mg (17%) product (**11**) was obtained. Mp. = 182–184 °C. TLC (dichloromethane-methanol = 20:1); R_f = 0.40. IR (KBr) 805; 1109; 1167; 1348; 1521; 1608; 1644; 3080 cm^{-1} . ^1H NMR (499.9 MHz; DMSO- d_6) δ (ppm) 5.27 (s; 2H; H₂-1''); 5.34 (s; 2H; H₂-1'); 5.83 (s; 2H; H₂-7'); 5.84 (s; 2H; H₂-7''); 6.76 (s; 1H; H-3); 6.82 (d; J = 2.3 Hz; 1H; H-6); 7.09 (d; J = 2.3 Hz; 1H; H-8); 7.53–7.61 (m; 7H; H-9', H-13', H-9'', H-13''); C(2)-Ph: 2x H_{meta}, H_{para}); 8.02–8.06 (m; 2H; C(2)-Ph: 2x H_{ortho});

8.22–8.26 (m; 4H; H-10', H-12', H-10'', H-12''); 8.39 (s; 1H; H-6''); 8.45 (s; 1H; H-6'). ¹³C NMR (125.7 MHz; DMSO-*d*₆) δ (ppm) 51.8 (C-7''); 51.9 (C-7'); 61.6 (C-1'); 62.6 (C-1''); 94.9 (C-8); 98.4 (C-6); 108.2 (C-3); 108.8 (C-10); 123.8 (C-10', C-12', C-10'', C-12''); 125.0 (C-6''); 125.4 (C-6'); 125.8 (C(2)-Ph: *C_{ortho}*); 129.0 (C-9', C-13', C-9'', C-13'', C(2)-Ph: *C_{meta}*); 130.7 (C(2)-Ph: *C_{ipso}*); 131.4 (C(2)-Ph: *C_{para}*); 142.2 (C-2'); 143.1 (C-2''); 143.2 (C-8'); 143.3 (C-8''); 147.2 (C-11', C-11''); 158.7 (C-5); 159.0 (C-9); 159.6 (C-2); 162.1 (C-7); 175.4 (C-4). ESI-HRMS: M+H = 687.19286 (δ = -2.6 ppm; C₃₅H₂₇O₈N₈). HR-ESI-MS-MS (CID = 35%; rel. int. %): 659(45); 631(10); 507(84); 471(100); 443(12); 343(3); 291(7).

3.2.7. O-Alkylation of Kaempferol (4) with Propargyl Bromide

(a) Kaempferol (4) (113 mg, 0.393 mmol) and cesium carbonate (129 mg, 0.393 mmol) were dissolved in dimethylformamide (5 mL) and after 10 min stirring propargyl bromide (0.043 mL, 0.393 mmol) was added in 80% toluene solution. The reaction mixture was stirred at room temperature for 2.5 hrs and was evaporated to dryness. The residue was dissolved in dichloromethane (20 mL), then water (20 mL) was added and the pH was adjusted to 1 with 2N hydrochloric solution. The water phase was washed with dichloromethane (2 × 10 mL), the combined organic phase was treated with water (20 mL), and then with saturated sodium chloride solution (20 mL). After drying with magnesium sulfate the solution was evaporated to dryness and using preparative TLC (dichloromethane-methanol = 20:1) two products were obtained: 8 mg (6%) of monopropargylated derivative (12), and 25 mg (19%) of 3,7-bis(O-propargyl) kaempferol (13).

(b) Kaempferol (4) (1130 mg, 3.93 mmol) and potassium carbonate (543 mg, 3.93 mg) were dissolved in dimethylformamide (15 mL). After 10 min stirring at room temperature propargyl bromide (0.43 mL, 3.93 mmol, in 80% toluene solution) dissolved in dimethylformamide (5 mL) was dropped into the reaction mixture. After 2.5 h further potassium carbonate (272 mg, 1.97 mmol) and propargyl bromide (0.22 mL, 1.97 mmol, in 80% toluene solution) dissolved in dimethylformamide (2 mL) were added. The reaction mixture was stirred for a further 5 hrs at room temperature, evaporated to dryness, and the residue was dissolved in chloroform (200 mL). Next, water (200 mL) was added, and the pH was adjusted to 1 with 2N hydrochloric acid. The water phase was extracted with chloroform (2 × 100 mL), and the combined organic phase was washed with water (200 mL) and with saturated sodium chloride solution (200 mL) and evaporated to dryness. Preparative TLC (dichloromethane-methanol = 20:1) separation of the residue 40 mg (3%) of 12 and 330 mg (23%) of 13 were obtained.

3-(O-Propargyl)kaempferol (12): M.p. = 180–182 °C. TLC (dichloromethane-methanol = 20:1); *R_f* = 0.19. IR (KBr) 821; 1180; 1235; 1557; 1660; 3293 cm⁻¹. ¹H NMR (499.9 MHz; DMSO-*d*₆) δ (ppm) 3.50 (t; *J* = 2.4 Hz; 1H; C(3)-OCH₂C≡CH); 4.89 (d; *J* = 2.4 Hz; 2H; C(3)-OCH₂); 6.22 (d; *J* = 2.1 Hz; 1H; H-6); 6.46 (d; *J* = 2.1 Hz; 1H; H-8); 6.90–6.95 (m; 2H; H-3', H-5'); 7.98–8.01 (m; 2H; H-2', H-6'); 10.28 (br s; 1H; C(4')-OH); 10.90 (br; 1H; C(7)-OH); 12.55 (s; 1H; C(5)-OH). ¹³C NMR (125.7 MHz; DMSO-*d*₆) δ (ppm) 58.8 (C(3)-OCH₂); 78.6 (C(3)-OCH₂C≡CH); 79.2 (C(3)-OCH₂C≡CH); 93.7 (C-8); 98.6 (C-6); 103.8 (C-10); 115.4 (C-3', C-5'); 120.4 (C-1'); 130.4 (C-2', C-6'); 134.8 (C-3); 156.25 (C-9); 156.34 (C-2); 160.1 (C-4'); 161.1 (C-5); 164.2 (C-7); 177.6 (C-4). EI-HRMS: M = 324.06174 (δ = -3.4 ppm; C₁₈H₁₂O₆).

3,7-Bis(O-propargyl)kaempferol (13): M.p. = 185–187 °C. TLC (dichloromethane-methanol = 20:1); *R_f* = 0.49. IR (KBr) 1180; 1289; 1332; 1493; 1602; 1662; 3259 cm⁻¹. ¹H NMR (499.9 MHz; DMSO-*d*₆) δ (ppm) 3.51 (t; *J* = 2.4 Hz; 1H; C(3)-OCH₂C≡CH); 3.68 (t; *J* = 2.4 Hz; 1H; C(7)-OCH₂C≡CH); 4.91 (d; *J* = 2.4 Hz; 2H; C(3)-OCH₂); 4.95 (d; *J* = 2.4 Hz; 2H; C(7)-OCH₂); 6.46 (d; *J* = 2.3 Hz; 1H; H-6); 6.82 (d; *J* = 2.3 Hz; 1H; H-8); 6.93–6.97 (m; 2H; H-3', H-5'); 8.01–8.05 (m; 2H; H-2', H-6'); 10.3–10.4 (br; 1H; C(4')-OH); 12.55 (s; 1H; C(5)-OH). ¹³C NMR (125.7 MHz; DMSO-*d*₆) δ (ppm) 56.2 (C(7)-OCH₂); 58.9 (C(3)-OCH₂); 78.3 (C(7)-OCH₂C≡CH); 78.5 (C(3)-OCH₂C≡CH); 79.0 (C(7)-OCH₂C≡CH); 79.3 (C(3)-OCH₂C≡CH); 93.3 (C-8); 98.4 (C-6); 105.2 (C-10); 115.4 (C-3', C-5'); 120.3 (C-1'); 130.5 (C-2', C-6'); 135.1 (C-3); 155.9 (C-9); 156.8 (C-2); 160.3 (C-4'); 160.8 (C-5); 162.9 (C-7); 177.8 (C-4). EI-HRMS: M = 362.07804 (δ = -1.2 ppm; C₂₁H₁₄O₆).

(c) Kaempferol (**4**) (200 mg, 0.699 mmol) and potassium carbonate (106 mg, 0.769 mg) were dissolved in acetone (7 mL). After 10 min stirring at room temperature propargyl bromide (0.076 mL, 0.699 mmol, in 80% toluene solution) dissolved in acetone (3 mL) was dropped into the reaction mixture. After 7 hrs reflux further potassium carbonate (53 mg, 0.35 mmol) and propargyl bromide (0.038 mL, 0.35 mmol, in 80% toluene solution) dissolved in acetone (1.5 mL) were added. The reaction mixture was refluxed for a further 6 hrs, evaporated to dryness, and the residue was dissolved in dichloromethane (40 mL). Next, water (40 mL) was added and the pH was adjusted to 1 with 2*N* hydrochloric acid. The water phase was extracted with dichloromethane (2 × 20 mL), the combined organic phase was washed with water (40 mL) and with saturated sodium chloride solution (40 mL) and evaporated to dryness. After preparative TLC (dichloromethane-methanol = 20:1) separation of the residue, 10 mg (3%) of product **14** was obtained. M.p. = 158–160 °C. TLC (dichloromethane-methanol = 20:1); R_f = 0.82. IR (KBr) 1174; 1185; 1509; 1605; 1627; 3287 cm^{-1} . ^1H NMR (499.9 MHz; DMSO- d_6) δ (ppm) 3.47 (t; J = 2.4 Hz; 1H; C(3)-OCH₂C≡CH); 3.64 (t; J = 2.4 Hz; 1H; C(4′)-OCH₂C≡CH); 3.65 (t; J = 2.4 Hz; 1H; C(5)-OCH₂C≡CH); 3.69 (t; J = 2.4 Hz; 1H; C(7)-OCH₂C≡CH); 4.91 (d; J = 2.4 Hz; 2H; C(3)-OCH₂); 4.92 (d; J = 2.4 Hz; 2H; C(4′)-OCH₂); 4.93 (d; J = 2.4 Hz; 2H; C(5)-OCH₂); 4.97 (d; J = 2.4 Hz; 2H; C(7)-OCH₂); 6.64 (d; J = 2.3 Hz; 1H; H-6); 6.96 (d; J = 2.3 Hz; 1H; H-8); 7.15–7.19 (m; 2H; H-3′, H-5′); 8.07–8.11 (m; 2H; H-2′, H-6′). ^{13}C NMR (125.7 MHz; DMSO- d_6) δ (ppm) 55.5 (C(4′)-OCH₂); 56.2 (C(7)-OCH₂); 56.5 (C(5)-OCH₂); 58.2 (C(3)-OCH₂); 78.2 (C(7)-OCH₂C≡CH); 78.5 (C(5)-OCH₂C≡CH); 78.6 (C(4′)-OCH₂C≡CH); 78.76 (C(4′)-OCH₂C≡CH); 78.79 (C(3)-OCH₂C≡CH); 78.9 (C(5)-OCH₂C≡CH); 79.05 (C(7)-OCH₂C≡CH); 79.10 (C(3)-OCH₂C≡CH); 94.7 (C-8); 98.4 (C-6); 108.8 (C-10); 114.7 (C-3′, C-5′); 123.0 (C-1′); 129.8 (C-2′, C-6′); 137.4 (C-3); 152.7 (C-2); 157.80 (C-9); 157.82 (C-5); 158.8 (C-4′); 161.2 (C-7); 171.9 (C-4). EI-HRMS: M = 438.10893 (δ = −2.0 ppm; C₂₇H₁₈O₆).

3.2.8. Click Reaction of 3,7-Bis(O-propargyl)kaempferol (**13**) with 4-Fluorobenzyl Azide; Preparation of **15**

(a) To 3,7-bis(O-propargyl) kaempferol (**13**) (140 mg, 0.387 mmol) was added 4-fluorobenzyl azide (117 mg, 0.773 mmol) in toluene solution (10 mL) prepared in situ [30], triphenylphosphine (41 mg, 0.155 mmol), copper(I) iodide (15 mg, 0.077 mmol), 0.43 mL (2.322 mmol) diisopropylethylamine and 13 mL toluene. After reflux for 5.5 hrs, the reaction mixture was diluted with toluene (70 mL), and the mixture was washed with water (45 mL), then the water phase was washed with toluene (15 mL). The combined organic phase was dried with magnesium sulfate and after preparative TLC (dichloromethane-methanol = 20:1) of the residue, 17 mg (7%) product (**15**) was obtained.

(b) To 3,7-bis(O-propargyl) kaempferol (**13**) (193 mg, 0.532 mmol) was added 4-fluorobenzyl azide (161 mg, 1.064 mmol) in dichloromethane solution (18 mL) prepared in situ [30], copper(II) sulfate pentahydrate (222 mg, 0.888 mmol), sodium L-ascorbate (351 mg, 1.77 mmol) and water (18 mL). After 8 h of intensive stirring at room temperature, the reaction mixture was diluted with water (70 mL) and extracted with dichloromethane (3 × 80 mL). The combined organic phase was washed with saturated sodium chloride solution (200 mL), and after drying with magnesium sulfate the solution was evaporated. The residue was separated with preparative TLC (dichloromethane-methanol = 20:1) and 18 mg (5%) product (**15**) was obtained (Figure 3). M.p. = 151–153 °C. TLC (dichloromethane-methanol = 20:1); R_f = 0.31. IR (KBr) 1172; 1225; 1512; 1587; 1602; 1665; 3139 cm^{-1} . ^1H NMR (499.9 MHz; DMSO- d_6) δ (ppm) 5.20 (s; 2H; H₂-1′′); 5.27 (s; 2H; H₂-1′); 5.51 (s; 2H; H₂-7′′); 5.62 (s; 2H; H₂-7′); 6.47 (d; J = 2.2 Hz; 1H; H-6); 6.85–6.87 (m; 2H; C(2)-Ar: 2x H_{meta}); 6.88 (d; J = 2.2 Hz; 1H; H-8); 7.14–7.19 (m; 2H; H-10′′, H-12′′); 7.19–7.25 (m; 4H; H-10′, H-12′, H-9′′, H-13′′); 7.39–7.44 (m; 2H; H-9′, H-13′); 7.88–7.92 (m; 2H; C(2)-Ar: 2x H_{ortho}); 8.14 (s; 1H; H-6′′); 8.34 (s; 1H; H-6′); 10.30 (br s; 1H; C(2)-Ar: C_{para}-OH); 12.68 (s; 1H; C(5)-OH). ^{13}C NMR (125.7 MHz; DMSO- d_6) δ (ppm) 51.7 (C-7′′); 52.0 (C-7′); 61.7 (C-1′); 64.1 (C-1′′); 93.0 (C-8); 98.3 (C-6); 105.2 (C-10); 115.3 (C(2)-Ar: C_{meta}); 115.4 (d; $^2J_{\text{CF}}$ = 21.6 Hz; C-10′′, C-12′′); 115.5 (d; $^2J_{\text{CF}}$ = 21.6 Hz; C-10′, C-12′); 120.3 (C(2)-Ar: C_{ipso}); 124.9 (C-6′); 125.0 (C-6′′);

129.8 (d; $^3J_{CF} = 8.4$ Hz; C-9', C-13'); 130.27 (C(2)-Ar: C_{ortho}); 130.30 (d; $^3J_{CF} = 8.3$ Hz; C-9', C-13'); 132.1 (d; $^4J_{CF} = 3.0$ Hz; C-8', C-8''); 135.6 (C-3); 142.1 (C-2'); 142.4 (C-2''); 156.1 (C-9); 156.5 (C-2); 160.1 (C(2)-Ar: C_{para}); 160.9 (C-5); 161.4 (d; $^1J_{CF} = 244.2$ Hz; C-11'); 161.7 (d; $^1J_{CF} = 244.4$ Hz; C-11''); 163.7 (C-7); 178.0 (C-4). ESI-HRMS: M + H = 665.19497 (delta = -0.7 ppm; C₃₅H₂₇O₆N₆F₂). HR-ESI-MS-MS (CID = 35%; rel. int. %): 637(51); 620(5); 584(8); 530(20); 512(51); 484(26); 476(100); 456(7); 448(51); 431(8); 299(4).

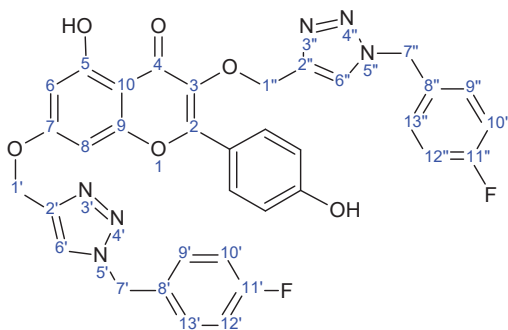


Figure 3. The skeleton numbering of compound 15 used for NMR assignment.

3.3. Biological Evaluation

3.3.1. One-Dose Screen

All compounds were tested initially at a single high dose (10^{-5} M) in the full NCI60 cell panel [31–35]. The number reported for the one-dose assay is growth relative to the no-drug control and relative to the time zero number of cells. This allowed the detection of both growth inhibition (values between 0 and 100) and lethality (values less than 0). For example, a value of 100 means no growth inhibition. A value of 30 would mean 70% growth inhibition. A value of 0 means no net growth over the course of the experiment. A value of -30 would mean 30% lethality. A value of -100 means all cells are dead.

3.3.2. Five-Dose Screen

Compounds that exhibited significant growth inhibition in the one-dose screen were evaluated against the 60-cell panel at five concentration levels. The human tumor cell lines of the cancer screening panel were grown in RPMI 1640 medium containing 5% fetal bovine serum and 2 mM l-glutamine. Typically, cells were inoculated in 96-well microtiter plates in 100 μ L at plating densities ranging from 5000 to 40,000 cells/well, depending on the doubling time of individual cell lines. After cell inoculation, the microtiter plates were incubated at 37 $^{\circ}$ C, 5% CO₂, 95% air, and 100% relative humidity for 24 h prior to the addition of experimental drugs. After 24 h, two plates of each cell line were fixed in situ with trichloroacetic acid (TCA), to represent a measurement of the cell population for each cell line at the time of drug addition (t_2). Experimental drugs were solubilized in dimethyl sulfoxide at 400-fold the desired final maximum test concentration and stored frozen prior to use. At the time of drug addition, an aliquot of frozen concentrate was thawed and diluted to twice the desired final maximum test concentration with complete medium containing 50 μ g ml⁻¹ gentamicin. Additional four, 10-fold or $\frac{1}{2}$ log serial dilutions were made to provide a total of five drug concentrations plus control. Aliquots of 100 μ L of these different drug dilutions were added to the appropriate microtiter wells already containing 100 μ L of medium, resulting in the required final drug concentrations.

Following drug addition, the plates were incubated at 37 $^{\circ}$ C, 5% CO₂, 95% air, and 100% relative humidity for an additional 48 h. For adherent cells, the assay was terminated by the addition of cold TCA. Cells were fixed in situ by the addition of 50 μ L of cold 50% (*w/v*) TCA, and incubated at 4 $^{\circ}$ C for 60 min. The supernatant was discarded, and the plates were washed with water (5 \times) and dried in air. Sulforhodamine B (SRB) solution

(100 μ L) at 0.4% (*w/v*) in 1% acetic acid was added to each well, and plates were incubated at room temperature for 10 min. After staining, the unbound dye was removed by washing five times with 1% acetic acid, and the plates were dried in the air. The bound stain is subsequently solubilized with 10 mM trizma base, and the absorbance is read on an automated plate reader at $\lambda = 515$ nm. Using the seven absorbance measurements [time zero (t_z), control growth (c), and test growth in the presence of drug at the five concentration levels (t_i)], the percentage growth was calculated at each of the drug concentration levels. Growth inhibition (%) was calculated as:

$$[(t_i - t_z)/(c - t_z)] \times 100, \text{ for concentrations where } t_i \geq t_z \quad (1)$$

$$[(t_i - t_z)/(t_z)] \times 100, \text{ for concentrations where } t_i < t_z. \quad (2)$$

Three dose-response parameters were calculated as follows. GI_{50} (growth inhibition of 50%) was calculated from Equation (3), which is the drug concentration resulting in a 50% reduction in the net protein increase (as measured by SRB staining) in control cells during the drug incubation. The drug concentration resulting in total growth inhibition (TGI) was calculated from Equation (4), where $t_i = t_z$. The LC_{50} indicating a 50% net loss of cells following treatment was calculated from Equation (5):

$$[(t_i - t_z)/(c - t_z)] \times 100 = 50 \quad (3)$$

$$[(t_i - t_z)/(c - t_z)] \times 100 = 0 \quad (4)$$

$$[(t_i - t_z)/(t_z)] \times 100 = -50. \quad (5)$$

3.3.3. Antiproliferative Assay on HeLa and SiHa Cells

Cervical adenocarcinoma (HeLa) and cervical carcinoma (SiHa) cells were obtained from the European Collection of Cell Cultures (Salisbury, UK) and the American Type Tissue Culture Collection (Manassas, VA, USA), respectively. The cells were cultured in Minimum Essential Medium supplemented with 10% fetal bovine serum, 1% non-essential amino acids, and 1% penicillin-streptomycin at 37 °C in a humidified atmosphere. Media and supplements were purchased from Lonza Group Ltd. (Basel, Switzerland). Cell viability was assessed by the MTT assay as published before [36]. Briefly, the cells were seeded in 96 well plates at 5000 cells/well density. After 24 h, 100 μ L of new media containing the test samples was added. After incubation for 72 h, an aliquot of 44 μ L of MTT solution (5 mg/mL) was added. After incubation for a further 4 h, the medium was removed by aspiration, the precipitated formazan crystals were dissolved by adding 100 μ L of DMSO to each well, and the plates were shaken at 37 °C for 1 h. The absorbance was measured at 545 nm with a microplate reader. IC_{50} values were calculated by fitting sigmoidal dose-response curves by the nonlinear regression model log (inhibitor) vs. normalized response and variable slope fit of GraphPad Prism 6 (GraphPad Software Inc., San Diego, CA, USA). Clinically utilized anticancer agent cisplatin (Ebewe GmbH, Unterach, Austria) was included as a reference molecule.

4. Conclusions

As a result of the current study, hybrid compounds containing chrysin coupled with substituted 1,2,3-triazole pharmacophores showed significant *in vitro* anticancer activities on several cell lines of different types of cancer. Moreover, the activity of the bis-conjugated derivatives of chrysin was also considerable. Therefore, it may be a reasonable strategy to prepare further hybrid molecules of flavones with more complex structures to obtain potentially valuable new antitumor leads.

Author Contributions: A.N.-R. performed the experiments; P.K. and L.H. conceived and designed the experiments; A.D.L. performed bioactivity testing supervised by I.Z. and A.H.; L.H. wrote the paper. All authors have read and agreed to the published version of the manuscript.

Funding: This research received no external funding.

Institutional Review Board Statement: Not applicable.

Informed Consent Statement: Not applicable.

Data Availability Statement: Not available.

Acknowledgments: Project no. RRF-2.3.1-21-2022-00015 has been implemented with the support provided by the European Union. A.H. acknowledges support from the Ministry of Innovation and Technology of Hungary (TKP2021-EGA-32). We thank Áron Szigetvári, Miklós Dékány and Csaba Szántay Jr., Gedeon Richter Plc., for the NMR and MS measurements and interpretations.

Conflicts of Interest: The authors declare no conflict of interest.

Sample Availability: Samples of the compounds are not available from the authors.

References

- Nepali, K.; Sharma, S.; Sharma, M.; Bedi, P.M.S.; Dhar, K.L. Rational approaches, design strategies, structure activity relationship and mechanistic insights for anticancer hybrids. *Eur. J. Med. Chem.* **2014**, *77*, 422–487. [[CrossRef](#)] [[PubMed](#)]
- Choudhary, S.; Singh, P.K.; Verma, H.; Singh, H.; Silakari, O. Success stories of natural product-based hybrid molecules for multi-factorial diseases. *Eur. J. Med. Chem.* **2018**, *151*, 62–97. [[CrossRef](#)] [[PubMed](#)]
- Mayer, S.; Keglevich, P.; Hazai, L. *Vinca* Hybrids with Antiproliferative Effect. *Med. Res. Arch.* **2022**, *10*, 2–11. [[CrossRef](#)]
- Keglevich, P.; Hazai, L.; Gorka-Kereskényi, Á.; Péter, L.; Gyenese, J.; Lengyel, Z.; Kalas, G.; Dubrovay, Z.; Dékány, M.; Orbán, E.; et al. Synthesis and *in vitro* antitumor effect of new vindoline derivatives coupled with amino acid esters. *Heterocycles* **2013**, *87*, 2299–2317. [[CrossRef](#)]
- Keglevich, A.; Dányi, L.; Rieder, A.; Horváth, D.; Szigetvári, Á.; Dékány, M.; Szántay, C., Jr.; Latif, A.D.; Hunyadi, A.; Zupkó, I.; et al. Synthesis and Cytotoxic Activity of New Vindoline Derivatives Coupled to Natural and Synthetic Pharmacophores. *Molecules* **2020**, *25*, 1010. [[CrossRef](#)]
- Keglevich, A.; Zsiros, V.; Keglevich, P.; Szigetvári, Á.; Dékány, M.; Szántay, C., Jr.; Mernyák, E.; Wölfling, J.; Hazai, L. Synthesis and *in vitro* Antitumor Effect of New Vindoline-Steroid Hybrids. *Curr. Org. Chem.* **2019**, *23*, 958–966. [[CrossRef](#)]
- Mayer, S.; Nagy, N.; Keglevich, P.; Szigetvári, Á.; Dékány, M.; Szántay, C., Jr.; Hazai, L. Synthesis of Novel Vindoline-Chrysin Hybrids. *Chem. Biodivers.* **2021**, *18*, e202100725. [[CrossRef](#)]
- Keglevich, A.; Szigetvári, Á.; Dékány, M.; Szántay, C., Jr.; Keglevich, P.; Hazai, L. Synthesis and *in vitro* Antitumor Effect of New Vindoline Derivatives Coupled with Triphenylphosphine. *Curr. Org. Chem.* **2019**, *23*, 852–858. [[CrossRef](#)]
- Mayer, S.; Keglevich, P.; Ábrányi-Balogh, P.; Szigetvári, Á.; Dékány, M.; Szántay, C., Jr.; Hazai, L. Synthesis and *In Vitro* Anticancer Evaluation of Novel Chrysin and 7-Aminochrysin Derivatives. *Molecules* **2020**, *25*, 888. [[CrossRef](#)]
- Kopustinskiene, D.M.; Jakstas, V.; Savickas, A.; Bernatoniene, J. Flavonoids as Anticancer Agents. *Nutrients* **2020**, *12*, 457. [[CrossRef](#)]
- Ren, W.; Qiao, Z.; Wang, H.; Zhu, L.; Zhang, L. Flavonoids: Promising Anticancer Agents. *Med. Res. Rev.* **2003**, *23*, 519–534. [[CrossRef](#)] [[PubMed](#)]
- Xu, Z.; Zhao, S.-J.; Liu, Y. 1,2,3-Triazole containing hybrids as potential anticancer agents: Current developments, action mechanisms and structure-activity relationship. *Eur. J. Med. Chem.* **2019**, *183*, 111700. [[CrossRef](#)] [[PubMed](#)]
- El Azab, I.H.; El-Sheshtawy, H.S.; Bakr, R.B.; Elkanzi, N.A.A. New 1,2,3-Triazole-Containing Hybrids as Antitumor Candidates: Design, Click Reaction Synthesis, DFT Calculations, and Molecular Docking Study. *Molecules* **2021**, *26*, 708. [[CrossRef](#)]
- Liang, T.; Sun, X.; Li, W.; Hou, G.; Gao, F. 1,2,3-Triazole-Containing Compounds as Anti-Lung Cancer Agents: Current Developments, Mechanisms of Action, and Structure-Activity Relationship. *Front. Pharmacol.* **2021**, *12*, 661173. [[CrossRef](#)] [[PubMed](#)]
- Çot, A.; Çeşme, M.; Onur, S.; Aksakal, E.; Şahin, İ.; Tümer, F. Rational design of 1,2,3-triazole hybrid structures as novel anticancer agents: Synthesis, biological evaluation and molecular docking studies. *J. Biomol. Struct. Dyn.* **2022**; ahead of print. [[CrossRef](#)]
- Pereira, D.; Pinto, M.; Correia-da-Silva, M.; Cidadae, H. Recent Advances in Bioactive Flavonoid Hybrids Linked by 1,2,3-Triazole Ring Obtained by Click Chemistry. *Molecules* **2022**, *27*, 230. [[CrossRef](#)]
- Kant, R.; Kumar, D.; Agarwal, D.; Gupta, R.D.; Tilak, R.; Awasthi, S.K.; Agarwal, A. Synthesis of newer 1,2,3-triazole linked chalcone and flavone hybrid compounds and evaluation of their antimicrobial and cytotoxic activities. *Eur. J. Med. Chem.* **2016**, *113*, 34–49. [[CrossRef](#)]
- Rao, Y.J.; Sowjanya, T.; Thirupathi, G.; Murthy, N.Y.S.; Kotapalli, S.S. Synthesis and biological evaluation of novel flavone/triazole/benzimidazole hybrids and flavone/isoxazole-annulated heterocycles as antiproliferative and antimycobacterial agents. *Mol. Divers.* **2018**, *22*, 803–814. [[CrossRef](#)]
- Qi, Y.; Ding, Z.; Yao, Y.; Ma, D.; Ren, F.; Yang, H.; Chen, A. Novel triazole analogs of apigenin-7-methyl ether exhibit potent antitumor activity against ovarian carcinoma cells via the induction of mitochondrial-mediated apoptosis. *Exp. Ther. Med.* **2019**, *17*, 1670–1676. [[CrossRef](#)]

20. Li, X.; Cai, Y.; Yang, F.; Meng, Q. Synthesis and molecular docking studies of chrysin derivatives as antibacterial agents. *Med. Chem. Res.* **2017**, *26*, 2225–2234. [[CrossRef](#)]
21. Mehdi, S.H.; Nafees, S.; Zafaryab, M.; Khan, M.A.; Rizvi, M.M.A. Chrysin: A Promising Anticancer Agent its Current Trends and Future Perspectives. *Eur. J. Exp. Biol.* **2018**, *8*, 3–16. [[CrossRef](#)]
22. Khoo, B.Y.; Chua, S.L.; Balam, P. Apoptotic Effects of Chrysin in Human Cancer Cell Lines. *Int. J. Mol. Sci.* **2010**, *11*, 2188–2199. [[CrossRef](#)] [[PubMed](#)]
23. Mei, Q.; Wang, C.; Yuan, W.; Zhang, G. Selective methylation of kaempferol via benzylation and deacetylation of kaempferol acetates. *Beilstein J. Org. Chem.* **2015**, *11*, 288–293. [[CrossRef](#)] [[PubMed](#)]
24. Agalave, S.G.; Maujan, S.R.; Pore, V.S. Click Chemistry: 1,2,3-Triazoles as Pharmacophores. *Chem. Asian J.* **2011**, *6*, 2696–2718. [[CrossRef](#)] [[PubMed](#)]
25. Bozorov, K.; Zhao, J.; Aisa, H.A. 1,2,3-Triazole-containing hybrids as leads in medicinal chemistry: A recent overview. *Bioorg. Med. Chem.* **2019**, *27*, 3511–3531. [[CrossRef](#)]
26. Alam, M.M. 1,2,3-Triazole hybrids as anticancer agents: A review. *Arch. Pharm.* **2022**, *355*, e2100158. [[CrossRef](#)]
27. Tian, L.; Zheshan, Q.; Yingquan, F.; Hongjing, Y. Design, Synthesis and Antiproliferative Activity of Chrysin Derivatives Bearing Triazole Moieties. *Chin. J. Org. Chem.* **2020**, *40*, 440–446. [[CrossRef](#)]
28. Kolb, H.C.; Sharpless, K.B. The growing impact of click chemistry on drug discovery. *Drug Discov. Today* **2003**, *8*, 1128–1137. [[CrossRef](#)]
29. Ruiz-Mendoza, F.J.; Mendoza-Espinoza, D.; Gonzalez-Montiel, S. Synthesis and Catalytic Activity of Coumarin- and Chrysin-Tethered Triazolylidene Gold(I) Complexes. *Eur. J. Inorg. Chem.* **2018**, *42*, 4622–4629. [[CrossRef](#)]
30. Rodriguez-Hernández, D.; Demuner, A.J.; Barbosa, L.C.A.; Heller, L.; Csuk, R. Novel hederagenin–triazolyl derivatives as potential anti-cancer agents. *Eur. J. Med. Chem.* **2016**, *115*, 257–267. [[CrossRef](#)]
31. Monks, A.; Scudiero, D.; Skehan, P.; Shoemaker, R.H.; Paull, K.; Vistica, D.; Hose, C.; Langley, J.; Cronise, P.; Vaigro-Wolff, A.; et al. Feasibility of a high-flux anticancer drug screen using a diverse panel of cultured human tumor cell lines. *J. Natl. Cancer Inst.* **1991**, *83*, 757–766. [[CrossRef](#)]
32. Shoemaker, R.H. The NCI60 human tumour cell line anticancer drug screen. *Nat. Rev. Cancer* **2006**, *6*, 813–823. [[CrossRef](#)] [[PubMed](#)]
33. Alley, M.C.; Scudiero, D.A.; Monks, A.M.; Hursey, L.; Czerwinski, M.J.; Fine, D.L.; Abbott, B.J.; Mayo, J.G.; Shoemaker, R.H.; Boyd, M.R. Feasibility of Drug Screening with Panels of Human Tumor Cell Lines Using a Microculture Tetrazolium Assay. *Cancer Res.* **1988**, *48*, 589–601. [[PubMed](#)]
34. Shoemaker, R.H.; Monks, A.; Alley, M.C.; Scudiero, D.A.; Fine, D.L.; McLemore, T.L.; Abbott, B.J.; Paull, K.D.; Mayo, J.G.; Boyd, M.R. Development of Human Tumor Cell Line Panels for Use in Disease-Oriented Drug Screening. *Prog. Clin. Biol. Res.* **1988**, *276*, 265–286. [[PubMed](#)]
35. NCI-60 Screening Methodology. Available online: https://dtp.cancer.gov/discovery_development/nci-60/methodology.htm (accessed on 14 December 2022).
36. Latif, A.D.; Gonda, T.; Vágvolgyi, M.; Kúsz, N.; Kulmány, A.; Ocsovszki, I.; Zomborszki, Z.P.; Zupkó, I. Synthesis and In Vitro Antitumor Activity of Naringenin Oxime and Oxime Ether Derivatives. *Int. J. Mol. Sci.* **2019**, *20*, 2184. [[CrossRef](#)] [[PubMed](#)]

Disclaimer/Publisher’s Note: The statements, opinions and data contained in all publications are solely those of the individual author(s) and contributor(s) and not of MDPI and/or the editor(s). MDPI and/or the editor(s) disclaim responsibility for any injury to people or property resulting from any ideas, methods, instructions or products referred to in the content.

Review

Therapeutic Potential of Phenolic Compounds in Medicinal Plants—Natural Health Products for Human Health

Wenli Sun ^{*,†} and Mohamad Hesam Shahrajabian [†]

Biotechnology Research Institute, Chinese Academy of Agricultural Sciences, Beijing 100081, China

* Correspondence: sunwenli@caas.cn; Tel.: +86-13-4260-83836

† These authors contributed equally to this work.

Abstract: Phenolic compounds and flavonoids are potential substitutes for bioactive agents in pharmaceutical and medicinal sections to promote human health and prevent and cure different diseases. The most common flavonoids found in nature are anthocyanins, flavones, flavanones, flavonols, flavanonols, isoflavones, and other sub-classes. The impacts of plant flavonoids and other phenolics on human health promoting and diseases curing and preventing are antioxidant effects, antibacterial impacts, cardioprotective effects, anticancer impacts, immune system promoting, anti-inflammatory effects, and skin protective effects from UV radiation. This work aims to provide an overview of phenolic compounds and flavonoids as potential and important sources of pharmaceutical and medical application according to recently published studies, as well as some interesting directions for future research. The keyword searches for flavonoids, phenolics, isoflavones, tannins, coumarins, lignans, quinones, xanthones, curcuminoids, stilbenes, curcumin, phenylethanoids, and secoiridoids medicinal plant were performed by using Web of Science, Scopus, Google scholar, and PubMed. Phenolic acids contain a carboxylic acid group in addition to the basic phenolic structure and are mainly divided into hydroxybenzoic and hydroxycinnamic acids. Hydroxybenzoic acids are based on a C6-C1 skeleton and are often found bound to small organic acids, glycosyl moieties, or cell structural components. Common hydroxybenzoic acids include gallic, syringic, protocatechuic, *p*-hydroxybenzoic, vanillic, gentistic, and salicylic acids. Hydroxycinnamic acids are based on a C6-C3 skeleton and are also often bound to other molecules such as quinic acid and glucose. The main hydroxycinnamic acids are caffeic, *p*-coumaric, ferulic, and sinapic acids.

Citation: Sun, W.; Shahrajabian, M.H. Therapeutic Potential of Phenolic Compounds in Medicinal Plants—Natural Health Products for Human Health. *Molecules* **2023**, *28*, 1845. <https://doi.org/10.3390/molecules28041845>

Academic Editor: Giovanni Ribaudo

Received: 6 January 2023

Revised: 11 February 2023

Accepted: 13 February 2023

Published: 15 February 2023



Copyright: © 2023 by the authors. Licensee MDPI, Basel, Switzerland. This article is an open access article distributed under the terms and conditions of the Creative Commons Attribution (CC BY) license (<https://creativecommons.org/licenses/by/4.0/>).

Keywords: phenolics; curcumin; protocatechuic; quinones; stilbenes; curcuminoids

1. Introduction

Medicinal plants are very important worldwide, both when used alone and as a supplement to traditional medication [1–5]. For many years, humans have employed plants as a source of food, flavoring, and medicines [6–10]. Various parts of medicinal plants such as seeds, leaves, flowers, fruits, stems, and roots are rich sources of bioactive compounds [11–13]. Bioactive compounds should be considered as important dietary supplements [14–19]. Polyphenols are a group of secondary metabolites involved in the hydrogen peroxide scavenging in plant cells [20]. Phenolic compounds are second only to carbohydrates in abundance in higher plants, and they display a great variety of structures, varying from derivatives of simple phenols to complex polymeric materials such as lignin [21–26]. Phenolic compounds are known for their notable potential activity against various human viruses, and phenolic compounds also have immunomodulatory and anti-inflammatory activity [27]. The most abundant phenolic compounds are phenolic monoterpenes (carvacrol and thymol) and diterpenes (carnosol, carnosic acid, and methyl carnosate), hydroxybenzoic acids (*p*-hydroxybenzoic, protocatechuic, gallic, vanillic, catechol, and ellagic), phenylpropanoic acids (*p*-coumaric, caffeic, rosmarinic, chlorogenic, ferulic, cryptochlorogenic, and neochlorogenic), phenylpropenes (eugenol), coumarins

(herniarin and coumarin), flavanones (naringenin, eriocitrin, naringin, and hesperidin), flavones (apigenin, apigenin, genkwanin, luteolin, luteolin 7-glucuronide, cynaroside, scolymoside, salvigenin, and cirsimaritin), and flavanols (catechin, astragalol, kaempferol, methyl ethers, quercetin, hyperoside, isoquercetin, miquelianin, and rutin) [28,29].

Plant phenolics are considered promising antibiofilm and antifungal agents [30,31]. Diaz et al. [32] also reported that the levels of phenolic and flavonoid compounds were correlated with the anti-inflammatory and antioxidant activities of medicinal plants. Tukun et al. [33] reported that phenolic content is significantly connected to antioxidant activity, and halophytes have high content of nutrients and phenolic metabolites. Some of the most important phenolic compounds recognized from medicinal plants are syringic acid and gallic acid from *Moringa oleifera* [34]; gallic acid, vanillic acid, 4-hydroxybenzoic acid, and syringic acid from *Peganum harmala* [35]; rosmarinic acid from *Rosmarinus officinalis* L. and *Mentha canadensis* L. [36]; vanillin from *Thymus vulgaris* [37]; caffeic acid and *p*-coumaric acid from *Ocimum basilicum* L., *Thymus vulgaris* L., *Salvia officinalis* L., and *Origanum vulgare* L. [36]; piceatannol glucoside, resveratrolsides, and piceid from *Polygonum cuspidatum* [38]; trans-rhapontin, cis-rhapontin, and trans-desoxyrhaponticin from *Rheum tanguticum* Maxim. Ex Balf. [39]; herniarin from *Matricaria chamomilla* [40]; kayeassamin I, mammeasin E, and mammeasin E from *Mammea siamensis* [41]; scopoletin, fraxetin, aesculetin, fraxin, and aesculin from *Fraxinus rhynchophylla* [42]; phyllanthin, niranthin, hypophyllanthin, nirtetralin, virgastusin, heliobupphthalmin lactone, and bursehennin from *Phyllanthus amarus* [43]; schisanchinin A, schisanchinin B, schisanchinin C, and schisanchinin D from *Schisandra chinensis* [44]; 7-methyljuglone from *Drosera rotundifolia* [45]; rhein, physcion, chrysophanol, emodin, and aloe-emodin from *Rheum palmatum* and *Rheum hotaoense* [46]; curcumin, demethoxycurcumin, and bis-demethoxycurcumin from *Curcuma longa* [47]; luteolin, apigenin, orientin, apigenin-O-glucuronide, and luteolin-O-glycoside from *Origanum majorana* [48]; glycitein, genistein, formononetin, daidzein, prunetin, biochanin A and daidzin, and genistin from *Medicago* spp. [49]; kaempferol 3-O-glucoside and isorhamnetin 3-O-galactoside from *Tephrosia vogelii* [50]; rutin, kaempferol 3-O-rhamnoside, and quercetin 3-O-glucoside from *M. oleifera* [34]; gallo catechin and catechin from *Mentha pulegium* [48]; taxifolin, taxifolin methyl ether, and dihydrokaempferide from *Origanum majorana* [48]; hesperidin, naringenin-O-rhamnoglucoside, and isosakuranetin-O-rutinoside from *Mentha pulegium* [48]; and punicalagin, pedunculagin I, granatin A, ellagic acid, ellagic acid pentoside, ellagic acid glucoside, and punigluconin from *Punica granatum* [51]. Phenolic phytochemicals include flavonoids, flavonols, flavanols, flavanones, flavones, phenolic acids, chalcones, isoflavones, tannins, coumarins, lignans, quinones, xanthenes, curcuminoids, stilbenes, curcumin, phenylethanoids, and several other plant compounds, owing to the hydroxyl group bonded directly to an aromatic hydrocarbon group [52]. The classes of phenolic compounds in plants are shown in Table 1.

Table 1. Classes of phenolic compounds in plants [53].

Class	Structure
Simple phenolics, benzoquinones	C ₆
Hydroxybenzoic acids	C ₆ -C ₁
Acetophenones, phenylacetic acids	C ₆ -C ₂
Hydroxycinnamic acids, phenylpropanoids (coumarins, isocoumarins, chromones, chromenes)	C ₆ -C ₃
Naphthoquinones	C ₆ -C ₄
Xanthenes	C ₆ -C ₁ -C ₆
Stilbenes, anthraquinones	C ₆ -C ₂ -C ₆
Flavonoids, isoflavonoids	C ₆ -C ₃ -C ₆
Lignans, neolignans	(C ₆ -C ₃) ₂
Biflavonoids	(C ₆ -C ₃ -C ₆) ₂
Lignins	(C ₆ -C ₃) _n
Condensed tannins (proanthocyanidins or flavolans)	(C ₆ -C ₃ -C ₆) _n

Phenolic acids include two subgroups, i.e., hydroxybenzoic and hydroxycinnamic acids [53]. Hydroxybenzoic acids consist of gallic, *p*-hydroxybenzoic, vanillic, protocatechuic, and syringic acid, which, in common, have the C₆-C₁ structure [53]. Hydroxycinnamic acids, on the other hand, are aromatic compounds with a three-carbon side chain (C₆-C₃), with caffeic, *p*-coumaric, ferulic, and sinapic acids being the most common [52]. Gallic acid is present in cloves (*Eugenia caryophyllata* Thunb.), while protocatechuic acid can be found in coriander (*Coriandrum sativum* L.), dill (*Anethum graveolens* L.), and star anise (*Illicium verum* Hook. f.) [54]. Caffeic acid is found among others in parsley (*Petroselinum crispum* L.), ginger (*Zingiber officinale* Rosc.), and sage (*Salvia officinalis* L.), and *p*-coumaric acid is found in oregano (*Origanum vulgare* L.), basil (*Ocimum basilicum* L.), and thyme (*Thymus vulgaris* L.) [54]. Some samples of hydroxybenzoic and hydroxycinnamic acids are presented in Table 2.

Table 2. Examples of hydroxybenzoic and hydroxycinnamic acids.

Phenolic Acids	Examples	Molecular Formula
Hydroxybenzoic acids	Gallic acid	C ₇ H ₆ O ₅
	Protocatechuic acid	C ₇ H ₆ O ₄
	<i>p</i> -coumaric acid	C ₉ H ₈ O ₃
Hydroxycinnamic acids	Caffeic acid	C ₉ H ₈ O ₄
	Ferulic acid	C ₁₀ H ₁₀ O ₄
	Sinapic acid	C ₁₁ H ₁₂ O ₅
Other components		
Coumarins	Umbelliferone	C ₉ H ₆ O ₃
	Esculetin	C ₉ H ₆ O ₄
	Scopoletin	C ₁₀ H ₈ O ₄
Stilbenes	Resveratrol	C ₁₄ H ₁₂ O ₃
	Piceatannol	C ₁₄ H ₁₂ O ₄
	Pterostilbene	C ₁₆ H ₁₆ O ₃
Curcuminoids	Curcumin	C ₂₁ H ₂₀ O ₆
	Demethoxycurcumin	C ₂₀ H ₁₈ O ₅
	Bisdemethoxycurcumin	C ₁₉ H ₁₆ O ₄
Condensed tannins or proanthocyanidins	Procyanidin B1	C ₃₀ H ₂₆ O ₁₂
	Lignan Sesamin	C ₂₀ H ₁₈ O ₆

Flavonoids include the largest group of plant phenolics, responsible for over half of the eight thousand naturally occurring phenolic constituents [55,56]. Flavonoids are low molecular weight compounds, including fifteen carbon atoms, arranged in a C₆-C₃-C₆ configuration [53]. The genetic structure of main classes of flavonoids are shown in Table 3.

Phenolic phytochemicals play a variety of protective roles against abiotic stresses, such as UV light, or abiotic stresses, namely predator and pathogen attacks [57]. Phenolic phytochemicals are utilized by humans to treat several ailments including bacterial, protozoal, fungal, and viral infections, inflammation, diabetes, and cancer. Biosynthesis and accumulation of polyphenol and other secondary metabolites in plants is considered as an evolutionary reaction of biochemical pathways under adverse environmental influences, i.e., biotic/abiotic limitations, including increased salinity and drought stress [58–60]. Some of the extraction methodologies of phenolic components from medicinal and aromatic plants are maceration, digestion, infusion, decoction, Soxhlet extraction, percolation, aqueous alcoholic extraction by fermentation, counter-current extraction, ultrasound extraction, supercritical fluid extraction, and phytomics stage. The principle factors shaping the production of phenolic components are the water supplied to plants and the time of stress exposure, and, among the various quantification methods, HPLC and colorimetric tests are the most utilized to quantify the phenolic compounds analyzed [61]. Djeridane et al. [62] reported that the phenolics in medicinal plants provide substantial antioxidant activity. A positive, significant linear connection between antioxidant activity and total phenolic content revealed that phenolic components were the dominant antioxidant constituents in medicinal plants [63,64]. Various groups of tests on phenolics indi-

cated significant mean alterations in radical scavenging activity; tannins demonstrated the strongest activity, while most quinones, isoflavones, and lignans tested revealed the weakest activity [65,66]. The most abundant flavone in *Cytisus multiflorus* is the chrysin derivative, Kaempferol-3-*O*-rutinoside is the major flavonol in *Malva sylvestris*, and Quercetin-3-*O*-rutinoside is the principle flavonol in *Sambucus nigra* [66]. *Nepeta italica* subsp. *cadmea* and *Teucrium sandrasicum* are rich in phenolics, which indicated antioxidant and cytotoxic properties [67]. Through LC-ESI-MS analysis, five phenolic acids (quinic acid, syringic acid, gallic acid, *p*-coumaric acid, and trans-ferulic acid) and five flavonoids (catechin, epicatechin, quercetin, rutin, and naringenin) were predominant and common in some desert shrubs of Tunisian flora (*Pituranthos tortuosus*, *Ephedra alata*, *Retama raetam*, *Ziziphus lotus*, *Calligonum comosum*, and *Capparis spinosa*) [68].

Table 3. Generic structure of major classes of flavonoids.

Flavonoids		Molecular Formula
Flavones	Apigenin	C ₁₅ H ₁₀ O ₅
	Luteolin	C ₁₅ H ₁₀ O ₆
	Chrysin	C ₁₅ H ₁₀ O ₄
Flavonols	Kaempferol	C ₁₅ H ₁₀ O ₆
	Quercetin	C ₁₅ H ₁₀ O ₇
	Isorhamnetin	C ₁₆ H ₁₂ O ₇
Flavanones	Naringenin	C ₁₅ H ₁₂ O ₅
	Eriodictyol	C ₁₅ H ₁₂ O ₆
	Hesperetin	C ₁₆ H ₁₄ O ₆
Flavanols		C ₁₅ H ₁₄ O ₂
Anthocyanidin		C ₁₅ H ₁₁ O ⁺
Flavanonols	Taxifolin	C ₁₅ H ₁₂ O ₇
	Aromadendrin	C ₁₅ H ₁₂ O ₆
Flavan-3-ols	Gallocatechin	C ₁₅ H ₁₄ O ₇
	Catechin	C ₁₅ H ₁₄ O ₆
	Genistein	C ₁₅ H ₁₀ O ₅
Isoflavones	Daidzein	C ₁₅ H ₁₀ O ₄
	Formononetin	C ₁₆ H ₁₂ O ₄

The main phenolic compounds in Matico (*Piper angustifolium* R.), Guascas (*Galinsoga parviflora*), and Huacatay were chlorogenic acid and hydroxycinnamic acid derivatives [69]. High phenolic and antioxidant activity-containing medicinal plants and species such as Chanca Piedra (*Phyllanthus nirui* L.), Yerba Mate (*Ilex paraguariensis* St-Hil), Zarzaparrilla (*Smilax officinalis*), and Huacatay (*Tagetes minuta*) have the highest anti-hyperglycemia-relevant in vitro α -glucosidase inhibitory activities with no effect on α -amylase [69]. Nineteen phenolic compounds from different groups are used in wound treatment, and the compounds are tyrosol, curcumin, hydroxytyrosol, luteolin, rutin, chrysin, kaempferol, quercetin, icariin, epigallocatechin gallate, morin, silymarin, taxifolin, hesperidin, naringin, puerarin, isoliquiritin, genistein, and daidzein [70–73]. The most important identified phenolics in *Phlomis angustissima* and *Phlomis fruticosa*, medicinal plants from Turkey, by RP-HPLC-DAD were hesperidin, catechin, kaempferol, epicatechin, eupatorin, and epigallocatechin, and chlorogenic, syringic, vanillic, *p*-coumaric, ferulic, and benzoic acids [74]. Quercetin of *Cordia dichotoma* G. Forst. (Lashusa) is the most notable phytoconstituent responsible for the therapeutic efficacy [75]. Vanillic acid, nepetin, verbascoside, and hispidulin, of *Clerodendrum petasites* S. Moore (CP) were chosen as potential phenolic active compounds in Thai traditional medicine for the treatment of different kinds of skin diseases [76–78]. Bouyahya et al. [79] reported that compounds such as terpenoids, alkaloids, flavonoids, phenolic acids, and fatty acids of *Arbutus unedo* L., *Thymus capitatus* managed diabetes by several mechanisms such as enzymatic inhibition, interference with

glucose and lipid metabolism signaling pathways, and the inhibition and the activation of gene expression involved in glucose homeostasis.

Grewia tenax, *Terminalia sericea*, *Albizia anthelmintica*, *Corchorus tridens*, and *Lantana camara* are frequently used to treat gastroenteritis and include higher total phenolic and flavonoid contents in Namibia [80–85]. The most important phenolics identified from pomegranate are punicalin, gallic acid, ellagic acid, pyrogallol, salicylic acid, coumaric acid, vanillic acid, sesamin, and caffeic [86], and phenolic compounds have been discovered to have inhibitory effects against α -glucosidase activities [87]. Two new phenolics, leucoxenols A and B, were obtained and identified as major secondary metabolites from the leaves of *Syzygium leucoxylon* [88]. Phenolics are main phytochemicals found in *Cyathea* species, and *Cyathea* has been considered to be a potential source of novel cancer therapeutic compounds [89]. Purified phenolic compounds from the bark of *Acacia nilotica* showed insecticidal potential against *Spodoptera litura*, and they could provide substitutes to synthetic pesticides for controlling various pests [90]. Bellumori et al. [91] reported that the roots of *Acmella oleracea* L. had about twice as many phenols as the aerial parts, and caffeic acid derivatives were the main phenolic compounds in roots and aerial parts. Kaempferol was found as the most abundant phenolic compound in basil leaf extract after using an HPLC-UC method ($61.4 \text{ mg}\cdot\text{kg}^{-1}$) [92]. Apple fruit (*Annona squamosa* L.) has a specific spatial distribution of microbes and phenolics, its peel phenolics contain antimicrobial activity against several Gram-positive bacteria, and its peel phenolics had a growth-promoting effect toward autochthonous yeasts [93–96]. The phenolic contents of *Cyathea dregei* (root and leaves), *Felicia erigeroides* (leaves and stems), *Felicia erigeroides* (leaves and stems), *Hypoxis colchicifolia* (leaves), *Hypoxis colchicifolia* (leaves), and *Senna petersiana* (leaves) have shown high antimicrobial and cyclooxygenase (COX) inhibitory activities [97].

The most important techniques for analysis of phenolic compounds and extracts are nuclear magnetic resonance (NMR), high performance liquid chromatography (HPLC) with ultraviolet-visible (UV-Vis) or photodiode array (PDA) detector or coupled to mass spectrometry (MS), derivatization (silylation, alkylation, etc.) as well as gas chromatography (GC) or GC-MS analysis, phytochemical screening such as total flavonoid content (TFC), total phenolic content (TPC), etc., and antioxidant potential tests such as 2,2-diphenyl-1-picrylhydrazyl (DPPH), etc. [97–107]. Solid-liquid extraction (SLE) is one of the main methods for extraction of phenolic compounds, specially syringic acid, catechin, and *p*-coumaric acid, which is simple, well established, and widely used [108]. Ultrasound-assisted extraction (UAE) is often used for extraction of gallic acid and rutin, which is easy to execute, uses inexpensive equipment, and consumes less solvents, and has fast extraction, good extraction yield, and low impacts on the environment [109]. Supercritical fluid extraction (SFE) usually applies for gallic acid, anthocyanin, and protocatechuic acid, which has high selectivity, cheaper and safer solvent, easily controlled extraction conditions, environmental friendliness, low operating temperature, and easy separation of solvent from solutes [110]. Microwave-assisted extraction (MAE) is used for extraction of 3-caffeoylquinic acid, 5-caffeoylquinic acid, and ellagic acid, which has short extraction time and low solvent consumption [111]. Pressurized liquid extraction (PLE) applies for extraction of rutin and quercetin, which consumes fewer organic solvents, has higher probability to avoid organic solvents by using water only, and is fast and efficient [112]. For extraction of proanthocyanidin, naringin, and hesperidin, enzyme-assisted extraction (EAE) is proposed, which is safe and green and does not need complex paraphernalia [113]. Key points about phenolic acids and their derivatives are shown in Table 4. This work aims to provide an overview of phenolic compounds and flavonoids as potential sources of pharmaceutical and medical application from recently published studies, as well as some interesting directions for future research.

Table 4. Important points about phenolic acids and their derivatives.

The Derivatives of Phenolic Acids	Key Points	References
Flavonoids	The largest group of natural phenolic compounds.	[54,114]
	Their structure is based on a 15-carbon phenyl benzopyran skeleton (C6-C3-C6, i.e., A-C-B rings).	[54,114]
	Based on differences in the pyran ring, flavonoids can be categorized into flavones, isoflavones, flavanonols, flavonols, flavanones, flavan-3-ols, and anthocyanidins.	[54,114]
	The majority occur as glycosides, except for flavan-3-ols, which are rarely glycosylated.	[54,114]
	Different patterns of hydroxylation and methylation of the A and B rings consequently result in a variety of compounds for each flavonoid category.	[54,114]
	Flavones have a double bond between C-2 and C-3, a keto function in C-4, and the B ring is attached at C-2.	[54,114]
	The most common flavonoids in medicinal and aromatic plants are luteolin, apigenin, and glycosides.	[54,114]
	In isoflavones, the B ring is attached at C-3 and the main components are daidzein, genistein, and glycitein.	[54,114]
	Flavonols are flavones bearing a hydroxyl group at C-3, such as kaempferol, quercetin, and myricetin.	[54,114]
	In flavanones, the C-ring has no double bond between C2 and C3, such as in naringenin, eriodictyol, and hesperetin.	[54,114]
	Flavanonols, also called dihydroflavonols, have the same saturated C-ring as flavanones but are hydroxylated at C-3.	[54,114]
	Flavan-3-ols, also referred to as flavanols, also contain a saturated C-ring, but lack the keto group at C-4, and are hydroxylated at C-3, such as catechin and gallocatechin, or as oligomers and polymers.	[54]
Stilbenes	In anthocyanidins, the C-ring lacks the keto group at C-4, is hydroxylated at C-3, and, uniquely, has two double bonds forming the flavylium cation, such as in cyanidin, petunidin, malvidin, pelargonidin, peonidin, and delphinidin.	[54]
	They are based on 1,2-diphenylethylene, which has a C6-C2-C6 skeleton.	[115]
Tannins	They can be found as aglycones, monomers, oligomers, or glycosylated derivatives.	[116]
	Tannins are high molecular weight polyphenolic compounds.	[117,118]
	They can be synthesized as a defensive mechanism in response to pathogen attack and abiotic stresses such as UV radiation.	[117,118]
Quinones	Based on their structures, tannins in plants can be classified into mainly hydrolysable tannins and condensed tannins, also known as proanthocyanidins.	[117,118]
	Hydrolysable tannins are built based on gallic acid and are divided into the gallotannins and ellagitannins.	[117,118]
	They contain a di-one or di-ketone group.	[119]
Coumarins	They are distinguished into benzoquinones and naphthoquinones and are based on their derivative molecules.	[119]
	They may occur as monomers, dimers, trimers, glycosides, or in reduced forms.	[119]
Curcuminoids	They may occur in a free or glycosylated state.	[120]
	They are divided into six categories, namely simple coumarins, furanocoumarins, dihydrofuranocoumarins, pyranocoumarins, phenylcoumarins, and bicoumarins.	[120]
Lignins	They widely occur in <i>Curcuma</i> spp., especially in the rhizomes of <i>Curcuma longa</i> (turmeric).	[121,122]
	There are three major curcuminoids, namely curcumin, demethoxycurcumin, and bis-demethoxycurcumin.	[121,122]
Lignins	The structure of curcumin consists of a keto-enol tautomeric unsaturated chain linking two aromatic rings bearing a hydroxyl and methoxy group.	[121,122]
	Lignans consist of two phenylpropane units joined together by a β - β' bond.	[123]
	They are divided into eight categories, namely dibenzylbutyrolactols, dibenzocyclooctadienes, dibenzylbutanes, dibenzylbutyrolactones, aryl-naphthalene, aryl-tetralins, furans, and furofurans.	[123]

2. The Important Health Benefits of Phenolic Components

Flavonoids and phenolics are commonly known as the largest phytochemical molecules with antioxidant characteristics [124]. Traditional Chinese medicinal plants that contain phenolic acids and flavonoids have shown high antioxidant activity. *Nepeta italica* subsp. *Cad-*

mea and *Teucrium sandracicum* are rich in phenolic, tannin, and flavonoids content, which showed antioxidant and cytotoxic properties. *Bauhinia variegata* L. contained flavonoid compounds and revealed antioxidant properties against oxidative damage by radical neutralization, iron binding, and decreasing power abilities [125]. The rhizome extracts of *Polygonatum verticillatum* (L.) All. exhibited antioxidant activity, which is connected to the level of phenolic composition [126]. Singh and Yadav [127] have reported that, among medicinal plants, oregano, clove, thyme, and rosemary contain the highest amounts of phenolic compounds. Flavan-3-ol oligomers and monomers were potent antioxidant compounds abundantly identified in *Camellia fangchengensis* [128].

Bellis perennis L. was rich in phenolic compounds, and it can be used for wounds, cancer, inflammation, and eye diseases [129]. A total of 27 kinds of phenolic compounds were identified by HPLC-ESI-QTOF-MS/MS, and okra (*Abelmoschus esculentus*) polyphenols exhibited great antioxidant activity in vitro [130]. The *Althaea officinalis* extracts showed stronger antioxidant activity and excellent α -glucosidase, 5-lipoxygenase, and nitric oxide inhibitory properties [131]. *Dendrobium densiflorum* was rich in flavonoid, alkaloid, and antioxidant activity, *Acampe papillosa* was rich in total phenol, total tannin, and total saponin content, and *Coelogyne nitida* exhibited higher antioxidant activity because of its higher quercetin content [132]. Cirak et al. [133] showed that *Achillea arabica* Kotschy is an important source of natural antioxidants. The antioxidant property and bioactive constituents from the fruits of *Aesculus indica* (Wall. Ex Cambess.) Hook, which were quercetin and mandelic acid, were the major bioactive molecules with notable antioxidant properties to decrease oxidative stress caused by reactive oxygen species (ROS) [134]. The phytochemical compounds and biological activity of *Pinus cembra* L. contain higher concentration of total phenolics and flavonoids than that of needle extract, and its bark extract showed better ability as a free radical scavenger [135]. Higher antioxidant activity in normal-tannin lentil seed coats than low-tannin ones was reported; kaempferol tetraglycoside was dominant in low-tannin seed coats, and procyanidins, kaempferol tetraglycoside, and catechin-3-*O*-glucoside in normal-tannin has been found [136]. Zhang et al. [137] also reported that antioxidant activity and prebiotic impacts were positively correlated for oat phenolic compounds. 3,4-dihydroxybenzoic, rutin, vanillic acid, and quercetin were detected from aqueous extracts of *azendjar* and *taamriouth* figs, and a dark peel variety consisted of more phenolics and exerted a higher antioxidant capacity [138]. Although gallic acid was the most important compound in carob (*Ceratonia siliqua* L.) pulp extract, geographic origin strongly influenced the contents of bioactive compounds and antioxidant activities [139].

Asplenium nidus L. contained gliricidin 7-*O*-hexoside and quercetin-7-*O*-rutinoside that can fight against three pathogens, i.e., *Proteus vulgaris* Hauser, *Proteus mirabilis* Hauser, and *Pseudomonas aeruginosa* (Schroeter) Migula [140]. Flavones, which were extracted from the root of *Scutellaria baicalensis* Georgi, were proven as potential antibacterial agents against *Propionibacterium acnes*-induced skin inflammation both in in vitro and in vivo models [141]. Kaempferol that was isolated from the *Impatiens balsamina* L. exhibited potential activity to inhibit the growth of *P. acnes* [142]. Phenolics from kernel extract *Mangifera indica* L. also showed anti-acne properties to inhibit the growth of *P. acnes* [143]. Medicinal plants such as *Albizia procera*, *Atalantia monophylla*, *Asclepias curassavica*, *Azima tetracantha*, *Cassia fistula*, *Costus speciosus*, *Cinnamomum verum*, *Nymphaea stellata*, *Osbeckia chinensis*, *Punica granatum*, *Piper argyrophyllum*, *Tinospora cordifolia*, and *Toddalia asiatica* have shown antifungal activity [144]. The strictinin isolated from the leaves of *Camellia sinensis* var. *assamica* (J.W. Mast.) Kitam was a good substitute for antibacterial activities [145]. Phenolic compounds, especially flavonoids, have long been reported as chemopreventive factors in cancer therapy [146–148]. The extract of *Curcuma longa* L. rhizome has been suggested as a promising source of natural active compounds to fight against malignant melanoma due to its potential anticancer property in the B164A5 murine melanoma cell line [149]. Gliricidia 7-*O*-hexoside and Quercetin 7-*O*-rutinoside, which were flavonoids isolated from the medicine fern (*Asplenium nidus*), were also proposed as potential chemopreventives against human hepatoma HepG2 and human carcinoma HeLa cells [140]. Quercetin can

induce miR-200b-3p to regulate the mode of self-renewing divisions of the tested pancreatic cancer [150], and a soy isoflavone genistein inhibited the activation of the nuclear factor kappa B (NF- κ B) signaling pathway that maintains the balance of cell survival and apoptosis; this soy isoflavone could also take its action to fight against cell growth, apoptosis, and metastasis, including epigenetic modifications in prostate cancer [151]. Curcumin exhibits anticancer impacts towards skin cancers, as this phenolic can influence the cell cycle by acting as a pro-apoptotic agent [152]. Curcumin acts as a non-selective cyclic nucleotide phosphodiesterase (PDE) inhibitor to inhibit melanoma cell proliferation, which is associated with epigenetic integrator UHRF1 [153]. Curcumin inhibited proliferation of the selected cell lines in prostate cancer and induced apoptosis of the cancer cells with a dose-dependent response [154].

The cardioprotective impacts from various kinds of phenolics and flavonoids occurring in medicinal plants have been investigated in many studies [155,156]. Many phenolic and flavonoid compounds have been studied and had reported their cardioprotective properties via different mechanisms including inhibition of ROS generation, apoptosis, mitochondrial dysfunction, NF- κ B, p53, and DNA damage both in vitro and in vivo, and clinical studies [157]. Kaempferol, luteolin, rutin, and resveratrol showed their efficacy against doxorubicin-induced cardiotoxicity [158,159]. Isorhamnetin provided a cardioprotective effect against cardiotoxicity of doxorubicin and potentiated the anticancer efficacy of this drug [160]. The total phenolic and flavonoid contents of the aqueous fraction from *Marrubium vulgare* L. have effects on ischemia-reperfusion injury of rat hearts, which proved that the aqueous fraction from *M. vulgare* had cardioprotective potential [156]. Aspalathin and phenylpyruvic acid-2-O- β -D-glucoside, two of the major compounds from *Aspalathus linearis* (Burm.f.) R. Dahlgren, were demonstrated as potential protective compounds to protect myocardial infarction caused by chronic hyperglycemia [155]. Puerarin is a potential isoflavone that was reported as an interesting candidate for cardioprotection by protecting myocardium from ischemia and reperfusion damage by means of opening the Ca²⁺-activated K⁺ channel and activating the protein kinase C [161]. Quercetin, hesperidin, apigenin, and luteolin were reported as flavonoids containing potential anti-inflammatory impacts [162]. The flavonoids and phenolic compounds of *Phyllanthus acidus* leaves could be correlated with the analgesic, antioxidant, and anti-inflammatory activities [163]. Hydroxytyrosol and quercetin 7-O- α -L-rhamnopyranoside exhibited anti-inflammatory activity through lowering the levels of TNF- α , and hydroxytyrosol and caffeic acid showed significant anti-inflammatory activity at 100 μ m by reducing the release of NO in LPS-stimulated macrophages comparable to positive control indomethacin [164].

The most important chemical compounds extracted from ethanol of *Cardiospermum halicacabum* were chrysoeriol, kaempferol, apigenin, luteolin, methyl 3,4-dihydroxybenzoate, 4-hydroxybenzoic acid, quercetin, hydroquinone, protocatechuic acid, gallic acid, and indole 3-carboxylic acid, which have shown high anti-inflammatory and antioxidant activities [165]. The most important phenolic components with antiviral effects against COVID-19 were curcumin, Theaflavin-3,3'-digallate, EGCG, Paryriflavonol A, Resveratrol, Quercetin, Luteolin, Scutellarein, Myricetin, and Forsythoside A [166]. In traditional Persian medicinal science, medicinal plants such as *Glycyrrhiza glabra* L., *Rheum palmatum* L., *Punica granatum* L., and *Nigella sativa* L. have been introduced for treating respiratory disorders and infections because of their phenolic compounds [167]. The anti-inflammatory activity of polyphenolic compounds in *Gaillardia grandiflora* Hort. Ex Van Houte and *Gaillardia pulchella* Foug from Egypt were reported [168]. Anti-inflammatory properties of two medicinal plant species, *Bidens engleri* O.E. Schulz from Asteraceae family as well as *Boerhavia erecta* L. from Nyctaginaceae family, were identified and reported in various fractions [169]. *Plantago subulata* has shown anti-inflammatory properties on macrophages and a protective effect against H₂O₂ injury [170]. Phenolic content changes with aromatic and medicinal plant species and extraction method used [171]. Astilbin, a dihydroflavonol, from *Smilax glabra* Roxb significantly inhibited nitric oxide production, tumor necrosis factor- α (TNF- α), and mRNA expression of inducible nitric oxide synthase in the tested cells [172]. Apigenin is a

main flavone with skin protective impact against UV light; this flavone can be identified in various edible medicinal plants or plants-derived beverages, e.g., beer, red wine, and chamomile tea [173,174]. Quercetin is a flavonol that can be discovered in apple peel, onion skin, and *Hypericum perforatum* L. leaves [175]. Silymarin, a standardized extract of flavonolignans from the milk thistle (*Silybum marianum* (L.) Gaernt.) fruits, consists of silybin, a principle active component [176]. Genistein is a soybean isoflavone that was also reported as photoprotective molecule against photocarcinogenesis by inhibiting UV-induced DNA damage in human skin-equivalent in vitro model [177]. Equol is considered as an isoflavonoid metabolite from isoflavone daidzein or genistein produced by gut microflora [178,179]. Genistein is an obvious example of an interesting choice of a flavonoid phytoestrogen for improving endothelial roles in postmenopausal women with MetS [180]. A chrysin derivative was the most abundant flavone in *Cytisus multiflorus*, quercetin-3-O-rutinoside was the main flavonol in *Sambucus nigra*, and kaempferol-3-O-rutinoside was the main flavonol in *Malva sylvestris* [181]. Biological properties of phenolic compounds are presented in Table 5.

Table 5. Biological activities of phenolic compounds.

Health Benefits	Key Points	References	
Antioxidant activity	* The stem of <i>Dendrophthoe falcata</i> (Loranthaceae) plant had a high content of phenolic and flavonoid compounds and very high antioxidant activities.	[182]	
	* The phenolic compounds of <i>Buchenavia tetraphylla</i> , <i>Buchenavia tomentosa</i> , and <i>Lippia sidoides</i> provided the main contributions to the antioxidant potential.	[183]	
	* The total phenolic, flavonoid, and antioxidant capacity of all blueberry cultivars increased nonlinearly with ripening.	[184]	
	* Cynaroside, rosmarinic acid, cosmosiin, luteolin, apigenin, and acacetin were the main components in ethyl acetate extracts of <i>Salvia absconditiflora</i> , <i>Salvia sclarea</i> , and <i>Salvia palaestina</i> with antioxidant activity.	[185]	
	* Phenolic compounds from <i>Pistacia lentiscus</i> L. black fruits exhibited potent antioxidant properties.	[186]	
	* Lycium berries of different species contained a total of 186 phenolic compounds, which exhibited potent antioxidant activities.	[187,188]	
	* <i>Stachys</i> species contained important bioactive phenolics and had promising antioxidant impacts.	[189]	
	* <i>Acacia nilotica</i> pods and bark had potent total phenolic content, antioxidant activity, and tyrosinase inhibitory properties.	[190]	
	* <i>Bersama abyssinica</i> (Meliaceae) was rich in phenolic compounds, flavonoids and coumarin, and 7,8-Dimethoxycoumarin with high antioxidant activity.	[191]	
	* Epicatechin was the main monomeric polyphenol in the profile of longan phenolics.	[192]	
	* Epicatechin, quercetin 3-O-rhamnoside, and kaempferol were responsible for the high antioxidant activity of <i>Litsea glaucescens</i> .	[193]	
	* The water extract of <i>Amsonia orientalis</i> leaves exhibited promising antioxidant activity when used at low concentration.	[194]	
	* The ethanolic extract of <i>Amsonia orientalis</i> leaves had the highest phenolic substance content and 2,2-diphenyl-1-picrylhydrazyl (DPPH) scavenging activity.	[194]	
	* A variety of phenolic compounds and stilbene derivatives in different parts of germinated peanut suggested that the peanut sprout exerted high anti-inflammatory effects and may be related to the polyphenolic content and antioxidant properties.	[195]	
	Anti-inflammatory activity	* Fermented olive cream and <i>Lactiplantibacillus</i> (Lpb.) plantarum IMC513 reduced proinflammatory cytokine levels.	[196]
		* <i>Allium scorodoprasum</i> L. subsp. <i>rotundum</i> extract showed high anti-inflammatory inhibitory effects against xanthine oxidase activity.	[197]
* <i>Helleborus purpurascens</i> demonstrated the strongest anti-inflammatory potential, especially because of fatty acids.		[198]	
* <i>Thalictrum minus</i> possessed combined anti-inflammatory and antioxidant effects.		[198]	
* The leaf of <i>Aurea helianthus</i> demonstrated strong anti-inflammatory activity that reduced NO production.		[199]	

Table 5. Cont.

Health Benefits	Key Points	References
Antifungal activity	* <i>Hypericum empetrifolium</i> aerial parts extract (HEA) exhibited antifungal activity against <i>Candida tropicalis</i> with 19.53 µg/mL.	[200]
	* <i>Allium sativum</i> extract revealed strong antifungal activity effects against <i>Curcularia</i> spp., <i>Trichophyton</i> spp., and <i>Geotrichum</i> spp.	[201]
	* <i>Rosa micrantha</i> flowers extract revealed fungicide effects in <i>Candida glabrata</i> .	[202]
	* Phenolic compounds of <i>Ulmus davidiana</i> var. <i>japonica</i> showed antifungal activity against <i>Cryptococcus neoformans</i> and <i>Candida albicans</i> .	[203]
	* <i>Zataria multiflora</i> essential oils could act as natural fungicides; carvacrol and thymol chemotypes of <i>Zataria multiflora</i> inhibited five important fungal plant pathogens.	[204]
	* <i>Aconitum heterophyllum</i> and <i>Polygonum bistorta</i> exhibited significant antimicrobial and antioxidant activity.	[205]
Antimicrobial activity	* The antimicrobial activities of mint and thyme were due to a wide range of diverse phenolics such as menthone, menthyl acetate, menthol, terpenes, and thyme.	[206]
	* Phenolic compounds of <i>Codonopsis lanceolata</i> plants exhibited notable antimicrobial activity.	[207]
	* Phenolic compounds of cashew (<i>Anacardium occidentale</i> L.) compounds identified included mainly flavanols, which showed high antimicrobial activity.	[208]
Antibacterial activity	* <i>Ixora coccinea</i> Linn. root contained bioactive phenolic compounds including pyrocatechol, catechin, and chlorogenic acid with potent antimicrobial effects.	[209]
	* The ethyl acetate fraction of <i>Scirpus holoschoenus</i> showed the highest antioxidant activity and antibacterial effect for <i>Staphylococcus aureus</i> and <i>Bacillus subtilis</i> .	[210]
	* <i>Rhanterium adpressum</i> showed antibacterial activity.	[211]
	* The lignum of <i>Rhus verniciflua</i> contained high content of phenolic compounds with less urushiols, which suggests efficient antibacterial activity with less toxicity.	[212]
	* Phenolic compounds of <i>Scrophularia ningpoensis</i> Hemsl. showed antibacterial activity.	[213]
	* Flavonoids, saponin, alkaloids, tannins, steroids, and terpenoids of <i>Solanum incanum</i> L. and <i>Harrisonia abyssinica</i> Oliv. exhibited antibacterial activity.	[214]
	* The phenolic extracts from <i>Cerbera manghas</i> , <i>Commelina diffusa</i> , <i>Peperomia pellucida</i> , <i>Kleinhovia hospita</i> , <i>Mikania micrantha</i> , <i>Homalanthus nutans</i> , <i>Psychotria insularum</i> , <i>Phymatosorus scolopendria</i> , <i>Piper graeffei</i> , and <i>Schizostachyum glaucifolium</i> exhibited antibacterial activities.	[215]
	* Curcumin has been suggested as a potential treatment choice for patients with COVID-19 because it inhibits ACE2 and suppresses the entry of SARS-CoV-2 into the cells.	[216]
Anti-Coronavirus Properties	* Theaflavin, the compound responsible for the orange/black color of black tea, is a potent inhibitor of the RNA polymerase of SARS-CoV-2.	[217]
	* Catechin gallate and gallic acid also showed high inhibitory activity against SARS-CoV-2 N protein in a concentration-dependent manner and affected virus replication.	[218]
	* Myricetin could be further tested and developed as a potential SARS-CoV-2 antiviral.	[219]
	* The phenolic compounds <i>Kadsurenin</i> L. and <i>Methysticin</i> of <i>Piper nigrum</i> are candidate ligands for inhibiting COVID-19.	[220]
	* Plant-derived phenolic compounds of <i>Isatis indigotica</i> root were frequently used for the prevention of SARS during the SARS outbreaks in east Asia.	[221]
	* Among phenolic acid constituents, chlorogenic acid, caffeic acid, and gallic acid of <i>Sambucus Formosana Nakai</i> reduced cytopathicity and virus yield in HCoV-NL63-infected cells.	[222]
	* Some phenolic compounds such as diethylstilbestrol, enterodiol, enterolactone, flavokawain A, flavokawain B, and flavokawain C showed excellent to good inhibitory activities against collagenase, elastase enzymes, and SARS-CoV-2.	[223]
	* The phenolic compounds of blackcurrant (<i>Ribes nigrum</i> L.) had antiviral activity in Coxsackievirus A9 and human coronavirus HCoV-OC-43.	[224]

Table 5. Cont.

Health Benefits	Key Points	References
Neuroprotective potential	* Hydroxytyrosol obtained from olive exhibited neuroprotective impacts on multiple chronic neurodegenerative diseases including Alzheimer's, Parkinson's, and multiple sclerosis.	[225]
	* The protective impacts of oil palm phenolics against neurodegenerative diseases have been recently identified.	[226]
	* Phenolic compounds of <i>Hypericum wightianum</i> , namely Hyperwightin E and petiolin G, revealed noticeable neuroprotection at 10 μ M.	[227]
	* <i>Inula viscosa</i> (L.) Greuter has high total phenolics and flavonoids and demonstrated neuroprotective properties.	[228]
	* <i>Maclura tinctoria</i> leaf aqueous extract contained high phenolic components, and it has been found that neuroprotective effects of it could be associated with the presence of the phenolic compounds identified.	[229]
Skin health	* Phenolic compounds from <i>Lippia microphylla</i> and <i>Dimorphandra gardneriana</i> presented a high sun protector factor because of the presence of sakuranetin flavonoids and quercetin glycosides.	[230]
	* Among Moroccan medicinal plants, <i>Allium cepa</i> L., <i>Chamaeleon gummiifer</i> (L.) Cass, and <i>Salvia rosmarinus</i> Schleid. Mill. leaves were the most commonly used for different types of skin diseases.	[231]
	* <i>Panax ginseng</i> C.A. Meyer and <i>Nardostachys chinensis</i> Bat. have been confirmed for the treatment of skin pigmentary disorders.	[232]
	* The protective effects on skin cells associated with blueberry phenolic compounds that included inhibition of proliferation and cell cycle arrest in malignant cells decreased oxidized macromolecules, down-regulated inflammatory cytokine genes, and mitigated oxidative stress.	[233]
Wound healing	* Gel containing <i>Ipomoea pes-caprae</i> (Ipc) phenolic-rich leaf extract accelerated the wound-healing process.	[234]
	* <i>Loranthus acaciae</i> exhibited high phenolic contents and wound healing activities.	[235]
	* <i>Haworthia limifolia</i> showed excellent wound-healing properties because of high phenolic contents.	[236]
	* <i>Lawsonia inermis</i> and <i>Azadirachta indica</i> are well known for wound healing.	[237]
	* Aloe vera (<i>Aloe barbadensis</i>) is one of the oldest medicinal plants with wound healing activity for a variety of skin disorders including burns as well as infections and diabetic dermal wounds.	[238]
	* <i>Amphimas pterocarpoides</i> leaves and stem bark have high phenolic and flavonoid contents, and it has been proven that leaf and stem bark ointments increased the rate of wound healing in rats.	[239]
Anticancer activity	* <i>Sedum dendroideum</i> showed anti-proliferative activity in breast cancer cells.	[240]
	* <i>Hypericum perforatum</i> extract exhibited a remarkable total phenol content, which showed high anticancer activity.	[241]
	* <i>Ficus palmata</i> Forssk. exhibited high total phenolic and flavonoids contents, which showed its high anticancer activity.	[242]
	* <i>Euphorbia thymifolia</i> and <i>Euphorbia hirta</i> showed anticancer activity against ascites carcinoma in mice models.	[243]
	* <i>Vitis vinifera</i> L. contained high phenolic components, which can be considered as a promising potential for an anticancer drug.	[244]
	* Phenolic compounds and alkaloid compounds of <i>Dysphania ambrosioides</i> might have significantly contributed to anticancer activity.	[245]
	* <i>Sisymbrium officinale</i> had considerable phenolic and flavonoids contents, which was why it showed anticancer activity.	[246]

3. Hydroxybenzoic Acids (Gallic Acid and Protocatechuic Acid)

Hydroxybenzoic acids (HBAs) are antioxidant phytochemicals found in many medicinal plants and are efficient for prevention of various human diseases [247,248]. Joshi et al. [249] reported that 4-hydroxybenzoic acid (4HBA) is a potential antidiabetic, anticancer, antifungal, antioxidant, and cardioprotective, etc. *Piper garagaranum* C. DC contains prenylated hydroxybenzoic acids, and prenylated hydroxybenzoic acids indicated anti-inflammatory characteristics, as determined in murine macrophage assays [250].

3.1. Gallic Acid

Gallic acid is one of the most abundant polyphenols identified in nature [251,252]. Behera et al. [253] reported that gallic acid reveals antioxidant or free radical scavengers in adipocyte proliferation. Gallic acid is found in a wide range of natural plants, it is associated with the health of human beings, and it has well-documented anticancer, antibacterial, anti-inflammatory, and antifungal activities [254,255]. Gallic acid in *Emblica officinalis* mediated antidiabetic potential and delineated the upregulation of pAkt, PPAR- γ , and Glut4 through gallic acid-mediated antidiabetic properties, thus providing potent therapy for diabetes [256]. Gallic acid inhibited about 44–57% of the total CaOx crystal formations, and it is a promising agent with antiurolithiatic properties for the treatment and prevention of urinary or kidney stones [257]. Gallic acid supplementation adjusted serum lipid metabolism by decreasing serum triglyceride, fat digestibility, and bacteroidetes/firmicutes ratio [258]. Gallic acid prevents the development and occurrence of gastric precancerous lesions (GPL) by inhibiting the Wnt/ β -catenin signaling pathway and then suppressing the epithelial–mesenchymal transition (EMT) process [259]. Gallic acid is a direct thrombin inhibitor with a platelet aggregation inhibitory effect [260]. Gallic acid shows significant binding and disruption of protease structure, and gallic acid has a potential phytotherapeutic effect against fungal protease, which is a notable virulence factor [261]. Gallic acid can boost gut microbiota alterations connected with cardiovascular disease (CVD) and suggests that males suffering from atherosclerosis may benefit from gallic acid supplementation, as this polyphenol partially restored microbiome dysbiosis [262]. Gallic acid could decrease the noxious impacts of diclofenac (DIC) on the antioxidant defense system and renal tissue [263].

3.2. Protocatechuic Acid

Protocatechuic acid (3,4-dihydroxybenzoic acid) is a natural phenolic acid, and one of the chief metabolites of complex polyphenols [264]. It can be identified in many plants such as bran and grain brown rice, particularly in the scales of onion, plums, grapes, gooseberries, and nuts such as ordinary almonds [265,266]. Da-Costa-Roch et al. [267] and Adedara et al. [268] reported that protocatechuic acid can be found in many medicinal plants, especially *Hibiscus sabdariffa* L. (Hs, roselle; Malvaceae). Protocatechuic acid has different activities such as neuroprotective activities, antiosteoporotic activities, antitumor activities, and the protective effects against hepatotoxic and nephrotoxic activities [269,270]. It has also antibacterial, antiulcer, anti-aging, antidiabetic, anticancer, antiviral, antifibrotic, analgesic, anti-inflammatory, anti-atherosclerotic, and cardiac activity [271,272]. Protocatechuic acid from bitter melon (*Momordica charantia*) alleviates cisplatin-induced oxidative renal damage, which proves it has protective activity against anticancer drug-induced oxidative nephrotoxicity [273]. Protocatechuic acid inhibits Cd-induced neurotoxicity in rats, increases the Nrf2 signaling pathway, and exhibits anti-apoptotic and anti-inflammatory activities [274]. *Veronica montana* has protocatechuic acid as the main phenolic molecule, and it kills bacteria by affecting its cytoplasmic membrane [275].

4. Hydroxycinnamic Acids (*p*-Coumaric Acid, Caffeic Acid, Ferulic Acid, Sinapic Acid)

Hydroxycinnamic acid derivatives are a notable class of polyphenols found in vegetables, fruits, and medicinal plants, and extensively consumed in human diet [276,277]. Hydroxycinnamic acids significantly contribute to antioxidant capacity [278]. Hydroxycinnamic acids are widely found in plants and their products such as cereals, fruits, coffee, vegetables, etc. [279,280].

4.1. *p*-Coumaric Acid

p-Coumaric acid is a plant metabolite with antioxidant and anti-inflammatory impacts [281,282]. *p*-Coumaric acid boosts hepatic fatty acid oxidation and fecal lipid excretion, and it affects inflammatory and insulin resistance-related adipokines. *p*-Coumaric acid stimulates electrical factors of biological and model lipid membranes [283].

4.2. Caffeic Acid

Caffeic acid (3,4-dihydroxycinnamic acid) has been known as an important source of natural antioxidants in different agricultural products [284,285]. It has immense use in cancer treatment [286,287], and it could be known as an important natural antioxidant [288]. Caffeic acid can induce apoptosis in cancer cells through increasing ROS levels and impairing mitochondrial function, and it also benefits from reducing aggressive behavior of tumors via suppressing metastasis [289]. Caffeic acid has anti-inflammatory and antioxidant properties against 6-propyl-thiouracil (PTU)-induced hypothyroidism [290]. Meinhart et al. [291] reported that higher sums of mono-caffeoylquinic acids were found in mulberry, quince, and bilberry, and the dicaffeoylquinic acids sum was higher in granadilla, passion fruit, and kumquat. It is a phenolic compound extensively discovered in commonly consumed foods such as apples, pears, and coffee [292]. The biosynthesis pathway of caffeic acid can be categorized into two modules, (1) L-tyrosine is synthesized from carbon sources via the glycolytic pathway, the pentose phosphate pathway, and the shikimate pathway; (2) caffeic acid is generated by the continuous deamination and hydroxylation of L-tyrosine [293]. Trifan et al. [294] found that caffeic acid oligomers reported in *Symphytum officinale* L. root may contribute to the anti-inflammatory activity for which comfrey preparations are used in traditional medicine. Caffeic acid phenethyl ester extracted from *Rhodiola sacra* could provide health benefits, decreasing the magnitude of the inflammatory process triggered by endotoxin shock and the production of inflammatory mediators [295]. Caffeic acid from the leaves of *Annona coriacea* have shown antidepressant-like impacts, which involve important neurotransmitter systems [296]. Spagnol et al. [297] reported that caffeic acid presented antioxidant activity greater than ascorbic acid and trolox. Caffeic acid regulates lipogenesis-related protein expression in high-fat diet (HFD)-fed mice, alleviates endotoxemia and the proinflammatory response in HFD-fed mice, and attenuates gut microbiota dysbiosis in HFD-fed mice [298]. Caffeic acid decreases oxidative stress levels in the hippocampus and regulates microglial activation in the hippocampus [299].

4.3. Ferulic Acid

Ferulic acid (4-hydroxy-3-methoxycinnamic acid) is a polyphenol that is widely known for its therapeutic potential, showing anti-aging, anti-inflammatory, and neuroprotective impacts [300,301]. The ferulic acid molecule reveals cis-trans isomerism, with the most abundant form in nature being the trans isomer, and both isomers have proven results in the treatment of several pathologies such as diabetes, cancer, and neurodegenerative and cardiac diseases [302]. Ferulic acid is important for the synthesis of significant chemical molecules such as coniferyl alcohol, di ferulic acid, vanillin, synaptic, and curcumin, as well as for giving the cell wall stiffness [303]. Ferulic acid can be applied as an antioxidant to prevent damage from ultraviolet (UV) radiation and skin carcinogenesis [304]. It is ample in numerous fruits and vegetables, including bananas, eggplant, citrus fruits, and cabbage, as well as in seeds and leaves [305,306]. In Chinese medicinal science, ferulic is normally joined with polysaccharides by covalent bonds in various plant cell walls such as cereal bran and regarded as the main bioactive compound of *Angelica sinensis*, chuanxiong rhizoma, and ferula [307], and it has several biological activities such as anti-apoptosis, anticancer, antioxidant, and anti-inflammatory impacts [308]. Free ferulic acid is related to the natural content of ferulic acid in herbs, and total ferulic acid refers to the sum of free ferulic acid plus the amount of related hydrolyzed components [309,310]. *Angelica sinensis* is a perennial herbaceous species that creates the bioactive metabolite ferulic acid [311,312]. The ferulic compounds of *Salvia officinalis* could be useful as a safe natural source for estrogenic characteristics [313]. Singh et al. [314] indicated that ferulic acid is a phenol derivative from natural sources and applied it as a potential pharmacophore that exerts multiple pharmacological properties such as neuroprotection, A β aggregation modulation, antioxidant, and anti-inflammatory. Ferulic acid increases cerebellar functional and histopathological changes induced by diabetes, which can be attributed to its antioxidative effect and its ability to modulate nitric oxide synthase (NOS) isoforms [315]. Ramar et al. [316] showed that

ferulic acid and resveratrol revealed antioxidant as well as antidiabetic effects, consequently modulating liver, kidney, and pancreas damage caused by alloxan-induced diabetes, possibly via inhibition of the proinflammatory factor, NF-KB. Ferulic acid treatment prevents radiation-induced lipid peroxidation and DNA damage and restores antioxidant status and histopathological alterations in experimental animals [317]. Hu et al. [318] found that ferulic acid could alleviate inflammation and oxidative stress. Ferulic acid can inhibit cancer proliferation through various mechanisms, including changing the cancer cell cycle, inducing apoptosis, and regulating proteins involved in cell proliferation [319], and ferulic acid could be used as a potential official adjuvant for breast cancer treatment [320].

4.4. Sinapic Acid

Sinapic acid, a widely prevalent hydroxycinnamic acid, contains numerous biological activities related to its antioxidant property [321,322]. It protects lysosomes and prevents lysosomal dysfunction [323]. Saeedavi et al. [324] reported that sinapic acid may be a new therapeutic potential to treat allergic asthma through suppressing T-helper 2 immune responses. Sinapic acid phenethyl ester boosts gene expression related to the cholesterol metabolic process [325]. Hu et al. [326] indicated that sinapic acid can be utilized as an effective chemo preventive agent against lung carcinogenesis. It can also alleviate blood glucose levels by improving insulin production in pancreatic β -cells, and it can exhibit an antioxidative impact by suppressing lipid peroxidation and increasing the activity of antioxidant enzymes [327]. Sinapic acid significantly increases caspase-3 activity and inhibits cell invasion, and it has anticancer impacts on prostate cancer cells [328]. Sinapic acid pretreatment mitigates renal impairment and structural injuries through the downregulation of oxidative/nitrosative stress, inflammation, and apoptosis in the kidney [329]. Raish et al. [330] indicated the ability of sinapic acid to restore the antioxidant system and to suppress oxidative stress, pro-inflammatory cytokines, extracellular matrix, and TGF- β , and showed that sinapic acid treatment (10 and 20 mg/kg) significantly ameliorated bleomycin (BML)-induced lung injuries. Singh and Verma [331] revealed that sinapic acid increases streptozotocin (STZ)-induced cognitive impairment by ameliorating oxidative stress and neuro inflammation in the cortex and hippocampus. Sinapic acid can modulate the redox state in high-fat diet (HFD) rats [332].

5. The Health Benefits of Coumarins (Umbelliferone, Esculetin, Scopoletin)

Coumarins (2H-chromen-2-one ring) with the molecular formula $C_9H_6O_2$ are an important group of natural compounds and are used as additives in both cosmetics and foods [333], and they constitute a notable class of heterocyclic compounds with the characteristic benzo- α -pyrone moiety in its structure [334]. Coumarin has been reported to have antibacterial, anticancer, antioxidant, anti-inflammatory, anticoagulant, and anti-Alzheimer's disease (AD) activities [335,336]. Coumarin derivatives are found naturally as secondary metabolites in more than 150 species of plants and in over 30 plant families such as *Clusiaceae*, *Umbelliferae*, *Guttiferae*, *Rutaceae*, *Oleaceae*, *Fabaceae*, and many more [337]. Seo et al. [338] reported that different coumarins were identified from the roots of *Angelica dahurica* using NMR spectroscopy, and each coumarin revealed remarkable differences in content and inhibitory effect. Kassim et al. [339] indicated that the good antioxidant activity of *Melicope glabra* (Rutaceae) is because of umbelliferone, glabranin, and scopoletin. Coumarin-based compounds extracted from the medicinal plants are shown in Table 6.

Table 6. Coumarin-based compounds obtained from the medicinal plants used by various ancient medical systems [340].

Compounds	Molecular Formula	Pharmaceutical Activity
6-hydroxy-4-methoxy-5-methylcoumarin	$C_{11}H_{10}O_4$	Microtubule stabilizing agent
(+)-Calanolide	$C_{22}H_{26}O_5$	Anti-HIV agent
Inophyllum	$C_{25}H_{24}O_5$	Anti-HIV agent
Theraphin	$C_{22}H_{28}O_6$	Anticancer agent Antimalarial agent

5.1. Umbelliferone

Umbelliferone is a 7-hydroxycoumarin and an isomer of caffeic acid [341], and it has been reported for different pharmacological activities against numerous diseases such as cancer [342]. The plant sources of umbelliferone are *Acacia nilotica*, *Angelica decursiva*, *Aegle marmelos*, *Artemisia tridentata*, *Aster praelatus*, *Balsamocitrus camerunensis*, *Chamomilla recutita*, *Citrus aurantium*, *Cirtus natsudaikai*, *Citrus paradise*, *Coriandrum sativum*, *Diospyros oocarpa*, *Diplostephium foliosissimum*, *Dystaenia takeshimana*, *Edgeworthia chrysantha*, *Edgeworthia gardneri*, *Eriostemon apiculatus*, *Ferula communis*, *Ferula communis*, *Ferula assafoetida*, *Fructus Aurantii*, *Glycyrrhiza glabra*, *Angelica archangelica*, *Haplophyllum villosum*, *Harbouria trachypleura*, *Haplopappus deserticola*, *Haplophyllum patavinum*, *Hydrangea chinensis*, *Hydrangea macrophylla*, *Hieracium pilosella*, *Ipomoea mauritiana*, *Justicia pectoralis*, *Matricaria recutita*, *Melicope glabra*, *Musa spp.*, *Parkinsonia aculeata*, *Peucedanum praeruptorum*, *Picea abies*, *Potentilla evestita*, *Rhododendron lepidotum*, *Platanus acerifolia*, *Selaginella stautoniana*, *Saussurea copygmaea*, *Stellera chamaejasme*, and *Typha domingensis* [343]. It has been reported to have antioxidant, anti-inflammatory, free radical scavenging, and antihyperglycemic properties [344], and antifungal characteristics [345]. Althunibat et al. [346] reported that umbelliferone prevented isoproterenol cardiotoxicity in rats, and it decreased isoproterenol-induced oxidative stress and inflammation. Kutlu et al. [347] reported that umbelliferone has a strong antioxidant and anti-inflammatory effect on sepsis, and it can be considered as a new treatment for organ dysfunction. Umbelliferone ameliorates atopic dermatitis (AD)-associated symptoms and inflammation via regulation of various signaling pathways, suggesting that umbelliferone might be a potential therapeutic of AD [348]. Umbelliferone downregulates TGF- β 1 levels in kidney tissue and it may promote kidney function and ameliorate renal oxidative stress [349]. Mohamed et al. [350] indicated that umbelliferone ameliorated oxidative stress-related hepatotoxicity via its ability to augment cellular antioxidant defenses by activating Nrf2-mediated HO-1 expression. Umbelliferone exhibits anticancer impacts on human oral carcinoma (KB) cell lines, with the increased generation of intracellular reactive oxygen species (ROS) triggering oxidative stress-mediated depolarization of mitochondria [351]. Umbelliferone has gastric protective activity in vivo, and it has antidiarrheal activity in vivo [352].

5.2. Esculetin

Esculetin (6,7-dihydroxycoumarin), a natural coumarin derived from herbs, has shown different pharmacological activities [353]. Kadakol et al. [354] reported that esculetin, a naturally occurring 6,7-dihydroxy derivative of coumarin, has revealed its potential function in various non-communicable diseases (NCDs) including obesity, diabetes, renal failure, cardiovascular disease, cancer, and neurological disorders. Esculetin reduced both chronic and acute topic skin inflammation, and mitigated inflammation by suppressing infiltration of inflammatory cells [355]. It can be found in many medicinal plants such as *Artemisia capillaris*, *Matricaria chamomilla* L., *Artemisia scoparia*, *Citrus limonia*, *Cortex Fraxini*, and *Ceratostigma willmottianum* [356–358]. Esculetin supplementation could protect against development of non-alcoholic fatty liver in diabetes via regulation of glucose, lipids, and inflammation [359]. The esculetin protects human hepatoma HepG2 cells from hydrogen peroxide-induced oxidative injury, and the production is provided via the induction of protective enzymes as part of an adaptive response mediated by Nrf2 nuclear accumulation [360]. Esculetin prevents progressive renal fibrosis under insulin resistance (IR) and type 2 diabetic nephropathy (T2D) conditions, and it decreases oxidative stress in the kidney under IR and T2D conditions [361]. Esculetin has the ability to suppress tumor growth and metastasis via Axin2 suppression, which can be an attractive therapeutic strategy for the treatment of metastatic colorectal cancer (CRC) [362]. Esculetin treatment decreased neurological defects and improved cognitive impairments in transient bilateral common carotid artery occlusion (tBCCAO)-treated mice, and the mechanism underlying the pharmacological impacts of esculetin involved its action on mitochondrial autophagy and the apoptosis triggered by mitochondrial oxidative stress via mediation of mitochondrial frag-

mentation during transient cerebral ischaemia and reperfusion injury [363]. Zhang et al. [364] reported that esculentin could be a potential therapeutic drug for the treatment of hepatic fibrosis by inducing stellate cell senescence. Wang et al. [365] indicated that esculentin is safe and reliable, is easy to be absorbed by the body, and can be synthesized in a variety of ways. Esculetin inhibits the pyroptosis of microvascular endothelial cells through the NF-KB/NLFP3 signaling pathway and is expected to be conducive in treating pyroptosis-related diseases [366]. Esculetin directly binds to hnRNPA1 and decreases the concentration of hnRNPA1 in endometrial cancer cells, and it downregulates the levels of BCL-XL and XIAP expression, resulting in apoptosis and an arrest in proliferation [367]. Esculetin inhibits clear cell renal cell carcinoma growth in a dose- and time-dependent manner, and it induces apoptosis and cell cycle arrest [368]. Esculetin could be used as a dietary therapy for the prevention of alcoholic liver disease, and it can markedly prevent ethanol-induced liver injury in mice [369].

5.3. Scopoletin

Scopoletin (6-methoxyl-7-hydroxy coumarin) has a phenolic hydroxyl structure and is a member of the coumarin family [370]. It has a long history of use for its medicinal characteristics in traditional Chinese medicine [371]. Scopoletin is one of the main bioactive components of *Convolvulus prostratus* Forssk, known to have a role in acetylcholinesterase inhibitor, antimicrobial, memory enhancer, and antioxidative properties [372]. It is a major component of noni (*Morinda citrifolia* L.), which contributes to the anti-inflammatory, antioxidative, immunomodulatory, and hepatoprotective properties [373]. Scopoletin could be a potential phagocytic enhancer, and it can increase immunity through enhancing macrophage phagocytic capabilities [374]. Scopoletin improved vancomycin-induced renal injury via restoring the antioxidant defense system [375]. Scopoletin reduces non-alcoholic fatty liver disease in high-fat diet-fed mice [376]. It has been reported that scopoletin could exert a positive impact on anti-aging related to autophagy via modulation of p53 in human lung fibroblasts [377].

6. The Health Benefits of Stilbenes (Resveratrol, Piceatannol, Pterostilbene)

Stilbenes (based on the 1,2-diphenylethylene skeleton) are a group of plant polyphenols with rich structural and bioactive diversity [378]. They originate from plant families such as Vitaceae, Gnetaceae, Leguminaceae, and Dipterocarpaceae, and, structurally, they have a C6-C2-C6 skeleton, normally with two isomeric forms [379,380]. They have wonderful potential for anti-inflammatory, antiviral, anticancer, and antioxidant activities, as well as an application as cosmetic materials, coloring agents, and dietary supplements [381–383]. Wine and grapes are the main dietary source of stilbenes [384]. These compounds are synthesized by plants in response to abiotic or biotic stress situations [385]. Most stilbene compounds reveal antimicrobial properties, acting as phytoalexins in response to pathogen or herbivore attack [386]. Phytochemical phenols of stilbene families indicated good stability at elevated temperatures [387].

6.1. Resveratrol

Resveratrol (3,5,4'-trihydroxy-trans-stilbene) is a plant polyphenol, extensively popularized during the last decades, owing to its promising beneficial effects on human health [388]. It is a famous non-flavonoid polyphenol, related to the family of stilbenes whose structure consists of two phenolic rings linked by a double bond, which promotes two isomeric conformations: trans- and cis-resveratrol [389,390]. Resveratrol's cis-isomer is unstable, and its trans-isomer contains greater stability, but converts to the cis-isomer under exposure to high pH or UV light [391,392], with heat increasing the degradation process [391]. It exists in many traditional herbs, and in several types of fruits, especially in the muscadine grape, red wine, cranberry, lingonberry, and redcurrant [393], and roots of various plant species including *Polygonum cuspidatum* and rhubarb (*Rheum rhaponticum*) [394]. It is also useful in common age-related diseases such as cancer, cardiovascular diseases,

type 2 diabetes, and neurological conditions, and it has also positive impacts on metabolism and can boost the lifespan of various organisms [395]. Resveratrol supplementation can be considered as an adjuvant therapy for relieving inflammation [396]. It has great potency in treating cardiovascular diseases [397]. Resveratrol attenuates kidney damage in malignant hypertension rats, and it can increase glomerular filtration while decreases proteinuria [398]. It inhibits the release of proinflammatory cytokines and leads to the release of anti-inflammatory cytokines, and it scavenges free radicals and upregulates antioxidant enzymes [399]. Chowdhury et al. [400] indicated that resveratrol treatment indicated beneficial impacts on preventing oxidative stress and fibrosis in the kidneys of high-fat (HF) diet-fed rats, probably by modulating the gene expression of oxidative stress and inflammation-related parameters and enzymes. Resveratrol can downregulate the pro-inflammatory cytokine release decreasing lung injury [401]. Resveratrol-containing fruits could be a promising substitute for the management of Alzheimer's disease [402]. It can be more effective in cardiotoxicity prevention [403]. *Polygonum cuspidatum* is an important medicinal plant in China and a rich source of resveratrol compounds, which is a secondary metabolite formed in the long-term evolution procedure of plants to increase their response to adverse environments such as pathogens and ultraviolet radiation [404]. As an anticancer parameter, resveratrol promotes apoptosis in hepatocellular carcinoma cells [405]. Bhaskara et al. [406] reported that resveratrol is a potential reducing factor that can prevent carcinogenesis due to its antioxidant abilities, and it acts as an immunomodulatory agent for treating cancer. Resveratrol can exhibit anti-aging activity through a variety of signaling pathways [407]. Resveratrol shows potent anti-rotavirus efficacy in vitro and in vivo, and it blocks viral structural expression and genomic RNA synthesis [408]. Resveratrol oligomers from *Paeonia suffruticosa* indicate neuroprotective effects in vitro and in vivo by regulating cholinergic, antioxidant, and anti-inflammatory pathways, and they may have promising applications in the treatment of Alzheimer's disease [409]. Resveratrol is also involved in neurodegenerative diseases (NDs) with multiple neuroprotective activities [410]. Antimicrobial activity of resveratrol against many bacteria and fungi has been reported, such as antimicrobial activity against Gram-positive bacteria such as *Bacillus cereus*, *Bacillus megaterium*, *Staphylococcus aureus*, *Enterococcus faecalis*, *Enterococcus faecium*, *Mycobacterium tuberculosis*, *Mycobacterium smegmatis*, *Streptococcus pneumoniae*, *Streptococcus pyogenes*, *Propionibacterium acnes*, and *Listeria monocytogenes*; against Gram-negative bacteria such as *Escherichia coli*, *Klebsiella pneumoniae*, *Salmonella enterica* serovar *Typhimurium*, *Pseudomonas aeruginosa*, *Helicobacter pylori*, *Arcobacter butzleri*, *Arcobacter cryaerophilus*, *Haemophilus ducreyi*, *Neisseria gonorrhoeae*, *Neisseria meningitidis*, *Vibrio cholerae*, *Fusobacterium nucleatum*, *Campylobacter jejuni*, and *Campylobacter coli*; and against fungi such as *Trichophyton mentagrophytes*, *Trichophyton tonsurans*, *Trichophyton rubrum*, *Epidermophyton floccosum*, *Microsporum gypseum*, *Candida albicans*, *Saccharomyces cerevisiae*, *Botrytis cinerea*, and *Trichosporon beigelii* [411]. Resveratrol has powerful anticancer characteristics in different cancer cells and organs such as pancreatic cancer, colorectal cancer, gastric cancer, esophageal cancer, hepatocellular cancer, oral cancer, and biliary tract cancer [412]. Resveratrol decreases damage to pancreatic tissue via suppression of calcium overload; it suppresses calcium overload and, thereby, decreases trypsinogen activation, oxidative stress, mitochondrial dysfunction, and disorders, and it also reduces damage to other organs such as lung and heart by decreasing microcirculatory dysfunction [413].

6.2. Piceatannol

Piceatannol (3,4,3',5'-tetrahydroxy-trans-stilbene), a natural polyphenolic stilbene, has pleiotropic pharmacological potentials [414]. It can be found in different kinds of fruits and vegetables such as blueberries, grapes, and passion fruit [415]. Piceatannol is a metabolite of resveratrol found in red wine, which prevents cardiac hypertrophy in rat neonatal cardiomyocytes [416]. It has previously been known as an antileukemic principle, which has been shown to be an inhibitor of protein-tyrosine kinase activity [417]. It has been reported that its low water-solubility and bioavailability could limit its application in both food and

pharmaceutical fields [418]. Piceatannol, compared with the renowned resveratrol, is a better anticancer factor and a superior agent with other biological properties [419]. Piceatannol lightened oxidative injury and collagen synthesis in lung tissues during pulmonary fibrosis, and it suppressed the activation and collagen synthesis of TGF- β -induced lung fibroblasts [420]. It appears to be an appropriate nutritional or pharmacological biomolecule that modulates effector T cell functions, namely cytokine production, differentiation, and proliferation [421]. Piceatannol attenuates fat accumulation in steatosis-induced HepF2 cells, it suppressed lipogenesis and fatty acid uptake in steatosis-induced HepG2 hepatocytes, and it suppressed fatty acid-induced oxidative stress [422]. It shows anti-aggregation activity, and it increases catalase and glutathione peroxidase activity [423]. It can also be considered as a potential chemotherapeutic factor in the treatment of leukemia, but it may be connected with the risk of multi-drug resistance [424]. Passion fruit seed extract and piceatannol could exert anticancer activity via human glyoxalase I (GLO I) inhibition [425]. Piceatannol is a promising medication for preventing acute liver failure and the mechanisms may be associated to its inhibitory impacts on ER stress, inflammation, and oxidative stress [426]. Piceatannol has a potential inhibitory activity against human glyoxalase I (GLO I), and it inhibits the proliferation of GLO I-dependent human lung cancer [427]. It protects ARPE-19 cells against apoptosis induced by photo-oxidation, and the protective effect of piceatannol is because of the activation of the Nrf2/NQO1 pathway [428]. Piceatannol is a potent enhancer of cisplatin-induced apoptosis, and it reveals the potential for clinical development for the treatment of ovarian cancer [429]. It has been reported that piceatannol significantly decreases the degree of bovine serum albumin (BSA) glycosylation, and this suggests its potential impact on preventing the progression of diabetes mellitus [430].

6.3. Pterostilbene

Pterostilbene, a dimethyl ester derivative of resveratrol, may act as a cytotoxic and anticancer factor [431]. It primarily exists in blueberries, grapevines, and heartwood of red sandalwood [432,433]. Phenolic resveratrol, pterostilbene has been reported to have antifungal activity against a broad range of important phytopathogenic fungi such as *Leptosphaeria maculans* and *Peronophythora litchii* [434]. It is an anti-inflammatory and antioxidant agent with preventive effects toward skin disorders, and its anticancer impacts include inducing necrosis, apoptosis, and autophagy [435]. It can alleviate hepatic damage and oxidative stress and increase hepatic antioxidant function in piglets [436]. It possesses the abilities of antiproliferation, reversing epithelial to mesenchymal transition (EMT), and suppression of cancer stemness, and it could suppress tumor growth and inhibit the metastasis of tumor cells to livers and lungs with therapeutic safety in BALB/C mice [437].

7. The Important Health Benefits of Lignan (Sesamin)

Lignans are naturally occurring compounds produced and accumulated in different edible and medicinal plants, which can be subdivided bio-synthetically into neolignan and lignans [438,439]. Lignans, as the notable subgroup of phenylpropanoids, are involved in the plant defense responses to numerous biotic and abiotic stresses [440]. Lignans, with different biological activities, such as antitumor, antibacterial, antioxidant, and antiviral activities, are generally distributed in nature and mostly exist in the xylem of plants [441,442]. The level of lignans varies between plant parts of all species [443].

Sesamin, a major lignan derived from sesame seeds, has several benefits and medicinal characteristics [444]. It exerts various pharmacological impacts, such as prevention of hyperlipidemia, hypertension, and carcinogenesis, as well as anticancer and chemopreventive activity in vitro and in vivo [445,446], and antioxidant and anti-inflammatory characteristics [447,448]. Plants reported to contain sesamin are *Paulownia tomentosa* Staud., *Phyllarthron comorense*, *Justicia simplex*, *Hyptis tomentosa*, *Anacyclus pyrethrum*, *Artemisia absinthium*, *Artemisia gorgonum*, *Chrysanthemum cinerariaefolium*, *C. frutescens*, *C. indicum*, *Diotis maritima*, *Eupatorium aegeratina*, *E. ritionia*, *E. fleischmannia*, *Otanthus maritimus*, *Aptosimum*

spinescens, *Gmelina arborea* Roxb., *Acanthopanax senticosus*, *A. sessiliflorum*, *Eleutherococcus divaricatus*, *Asarum sieboldii*, *Aristolochia cymbifera*, *Alnus glutinosa*, *Salicornia europaea*, *Austrocedrus chilensis*, *Evodia micrococca*, *Fagara xanthoxyloides*, *Fagara tessmannii*, *Fagara heitzii*, *Micromelum minutum*, *Melicope glabra*, *Spiranthera odoratissima*, *Flindersia pubescens*, *Zanthoxylum naranjillo*, *Zanthoxylum tingoassuiba*, *Zanthoxylum piperitum*, *Zanthoxylum nitidum*, *Zanthoxylum flavum*, *Zanthoxylum alatum* Roxb., *Zanthoxylum bungeanum*, *Ginkgo biloba*, *Machilus glaucescens*, *Ocotea usambarensis*, *Aiouea trinervis* Meisn., *Talauma hodgsonii*, *Magnolia* spp., *Picea abies*, *Macropiper excelsum*, *Piper sarmentosum*, *Sesamum indicum*, *S. radiatum*, *S. mulayanum*, *S. malabaricum*, *S. alatum*, *S. angustifolium*, *S. angolense*, *S. calycinum*, *Anemopsis californica*, *Quercus frainetto* Ten., *Vernicia fordii*, *Jatropha curcas*, *Larrea tridentata*, *Morinda citrifolia*, *Glossostemon bruguieri*, *Ligustrum japonicum*, and *Triclisia sacleuxii* [449]. Sesamin could boost the proliferation and adhesion of intestinal probiotics, leading to modulating gut microbiota, which provided the basis for sesamin as a food-borne functional parameter for improving intestinal health [450]. Sesamin suppressed breast cancer proliferation, and it downregulated programmed death ligand 1 (PD-L1) expression, which is mediated by NF-KB and AKT [451]. Sesamin increased osteoblast differentiation by the increase of type I collagen (COL1A1) and alkaline phosphatase (ALP) gene expression as well as ALP activity [452]. Sesamin ameliorated lead-induced neuroinflammation in rats, and decreased accumulation of lead in blood and neuronal tissues of rats [453]. It ameliorated polymorphonuclear neutrophils infiltration and exudate volume [454]. Majdalawieh et al. [455] reported that sesamin can potentially be utilized as an effectual adjuvant therapeutic agent in ameliorating tumor development and progression, and it could be utilized in the prevention and treatment of different types of cancer. It has been reported that sesamin promoted diabetes-induced neuroinflammation in rats, exhibited neurotrophic supportive action in diabetic rats, and prevented neuronal loss in diabetic rats [456]. Sesamin has a chondroprotective effect through inhibition of proteoglycans (PGs) degradation induced by IL-1beta and inhibition of collagen degradation [457].

8. The Health Benefits of Condensed Tannins or Proanthocyanidins (Procyanidin B1)

Proanthocyanidins, also known as condensed tannins [458,459], belong to the oldest of plant secondary metabolites, and these constituents are widespread in woody plants, but are also discovered in certain forages, as well as fruits, seeds, nuts, and bark [460,461]. Yu et al. [462] reported that proanthocyanidins were prevalent in lotus seed coats. They can be categorized into three groups according to their component units and the linkages between them: procyanidins, prodelfinidins, and propelargonidins [463]. The biological activity of plant proanthocyanidins is associated with their chemical concentration and structure [464]. Proanthocyanidins from *Pinus thunbergii* mainly included catechin/epicatechin, and they showed significant antioxidant capacity [465]. Proanthocyanidins in tea, black currant, grapes, bilberry, pine bark, cranberry, and peanut skin may lead to a decrease in the oxidative stress (ROS), induce lower iNOS and COX-2 overexpression, then lower inflammation, and, lastly, show activities against diabetes, asthma, neuropathologies, cardiovascular ailments, obesity, and cancer [466]. The precursors of proanthocyanidins are produced by the phenyl propanoid pathway in the cytosol and are converted to the vacuole, where they polymerize to create proanthocyanidins [467]. They have various bioactivities, such as anticancer, antibacterial, and antioxidant [468]. Proanthocyanidins stimulate antioxidant capacity and increase resistance against oxidative stress-induced senescence in fruits after harvest [469].

Procyanidins are associated with the class of natural products known as proanthocyanidins or condensed polyphenols [470]. They have been reported to reveal broad advantages to human health and are applied in the prevention of cancers, diabetes, cardiovascular diseases, etc. [471]. They are structurally diverse constituents and can be divided into monomeric, oligomeric, or polymeric variants associated with degree of polymerization, which plays a role in manifesting various impacts that are associated with human health [471]. The anti-digestion and antioxidant impacts of grape seed procyanidins have

been proven [472]. Procyanidin B1 is also a promising liver cancer antitumor drug [473] (Na et al., 2020). Procyanidins increase the glycometabolism and decrease the secretion of inflammatory factors of postpartum mice with gestational diabetes mellitus (GDM) [474].

9. The Health Benefits of Curcuminoids (Curcumin, Demethoxycurcumin, Bisdemethoxycurcumin)

9.1. Curcuminoids

Curcuminoids are a group of polyphenol coloring constituents that exist in the plant species *Curcuma*, such as *Curcuma longa*, *C. Wenyujin*, *C. zedoaria*, etc. [475,476]. They are synthesized in turmeric from cinnamic acid precursors obtained via the phenylpropanoid biosynthetic pathway, and there are three different precursors, namely curcuminoids biosynthesis-cinnamic acid, ferulic acid, and coumaric acid [477]. Ramirez-Ahumada et al. [478] reported that curcuminoid synthase activity in turmeric crude protein extracts converts feruloyl-CoA into curcumin. Curcumins are the commercially available component in curcuminoids, as the principle constituents, and the other two, demethoxycurcumin and bisdemethoxycurcumin, as minor components [479,480]. Curcumin and demethoxycurcumin are distinctive because of the phenylmethoxy group [481]. Curcuminoids share important pharmacological characteristics possessed by turmeric, a distinguished curry spice, considered as an important factor in Alzheimer's disease [482]. It has been reported that curcuminoids of turmeric can be considered as a modern medicine for the treatment of knee osteoarthritis [483] as well as a potential anticancer agent [484]. Zhou et al. [485] also reported that turmeric rhizomes exhibit versatile biological activities such as a significant anticancer property. Three curcuminoids, namely curcumin, demethoxycurcumin, and bisdemethoxycurcumin, in turmeric were found and were shown to contain significant synergistic anticancer activities [486]. Curcuminoids rescued neurotoxin-induced inflammatory gene expression and rescued neurotoxin-induced apoptotic gene expression, and individual curcuminoids showed significant function useful for Alzheimer's disease [482].

9.2. Curcumin

Curcumin (bis- α,β -unsaturated β -diketone), also known as diferuloylmethane, is a hydrophobic polyphenol obtained from the rhizome of the perennial herb genus *Curcuma*, which belongs to the ginger family (Zingiberaceae) and consists of species such as *Curcuma longa*, *Curcuma amada*, *Curcuma aromatic*, *Curcuma zedoaria*, and *Curcuma raktakanta* [487,488]. Curcumins contain different medicinal values such as antioxidant, anti-pulmonary fibrosis, anti-inflammation, antiviral, and chronic obstructive pulmonary disease impacts, and attractively docked with multi-target molecular proteins related to diabetes [489–494]. Curcumin is insoluble in water and easily efficient in organic solvents [495]; the active functional groups of curcumin can be oxidized by electron transfer and hydrogen abstraction [496], and curcumin is more durable in acidic to neutral conditions than in alkaline circumstances [495–497]. Curcumin, as an enzyme inhibitor, has proper structural characteristics including a flexible backbone, hydrophobic nature, and different available hydrogen bond (H-bond) donors and acceptors [498]. Curcumin is stable to heat but is light-sensitive and produces singlet oxygen and other reactive oxygen species (ROS) when exposed to the sun, which is also a photodynamic and photobiological property of curcumin [499]. Curcumin decreases inflammation by inhibiting lipopolysaccharide-induced nuclear factor-KB (NF-KB) p65 translocation and mitogen-activated protein kinase activation in dendritic cells [500]. Curcumin decreases morphine dependence in rats through an inhibitory influence on neuroinflammation and a decline in the expression of μ -opioid receptors in the prefrontal cortex [501]. Curcumin influences synaptic plasticity genes (Arc and Fmr1) to decrease amnesia [502]. Xie et al. [503] reported that curcumin together with photodynamic therapy have been confirmed as effective in many kinds of cancer cells in vitro and animal models. It has been extensively applied in cancer treatment because of its ability to trigger cell death and suppress metastasis [504]. Mahjoob and Stochaj [505] reported that curcumin improves aging-related cellular and

organ dysfunctions. Curcumin can be a promising antifatigue substitute for improving exercise performance [506]. Its derivatives have anti-inflammatory actions for drug repurposing in traumatic brain injury (TBI), but their molecular targets are not clear [507].

9.3. Demethoxycurcumin

Demethoxycurcumin is one of the principle active compounds of curcuminoids discovered in turmeric powder, which is used as a spice in Asian cooking and traditional medicine [508]. Recent studies reveal that demethoxycurcumin has various biological activities including antioxidant, anti-inflammation, and anticancer activities [509–511]. Lin et al. [512] reported that demethoxycurcumin is the most active constituent against various kinds of breast cancer cell lines and induces apoptosis and autophagy. Demethoxycurcumin, a natural derivative of curcumin, revealed stronger inhibitory activity on nitric oxide and tumor necrosis factor- α production in comparison with curcumin in lipopolysaccharide-activated rat primary microglia [513]. Demethoxycurcumin remitted the inflammation of nucleus pulposus cells without overt cytotoxic impacts [514].

9.4. Bisdemethoxycurcumin

Bisdemethoxycurcumin is a demethoxy derivative of curcumin and is much more stable than curcumin in physiological media [514–516]. It can scavenge free radicals and control cellular redox balance because of its antioxidant property [517,518], and it has potential anti-allergic effects [519]. Mahattanadul et al. [520] reported that bisdemethoxycurcumin's antiulcer impacts might be because of its characteristics of decreasing gastric acid secretion and increasing the mucosal defensive mechanism via suppression of inducible nitric oxide synthase (iNOS)-mediated inflammation. Bisdemethoxycurcumin inhibits human pancreatic α -amylase (HPA) [521].

10. Conclusions

Phenolic compounds are one of the most important types of compounds with an important role in growth and reproduction, providing protection against pathogens and predators, and they could be the main determinant of antioxidant potential of foods. Phenolics are a heterogeneous collection of compounds generated as secondary metabolites in plants. Phenolic compounds are aromatic or aliphatic compounds with at least one aromatic ring to which one or more OH groups are connected. They are subdivided into different groups depending on the number of phenolic rings that they possess and the structural elements joined to them. They are naturally occurring compounds present in several foods such as cereals, fruits, vegetables, and beverages. Polyphenols can also be found in dried legumes and chocolate. The distribution of phenolic compounds in plant tissues and cells change considerably according to the type of chemical compound. They also contribute towards the color and sensory characteristics of fruits and vegetables. Different classes of phenolic compounds in plants are simple phenolics, benzoquinones, hydroxybenzoic acids, acetophenones, phenylacetic acids, hydroxycinnamic acids, phenylpropanoids, naphthoquinones, xanthenes, stilbenes, anthraquinones, flavonoids, isoflavonoids, lignans, neolignans, biflavonoids, lignins, and condensed tannins. Hydroxybenzoic acids are gallic acid and Protocatechuic acid. Hydroxycinnamic acids are *p*-coumaric acid, caffeic acid, ferulic acid, sinapic acid, and other components such as coumarins (umbelliferone, esculetin, scopoletin, resveratrol, piceatannol, pterostilbene), curcuminoids (curcumin, demethoxycurcumin, bisdemethoxycurcumin), condensed tannins or proanthocyanidins (procyanidin B1), and lignan (sesamin). From a human physiological viewpoint, phenolic compounds are important in defense responses such as antioxidant, anti-aging, antiproliferative, and anti-inflammatory. High phenolic activity in many species could prove to be beneficial towards human health if included as part of food designs for a healthy diet.

Flavonoids are the largest group of natural phenolic compounds, and, based on the differences in the pyran ring, flavonoids can be divided into flavones, isoflavones, flavanols, flavonols, flavanones, flavan-3-ols, and anthocyanidins. They can be subdivided

into different subgroups on the basis of the carbon of the C ring on which the B ring is attached and the degree of unsaturation and oxidation of the C ring. Flavonoids in which the B ring is linked in position 3 of the C ring are called isoflavones. Those in which the B ring is linked in position 4 are called neoflavonoids, while those in which the B ring is linked in position 2 can be further subdivided into several subgroups on the basis of the structural characteristics of the C ring. The most prominent health benefits of phenolic compounds are antioxidant activity, anti-inflammatory properties, antifungal activity, antimicrobial activity, antibacterial properties, anti-coronavirus activities, neuroprotective potential, appropriate for skin health, suitable for wound healing, and anticancer activities. Flavonoids, a group of natural substances with variable phenolic structure, are found in vegetables, fruits, grains, bark, stems, roots, flowers, wine, and tea. Flavonoids are considered as an important constituent in different pharmaceutical, medicinal, nutraceutical, and cosmetic applications. They belong to a class of low-molecular-weight phenolic compounds that are extensively distributed in the plant kingdom. Future research is needed to determine the pharmaceutical benefits of phenolic and flavonoid compounds of medicinal plants, especially traditional Chinese medicinal plants, and to gain a better understanding of these chemical compounds in medicinal plants and herbs. It is also important to increase analytic techniques to allow the collection of more data on excretion and absorption.

Author Contributions: W.S., writing—original draft preparation; M.H.S., writing—original draft preparation and editing. All authors have read and agreed to the published version of the manuscript.

Funding: This research was funded by the Natural Science Foundation of Beijing, China (Grant No.M21026). This research was also supported by the National Key R&D Program of China (Research grant 2019YFA0904700).

Institutional Review Board Statement: Not applicable.

Informed Consent Statement: Not applicable.

Data Availability Statement: Not applicable.

Conflicts of Interest: The authors declare no conflict of interest.

References

- Marmitt, D.; Shahrajabian, M.H. Plant species used in Brazil and Asia regions with toxic properties. *Phytother. Res.* **2021**, *35*, 4703–4726. [[CrossRef](#)] [[PubMed](#)]
- Shahrajabian, M.H.; Sun, W.; Cheng, Q. Clinical aspects and health benefits of ginger (*Zingiber officinale*) in both traditional Chinese medicine and modern industry. *Acta Agric. Scand. B Soil Plant Sci.* **2019**, *69*, 546–556. [[CrossRef](#)]
- Shahrajabian, M.H.; Sun, W.; Shen, H.; Cheng, Q. Chinese herbal medicine for SARS and SARS-CoV-2 treatment and prevention, encouraging using herbal medicine for COVID-19 outbreak. *Acta Agric. Scand. B Soil Plant Sci.* **2020**, *70*, 437–443. [[CrossRef](#)]
- Shahrajabian, M.H.; Sun, W. Using sumac (*Rhus coriaria* L.), as a miraculous spice with outstanding pharmacological activities. *Not. Sci. Biol.* **2022**, *14*, 11118. [[CrossRef](#)]
- Shahrajabian, M.H.; Sun, W. Medicinal plants, economical and natural agents with antioxidant activity. *Curr. Nutr. Food. Sci.* **2022**, *18*, 1. [[CrossRef](#)]
- Shahrajabian, M.H.; Sun, W.; Cheng, Q. Product of natural evolution (SARS, MERS, and SARS-CoV-2); deadly diseases, from SARS to SARS-CoV-2. *Hum. Vaccines Immunother.* **2020**, *17*, 62–83. [[CrossRef](#)] [[PubMed](#)]
- Shahrajabian, M.H.; Sun, W.; Soleymani, A.; Cheng, Q. Traditional herbal medicines to overcome stress, anxiety and improve mental health in outbreaks of human coronaviruses. *Phytother. Res.* **2020**, *35*, 1237–1247. [[CrossRef](#)] [[PubMed](#)]
- Marmitt, D.; Shahrajabian, M.H.; Goettert, M.I.; Rempel, C. Clinical trials with plants in diabetes mellitus therapy: A systematic review. *Expert Rev. Clin. Pharmacol.* **2021**, *14*, 735–747. [[CrossRef](#)]
- Sun, W.; Shahrajabian, M.H.; Cheng, Q. Barberry (*Berberis vulgaris*), a medicinal fruit and food with traditional and modern pharmaceutical uses. *Isr. J. Plant Sci.* **2021**, *68*, 61–71. [[CrossRef](#)]
- Sun, W.; Shahrajabian, M.H.; Cheng, Q. Fenugreek cultivation with emphasis on historical aspects and its uses in traditional medicine and modern pharmaceutical sciences. *Mini Rev. Med. Chem.* **2021**, *21*, 724–730. [[CrossRef](#)] [[PubMed](#)]
- Sun, W.; Shahrajabian, M.H.; Cheng, Q. Anise (*Pimpinella anisum* L.), a dominant spice and traditional medicinal herb for both food and medicinal purposes. *Cogent Biol.* **2019**, *5*, 1673688. [[CrossRef](#)]
- Barragan-Zarate, G.S.; Lagunez-Rivera, L.; Solano, R.; Carranza-Alvarez, C.; Hernandez-Benavides, D.M.; Vilarem, G. Validation of the traditional medicinal use of a Mexican endemic orchid (*Prosthechea karwinskii*) through UPLC-ESI-qTOF-MS/MS characterization of its bioactive compounds. *Heliyon* **2022**, *8*, e09867. [[CrossRef](#)]

13. Shahrajabian, M.H. Medicinal herbs with anti-inflammatory activities for natural and organic healing. *Curr. Org. Chem.* **2021**, *25*, 2885–2901. [[CrossRef](#)]
14. Shahrajabian, M.H.; Sun, W.; Cheng, Q. Exploring *Artemisia annua* L., artemisinin and its derivatives, from traditional Chinese wonder medicinal science. *Not. Bot. Horti Agrobot.* **2020**, *48*, 1719–1741. [[CrossRef](#)]
15. Shahrajabian, M.H.; Sun, W.; Cheng, Q. Chemical components and pharmacological benefits of Basil (*Ocimum basilicum*): A review. *Int. J. Food Prop.* **2020**, *23*, 1961–1970. [[CrossRef](#)]
16. Shahrajabian, M.H.; Sun, W.; Cheng, Q. Traditional herbal medicine for the prevention and treatment of cold and flu in the autumn of 2020, overlapped with COVID-19. *Nat. Prod. Commun.* **2020**, *15*, 1431. [[CrossRef](#)]
17. Shahrajabian, M.H.; Sun, W. Sustainable approaches to boost yield and chemical constituents of aromatic and medicinal plants by application of biostimulants. *Recent Adv. Food Nutr. Agric.* **2022**, *13*, 72–92. [[CrossRef](#)]
18. Shahrajabian, M.H.; Sun, W. Importance of thymoquinone, sulfuraphane, phloretin, and epigallocatechin and their health benefits. *Lett. Drug Des. Discov.* **2022**, *19*, ahead of print. [[CrossRef](#)]
19. Shahrajabian, M.H.; Sun, W. Survey on medicinal plants and herbs in traditional Iranian medicine with antioxidant, antiviral and antimicrobial, and antiinflammation properties. *Lett. Drug Des. Discov.* **2022**, *19*, ahead of print. [[CrossRef](#)]
20. Supriha, P.; Radha, K.V. Estimation of phenolic compounds present in the plant extracts using high pressure liquid chromatography, antioxidant properties, and its antibacterial activity. *Indian J. Pharm. Educ. Res.* **2018**, *52*, 321–326. [[CrossRef](#)]
21. Amessis-Ouchemoukh, N.; Madani, K.; Fale, P.L.V.; Serralheiro, M.L.; Araujo, M.E.M. Antioxidant capacity and phenolic contents of some Mediterranean medicinal plants and their potential role in the inhibition of cyclooxygenase-1 and acetylcholinesterase activities. *Ind. Crop. Prod.* **2014**, *53*, 6–15. [[CrossRef](#)]
22. El-Haci, I.A.; Bekkara, F.A.; Mazari, W.; Gherib, M. Phenolic content and antioxidant activity of some organic extracts of endemic medicinal plant *Anabasis aetioioides* Coss. & Moq. From Algerian Sahara. *Pharmacogn. J.* **2013**, *5*, 108–112. [[CrossRef](#)]
23. Subedi, L.; Timalsena, S.; Duwadi, P.; Thapa, R.; Paudel, A.; Parajuli, K. Antioxidant activity and phenol and flavonoid contents of eight medicinal plants from Western Nepal. *J. Tradit. Chin. Med.* **2014**, *34*, 584–590. [[CrossRef](#)]
24. Skotti, E.; Anastasaki, E.; Kanellou, G.; Polissiou, M.; Tarantilis, P.A. Total phenolic content, antioxidant activity and toxicity of aqueous extracts from selected Greek medicinal and aromatic plants. *Ind. Crop. Prod.* **2014**, *53*, 46–54. [[CrossRef](#)]
25. Jimenez, N.; Carrillo-Hormaza, L.; Pujol, A.; Alzate, F.; Osorio, E.; Lara-Guzman, O. Antioxidant capacity and phenolic content of commonly used anti-inflammatory medicinal plants in Colombia. *Ind. Crop. Prod.* **2015**, *70*, 272–279. [[CrossRef](#)]
26. Cisneros, H.S.; Bertiller, M.B.; Furlong, J.J.P.; Carrera, A.L. Similar structural complexity of phenols in plant morphotypes with contrasting soluble phenol concentration and richness in arid rangelands of Patagonia. *Flora* **2022**, *295*, 152134. [[CrossRef](#)]
27. Tirado-Kulieva, V.A.; Hernandez-Martinez, E.; Choque-Rivera, T.J. Phenolic compounds versus SARS-CoV-2: An update on the main findings against COVID-19. *Heliyon* **2022**, *8*, e10702. [[CrossRef](#)] [[PubMed](#)]
28. Sun, W.; Shahrajabian, M.H.; Cheng, Q. Natural dietary and medicinal plants with anti-obesity therapeutics activities for treatment and prevention of obesity during lock down and in post-COVID-19 era. *Appl. Sci.* **2021**, *11*, 7889. [[CrossRef](#)]
29. Sun, W.; Shahrajabian, M.H.; Lin, M. Research progress of fermented functional foods and protein factory-microbial fermentation technology. *Fermentation* **2022**, *8*, 688. [[CrossRef](#)]
30. Macharia, J.M.; Mwangi, R.W.; Rozmann, N.; Zsolt, K.; Varjas, T.; Uchechukwu, P.O.; Wagara, I.N.; Raposa, B.L. Medicinal plants with anti-colorectal cancer bioactive compounds: Potential game-changers in colorectal cancer management. *Biomed. Pharmacother.* **2022**, *153*, 113383. [[CrossRef](#)]
31. Jaiswal, N.; Kumar, A. HPLC in the discovery of plant phenolics as antifungal molecules against *Candida* infection related biofilms. *Microchem J.* **2022**, *179*, 107572. [[CrossRef](#)]
32. Diaz, P.; Jeong, S.C.; Lee, S.; Khoo, C.; Koyyalamudi, S.R. Antioxidant and anti-inflammatory activities of selected medicinal plants and fungi containing phenolic and flavonoids compounds. *Chin. Med.* **2012**, *7*, 26. [[CrossRef](#)]
33. Tukun, A.B.; Shaheen, N.; Banu, C.P.; Mohiduzzaman, M.D.; Islam, S.; Begum, M. Antioxidant capacity and total phenolic contents in hydrophilic extracts of selected Bangladeshi medicinal plants. *Asian Pac. J. Trop. Med.* **2014**, *7* (Suppl. 1), S568–S573. [[CrossRef](#)] [[PubMed](#)]
34. Manguro, L.O.A.; Lemmen, P. Phenolics of *Moringa oleifera* leaves. *Nat. Prod. Res.* **2007**, *21*, 56–68. [[CrossRef](#)]
35. Sodaiezadeh, H.; Rafieihoossaini, M.; Havlik, J.; van Damme, P. Allelopathic activity of different plant parts of *Peganum harmala* L. and identification of their growth inhibitors substances. *Plant Growth Regul.* **2009**, *59*, 227–236. [[CrossRef](#)]
36. Shah, B.; Cai, Y.Z.; Sun, M.; Corke, H. Antioxidant capacity of 26 spice extracts and characterization of their phenolic constituents. *J. Agric. Food Chem.* **2005**, *53*, 7749–7759. [[CrossRef](#)]
37. Koksall, E.; Bursal, E.; Gulcin, I.; Korkmaz, M.; Caglayan, C.; Goren, A.C.; Alwasel, S.H. Antioxidant activity and polyphenol content of Turkish thyme (*Thymus vulgaris*) monitored by liquid chromatography and tandem mass spectrometry. *Int. J. Food Prop.* **2017**, *20*, 514–525. [[CrossRef](#)]
38. Vastano, B.C.; Chen, Y.; Zhu, N.Q.; Ho, C.T.; Zhou, Z.Y.; Rosen, R.T. Isolation and identification of stilbenes in two varieties of *Polygonum cuspidatum*. *J. Agric. Food* **2000**, *48*, 253–256. [[CrossRef](#)]
39. Zhao, X.H.; Han, F.; Li, Y.L.; Yue, H.L. Preparative isolation and purification of three stilbene glycosides from the Tibetan medicinal plant *Rheum tanguticum* Maxim. Ex Balf. by high-speed counter-current chromatography. *Phytochem. Anal.* **2013**, *24*, 171–175. [[CrossRef](#)]

40. Ahmad, A.; Misra, L.N. Isolation of herniarin and other constituents from *Matricaria chamomilla* flowers. *Int. J. Pharmacogn.* **1997**, *35*, 121–125. [[CrossRef](#)]
41. Morikawa, T.; Luo, F.L.; Manse, Y.; Sugita, H.; Saeki, S.; Chaipech, S.; Pongiriyadacha, Y.; Muraoka, O.; Ninomiya, K. Geranylated coumarins from Thai medicinal plant *Mammea siamensis* with testosterone 5 alpha-reductase inhibitory activity. *Front. Chem.* **2020**, *8*, 199. [[CrossRef](#)]
42. Thuong, P.T.; Hung, T.M.; Ngoc, T.M.; Ha, D.T.; Min, B.S.; Kwak, S.J.; Kang, T.S.; Choi, J.S.; Bae, K. Antioxidant activities of coumarins from Korean medicinal plants and their structure-activity relationships. *Phytother. Res.* **2010**, *24*, 101–106. [[CrossRef](#)] [[PubMed](#)]
43. Singh, M.; Tiwari, N.; Shanker, K.L.; Verma, R.K.; Gupta, A.K.; Gupta, M.M. Two new lignans from *Phyllanthus amarus*. *J. Asian Nat. Prod. Res.* **2009**, *11*, 562–568. [[CrossRef](#)] [[PubMed](#)]
44. Hu, D.; Yang, Z.Y.; Yao, X.C.; Wang, H.; Han, N.; Liu, Z.H.; Wang, Y.; Yang, J.Y.; Yin, J. Dibenzocyclooctadiene lignans from *Schisanra chinensis* and their inhibitory activity on No production in lipopolysaccharide-activated microglia cells. *Phytochemistry* **2014**, *104*, 72–78. [[CrossRef](#)] [[PubMed](#)]
45. Baranyai, B.; Backer, C.; Reich, C.; Lindequist, U. The production of 7-methyljuglone, plumbagin, and quercetin in wild and cultivated *Drosera rotundifolia* and *Drosera intermedia*. *Mires Peat* **2016**, *18*, 1–8. [[CrossRef](#)]
46. Tian, K.; Zhang, H.G.; Chen, X.G.; Hu, Z.D. Determination of five anthraquinones in medicinal plants by capillary zone electrophoresis with beta-cyclodextrin addition. *J. Chromatogr. A* **2006**, *1123*, 134–137. [[CrossRef](#)]
47. Ali, I.; Haque, A.; Saleem, K. Separation and identification of curcuminoids in turmeric powder by HPLC using phenyl column. *Anal. Methods* **2014**, *6*, 2526–2536. [[CrossRef](#)]
48. Taamalli, A.; Arraez-Roman, D.; Abaza, L.; Iswaldi, I.; Fernandez-Gutierrez, A.; Zarrouk, M.; Segura-Carretero, A. LC-MS-based metabolite profiling of methanolic extracts from the medicinal and aromatic species *Mentha pulegium* and *Origanum majorana*. *Phytochem Anal.* **2015**, *26*, 320–330. [[CrossRef](#)]
49. Rodrigues, F.; Almeida, I.; Sarmiento, B.; Amaral, M.H.; Oliveira, M. Study of the isoflavone content of different extracts of *Medicago* spp. as potential active ingredient. *Ind. Crop. Prod.* **2014**, *57*, 110–115. [[CrossRef](#)]
50. Stevenson, P.C.; Kite, G.C.; Lewis, G.P.; Forest, F.; Nyirenda, S.P.; Belmain, S.R.; Sileshi, G.W.; Veitch, N.C. Distinct chemotypes of *Tephrosia vogelii* and implications for their use in pest control and soil enrichment. *Phytochemistry* **2012**, *78*, 135–146. [[CrossRef](#)]
51. Russo, M.; Fanali, C.; Tripodo, G.; Dugo, P.; Muleo, R.; Dugo, L.; de Gara, L.; Mondello, L. Analysis of phenolic compounds in different parts of pomegranate (*Punica granatum*) fruit by HPLC-PDA-ESI/MS and evaluation of their antioxidant activity: Application to different Italian varieties. *Anal. Bioanal. Chem.* **2018**, *410*, 3507–3520. [[CrossRef](#)] [[PubMed](#)]
52. Bravo, L. Polyphenols: Chemistry, dietary sources, metabolism, and nutritional significance. *Nutr. Rev.* **1998**, *56*, 317–333. [[CrossRef](#)] [[PubMed](#)]
53. Balasundram, N.; Sundram, K.; Samman, S. Phenolic compounds in plants and agri-industrial by-products: Antioxidant activity, occurrence, and potential uses. *Food Chem.* **2006**, *99*, 191–203. [[CrossRef](#)]
54. De la Rosa, L.A.; Moreno-Escamilla, J.O.; Rodrigo-Garcia, J.; Alvarez-Parrilla, E. Chapter 12—Phenolic Compounds. In *Postharvest Physiology and Biochemistry of Fruits and Vegetables*; Yahia, E.M., Ed.; Woodhead Publishing: Sawston, UK, 2019; pp. 253–271. [[CrossRef](#)]
55. Soleymani, A.; Shahrajabian, M.H.; Naranjani, L. Yield and yield components of berseem clover cultivars in low nitrogen fertilizer input farming. *J. Food Agric. Environ.* **2011**, *9*, 281–283.
56. Soleymani, A.; Shahrajabian, M.H.; Naranjani, L. Effect of planting dates and different levels of nitrogen on seed yield and yield components of nuts sunflower (*Helianthus annuus* L.). *Afr. J. Agric. Res.* **2013**, *8*, 5802–5805. [[CrossRef](#)]
57. Paine, C.S.; van Staden, J.; Finnie, J.F. Elicitation of phenolic compounds of medicinal value in plants. *S. Afr. J. Bot.* **2017**, *109*, 362. [[CrossRef](#)]
58. Salem, M.M.; Davidorf, F.H.; Abdel-Rahman, M.H. In vitro anti-uvéal melanoma activity of phenolic compounds from the Egyptian medicinal plant *Acacia nilotica*. *Fitoterapia* **2011**, *82*, 1279–1284. [[CrossRef](#)]
59. Carbonell-Capella, J.M.; Buniowska, M.; Barba, F.J.; Esteve, M.J.; Frigola, A. Analytical methods for determining bioavailability and bioaccessibility of bioactive compounds from fruits and vegetables: A review. *Compr. Rev. Food Sci. Food Saf.* **2014**, *13*, 155–171. [[CrossRef](#)]
60. Rein, M.J.; Renouf, M.; Cruz-Hernandez, C.; Actis-Goretta, L.; Thakkar, S.K.; da Silva Pinto, M. Bioavailability of bioactive food compounds: A challenging journey of bioefficacy. *Br. J. Clin. Pharmacol.* **2013**, *75*, 588–602. [[CrossRef](#)]
61. Albergaria, E.T.; Oliveira, A.F.M.; Albuquerque, U.P. The effect of water deficit stress on the composition of phenolic compounds in medicinal plants. *S. Afr. J. Bot.* **2020**, *131*, 12–17. [[CrossRef](#)]
62. Djeridane, A.; Yousfi, M.; Nadjemi, B.; Boutassouna, D.; Stocker, P.; Vidal, N. Antioxidant activity of some algerian medicinal plants extracts containing phenolic compounds. *Food Chem.* **2006**, *97*, 654–660. [[CrossRef](#)]
63. Cai, Y.; Luo, Q.; Sun, M.; Corke, H. Antioxidant activity and phenolic compounds of 112 traditional Chinese medicinal plants associated with anticancer. *Life Sci.* **2004**, *74*, 2157–2184. [[CrossRef](#)] [[PubMed](#)]
64. Chirinos, R.; Pedreschi, R.; Rogez, H.; Larondelle, Y.; Campos, D. Phenolic compounds contents and antioxidant activity in plants with nutritional and/or medicinal properties from the Peruvian Andean region. *Ind. Crop. Prod.* **2013**, *47*, 145–152. [[CrossRef](#)]
65. Cai, Y.-Z.; Sun, M.; Xing, J.; Luo, Q.; Corke, H. Structure—Radical scavenging activity relationships of phenolic compounds from traditional Chinese medicinal plants. *Life Sci.* **2006**, *78*, 2872–2888. [[CrossRef](#)] [[PubMed](#)]

66. Barros, L.; Duenas, M.; Carvalho, A.M.; Ferreira, I.C.F.R.; Santos-Buelga, C. Characterization of phenolic compounds in flowers of wild medicinal plants from Northeastern Portugal. *Food Chem. Toxicol.* **2012**, *50*, 1576–1582. [[CrossRef](#)] [[PubMed](#)]
67. Kaska, A.; Cicek, M.; Mammadov, R. Biological activities, phenolic constituents and mineral element analysis of two endemic medicinal plants from Turkey: *Nepeta italica* subsp. *cadmea* and *Teucrium sandracicum*. *S. Afr. J. Bot.* **2019**, *124*, 63–70. [[CrossRef](#)]
68. Benabderrahim, M.A.; Yahia, Y.; Bettaieb, I.; Elfalleh, W.; Nagaz, K. Antioxidant activity and phenolic profile of a collection of medicinal plants from Tunisian arid and Saharan regions. *Ind. Crop. Prod.* **2019**, *138*, 111427. [[CrossRef](#)]
69. Ranilla, L.G.; Kwon, Y.-I.; Apostolidis, E.; Shetty, K. Phenolic compounds, antioxidant activity and in vitro inhibitory potential against key enzymes relevant for hyperglycemia and hypertension of commonly used medicinal plants, herbs, and species in Latin America. *Bioresour. Technol.* **2010**, *101*, 4676–4689. [[CrossRef](#)]
70. Ng, M.H.; Nu/man, A.H. Investigation on the use of deep eutectic solvent with microwave assistance for the extraction of ferulic acid from palm pressed fibre. *Curr. Res. Green Sustain. Chem.* **2021**, *4*, 100155. [[CrossRef](#)]
71. Chahal, S.; Kaur, H.; Lekhak, M.M.; Shekhawat, M.S.; Goutam, U.; Singh, S.K.; Ochatt, S.J.; Kumar, V. Meta-topolin-mediated regeneration and accumulation of phenolic acids in the critically endangered medicinal plant *Crinum malabaricum* (Amaryllidaceae): A potent source of galanthamine. *S. Afr. J. Bot.* **2022**, *149*, 853–859. [[CrossRef](#)]
72. Mssillou, I.; Bakour, M.; Slighoua, M.; Laaroussi, H.; Saghrouchni, H.; Amrati, F.E.-Z.; Lyoussi, B.; Derwich, E. Investigation on wound healing effect of Mediterranean medicinal plants and some related phenolic compounds: A review. *J. Ethnopharmacol.* **2022**, *298*, 115663. [[CrossRef](#)]
73. Silva, R.F.D.; Carneiro, C.N.; Sousa, C.B.D.C.; Gomez, F.J.V.; Espino, M.; Boiteux, J.; Fernandez, M.D.I.A.; Silva, M.F.; Dias, F.D.S. Sustainable extraction bioactive compounds procedures in medicinal plants based on the principles of green analytical chemistry: A review. *Microchem. J.* **2022**, *175*, 107184. [[CrossRef](#)]
74. Tarhan, L.; Urek, R.O.; Oner, A.; Nakiboglu, M. Evaluation of phenolic profiles, antioxidant activities, and cytotoxic and apoptotic potentials of *Phlomis angustissima* and *Phlomis fruticosa*, medicinal plants from Turkey. *Eur. J. Integr. Med.* **2022**, *55*, 102188. [[CrossRef](#)]
75. Raghuvanshi, D.; Sharma, K.; Verma, R.; Kumar, D.; Kumar, H.; Khan, A.; Valko, M.; Almoar, S.Y.; Alwasel, S.H.; Nepovimova, E.; et al. Phytochemistry, and pharmacological efficacy of *Cordia dichotoma* G. Forst. (Lashuda): A therapeutic medicinal plant of Himachal Pradesh. *Biomed. Pharmacother.* **2022**, *153*, 113400. [[CrossRef](#)] [[PubMed](#)]
76. Thitilertdecha, P.; Rowan, M.G.; Guy, R.H. Topical formulation and dermal delivery of active phenolic compounds in the Thai medicinal plant-*Clerodendrum petasites* S. Moore. *Int. J. Pharm.* **2015**, *478*, 39–45. [[CrossRef](#)] [[PubMed](#)]
77. Sprea, R.M.; Caleja, C.; Pinela, J.; Finimundy, T.C.; Calhelha, R.C.; Kostic, M.; Sokovic, M.; Prieto, M.A.; Pereira, E.; Amaral, J.S.; et al. Comparative study on the phenolic composition and in vitro bioactivity of medicinal and aromatic plants from the Lamiaceae family. *Food Res. Int.* **2022**, *161*, 111875. [[CrossRef](#)] [[PubMed](#)]
78. Garcia-Perez, P.; Ayuso, M.; Lozano-Milo, E.; Pereira, C.; Dias, M.I.; Ivanov, M.; Calhelha, R.C.; Sokovic, M.; Ferreira, I.C.F.R.; Barros, L.; et al. Phenolic profiling and in vitro bioactivities of three medicinal *Bryophyllum* plants. *Ind. Crop. Prod.* **2021**, *162*, 113241. [[CrossRef](#)]
79. Bouyahya, A.; El Omari, N.; Elmenyiy, N.; Guaougaou, F.-E.; Balahbib, A.; Belmehdi, O.; Salhi, N.; Imtara, H.; Mrabti, H.N.; El-Shazly, M.; et al. Moroccan antidiabetic medicinal plants: Ethnobotanical studies, phytochemical bioactive compounds, preclinical investigations, toxicological validations and clinical evidences; challenges, guidance, and perspectives for future management of diabetes worldwide. *Trends Food Sci. Technol.* **2021**, *115*, 147–254. [[CrossRef](#)]
80. Shatri, A.M.N.; Mumbengegwi, D.R. Ethnomedicinal use and phytochemical analysis of medicinal plants used to treat gastrointestinal conditions by Awambo people in Iikokola village, Namibia. *Sci. Afr.* **2022**, *18*, e01428. [[CrossRef](#)]
81. Pesaraklu, A.; Radjabian, T.; Salami, S.A. Methyl jasmonate and Ag⁺ effective elicitors for enhancement of phenolic acids contents in *Salvia officinalis* and *Salvia verticillata*, as two traditional medicinal plants. *S. Afr. J. Bot.* **2021**, *141*, 105–115. [[CrossRef](#)]
82. Tavakoli, M.; Esfahani, M.T.; Soltani, S.; Karamian, R.; Aliarabi, H. Effects of ecological factors on phenolic compounds in *Salvia multicaulis* Vahl (Lamiaceae). *Biochem. Syst. Ecol.* **2022**, *104*, 104484. [[CrossRef](#)]
83. Milevskaya, V.V.; Prasad, S.; Temerdashev, Z.A. Extraction and chromatographic determination of phenolic compounds from medicinal herbs in the Lamiaceae and Hypericaceae families: A review. *Microchem. J.* **2019**, *145*, 1036–1049. [[CrossRef](#)]
84. Fawole, O.A.; Opara, U.L. Stability of total phenolic concentration and antioxidant capacity of extracts from pomegranate co-products subjected to in vitro digestion. *BMC Complement. Altern. Med.* **2016**, *16*, 358. [[CrossRef](#)]
85. Guerrero, R.F.; Aliano-Gonzalez, M.J.; Puertas, B.; Richard, T.; Cantos-Villar, E. Comparative analysis of stilbene concentration in grapevine shoots of thirteen *Vitis* during a three-year study. *Ind. Crop. Prod.* **2020**, *156*, 112852. [[CrossRef](#)]
86. Maphet, N.; Unuofin, J.O.; Masuku, N.P.; Olisah, C.; Lebelo, S.L. Medicinal uses, pharmacological activities, phytochemistry, and the molecular mechanisms of *Punica granatum* L. (pomegranate) plant extracts: A review. *Biomed. Pharmacother.* **2022**, *153*, 113256. [[CrossRef](#)]
87. Topalovic, A.; Knezevic, M.; Ivanovic, L.; Gachnik, S.; Mikulic-Petkovsek, M. Phytochemical screening of wild pomegranate (*Punica granatum* L.) juices from the market. *J. Food Compos. Anal.* **2021**, *100*, 103933. [[CrossRef](#)]
88. Shamsudin, K.J.; Phan, C.-S.; Kulip, J.; Hatai, K.; Vairappan, C.S.; Kamada, T. Leucoxenols A and B, two new phenolics from Bornean medicinal plant *Syzygium leucocylon*. *J. Asian Nat. Prod. Res.* **2019**, *21*, 435–441. [[CrossRef](#)]
89. Chaparro-Hernandez, I.; Rodriguez-Ramirez, J.; Barriada-Bernal, L.G.; Mendez-Lagunas, L. Tree ferns (Cyatheaceae) as a source of phenolic compounds—A review. *J. Herb. Med.* **2022**, *35*, 100587. [[CrossRef](#)]

90. Gautam, S.; Chimni, S.S.; Arora, S.; Sohal, S.K. Toxic effects of purified phenolic compounds from *Acacia nilotica* against common cutworm. *Toxicon* **2021**, *203*, 22–29. [[CrossRef](#)] [[PubMed](#)]
91. Bellumori, M.; Zonfrillo, B.; Maggini, V.; Bogani, P.; Gallo, E.; Firenzuoli, F.; Mulinacci, N.; Innocenti, M. *Acmella oleracea* (L.) R.K. Jansen: Alkylamides and phenolic compounds in aerial parts and roots of in vitro seedlings. *J. Pharm. Biomed. Anal.* **2022**, *220*, 114991. [[CrossRef](#)] [[PubMed](#)]
92. Parkes, R.; McGee, D.; McDonnell, A.; Gillespie, E.; Touzet, N. Rapid screening of phenolic compounds in extracts of photo-synthetic organisms separated using C18 monolithic column based HPLC-UV method. *J. Chromatogr. B* **2022**, *1213*, 123521. [[CrossRef](#)]
93. Thais, A.Z.A.; Rantsiou, K.; Filannino, P.; Cocolin, L.S.; Cavoski, I.; Gobetti, M.; Cagno, R.D. Ecological linkages between biotechnologically relevant autochthonous microorganisms and phenolic compounds in sugar apple fruit (*Annona squamosa* L.). *Int. J. Food Microbiol.* **2022**, *387*, 110057. [[CrossRef](#)]
94. Sytar, O.; Hemmerich, I.; Zivcak, M.; Rauh, C.; Brestic, M. Comparative analysis of bioactive phenolic compounds composition from 26 medicinal plants. *Saudi J. Biol. Sci.* **2018**, *25*, 631–641. [[CrossRef](#)]
95. Kasmi, S.; Hamdi, A.; Atmani-Kilani, D.; Debbache-Benaida, N.; Jaramillo-Carmona, S.; Rodriguez-Arcos, R.; Jimenez-Araujo, A.; Ayouni, K.; Atmani, D.; Guillen-Bejarano, R. Characterization of phenolic compounds isolated from the *Fraxinus angustifolia* plant and several associated bioactivities. *J. Herb. Med.* **2021**, *29*, 100485. [[CrossRef](#)]
96. Hossain, M.A.; Shah, M.D.; Gnanaraj, C.; Iqbal, M. In vitro total phenolics, flavonoids contents and antioxidant activity of essential oil, various organic extracts from the leaves of tropical medicinal plant *Tetrastigma* from Sabah. *Asian Pac. J. Trop. Med.* **2011**, *4*, 717–721. [[CrossRef](#)]
97. Aremu, A.O.; Ndhkala, A.R.; Fawole, O.A.; Light, M.E.; Finnie, J.F.; van Staden, J. In vitro pharmacological evaluation and phenolic content of ten South African medicinal plants used as anthelmintics. *S. Afr. J. Bot.* **2010**, *76*, 558–566. [[CrossRef](#)]
98. Golkar, P.; Fotoohi, A. Preliminary phytochemical screening of the phenolic compounds and antioxidant activity of six *Plantago* species from Iran. *J. Plant Process Funct.* **2021**, *10*, 1–10. [[CrossRef](#)]
99. Tauchen, J.; Bortil, L.; Huml, L.; Miksatkova, P.; Doskocil, I.; Marsik, P.; Villegas, P.P.P.; Flores, Y.B.; van Damme, P.V.; Lojka, B.; et al. Phenolic composition, antioxidant and anti-proliferative activities of edible and medicinal plants from the Peruvian Amazon. *Rev. Bras. Farmacogn.* **2016**, *26*, 728–737. [[CrossRef](#)]
100. Stalikas, C.D. Extraction, separation, and detection methods for phenolic acids and flavonoids. *J. Sep. Sci.* **2007**, *30*, 3268–3295. [[CrossRef](#)] [[PubMed](#)]
101. Khalafallah, A.K.; Suleiman, S.A.; Yousef, A.H.; El-Kaniz, N.A.A.; Mohamed, A. Prenylated flavonoids from *Tephrosia apollinea*. *Chin. Chem. Lett.* **2009**, *20*, 1465–1468. [[CrossRef](#)]
102. Rebey, I.B.; Bourgou, S.; Debez, I.B.; Karoui, I.J.; Sellami, I.H.; Msaada, K.; Limam, F.; Marzouk, B. Effects of extraction solvents and provenances on phenolic contents and antioxidant activities of cumin (*Cuminum cyminum* L.) seeds. *Food Bioprocess Technol.* **2012**, *5*, 2827–2836. [[CrossRef](#)]
103. Rayyan, S.; Fossen, T.; Andersen, Q.M. Flavone C-Glycosides from seeds of fenugreek, *Trigonella foenum-graecum* L. *J. Agric. Food Chem.* **2010**, *58*, 7211–7217. [[CrossRef](#)]
104. Dona, A.C.; Kyriakides, M.; Scott, F.; Shephard, E.A.; Varshavi, D.; Veselkov, K.; Everett, J.R. A guide to the identification of metabolites in NMR-based metabolomics/metabolomics experiments. *Comput. Struct. Biotechnol. J.* **2016**, *14*, 135–153. [[CrossRef](#)]
105. Arceusz, A.; Wesolowski, M.; Konieczynski, P. Methods for extraction and determination of phenolic acids in medicinal plants: A review. *Nat. Prod. Commun.* **2013**, *8*, 1821–1829. [[CrossRef](#)] [[PubMed](#)]
106. Castillo-Lopez, R.I.; Leon-Felix, J.; Angulo-Escalante, M.A.; Gutierrez-Dorado, R.; Muy-Rangel, M.D.; Heredia, J.B. Nutritional and phenolic characterization of *Moringa oleifera* leaves grown in Sinaloa, Mexico. *Pak. J. Bot.* **2017**, *49*, 161–168. [[CrossRef](#)]
107. Xu, C.-C.; Wang, B.; Pu, Y.-Q.; Tao, J.-S.; Zhang, T. Advances in extraction and analysis of phenolic compounds from plant materials. *Chin. J. Nat. Med.* **2017**, *15*, 721–731. [[CrossRef](#)]
108. Koleva, V.; Simeonov, E. Solid liquid extraction of phenolic and flavonoid compounds from *Cotinus coggygria* and concentration by nanofiltration. *Chem. Biochem. Eng. Q.* **2014**, *28*, 545–551. [[CrossRef](#)]
109. Ameer, K.; Shahbaz, H.M.; Kwon, J.H. Green extraction methods for polyphenols from plant matrices and their byproducts: A review. *Compr. Rev. Food Sci. Food Saf.* **2017**, *16*, 295–315. [[CrossRef](#)]
110. Pimentel-Moral, S.; Borrás-Linares, I.; Lozano-Sanchez, J.; Arraez-Roman, D.; Martinez-Ferez, A.; Segura-Carretero, A. Supercritical CO₂ extraction of bioactive compounds from *Hibiscus sabdariffa*. *J. Supercrit. Fluids* **2019**, *147*, 213–221. [[CrossRef](#)]
111. Dahmoune, F.; Nayak, B.; Moussi, K.; Remini, H.; Madani, K. Optimization of microwave-assisted extraction of polyphenols from *Myrtus communis* L. leaves. *Food Chem.* **2015**, *166*, 585–595. [[CrossRef](#)] [[PubMed](#)]
112. Fernandez-Ponce, M.T.; Parjikolaie, B.R.; Lari, H.N.; Casas, L.; Mantell, C.; de la Ossa, E.J.M. Pilot-plant scale extraction of phenolic compounds from mango leaves using different green techniques: Kinetic and scale up study. *Chem. Eng. J.* **2016**, *299*, 420–430. [[CrossRef](#)]
113. Kitryte, V.; Povilaitis, D.; Kraujaliene, V.; Sulniute, V.; Pukalskas, A.; Venskutonis, P.R. Fractionation of sea buckthorn pomace and seeds into valuable components by using high pressure and enzyme-assisted extraction methods. *LWT Food Sci. Technol.* **2017**, *85*, 534–538. [[CrossRef](#)]
114. Santos, E.L.; Maia, B.H.L.N.S.; Ferriani, A.P.; Teixeira, S.D. Flavonoids: Classification, Biosynthesis and Chemical Ecology. In *Flavonoids-From Biosynthesis to Human Health*; Justino, G., Ed.; IntechOpen: London, UK, 2017; pp. 3–16.

115. Niesen, D.B.; Hessler, C.; Seeram, N.P. Beyond resveratrol: A review of natural stilbenoids identified from 2009–2013. *J. Berry Res.* **2013**, *3*, 181–196. [[CrossRef](#)]
116. Chong, J.; Poutaraud, A.; Huguency, P. Metabolism and roles of stilbenes in plants. *Plant Sci.* **2009**, *177*, 143–155. [[CrossRef](#)]
117. Chang, Z.; Zhang, Q.; Liang, W.; Zhou, K.; Jian, P.; She, G.; Zhang, L. A Comprehensive Review of the Structure Elucidation of Tannins from *Terminalia* Linn. Evidence-Based Complement. *Altern. Med.* **2019**, *2019*, 8623909. [[CrossRef](#)]
118. Fraga-Corral, M.; Garcia-Oliveira, P.; Pereira, A.G.; Lourenco-Lopes, C.; Jimenez-Lopez, C.; Prieto, M.A.; Simal-Gandara, J. Technological application of tannin-based extracts. *Molecules* **2020**, *25*, 614. [[CrossRef](#)] [[PubMed](#)]
119. Babula, P.; Adam, V.; Havel, L.; Kizek, R. Noteworthy secondary metabolites naphthoquinones—Their occurrence, pharmacological properties and analysis. *Curr. Pharm. Anal.* **2009**, *5*, 47–68. [[CrossRef](#)]
120. Venugopala, K.N.; Rashmi, V.; Odhav, B. Review on natural coumarin lead compounds for their pharmacological activity. *BioMed Res. Int.* **2013**, *2013*, 963248. [[CrossRef](#)]
121. Itokawa, H.; Shi, Q.; Akiyama, T.; Morris-Natschke, S.L.; Lee, K.H. Recent advances in the investigation of curcuminoids. *Chin. Med.* **2008**, *3*, 11. [[CrossRef](#)]
122. Amalraj, A.; Pius, A.; Gopi, S. Biological activities of curcuminoids, other biomolecules from turmeric and their derivatives—A review. *J. Tradit. Complement. Med.* **2017**, *7*, 205–233. [[CrossRef](#)] [[PubMed](#)]
123. Rodriguez-Garcia, C.; Sanchez-Quesada, C.; Toledo, E.; Delgado-Rodriguez, M.; Gaforio, J.J. Naturally lignan-rich foods: A dietary tool for health promotion? *Molecules* **2019**, *24*, 917. [[CrossRef](#)] [[PubMed](#)]
124. Choudhary, P.; Guleria, S.; Sharma, N.; Salaria, K.H.; Chalotra, R.; Ali, V.; Vyas, D. Comparative phenolic content and antioxidant activity of some medicinal plant extracts prepared by choline chloride based green solvents and methanol. *Curr. Res. Green Sustain. Chem.* **2021**, *4*, 100224. [[CrossRef](#)]
125. Mishra, A.; Sharma, A.K.; Kumar, S.; Saxena, A.K.; Pandey, A.K. *Bauhinia variegata* leaf extracts exhibit considerable antibacterial, antioxidant, and anticancer activities. *BioMed Res. Int.* **2013**, *2013*, 915436. [[CrossRef](#)]
126. Kumar Singh, S.; Patra, A. Evaluation of phenolic composition, antioxidant, anti-inflammatory and anticancer activities of *Polygonatum verticillatum* (L.). *J. Integr. Med.* **2018**, *16*, 273–282. [[CrossRef](#)] [[PubMed](#)]
127. Singh, N.; Yadav, S.S. A review on health benefits of phenolics derived from dietary spices. *Curr. Res. Food Sci.* **2022**, *5*, 1508–1523. [[CrossRef](#)] [[PubMed](#)]
128. Meng, X.-H.; Liu, C.; Zhug, L.Z.; Zhu, L.-F.; Yang, S.-X.; Zhu, H.-T.; Wang, D.; Yang, C.-R.; Zhang, Y.-J. Antioxidative Flavan-3-ol Dimers from the Leaves of *Camellia fangchengensis*. *J. Agric. Food Chem.* **2018**, *66*, 247–254. [[CrossRef](#)] [[PubMed](#)]
129. Karakas, F.P.; Turker, A.U.; Karakas, A.; Mshvildadze, V.; Pichette, A.; Legault, J. *In vitro* cytotoxic, antibacterial, anti-inflammatory and antioxidant activities and phenolic content in wild-grown flowers of common daisy—A medicinal plant. *J. Herb. Med.* **2017**, *8*, 31–39. [[CrossRef](#)]
130. Wang, L.; Li, N.; Yu, S.; Zhou, J. Enhancing caffeic acid production in *Escherichia coli* by engineering the biosynthesis pathway and transporter. *Bioresour. Technol.* **2023**, *368*, 128320. [[CrossRef](#)] [[PubMed](#)]
131. Xue, T.-T.; Yang, Y.-G.; Tang, Z.-S.; Duan, J.-A.; Song, Z.-X.; Hu, X.-H.; Yang, H.-D.; Xu, H.-B. Evaluation of antioxidant, enzyme inhibition, nitric oxide production inhibitory activities and chemical profiles of the active extracts from the medicinal and edible plant: *Althaea officinalis*. *Food Res. Int.* **2022**, *156*, 111166. [[CrossRef](#)]
132. Natta, S.; Mondol, S.A.; Pal, K.; Mandal, S.; Sahana, N.; Pal, R.; Pandit, G.K.; Alam, B.K.; Das, S.S.; Biswas, S.S.; et al. Chemical composition, antioxidant activity and bioactive constituents of six native endangered medicinal orchid species from north-eastern Himalayan region of India. *S. Afr. J. Bot.* **2022**, *150*, 248–259. [[CrossRef](#)]
133. Cirak, C.; Radusiene, J.; Raudone, L.; Vilkickyte, G.; Seyis, F.; Marksa, M.; Ivanauskas, L.; Yayla, F. Phenolic compounds and antioxidant activity of *Achillea arabica* populations. *S. Afr. J. Bot.* **2022**, *147*, 425–433. [[CrossRef](#)]
134. Zahoor, M.; Shafiq, S.; Ullah, H.; Sadiq, A.; Ullah, F. Isolation of quercetin and mandelic acid from *Aesculus indica* fruit and their biological activities. *BMC Biochem.* **2018**, *19*, 5. [[CrossRef](#)]
135. Lungu, C.; Tuchilus, C.; Aprotosoae, A.C.; Oprea, A.; Malterud, K.E.; Miron, A. Chemical, antioxidant and antimicrobial investigations of *Pinus cembra* L. bark and needles. *Molecules* **2011**, *16*, 7773–7788. [[CrossRef](#)]
136. Pathiraja, D.; Wanasundara, J.P.D.; Elessawy, F.M.; Purves, R.W.; Vandenberg, A.; Shand, P.J. Water-soluble phenolic compounds and their putative antioxidant activities in the seed coats from different lentin (*Lens culinaris*) genotypes. *Food Chem.* **2023**, *407*, 135145. [[CrossRef](#)] [[PubMed](#)]
137. Zhang, Y.; Li, Y.; Ren, X.; Zhang, X.; Wu, Z.; Liu, L. The positive correlation of antioxidant activity and prebiotic effect about oat phenolic compounds. *Food Chem.* **2023**, *402*, 134231. [[CrossRef](#)]
138. Kebal, L.; Pokajewicz, K.; Djebli, N.; Mostefa, N.; Poliwoda, A.; Wieczorek, P.P. HPLC-DAD profile of phenolic compounds and *in vitro* antioxidant activity of *Ficus carica* L. fruits from two Algerian varieties. *Biomed. Pharmacother.* **2022**, *155*, 113738. [[CrossRef](#)] [[PubMed](#)]
139. Richane, A.; Rim, B.M.; Wided, M.; Riadh, K.; Khaoula, A.; Nizar, M.; Hanen, B.I. Variability of phenolic compounds and antioxidant activities of ten *Ceratonia siliqua* L. provenances. *Biochem. Syst. Ecol.* **2022**, *104*, 104486. [[CrossRef](#)]
140. Jarial, R.; Thakur, S.; Sakinah, M.; Zularisam, A.W.; Sharad, A.; Kanwar, S.S.; Singh, L. Potent anticancer, antioxidant and antibacterial activities of isolated flavonoids from *Asplenium nidus*. *J. King Saud. Univ. Sci.* **2018**, *30*, 185–192. [[CrossRef](#)]
141. Tsai, P.J.; Huang, W.C.; Hsieh, M.C.; Sung, P.J.; Kuo, Y.H.; Wu, W.H. Flavones isolated from *Scutellariae radix* suppress *Propionibacterium acnes*-induced cytokine production *in vitro* and *in vivo*. *Molecules* **2016**, *21*, 15. [[CrossRef](#)]

142. Lim, Y.-H.; Kim, I.-H.; Seo, J.-J. In vitro activity of kaempferol isolated from the *Impatiens balsamina* alone and in combination with erythromycin or clindamycin against *Propionibacterium acnes*. *J. Microbiol.* **2007**, *45*, 473–477.
143. Poomanee, W.; Chaiyana, W.; Mueller, M.; Viernstein, H.; Khunkitti, W.; Leelapornpisid, P. In vitro investigation of anti-acne properties of *Mangifera indica* L. kernel extract and its mechanism of action against *Propionibacterium acnes*. *Anaerobe* **2018**, *52*, 64–74. [[CrossRef](#)]
144. Duraipandiyar, V.; Ignacimuthu, S. Antifungal activity of traditional medicinal plants from Tamil Nadu, India. *Asian Pac. J. Trop. Biomed.* **2011**, *1*, S204–S215. [[CrossRef](#)]
145. Hsieh, S.K.; Xu, J.R.; Lin, N.H.; Li, Y.C.; Chen, G.H.; Kuo, P.C.; Chen, W.Y.; Tzen, J.T.C. Antibacterial and laxative activities strictinin isolated from Pu er tea (*Camellia sinensis*). *J. Food Drug Anal.* **2016**, *24*, 722–729. [[CrossRef](#)] [[PubMed](#)]
146. Ahmed, S.I.; Hayat, M.Q.; Tahir, M.; Mansoor, Q.; Ismail, M.; Keck, K.; Bates, R.B. Pharmacologically active flavonoids from the anticancer, antioxidant, and antimicrobial extracts of *Cassia angustifolia* Vahl. *BMC Complement. Altern. Med.* **2016**, *16*, 460. [[CrossRef](#)] [[PubMed](#)]
147. Block, V.; Patterson, B.; Subar, A. Fruit, vegetables, and cancer prevention: A review of the epidemiological evidence. *Nutr. Cancer* **1992**, *18*, 1–29. [[CrossRef](#)]
148. Brusselmans, K.; de Schrijver, E.; Heyns, W.; Verhoeven, G.; Swinnen, J.V. Epigallocatechin-3-gallate is a potent natural inhibitor of fatty acid synthase in intact cells and selectively induces apoptosis in prostate cancer cells. *Int. J. Cancer* **2003**, *106*, 856–862. [[CrossRef](#)]
149. Danciu, C.; Vlaia, L.; Fetea, F.; Hancianu, M.; Coricovac, D.E.; Ciurlea, S.A.; Soica, C.M.; Marincu, I.; Vlaia, V.; Dehelean, C.A.; et al. Evaluation of phenolic profile, antioxidant, and anticancer potential of two main representants of Zingiberaceae family against B16A5 murine melanoma cells. *Biol. Res.* **2015**, *48*, 1. [[CrossRef](#)]
150. Nwaeburu, C.C.; Abukiwan, A.; Zhao, Z.; Herr, I. Quercetin-induced miR-200b-3p regulates the mode of self-renewing divisions in pancreatic cancer. *Mol. Cancer* **2017**, *16*, 23. [[CrossRef](#)]
151. Adjakly, M.; Ngollo, M.; Boiteux, J.P.; Bignon, Y.J.; Guy, L.; Bernard-Gallon, D. Genistein and daidzein: Different molecular effects on prostate cancer. *Anticancer Res.* **2013**, *33*, 39–44. [[CrossRef](#)]
152. Dazialo, M.; Mierziak, J.; Korzun, U.; Preisner, M.; Szopa, J.; Kulma, A. The potential of plant phenolics in prevention and therapy of skin disorders. *Int. J. Mol. Sci.* **2016**, *17*, 160. [[CrossRef](#)] [[PubMed](#)]
153. Abusnina, A.; Keravis, T.; Yougbare, I.; Bronner, C.; Lugnier, C. Anti-proliferative effect of curcumin on melanoma cells is mediated by PDE1A inhibition that regulates the epigenetic integrator UHRF1. *Mol. Nutr. Food Res.* **2011**, *55*, 1677–1689. [[CrossRef](#)] [[PubMed](#)]
154. Ide, H.; Lu, Y.; Noguchi, T.; Muto, S.; Okada, H.; Kawato, S.; Horie, S. Modulation of AKR1C2 by curcumin decreases testosterone production in prostate cancer. *Cancer Sci.* **2018**, *109*, 1230–1238. [[CrossRef](#)] [[PubMed](#)]
155. Dłudla, P.V.; Joubert, E.; Muller, C.J.F.; Louw, J.; Johnson, R. Hyperglycemia-induced oxidative stress and heart disease—cardioprotective effects of rooibos flavonoids and phenylpyruvic acid-2-O-β-D-glucoside. *Nutr. Metab.* **2017**, *14*, 45. [[CrossRef](#)] [[PubMed](#)]
156. Garjani, A.; Tila, D.; Hamedeyazdan, S.; Vaez, H.; Rameshrad, M.; Pashaii, M.; Fathiazad, F. An investigation on cardioprotective potential of *Marrubium vulgare* aqueous fraction against ischaemia-reperfusion injury in isolated rat heart. *Folia Morphol.* **2017**, *76*, 361–371. [[CrossRef](#)]
157. Razvani-Azarkhiavi, K.; Iranshahy, M.; Sahebkar, A.; Shirani, K.; Karimi, G. The protective role of phenolic compounds against doxorubicin-induced cardiotoxicity: A comprehensive review. *Nutr. Cancer* **2016**, *68*, 892–917. [[CrossRef](#)]
158. Han, X.; Gao, S.; Cheng, Y.; Sun, Y.; Liu, W.; Tang, L.; Ren, D. Protective effect of naringenin-7-O-glucoside against oxidative stress induced by doxorubicin in H9c2 cardiomyocytes. *Biosci. Trends* **2012**, *6*, 19–25. [[CrossRef](#)]
159. Morrison, D.K. MAP kinase pathways. *Cold Spring Harb. Perspect. Biol.* **2012**, *4*, a011254. [[CrossRef](#)]
160. Sun, J.; Sun, G.; Meng, X.; Wang, H.; Luo, Y.; Qin, M.; Ma, B.; Wang, M.; Cai, D.; Guo, P.; et al. Isorhamnetin protects against doxorubicin-induced cardiotoxicity in vivo and in vitro. *PLoS ONE* **2013**, *8*, e64526. [[CrossRef](#)]
161. Gao, Q.; Yang, B.; Ye, Z.-C.; Wang, J.; Bruce, I.C.; Xia, Q. Opening the calcium-activated potassium channel participates in the cardioprotective effect of puerarin. *Eur. J. Pharmacol.* **2007**, *574*, 179–184. [[CrossRef](#)]
162. Kumar, S.; Pandey, A.K. Chemistry and biological activities of flavonoids: An overview. *Sci. World J.* **2013**, *2013*, 162750. [[CrossRef](#)]
163. Chakraborty, R.; Biplab, D.; Devanna, N.; Sen, S. Antiinflammatory, antinociceptive and antioxidant activities of *Phyllanthus acidus* L. extracts. *Asian Pac. J. Trop. Biomed.* **2012**, *2*, S953–S961. [[CrossRef](#)]
164. Kirmizibekmez, H.; Inan, Y.; Reis, R.; Sipahi, H.; Goren, A.C.; Yesilada, E. Phenolic compounds from the aerial parts of *Clematis viticella* L. and their in vitro anti-inflammatory activities. *Nat. Prod. Res.* **2019**, *33*, 2541–2544. [[CrossRef](#)] [[PubMed](#)]
165. Cheng, H.-L.; Zhang, L.-J.; Liang, Y.-H.; Hsu, Y.-W.; Lee, I.-J.; Liaw, C.-C.; Hwang, S.-Y.; Kuo, Y.-H. Antiinflammatory and antioxidant flavonoids and phenols from *Cardiospermum halicacabum*. *J. Tradit. Complement. Med.* **2013**, *3*, 33–40. [[CrossRef](#)]
166. Augusti, P.R.; Conterato, G.M.M.; Denardin, C.C.; Prazeres, I.D.; Serra, A.T.; Bronze, M.R.; Emanuelli, T. Bioactivity, bioavailability, and gut microbiota transformations of dietary phenolic compounds: Implications for COVID-19. *J. Nutr. Biochem.* **2021**, *97*, 108787. [[CrossRef](#)] [[PubMed](#)]
167. Setayesh, M.; Karimi, M.; Zargarani, A.; Abousaidi, H.; Shahesmaeili, A.; Amiri, F.; Hasheminasab, F.S. Efficacy of a persian herbal medicine compound on coronavirus disease 2019 (COVID-19): A randomized controlled trial. *Integr. Med. Res.* **2022**, *11*, 100869. [[CrossRef](#)]

168. Moharram, F.A.; El Dib, R.A.E.M.; Marzouk, M.S.; El-Shenawy, S.M.; Ibrahim, H.A. New apigenin glycoside, polyphenolic constituents, anti-inflammatory and hepatoprotective activities of *Gaillardia grandiflora* and *Gaillardia pulchella* aerial parts. *Pharmacogn. Mag.* **2017**, *13*, S244–S249. [CrossRef] [PubMed]
169. Compaore, M.; Bakasso, S.; Meda, R.; Nacoulma, O. Antioxidant and anti-inflammatory activities of fractions from *Bidens engleri* O.E. Schulz (Asteraceae) and *Boerhavia erecta* L. (Nyctaginaceae). *Medicines* **2018**, *5*, 53. [CrossRef] [PubMed]
170. Genc, Y.; Harput, U.S.; Saracoglu, I. Active compounds isolated from *Plantago subulata* L. via wound healing and antiinflammatory activity guided studies. *J. Ethnopharmacol.* **2019**, *241*, 112030. [CrossRef]
171. Skendi, A.; Irakli, M.; Chatzopoulou, P.; Bouloumpasi, E.; Biliaderis, C.G. Phenolic extracts from solid wastes of the aromatic plant essential oil industry: Potential uses in food applications. *Food Chem. Adv.* **2022**, *1*, 100065. [CrossRef]
172. Lu, C.L.; Zhu, Y.F.; Hu, M.M.; Wang, D.M.; Xu, X.J.; Lu, C.J.; Zhu, W. Optimization of astilbin extraction from the rhizome of *Smilax glabra*, and evaluation of its anti-inflammatory effect and probably underlying mechanism in lipopolysaccharide-induced RAW264.7 macrophages. *Molecules* **2015**, *20*, 625–644. [CrossRef]
173. Gerhauser, C. Beer constituents as potential cancer chemopreventive agents. *Eur. J. Cancer.* **2005**, *41*, 1941–1954. [CrossRef] [PubMed]
174. McKay, D.L.; Blumberg, J.B. A review of the bioactivity and potential health benefits of chamomile teas (*Matricaria recutita* L.). *Phytother. Res.* **2006**, *20*, 519–530. [CrossRef]
175. Wäch, A.; Pyrzyńska, K.; Biesaga, M. Quercetin content in some food and herbal samples. *Food Chem.* **2007**, *100*, 699–704. [CrossRef]
176. Bijak, M. Silybin, a major bioactive component of milk thistle (*Silybum marianum* L. Gaertn.)—Chemistry, bioavailability, and metabolism. *Molecules* **2017**, *22*, 1942. [CrossRef] [PubMed]
177. Moore, J.O.; Wang, Y.; Stebbins, W.G.; Gao, D.; Zhou, X.; Phelps, R.; Lebwohl, M.; Wei, H. Photoprotective effect of isoflavone genistein on ultraviolet B-induced pyrimidine dimer formation and PCNA expression in human reconstituted skin and its implications in dermatology and prevention of cutaneous carcinogenesis. *Carcinogenesis* **2006**, *27*, 1627–1635. [CrossRef]
178. Widyarani, S. Protective effect of the isoflavone equol against DNA damage induced by ultraviolet radiation to hairless mouse skin. *J. Vet. Sci.* **2006**, *7*, 217–223. [CrossRef]
179. Setchell, K.D.R.; Clerici, C. Equol: History, chemistry, and formation. *J. Nutr.* **2010**, *140*, 1355S–1362S. [CrossRef] [PubMed]
180. Irace, C.; Marini, H.; Bitto, A.; Altavilla, D.; Polito, F.; Adamo, E.B.; Arcoraci, V.; Minutoli, L.; Di Benedetto, A.; Di Vieste, G. Genistein and endothelial function in postmenopausal women with metabolic syndrome. *Eur. J. Clin. Investig.* **2013**, *43*, 1025–1031. [CrossRef]
181. Shahrajabian, M.H.; Petropoulos, S.A.; Sun, W. Survey of the influences of microbial biostimulants on horticultural crops: Case studies and successful paradigms. *Horticulturae* **2023**, *9*, 1–24. [CrossRef]
182. Atun, S.; Handayani, S.; Rakhmawati, A.; Aini Purnamaningish, N.; An Naila, B.I.; Lestari, A. Study of potential phenolic compounds from stems of *Dendrophthoe falcata* (Loranthaceae) plant as antioxidant and antimicrobial agents. *Orient. J. Chem.* **2018**, *34*, 2342–2349. [CrossRef]
183. Teixeira, T.S.; Vale, R.C.; Almeida, R.R.; Ferreira, T.P.S.; Guimaraes, G.L. Antioxidant potential and its correlation with the contents of phenolic compounds and flavonoids of methanolic extracts from different medicinal plants. *Rev. Virtual Química* **2017**, *9*, 1546–1559. [CrossRef]
184. Xie, G.F.; Xu, X.Y.; Zhou, X.L.; Liu, Y.L.; Zhao, Z.B. Changes in phenolic profiles and antioxidant activity in rabbiteye blue berries during ripening. *Int. J. Food Prop.* **2019**, *22*, 320–329.
185. Onder, A.; Izgi, M.N.; Cinar, A.S.; Zengin, G.; Yilmaz, M.A. The characterization of phenolic compounds via LC-ESI-MS/MS, antioxidant, enzyme inhibitory activities of *Salvia absconditiflora*, *Salvia sclarea*, and *Salvia palaestina*: A comparative analysis. *S. Afr. J. Bot.* **2022**, *150*, 313–322. [CrossRef]
186. Tebii, S.O.; Debbache-Benaida, N.; Kadri, N.; Kadi, R.; Zaidi, S. A novel strategy to improve the recovery of phenolic compounds from *Pistacia lentiscus* L. fruits using design-based statistical modeling for ultrasound-deep eutectic solvents extraction and the evaluation of their antioxidant potential. *Sustain. Chem. Pharm.* **2023**, *31*, 100933. [CrossRef]
187. Jiang, R.; Su, G.; Chen, X.; Chen, S.; Li, Q.; Xie, B.; Zhao, Y. Esculetin inhibits endometrial cancer proliferation and promotes apoptosis via hnRNPA1 to downregulate BCLXL and XIAP. *Cancer Lett.* **2021**, *521*, 308–321. [CrossRef] [PubMed]
188. Ma, Y.-L.; Wang, Y.; Wu, Z.-F.; Mei, J.; Zhang, W.-Q.; Shang, Y.-F.; Thakur, K.; Wei, Z.-J. Exploring the effect of in vitro digestion on the phenolics and antioxidant activity of *Lycium barbarum* fruit extract. *Food Biosci.* **2023**, *51*, 102255. [CrossRef]
189. Bahadori, M.B.; Zengin, G.; Dinparast, L.; Eskandani, M. The health benefits of three Hedgenettle herbal teas (*Stachys byzantina*, *Stachys inflata*, and *Stachys lavandulifolia*)—profiling phenolic and antioxidant activities. *Eur. J. Integr. Med.* **2020**, *36*, 101134. [CrossRef]
190. Muddathir, A.M.; Yamauchi, K.; Batubara, I.; Mohieldin, E.A.M.; Mitsunaga, T. Anti-tyrosinase, total phenolic content and antioxidant activity of selected Sudanese medicinal plants. *S. Afr. J. Bot.* **2017**, *109*, 9–15. [CrossRef]
191. Zekeya, N.; Ibrahim, M.; Mamiro, B.; Ndossi, H.; Kilonzo, M.; M Kangara, M.; Chacha, M.; Chilongola, J.; Kideghesho, J. Potential of natural phenolic antioxidant compounds from *Bersama abyssinica* (Meliathacea) for treatment of chronic diseases. *Saudi J. Biol. Sci.* **2022**, *29*, 103273. [CrossRef]
192. Lin, Y.; Tang, D.; Liu, X.; Cheng, J.; Wang, X.; Guo, D.; Zou, J.; Yang, H. Phenolic profile and antioxidant activity of longan pulp of different cultivars from South China. *LWT* **2022**, *165*, 113698. [CrossRef]

193. Cesar, L.-R.J.; Javier, H.; Fernando, A.-Z.J.; Carlos, V.; Enrique, R.-Z.R.; Efrain, A.; Evelin, M.-B.; Inocencio, H.-C.; Luis, O.J.; Zaira, D.; et al. Identification of the main phenolic compounds responsible for the antioxidant activity of *Litsea glaucescens* Kunth. *S. Afr. J. Bot.* **2022**, *147*, 208–214. [[CrossRef](#)]
194. Acemi, R.K.; Acemi, A.; Cakir, M.; Polat, E.G.; Ozen, F. Preliminary screening the antioxidant potential of in vitro-propagated *Amsonia orientalis*: An example to sustainable use of rare medicinal plants in pharmaceutical studies. *Sustain. Chem. Pharm.* **2020**, *17*, 100302. [[CrossRef](#)]
195. Limmongkon, A.; Nopprang, P.; Chaikandee, P.; Somboon, T.; Wongshaya, P.; Pilaisangsuee, V. LC-MS/MS profiles and interrelationships between the anti-inflammatory activity, total phenolic content, and antioxidant potential of Kalasin 2 cultivar peanut sprout crude extract. *Food Chem.* **2018**, *239*, 569–578. [[CrossRef](#)]
196. Vetuschi, A.; Battista, N.; Pompili, S.; Cappariello, A.; Prete, R.; Taticchi, A.; Selvaggini, R.; Latella, G.; Corsetti, A.; Sferra, R. The antiinflammatory and antifibrotic effect of olive phenols and *Lactiplantibacillus plantarum* IMC513 in dextran sodium sulfate-induced chronic colitis. *Nutrition* **2022**, *94*, 111511. [[CrossRef](#)]
197. Demir, T.; Akpinar, O.; Kara, H.; Gungor, H. Phenolic profile and investigation of biological activities of *Allium scorodoprasum* L. subsp. *rotundum*. *Food Biosci.* **2022**, *46*, 101548. [[CrossRef](#)]
198. Malik, J.; Tauchen, J.; Landa, P.; Kutil, Z.; Marsik, P.; Kloucek, P.; Havlik, J.; Kokoska, L. In vitro antiinflammatory and antioxidant potential of root extracts from Ranunculaceae species. *S. Afr. J. Bot.* **2017**, *109*, 128–137. [[CrossRef](#)]
199. Kim, H.-J.; Park, C.-G.; Varghese, R.; Lee, J.Y.; Kim, Y.O.; Sung, G.-H. In-vitro antioxidative, antiinflammatory properties of *Aurea helianthus* leaf extract a Korean traditional medicinal plant. *Saudi J. Biol. Sci.* **2017**, *24*, 1943–1947. [[CrossRef](#)] [[PubMed](#)]
200. Boga, M.; Ersoy, E.; Ozkan, E.E.; Cinar, E.; Kara, E.M.; Canturk, Y.Y.; Zengin, G. Volatile and phenolic profiling of a traditional medicinal plant, *Hypericum empetrifolium* with in vitro biological activities. *J. Ethnopharmacol.* **2021**, *272*, 113933. [[CrossRef](#)]
201. Abirami, S.; Raj, B.E.; Soundarya, T.; Kannan, M.; Sugapriya, D.; Al-Dayan, N.; Mohammed, A.A. Exploring antifungal activities of acetone extract of selected Indian medicinal plants against human dermal fungal pathogens. *Saudi J. Biol. Sci.* **2021**, *28*, 2180–2187. [[CrossRef](#)]
202. Barros, L.; Alves, C.T.; Dueñas, M.; Silva, S.; Oliveira, R.; Carvalho, A.M.; Henriques, M.; Santos-Buelga, C.; Ferreira, I.C.F.R. Characterization of phenolic compounds in wild medicinal flowers from Portugal by HPLC-DAD-ESI/MS and evaluation of antifungal properties. *Ind. Crop. Prod.* **2013**, *44*, 104–110. [[CrossRef](#)]
203. Alishir, A.; Yu, J.S.; Park, M.; Kim, J.-C.; Pang, C.; Kim, J.K.; Jang, T.S.; Jung, W.H.; Kim, K.H. Ulmusakidian, a new coumarin glycoside and antifungal phenolic compounds from the root bark of *Ulmus davidiana* var. *japonica*. *Bioorg. Med. Chem. Lett.* **2021**, *36*, 127828. [[CrossRef](#)]
204. Karimi, A.; Meiners, T. Antifungal activity of *Zataria multiflora* Boiss. Essential oils and changes in volatile compound composition under abiotic stress conditions. *Ind. Crop. Prod.* **2021**, *171*, 113888. [[CrossRef](#)]
205. Munir, N.; Jiaz, W.; Altaf, I.; Naz, S. Evaluation of antifungal and antioxidant potential of two medicinal plants: *Aconitum heterophyllum* and *Polygonum bistorta*. *Asian Pac. J. Trop. Biomed.* **2014**, *4*, S639–S643. [[CrossRef](#)]
206. Soleimani, M.; Arzani, A.; Arzani, V.; Roberts, T.H. Phenolic compounds and antimicrobial properties of mint and thyme. *J. Herb. Med.* **2022**, *36*, 100604. [[CrossRef](#)]
207. Ghimire, B.K.; Seong, E.S.; Yu, C.Y.; Kim, S.-H.; Chung, I.-M. Evaluation of phenolic compounds and antimicrobial activities in transgenic *Codonopsis lanceolata* plans via overexpression of the γ -tocopherol methyltransferase (γ -tmt) gene. *S. Afr. J. Bot.* **2017**, *109*, 25–33. [[CrossRef](#)]
208. Sruthi, P.; Roopavathi, C.; Naidu, M.M. Profiling of phenolics in cashew nut (*Anacardium occidentale* L.) testa and evaluation of their antioxidant and antimicrobial properties. *Food Biosci.* **2023**, *51*, 102246. [[CrossRef](#)]
209. Muhammad, H.; Qasim, M.; Ikram, A.; Versiani, M.A.; Tahiri, I.A.; Yasmeen, K.; Abbasi, M.W.; Azeem, M.; Ali, S.T.; Gul, B. Antioxidant and antimicrobial activities of *Ixora coccinea* root and quantification of phenolic compounds using HPLC. *S. Afr. J. Bot.* **2020**, *135*, 71–79. [[CrossRef](#)]
210. Oussaid, S.; Chibane, M.; Madani, K.; Amrouche, T.; Achat, S.; Dahmoune, F.; Houali, K.; Rendueles, M.; Diaz, M. Optimization of the extraction of phenolic compounds from *Scripus holoschoenus* using a simplex centroid design for antioxidant and antibacterial applications. *LWT Food Sci. Technol.* **2017**, *86*, 635–642. [[CrossRef](#)]
211. Boussoussa, H.; Khacheba, I.; Djeridane, A.; Mellah, N.; Yousofi, M. Antibacterial activity from *Rhanterium adpressum* flowers extracts depending on seasonal variations. *Ind. Crop. Prod.* **2016**, *83*, 44–47. [[CrossRef](#)]
212. Jang, J.Y.; Shin, H.; Lim, J.W.; Ahn, J.H.; Jo, Y.H.; Lee, K.Y.; Hwang, B.Y.; Jung, S.-J.; Kang, S.Y.; Lee, M.K. Comparison of antibacterial activity and phenolic constituents of bark, lignum, leaves, and fruit of *Rhus verniciflua*. *PLoS ONE* **2018**, *13*, e0200257. [[CrossRef](#)]
213. Lin, T.; Huang, L.; Cheng, N.; Wang, Y.; Ning, Z.; Huang, S.; Wu, Y.; Chen, T.; Su, S.; Lin, Y. The in vitro and in vivo antibacterial activities of unilorous honey from a medicinal plant, *Scrophularia ningpoensis* Hemsl., and characterization of its chemical profile with UPLC-MS/MS. *J. Ethnopharmacol.* **2022**, *296*, 115499. [[CrossRef](#)]
214. Guadie, A.; Dakone, D.; Unbushe, D.; Wang, A.; Xia, S. Antibacterial activity of selected medicinal plants used by traditional healers in Genta Meyche (Southern Ethiopia) for the treatment of gastrointestinal disorders. *J. Herb. Med.* **2020**, *22*, 100338. [[CrossRef](#)]

215. Frankova, A.; Vistejnova, L.; Merinas-Amo, T.; Leheckova, Z.; Duskocil, I.; Soon, J.W.; Kudara, T.; Laupua, F.; Alonso-Moraga, A.; Kokoska, L. In vitro antibacterial activity of extracts from Samoan medicinal plants and their effect on proliferation and migration of human fibroblasts. *J. Ethnopharmacol.* **2021**, *264*, 113220. [[CrossRef](#)] [[PubMed](#)]
216. Zahedipour, F.; Hosseini, S.A.; Sathyapalan, T.; Majeed, M.; Jamialahmadi, T.; Al-Rasadi, K.; Banach, M.; Sahebkar, A. Potential effects of curcumin in the treatment of COVID-19 infection. *Phytother. Res.* **2020**, *34*, 2911–2920. [[CrossRef](#)] [[PubMed](#)]
217. Lung, J.; Lin, Y.-S.; Yang, Y.-H.; Chou, Y.-L.; Shu, L.-H.; Cheng, Y.-C.; Liu, H.T.; Wu, C.-Y. The potential chemical structure of anti-SARS-CoV-2 RNA-dependent RNA polymerase. *J. Med. Virol.* **2020**, *92*, 693–697. [[CrossRef](#)]
218. Ghosh, R.; Chakraborty, A.; Biswas, A.; Chowdhuri, S. Evaluation of green tea polyphenols as novel corona virus (SARS CoV-2) main protease (Mpro) inhibitors—An in silico docking and molecular dynamics simulation study. *J. Biomol. Struct. Dyn.* **2021**, *39*, 4362–4374. [[CrossRef](#)] [[PubMed](#)]
219. Xiao, T.; Cui, M.; Zheng, C.; Wang, M.; Sun, R.; Gao, D.; Bao, J.; Ren, S.; Lin, J.; Li, X. Myricetin inhibits SARS-CoV-2 viral replication by targeting M-pro and ameliorates pulmonary inflammation. *Front. Pharmacol.* **2021**, *12*, 1012. [[CrossRef](#)]
220. Davella, R.; Gurrapu, S.; Mamidala, E. Phenolic compounds as promising drug candidates against COVID-19 an integrated molecular docking and dynamics simulation study. *Mater. Today* **2022**, *51*, 522–527. [[CrossRef](#)]
221. Lin, C.-W.; Tsai, F.-J.; Tsai, C.-H.; Lai, C.-C.; Wang, L.; Ho, T.-Y.; Hsieh, C.-C.; Chao, P.-D.L. Anti-SARS coronavirus 3C-like protease effects of Isatis indigotica root and plant-derived phenolic compounds. *Antivir. Res.* **2005**, *68*, 36–42. [[CrossRef](#)]
222. Weng, J.-R.; Lin, C.-S.; Lai, H.-C.; Lin, Y.-P.; Wang, C.-Y.; Tsai, Y.-C.; Wu, K.-C.; Huang, S.-H.; Lin, C.-W. Antiviral activity of *Sambucus Formosana Nakai* ethanol extract and related phenolic acid constituents against human coronavirus NL63. *Virus Res.* **2019**, *273*, 197767. [[CrossRef](#)]
223. Wei, L.; Liao, Z.; Ma, H.; Wei, J.; Peng, C. Antioxidant properties, anti-SARS-CoV-2 study, collagenase and elastase inhibition effects, anti-human lung cancer potential of some phenolic compounds. *J. Indian Chem. Soc.* **2022**, *99*, 100416. [[CrossRef](#)]
224. Granato, D.; Fidelis, M.; Haapakoski, M.; Lima, A.D.S.; Viil, J.; Hellstrom, J.; Ratsep, R.; Kaldmae, H.; Bleive, U.; Azevedo, L.; et al. Enzyme-assisted extraction of anthocyanins and other phenolic compounds from blackcurrant (*Ribes nigrum* L.) press cake: From processing to bioactivities. *Food Chem.* **2022**, *391*, 133240. [[CrossRef](#)]
225. Conde, C.; Escribano, B.M.; Luque, E.; Aguilar-Luque, M.; Feijóo, M.; Ochoa, J.; Latorre, M.; Giraldo, A.; Lillo, R.; Aguera-Morales, E.; et al. The protective effect of extra-virgin olive oil in the experimental model of multiple sclerosis in the rat. *Nutr. Neurosci.* **2020**, *23*, 37–48. [[CrossRef](#)]
226. Ibrahim, N.; Tadj, N.M.I.; Sarker, R.; Mohamed, I.N. The potential mechanisms of the neuroprotective actions of oil palm phenolics: Implications for neurodegenerative diseases. *Molecules* **2020**, *25*, 5159. [[CrossRef](#)]
227. Yang, L.; Wang, Z.-M.; Wang, Y.; Li, R.-S.; Wang, F.; Wang, K. Phenolic constituents with neuroprotective activities from *Hypericum wightianum*. *Phytochemistry* **2019**, *16*, 112049. [[CrossRef](#)] [[PubMed](#)]
228. Qneibi, M.; Hanania, M.; Jaradat, N.; Emwas, N.; Radwan, S. *Inula viscosa* (L.) Greuter, phytochemical composition, antioxidant, total phenolic content, total flavonoids content and neuroprotective effects. *Eur. J. Integr. Med.* **2021**, *42*, 101291. [[CrossRef](#)]
229. Camargo, A.; Dalmagro, A.P.; Rebelo, A.M.; Reinke, C.K.; Zeni, A.L.B. Phenolic profile, antidepressant-like and neuroprotective effects of *Maclura tinctoria* leaves extract. *Nat. Prod. Res.* **2021**, *36*, 4692–4695. [[CrossRef](#)]
230. Nunes, A.R.; Rodrigues, A.L.M.; Queiroz, D.B.D.; Vieira, I.G.P.; Neto, J.F.C.; Calixto Junior, J.T.; Tintino, S.R.; de Moraes, S.M.; Coutinho, H.D.M. Photoprotective potential of medicinal plants from Cerrado biome (Brazil) in relation to phenolic content and antioxidant activity. *J. Photochem. Photobiol. B Biol.* **2018**, *189*, 119–123. [[CrossRef](#)]
231. Ajjour, M.; Kharchoufa, L.; Merrouni, I.A.; Elachouri, M. Moroccan medicinal plants traditionally used for the treatment of skin diseases: From ethnobotany to clinical trials. *J. Ethnopharmacol.* **2022**, *297*, 115532. [[CrossRef](#)]
232. Li, Y.; Huang, J.; Lu, J.; Ding, Y.; Jiang, L.; Hu, S.; Chen, J.; Zeng, Q. The role and mechanism of Asian medicinal plants in treating skin pigmentary disorders. *J. Ethnopharmacol.* **2019**, *245*, 112173. [[CrossRef](#)]
233. Maya-Cano, D.A.; Arango-Varela, S.; Santa-Gonzalez, G.A. Phenolic compounds of blueberries (*Vaccinium* spp.) as a protective strategy against skin cell damage induced by ROS: A review of antioxidant potential and antiproliferative capacity. *Heliyon* **2021**, *7*, e06297. [[CrossRef](#)]
234. Xavier-Santos, J.B.; Passos, J.G.R.; Gomes, J.A.S.; Cruz, J.V.C.; Alves, J.S.F.; Garcia, V.B.; da Silva, R.M.; Lopes, N.P.; Araujo-Junior, R.F.; Zucolotto, S.M.; et al. Topical gen containin phenolic-rich extract from *Ipomoea pes-capre* leaf (Convolvulaceae) has anti-inflammatory, wound healing, and antiophidic properties. *BioMed Pharmacother.* **2022**, *149*, 112921. [[CrossRef](#)] [[PubMed](#)]
235. Moglad, E.H.; Hamad, A.M.; Fatima, F.; Seshadri, V.D.; Naz, M. Antimicrobial and wound healing activities of certain Sudanese medicinal plants. *Saudi J. Biol. Sci.* **2020**, *27*, 1766–1772. [[CrossRef](#)] [[PubMed](#)]
236. Ghuman, S.; Ncube, B.; Finnie, J.F.; McGaw, L.J.; Njoya, E.M.; Cooposamy, R.M.; van Staden, J. Antioxidant, anti-inflammatory and wound healing properties of medicinal plant extracts used to treat wounds and dermatological disorders. *S. Afr. J. Bot.* **2019**, *126*, 232–240. [[CrossRef](#)]
237. Nigussie, D.; Makonnen, E.; Tufa, T.B.; Brewster, M.; Legesse, B.A.; Fekadu, A.; Davey, G. Systematic review of Ethiopian medicinal plants used for their anti-inflammatory and wound healing activities. *J. Ethnopharmacol.* **2021**, *276*, 114179. [[CrossRef](#)] [[PubMed](#)]
238. Yazarlu, O.; Iranshahi, M.; Kashani, H.R.K.; Reshadat, S.; Habtemariam, S.; Iranshahi, M.; Hasanpour, M. Perspective on the application of medicinal plants and natural products in wound healing: A mechanistic review. *Pharmacol. Res.* **2021**, *174*, 105841. [[CrossRef](#)] [[PubMed](#)]

239. Asante-Kwatia, E.; Adjei, S.; Jibira, Y.; Gyimah, L.; Adjei-Hinne, G.; Amponsah, I.K.; Mensah, A.Y. *Amphimas pterocarpoides* harms.: An evaluation of flavonoids and phenolic contents, wound healing, anthelmintic and antioxidant activities of the leaves and stem bark. *Heliyon* **2021**, *7*, e08261. [[CrossRef](#)] [[PubMed](#)]
240. Enriquez-Ochoa, D.; Sanchez-Trasvina, C.; Hernandez-Sedas, B.; Mayolo-Deloisa, K.; Zavala, J.; Rito-Palomares, M.; Valdez-Garcia, J.E. Aqueous two-phase extraction of phenolic compounds from *Sedum dendroideum* with antioxidant activity and anti-proliferative properties against breast cancer cells. *Sep. Purif. Technol.* **2020**, *251*, 117341. [[CrossRef](#)]
241. Eroglu, E.; Girin, S.N. A unique phenolic extraction method from oil macerate of *Hypericum perforatum* using DMSO: Assessment of in vitro anticancer activity, LC-MS/MS profile, total phenolic content and antioxidant capacity. *S. Afr. J. Bot.* **2021**, *139*, 6–11. [[CrossRef](#)]
242. Al-Qahtani, J.; Abbasi, A.; Aati, H.Y.; Al-Taweel, A.; Al-Abdali, A.; Atai, S.; Yanbawi, A.N.; Khan, M.A.; Ghalloo, B.A.; Anwar, M.; et al. Phytochemical, antimicrobial, antidiabetic, thrombolytic, anticancer activities, and in silico studies of *Ficus palmata* Forssk. *Arab. J. Chem.* **2023**, *16*, 104455. [[CrossRef](#)]
243. Sulaiman, C.T.; Deepak, M.; Praveen, T.K.; Lijini, K.R.; Salman, M.; Kumari, S.; Balachandran, I. Metabolite profiling and anti-cancer activity of two medicinally important Euphorbia species. *Med. Omics* **2022**, *7*, 100018. [[CrossRef](#)]
244. Salehi, B.; Vlaisavljevic, S.; Adetunji, C.O.; Adetunji, J.B.; Kregiel, D.; Antolak, H.; Pawlikowska, E.; Uprety, Y.; Mileski, K.S.; Devkota, H.P.; et al. Plants of the genus *Vitis*: Phenolic compounds, anticancer properties and clinical relevance. *Trends Food Sci. Technol.* **2019**, *91*, 362–379. [[CrossRef](#)]
245. Tauchen, J.; Huml, L.; Bortl, L.; Duskocil, I.; Jarosova, V.; Marsik, P.; Frankova, A.; Peralta, Z.M.C.; Zans, M.-E.C.; Havlik, J.; et al. Screening of medicinal plants traditionally used in Peruvian Amazon for in vitro antioxidant and anticancer potential. *Nat. Prod. Res.* **2019**, *33*, 2718–2721. [[CrossRef](#)] [[PubMed](#)]
246. Khalid, M.; Amayreh, M.; Sanduka, S.; Salah, Z.; Al-Rimawi, F.; Al-Mazaideh, G.M.; Alanezi, A.A.; Wedian, F.; Alasmari, F.; Shalayel, M.H.F. Assessment of antioxidant, antimicrobial, and anticancer activities of *Sisymbrium officinale* plant extract. *Heliyon* **2022**, *8*, e10477. [[CrossRef](#)]
247. Ogawa, S.; Takafuji, K.; Tsubuku, S.; Horie, Y.; Ikegawa, S.; Higashi, T. Isotope-coded derivatization based LC/ESI-MS/MS methods using a pair of novel reagents for quantification of hydroxycinnamic acids and hydroxybenzoic acids in fermented brown rice product. *J. Pharm. Biomed. Anal.* **2017**, *142*, 162–170. [[CrossRef](#)]
248. Ossipov, V.; Zubova, M.; Nechaeva, T.; Zagoskina, N.; Salminen, J.-P. The regulating effect of light on the content of flavan-3-ols and derivatives of hydroxybenzoic acids in the callus culture of the tea plant, *Camellia sinensis* L. *Biochem. Syst. Ecol.* **2022**, *101*, 104384. [[CrossRef](#)]
249. Joshi, A.N.; Chandrakar, A.K.; Wasewar, K.L. Extractive separation of 4-hydroxybenzoic acid from aqueous solution using non-toxic and conventional solvents. *Chem. Data Collect.* **2021**, *36*, 100782. [[CrossRef](#)]
250. Saenz-Castillo, A.; Sanabria-Chinchilla, J.; Garcia-Pineres, A.J.; Tamayo-Castillo, G. Bioactivity of prenylated hydroxybenzoic acids from *Piper garagaranum* C. DC. *Phytochem. Lett.* **2022**, *47*, 28–33. [[CrossRef](#)]
251. Osamudiamen, P.M.; Oluremi, B.B.; Oderinlo, O.O.; Aiyelaagbe, O.O. *Trans-resveratrol*, piceatannol and gallic acid: Potent polyphenols isolated from *Mezoneuron benthamianum* effective as anticaries, antioxidant and cytotoxic agents. *Sci. Afr.* **2020**, *8*, e00244. [[CrossRef](#)]
252. Asdaq, S.M.B.; Alamri, A.S.; Alsanie, W.F.; Alhomrani, M.; Yasmin, F. Potential benefits of gallic acid as skeletal muscle relaxant in animal experimental models. *Saudi J. Biol. Sci.* **2021**, *28*, 7575–7580. [[CrossRef](#)]
253. Behera, P.K.; Devi, S.; Mittal, N. Therapeutic potential of gallic acid in obesity: Considerable shift. *Obes. Med.* **2023**, *37*, 100473. [[CrossRef](#)]
254. Gong, W.; Wang, R.; Huang, H.; Hou, Y.; Wang, X.; He, W.; Gong, X.; Hu, J. Construction of double network hydrogels using agarose and gallic acid with antibacterial and anti-inflammatory properties for wound healing. *Int. J. Biol. Macromol.* **2023**, *227*, 698–710. [[CrossRef](#)] [[PubMed](#)]
255. Tan, Q.; An, X.; Pan, S.; Zhen, S.; Hu, Y.; Hu, X. A facile and sensitive ratiometric fluorescent sensor for determination of gallic acid. *Microchem. J.* **2022**, *172 Pt B*, 106922. [[CrossRef](#)]
256. Variya, B.C.; Bakrania, A.K.; Patel, S.S. Antidiabetic potential of gallic acid from *Emblica officinalis*: Improved glucose transporters and insulin sensitivity through PPAR- γ and Akt signaling. *Phytomedicine* **2020**, *73*, 152906. [[CrossRef](#)] [[PubMed](#)]
257. Cechinel-Zanchett, C.C.; Mariano, L.N.B.; Schlickmann, F.; Cechinel-Filho, V.; de Souza, P. In vitro effects of two bioactive compounds, gallic acid and methyl gallate, on urolithiasis Efecto in vitro de dos compuestos bioactivos, el acido galico y el galato de metilo, sobre la urolitiasis. *Actas Urol. Esp.* **2021**, *45*, 604–608. [[CrossRef](#)]
258. Yang, K.; Jian, S.; Guo, D.; Wen, C.; Xin, Z.; Zhang, L.; Kuang, T.; Wen, J.; Yin, Y.; Deng, B. Fecal microbiota and metabolomics revealed the effect of long-term consumption of gallic acid on canine lipid metabolism and gut health. *Food Chem.* **2022**, *15*, 100377. [[CrossRef](#)]
259. Liao, W.; Wen, Y.; Wang, J.; Zhao, M.; Iv, S.; Chen, N.; Li, Y.; Wang, L.; Zheng, Q.; Mou, Y.; et al. Gallic acid alleviates gastric precancerous lesions through inhibition of epithelial mesenchymal transition via Wnt/ β -catenin signaling pathway. *J. Ethnopharmacol.* **2023**, *302 Pt A*, 115885. [[CrossRef](#)]
260. Zhang, Y.; Wang, X.; Lu, B.; Gao, Y.; Zhang, Y.; Li, Y.; Niu, H.; Fan, L.; Pang, Z.; Qiao, Y. Functional and binding studies of gallic acid showing platelet aggregation inhibitory effect as a thrombin inhibitor. *Chin. Herb. Med.* **2022**, *14*, 303–309. [[CrossRef](#)]

261. Hasan, Z.; Islam, A.; Khan, L.A. Spectroscopic investigations on fungal aspartic protease as target of gallic acid. *Int. J. Biol. Macromol.* **2022**, *228*, 333–345. [CrossRef]
262. Clark, M.; Centner, A.M.; Ukhanov, V.; Nagpal, R.; Salazar, G. Gallic acid ameliorates atherosclerosis and vascular senescence and remodels the microbiome in a sex-dependent manner in ApoE^{-/-} mice. *J. Nutr. Biochem.* **2022**, *110*, 109132. [CrossRef]
263. Moradi, A.; Abolfathi, M.; Javadian, M.; Heidarian, E.; Roshanmehr, H.; Khaledi, M.; Nouri, A. Gallic acid exerts nephroprotective, anti-oxidative stress, and anti-inflammatory effects against diclofenac-induced renal injury in malerats. *Arch. Med. Res.* **2021**, *52*, 380–388. [CrossRef]
264. Erukainure, O.L.; Hafizur, R.M.; Choudhary, M.I.; Adhikari, A.; Mesaik, A.M.; Atolani, O.; Banerjee, P.; Preissner, R.; Muhammad, A.; Islam, S. Anti-diabetic effect of the ethyl acetate fraction of *Clerodendrum volubile*: Protocatechuic acid suppresses phagocytic oxidative burst and modulates inflammatory cytokines. *Biomed. Pharmacother.* **2017**, *86*, 307–315. [CrossRef] [PubMed]
265. Dare, R.G.; Oliveira, M.M.; Truitt, M.C.T.; Nakamura, C.V.; Ximenes, V.F.; Lautenschlager, S.O.S. Abilities of protocatechuic acid and its alkylesters, ethyl and heptyl protocatechuates, to counteract UVB-induced oxidative injuries and photoaging in fibroblasts L929 cell line. *J. Photochem. Photobiol. B Biol.* **2020**, *203*, 111771. [CrossRef] [PubMed]
266. Krishna, P.U.N.; Muraleedharan, K. Metal chelation ability of protocatechuic acid anion with ²¹⁰Po₈₄: A theoretical insight. *Comput. Theor. Chem.* **2022**, *1220*, 113996. [CrossRef]
267. Da-Costa-Rocha, I.; Bonnlaender, B.; Sievers, H.; Pischel, I.; Heinrich, M. *Hibiscus sabdariffa* L.—A phytochemical and pharmacological review. *Food Chem.* **2014**, *165*, 424–443. [CrossRef] [PubMed]
268. Adedara, I.A.; Omole, O.; Okpara, E.S.; Fasina, O.B.; Ayeni, M.F.; Ajayi, O.M.; Busari, E.O.; Farombi, E.O. Impact of prepubertal exposure to dietary protocatechuic acid on the hypothalamic-pituitary-testicular axis in rats. *Chem. Biol. Interact.* **2018**, *290*, 99–109. [CrossRef]
269. Salama, A.; Elgohary, R.; Amin, M.M.; Elwahab, S.A. Immunomodulatory effect of protocatechuic acid on cyclophosphamide induced brain injury in rat: Modulation of inflammosomes NLRP3 and SIRT1. *Eur. J. Pharmacol.* **2022**, *932*, 175217. [CrossRef]
270. Song, J.; He, Y.; Luo, C.; Feng, B.; Ran, F.; Xu, H.; Ci, Z.; Xu, R.; Han, L.; Zhang, D. New progress in the pharmacology of protocatechuic acid: A compounds ingested in daily foods and herbs frequently and heavily. *Pharmacol. Res.* **2020**, *161*, 105109. [CrossRef]
271. Antony, F.M.; Wasewar, K. Effect of temperature on equilibria for physical and reactive extraction of protocatechuic acid. *Heliyon* **2020**, *6*, e03664. [CrossRef]
272. Chen, J.; Dai, X.; Jiang, C.; Fu, Y.; Jiang, T.; Tang, L.; Wang, L.; Wang, Q.; Huang, G.; Cao, J. One new protocatechuic acid methyl ester and one enantiomeric pair of dihydroflavones isolated from *Phymatopteris hastata*. *Phytochem. Lett.* **2021**, *43*, 130–134. [CrossRef]
273. Yamabe, N.; Park, J.Y.; Lee, S.; Cho, E.-J.; Lee, S.; Kang, K.S.; Hwang, G.S.; Kim, S.-N.; Kim, H.Y.; Shibamoto, T. Protective effects of protocatechuic acid against cisplatin-induced renal damage in rats. *J. Funct. Foods* **2015**, *19 Pt A*, 20–27. [CrossRef]
274. Al-Olayan, E.M.; Aloufi, A.S.; Al-Amri, O.D.; El-Habit, O.H.; Moneim, A.E.A. Protocatechuic acid mitigates cadmium-induced neurotoxicity in rats: Role of oxidative stress, inflammation and apoptosis. *Sci. Total Environ.* **2020**, *723*, 137969. [CrossRef] [PubMed]
275. Stojkovic, D.S.; Zivkovic, J.; Sokovic, M.; Glamoclija, J.; Ferreira, I.C.F.R.; Jankovic, T.; Maksimovic, Z. Antibacterial activity of *Veronica montana* L. extract and protocatechuic acid incorporated in a food system. *Food Chem. Toxicol.* **2013**, *55*, 209–213. [CrossRef] [PubMed]
276. Yuan, Y.; Xiang, J.; Zheng, B.; Sun, J.; Luo, D.; Li, P.; Fan, J. Diversity of phenolics including hydroxycinnamic acid amide derivatives phenolic acids contribute to antioxidant properties of proso millet. *LWT* **2022**, *154*, 112611. [CrossRef]
277. Schroter, D.; Baldermann, S.; Schreiner, M.; Witzel, K.; Maul, R.; Rohn, S.; Neugart, S. Natural diversity of hydroxycinnamic acid derivatives, flavonoid glycosides, carotenoids and chlorophylls in leaves of six different amaranth species. *Food Chem.* **2018**, *267*, 376–386. [CrossRef]
278. Xiang, J.; Zhang, M.; Apea-Bah, F.; Beta, T. Hydroxycinnamic acid amide (HCAA) derivatives, flavonoid C-glycosides, phenolic acids and antioxidant properties of foxtail millet. *Food Chem.* **2019**, *295*, 214–223. [CrossRef]
279. Bijalwan, V.; Ali, U.; Kesarwani, A.K.; Yadav, K.; Mazumder, K. Hydroxycinnamic acid bound arabinoxylans from millet brans-structural features and antioxidant activity. *Int. J. Biol. Macromol.* **2016**, *88*, 296–305. [CrossRef] [PubMed]
280. Ribas-Agusti, A.; Martin-Belloso, O.; Soliva-Fortuny, R.; Elez-Martinez, P. Enhancing hydroxycinnamic acids and flavan-3-ol contents by pulsed electric fields without affecting quality attributes of apple. *Food Res. Int.* **2019**, *121*, 433–440. [CrossRef]
281. Bal, S.S.; Leishangthem, G.D.; Sethi, R.S.; Singh, A. *p*-coumaric acid ameliorates fipronil induced liver injury in mice through attenuation of structural changes, oxidative stress and inflammation. *Pestic. Biochem. Physiol.* **2022**, *180*, 104997. [CrossRef]
282. Combes, J.; Imatoukene, N.; Couvreur, J.; Godon, B.; Fojcik, C.; Allais, F.; Lopez, M. An optimized semi-defined medium for *p*-coumaric acid production in extractive fermentation. *Process. Biochem.* **2022**, *122 Pt 2*, 357–362. [CrossRef]
283. Naumowicz, M.; Kusaczuk, M.; Kruszewski, M.A.; Gal, M.; Kreowski, R.; Cechowska-Pasko, M.; Kotynska, J. The modulating effect of lipid bilayer/*p*-coumaric acid interactions on electrical properties of model lipid membranes and human glioblastoma cells. *Bioorg. Chem.* **2019**, *92*, 103242. [CrossRef] [PubMed]
284. Grodzicka, M.; Pena-Gonzalez, C.E.; Ortega, P.; Michlewska, S.; Lozano, R.; Bryszewska, M.; Mata, F.J.D.I.; Ionov, M. Heterofunctionalized polyphenolic dendrimers decorated with caffeic acid: Synthesis, characterization and antioxidant activity. *Sustain. Mater. Technol.* **2022**, *33*, e00497. [CrossRef]

285. Kfoury, M.; Geagea, C.; Ruellan, S.; Greige-Gerges, H.; Fourmentin, S. Effect of cyclodextrin and cosolvent on the solubility and antioxidant activity of caffeic acid. *Food Chem.* **2019**, *278*, 163–169. [\[CrossRef\]](#)
286. Raviadarani, R.; Ng, M.H.; Chandran, D.; Ooi, K.K.; Manickam, S. Stable W/O/W multiple nanoemulsion encapsulating natural tocotrienols and caffeic acid with cisplatin synergistically treated cancer cell lines (A549 and HEP G2), and reduced toxicity on normal cell line (HEK 293). *Mater. Sci. Eng. C* **2021**, *121*, 111808. [\[CrossRef\]](#) [\[PubMed\]](#)
287. Tabakam, G.T.; Kodama, T.; Donfack, A.R.N.; Nguekeu, Y.M.M.; Nomin-Erdene, B.; Htoo, Z.P.; Do, K.M.; Ngouela, S.A.; Tene, M.; Morita, H.; et al. A new caffeic acid ester and a new ceramide from the roots of *Eriosema glomeratum*. *Phytochem. Lett.* **2021**, *45*, 82–87. [\[CrossRef\]](#)
288. Salsabila, R.; Perdani, M.S.; Kitakawa, N.S.; Hermansyah, H. Production of methyl caffeate as an intermediate product to produce caffeic acid phenethyl ester by esterification using cation-exchange resin. *Energy Rep.* **2020**, *6*, 528–533. [\[CrossRef\]](#)
289. Mirzaei, S.; Gholami, M.H.; Zabolian, A.; Saleki, H.; Farahani, M.V.; Hamzehlou, S.; Bakhtiari Far, F.; Sharifzadeh, S.O.; Samarghandian, S.; Khan, H.; et al. Caffeic acid and its derivatives as potential modulators of oncogenic molecular pathways: New hope in the fight against cancer. *Pharmacol. Res.* **2021**, *171*, 105759. [\[CrossRef\]](#)
290. Kar, A.; Panda, S.; Singh, M.; Biswas, S. Regulation of PTU-induced hypothyroidism in rats by caffeic acid primarily by activating thyrotropin receptors and by inhibiting oxidative stress. *Phytomed. Plus* **2022**, *2*, 100298. [\[CrossRef\]](#)
291. Meinhart, A.D.; Damin, F.M.; Caldeirao, L.; Filho, M.D.J.; da Silva, L.C.; Constant, L.D.S.; Filho, J.T.; Wagner, R.; Godoy, H.T. Chlorogenic and caffeic acids in 64 fruits consumed in Brazil. *Food Chem.* **2019**, *286*, 51–63. [\[CrossRef\]](#)
292. Silva, A.D.S.; Pereira-de-Morais, L.; da Silva, R.E.R.; Dantas, D.D.M.; Milfont, C.G.B.; Gomes, M.F.; Araujo, I.M.; Kerntopf, M.R.; Menezes, I.R.A.D.; Barbosa, R. Pharmacological screening of the phenolic compound caffeic acid using rat aorta, uterus and ileum smooth muscle. *Chem. Biol. Interact.* **2020**, *332*, 109269. [\[CrossRef\]](#)
293. Wang, X.; Liu, X.; Shi, N.; Zhang, Z.; Chen, Y.; Yan, M.; Li, Y. Response surface methodology optimization and HPLC-ESI-QTOF-MS/MS analysis on ultrasonic-assisted extraction of phenolic compounds from okra (*Abelmoschus esculentus*) and their antioxidant activity. *Food Chem.* **2023**, *405 Pt B*, 134966. [\[CrossRef\]](#) [\[PubMed\]](#)
294. Trifan, A.; Skalicka-Wozniak, K.; Granica, S.; Czerwinska, M.E.; Kruk, A.; Marcourt, L.; Wolfender, J.-L.; Wolfram, E.; Esslinger, N.; Grubelnik, A.; et al. *Symphytum officinale* L.: Liquid-liquid chromatography isolation of caffeic acid oligomers and evaluation of their influence on pro-inflammatory cytokine release in LPS-stimulated neutrophils. *J. Ethnopharmacol.* **2020**, *262*, 113169. [\[CrossRef\]](#) [\[PubMed\]](#)
295. Jung, W.-K.; Lee, D.-Y.; Kim, J.-H.; Choi, I.; Park, S.-G.; Seo, S.-K.; Lee, S.-W.; Lee, C.-M.; Park, Y.-M.; Jeon, Y.-J.; et al. Anti-inflammatory activity of caffeic acid phenethyl ester (CAPE) extracted from *Rhodiola sacra* against lipopolysaccharide-induced inflammatory responses in mice. *Process. Biochem.* **2008**, *43*, 783–787. [\[CrossRef\]](#)
296. Monteiro, A.B.; Rodrigues, C.K.D.S.; Nascimento, E.P.D.; Sales, V.D.S.; Delmondes, G.D.A.; Costa, M.H.N.D.; Oliveira, V.A.P.D.; Morais, L.P.D.; Boligon, A.A.; Barbosa, R.; et al. Anxiolytic and antidepressant-like effects of *Annona coriacea* (Mart.) and caffeic acid in mice. *Food Chem. Toxicol.* **2020**, *136*, 111049. [\[CrossRef\]](#)
297. Spagnol, C.M.; Assis, R.P.; Brunetti, I.L.; Isaac, V.L.B.; Salgado, H.R.N.; Correa, M.A. In vitro methods to determine the antioxidant activity of caffeic acid. *Spectrochim. Acta Part A Mol. Biomol. Spectrosc.* **2019**, *219*, 358–366. [\[CrossRef\]](#)
298. Mu, H.-N.; Zhou, Q.; Yang, R.-Y.; Tang, W.-Q.; Li, H.-X.; Wang, S.-M.; Li, J.; Chen, W.-X.; Dong, J. Caffeic acid prevents non-alcoholic fatty liver disease induced by a high-fat diet through gut microbiota modulation in mice. *Food Res. Int.* **2021**, *143*, 110240. [\[CrossRef\]](#)
299. Koga, M.; Nakagawa, S.; Kato, A.; Kusumi, I. Caffeic acid reduces oxidative stress and microglial activation in the mouse hippocampus. *Tissue Cell* **2019**, *60*, 14–20. [\[CrossRef\]](#)
300. Bao, Y.; Chen, Q.; Xie, Y.; Tao, Z.; Jin, K.; Chen, S.; Bai, Y.; Yang, J.; Shan, S. Ferulic acid attenuates oxidative DNA damage and inflammatory responses in microglia induced by benzo(a)pyrene. *Int. Immunopharmacol.* **2019**, *77*, 105980. [\[CrossRef\]](#)
301. Calabrese, E.J.; Agathokleous, E.; Calabrese, V. Ferulic acid and hormesis: Biomedical and environmental implications. *Mech. Ageing Dev.* **2021**, *198*, 111544. [\[CrossRef\]](#)
302. Pinheiro, P.G.; Santiago, G.M.P.; Silva, F.E.F.D.; Araujo, A.C.J.D.; Oliveira, C.R.T.D.; Freitas, P.R.; Rocha, J.E.; Neto, J.B.D.A.; da Silva, M.M.C.; Tintino, S.R.; et al. Ferulic acid derivatives inhibiting *Staphylococcus aureus* tetK and MsrA efflux pumps. *Biotechnol. Rep.* **2022**, *34*, e00717. [\[CrossRef\]](#)
303. Raj, N.D.; Singh, D. A critical appraisal on ferulic acid: Biological profile, biopharmaceutical challenges nano formulations. *Health Sci. Rev.* **2022**, *5*, 100063. [\[CrossRef\]](#)
304. Zhang, L.-W.; Al-Sywayeh, S.A.; Hsieh, P.-W.; Fang, J.-Y. A comparison of skin delivery of ferulic acid and its derivatives: Evaluation of their efficacy and safety. *Int. J. Pharm.* **2010**, *399*, 44–51. [\[CrossRef\]](#)
305. Ali, S.A.; Saifi, M.a.; Pulivendala, G.; Godugu, C.; Talla, V. Ferulic acid ameliorates the progression of pulmonary fibrosis via inhibition of TGF- β /smad signalling. *Food Chem. Toxicol.* **2021**, *149*, 111980. [\[CrossRef\]](#)
306. Cao, C.-N.; Liu, C.-F.; Zhao, L.; Rao, G.-W. New insight into the photoinduced wavelength dependent decay mechanisms of the ferulic acid system on the excited states. *Spectrochim. Acta Part A Mol. Biomol. Spectrosc.* **2020**, *240*, 118565. [\[CrossRef\]](#)
307. Rosa, L.; Jordao, N.; Soares, N.; de Mesquita, J.; Monteiro, M.; Teodoro, A. Pharmacokinetic, antiproliferative and apoptotic effects of phenolic acids in human colon adenocarcinoma cells using in vitro and in silico approaches. *Molecules* **2018**, *23*, 2569. [\[CrossRef\]](#)

308. Wang, X.; He, Y.; Tian, J.; Muhammad, I.; Liu, M.; Wu, C.; Xu, C.; Zhang, X. Ferulic acid prevents aflatoxin B1-induced liver injury in rats via inhibiting cytochrome P450 enzyme, activating Nrf2/GST pathway and regulating mitochondrial pathway. *Ecotoxicol. Environ. Saf.* **2021**, *224*, 112624. [[CrossRef](#)] [[PubMed](#)]
309. Pazo-Cepeda, M.V.; Aspromonte, S.G.; Alonso, E. Extraction of ferulic acid and feruloylated arabinosylo-oligosaccharides from wheat bran using pressurized hot water. *Food Biosci.* **2021**, *44*, 101374. [[CrossRef](#)]
310. Singh, S.; Arthur, R.; Upadhayay, S.; Kumar, P. Ferulic acid ameliorates neurodegeneration via the Nrf2/ARE signalling pathways: A review. *Pharmacol. Res. Mod. Chin. Med.* **2022**, *5*, 100190. [[CrossRef](#)]
311. Li, J.; Wang, C.; Chen, X.; Huang, M.; Fu, Q.; Li, R.; Wang, Y.; Li, C.; Zhao, P.; Xie, Y.; et al. A non-enzymatic photoelectrochemical sensor based on g-C₃N₄@CNT heterojunction for sensitive detection of antioxidant gallic acid in food. *Food Chem.* **2022**, *389*, 133086. [[CrossRef](#)]
312. Wang, Q.-H.; Qin, S.-W.; Jiang, J.-G. Improvement effects of esculetin on the formation and development of atherosclerosis. *Biomed. Pharmacother.* **2022**, *150*, 113001. [[CrossRef](#)] [[PubMed](#)]
313. Sabry, M.M.; Abdel-Rahman, R.F.; El-Shenawy, S.; Hassan, A.M.; El-Gayed, S.H. Estrogenic activity of Sage (*Salvia officinalis* L.) aerial parts and its isolated ferulic acid in immature ovariectomized female rats. *J. Ethnopharmacol.* **2022**, *282*, 114579. [[CrossRef](#)] [[PubMed](#)]
314. Singh, Y.P.; Rai, H.; Singh, G.; Singh, G.K.; Mishra, S.; Kumar, S.; Srikrishna, S.; Modi, G. A review on ferulic acid and analogs based scaffolds for the management of Alzheimers disease. *Eur. J. Med. Chem.* **2021**, *215*, 113278. [[CrossRef](#)] [[PubMed](#)]
315. Elhessy, H.M.; Eltahry, H.; Erfan, O.S.; Mahdi, M.R.; Hazem, N.M.; El-Shahat, M.A. Evaluation of the modulation of nitric oxide synthase expression in the cerebellum of diabetic albino rats and the possible protective effect of ferulic acid. *Acta Histochem.* **2020**, *122*, 151633. [[CrossRef](#)]
316. Ramar, M.; Manikandan, B.; Raman, T.; Priyadarsini, A.; Palanisamy, S.; Velayudam, M.; Munusamy, A.; Prabhu, N.M.; Vaseeharan, B. Protective effect of ferulic acid and resveratrol against alloxan-induced diabetes mice. *Eur. J. Pharmacol.* **2012**, *690*, 226–235. [[CrossRef](#)] [[PubMed](#)]
317. Shanthakumar, J.; Karthikeyan, A.; Bandugula, V.R.; Prasad, N.R. Ferulic acid, a dietary phenolic acid, modulates radiation effects in Swiss albino mice. *Eur. J. Pharmacol.* **2012**, *691*, 268–274. [[CrossRef](#)] [[PubMed](#)]
318. Hu, R.; Wu, S.; Li, B.; Tan, J.; Yan, J.; Wang, Y.; Tang, Z.; Liu, M.; Fu, C.; Zhang, H.; et al. Dietary ferulic acid and vanillic acid on inflammation, gut barrier function and growth performance in lipopolysaccharide-challenged piglets. *Anim. Nutr.* **2022**, *8*, 144–152. [[CrossRef](#)]
319. Alam, M.A.; Sernia, C.; Brown, L. Ferulic acid improves cardiovascular and kidney structure and function in hypertensive rats. *J. Cardiovasc. Pharmacol.* **2013**, *61*, 240–249. [[CrossRef](#)]
320. Cheng, W.-J.; Zhang, P.-P.; Luo, Q.-Q.; Deng, S.-M.; Jia, A.-Q. The chemosensitizer ferulic acid enhances epirubicin-induced apoptosis in MDA-MB-231 cells. *J. Funct. Foods.* **2020**, *73*, 104130. [[CrossRef](#)]
321. Von Danwitz, A.; Schulz, C. Effects of dietary rapeseed glucosinolates, sinapic acid and phytic acid on feed intake growth performance and fish health in turbot (*Psetta maxima* L.). *Aquaculture* **2020**, *516*, 734624. [[CrossRef](#)]
322. Kaur, J.; Mehta, V.; Kaur, G. Preparation, development and characterization of *Leucaena leucocephala* galactomannan (LLG) conjugated sinapic acid: A potential colon targeted prodrug. *Int. J. Biol. Macromolecul.* **2021**, *178*, 29–40. [[CrossRef](#)]
323. Roy, S.J.; Prince, P.S.M. Protective effects of sinapic acid on lysosomal dysfunction in isoproterenol induced myocardial infarcted rats. *Food Chem. Toxicol.* **2012**, *50*, 3984–3989. [[CrossRef](#)] [[PubMed](#)]
324. Saeedavi, M.; Goudarzi, M.; Mehrzadi, S.; Basir, Z.; Hasanvand, A.; Hosseinzadeh, A. Sinapic acid ameliorates airway inflammation in murine ovalbumin-induced allergic asthma by reducing Th2 cytokine production. *Life Sci.* **2022**, *307*, 120858. [[CrossRef](#)]
325. Basque, A.; Touaibia, M.; Martin, L.J. Sinapic and ferulic acid phenethyl esters increase the expression of steroidogenic genes in MA-10 tumor Leydig cells. *Toxicol. In Vitro* **2023**, *86*, 105505. [[CrossRef](#)] [[PubMed](#)]
326. Hu, X.; Geetha, R.V.; Surapaneni, K.M.; Veeraraghavan, V.P.; Chinnathambi, A.; Alahmadi, T.A.; Manikandan, V.; Manokaran, K. Lung cancer induced by Benzo(A)Pyrene: Chemo-protective effect of sinapic acid in swiss albino mice. *Saudi J. Biol. Sci.* **2021**, *28*, 7125–7133. [[CrossRef](#)]
327. Altindag, F.; Ragetli, M.C.; Ozdek, U.; Koyun, N.; Alhalboosi, J.K.I.; Elasan, S. Combined treatment of sinapic acid and ellagic acid attenuates hyperglycemia in streptozotocin-induced diabetic rats. *Food Chem. Toxicol.* **2021**, *156*, 112443. [[CrossRef](#)]
328. Eroglu, C.; Avci, E.; Vural, H.; Kurar, E. Anticancer mechanism of Sinapic acid in PC-3 and LNCaP human prostate cancer cell lines. *Gene* **2018**, *671*, 127–134. [[CrossRef](#)] [[PubMed](#)]
329. Ansari, M.A.; Raish, M.; Ahmad, A.; Ahmad, S.F.; Mudassar, S.; Mohsin, K.; Shakeel, F.; Korashy, H.M.; Bakheet, S.A. Sinapic acid mitigates gentamicin-induced nephrotoxicity and associated oxidative/nitrosative stress, apoptosis, and inflammation in rats. *Life Sci.* **2016**, *165*, 1–8. [[CrossRef](#)] [[PubMed](#)]
330. Raish, M.; Ahmad, A.; Ansari, M.A.; Ahad, A.; Al-Jenoobi, F.I.; Al-Mohizea, A.M.; Khan, A.; Ali, N. Sinapic acid ameliorates bleomycin-induced lung fibrosis in rats. *Biomed. Pharmacother.* **2018**, *108*, 224–231. [[CrossRef](#)]
331. Singh, D.; Verma, R.K. Sinapic acid mitigates intracerebroventricular streptozotocin induced oxidative stress and neuro-inflammatory changes in rats. *J. Neurol. Sci.* **2019**, *405*, 109. [[CrossRef](#)]
332. Yang, C.; Deng, Q.; Xu, J.; Wang, X.; Hu, C.; Tang, H.; Huang, F. Sinapic acid and resveratrol alleviate oxidative stress with modulation of gut microbiota in high-fat diet-fed rats. *Food Res. Int.* **2019**, *116*, 1202–1211. [[CrossRef](#)] [[PubMed](#)]

333. Bezerra, J.J.L.; Pinheiro, A.A.V.; Barreto, E.D.O. Medicinal plants used in the treatment of asthma in different regions of Brazil: A comprehensive review of ethnomedicinal evidence, preclinical pharmacology and clinical trials. *Phytomed. Plus* **2022**, *2*, 100376. [[CrossRef](#)]
334. Borah, B.; Dwivedi, K.D.; Kumar, B.; Chowhan, L.R. Recent advances in the microwave- and ultrasound-assisted green synthesis of coumarin-heterocycles. *Arab. J. Chem.* **2022**, *15*, 103654. [[CrossRef](#)]
335. Alagesan, V.; Ramalingam, S.; Kim, M.; Venugopal, S. Antioxidant activity guided isolation of a coumarin compound from *Ipomoea pes-caprea* (Convolvulaceae) leaves acetone extract and its biological and molecular docking studies. *Eur. J. Integr. Med.* **2019**, *32*, 100984. [[CrossRef](#)]
336. Cakmakci, E.; Ozdemir, M.; Sen, F.; Bulut, M.; Talcin, B. Vegetable oil-based, coumarin-containing antibacterial thermosets with improved thermal stability via copper-free thermal stability via copper-free thermal azide-alkyne click polymerization. *Ind. Crop. Prod.* **2022**, *182*, 114870. [[CrossRef](#)]
337. Dandriyal, J.; Singla, R.; Kumar, M.; Jaitak, V. Recent developments of C-4 substituted coumarin derivatives as anticancer agents. *Eur. J. Med. Chem.* **2016**, *119*, 141–168. [[CrossRef](#)] [[PubMed](#)]
338. Seo, W.D.; Kim, J.Y.; Ryu, H.W.; Kim, J.H.; Han, S.-I.; Ra, J.-E.; Seo, K.H.; Jang, K.C.; Lee, J.H. Identification and characterisation of coumarins from the roots of *Angelica dahurica* and their inhibitory effects against cholinesterase. *J. Funct. Foods* **2013**, *5*, 1421–1431. [[CrossRef](#)]
339. Kassim, N.K.; Rahmani, M.; Ismail, A.; Sukari, M.A.; Ee, G.C.L.; Nasir, N.M.; Awang, K. Antioxidant activity-guided separation of coumarins and lignan from *Melicope glabra* (Rutaceae). *Food Chem.* **2013**, *139*, 87–92. [[CrossRef](#)] [[PubMed](#)]
340. Sharma, M.; Vyas, V.K.; Bhatt, S.; Ghate, M.D. Therapeutic potential of 4-substituted coumarins: A conspectus. *Eur. J. Med. Chem. Rep.* **2022**, *6*, 100086. [[CrossRef](#)]
341. Salau, V.F.; Erukainure, O.L.; Ibeji, C.U.; Koorbanally, N.A.; Islam, S. Umbelliferone stimulates glucose uptake; modulates gluconeogenic and nucleotide-hydrolyzing enzymes activities, and dysregulated lipid metabolic pathways in isolated psoas muscle. *J. Funct. Food* **2020**, *67*, 103847. [[CrossRef](#)]
342. Seong, S.H.; Ali, Y.; Jung, H.A.; Choi, J.S. Umbelliferone derivatives exert neuroprotective effects by inhibiting monoamine oxidase A, self-amyloid β aggregation, and lipid peroxidation. *Bioorg. Chem.* **2019**, *92*, 103293. [[CrossRef](#)]
343. Mazimba, O. Umbelliferone: Sources, chemistry and bioactivities review. *Bull. Fac. Pharm. Cairo Univ.* **2017**, *55*, 223–232. [[CrossRef](#)]
344. Kundu, M.; Chatterjee, S.; Ghosh, N.; Manna, P.; Das, J.; Sil, P.C. Tumor targeted delivery of umbelliferone via a smart mesoporous silica nanoparticles controlled-release drug delivery system for increased anticancer efficiency. *Mater. Sci. Eng. C* **2020**, *116*, 111239. [[CrossRef](#)]
345. Pan, L.; Li, X.; Jin, H.; Yang, X.; Qin, B. Antifungal activity of umbelliferone derivatives: Synthesis and structure-activity relationships. *Microb. Pathog.* **2017**, *104*, 110–115. [[CrossRef](#)] [[PubMed](#)]
346. Althunibat, O.Y.; Abduh, M.S.; Abukhalil, M.H.; Aladaileh, S.H.; Hanieh, H.; Mahmoud, A.M. Umbelliferone prevents isoproterenol-induced myocardial injury by upregulating Nrf2/HO-1 signaling, and attenuating oxidative stress, inflammation, and cell death in rats. *Biomed. Pharmacother.* **2022**, *149*, 112900. [[CrossRef](#)] [[PubMed](#)]
347. Kutlu, Z.; Celik, M.; Bilen, A.; Halici, Z.; Yildirim, S.; Karabulut, S.; Karakaya, S.; Bostanlik, D.F.; Aydin, P. Effects of umbelliferone isolated from the *Ferulago pauciradiata* Boiss. & Heldr. plant on cecal ligation and puncture-induced sepsis model in rats. *Biomed. Pharmacother.* **2020**, *127*, 110206. [[CrossRef](#)] [[PubMed](#)]
348. Lim, J.-Y.; Lee, J.-H.; Lee, D.-H.; Lee, J.-H.; Kim, D.-K. Umbelliferone reduces the expression of inflammatory chemokines in HaCaT cells and DNCB/DFE-induced atopic dermatitis symptoms in mice. *Int. Immunopharmacol.* **2019**, *75*, 105830. [[CrossRef](#)]
349. Garud, M.S.; Kulkarni, Y.A. Attenuation of renal damage in type I diabetic rats by umbelliferone—A coumarin derivative. *Pharmacol. Rep.* **2017**, *69*, 1263–1269. [[CrossRef](#)]
350. Mohamed, M.R.; Emam, M.A.; Hassan, N.S.; Mogadem, A.I. Umbelliferone and daphnetin ameliorate carbon tetrachloride-induced hepatotoxicity in rats via nuclear factor erythroid 2-related factor 2-mediated heme oxygenase-2 expression. *Environ. Toxicol. Pharmacol.* **2014**, *38*, 531–541. [[CrossRef](#)]
351. Vijayalakshmi, A.; Sindhu, G. Umbelliferone arrest cell cycle at G0/G1 phase and induces apoptosis in human oral carcinoma (KB) cells possibly via oxidative DNA damage. *Biomed. Pharmacother.* **2017**, *92*, 661–671. [[CrossRef](#)]
352. Cruz, L.F.; de Figueiredo, G.F.; Pedro, L.P.; Amarin, Y.M.; Andrade, J.T.; Passos, T.F.; Rodrigues, F.F.; Souza, I.L.A.; Goncalves, T.P.R.; Lima, L.A.R.D.S.; et al. Umbelliferone (7-hydroxycoumarin): A non-toxic antiarrheal and antiulcerogenic coumarin. *Biomed. Pharmacother.* **2020**, *129*, 110432. [[CrossRef](#)]
353. Park, C.; Jin, C.-Y.; Kim, G.-Y.; Choi, I.-W.; Kwon, T.K.; Choi, B.T.; Lee, S.J.; Lee, W.H.; Choi, Y.H. Induction of apoptosis by esculetin in human leukemia U937 cells through activation of JNK and ERK. *Toxicol. Appl. Pharmacol.* **2008**, *227*, 219–228. [[CrossRef](#)] [[PubMed](#)]
354. Kadakol, A.; Sharma, N.; Kulkarni, Y.A.; Gaikwad, A.B. Esculetin: A phytochemical endeavor fortifying effect against non-communicable diseases. *Biomed. Pharmacother.* **2016**, *84*, 1442–1448. [[CrossRef](#)]
355. Jeong, N.-H.; Yang, E.-J.; Jin, M.; Lee, J.Y.; Choi, Y.-A.; Park, P.-H.; Lee, S.-R.; Kim, S.-U.; Shin, T.-Y.; Kwon, T.K.; et al. Esculetin from *Fraxinus rhynchophylla* attenuates atopic skin inflammation by inhibiting the expression of inflammatory. *Int. Immunopharmacol.* **2018**, *59*, 209–216. [[CrossRef](#)]

356. Prabakaran, D.; Ashokkumar, N. Antihyperglycemic effect of esculetin modulated carbohydrate metabolic enzymes activities in streptozotocin induced diabetic rats. *J. Funct. Food* **2012**, *4*, 776–783. [[CrossRef](#)]
357. Prabakaran, D.; Ashokkumar, N. Protective effect of esculetin on hyperglycemia-mediated oxidative damage in the hepatic and renal tissues of experimental diabetic rats. *Biochimie* **2013**, *95*, 366–373. [[CrossRef](#)]
358. Yang, J.; Han, J.; Li, Y.; Dong, B. Esculetin inhibits the apoptosis in H9c2 cardiomyocytes via the MAPK signaling pathway following hypoxia/reoxygenation injury. *Biomed. Pharmacother.* **2017**, *88*, 1206–1210. [[CrossRef](#)]
359. Choi, R.-Y.; Ham, J.R.; Lee, M.-K. Esculetin prevents non-alcoholic fatty liver in diabetic mice fed high-fat diet. *Chem. Biol. Interact.* **2016**, *260*, 13–21. [[CrossRef](#)]
360. Subramaniam, S.R.; Ellis, E.M. Esculetin-induced protection of human hepatoma HepG2 cells against hydrogen peroxide is associated with the Nrf2-dependent induction of the NAD(P)H: Quinone oxidoreductase 1 gene. *Toxicol. Appl. Pharmacol.* **2011**, *250*, 130–136. [[CrossRef](#)]
361. Kadakol, A.; Malek, V.; Goru, S.K.; Pandey, A.; Sharma, N.; Gaikwad, A.B. Esculetin ameliorates insulin resistance and type 2 diabetic nephropathy through reversal of histone H3 acetylation and H2A lysine 119 monoubiquitination. *J. Funct. Food* **2017**, *35*, 256–266. [[CrossRef](#)]
362. Kim, W.K.; Byun, W.S.; Chung, H.-J.; Oh, J.; Park, H.J.; Choi, J.S.; Lee, S.K. Esculetin suppresses tumor growth and metastasis by targeting Axin2/E-cadherin axis in colorectal cancer. *Biochem. Pharmacol.* **2018**, *152*, 71–83. [[CrossRef](#)]
363. Xu, B.; Zhu, L.; Chu, J.; Ma, Z.; Fu, Q.; Wei, W.; Deng, X.; Ma, S. Esculetin improves cognitive impairments induced by transient cerebral ischaemia and reperfusion in mice via regulation of mitochondrial fragmentation and mitophagy. *Behav. Brain Res.* **2019**, *372*, 112007. [[CrossRef](#)] [[PubMed](#)]
364. Zhang, M.; Damba, T.; Wu, Z.; Serna-Salas, S.; Buist-Homan, M.; Faber, K.N.; Moshage, H. Bioactive coumarin-derivative esculetin decreases hepatic stellate cell activation via induction of cellular senescence via the PI3K-Akt-GSK3 β pathway. *Food Biosci.* **2022**, *50*, 102164. [[CrossRef](#)]
365. Wang, J.; Lai, X.; Yuan, D.; Liu, Y.; Wang, J.; Liang, Y. Effects of ferulic acid, a major component of rice bran, on proliferation, apoptosis, and autophagy of HepG2 cells. *Food Res. Int.* **2022**, *161*, 111816. [[CrossRef](#)] [[PubMed](#)]
366. Ren, W.; Zhou, Q.; Yu, R.; Liu, Z.; Hu, Y. Esculetin inhibits the pyroptosis of microvascular endothelial cells through NF-KB/NLRP3 signaling pathway. *Arch. Biochem. Biophys.* **2022**, *720*, 109173. [[CrossRef](#)] [[PubMed](#)]
367. Jiang, Y.; Fang, Z.; Leonard, W.; Zhang, P. Phenolic compounds in *Lycium* berry: Composition, health benefits and industrial applications. *J. Funct. Food* **2021**, *77*, 104340. [[CrossRef](#)]
368. Duan, J.; Shi, J.; Ma, X.; Xuan, Y.; Li, P.; Wang, H.; Fan, Y.; Gong, H.; Wang, L.; Pang, Y.; et al. Esculetin inhibits proliferation, migration, and invasion of clear cell renal cell carcinoma cells. *Biomed. Pharmacother.* **2020**, *125*, 110031. [[CrossRef](#)] [[PubMed](#)]
369. Lee, J.; Yang, J.; Jeon, J.; Jeong, H.S.; Lee, J.; Sung, J. Hepatoprotective effect of esculetin on ethanol-induced liver injury in human HepG2 cells and C57BL/6J mice. *J. Funct. Food* **2018**, *40*, 536–543. [[CrossRef](#)]
370. Dou, Y.; Tong, B.; Wei, Z.; Li, Y.; Xia, Y.; Dai, Y. Scopoletin suppresses IL-6 production from fibroblast-like synoviocytes of adjuvant arthritis rats induced by IL-1 β stimulation. *Int. Immunopharmacol.* **2013**, *17*, 1037–1043. [[CrossRef](#)]
371. Connell, B.J.; Saleh, M.C.; Rajagopal, D.; Saleh, T.M. UPEI-400, a conjugate of lipoic acid and scopoletin, mediates neuroprotection in a rat model of ischemia/reperfusion. *Food Chem. Toxicol.* **2017**, *100*, 175–182. [[CrossRef](#)]
372. Rutul, R.; Amar, S.; Mithil, P.; Sushil, K.; Singh, A.; Parth, D.; Ghanshyam, P.; Mistri, J.; Subhash, N. Study of dynamics of genes involved in biosynthesis and accumulation of scopoletin at different growth stages of *Convolvulus prostratus* Forssk. *Phytochemistry* **2021**, *182*, 112594. [[CrossRef](#)] [[PubMed](#)]
373. Tasfiyati, A.N.; Antika, L.D.; Dwei, R.T.; Spetama, A.W.; Sabarudin, A.; Ernawati, T. An experimental design approach for the optimization of scopoletin extraction from *Morinda citrifolia* L. using accelerated solvent extraction. *Talanta* **2022**, *238*, 123010. [[CrossRef](#)] [[PubMed](#)]
374. Alkorashy, A.I.; Doghish, A.S.; Abulsoud, A.I.; Ewees, M.G.; Abdelghany, T.M.; Elshafey, M.M.; Elkhatib, W.F. Effect of scopoletin on phagocytic activity of U937-derived human macrophages: Insights from transcriptomic analysis. *Genomics* **2020**, *112*, 3518–3524. [[CrossRef](#)] [[PubMed](#)]
375. Khalaf, M.M.; Hassan, S.M.; Sayed, A.M.; Abo-Youssef, A.M. Ameliorate impacts of scopoletin against vancomycin-induced intoxication in rat model through modulation of Keap1-Nrf2/HO-1 and IKK α -P65 NF-KB/P38 MAPK signaling pathways: Molecular study, molecular docking evidence and network pharmacology analysis. *Int. Immunopharmacol.* **2022**, *102*, 108382. [[CrossRef](#)] [[PubMed](#)]
376. Ham, J.R.; Lee, H.-I.; Choi, R.-Y.; Sim, M.-O.; Choi, M.-S.; Kwon, E.-Y.; Yun, K.W.; Kim, M.-J.; Lee, M.-K. Anti-obesity and anti-hepatosteatosis effects of dietary scopoletin in high-fat diet fed mice. *J. Funct. Food* **2016**, *25*, 433–446. [[CrossRef](#)]
377. Nam, H.; Kim, M.-M. Scopoletin has a potential activity for anti-aging via autophagy in human lung fibroblasts. *Phytomedicine* **2015**, *22*, 362–368. [[CrossRef](#)]
378. Oyama, T.; Yoshimori, A.; Ogawa, H.; Shirai, Y.; Abe, H.; Kamiya, T.; Tanuma, S.-I. The structural differences between mushroom and human tyrosinase cleared by investigating the inhibitory activities of stilbenes. *J. Mol. Struct.* **2023**, *1272*, 134180. [[CrossRef](#)]
379. Avendano-Godoy, J.; Ortega, E.; Urrutia, M.; Escobar-Avello, D.; Luengo, J.; Baer, D.V.; Mardones, C.; Gomez-Gaete, C. Prototype of nutraceutical products from microparticles loaded with stilbenes extracted from grape cane. *Food Bioprod. Process.* **2022**, *134*, 19–29. [[CrossRef](#)]

380. Fu, Y.-H.; Hou, Y.-D.; Duan, Y.-Z.; Sun, X.-Y.; Chen, S.-Q. Six undescribed derivatives of stilbene isolated from *Lindera reflexa* hemsl. And their anti-tumor and anti-inflammatory activities. *Fitoterapia* **2022**, *163*, 105331. [CrossRef]
381. Choi, Y.S.; Yoon, D.H.; Kim, S.Y.; Kim, C.S.; Lee, K.R. Stilbene oligomers from the stems of *Parthenocissus tricuspidata* and their potential anti-neuroinflammatory and neuroprotective activity. *Tetrahedron Lett.* **2021**, *71*, 153027. [CrossRef]
382. Brianceau, S.; Turk, M.; Vitrac, X.; Vorobiev, E. High voltage electric discharges assisted extraction of phenolic compounds from grape stems: Effect of processing parameters on flavan-3-ols, flavonols and stilbenes recovery. *Innov. food Sci. Emerg. Technol.* **2016**, *35*, 67–74. [CrossRef]
383. Robb, E.L.; Stuart, J.A. The stilbenes resveratrol, pterostilbene and piceid affect growth and stress resistance in mammalian cells via a mechanism requiring estrogen receptor beta and the induction of Mn-superoxide dismutase. *Phytochemistry* **2014**, *98*, 164–173. [CrossRef] [PubMed]
384. Fernandez-Marin, M.I.; Guerrero, R.F.; Garcia-Parrilla, M.C.; Puertas, B.; Richard, T.; Rodriguez-Werner, M.A.; Winterhalter, P.; Monti, J.-P.; Cantos-Villar, E. Isorhapontigenin: A novel bioactive stilbene from wine grapes. *Food Chem.* **2012**, *135*, 1353–1359. [CrossRef] [PubMed]
385. Benbouguerra, N.; Hornedo-Ortega, R.; Garcia, F.; Khawand, T.E.; Saucier, C.; Richard, T. Stilbenes in grape berries and wine and their potential role as anti-obesity agents: A review. *Trends Food Sci. Technol.* **2021**, *112*, 362–381. [CrossRef]
386. Guerrero-Solao, J.; Jaramillo-Morales, O.A.; Jimenez-Cabrera, T.; Urrutia-Hernandez, T.A.; Chehue-Romero, A.; Olvera-Hernandez, E.G.; Bautista, M. Punica protopunica Balf., the forgotten sister of the common pomegranate (*Punica granatum* L.): Features and medicinal properties—A review. *Plants* **2020**, *9*, 1214. [CrossRef] [PubMed]
387. Runeberg, P.; Ryabukhin, D.; Lagerquist, L.; Rahkila, J.; Eklund, P. Transformations and antioxidative activities of lignans and stilbenes at high temperatures. *Food Chem.* **2023**, *4040*, 134641. [CrossRef] [PubMed]
388. Thriumalaisamy, R.; Bhuvaneswari, M.; Haritha, S.; Jeevarathna, S.; Janani, K.S.S.; Suresh, K. Curcumin, Naringenin and resveratrol from natural plant products hold promising solutions for modern world diseases—A recent review. *S. Afr. J. Bot.* **2022**, *151*, 567–580. [CrossRef]
389. Pinilla-Penalver, E.; Garcia-Bejar, B.; Contento, A.M.; Rios, A. Graphene quantum dots an efficient nanomaterial for enhancing the photostability of *trans*-resveratrol in food samples. *Food Chem.* **2022**, *386*, 132766. [CrossRef]
390. Pirola, L.; Frojdo, S. Resveratrol: One molecule, many targets IUBMB. *Life* **2008**, *60*, 323–332. [CrossRef]
391. Zupancic, S.; Lavric, Z.; Kristl, J. Stability and solubility of *trans*-resveratrol are strongly influenced by pH and temperature. *Eur. J. Pharm. Biopharm.* **2015**, *93*, 196–204. [CrossRef] [PubMed]
392. Vian, M.A.; Tomao, V.; Gallet, S.; Coulomb, P.O.; Lacombe, J.M. Simple and rapid method for *cis*- and *trans*-resveratrol and piceid isomers determination in wine by high-performance liquid chromatography using chromolith columns. *J. Chromatogr. A* **2005**, *1085*, 224–229. [CrossRef]
393. Shen, L.; Ji, H.-F. Reciprocal interactions between resveratrol and gut microbiota deepen our understanding of molecular mechanisms underlying its health benefits. *Trends Food Sci. Technol.* **2018**, *81*, 232–236. [CrossRef]
394. Nicolau, A.L.A.; Peres, G.B.; Silva, J.D.S.; Nunes, S.H.; Fortes, T.M.L.; Suffredini, I.B. Pilot project. Resveratrol intake by physical active and sedentary older adult women and blood pressure. *Exp. Gerontol.* **2022**, *166*, 111883. [CrossRef]
395. Marques, F.Z.; Markus, M.A.; Morris, B.J. Resveratrol: Cellular actions of a potent natural chemical that confers a diversity of health benefits. *Int. J. Biochem. Cell Biol.* **2009**, *41*, 2125–2128. [CrossRef] [PubMed]
396. Shoura, S.M.S.; Naghsh, N.; Moslemi, E.; Kayvani, Z.; Moridpour, A.H.; Musazadeh, V.; Dehghan, P. Can resveratrol supplementation affect biomarkers of inflammation and oxidative stress? An umbrella meta-analysis. *J. Funct. Food* **2022**, *99*, 105360. [CrossRef]
397. Guo, S.; Zhou, Y.; Xie, X. Resveratrol inhibiting TGF/ERK signaling pathway can improve atherosclerosis: Backgrounds, mechanisms and effects. *Biomed. Pharmacother.* **2022**, *155*, 113775. [CrossRef]
398. Grujic-Milanovic, J.; Jacevic, V.; Miloradovic, Z.; Milanovic, S.D.; Jovovic, D.; Ivanov, M.; Karanovic, D.; Vajic, U.-J.; Mihailovic-Stanojevic, N. Resveratrol improved kidney function and structure in malignantly hypertensive rats by restoration of antioxidant capacity and nitric oxide bioavailability. *Biomed. Pharmacother.* **2022**, *154*, 113642. [CrossRef]
399. Nath, J.; Roy, R.; Sathyamoorthy, Y.K.; Paul, S.; Goswami, S.; Chakravarty, H.; Paul, R.; Borah, A. Resveratrol as a therapeutic choice for traumatic brain injury: An insight into its molecular mechanism of action. *Brain Disord.* **2022**, *6*, 100038. [CrossRef]
400. Chowdhury, F.I.; Yasmin, T.; Akter, R.; Islam, N.; Hossain, M.M.; Khan, F.; Aldahrani, A.; Soliman, M.M.; Subhan, N.; Haque, A.; et al. Resveratrol treatment modulates several antioxidant and anti-inflammatory genes expression and ameliorated oxidative stress mediated fibrosis in the kidneys of high-fat diet-fed rats. *Saudi Pharm. J.* **2022**, *30*, 1454–1463. [CrossRef]
401. Van Brummelen, R.; Brummelen, A.C.V. The potential role of resveratrol as supportive antiviral in treating conditions such as COVID-19—A formulator’s perspective. *Biomed. Pharmacother.* **2022**, *148*, 112767. [CrossRef]
402. Kotta, S.; Aldawsari, H.M.; Badr-Eldin, S.M.; Alhakamy, N.A.; Shadab, M. Coconut oil-based resveratrol nanoemulsion: Optimization using response surface methodology, stability assessment and pharmacokinetic evaluation. *Food Chem.* **2021**, *357*, 129721. [CrossRef]
403. Monahan, D.S.; Flaherty, E.; Hameed, A.; Duffy, G.P. Resveratrol significantly improves cell survival in comparison to dexrazoxane and carvedilol in a h9c2 model of doxorubicin induced cardiotoxicity. *Biomed. Pharmacother.* **2021**, *140*, 111702. [CrossRef]
404. Dai, M.; Yuan, D.; Lei, Y.; Li, J.; Ren, Y.; Zhang, Y.; Cang, H.; Gao, W.; Tang, Y. Expression, purification and structural characterization of resveratrol synthase from *Polygonum cuspidatum*. *Protein Expr. Purif.* **2022**, *191*, 106024. [CrossRef] [PubMed]

405. Catalogna, G.; Moraca, F.; D'Antona, L.; Dattilo, V.; Perrotti, G.; Lupia, A.; Costa, G.; Ortuso, F.; Iuliano, R.; Trapasso, F.; et al. Review about the multi-target profile of resveratrol and its implication in the SGK1 inhibition. *Eur. J. Med. Chem.* **2019**, *183*, 111675. [[CrossRef](#)]
406. Bhaskara, V.K.; Mittal, B.; Mysorekar, V.V.; Amaresh, N.; Simal-Gandara, J. Resveratrol, cancer and cancer stem cells: A review on past to future. *Curr. Res. Food Sci.* **2020**, *3*, 284–295. [[CrossRef](#)]
407. Chu, S.-H.; Yang, D.; Wang, Y.-P.; Yang, R.; Qu, L.; Zeng, H.-J. Effect of resveratrol on their repair kidney and brain injuries and its regulation on klotho gene in D-galactose-induced aging mice. *Bioorg. Med. Chem. Lett.* **2021**, *40*, 127913. [[CrossRef](#)] [[PubMed](#)]
408. Huang, H.; Liao, D.; Zhou, G.; Zhu, Z.; Cui, Y.; Pu, R. Antiviral activities of resveratrol against rotavirus in vitro and in vivo. *Phytomedicine* **2020**, *77*, 153230. [[CrossRef](#)] [[PubMed](#)]
409. Liu, S.; Li, Y.; Yi, F.; Liu, Q.; Chen, N.; He, X.; He, C.; Xiao, P. Resveratrol oligomers from *Paeonia suffruticosa* protect mice against cognitive dysfunction by regulation cholinergic, antioxidant and anti-inflammatory pathways. *J. Ethnopharmacol.* **2020**, *260*, 112983. [[CrossRef](#)]
410. Fantacuzzi, M.; Amoroso, R.; Carradori, S.; Filippis, B.D. Resveratrol-based compounds and neurodegeneration: Recent insight in multitarget therapy. *Eur. J. Med. Chem.* **2022**, *233*, 114242. [[CrossRef](#)]
411. Vestergaard, M.; Ingmer, H. Antibacterial and antifungal properties of resveratrol. *Int. J. Antimicrob. Agents* **2019**, *53*, 716–723. [[CrossRef](#)]
412. Roshani, M.; Jafari, A.; Loghman, A.-H.; Sheida, A.H.; Taghavi, T.; Tamehri Zadeh, S.S.; Hamblin, M.R.; Homayounfal, M.; Mirzaei, H. Application of resveratrol in the treatment of gastrointestinal cancer. *Biomed. Pharmacother.* **2022**, *153*, 113274. [[CrossRef](#)] [[PubMed](#)]
413. Agah, S.; Akbari, A.; Sadeghi, E.; Morvaridzadeh, M.; Basharat, Z.; Palmowski, A.; Heshmati, J. Resveratrol supplementation and acute pancreatitis: A comprehensive review. *Biomed. Pharmacother.* **2021**, *137*, 111268. [[CrossRef](#)]
414. Algandaby, M.M.; Al-Sawahli, M.M. Augmentation of anti-proliferative, pro-apoptotic and oxidant profiles induced by piceatannol in human breast carcinoma MCF-7 cells using zein nanostructures. *Biomed. Pharmacother.* **2021**, *138*, 111409. [[CrossRef](#)]
415. Takei, M.; Umeyama, A.; Arihara, S.; Matsumoto, H. Effect of piceatannol in human monocyte-derived dendritic cells in vitro. *J. Pharm. Sci.* **2005**, *94*, 974–982. [[CrossRef](#)] [[PubMed](#)]
416. Kee, H.J.; Park, S.; Kang, W.; Lim, K.S.; Kim, J.H.; Ahn, Y.; Jeong, M.H. Piceatannol attenuates cardiac hypertrophy in an animal model through regulation of the expression and binding of the transcription factor GATA binding factor 6. *FEBS Lett.* **2014**, *588*, 1529–1536. [[CrossRef](#)]
417. Geahlen, R.; McLaughlin, J.L. Piceatannol (3,4,3',5'-tetrahydroxy-trans-stilbene) is a naturally occurring protein-tyrosine kinase inhibitor. *Biochem. Biophys. Res. Commun.* **1989**, *164*, 241–245. [[CrossRef](#)]
418. Messiad, H.; Amira-Guebailia, H.; Houache, O. Reversed phase high performance liquid chromatography used for the physico-chemical and thermodynamic characterization of piceatannol/ β -cyclodextrin complex. *J. Chromatogr. B* **2013**, *926*, 21–27. [[CrossRef](#)]
419. Wang, D.; Zhang, Y.; Zhang, C.; Gao, L.; Li, J. Piceatannol pretreatment alleviates acute cardiac injury via regulating PI3K-Akt-eNOS signaling in H9c2 cells. *Biomed. Pharmacother.* **2019**, *109*, 886–891. [[CrossRef](#)] [[PubMed](#)]
420. Tieyuan, Z.; Ying, Z.; Xinghua, Z.; Huimin, W.; Huagang, L. Piceatannol-mediated JAK2/STAT3 signaling pathway inhibition contributes to the alleviation of oxidative injury and collagen synthesis during pulmonary fibrosis. *Int. Immunopharmacol.* **2022**, *111*, 109107. [[CrossRef](#)] [[PubMed](#)]
421. Kim, D.-H.; Lee, Y.-G.; Park, H.-J.; Lee, J.-A.; Kim, H.J.; Hwang, J.-K.; Choi, J.-M. Piceatannol inhibits effector T cell functions by suppressing TcR signaling. *Int. Immunopharmacol.* **2015**, *25*, 285–292. [[CrossRef](#)]
422. Yang, J.S.; Tongson, J.; Kim, K.-H.; Park, Y. Piceatannol attenuates fat accumulation and oxidative stress in steatosis-induced HepG2 cells. *Curr. Res. Food Sci.* **2020**, *3*, 92–99. [[CrossRef](#)] [[PubMed](#)]
423. Gerszon, J.; Wojtala, M.; Michlewska, S.; Rodacka, A. Piceatannol effectively counteracts glyceraldehyde-3-phosphate dehydrogenase aggregation and nuclear translocation in hippocampal cells. *J. Funct. Food* **2019**, *58*, 180–188. [[CrossRef](#)]
424. Siedleck-Kroplewska, K.; Slebioda, T.; Kmiec, Z. Induction of autophagy, apoptosis and acquisition of resistance in response to piceatannol toxicity in MOLT-4 human leukemia cells. *Toxicol In Vitro* **2019**, *59*, 12–25. [[CrossRef](#)]
425. Yamamoto, T.; Sato, A.; Takai, Y.; Yoshimori, A.; Umehara, M.; Ogino, Y.; Inada, M.; Shimada, N.; Nishida, R.; et al. Effect of piceatannol-rich passion fruit seed extract on human glyoxalase I-mediated cancer cell growth. *Biochem. Biophys. Rep.* **2019**, *20*, 100684. [[CrossRef](#)] [[PubMed](#)]
426. Wen, J.; Lin, H.; Zhao, M.; Tao, L.; Yang, Y.; Xu, X.; Jia, A.; Zhang, J.; Weng, D. Piceatannol attenuates D-Ga1N/LPS-induced hepatotoxicity in mice: Involvement of ER stress, inflammation and oxidative stress. *Int. Immunopharmacol.* **2018**, *64*, 131–139. [[CrossRef](#)]
427. Takasawa, R.; Akahane, H.; Tanaka, H.; Shimada, N.; Yamamoto, T.; Uchida-Maruki, H.; Sai, M.; Yoshimori, A.; Tanuma, S.-I. Piceatannol, a natural *trans*-stilbene compound, inhibits human glyoxalase I. *Bioorg. Med. Chem. Lett.* **2017**, *27*, 1169–1174. [[CrossRef](#)] [[PubMed](#)]
428. Lu, B.; Sun, T.; Li, W.; Sun, X.; Yao, X.; Sun, X. Piceatannol protects ARPE-19 cells against vitamin A dimer-mediated photo-oxidative damage through activation of Nrf2/NQO1 signaling. *J. Funct. Food* **2016**, *26*, 739–749. [[CrossRef](#)]
429. Farrand, L.; Byun, S.; Kim, J.Y.; Im-Aram, A.; Lee, J.; Lim, S.; Lee, K.W.; Suh, J.-Y.; Lee, H.J.; Tsang, B.K. Piceatannol enhances cisplatin sensitivity in ovarian cancer via modulation of p53, X-linked inhibitor of apoptosis protein (XIAP), and mitochondrial fission. *J. Biol. Chem.* **2013**, *288*, 23740–23750. [[CrossRef](#)]

430. Xu, X.; Zhao, M.; Han, Q.; Wang, H.; Zhang, H.; Wang, Y. Effects of piceatannol on the structure and activities of bovine serum albumin: A multi-spectral and molecular modeling studies. *Spectrochim. Acta Part A Mol. Biomol. Spectrosc.* **2020**, *228*, 117706. [CrossRef]
431. Ren, G.; Rimando, A.M.; Mathews, S.T. AMPK activation by pterostilbene contributes to suppression of hepatic gluconeogenic gene expression and glucose production in H4IIE cells. *Biochem. Biophys. Res. Commun.* **2018**, *498*, 640–645. [CrossRef] [PubMed]
432. Rodriguez-Bonilla, P.; Lopez-Nicolas, J.M.; Mendez-Cazorla, L.; Garcia-Carmona, F. Development of a reversed phase high performance liquid chromatography method based on the use of cyclodextrins as mobile phase additives to determine pterostilbene in blueberries. *J. Chromatogr. B* **2011**, *879*, 1091–1097. [CrossRef]
433. Azzolini, M.; Mattarei, A.; Spina, M.L.; Fanin, M.; Chiodarelli, G.; Romio, M.; Zoratti, M.; Paradisi, C.; Biasutto, L. New natural amino acid-bearing prodrugs boost pterostilbene's oral pharmacokinetic and distribution profile. *Eur. J. Pharm. Biopharm.* **2017**, *115*, 149–158. [CrossRef]
434. Xu, D.; Qiao, F.; Xi, P.; Lin, Z.; Jiang, Z.; Romanazzi, G.; Gao, L. Efficacy of pterostilbene suppression of postharvest gray mold in table grapes and potential mechanisms. *Postharvest Biol. Technol.* **2022**, *183*, 111745. [CrossRef]
435. Chen, R.-J.; Lee, Y.-H.; Yeh, Y.-L.; Wu, W.-S.; Ho, C.-T.; Li, C.-Y.; Wang, B.-J.; Wang, Y.-J. Autophagy-inducing effect of pterostilbene: A prospective therapeutic/preventive option for skin diseases. *J. Food Drug Anal.* **2017**, *25*, 125–133. [CrossRef]
436. Zhang, H.; Chen, Y.; Chen, Y.; Ji, S.; Jia, P.; Xu, J.; Li, Y.; Wang, T. Pterostilbene attenuates liver injury and oxidative stress in intrauterine growth-retarded weanling piglets. *Nutrition* **2021**, *81*, 110940. [CrossRef] [PubMed]
437. Ma, K.; Chen, H.; Wang, K.; Han, X.; Zhang, Y.; Wang, H.; Hu, Z.; Wang, J. Pterostilbene inhibits the metastasis of TNBC via suppression of β -catenin-mediated epithelial to mesenchymal transition and stemness. *J. Funct. Food* **2022**, *96*, 105219. [CrossRef]
438. Zalesak, F.; Bon, D.J.-Y.D.; Pospisil, J. Lignans and neolignans: Plant secondary metabolites as a reservoir of biologically active substances. *Pharmacol. Res.* **2019**, *146*, 104284. [CrossRef]
439. Su, J.-H.; Wang, M.-Q.; Zhu, L.-P.; Yang, W.-Q.; Jiang, S.-Q.; Zhao, Z.-X.; Sun, Z.-H. Coumarins and lignans from the roots of *Zanthoxylum nitidum*. *Biochem. Syst. Ecol.* **2022**, *101*, 104399. [CrossRef]
440. Samari, E.; Chashmi, N.A.; Ghanati, F.; Sajedi, R.H.; Gust, A.A.; Haghdoust, F.; Sharifi, M.; Fuss, E. Interactions between second messengers, SA and MAPK6 signaling pathways lead to chitosan-induced lignan production in *Linum album* cell culture. *Ind. Crop. Prod.* **2022**, *177*, 114525. [CrossRef]
441. Tannous, S.; Haykal, T.; Dhaini, J.; Hodroj, M.H.; Rizk, S. The anti-cancer effect of flaxseed lignan derivatives on different acute myeloid leukemia cancer cells. *Biomed. Pharmacother.* **2020**, *132*, 110884. [CrossRef]
442. Torres-Moreno, H.; Lopez-Romero, J.C.; Vidal-Gutierrez, M.; Rodriguez-Martinez, K.; Robles-Zepeda, R.E.; Vilegas, W.; Velarde-Rodriguez, G.M. Seasonality impact on the anti-inflammatory, antiproliferative potential and the lignan composition of *Bursera microphylla*. *Ind. Crop. Prod.* **2022**, *184*, 115095. [CrossRef]
443. Kalinova, J.P.; Maresova, I.; Triska, J.; Vrchotova, N. Distribution of lignans in *Panicum miliaceum*, *Fagopyrum esculentum*, *Fagopyrum tataricum*, and *Amaranthus hypochondriacus*. *J. Food Compos. Anal.* **2022**, *106*, 104283. [CrossRef]
444. Rangkadilok, N.; Pholphana, N.; Mahidol, C.; Wongyai, W.; Saengsooksree, K.; Nookabkaew, S.; Satayavivad, J. Variation of sesamin, sesamolins, and tocopherols in sesame (*Sesamum indicum* L.) seeds and oil products in Thailand. *Food Chem.* **2010**, *122*, 724–730. [CrossRef]
445. Anju, V.T.; Busi, S.; Ranganathan, S.; Ampasala, D.R.; Kumar, S.; Suchiang, K.; Kumavath, R.; Dyavaiah, M. Sesamin and sesamolins rescue *Caenorhabditis elegans* from *pseudomonas aeruginosa* infection through the attenuation of quorum sensing regulated virulence factors. *Microb. Pathog.* **2021**, *155*, 104912. [CrossRef] [PubMed]
446. Dong, Z.-Y.; Wei, L.; Lu, H.-Q.; Zeng, Q.-H.; Meng, F.-C.; Wang, G.-W.; Lan, X.-Z.; Liao, Z.-H.; Chen, M. Pterostilbenes A and B: Two new sesamin-type sesquiligans with antiangiogenic activity from *Pteroccephalus hookeri* (C.B. Clarke) Hoeck. *Fitoterapia* **2021**, *151*, 104886. [CrossRef]
447. Dalibalta, S.; Majdalawieh, A.F.; Manjikian, H. Health benefits of sesamin on cardiovascular disease and its associated risk factors. *Saudi Pharm. J.* **2020**, *28*, 1276–1289. [CrossRef]
448. Hata, N.; Hayashi, Y.; Okazawa, A.; Ono, E.; Satake, H.; Kobayashi, A. Comparison of sesamin contents and CYP81Q1 gene expressions in aboveground vegetative organs between two Japanese sesame (*Sesamum indicum* L.) varieties differing in seed sesamin contents. *Plant Sci.* **2010**, *178*, 510–516. [CrossRef]
449. Dossou, S.S.K.; Xu, F.-T.; Dossa, K.; Zhou, R.; Zhao, Y.-Z.; Wang, L.-H. Antioxidant lignans sesamin and sesamolins in sesame (*Sesamum indicum* L.): A comprehensive review and future prospects. *J. Integr. Agric.* **2022**. [CrossRef]
450. Wang, M.; Liu, P.; Kong, L.; Xu, N.; Lei, H. Promotive effects of sesamin on proliferation and adhesion of intestinal probiotics and its mechanism of action. *Food Chem. Toxicol.* **2021**, *149*, 112049. [CrossRef] [PubMed]
451. Kongtawelert, P.; Wudtiwai, B.; Shwe, T.H.; Pothacharoen, P.; Phitak, T. Inhibition of programmed death ligand 1 (PD-L1) expression in breast cancer cells by sesamin. *Int. Immunopharmacol.* **2020**, *86*, 106759. [CrossRef]
452. Wanachewin, O.; Klangjorhor, J.; Pothacharoen, P.; Phitak, T.; Laohapoonrunsee, A.; Pruksakorn, D.; Kongtawelert, P. The promoting effects of sesamin on osteoblast differentiation of human mesenchymal stem cells. *J. Funct. Foods.* **2015**, *14*, 395–406. [CrossRef]
453. Rashno, M.; Sarkaki, A.; Ghaderi, S.; Khoshnam, S.E. Sesamin: Insights into its protective effects against lead-induced learning and memory deficits in rats. *J. Trace Elem. Med. Biol.* **2022**, *72*, 126993. [CrossRef]

454. Ye, H.; Sun, L.; Li, J.; Wang, Y.; Bai, J.; Wu, L.; Han, Q.; Yang, Z.; Li, L. Sesamin attenuates carrageenan-induced lung inflammation through upregulation of A20 and TAX1BP1 in rats. *Int. Immunopharmacol.* **2020**, *88*, 107009. [[CrossRef](#)] [[PubMed](#)]
455. Majdalawieh, A.F.; Massri, M.; Nasrallah, G.K. A comprehensive review on the anti-cancer properties and mechanisms of action of sesamin, a lignan in sesame seeds (*Sesamum indicum*). *Eur. J. Pharmacol.* **2017**, *815*, 512–521. [[CrossRef](#)] [[PubMed](#)]
456. Ghaderi, S.; Rashno, M.; Nesari, A.; Khoshnam, S.E.; Sarkaki, A.; Khorsandi, L.; Farbood, Y.; Rashidi, K. Sesamin alleviates diabetes-associated behavioral deficits in rats: The role of inflammatory and neurotrophic factors. *Int. Immunopharmacol.* **2021**, *92*, 107356. [[CrossRef](#)]
457. Phitak, T.; Potacharoen, P.; Settakorn, J.; Poompimol, W.; Catterson, B.; Kongtawelert, P. Chondroprotective and anti-inflammatory effects of sesamin. *Phytochemistry* **2012**, *80*, 77–88. [[CrossRef](#)] [[PubMed](#)]
458. Ju, Y.-I.; Yang, L.; Yue, X.-F.; He, R.; Deng, S.-L.; Yang, X.; Liu, X.; Fang, Y.-L. The condensed tannin chemistry and astringency properties of fifteen *Vitis davidii* Foex grapes and wines. *Food Chem.* **2021**, *11*, 100125. [[CrossRef](#)]
459. Han, S.; Kong, X.; Xia, S.; Jia, B.; Dong, M.; Gan, L. UV light-driven controlled photodegradation of condensed tannins from larch bark. *Ind. Crop. Prod.* **2022**, *177*, 114403. [[CrossRef](#)]
460. Abhijit, S.; Tripathi, S.J.; Rao, B.S.S.; Devi, S.A. Grape seed proanthocyanidin extract and swimming training enhances neuronal number in dorso-medial prefrontal cortex in middle-aged male rats by alleviating oxidative stress. *J. Funct. Food* **2020**, *64*, 103693. [[CrossRef](#)]
461. Sangiovanni, E.; Piazza, S.; Vrhovsek, U.; Fumagalli, M.; Khalilpour, S.; Masuero, D.; Lorenzo, C.D.; Colombo, L.; Mattivi, F.; Fabiani, E.D.; et al. A bio-guided approach for the development of a chestnut-based proanthocyanidin-enriched nutraceutical with potential anti-gastritis properties. *Pharmacol. Res.* **2018**, *134*, 145–155. [[CrossRef](#)]
462. Yu, G.-H.; Fang, Y. Resveratrol attenuates atherosclerotic endothelial injury through the Pin1/Notch1 pathway. *Toxicol. Appl. Pharmacol.* **2022**, *446*, 116047. [[CrossRef](#)]
463. Tao, W.; Pan, H.; Jiang, H.; Wang, M.; Ye, X.; Chen, S. Extraction and identification of proanthocyanidins from the leaves of persimmon and loquat. *Food Chem.* **2022**, *372*, 130780. [[CrossRef](#)] [[PubMed](#)]
464. Zhang, X.; Song, X.; Hu, X.; Chen, F.; Ma, C. Health benefits of proanthocyanidins linking with gastrointestinal modulation: An updated review. *Food Chem.* **2023**, *4040*, 134596. [[CrossRef](#)]
465. Yang, J.; Chen, J.; Hao, Y.; Liu, Y. Identification of the DPPH radical scavenging reaction adducts of ferulic acid and sinapic acid and their structure-antioxidant activity relationship. *LWT* **2021**, *146*, 111411. [[CrossRef](#)]
466. Rauf, A.; Imran, M.; Abu-Izneid, T.; Ul-Haq, I.; Patel, S.; Pan, X.; Naz, S.; Silva, A.S.; Saeed, F.; Suleria, H.A.R. Proanthocyanidins: A comprehensive review. *Biomed. Pharmacother.* **2019**, *116*, 108999. [[CrossRef](#)] [[PubMed](#)]
467. Rippin; Sharma, A.K.; Beniwal, V. Biosynthesis and medicinal applications of proanthocyanidins: A recent update. *Biocatal. Agric. Biotechnol.* **2022**, *45*, 102500. [[CrossRef](#)]
468. Morimoto, H.; Hatanaka, T.; Narusaka, M.; Narusaka, Y. Molecular investigation of proanthocyanidin from *Alpinia zerumbet* against the influenza A virus. *Fitoterapia* **2022**, *158*, 105141. [[CrossRef](#)] [[PubMed](#)]
469. Shen, W.; Li, W.; Shao, Y.; Zeng, J. Proanthocyanidin delays litchi peel browning by inhibiting ethylene biosynthesis, respiratory metabolism, and phenol oxidase activities. *Sci. Hortic.* **2023**, *309*, 111677. [[CrossRef](#)]
470. Rohr, G.E.; Meier, B.; Sticher, O. Analysis of procyanidins. *Stud. Nat. Prod. Chem.* **2000**, *21*, 497–570. [[CrossRef](#)]
471. Yang, H.; Tuo, X.; Wang, L.; Tundis, R.; Portillo, M.P.; Simal-Gandara, J.; Yu, Y.; Zou, L.; Xiao, J.; Deng, J. Bioactive procyanidins from dietary sources: The relationship between bioactivity and polymerization degree. *Trends Food Sci. Technol.* **2021**, *111*, 114–127. [[CrossRef](#)]
472. Zhou, P.; Zhang, L.; Li, W.; Zhang, S.; Luo, L.; Wang, J.; Sun, B. In vitro evaluation of the anti-digestion and antioxidant effects of grape seed procyanidins according to their degrees of polymerization. *J. Funct. Food* **2018**, *49*, 85–95. [[CrossRef](#)]
473. Na, W.; Ma, B.; Shi, S.; Chen, Y.; Zhang, H.; Zhan, Y.; An, H. Procyanidin B1, a novel and specific inhibitor of Kv10.1 channel, suppresses the evolution of hepatoma. *Biochem. Pharmacol.* **2020**, *178*, 114089. [[CrossRef](#)]
474. Liu, Y.; Sun, R.; Li, X.-P.; Wu, L.; Chen, H.; Shen, S.; Li, Y.; Wei, Y.; Deng, G. Procyanidins and its metabolites by gut microbiome improves insulin resistance in gestational diabetes mellitus mice model via regulating NF-KB and NLRP3 inflammasome pathway. *Biomed. Pharmacother.* **2022**, *151*, 113078. [[CrossRef](#)]
475. Chen, R.; Hu, T.; Wang, M.; Hu, Y.; Chen, S.; Wei, Q.; Yin, X.; Xie, T. Functional characterization of key polyketide synthases by integrated metabolome and transcriptome analysis on curcuminoid biosynthesis in *Curcuma wenyujin*. *Syn. Sys. Biotechnol.* **2022**, *7*, 849–861. [[CrossRef](#)] [[PubMed](#)]
476. Wu, J.-N.; Tu, Q.-K.; Xiang, X.-L.; Shi, Q.-X.; Chen, G.-Y.; Dai, M.-X.; Zhang, L.-J.; Yang, M.; Song, C.-W.; Huang, R.-Z.; et al. Changes in curcuminoids between crude and processed turmeric based on UPLC-QTOF-MS/MS combining with multivariate statistical analysis. *Chin. J. Anal. Chem.* **2022**, *50*, 100108. [[CrossRef](#)]
477. El-Hawaz, R.; Tharayil, N.; Bridges, W.; Adelberg, J. Mineral nutrition of *Curcuma longa* L. in bioreactors affects subsequent development of curcuminoids following transfer to the greenhouse. *Ind. Crop. Prod.* **2016**, *83*, 186–193. [[CrossRef](#)]
478. Ramirez-Ahumada, M.D.; Timmermann, B.N.; Gang, D.R. Biosynthesis of curcuminoids and gingerols in turmeric (*Curcuma longa*) and ginger (*Zingiber officinale*). Identification of curcuminoid synthase and hydroxycinnamoyl-CoA thioesterases. *Phytochemistry* **2006**, *67*, 2017–2029. [[CrossRef](#)]
479. Aarthi, S.; Suresh, J.; Leela, N.K.; Prasath, D. Multi environment testing reveals genotype-environment interaction for curcuminoids in turmeric (*Curcuma longa* L.). *Ind. Crop. Prod.* **2020**, *145*, 112090. [[CrossRef](#)]

480. Abouheif, S.A.; Sallam, S.M.; El Shoafy, S.M.; Kassem, F.F.; Shawky, E. A green extraction approach using natural deep eutectic solvents enhances the in-vivo bioavailability of curcuminoids from turmeric extracts. *Ind. Crop. Prod.* **2022**, *189*, 115790. [[CrossRef](#)]
481. Wang, H.; Luo, J.; Zhang, Y.; He, D.; Jiang, R.; Xie, X.; Yang, Q.; Li, K.; Xie, J.; Zhang, J. Phospholipid/hydroxypropyl- β -cyclodextrin supramolecular complexes are promising candidates for efficient oral delivery of curcuminoids. *Int. J. Pharm.* **2020**, *582*, 119301. [[CrossRef](#)]
482. Ahmed, T.; Gilani, A.-H. A comparative study of curcuminoids to measure their effect on inflammatory and apoptotic gene expression in an A β plus ibotenic acid-infused rat model of Alzheimer's disease. *Brain Res.* **2011**, *1400*, 1–18. [[CrossRef](#)]
483. Monton, C.; Charoenchai, L.; Sukasaeree, J.; Sueree, L. Quantitation of curcuminoid contents, dissolution profile, and volatile oil content of turmeric capsules produced at some secondary government hospitals. *J. Food Drug Anal.* **2016**, *24*, 493–499. [[CrossRef](#)]
484. Solani, L.N.; Nelson, G.L.; Ronayne, C.T.; Lueth, E.A.; Foxley, M.A.; Jonnalagadda, S.K.; Gurrapu, S.; Mereddy, V.R. Synthesis, in vitro, and in vivo evaluation of novel functionalized quaternary ammonium curcuminoids as potential anti-cancer agents. *Bioorg. Med. Chem. Lett.* **2015**, *25*, 5777–5780. [[CrossRef](#)] [[PubMed](#)]
485. Zhou, J.-L.; Zheng, J.-Y.; Cheng, X.-Q.; Xin, G.-Z.; Wang, S.-L.; Xie, T. Chemical markers' knockout coupled with UHPLC-HRMS-based metabolomics reveals anti-cancer integration effect of the curcuminoids of turmeric (*Curcuma longa* L.) on lung cancer cell line. *J. Pharm. Biomed. Anal.* **2019**, *175*, 112738. [[CrossRef](#)] [[PubMed](#)]
486. Wei, M.-M.; Zhao, S.-J.; Dong, X.-M.; Wang, Y.-J.; Fang, C.; Wu, P.; Song, G.-Q.; Gao, J.-N.; Huang, Z.-H.; Xie, T.; et al. A combination index and glycoproteomics-based approach revealed synergistic anticancer effects of curcuminoids of turmeric against prostate cancer PC3 cells. *J. Ethnopharmacol.* **2021**, *267*, 113467. [[CrossRef](#)] [[PubMed](#)]
487. Feng, Y.; Li, B.; Yang, L.; Liu, Y. Co-amorphous delivery systems based on curcumin and hydroxycinnamic acids: Stabilization, solubilization, and controlled release. *LWT* **2022**, *170*, 114091. [[CrossRef](#)]
488. Vafaiepour, Z.; Razavi, B.M.; Hosseinzadeh, H. Effects of turmeric (*Curcuma longa*) and its constituent (Curcumin) on the metabolic syndrome: An updated review. *J. Integr. Med.* **2022**, *20*, 193–203. [[CrossRef](#)]
489. Aguiar, D.D.; Gonzaga, A.C.R.; Teofilo, A.L.H.; Miranda, F.A.; Perez, A.D.C.; Duarte, I.D.G.; Romero, T.R.L. Curcumin induces peripheral antinociception by opioidergic and cannabinoidergic mechanism: Pharmacological evidence. *Life Sci.* **2022**, *293*, 120279. [[CrossRef](#)]
490. Fu, Y.-S.; Chen, T.-H.; Weng, L.; Huang, L.; Lai, D.; Weng, C.-F. Pharmacological properties and underlying mechanisms of curcumin and prospects in medicinal potential. *Biomed. Pharmacother.* **2021**, *141*, 111888. [[CrossRef](#)]
491. Yixuan, L.; Qaria, M.A.; Sivasamy, S.; Jianzhong, S.; Daochen, Z. Curcumin production and bioavailability: A comprehensive review of curcumin extraction, synthesis, biotransformation and delivery systems. *Ind. Crop. Prod.* **2021**, *172*, 114050. [[CrossRef](#)]
492. Wang, Y.; Xu, S.; Han, C.; Wang, L.; Zheng, Q.; Wang, S.; Huang, Y.; Wei, S.; Qin, Q. Curcumin inhibits Singapore grouper iridovirus infection through multiple antiviral mechanisms. *Aquaculture* **2023**, *562*, 738870. [[CrossRef](#)]
493. Liu, Z.; Shi, B.; Wang, Y.; Xu, Q.; Gao, H.; Ma, J.; Jiang, X.; Yu, W. Curcumin alleviates aristolochic acid nephropathy based on SIRT1/Brf2/HO-1 signaling pathway. *Toxicology* **2022**, *479*, 153297. [[CrossRef](#)] [[PubMed](#)]
494. Lu, K.-H.; Lu, P.W.-A.; Lin, C.-W.; Yang, S.-F. Curcumin in human osteosarcoma: From analogs to carriers. *Drug Discov. Today* **2023**, *28*, 103437. [[CrossRef](#)]
495. Ming, T.; Tao, Q.; Tang, S.; Zhao, H.; Yang, H.; Liu, M.; Ren, S.; Xu, H. Curcumin: An epigenetic regulator and its application in cancer. *Biomed. Pharmacother.* **2022**, *156*, 113956. [[CrossRef](#)] [[PubMed](#)]
496. Priyadarsini, K.I. The chemistry of curcumin: From extraction to therapeutic agent. *Molecules* **2014**, *19*, 20091–20112. [[CrossRef](#)]
497. Zagury, Y.; David, S.; Edelman, R.; Brill, R.H.; Livney, Y.D. Sugar beet pectin as a natural carrier for curcumin, a water-insoluble bioactive for food and beverage enrichment: Formation and characterization. *Innov. Food Sci. Emerg. Technol.* **2021**, *74*, 102858. [[CrossRef](#)]
498. Ezati, M.; Ghavamipour, F.; Adibi, H.; Pouraghajan, K.; Arab, S.S.; Sajedi, R.H.; Khodarahmi, R. Design, synthesis, spectroscopic characterizations, antidiabetic, in silico and kinetic evaluation of novel curcumin-fused aldohexoses. *Spectrochim. Acta Part A Mol. Biomol. Spectrosc.* **2023**, *285*, 121806. [[CrossRef](#)] [[PubMed](#)]
499. Elanthendral, G.; Shobana, N.; Meena, R.; Prakash, P.; Samrot, A.V. Utilizing pharmacological properties of polyphenolic curcumin in nanotechnology. *Biocatal. Agric. Biotechnol.* **2021**, *38*, 102212. [[CrossRef](#)]
500. Jena, A.B.; Dash, U.C.; Duttaroy, A.K. An in silico investigation on the interactions of curcumin and epigallocatechin-3-gallate with NLRP3 inflammasome complex. *Biomed. Pharmacother.* **2022**, *156*, 113890. [[CrossRef](#)]
501. Sheikholeslami, M.A.; Parvardeh, S.; Ghafghazi, S.; Sabetkasaei, M. Curcumin attenuates morphine dependence by modulating μ -opioid receptors and glial cell-activated neuroinflammation in rat. *Neuropeptides* **2022**, *98*, 102318. [[CrossRef](#)]
502. Bhavani, T.; Gautam, A. Expression analysis of synaptic plasticity genes in curcumin-treated amnesic mice model. *Mater. Today Proc.* **2023**, *73*, 307–311. [[CrossRef](#)]
503. Xie, L.; Ji, X.; Zhang, Q.; Wei, Y. Curcumin combined with photodynamic therapy, promising therapies for the treatment of cancer. *Biomed. Pharmacother.* **2022**, *146*, 112567. [[CrossRef](#)] [[PubMed](#)]
504. Hashemi, M.; Mirzaei, S.; Barati, M.; Hejazi, E.S.; Kakavand, A.; Entezari, M.; Salimimoghadam, S.; Kalbasi, A.; Rashidi, M.; Taheriazam, A.; et al. Curcumin in the treatment of urological cancers: Therapeutic targets, challenges and prospects. *Life Sci.* **2022**, *309*, 120984. [[CrossRef](#)]
505. Mahjoob, M.; Stochaj, U. Curcumin nanoformulations to combat aging-related diseases. *Ageing Res. Rev.* **2021**, *69*, 101364. [[CrossRef](#)] [[PubMed](#)]

506. Chen, Y.; Wang, J.; Jing, Z.; Ordovas, J.M.; Wang, J.; Shen, L. Anti-fatigue and anti-oxidant effects of curcumin supplementation in exhaustive swimming mice via Nrf2/Keap1 signal pathway. *Curr. Res. Food Sci.* **2022**, *5*, 1148–1157. [[CrossRef](#)] [[PubMed](#)]
507. Sahebkar, A.; Sathyapalan, T.; Guest, P.C.; Barreto, G.E. Identification of difluorinated curcumin molecular targets linked to traumatic brain injury pathophysiology. *Biomed. Pharmacother.* **2022**, *148*, 112770. [[CrossRef](#)]
508. Huang, W.-T.; Larsson, M.; Lee, Y.-C.; Liu, D.-M.; Chiou, G.-Y. Dual drug-loaded biofunctionalized amphiphilic chitosan nanoparticles: Enhanced synergy between cisplatin and demethoxycurcumin against multidrug-resistant stem-like lung cancer cells. *Eur. J. Pharm. Biopharm.* **2016**, *109*, 165–173. [[CrossRef](#)]
509. Gullaiya, S.; Nagar, A.; Dubey, V.; Singh, V.; Kumar, A.; Tiwari, P.; Agrawal, S.S. Modulation of disease related immune events by demethoxycurcumin against autoimmune arthritis in rats. *Biomed. Aging Pathol.* **2013**, *3*, 7–13. [[CrossRef](#)]
510. Yodkeeree, S.; Ampasavate, C.; Sung, B.; Aggarwal, B.B.; Limtrakul, P. Demethoxycurcumin suppresses migration and invasion of MDA-MB-231 human breast cancer cell line. *Eur. J. Pharmacol.* **2010**, *627*, 8–15. [[CrossRef](#)]
511. Kumar, R.; Lal, N.; Nemaish, V.; Luthra, P.M. Demethoxycurcumin mediated targeting of MnSOD leading to activation of apoptotic pathway and inhibition of Akt/NF-KB survival signalling in human glioma U87 MG cells. *Toxicol. Appl. Pharmacol.* **2018**, *345*, 75–93. [[CrossRef](#)]
512. Lin, H.-Y.; Lin, J.-N.; Ma, J.-W.; Yang, N.-S.; Ho, C.-T.; Kuo, S.-C.; Way, T.-D. Demethoxycurcumin induces autophagic and apoptotic responses on breast cancer cells in photodynamic therapy. *J. Funct. Food* **2015**, *12*, 439–449. [[CrossRef](#)]
513. Zhang, L.; Wu, C.; Zhao, S.; Yuan, D.; Lian, G.; Wang, X.; Wang, L.; Yang, J. Demethoxycurcumin, a natural derivative of curcumin attenuates LPS-induced pro-inflammatory responses through down-regulation of intracellular ROS-related MAPK/NF-KB signaling pathways in N9 microglia induced by lipopolysaccharide. *Int. Immunopharmacol.* **2010**, *10*, 331–338. [[CrossRef](#)]
514. Lu, B.; Chen, X.; Chen, H.; Li, Q.; Li, H.; Xu, Y.; Li, Y.; Shen, X.; Jiang, R. Demethoxycurcumin mitigates inflammatory responses in lumbar disc herniation via MAPK and NF-KB pathways in vivo and in vitro. *Int. Immunopharmacol.* **2022**, *108*, 108914. [[CrossRef](#)] [[PubMed](#)]
515. Mehanny, M.; Hathout, R.M.; Geneidi, A.S.; Mansour, S. Bisdemethoxycurcumin loaded polymeric mixed micelles as potential anti-cancer remedy: Preparation, optimization and cytotoxic evaluation in a HepG-2 cell model. *J. Mol. Liq.* **2016**, *214*, 162–170. [[CrossRef](#)]
516. Paul, M.; Manikanta, K.; Hemshekhar, M.; Sundaram, M.S.; Naveen, S.; Ramesh, T.N.; Kemparaju, K.; Girish, K.S. Bisdemethoxycurcumin promotes apoptosis in human platelets via activation of ERK signaling pathway. *Toxicol. In Vitro* **2020**, *63*, 104743. [[CrossRef](#)]
517. Liu, J.; Wang, Q.; Omari-Siaw, E.; Adu-Frimpong, M.; Liu, J.; Xu, X.; Yu, J. Enhanced oral bioavailability of bisdemethoxycurcumin-loaded self-microemulsifying drug delivery system; Formulation design, in vitro and in vivo evaluation. *Int. J. Pharm.* **2020**, *590*, 119887. [[CrossRef](#)] [[PubMed](#)]
518. Zhang, J.; Han, H.; Zhang, L.; Wang, T. Dietary bisdemethoxycurcumin supplementation attenuates lipopolysaccharide-induced damages on intestinal redox potential and redox status of broilers. *Poult. Sci.* **2021**, *100*, 101061. [[CrossRef](#)]
519. Fu, M.; Fu, S.; Ni, S.; Wang, D.; Hong, T. Inhibitory effects of bisdemethoxycurcumin on mast cell-mediated allergic diseases. *Int. Immunopharmacol.* **2018**, *65*, 182–189. [[CrossRef](#)]
520. Mahattanadul, S.; Nakamura, T.; Panichayupakaranant, P.; Phdoongsombut, N.; Tungsinmunkong, K.; Bouking, P. Comparative antiulcer effect of bisdemethoxycurcumin and curcumin in a gastric ulcer model system. *Phytomedicine* **2009**, *16*, 342–351. [[CrossRef](#)]
521. Ponnusamy, S.; Zinjarde, S.; Bhargava, S.; Rajamohanam, P.R.; RaviKumar, A. Discovering bisdemethoxycurcumin from *Curcuma longa* rhizome as a potent small molecule inhibitor of human pancreatic α -amylase, a target for type-2 diabetes. *Food Chem.* **2012**, *135*, 2638–2642. [[CrossRef](#)]

Disclaimer/Publisher’s Note: The statements, opinions and data contained in all publications are solely those of the individual author(s) and contributor(s) and not of MDPI and/or the editor(s). MDPI and/or the editor(s) disclaim responsibility for any injury to people or property resulting from any ideas, methods, instructions or products referred to in the content.

Review

The Role of Natural and Semi-Synthetic Compounds in Ovarian Cancer: Updates on Mechanisms of Action, Current Trends and Perspectives

Md. Rezaul Islam ¹, Md. Mominur Rahman ¹, Puja Sutro Dhar ¹, Feana Tasmim Nowrin ¹, Nasrin Sultana ¹, Muniya Akter ¹, Abdur Rauf ^{2,*}, Anees Ahmed Khalil ³, Alessandra Gianoncelli ⁴ and Giovanni Ribaldo ^{4,*}

¹ Department of Pharmacy, Faculty of Allied Health Sciences, Daffodil International University, Dhaka 1207, Bangladesh

² Department of Chemistry, University of Swabi, Anbar 23430, Pakistan

³ University Institute of Diet and Nutritional Sciences, Faculty of Allied Health Sciences, The University of Lahore, Lahore 54000, Pakistan

⁴ Dipartimento di Medicina Molecolare e Traslationale, Università degli Studi di Brescia, Viale Europa 11, 25123 Brescia, Italy

* Correspondence: abdurrauf@uoswabi.edu.pk (A.R.); giovanni.ribaldo@unibs.it (G.R.)

Abstract: Ovarian cancer represents a major health concern for the female population: there is no obvious cause, it is frequently misdiagnosed, and it is characterized by a poor prognosis. Additionally, patients are inclined to recurrences because of metastasis and poor treatment tolerance. Combining innovative therapeutic techniques with established approaches can aid in improving treatment outcomes. Because of their multi-target actions, long application history, and widespread availability, natural compounds have particular advantages in this connection. Thus, effective therapeutic alternatives with improved patient tolerance hopefully can be identified within the world of natural and nature-derived products. Moreover, natural compounds are generally perceived to have more limited adverse effects on healthy cells or tissues, suggesting their potential role as valid treatment alternatives. In general, the anticancer mechanisms of such molecules are connected to the reduction of cell proliferation and metastasis, autophagy stimulation and improved response to chemotherapeutics. This review aims at discussing the mechanistic insights and possible targets of natural compounds against ovarian cancer, from the perspective of medicinal chemists. In addition, an overview of the pharmacology of natural products studied to date for their potential application towards ovarian cancer models is presented. The chemical aspects as well as available bioactivity data are discussed and commented on, with particular attention to the underlying molecular mechanism(s).

Keywords: ovarian cancer; natural compounds; semi-synthetic compounds; medicinal chemistry; anti-metastasis; apoptosis

Citation: Islam, M.R.; Rahman, M.M.; Dhar, P.S.; Nowrin, F.T.; Sultana, N.; Akter, M.; Rauf, A.; Khalil, A.A.; Gianoncelli, A.; Ribaldo, G. The Role of Natural and Semi-Synthetic Compounds in Ovarian Cancer: Updates on Mechanisms of Action, Current Trends and Perspectives. *Molecules* **2023**, *28*, 2070. <https://doi.org/10.3390/molecules28052070>

Academic Editor: Ionel Mangalagiu

Received: 31 January 2023

Revised: 16 February 2023

Accepted: 21 February 2023

Published: 22 February 2023



Copyright: © 2023 by the authors. Licensee MDPI, Basel, Switzerland. This article is an open access article distributed under the terms and conditions of the Creative Commons Attribution (CC BY) license (<https://creativecommons.org/licenses/by/4.0/>).

1. Introduction

Among gynecologic cancers, ovarian cancer is categorized as the third most prevalent cancer after cervical and uterine cancer, having high mortality rates in female subjects [1]. Epithelial ovarian malignancies, which include serous, mucinous, endometrioid, metastatic and clear cell carcinoma, represent the majority of ovarian diseases [2]. Intracavitary implantation, hematic and lymphatic pathways can all be exploited to transmit epithelial ovarian cancer, and the main route of spread is intraperitoneal metastases [3,4]. In the initial phases of the disease, patients are commonly asymptomatic, and 70% of patients are diagnosed at a later stage [5].

Nowadays, cytoreductive surgeries followed by platinum/paclitaxel-based chemotherapy are being considered as first-line approaches. Patients who receive this treatment, on the other hand, are prone to develop chemotherapeutic resistance and cumulative adverse

effects, including nephrotoxicity [6]. To date, treatment of ovarian cancer is considered among the most challenging tasks in the field of oncology owing to its low survival rate (5 years < 40%) [7]. Consequently, novel drugs and alternative therapeutics for treatment or prevention of progression of ovarian cancer are needed.

Due to the adverse side effects associated with standard anticancer treatment, plant-derived products, alone and/or in combination with conventional anticancer agents, are being explored nowadays as adjuvant treatment to minimize adverse side effects [8].

Recently, several ovarian cancer prevention and early detection strategies have not shown expected or satisfactory results, which is partially attributable to the disease's heterogeneity [9]. Increased DNA lesion repair, aberrant intracellular signal transmission, and drug metabolic inactivation are all promoted by genetic changes. Complete remission has instead been achieved by combining surgical intervention with genetic analysis [10]. In this context, the PARP inhibitor olaparib is administered to patients with *BRCA1* or *BRCA2* mutations [11]. It is also common practice to treat patients who have experienced a relapse after receiving platinum-based chemotherapy. Due to rapid tumor development and chemotherapy resistance, the period between treatments decreases progressively after a relapse.

As anticipated, to increase the survival quality of patients undergoing chemotherapeutic treatment, novel approaches are required. Botanical components are naturally occurring antioxidants or alkaloids with a long history in ethnopharmacology and characterized by the potential of being employed as therapeutic resources [12–14]. Natural products derived from plants are commonly thought of as nutritional supplements [15], meanwhile, plant-based constituents and products may be used as adjuvant therapies against ovarian cancer and for reduction of metastatic tumor size, and some examples have been reported in the literature.

With this review, we aim at highlighting the beneficial impacts of natural products, as single molecules and in combination, on ovarian cancer. Several scientific databases (Google Scholar, PubMed, Embase, etc.) were searched for records published from 2000 onwards by using the following keywords: ovarian cancer, etiology, risk of ovarian cancer incidence, natural products and ovarian cancer, ovarian cancer progression and chemopreventive potential of natural compounds [16–27]. The review is organized into sections covering etiology, risk factors and molecular mechanisms of ovarian cancer development. Then, cellular events and biochemical pathways targeted by natural compounds are discussed. Eventually, a focus on some relevant and widely studied molecules are presented.

2. Etiology of Ovarian Cancer

Each ovary is approximately 3.5 cm long, 2 cm wide and 1 cm thick. It has an oval, solid structure that is about the size of an almond. The ovaries are located in ovarian fossae, which are small depressions on either side of the uterus in the lateral walls of the pelvic cavity. Characterizing the variation in the ovarian surface epithelium (OSE) in accordance with pre-cancer lesions (intraepithelial neoplasia) is quite difficult owing to the intra-abdominal localization of the ovaries (Figure 1) and prevalence of disease [28]. Therefore, knowledge regarding earlier genetic and molecular events that are linked with ovarian cancer is still very limited. As a result, the causes of ovarian cancer are not very clear, and this is particularly true for epithelial ovarian cancer. The alterations in the OSE are a contributing factor in ovarian cancer, as shown by the following evidence: (1) the OCP, a widely used strategy of ovarian cancer prevention, triggers cancer-preventive molecular pathways in the OSE [29]; (2) evidence of dysplastic, premalignant alterations in the OSE can be detected using conventional techniques [30]; (3) colocalization of dysplastic specimens in the OSE of ovaries with loss of cancer-suppressing action or overexpression of cyclooxygenase 2 [31]; and (4) evolution from a nonmalignant to a cancerous OSE in a some early ovarian malignancies [32].

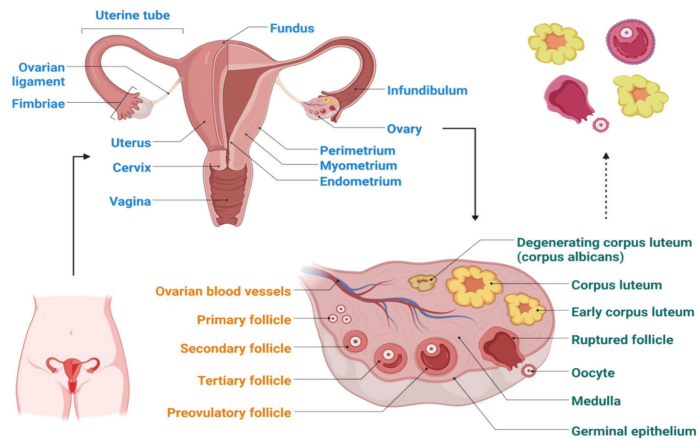


Figure 1. Schematic representation of the ovary structure.

Another hypothesis postulates that the cells that develop in the fallopian tube serve as the foundation for ovarian cancer growth [33]. This hypothesis, while it is still only a theory, is supported by the fact that the majority of ovarian cancer cells show histological features similar to those of the fallopian tube itself. Additionally, an abnormally high incidence of histologic and molecular markers linked to dysplasia at the fimbriated end of the fallopian tube is observed in preventive oophorectomy cases from high-risk women [34]. The probability of fallopian tube cancer development is noticeably increased in women who have a *BRCA*-related inherent ovarian disease risk. Furthermore, a thorough examination of the fallopian tubes in women with serous pelvic cancer has revealed a high likelihood of endosalpinx inclusion or concurrent tubal carcinomas. Similarly, p53 changes can be retrieved in both the pelvic and fallopian tube lesions, which suggests the possible hereditary character of the disease [35,36]. Additionally, p53 markers have been found in fallopian tubes removed for non-carcinogenic causes in women within a population bearing risk factors of ovarian cancer [37]. The fimbriated end of the fallopian chamber may evolve toward neoplasia when dysplastic cells shed from the OSE, or even when taking into consideration ovarian stromal materials provided during ovulation [38].

3. Risk Factors for Ovarian Cancer

Because of the rate of ovulatory cycles, it has been demonstrated that women who have early menarche (age < 12) and late menopause (age > 50) have a greater risk of ovarian cancer. In particular, early menarche and late menopause enhance the possibility of disease development by 1.1 to 1.5 times and 1.4–4.6 times, respectively. Breastfeeding, pregnancy, and the usage of ovulation-restricting oral contraceptives also all represent risk factors [39,40]. Endometriosis and ovarian cancer have been linked in epidemiological research, however the mechanism is uncertain [41]. Family history for ovarian cancer is known to be one of the most significant risk factors. *BRCA1* and *BRCA2* mutations have been associated with a high risk of ovarian and breast cancer development [39]. More specifically, women having mutations in *BRCA1* and *BRCA2* are thought to have elevated risk for the development of ovarian cancer [42]. Located on chromosome 17q21, *BRCA1* is an onco-suppressor gene, while *BRCA2* is located on chromosome 13q [39]. The codon is prematurely terminated when these genes are removed or inserted, resulting in a shortened protein. The mutation of such genes promotes uncontrolled cell proliferation because they play a role in chromatin remodeling. More specifically, *BRCA1* and *BRCA2* mutations have been linked to an increased risk of developing ovarian cancer by 50% and 20%, respectively [40,42–51].

4. Ovarian Cancer Carcinogenesis and Progression: Molecular Mechanisms

The stages of cancer progression are demonstrated in Figure 2: a higher number, such as stage 4, denotes that the cancer has progressed more widely. Several hypotheses have been formulated to explain the mechanisms underlying disease onset and progression.

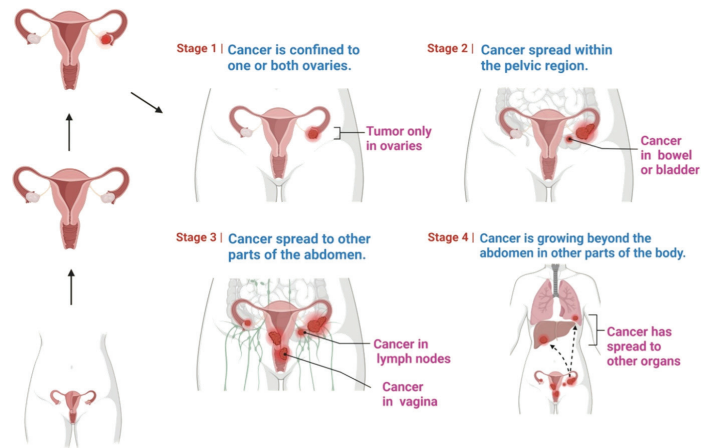


Figure 2. Stages of ovarian cancer, which vary from stage 1 to stage 4.

In this context, the cancer stem cell hypothesis deserves particular attention as it has been introduced to explain many cancer complications, resulting in drug resistance, metastases, and recurrence, that are related to disease progression. Cancer stem cells are a small population of tumor cells that contribute to the formation of phenotypically diverse tumors. Their hallmarks have been recently demonstrated to be targeted also by natural compounds to combat cell invasion and recurrence [52–54].

Several other hypotheses have been proposed to clarify the mechanism of ovarian cancer progression. Repeated ovulation, when associated with repetitive ovarian epithelial damage and repair, raises the risk of DNA damage and carcinogenesis, according to the so-called ovulation theory [55]. As a result, having a higher number of ovulations raises the risk of ovarian cancer. In rats, hyper-ovulation raises the chance of ovarian cancer progression substantially. According to experimental studies, ovulation may produce carcinogenesis by stimulating multiple cellular actions [56]. Therefore, incessant ovulation increases the risk of mutagenicity due to transformation of injured OSE cells. Bradykinin and other vasoactive mediators, as well as leukocytes and prostaglandins, are stimulated during ovulation [57].

The gonadotrophin hypothesis suggests that increased levels of gonadotrophins drive epithelial neoplastic change either straightforwardly or by implication through steroidogenesis [58]. On the other hand, it has been noted that progestins can induce apoptotic pathways and decrease the chance of growth alterations, while estrogens can promote the development of the disease [59]. In this context, carcinogenesis may also likewise connected to the use of contraceptive therapeutics [60].

Epithelial ovarian cancer cells can relocate to the peritoneal cavity, bringing about ascites and, potentially, immunosuppression that favors cancer development. Lysophosphatidic acid inhibits TNF receptor apoptosis-inducing ligand (TRAIL)-induced apoptosis by activating the PI3K/Akt pathway [61]. In ascites and plasma samples from epithelial ovarian cancer specimens, a recent report found a huge change in cytokines, demonstrating in particular a unique variety in ascites cytokines [62]. Additionally, it has been noted that protein kinase C (PKC), Akt, lysophosphatidyl acid (LPA), and interleukin-6 (IL-6) are increased in ovarian cancer [63]. According to another report, ovarian cancer cells use the Akt/nuclear factor kappa B (NF- κ B) pathway to produce IL-6, IL-8, and VEGF [64].

PKC likewise plays a critical role in the regulation of various pathways. More specifically, in ovarian cancer patients, PKC dysregulation has been related to carcinogenesis and resistance to treatments [65]. The abovementioned inflammatory agents and pathways result in increased ovarian cancer-related inflammation. Generally, inflammation then induces the production of various toxic oxidants that cause direct harm to DNA, proteins, and lipids, enhancing carcinogenesis [66]. In addition to this, inflammation is linked to increased cellular proliferation. Excessive cellular divisions then result in DNA repair replication errors, causing increasing mutagenesis [67]. Ovarian cancer cells release several inflammation mediators, including cytokines and interleukins [68]. In ovarian cancers, elevated levels of prostaglandins are observed as compared with normal cells [69], and prostaglandins promote cancer cell invasion at high concentrations [70]. Oxidative stress is another significant event associated with ovarian cancer. Compared with healthy women, patients with ovarian cancer show decreased antioxidant species and increased levels of oxidative stress [71]. More specifically, in ovarian cancer epithelial cells, some studies have reported oxidative stress conditions, with decreased concentrations of antioxidative enzymes. In addition to defective apoptosis, nitric oxide (NO), myeloperoxidase (MPO), NAD(P)H oxidase, and extended combinations of these enzymes have all been observed in ovarian cancer tissues. Besides, ovarian cancers have more elevated levels of caspase-3 nitrosylation, bringing about a huge decrease in caspase-3 capacity. MPO is a significantly relevant pro-oxidant chemical forming NO [72–74]. According to several experimental reports, high MPO levels have been detected in ovarian cancer cells [75]. At the molecular level, MPO directs apoptosis, severe reactions, and drug resistance [76]. MPO prompts the formation of reactive oxygen species (ROS), causing oxidative stress and influencing iron redox balance [72]. As a result, oxidative stress may play a crucial role in the progression of ovarian cancer [77].

5. Molecular Mechanisms Underlying Bioactivity of Natural Products

Mounting evidence demonstrates that plant-derived natural components like phytochemicals can have a role as adjuvants to conventional chemotherapy and may represent promising options for the future development of treatments against ovarian cancer [78,79].

The interest of researchers in the identification of small molecules acting as anticancer agents towards ovarian cancer is constantly growing, and this is testified by the increasing number of contributions in the field. In the 2019–2021 timeframe, some relevant reviews on this topic were published. Shafabakhsh and Asemi as well as Vafadar et al. reviewed the antiproliferative potential of one of the most widely studied natural compounds, quercetin, in the context of ovarian cancer [80,81]. On the other hand, Kubczak et al. reviewed the molecular targets for anticancer natural compounds identified so far, and organized their contribution into sections according to chemical classes [82]. Eventually, Wu et al. focused their attention on ovarian cancer, and classified the studied compounds according to the mechanisms by which natural molecules may act [83].

In this part of the review, we aim at providing a comprehensive and updated overview of natural compounds studied as anticancer agents in the context of ovarian cancer. With respect to previous contributions in the field, we expanded the list of possible molecular mechanisms according to the latest reports. Moreover, in the following sections, we provide a focus on the most promising compounds for which a higher amount of data can be retrieved in the recent literature. Eventually, we discuss the potential of semi-synthetic derivatives of natural compounds with enhanced anticancer activity.

More specifically, the current section briefly reports the role of natural constituents against ovarian cancer, and their proposed mode of action is also discussed herein. In general, natural compounds potentially modulate chemotherapeutic resistance, autophagy, inflammation, propagation, and apoptosis [84]. A brief overview of the several cellular events is reported below. The studied molecules have been grouped according to the proposed mechanism of action.

5.1. Compounds Inducing Apoptosis and Cytotoxicity and Inhibiting Proliferation

Apoptosis is a kind of organized cell death, and it represents a crucial process for maintenance of homeostasis [85]. The induction of apoptosis and inhibition of cell proliferation are the main general mechanisms through which several natural compounds exert their anticancer role [86,87], and the main examples in the field of ovarian cancer are reported below.

Pro-apoptotic activity in ovarian cancer cell lines has been reported for procyanidins from cocoa [88], zeylenone from *Uvaria grandiflora* Roxb [89], and sanguin H-6, a natural constituent present in red raspberry [90].

Similarly, methyl lucidone from *L. erythrocarpa* has cytotoxic effects and induced apoptosis in SKOV-3 and OVCAR-8 cell lines [91], while tanshinones from *Salvia miltiorrhiza* (Danshen), such as cryptotanshinone, tanshinone-I (Tan-I) and tanshinone-IIA (TII-A), were reported to induce apoptosis by interaction with TNF receptors. In particular, TII-A showed the highest activity [92].

Sulforafane (SFN) is a biologically relevant component found in cruciferous vegetables, including broccoli, and it suppressed cell growth by downregulating the cell cycle regulators cyclin D1 and cyclin-dependent kinases 4 and 6 [93].

Additionally, dihydroartemisinin (DHA), traditionally used to treat fever symptoms and recently investigated as a potential tool against severe acute respiratory syndrome-coronavirus 2 (SARS-CoV-2) [94,95], can be found in *Artemisia annua* [96] and induced apoptosis in ovarian cancer cells [97].

Reduced cell proliferation was also achieved with use of berbamine, an alkaloid obtained from *Berberis amurensis*, through the involvement of the Wnt/catenin signaling pathway [98].

Epigallocatechin gallate (EGCG), one of the main catechins found in green tea, inhibited the development and proliferation of OVCAR3 [99], as well as Pulchrin A from *Enicosanthellum pulchrum* [100].

Kadsuphilactone B, a nortriterpenoid from *Schisandra chinensis* (Turcz) B. [101], resveratrol [102] and curcumin [103], which will be discussed in a separate section of the review, represent other examples of compounds promoting ovarian cancer cell death.

Other naturally occurring mixtures, such as those containing silybin analogs, demonstrated a potential inhibitory effect on cancer development, including inhibition of elongation, pro-apoptotic effects, and cytotoxicity [104]. For a detailed list of extracts, the reader should refer to the review by Wu et al. [83].

Overall, the main involved mechanisms targeted by the abovementioned compounds include induction of DNA damage, caspase-3, reduction of Janus family tyrosine kinase (p-JAK), Akt phosphorylation and SERCA, increased apoptosis-inducing factor (AIF), PARP and Bcl-2 family proteins.

5.2. Interference with Reactive Oxygen Species (ROS) Damage and with Nucleic Acid Repair

Excessive oxidative stress is generally believed to play a role in a wide range of diseases, from inflammation to cancer. Carcinogenesis has been connected to enhanced ROS formation and damage [105], and several studies have highlighted the involvement of antioxidant and radical scavenger properties of natural and synthetic compounds [106,107].

In various experiments, the abovementioned antioxidant SFN induced apoptosis in the OVCAR3, OVCAR4, OVCAR5, and SKOV3 cell lines and diminished cancer development in vivo [108].

Several flavones, including quercetin [109], and isoflavones have been previously reported to show antiproliferative activity [110]. Quercetin is a relevant natural compound that has been widely studied, and the properties of this molecule will be overviewed in another section of this review. It has been demonstrated that the isoflavone formononetin (FMN), which is found in red clovers and soy, has anticancer and cancer-preventive actions in a variety of cell types. FMN combats ROS and cell division [83,111].

DNA can be harmed directly or indirectly by events such as oxidative stress, radiations, alkylating agents, and a range of other chemotherapeutic techniques, but the capability of ovarian cancer cells to repair DNA damage is believed to be a crucial element in determining the resistance to chemotherapy [112].

In this context, sideroxylin from *Callistemon lanceolatus* induced apoptosis and reduced proliferation in ovarian cancer cells by influencing lipid peroxidation and ROS activity [113].

Additionally, berberine, another example of a common alkaloid that can be retrieved from several natural sources [114], which has been proven to stop cell division by interfering with DNA repair processes, inhibited the effects of PARP1, which is involved in oxidative states of damaged DNA [115].

Besides, alone or in combination with cisplatin, the abovementioned compound WFA induced the formation of reactive oxygen species (ROS) in A2780 ovarian cancer cells, which caused DNA harm. The compound acted in a synergistic cytotoxic manner with cisplatin, which formed DNA adducts [116].

On the other hand, in the context of the role played by nucleic acid sequences as targets for anticancer agents, aberrant RNAs have been discovered to play critical oncogenic roles in several human cancers. For example, astragalus polysaccharide (APS), a bioactive substance from *Astragalus membranaceus*, increased apoptosis while decreasing cell invasion targeting such sequences [117].

5.3. Modulation of Inflammation

It is now widely accepted that inflammation has a direct association with carcinogenesis as it contributes in initiation, proliferation, invasion, and metastasis [118]. Pro-inflammatory cytokines like TNF- α and IL-6 are blocked by anti-inflammatory compounds including baicalein, apigenin, curcumin, EGCG, genistein, luteolin, and wogonin [83]. Alongside, signal transducer and activator of transcription 3 (STAT-3) prevention, cyclooxygenase-2 (COX-2) inhibition, and nitric oxide synthase (iNOS) downregulation are considered as the main anti-inflammatory mechanisms of phytochemicals [119].

5.4. Suppression of Events Related to Disease Progression: Cell Migration and Angiogenesis

Cell migration and invasion are among the hallmarks of disease progression, and some natural compounds have been reported to target such events.

Among these, tetramethylpyrazine (TMP) from *Ligusticum wallichii* decreased cell viability and motility in SKOV-3 cells [120], and emodin, which is contained in several preparations of Chinese herbs, was found to suppress cell division, invasion, and migration by hindering the ILK/GSK-3 β pathway [121].

Another event that contributes to disease progression is angiogenesis. BLP, the abovementioned mixture containing proanthocyanidins from Chinese bayberry leaves, is probably the most promising in this context, as it demonstrated an anti-angiogenic effect in the IOSE-364 ovarian cell line due to an inhibition of vascular endothelial growth factor (VEGF) [122].

Similarly, Tan-IIA, already mentioned above, interfered with disease progression in an A2780 xenograft model. Concerning the underlying mechanism of action, Tan-IIA promoted antiangiogenic effects, mediated by the interference with VEGF, and induced apoptosis in the ID-8 and A2780 cell lines [123].

Several natural flavonoids were also reported to act on the EGF/VEGF pathway, including apigenin, taxifolin, luteolin, quercetin, genistein, kaempferol [124], harmine [125], and cranberry proanthocyanidin-1 [126].

5.5. Regulation of Tumor Micro Environment

The tumor microenvironment is a complex and dynamic combination of elements in which cancer cells are embedded. It comprises nonmalignant cells, the extracellular matrix and several cytokines, chemokines, and growth factors. Considering their multi-target action, natural compounds can modulate several aspects of the microenvironment. In

particular, Dias et al. highlighted how natural derivatives can influence metabolic crosstalk to “re-educate” tumor microenvironment cells towards potential anticancer activity. In particular, curcumin, resveratrol, EGCG, shikonin, and phloretin were reported to alter the metabolism of stromal cells [127].

The abovementioned effect is achieved through the modulation of the expression of cancer-associated genes by the natural products, and this mechanism has also been reported to explain the anticancer activity of quercetin, berberine, and tanshinones [128].

In addition, β -escin was recently reported to combat ovarian cancer metastasis by targeting both cancer and stromal cells in the tumor microenvironment [129].

5.6. Other Mechanisms Related to Dysregulation of Cell Cycle

Dysregulation of the cell cycle is a relevant contributing factor in the carcinogenesis of ovarian cancer, and interference with the G0/G1 stages is the most commonly reported mechanism of natural compounds with an anticancer role targeting this process [130]. This mechanism was reported for asiatic acid from *Centella asiatica* [131], mentoflavone from *Selaginella tamariscina* [132], proanthocyanidins from Chinese bayberry leaves (BLPs) [133], and pulchrin A [134], which were found to combat cell proliferation and cancer progression, in particular by targeting such phases of the cell cycle.

Moreover, co-treatment with herbal extracts from *Fritillaria cirrhosa* (FC) and *Scutellaria baicalensis* (SB) resulted in G0/G1 stage cell cycle arrest also in OVCA 420 and OVCA 429 ovarian cancer cells [135].

Additionally, cucurbitacin-A, isolated from *Momordica charantia* L., was found to show anticancer potential, causing cell cycle arrest in the G2/M phase [136].

In this context, licorice plants contain large amounts of the flavonoid isoliquiritigenin (ISL). In OVCAR-5 and ES-2 cell lines, ISL also decreased cell proliferation in a dose- and time-dependent manner, targeting the G2/M phase of the cell cycle [137].

Autophagy is another physiological cell process that contributes to the maintenance of a normal cell cycle. According to increasing evidence, autophagy and ovarian cancer also appear to be connected [138]. Thus, natural compounds that help in modulating autophagy may find an application in ovarian cancer treatment. Among the natural constituents reported to act against ovarian cancer through this mechanism, *Embllica officinalis* (Amla) extracts [8], resveratrol [139], withaferin A (WFA) [140], and grifolin [141] were reported.

Moreover, Tan-I, a compound from the class of tanshinones, cited above, increased levels of the autophagy-related proteins beclin1, ATG7, and p62 as well as LC3II/LC3I and caspase-3 in A2780 and ID8, boosting apoptosis and inducing autophagy [142,143].

Finally, genistein promoted autophagy of caspase-independent cells [144] and induced apoptosis in cisplatin-sensitive and resistant ovarian cancer cells (A2780/CaOV3, ES-2).

5.7. Natural Constituents Modulating Resistance to Chemotherapeutic Agents

In ovarian cancer cells, plant-derived constituents were found to enhance sensitivity to chemotherapeutics, an aspect which, as anticipated, is crucial in this pathology.

For example, pre-treatment with either ellagic acid or resveratrol 48-h before cisplatin administration was reported to increase cytotoxicity of cisplatin itself in A2780CisR cisplatin-resistant cells, while synergistic treatment with either cisplatin–ellagic acid or cisplatin–resveratrol for 26 weekly cycles completely prevented cisplatin resistance in A2780 cells [145].

Moreover, in A2780 cells, SFN diminished the xenobiotic-reaction component (XRE). SFN also interferes with cell pH regulation and migration, and in this context it has been proposed as an agent to combat chemoresistance [146].

In doxorubicin-resistant human ovarian cancer cell lines (NCI/ADR-RES), treatment with RCM, also known as Korean dark raspberry, led to apoptosis through phosphorylation of c-Jun N-terminal kinase (JNK) [147]. In the same model, ellagic acid and quercetin, two phytochemicals also found in RCM as well as in many other natural sources, were shown to influence JNK and Akt phosphorylation, thus inducing apoptosis [148].

Finally, since therapy with WFA and doxorubicin reduced cell proliferation in xenograft mice models of ovarian cancer more effectively than WFA or doxorubicin alone, it has been postulated that WFA may be thought of as an adjuvant to standard doxorubicin therapy to minimize adverse effects [140].

A schematic representation and summary of the pathways targeted by natural compounds and mentioned in this section are reported in Figure 3. Moreover, Table 1 summarizes the most recently reported updates on the molecular mechanisms underlying the activity of natural compounds and their derivatives in the context of ovarian cancer.

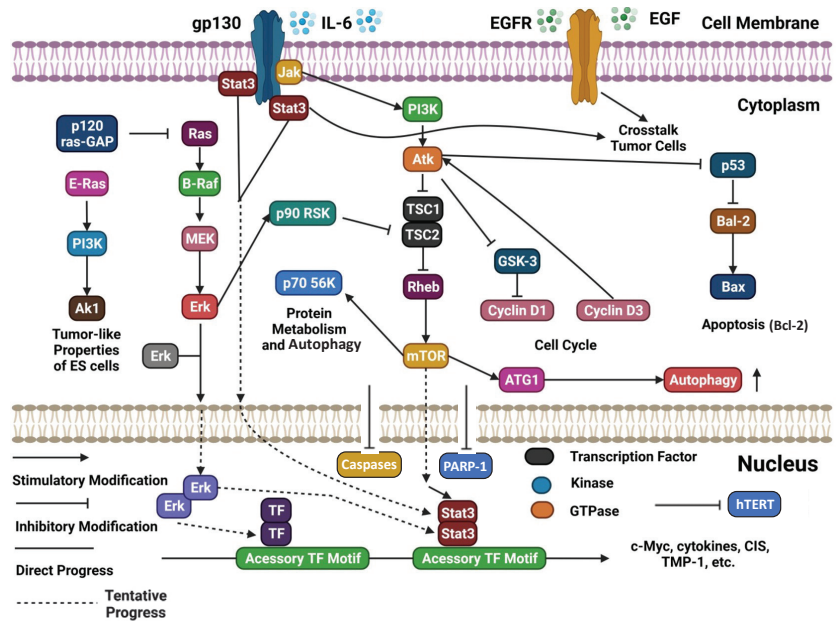


Figure 3. Schematic representation of several cellular signaling pathways potentially targeted by natural compounds (adapted and updated from [83]).

Table 1. Overview of natural substances showing anticancer properties against ovarian cancer models. This table is intended as an addendum to the one reported by Wu et al. [83], thus updated records were included. The reader is invited to refer to the abovementioned review for a more comprehensive overview with the corresponding references. The table also includes semi-synthetic derivatives of natural compounds that showed antiproliferative activity and that are discussed in Section 6.5 of the current review.

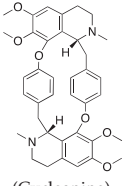
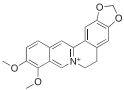
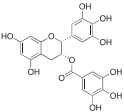
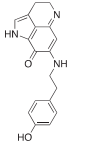
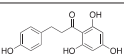
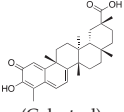
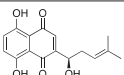
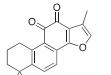
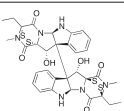
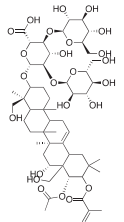
Compound	Source	Chemical Structure of the Representative Component	Classification	Model	Mechanism of Action	References
Aminoalkyl derivatives of cycleanine	Triclisia subcordata	 (Cycleanine)	Bisbenzylisoquinoline macrocyclic alkaloid	Cell lines	activation of caspases 3/7, cleavage of PARP	[149]

Table 1. Cont.

Compound	Source	Chemical Structure of the Representative Component	Classification	Model	Mechanism of Action	References
Berberine	European barberry, goldenseal, goldthread, Oregon grape, phellodendron, and tree turmeric		Alkaloid	A2780, HEY, HO8910	Triggering oxidative DNA damage, targeting of cancer stem cells	[52,115]
Epigallocatechin gallate (EGCG)	Green tea		Flavonoid	SKOV3-ip1, SKOV3TR-ip2	Reduction of hTERT and Bcl-2, alteration of the metabolism of stromal cells	[99,127,150]
FBA-TPQ (derivative of makaluvamines)	<i>Zyzygia</i> sponges	 (Makaluvamine scaffold)	Pyrroloimin-quinone alkaloid	in vitro and in vivo (xenograft)	ROS species, p53-MDM2 and PI3K-Akt pathways	[151]
Phloretin	Apple tree leaves		Dihydrochalcone	in vitro	Alteration of the metabolism of stromal cells	[127]
Semi-synthetic derivatives of celastrol	<i>Tripterygium</i> species	 (Celastrol)	Nortriterpenoid quinone	in vitro	STAT-3 pathway, induction of apoptosis, reduction of cell migration	[152]
Shikonin	<i>Alkanna tinctoria</i>		Naphthoquinone	A278 cells, in vitro	Alteration of the metabolism of stromal cells	[127,153]
Tanshinones	<i>Salvia miltiorrhiza</i>	 (Tanshinone IIA)	Terpenoid/ Abietane	A-549, TOV-21G	Growth capacity is inhibited by reducing cell viability, alteration of the microenvironment	[92,123,128,143]
Verticillin H esters	Fungi		Verticillins	OVCAR-3	Reduced cell proliferation	[154]
β -escin	horse chestnut seed		Pentacyclic triterpenoid saponin	in vitro and in vivo	Alteration of the microenvironment	[129]

6. A Focus on Selected Natural Compounds with Promising Activity against Ovarian Cancer

In the following part of the review, we focus on some of the most widely studied natural compounds, some of which have already been mentioned in previous paragraphs, with reported activity against ovarian cancer models (Figure 4). The compounds are presented to the reader according to a classification related to their chemical structure and natural origin. In particular, their potential as antiproliferative and anti-apoptotic agents, as well as the evidence concerning their anti-metastatic activity, are discussed. Eventually, a focus on semi-synthetic derivatives of natural compounds, designed to achieve improved anticancer activity, is presented.

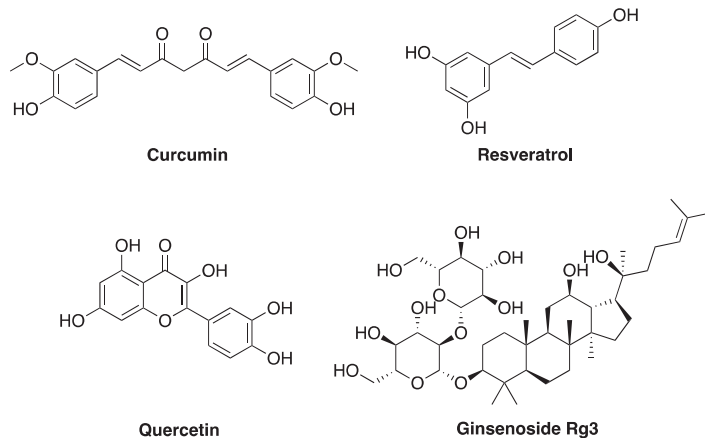


Figure 4. Chemical structures of curcumin, resveratrol, quercetin, and ginsenoside Rg3, the most promising natural compounds discussed in the review.

6.1. Curcumin

The primary ingredient in South Asian and Indian curries is turmeric, which comes from the root of *Curcuma longa*. Turmeric has a long history of usage in India and China as a traditional medicine [155]. Curcumin and two others related curcuminoids, namely demethoxycurcumin and bisdemethoxycurcumin, are well-known and widely studied compounds contained in this plant. As indicated by several reports published throughout the years, curcumin and curcuminoids have strong anticancer effects due to the interaction with a combination of intracellular targets [156].

6.1.1. Antiproliferative and Proapoptotic Activity

Excessive proliferation and unbalanced apoptosis are two signs of uncontrolled cell growth, and these events also occur in ovarian cancer, as discussed in the first part of this review. The protein kinase B/phosphatidylinositol 3-kinase (Akt/PI3K) signaling pathway is overactivated in ovarian cancer cells and supports cell proliferation and invasion [157].

In ovarian cancer cells, curcumin decreased Bcl-2 expression while it increased Bax and caspase-3, causing cell cycle arrest in the G2/M stage and consequent cell death [158]. According to Watson et al., curcumin activates caspase-8 and caspase-9 first, and then caspase-3 to exert this activity [159]. Moreover, the authors found that curcumin decreased Akt phosphorylation, Bcl-2, and survivin, an anti-apoptotic protein. When phosphorylated, STAT-3 advanced malignant growth by promoting cell proliferation and hindering apoptosis [160]. According to Saydmohammed et al., curcumin also reduced STAT-3 phosphorylation, which regulates the growth of ovarian cancer cells [161]. Curcumin regulated STAT-3 phosphorylation and enhanced interleukin (IL)-6 and IL-8 release, which decreased ovarian cell motility [162]. Seo et al. reported that curcumin influenced Ca^{2+} homeostasis

in ovarian cancer cells [103]. Curcumin also interferes with miRNAs, short non-coding RNA sequences regulating target genes post-transcriptionally [163]. According to Du et al., treatment with dimethoxy-curcumin sustained the levels of miR-551a, inducing apoptosis in ovarian cancer cells [164]. Additionally, when dihydroartemisinin and curcumin were combined, miR-124 was upregulated and its target, midkine, which promotes carcinogenesis and is overexpressed in infections, was downregulated [165], causing cell cycle arrest and apoptosis. Additionally, curcumin increased apoptosis and stopped the growth of ovarian cancer cells by targeting miR-9 [166].

Thus, as can be deduced from the results of the high number of reports concerning curcumin published in this context, it can be postulated that the compound may act through a combination of mechanisms at the molecular level to exert its antiproliferative activity.

6.1.2. Anti-Metastatic Activity

Unregulated cancer cells, also in the case of ovarian cancer, can spread to different organs [4], and in this context matrix metalloproteinases (MMPs), a type of proteolytic protein, promote the development of ovarian cancer [167]. By reducing the phosphorylation of FAK, MMP-9, and Rab coupling protein, curcumin inhibited SKOV3 cell invasion [168]. Moreover, bisdemethoxycurcumin reduced metastasis-related proteins such as MMP-2, MMP-9, and vascular cell bond particle 1 (VCAM-1) in SKOV3 cells by controlling oxidative stress and inactivating the NF- κ B pathway [169]. The cooperation of VCAM-1 and integrin has been shown to play a role in ovarian cancer cell intrusion and metastasis [170].

6.2. Resveratrol

Resveratrol is a polyphenolic compound that can be found in grapes, peanuts, and plants such as *Polygonum cuspidatum* [171]. Resveratrol improves heart disease and conditions affecting the nervous system and kidneys, and it is reported to have several other beneficial properties [172,173]. This compound has been widely studied throughout the years for its biological roles, and it has been cited previously in the current review. In this section, a brief overview of the reports concerning its antiproliferative and anti-metastatic activities are reported.

6.2.1. Antiproliferative and Proapoptotic Activity

In a mouse model, resveratrol diminished glucose uptake by cancer cells [174]. Resveratrol influenced GSK3 β in ovarian cancer cells, reducing protein glycosylation [175]. GSK3 β phosphorylated and deactivated glycogen synthase, thus regulating glucose storage [176]. Tino et al. [177] found that the combined use of resveratrol and acetyl resveratrol efficiently retarded the growth of ovarian cancer cells, and that this effect was accomplished by decreased NF- κ B protein [177]. Besides GSK3, in ovarian cancer cells, resveratrol reduced the phosphorylation of Akt, and increased the extracellular signal-coordinating kinase (ERK) [102].

6.2.2. Anti-Metastatic Activity

By reducing integrin levels, resveratrol has been shown to hinder the ability of ovarian cancer cells to invade the peritoneal mesothelium, thus preventing metastasis [178]. Resveratrol may limit the interaction between ovarian cancer cells and mesothelial cells by preventing the motility of the firsts, and, in particular, downregulation of VEGF in hypoxic conditions appears to be involved [179]. In fact, increased VEGF production has been shown to be related to metastasis in ovarian cancer cells [180].

6.3. Ginsenosides

The major pharmacologically active components of ginseng, ginsenosides, have antioxidant and anticancer properties [173,181]. Ginsenoside Rg3 and Rb1 especially have been reported to display anticancer activity [182].

6.3.1. Antiproliferative and Proapoptotic Activity

According to Li et al., ginsenoside Rg3 decreased ovarian disease cell glycolysis by downregulating phospho-STAT-3 [183]. Additionally, the compound triggered the upregulation of miR-603 in ovarian cancer cells by inhibiting DNA methylation. The same natural molecule also influenced hexokinase-2 activity [184].

However, the use of ginsenoside Rg3 is a rather debated issue, as recent reports showed that the use of low concentrations of the compound stimulated cell proliferation, while high concentrations were needed to achieve anticancer effects [185].

6.3.2. Anti-Metastatic Activity

HIF-1 α is a dimeric protein that plays a role in hypoxic conditions and metastasis [186]. Epithelial–mesenchymal transition (EMT), which is related to cell–cell adhesion, frequently takes place prior to the onset of ovarian cancer. Liu et al. observed that ginsenoside 20(S)-Rg3 counteracted EMT and downregulated HIF-1 through interference with the ubiquitin–proteasome pathway [183]. Additionally, it was discovered that ginsenoside Rg3 increased prolyl hydroxylase protein 1 and resulted in HIF-1 α degradation [187]. Moreover, a reduction in cell intrusion capability was observed upon treatment with this compound [184].

Furthermore, ginsenoside Rb1 reduced hypoxia-induced EMT in ovarian cancer cells by downregulating miR-25. More specifically, it prevented the production of EP300, a transcriptional activator of E-cadherin, a crucial molecule for epithelial cell attachment, from being suppressed by miR-25, which would have had an anti-metastatic impact [188]. By interaction with actin microfilaments in the cytoplasm through α - and β -catenin, E-cadherin is associated with the adhesion of epithelial cells [189].

6.4. Quercetin

Quercetin is one of the most widely studied naturally occurring flavonoids, which is known to possess a plethora of biological properties through several mechanisms including interaction with DNA (Figure 5) and several protein targets [190], and this section of the review is focused on the reports on anticancer activity of this compound in ovarian cancer models. Shafabakhsh and Asemi [93] and by Vafadar et al. [94] recently reviewed the anticancer properties of quercetin, and the reader is invited to refer to these reviews for a more comprehensive overview of the molecular mechanisms of this compound.

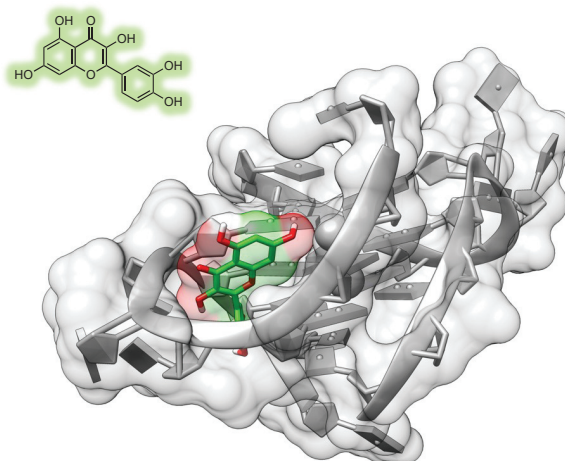


Figure 5. Quercetin structure and predicted binding mode to a G-quadruplex DNA sequence (Protein Data Bank ID: 3CE5; adapted from [190]). The artwork was produced using UCSF Chimera [191].

Liu et al. examined the effects of quercetin on apoptosis in an ovarian cancer mice xenograft model and demonstrated that quercetin caused mitochondrial apoptosis [192]. Furthermore, by causing endoplasmic reticulum (ER) stress, quercetin triggered mitochondria-mediated apoptosis in ovarian cancer cells. Quercetin affected ER stress, apoptosis, and autophagy via the p-STAT3/Bcl-2 center. In general, quercetin downregulates the growth of metastatic ovarian cancer cells through the induction of apoptotic conditions. In particular, the flavonoid increases the activity of apoptotic species including caspase-3, caspase-9, and cytochrome c. Moreover, pro-apoptotic proteins Bid, Bax, and Bad are also involved. Concerning this biomolecular mechanism, Bad and Bid promote the oligomerization of Bax and of the protein Bak, and this event triggers the permeabilization of the outer mitochondrial wall. Bid can directly trigger apoptosis, while Bad interacts with anti-apoptotic Bcl-2 proteins, thus lowering the threshold for induction of apoptosis. As a result, their equilibrium has an effect on the neoplastic shift in the human endometrium [193]. Like curcumin, quercetin causes mitochondrial-mediated apoptosis and thus limits the proliferation of metastatic ovarian cancer cells [194]. Moreover, our group recently demonstrated that quercetin, as well as its glycoside rutin, can target specific DNA sequences and arrangements in vitro, demonstrating that the compound could influence gene expression [190].

As for natural compounds and drugs in general, the bioavailability and formulation/delivery system may be crucial for obtaining the biological effects. In this context, another study investigated the antiproliferative potential of a quercetin-based nanoformulation. Both in vitro and in mice xenograft models, this specific form of quercetin reduced the development of ovarian cancer cells. Furthermore, it has been noted that quercetin from the nano-formulation activated caspase-3, caspase-9, and Bax while inhibiting MCL-1 and Bcl-2 to enhance apoptosis [195].

Additionally, several studies were aimed at understanding the synergistic benefits of quercetin when used in combination with various chemotherapeutics. In an in vitro/in vivo investigation, Gong et al. [196] examined the effects of quercetin combined with radiation on ovarian cancer. Exposure of quercetin made ovarian cancer cells undergo ER stress, and there was also an increase in p53, p21, and Bax expression, a reduction of Bcl-2 expression, and an increase in DNA damage.

Quercetin coupled with radiation dramatically decreased the growth of cancer cells and activated p53 in a xenograft ovarian cancer model. In another study, pretreatment with quercetin sustained the cytotoxic activity of cisplatin in ovarian cancer patients. In particular, quercetin increased ER stress, decreased STAT3 phosphorylation, and decreased Bcl-2 expression. Quercetin supported the anticancer impacts of cisplatin also in a xenograft mice model, suggesting a potential role for quercetin as a promising adjuvant medication for ovarian cancer treatment [197].

Other formulations of quercetin, such as PEGylated liposomal quercetin (lipo-quercetin), were tested in vitro and in vivo in models of both cisplatin-sensitive and cisplatin-resistant human ovarian cancer. Studies conducted in vitro revealed that the presence of lipo-quercetin caused cell cycle arrest and apoptosis in both kinds of cancer cells. Moreover, lipo-quercetin was more effective than free quercetin in mice xenograft models [198]. Several studies examined the impact of quercetin on cell cycle progression [199], and it was reported that the compound regulated 1-phosphatidylinositol 4-kinase (PI kinase) activity and lowered inositol-1,4,5-triphosphate (IP3) levels, thus confirming its effect on the cell cycle [200]. Moreover, quercetin was recently studied as an anti-metastatic agent in the context of ovarian cancer [201].

In the context of quercetin derivatives, an in vitro study examined the effects of 3,4',7-O-trimethylquercetin (34'7TMQ) on the growth and progression of ovarian cancer cells, and the compound diminished ovarian cancer cell invasion [202].

Importantly, recent studies showed that quercetin can help in mitigating the side effects of chemotherapeutic agents including cisplatin, 5-fluorouracil, taxol, and pirarubicin. While other, less recent, research reports showed quercetin to be directly effective in the treatment of ovarian cancer, especially when paired with other drugs; it has been later

demonstrated that low doses of quercetin increase antioxidant enzymes and reduce ROS-mediated anti-neoplastic drug toxicity [203]. In this context, another *in vitro* study in ovarian cancer cells supported the synergistic effect of quercetin when administered in combination with cisplatin [204].

The findings reported in this section suggest that quercetin and its formulations have anticancer potential against ovarian cancer through a combination of several mechanisms, which are outlined in Figure 6. Table 2 reports an update on findings concerning the potential of quercetin as an anticancer agent, in particular in the context of ovarian cancer. As can be noted from the records reported in the table, great efforts are currently focused on improving drug-likeness features and delivery strategies for this compound, together with the investigation of synergistic and potentiation effects with respect to traditional anticancer agents.

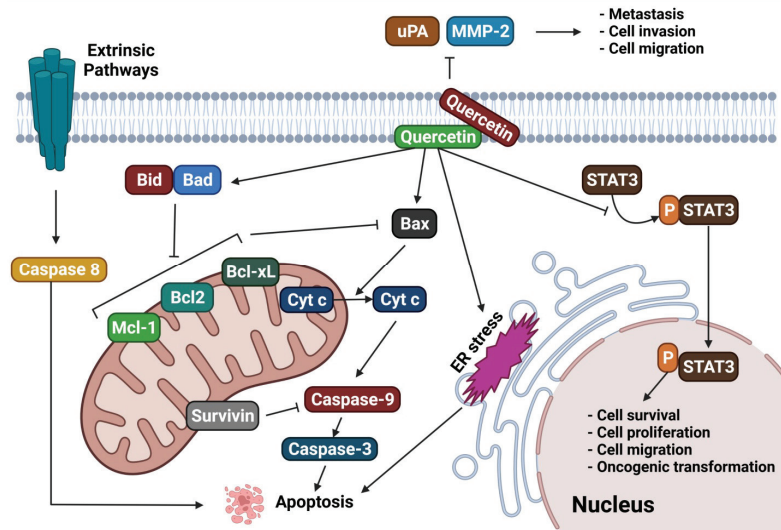


Figure 6. Quercetin targets several signaling pathways within the cells, representing a potential therapeutic agent against ovarian cancer (adapted from [80]).

Table 2. Update on experimental data reported in the literature for the activity of quercetin in the ovarian cancer model. This table is intended as an addendum to the ones reported by Shafabakhsh and Asemi [80] and by Vafadar et al. [81], thus updated records were included. The reader is invited to refer to the abovementioned reviews for a more comprehensive overview, with the corresponding references.

Compound/Formulation	Ovarian Cancer Model	Type of Study	Major Findings and Mechanisms	Reference
Graphene oxide polyvinylpyrrolidone-quercetin-gefitinib (GO-PVP-QSR-GEF)	Ovarian cancer cells	In vitro	Synergistic cytotoxic effect	[205]
Micellar(nanostructures) resveratrol (R):quercetin (Q) (mRQ)	Xenograft model	In vivo	Improvement of the efficacy of adriamycin	[206]
Quercetin	-	In vitro	Human telomeric G-quadruplex stabilization	[190]

Table 2. Cont.

Compound/Formulation	Ovarian Cancer Model	Type of Study	Major Findings and Mechanisms	Reference
Quercetin	Ovarian cancer cells	In vitro	Attenuation of metastatic ability	[201]
Quercetin micelle and thermosensitive hydrogel drug delivery system	SKOV-3 cells and animal model	In vitro and in vivo	Enhanced cytotoxicity	[207]

6.5. Semi-Synthetic Compounds

As anticipated, natural compounds are endowed with unique features in terms of chemical diversity and are often characterized, as highlighted by the overview presented in the previous sections of this review, by the capability of targeting a combination of biochemical pathways within the cell. Nevertheless, such compounds may also be characterized by poor bioavailability, lack of drug-likeness features, limited availability from natural sources, and poor specificity. Thus, research has recently focused on the design of semi-synthetic or synthetic derivatives of natural compounds with improved performances to address these issues [208].

Several examples of semi-synthetic investigational anticancer agents are presented in the literature. Napabucasin and other derivatives of naphthoquinones from *Handroanthus impetiginosus* were tested against cancer cells. The compounds inhibited STAT3, induced apoptosis, and stimulated ROS production [209]. Another example is represented by the paper from Nadysev et al. that reported the synthesis and characterized the biological activity profile of 4-aminomethyl derivatives of heliomycin, a metabolite from *Actinomyces flavochromogenes* var. *heliomycini* and *Streptomyces resistomycificus*. The molecules were tested against a set of cell lines and showed improved water solubility and antiproliferative efficacy with respect to the natural compound [210].

More specifically, concerning therapeutic approaches against ovarian cancer, Li et al. very recently reported a set of derivatives of celastrol, a compound isolated from *Tripterygium* species. This molecule has promising anticancer properties, but it is endowed with suboptimal pharmacological properties due to poor water stability, low bioavailability, and toxicity. The authors modified the structure to obtain drug-like compounds targeting the STAT3 pathway and showing anti-proliferative activity through induction of apoptosis and reduction of cell migration [152].

Previously, Chen et al. studied the synthetic compound FBA-TPQ, a derivative of the marine pyrroloiminoquinone alkaloid makaluvamine, which is isolated from sponges of the genera *Zyzzya*. FBA-TPQ exhibited anticancer activity against OVCAR-3 ovarian cancer cells through ROS species, p53-MDM2, and PI3K-Akt pathways. Moreover, minimal toxicity was observed in non-tumorigenic human IOSE-144 cells, and in vitro data were supported by in vivo studies in xenograft models [151].

Verticillins are another class of fungal metabolites, and several ester derivatives of verticillin H were prepared and tested against a panel of cancer cell lines, including OVCAR-3. The compounds showed cytotoxic activity in the nanomolar range [154].

Cycleanine is a bisbenzylisoquinoline macrocyclic alkaloid from *Triclisia subcordata*. Uche et al. synthesized a small pool of aminoalkyl derivatives that were tested against ovarian cancer cells. The molecules showed anticancer activity through activation of caspases 3/7 and cleavage of PARP [149].

The chemical structures of the most promising semi-synthetic compounds are shown in Figure 7, and the main findings in this context are outlined in Table 1.

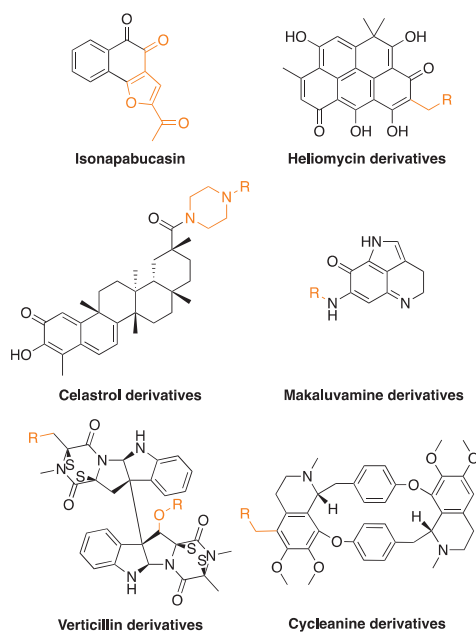


Figure 7. Chemical structures of the discussed semi-synthetic derivatives of natural compounds. The parts of the molecules that have been modified are highlighted in orange.

7. The Point of View of the Medicinal Chemist

Although it is widely established that first-line conventional chemotherapy has a therapeutic effect in many ovarian cancer patients, drug resistance typically limits the efficacy of treatment regimens. Natural products have been investigated in ovarian cancer models both per se and in adjuvant treatment, with positive outcomes in several cases, as overviewed in the previous paragraphs. As laid out in the reported studies, such compounds, belonging to several different chemical classes and acting through a combination of mechanisms, may effectively hinder cancer progression according to in vitro and in vivo studies. Importantly, moreover, natural compounds alone or in combination, boost chemotherapy efficacy while lowering toxic and side effects, potentially allowing a more promising outcome.

Three major observations can be drawn from this literature overview, considering the topic from the point of view of the medicinal chemist. First, the multi-target mechanism of natural compounds represents a valuable resource, but the lack of selectivity may represent a drawback for the development of novel therapeutic approaches. Second, it must be noted how many natural compounds, besides showing anticancer activity per se, also possess potentiating/synergistic properties with respect to other drugs. Additionally, they can help in re-sensitizing resistant cancer cells. Eventually, it must be considered that natural compounds should represent the starting point for compound optimization, as testified by the growing interest towards semi-synthetic derivatives with enhanced drug-likeness and performances. In fact, as overviewed in Section 6 of this review, the development of semi-synthetic compounds is pushing the efficacy of nature-derived molecules in the nanomolar range, even if every case is peculiar. Moreover, the efforts of medicinal chemists, besides improving antiproliferative activity, are pointed towards improving water solubility, stability, bioavailability, and toxicity profiles.

However, a major pitfall is still present and must not be ruled out, as very limited data support the clinical use of the natural compounds discussed in this paper. In fact, few clinical studies have assessed the anticancer effects of natural molecules, even for the most

studied ones such as quercetin, particularly in the field of ovarian cancer [81,211]. In other cases, compounds that have been demonstrated to be effective in in vivo models of ovarian cancer were tested in clinical trials, but with different anticancer indications. This is, for example, the case for β -escin [212]. Nevertheless, there are also compounds that have been more widely studied in clinical trials such as resveratrol, which, anyway, is affected by limitations in terms of bioavailability [213].

8. Conclusions and Future Perspectives

This review overviewed and summarized the anticancer potential of plant-derived molecules in ovarian cancer models. The compounds discussed in this paper bear a variety of different chemical scaffolds, as can be expected for molecules of natural origin. In this connection, the main classes comprise phenolic components, flavonoids, steroid glycosides, terpenoids, chalcones, and several alkaloids.

Similarly, the underlying molecular mechanisms for the different compounds are very diverse, and they include autophagy and apoptosis induction, ROS activity, inhibition of cell invasion, angiogenesis, and metastasis [214]. Most importantly, natural molecules often act through a combination of the abovementioned mechanisms.

Nevertheless, more exploration is required to estimate and understand the effective potential of natural substances in pre-clinical and clinical trials. In particular, some major points must be addressed, including (i) assessment of dose for use of natural compounds in ovarian cancer; (ii) usage of natural compounds as co-treatments with chemotherapy, radiotherapy, and other immunotherapies [215]; (iii) use of a combination of natural compounds acting through different and ideally synergistic mechanisms; and (iv) advanced formulation studies to improve bioavailability of the molecules, thus paving the way for the potential application of natural and nature-inspired compounds as antiproliferative agents against ovarian cancer.

Author Contributions: Conceptualization, A.R. and G.R.; investigation, M.R.I., M.M.R., P.S.D., F.T.N., N.S., M.A. and A.A.K.; writing—original draft preparation, M.R.I., M.M.R., P.S.D., F.T.N., N.S., M.A. and A.A.K.; writing—review and editing, A.R., A.G. and G.R.; funding acquisition, A.R., A.G. and G.R. All authors have read and agreed to the published version of the manuscript.

Funding: This work was funded by University of Brescia.

Institutional Review Board Statement: Not applicable.

Informed Consent Statement: Not applicable.

Data Availability Statement: Data sharing not applicable. No new data were created or analyzed in this study.

Conflicts of Interest: The authors declare no conflict of interest.

References

1. Bray, F.; Ferlay, J.; Soerjomataram, I.; Siegel, R.L.; Torre, L.A.; Jemal, A. Global Cancer Statistics 2018: GLOBOCAN Estimates of Incidence and Mortality Worldwide for 36 Cancers in 185 Countries. *CA Cancer J. Clin.* **2018**, *68*, 394–424. [[CrossRef](#)]
2. Duska, L.R.; Kohn, E.C. The New Classifications of Ovarian, Fallopian Tube, and Primary Peritoneal Cancer and Their Clinical Implications. *Ann. Oncol.* **2017**, *28*, viii8–viii12. [[CrossRef](#)] [[PubMed](#)]
3. Yousefi, M.; Dehghani, S.; Nosrati, R.; Ghanei, M.; Salmaninejad, A.; Rajaie, S.; Hasanzadeh, M.; Pasdar, A. Current Insights into the Metastasis of Epithelial Ovarian Cancer—Hopes and Hurdles. *Cell. Oncol.* **2020**, *43*, 515–538. [[CrossRef](#)] [[PubMed](#)]
4. Weidle, U.H.; Birzele, F.; Kollmorgen, G.; Rueger, R. Mechanisms and Targets Involved in Dissemination of Ovarian Cancer. *Cancer Genom. Proteom.* **2016**, *13*, 407–424. [[CrossRef](#)] [[PubMed](#)]
5. Falzone, L.; Scandurra, G.; Lombardo, V.; Gattuso, G.; Lavoro, A.; Distefano, A.B.; Scibilia, G.; Scollo, P. A Multidisciplinary Approach Remains the Best Strategy to Improve and Strengthen the Management of Ovarian Cancer (Review). *Int. J. Oncol.* **2021**, *59*, 53. [[CrossRef](#)]
6. Zhang, S.F.; Wang, X.Y.; Fu, Z.Q.; Peng, Q.H.; Zhang, J.Y.; Ye, F.; Fu, Y.F.; Zhou, C.Y.; Lu, W.G.; Cheng, X.D.; et al. TXNDC17 Promotes Paclitaxel Resistance via Inducing Autophagy in Ovarian Cancer. *Autophagy* **2015**, *11*, 225–238. [[CrossRef](#)]
7. Yang, M.-F.; Lou, Y.-L.; Liu, S.-S.; Wang, S.-S.; Yin, C.-H.; Cheng, X.-H.; Huang, O.-P. Capn4 Overexpression Indicates Poor Prognosis of Ovarian Cancer Patients. *J. Cancer* **2018**, *9*, 304–309. [[CrossRef](#)] [[PubMed](#)]

8. De, A.; De, A.; Papasian, C.; Hentges, S.; Banerjee, S.; Haque, I.; Banerjee, S.K. Emblica Officinalis Extract Induces Autophagy and Inhibits Human Ovarian Cancer Cell Proliferation, Angiogenesis, Growth of Mouse Xenograft Tumors. *PLoS ONE* **2013**, *8*, e72748. [[CrossRef](#)] [[PubMed](#)]
9. Kurman, R.J.; Shih, I.-M. The Origin and Pathogenesis of Epithelial Ovarian Cancer—a Proposed Unifying Theory. *Am. J. Surg. Pathol.* **2010**, *34*, 433–443. [[CrossRef](#)] [[PubMed](#)]
10. Ottevanger, P.B. Ovarian Cancer Stem Cells More Questions than Answers. *Semin. Cancer Biol.* **2017**, *44*, 67–71. [[CrossRef](#)]
11. Akilli, H.; Rahatli, S.; Tohma, Y.A.; Karakas, L.A.; Altundag, O.; Ayhan, A. Effect of Increased Number of Neoadjuvant Chemotherapy Cycles on Tumor Resectability and Pathologic Response in Advanced Stage Epithelial Ovarian Cancer. *J. BUON* **2018**, *23*, 111–115.
12. Ribaudo, G. Synthesis of Flavonoids or Other Nature-Inspired Small Molecules. *Molbank* **2022**, *2022*, M1313. [[CrossRef](#)]
13. Sharifi-Rad, J.; Rajabi, S.; Martorell, M.; López, M.D.; Toro, M.T.; Barollo, S.; Armanini, D.; Fokou, P.V.T.; Zagotto, G.; Ribaudo, G.; et al. Plant Natural Products with Anti-Thyroid Cancer Activity. *Fitoterapia* **2020**, *146*, 104640. [[CrossRef](#)] [[PubMed](#)]
14. Zorzan, M.; Collazuol, D.; Ribaudo, G.; Ongaro, A.; Scaroni, C.; Zagotto, G.; Armanini, D.; Barollo, S.; Galeotti, F.; Volpi, N.; et al. Biological Effects and Potential Mechanisms of Action of Pistacia Lentiscus Chios Mastic Extract in Caco-2 Cell Model. *J. Funct. Foods* **2019**, *54*, 92–97. [[CrossRef](#)]
15. Povo, C.; Foschini, A.; Ribaudo, G. Optimization of the Extraction of Bioactive Molecules from Lycium Barbarum Fruits and Evaluation of the Antioxidant Activity: A Combined Study. *Nat. Prod. Res.* **2018**, *33*, 2694–2698. [[CrossRef](#)]
16. Dutta, R.; Khalil, R.; Green, R.; Mohapatra, S.S.; Mohapatra, S. Withania Somnifera (Ashwagandha) and Withaferin A: Potential in Integrative Oncology. *Int. J. Mol. Sci.* **2019**, *20*, 5310. [[CrossRef](#)]
17. Mominur Rahman, M.; Islam, F.; Saidur Rahaman, M.; Sultana, N.A.; Fahim, N.F.; Ahmed, M. Studies on the Prevalence of HIV/AIDS in Bangladesh Including Other Developing Countries. *Adv. Tradit. Med.* **2021**, 1–12. [[CrossRef](#)]
18. Rahman, M.M.; Islam, M.R.; Akash, S.; Shohag, S.; Ahmed, L.; Supti, F.A.; Rauf, A.; Aljohani, A.S.M.; Al Abdulmonem, W.; Khalil, A.A.; et al. Naphthoquinones and Derivatives as Potential Anticancer Agents: An Updated Review. *Chem. Biol. Interact.* **2022**, *368*, 110198. [[CrossRef](#)]
19. Islam, M.R.; Akash, S.; Rahman, M.M.; Nowrin, F.T.; Akter, T.; Shohag, S.; Rauf, A.; Aljohani, A.S.M.; Simal-Gandara, J. Colon Cancer and Colorectal Cancer: Prevention and Treatment by Potential Natural Products. *Chem. Biol. Interact.* **2022**, *368*, 110170. [[CrossRef](#)]
20. Rahman, M.M.; Wang, X.; Islam, M.R.; Akash, S.; Supti, F.A.; Mitu, M.I.; Harun-Or-Rashid, M.; Aktar, M.N.; Khatun Kali, M.S.; Jahan, F.I.; et al. Multifunctional Role of Natural Products for the Treatment of Parkinson’s Disease: At a Glance. *Front. Pharmacol.* **2022**, *13*, 4207. [[CrossRef](#)]
21. Mukerjee, N.; Al-Khafaji, K.; Maitra, S.; Suhail Wadi, J.; Sachdeva, P.; Ghosh, A.; Buchade, R.S.; Chaudhari, S.Y.; Jadhav, S.B.; Das, P.; et al. Recognizing Novel Drugs against Keap1 in Alzheimer’s Disease Using Machine Learning Grounded Computational Studies. *Front. Mol. Neurosci.* **2022**, *15*, 638. [[CrossRef](#)]
22. Semwal, P.; Painuli, S.; Anand, J.; Martins, N.C.; Machado, M.; Sharma, R.; Batiha, G.E.S.; Yaro, C.A.; Lorenzo, J.M.; Rahman, M.M. The Neuroprotective Potential of Endophytic Fungi and Proposed Molecular Mechanism: A Current Update. *Evid. Based Complement. Altern. Med.* **2022**, *2022*, 6214264. [[CrossRef](#)]
23. Garg, S.; Singla, R.K.; Rahman, M.M.; Sharma, R.; Mittal, V. Evaluation of Ulcer Protective Activity of *Morus alba* L. Extract-Loaded Chitosan Microspheres in Ethanol-Induced Ulcer in Rat Model. *Evid. Based Complement. Altern. Med.* **2022**, *2022*, 4907585. [[CrossRef](#)]
24. Rahman, M.M.; Sarker, M.T.; Alam Tumpa, M.A.; Yamin, M.; Islam, T.; Park, M.N.; Islam, M.R.; Rauf, A.; Sharma, R.; Cavalu, S.; et al. Exploring the Recent Trends in Perturbing the Cellular Signaling Pathways in Cancer by Natural Products. *Front. Pharmacol.* **2022**, *13*, 3609. [[CrossRef](#)]
25. Rahman, M.M.; Islam, M.R.; Emran, T. Bin Impact of Nutrition in Brain Function and Development: Potential Brain Foods. *Int. J. Surg.* **2022**, *106*, 106908. [[CrossRef](#)]
26. Rahman, M.M.; Islam, M.R.; Akash, S.; Harun-Or-Rashid, M.; Ray, T.K.; Rahaman, M.S.; Islam, M.; Anika, F.; Hosain, M.K.; Aovi, F.I.; et al. Recent Advancements of Nanoparticles Application in Cancer and Neurodegenerative Disorders: At a Glance. *Biomed. Pharmacother.* **2022**, *153*, 113305. [[CrossRef](#)]
27. Rahman, M.M.; Islam, M.R.; Mim, S.A.; Sultana, N.; Chellappan, D.K.; Dua, K.; Kamal, M.A.; Sharma, R.; Emran, T. Bin Insights into the Promising Prospect of G Protein and GPCR-Mediated Signaling in Neuropathophysiology and Its Therapeutic Regulation. *Oxid. Med. Cell. Longev.* **2022**, *2022*, 8425640. [[CrossRef](#)] [[PubMed](#)]
28. Soong, T.R.; Dinulescu, D.M.; Xian, W.; Crum, C.P. Frontiers in the Pathology and Pathogenesis of Ovarian Cancer: Cancer Precursors and “Precursor Escape”. *Hematol. Oncol. Clin. N. Am.* **2018**, *32*, 915–928. [[CrossRef](#)] [[PubMed](#)]
29. Kotsopoulos, J.; Gronwald, J.; McCuaig, J.M.; Karlan, B.Y.; Eisen, A.; Tung, N.; Bordeleau, L.; Senter, L.; Eng, C.; Couch, F.; et al. Breastfeeding and the Risk of Epithelial Ovarian Cancer among Women with a BRCA1 or BRCA2 Mutation. *Gynecol. Oncol.* **2020**, *159*, 820–826. [[CrossRef](#)] [[PubMed](#)]
30. Shih, I.M.; Wang, Y.; Wang, T.L. The Origin of Ovarian Cancer Species and Precancerous Landscape. *Am. J. Pathol.* **2021**, *191*, 26–39. [[CrossRef](#)]

31. Yang, D.H.; Smith, E.R.; Cohen, C.; Wu, H.; Patriotis, C.; Godwin, A.K.; Hamilton, T.C.; Xu, X.X. Molecular Events Associated with Dysplastic Morphologic Transformation and Initiation of Ovarian Tumorigenicity. *Cancer* **2002**, *94*, 2380–2392. [[CrossRef](#)] [[PubMed](#)]
32. Imai, Y.; Hasegawa, K.; Matsushita, H.; Fujieda, N.; Sato, S.; Miyagi, E.; Kakimi, K.; Fujiwara, K. Expression of Multiple Immune Checkpoint Molecules on t Cells in Malignant Ascites from Epithelial Ovarian Carcinoma. *Oncol. Lett.* **2018**, *15*, 6457–6468. [[CrossRef](#)] [[PubMed](#)]
33. Crum, C.P.; Drapkin, R.; Kindelberger, D.; Medeiros, F.; Miron, A.; Lee, Y. Lessons from BRCA: The Tubal Fimbria Emerges as an Origin for Pelvic Serous Cancer. *Clin. Med. Res.* **2007**, *5*, 35–44. [[CrossRef](#)] [[PubMed](#)]
34. Roh, M.H.; Yassin, Y.; Miron, A.; Mehra, K.K.; Mehrad, M.; Monte, N.M.; Mutter, G.L.; Nucci, M.R.; Ning, G.; McKeon, F.D.; et al. High-Grade Fimbrial-Ovarian Carcinomas Are Unified by Altered P53, PTEN and PAX2 Expression. *Mod. Pathol.* **2010**, *23*, 1316–1324. [[CrossRef](#)] [[PubMed](#)]
35. Kindelberger, D.W.; Lee, Y.; Miron, A.; Hirsch, M.S.; Feltmate, C.; Medeiros, F.; Callahan, M.J.; Garner, E.O.; Gordon, R.W.; Birch, C.; et al. Intraepithelial Carcinoma of the Fimbria and Pelvic Serous Carcinoma: Evidence for a Causal Relationship. *Am. J. Surg. Pathol.* **2007**, *31*, 161–169. [[CrossRef](#)] [[PubMed](#)]
36. Chivukula, M.; Niemeier, L.A.; Edwards, R.; Nikiforova, M.; Mantha, G.; McManus, K.; Carter, G. Carcinomas of Distal Fallopian Tube and Their Association with Tubal Intraepithelial Carcinoma: Do They Share a Common “Precursor” Lesion? Loss of Heterozygosity and Immunohistochemical Analysis Using PAX 2, WT-1, and P53 Markers. *ISRN Obstet. Gynecol.* **2011**, *2011*, 858647. [[CrossRef](#)] [[PubMed](#)]
37. Shaw, P.A.; Rouzbahman, M.; Pizer, E.S.; Pintilie, M.; Begley, H. Candidate Serous Cancer Precursors in Fallopian Tube Epithelium of BRCA1/2 Mutation Carriers. *Mod. Pathol.* **2009**, *22*, 1133–1138. [[CrossRef](#)]
38. Hunn, J.; Rodriguez, G.C. Ovarian Cancer: Etiology, Risk Factors, and Epidemiology. *Clin. Obstet. Gynecol.* **2012**, *55*, 3–23. [[CrossRef](#)]
39. Koh, S.C.L.; Chan, Y.H.; Lutan, D.; Marpuang, J.; Ketut, S.; Budiana, N.G.; Saleh, A.Z.; Aziz, M.F.; Winarto, H.; Pradjatmo, H.; et al. Combined Panel of Serum Human Tissue Kallikreins and CA-125 for the Detection of Epithelial Ovarian Cancer. *J. Gynecol. Oncol.* **2012**, *23*, 175–181. [[CrossRef](#)]
40. Budiana, I.N.G.; Angelina, M.; Pelayun, T.G.A. Ovarian Cancer: Pathogenesis and Current Recommendations for Prophylactic Surgery. *J. Turk. Ger. Gynecol. Assoc.* **2019**, *20*, 47–54. [[CrossRef](#)]
41. Worley, M.J.; Welch, W.R.; Berkowitz, R.S.; Ng, S.W. Endometriosis-Associated Ovarian Cancer: A Review of Pathogenesis. *Int. J. Mol. Sci.* **2013**, *14*, 5367–5379. [[CrossRef](#)]
42. Mai, P.L.; Loud, J.T.; Greene, M.H. A Major Step Forward for BRCA1/2-Related Cancer Risk Management. *J. Clin. Oncol.* **2014**, *32*, 1531–1533. [[CrossRef](#)]
43. Akash, S.; Kumer, A.; Rahman, M.M.; Emran, T.B.; Sharma, R.; Singla, R.K.; Alhumaydhi, F.A.; Khandaker, M.U.; Park, M.N.; Idris, A.M.; et al. Development of New Bioactive Molecules to Treat Breast and Lung Cancer with Natural Myricetin and Its Derivatives: A Computational and SAR Approach. *Front. Cell. Infect. Microbiol.* **2022**, *12*, 1400. [[CrossRef](#)] [[PubMed](#)]
44. Akash, S.; Rahman, M.M.; Islam, M.R.; Sharma, R. Emerging Global Concern of Langya Henipavirus: Pathogenicity, Virulence, Genomic Features, and Future Perspectives. *J. Med. Virol.* **2023**, *95*, e28127. [[CrossRef](#)] [[PubMed](#)]
45. Rani, N.; Singla, R.K.; Narwal, S.; Tanushree; Kumar, N.; Mominur Rahman, M. Medicinal Plants Used as an Alternative to Treat Gingivitis and Periodontitis. *Evid. Based Complement. Altern. Med.* **2022**, *2022*, 2327641. [[CrossRef](#)]
46. Kazi, M.A.; Sahito, R.; Abbas, Q.; Ullah, S.; Majid, A.; Phull, A.R.; Rahman, M.M.; Kim, S.J. The Inhibitory Effect of Polyphenon 60 from Green Tea on Melanin and Tyrosinase in Zebrafish and A375 Human Melanoma Cells. *Evid. Based Complement. Altern. Med.* **2022**, *2022*, 7739023. [[CrossRef](#)]
47. Rhaman, M.; Islam, R.; Akash, S.; Mim, M.; Noor, A.; Nepovimova, E.; Valis, M.; Kuca, K.; Sharma, R. Exploring the Role of Nanomedicines for the Therapeutic Approach of Central Nervous System Dysfunction: At a Glance. *Front. Cell Dev. Biol.* **2022**, *10*, 1780. [[CrossRef](#)]
48. Shohag, S.; Akhter, S.; Islam, S.; Sarker, T.; Sifat, M.K.; Rahman, M.M.; Islam, M.R.; Sharma, R. Perspectives on the Molecular Mediators of Oxidative Stress and Antioxidant Strategies in the Context of Neuroprotection and Neurolongevity: An Extensive Review. *Oxid. Med. Cell. Longev.* **2022**, *2022*, 7743705. [[CrossRef](#)]
49. Rahman, M.M.; Islam, M.R.; Yamin, M.; Islam, M.M.; Sarker, M.T.; Meem, A.F.K.; Akter, A.; Emran, T.B.; Cavalu, S.; Sharma, R. Emerging Role of Neuron-Glia in Neurological Disorders: At a Glance. *Oxid. Med. Cell. Longev.* **2022**, *2022*, 3201644. [[CrossRef](#)]
50. Rauf, A.; Rahman, M.M. Potential Therapeutics against Neurological Disorders: Natural Products-Based Drugs. *Front. Pharmacol.* **2022**, *13*, 3178. [[CrossRef](#)]
51. Rahman, M.M.; Islam, M.R.; Rahman, F.; Rahaman, M.S.; Khan, M.S.; Abrar, S.; Ray, T.K.; Uddin, M.B.; Kali, M.S.K.; Dua, K.; et al. Emerging Promise of Computational Techniques in Anti-Cancer Research: At a Glance. *Bioengineering* **2022**, *9*, 335. [[CrossRef](#)] [[PubMed](#)]
52. Taylor, W.F.; Jabbarzadeh, E. The Use of Natural Products to Target Cancer Stem Cells. *Am. J. Cancer Res.* **2017**, *7*, 1588–1605.
53. Walcher, L.; Kistenmacher, A.-K.; Suo, H.; Kitte, R.; Dluczek, S.; Strauß, A.; Blandszun, A.-R.; Yevsa, T.; Fricke, S.; Kossatz-Boehlert, U. Cancer Stem Cells—Origins and Biomarkers: Perspectives for Targeted Personalized Therapies. *Front. Immunol.* **2020**, *11*, 1280. [[CrossRef](#)] [[PubMed](#)]
54. Telang, N. Stem Cell Models for Cancer Therapy. *Int. J. Mol. Sci.* **2022**, *23*, 7055. [[CrossRef](#)]

55. Jia, D.; Nagaoka, Y.; Katsumata, M.; Orsulic, S. Inflammation Is a Key Contributor to Ovarian Cancer Cell Seeding. *Sci. Rep.* **2018**, *8*, 12394. [[CrossRef](#)] [[PubMed](#)]
56. Yamulla, R.J.; Nalubola, S.; Flesken-Nikitin, A.; Nikitin, A.Y.; Schimenti, J.C. Most Commonly Mutated Genes in High-Grade Serous Ovarian Carcinoma Are Nonessential for Ovarian Surface Epithelial Stem Cell Transformation. *Cell Rep.* **2020**, *32*, 108086. [[CrossRef](#)]
57. Saed, G.M.; Diamond, M.P.; Fletcher, N.M. Updates of the Role of Oxidative Stress in the Pathogenesis of Ovarian Cancer. *Gynecol. Oncol.* **2017**, *145*, 595–602. [[CrossRef](#)]
58. Li, H.; Liu, Y.; Wang, Y.; Zhao, X.; Qi, X. Hormone Therapy for Ovarian Cancer: Emphasis on Mechanisms and Applications (Review). *Oncol. Rep.* **2021**, *46*, 223. [[CrossRef](#)] [[PubMed](#)]
59. Risch, H.A. Hormonal Etiology of Epithelial Ovarian Cancer, with a Hypothesis Concerning the Role of Androgens and Progesterone. *J. Natl. Cancer Inst.* **1998**, *90*, 1774–1786. [[CrossRef](#)]
60. Browning, L.; Patel, M.R.; Horvath, E.B.; Tawara, K.; Jorcyk, C.L. IL-6 and Ovarian Cancer: Inflammatory Cytokines in Promotion of Metastasis. *Cancer Manag. Res.* **2018**, *10*, 6685–6693. [[CrossRef](#)] [[PubMed](#)]
61. Kang, Y.C.; Kim, K.M.; Lee, K.S.; Namkoong, S.; Lee, S.J.; Han, J.A.; Jeoung, D.; Ha, K.S.; Kwon, Y.G.; Kim, Y.M. Serum Bioactive Lysophospholipids Prevent TRAIL-Induced Apoptosis via PI3K/Akt-Dependent CFLIP Expression and Bad Phosphorylation. *Cell Death Differ.* **2004**, *11*, 1287–1298. [[CrossRef](#)]
62. Giuntoli, R.L.; Webb, T.J.; Zoso, A.; Rogers, O.; Diaz-Montes, T.P.; Bristow, R.E.; Oelke, M. Ovarian Cancer-Associated Ascites Demonstrates Altered Immune Environment-2009. *Anticancer Res.* **2009**, *29*, 2875–2884. [[PubMed](#)]
63. Bast, R.C.; Hennessy, B.; Mills, G.B. The Biology of Ovarian Cancer: New Opportunities for Translation. *Nat. Rev. Cancer* **2009**, *9*, 415–428. [[CrossRef](#)]
64. Chou, C.H.; Wei, L.H.; Kuo, M.L.; Huang, Y.J.; Lai, K.P.; Chen, C.A.; Hsieh, C.Y. Up-Regulation of Interleukin-6 in Human Ovarian Cancer Cell via a Gi/PI3K-Akt/NF-KB Pathway by Lysophosphatidic Acid, an Ovarian Cancer-Activating Factor. *Carcinogenesis* **2005**, *26*, 45–52. [[CrossRef](#)]
65. Mackay, H.J.; Twelves, C.J. Targeting the Protein Kinase C Family: Are We There Yet? *Nat. Rev. Cancer* **2007**, *7*, 554–562. [[CrossRef](#)]
66. Kumari, S.; Badana, A.K.; Murali Mohan, G.; Shailender, G.; Malla, R.R. Reactive Oxygen Species: A Key Constituent in Cancer Survival. *Biomark. Insights* **2018**, *13*, 1177271918755391. [[CrossRef](#)] [[PubMed](#)]
67. Wong, R.S.Y. Role of Nonsteroidal Anti-Inflammatory Drugs (NSAIDs) in Cancer Prevention and Cancer Promotion. *Adv. Pharmacol. Sci.* **2019**, *2019*, 3418975. [[CrossRef](#)]
68. Chen, S.N.; Chang, R.; Lin, L.T.; Chern, C.U.; Tsai, H.W.; Wen, Z.H.; Li, Y.H.; Li, C.J.; Tsui, K.H. MicroRNA in Ovarian Cancer: Biology, Pathogenesis, and Therapeutic Opportunities. *Int. J. Environ. Res. Public Health* **2019**, *16*, 1510. [[CrossRef](#)]
69. Serhan, K.; Gartung, A.; Panigrahy, D. Drawing a Link between the Thromboxane A2 Pathway and the Role of Platelets and Tumor Cells in Ovarian Cancer. *Prostaglandins Other Lipid Mediat.* **2018**, *137*, 40–45. [[CrossRef](#)]
70. Rajagopal, C.; Lankadasari, M.B.; Aranjan, J.M.; Harikumar, K.B. Targeting Oncogenic Transcription Factors by Polyphenols: A Novel Approach for Cancer Therapy. *Pharmacol. Res.* **2018**, *130*, 273–291. [[CrossRef](#)] [[PubMed](#)]
71. Senthil, K.; Aranganathan, S.; Nalini, N. Evidence of Oxidative Stress in the Circulation of Ovarian Cancer Patients. *Clin. Chim. Acta* **2004**, *339*, 27–32. [[CrossRef](#)] [[PubMed](#)]
72. Fletcher, N.M.; Jiang, Z.; Ali-Fehmi, R.; Levin, N.K.; Belotte, J.; Tainsky, M.A.; Diamond, M.P.; Abu-Soud, H.M.; Saed, G.M. Myeloperoxidase and Free Iron Levels: Potential Biomarkers for Early Detection and Prognosis of Ovarian Cancer. *Cancer Biomark.* **2012**, *10*, 267–275. [[CrossRef](#)]
73. Jiang, Z.; Fletcher, N.M.; Ali-Fehmi, R.; Diamond, M.P.; Abu-Soud, H.M.; Munkarah, A.R.; Saed, G.M. Modulation of Redox Signaling Promotes Apoptosis in Epithelial Ovarian Cancer Cells. *Gynecol. Oncol.* **2011**, *122*, 418–423. [[CrossRef](#)]
74. Benhar, M. Roles of Mammalian Glutathione Peroxidase and Thioredoxin Reductase Enzymes in the Cellular Response to Nitrosative Stress. *Free Radic. Biol. Med.* **2018**, *127*, 160–164. [[CrossRef](#)] [[PubMed](#)]
75. Castillo-Tong, D.C.; Pils, D.; Heinze, G.; Braicu, I.; Sehouli, J.; Reinthaller, A.; Schuster, E.; Wolf, A.; Watrowski, R.; Maki, R.A.; et al. Association of Myeloperoxidase with Ovarian Cancer. *Tumor Biol.* **2014**, *35*, 141–148. [[CrossRef](#)] [[PubMed](#)]
76. Saed, G.M.; Ali-Fehmi, R.; Jiang, Z.L.; Fletcher, N.M.; Diamond, M.P.; Abu-Soud, H.M.; Munkarah, A.R. Myeloperoxidase Serves as a Redox Switch That Regulates Apoptosis in Epithelial Ovarian Cancer. *Gynecol. Oncol.* **2010**, *116*, 276–281. [[CrossRef](#)]
77. Kusriani, H.; Subarnas, A.; Diantini, A.; Iskandar, Y. Cytotoxicity of Quercetin and Quercetin-3-O-Rhamnoside of Etlingera Elatior (Jack) RM Sm. Leaves against HeLa Cervical Cancer Cells. *J. App. Pharm. Sci.* **2021**, *11*, 85–90.
78. Rais, J.; Jafri, A.; Siddiqui, S.; Tripathi, M.; Arshad, M. Phytochemicals in the Treatment of Ovarian Cancer. *Front. Biosci.* **2017**, *9*, 67–75. [[CrossRef](#)] [[PubMed](#)]
79. Hoseini Farzaei, M.; Bahramsoltani, R.; Rahimi, R. Phytochemicals as Adjunctive with Conventional Anticancer Therapies. *Curr. Pharm. Des.* **2016**, *22*, 4201–4218. [[CrossRef](#)]
80. Shafabakhsh, R.; Asemi, Z. Quercetin: A Natural Compound for Ovarian Cancer Treatment. *J. Ovarian Res.* **2019**, *12*, 55. [[CrossRef](#)] [[PubMed](#)]
81. Vafadar, A.; Shabaninejad, Z.; Movahedpour, A.; Fallahi, F.; Taghavipour, M.; Ghasemi, Y.; Akbari, M.; Shafiee, A.; Hajighadimi, S.; Moradzarmehri, S.; et al. Quercetin and Cancer: New Insights into Its Therapeutic Effects on Ovarian Cancer Cells. *Cell Biosci.* **2020**, *10*, 32. [[CrossRef](#)] [[PubMed](#)]

82. Kubczak, M.; Szustka, A.; Rogalińska, M. Molecular Targets of Natural Compounds with Anti-Cancer Properties. *Int. J. Mol. Sci.* **2021**, *22*, 13659. [[CrossRef](#)] [[PubMed](#)]
83. Wu, J.; Zhou, T.; Wang, Y.; Jiang, Y.; Wang, Y. Mechanisms and Advances in Anti-Ovarian Cancer with Natural Plants Component. *Molecules* **2021**, *26*, 5949. [[CrossRef](#)]
84. Pistollato, F.; Calderón Iglesias, R.; Ruiz, R.; Aparicio, S.; Crespo, J.; Dzul Lopez, L.; Giampieri, F.; Battino, M. The Use of Natural Compounds for the Targeting and Chemoprevention of Ovarian Cancer. *Cancer Lett.* **2017**, *411*, 191–200. [[CrossRef](#)] [[PubMed](#)]
85. Cheng, X.; Ferrell, J.E. Apoptosis Propagates through the Cytoplasm as Trigger Waves. *Science* **2018**, *361*, 607–612. [[CrossRef](#)] [[PubMed](#)]
86. Rajabi, S.; Maresca, M.; Yumashev, A.V.; Choopani, R.; Hajimehdipour, H. The Most Competent Plant-Derived Natural Products for Targeting Apoptosis in Cancer Therapy. *Biomolecules* **2021**, *11*, 534. [[CrossRef](#)]
87. Liu, C.; Zeng, Y.; Wen, Y.; Huang, X.; Liu, Y. Natural Products Modulate Cell Apoptosis: A Promising Way for the Treatment of Ulcerative Colitis. *Front. Pharmacol.* **2022**, *13*, 806148. [[CrossRef](#)] [[PubMed](#)]
88. Taparia, S.S.; Khanna, A. Procyanidin-Rich Extract of Natural Cocoa Powder Causes ROS-Mediated Caspase-3 Dependent Apoptosis and Reduction of pro-MMP-2 in Epithelial Ovarian Carcinoma Cell Lines. *Biomed. Pharmacother.* **2016**, *83*, 130–140. [[CrossRef](#)] [[PubMed](#)]
89. Xu, X.; Shi, J.; Gao, H.; Li, Q. Zeylenone Inhibits Proliferation and Promotes Apoptosis in Ovarian Carcinoma Cells via Janus Kinase 2 / Signal Transducers and Activators of Transcription 3 Pathways. *J. Obstet. Gynaecol. Res.* **2018**, *44*, 1451–1457. [[CrossRef](#)]
90. Lee, D.; Ko, H.; Kim, Y.J.; Kim, S.N.; Choi, K.C.; Yamabe, N.; Kim, K.H.; Kang, K.S.; Kim, H.Y.; Shibamoto, T. Inhibition of A2780 Human Ovarian Carcinoma Cell Proliferation by a Rubus Component, Sanguin H-6. *J. Agric. Food Chem.* **2016**, *64*, 801–805. [[CrossRef](#)]
91. Yoon, J.H.; Shin, J.W.; Pham, T.H.; Choi, Y.J.; Ryu, H.W.; Oh, S.R.; Oh, J.W.; Yoon, D.Y. Methyl Lucidone Induces Apoptosis and G2/M Phase Arrest via the PI3K/Akt/NF-KB Pathway in Ovarian Cancer Cells. *Pharm. Biol.* **2020**, *58*, 51–59. [[CrossRef](#)] [[PubMed](#)]
92. Chang, C.-C.; Kuan, C.-P.; Lin, J.-Y.; Lai, J.-S.; Ho, T.-F. Tanshinone IIA Facilitates TRAIL Sensitization by Up-Regulating DR5 through the ROS-JNK-CHOP Signaling Axis in Human Ovarian Carcinoma Cell Lines. *Chem. Res. Toxicol.* **2015**, *28*, 1574–1583. [[CrossRef](#)] [[PubMed](#)]
93. Taheri, M.; Roudbari, N.H.; Amidi, F.; Parivar, K. The Protective Effect of Sulforaphane against Oxidative Stress in Granulosa Cells of Patients with Polycystic Ovary Syndrome (PCOS) through Activation of AMPK/AKT/NRF2 Signaling Pathway. *Reprod. Biol.* **2021**, *21*, 100563. [[CrossRef](#)] [[PubMed](#)]
94. Ribaudo, G.; Coghi, P.; Yang, L.J.; Ng, J.P.L.; Mastinu, A.; Memo, M.; Wong, V.K.W.; Gianoncelli, A. Computational and Experimental Insights on the Interaction of Artemisinin, Dihydroartemisinin and Chloroquine with SARS-CoV-2 Spike Protein Receptor-Binding Domain (RBD). *Nat. Prod. Res.* **2022**, *36*, 5358–5363. [[CrossRef](#)] [[PubMed](#)]
95. Coghi, P.; Yang, L.J.; Ng, J.P.L.; Haynes, R.K.; Memo, M.; Gianoncelli, A.; Wong, V.K.W.; Ribaudo, G. A Drug Repurposing Approach for Antimalarials Interfering with SARS-CoV-2 Spike Protein Receptor Binding Domain (RBD) and Human Angiotensin-Converting Enzyme 2 (ACE2). *Pharmaceuticals* **2021**, *14*, 954. [[CrossRef](#)]
96. Abate, Z.; Zhang, L.; Pucci, M.; Morbini, G.; Mac Sweeney, E.; MacCarinelli, G.; Ribaudo, G.; Gianoncelli, A.; Uberti, D.; Memo, M.; et al. Phytochemical Analysis and Anti-Inflammatory Activity of Different Ethanolic Phyto-Extracts of Artemisia Annual. *Biomolecules* **2021**, *11*, 975. [[CrossRef](#)]
97. Liu, Y.; Gao, S.; Zhu, J.; Zheng, Y.; Zhang, H.; Sun, H. Dihydroartemisinin Induces Apoptosis and Inhibits Proliferation, Migration, and Invasion in Epithelial Ovarian Cancer via Inhibition of the Hedgehog Signaling Pathway. *Cancer Med.* **2018**, *7*, 5704–5715. [[CrossRef](#)]
98. Zhang, H.; Jiao, Y.; Shi, C.; Song, X.; Chang, Y.; Ren, Y.; Shi, X. Berbamine Suppresses Cell Proliferation and Promotes Apoptosis in Ovarian Cancer Partially via the Inhibition of Wnt/ β -Catenin Signaling. *Acta Biochim. Biophys. Sin.* **2018**, *50*, 532–539. [[CrossRef](#)]
99. Wang, F.; Chang, Z.; Fan, Q.; Wang, L. Epigallocatechin-3-Gallate Inhibits the Proliferation and Migration of Human Ovarian Carcinoma Cells by Modulating P38 Kinase and Matrix Metalloproteinase-2. *Mol. Med. Rep.* **2014**, *9*, 1085–1089. [[CrossRef](#)]
100. Ahmed, O.H.; Hamad, M.N.; Jaafar, N.S. Phytochemical Investigation of Chenopodium Murale (Family: Chenopodiaceae) Cultivated in Iraq, Isolation and Identification of Scopoletin and Gallic Acid. *Asian J. Pharm. Clin. Res.* **2017**, *10*, 70–77. [[CrossRef](#)]
101. Jeong, M.; Kim, H.M.; Kim, H.J.; Choi, J.-H.; Jang, D.S. Kudsuphilactone B, a Nortriterpenoid Isolated from Schisandra Chinensis Fruit, Induces Caspase-Dependent Apoptosis in Human Ovarian Cancer A2780 Cells. *Arch. Pharmacol. Res.* **2017**, *40*, 500–508. [[CrossRef](#)]
102. Vergara, D.; Simeone, P.; Toraldo, D.; Del Boccio, P.; Vergaro, V.; Leporatti, S.; Pieragostino, D.; Tinelli, A.; De Domenico, S.; Alberti, S.; et al. Resveratrol Downregulates Akt/GSK and ERK Signalling Pathways in OVCAR-3 Ovarian Cancer Cells. *Mol. Biosyst.* **2012**, *8*, 1078–1087. [[CrossRef](#)] [[PubMed](#)]
103. Seo, J.-A.; Kim, B.; Dhanasekaran, D.N.; Tsang, B.K.; Song, Y.S. Curcumin Induces Apoptosis by Inhibiting Sarco/Endoplasmic Reticulum Ca²⁺ ATPase Activity in Ovarian Cancer Cells. *Cancer Lett.* **2016**, *371*, 30–37. [[CrossRef](#)] [[PubMed](#)]
104. Manivannan, E.; Amawi, H.; Hussein, N.; Karthikeyan, C.; Fetcenko, A.; Narayana Moorthy, N.S.H.; Trivedi, P.; Tiwari, A.K. Design and Discovery of Silybin Analogues as Antiproliferative Compounds Using a Ring Disjunctive—Based, Natural Product Lead Optimization Approach. *Eur. J. Med. Chem.* **2017**, *133*, 365–378. [[CrossRef](#)] [[PubMed](#)]

105. Jiao, R.; Liu, Y.; Gao, H.; Xiao, J.; So, K.F. The Anti-Oxidant and Antitumor Properties of Plant Polysaccharides. *Am. J. Chin. Med.* **2016**, *44*, 463–488. [[CrossRef](#)] [[PubMed](#)]
106. Xu, D.-P.; Li, Y.; Meng, X.; Zhou, T.; Zhou, Y.; Zheng, J.; Zhang, J.-J.; Li, H.-B. Natural Antioxidants in Foods and Medicinal Plants: Extraction, Assessment and Resources. *IJMS* **2017**, *18*, 96. [[CrossRef](#)]
107. Ribaldo, G.; Bortoli, M.; Pavan, C.; Zagotto, G.; Orian, L. Antioxidant Potential of Psychotropic Drugs: From Clinical Evidence to In Vitro and In Vivo Assessment and toward a New Challenge for in Silico Molecular Design. *Antioxidants* **2020**, *9*, 714. [[CrossRef](#)]
108. Kwon, Y. Food-Derived Polyphenols Inhibit the Growth of Ovarian Cancer Cells Irrespective of Their Ability to Induce Antioxidant Responses. *Heliyon* **2018**, *4*, e00753. [[CrossRef](#)]
109. Sunil, C.; Xu, B. An Insight into the Health-Promoting Effects of Taxifolin (Dihydroquercetin). *Phytochemistry* **2019**, *166*, 112066. [[CrossRef](#)]
110. Ribaldo, G.; Coghi, P.; Zanforlin, E.; Law, B.Y.K.; Wu, Y.Y.J.; Han, Y.; Qiu, A.C.; Qu, Y.Q.; Zagotto, G.; Wong, V.K.W. Semi-Synthetic Isoflavones as BACE-1 Inhibitors against Alzheimer's Disease. *Bioorg. Chem.* **2019**, *87*, 474–483. [[CrossRef](#)] [[PubMed](#)]
111. Park, S.; Bazer, F.W.; Lim, W.; Song, G. The O-Methylated Isoflavone, Formononetin, Inhibits Human Ovarian Cancer Cell Proliferation by Sub G0/G1 Cell Phase Arrest through PI3K/AKT and ERK1/2 Inactivation. *J. Cell. Biochem.* **2018**, *119*, 7377–7387. [[CrossRef](#)] [[PubMed](#)]
112. Ai, Z.; Lu, Y.; Qiu, S.; Fan, Z. Overcoming Cisplatin Resistance of Ovarian Cancer Cells by Targeting HIF-1-Regulated Cancer Metabolism. *Cancer Lett.* **2016**, *373*, 36–44. [[CrossRef](#)]
113. Park, S.; Lim, W.; Jeong, W.; Bazer, F.W.; Lee, D.; Song, G. Sideroxylin (*Callistemon lanceolatus*) Suppressed Cell Proliferation and Increased Apoptosis in Ovarian Cancer Cells Accompanied by Mitochondrial Dysfunction, the Generation of Reactive Oxygen Species, and an Increase of Lipid Peroxidation. *J. Cell. Physiol.* **2018**, *233*, 8597–8604. [[CrossRef](#)]
114. Ribaldo, G.; Zanforlin, E.; Canton, M.; Bova, S.; Zagotto, G. Preliminary Studies of Berberine and Its Semi-Synthetic Derivatives as a Promising Class of Multi-Target Anti-Parkinson Agents. *Nat. Prod. Res.* **2018**, *32*, 1395–1401. [[CrossRef](#)] [[PubMed](#)]
115. Hou, D.; Xu, G.; Zhang, C.; Li, B.; Qin, J.; Hao, X.; Liu, Q.; Zhang, X.; Liu, J.; Wei, J.; et al. Berberine Induces Oxidative Dna Damage and Impairs Homologous Recombination Repair in Ovarian Cancer Cells to Confer Increased Sensitivity to Parp Inhibition. *Cell Death Dis.* **2017**, *8*, e3070. [[CrossRef](#)] [[PubMed](#)]
116. Kakar, S.S.; Jala, V.R.; Fong, M.Y. Synergistic Cytotoxic Action of Cisplatin and Withaferin A on Ovarian Cancer Cell Lines. *Biochem. Biophys. Res. Commun.* **2012**, *423*, 819–825. [[CrossRef](#)]
117. Guo, Y.; Zhang, Z.; Wang, Z.; Liu, G.; Liu, Y.; Wang, H. Astragalus Polysaccharides Inhibit Ovarian Cancer Cell Growth via MicroRNA-27a/FBXW7 Signaling Pathway. *Biosci. Rep.* **2020**, *40*, BSR20193396. [[CrossRef](#)]
118. Fernandes, J.V.; Cobucci, R.N.O.; Jatobá, C.A.N.; de Medeiros Fernandes, T.A.A.; de Azevedo, J.W.V.; de Araújo, J.M.G. The Role of the Mediators of Inflammation in Cancer Development. *Pathol. Oncol. Res.* **2015**, *21*, 527–534. [[CrossRef](#)]
119. Kim, M.K.; Kim, K.; Han, J.Y.; Lim, J.M.; Song, Y.S. Modulation of Inflammatory Signaling Pathways by Phytochemicals in Ovarian Cancer. *Genes Nutr.* **2011**, *6*, 109–115. [[CrossRef](#)]
120. Yin, J.; Yu, C.; Yang, Z.; He, J.L.; Chen, W.J.; Liu, H.Z.; Li, W.M.; Liu, H.T.; Wang, Y.X. Tetramethylpyrazine Inhibits Migration of SKOV3 Human Ovarian Carcinoma Cells and Decreases the Expression of Interleukin-8 via the ERK1/2, P38 and AP-1 Signaling Pathways. *Oncol. Rep.* **2011**, *26*, 671–679. [[CrossRef](#)]
121. Lu, J.; Xu, Y.; Wei, X.; Zhao, Z.; Xue, J.; Liu, P. Emodin Inhibits the Epithelial to Mesenchymal Transition of Epithelial Ovarian Cancer Cells via ILK/GSK-3 β /Slug Signaling Pathway. *BioMed Res. Int.* **2016**, *2016*, 6253280. [[CrossRef](#)]
122. Zhang, Y.; Chen, S.; Wei, C.; Rankin, G.O.; Rojanasakul, Y.; Ren, N.; Ye, X.; Chen, Y.C. Dietary Compound Proanthocyanidins from Chinese Bayberry (*Myrica Rubra* Sieb. et Zucc.) Leaves Inhibit Angiogenesis and Regulate Cell Cycle of Cisplatin-Resistant Ovarian Cancer Cells via Targeting Akt Pathway. *J. Funct. Foods* **2018**, *40*, 573–581. [[CrossRef](#)] [[PubMed](#)]
123. Zhou, J.; Jiang, Y.-Y.; Wang, X.-X.; Wang, H.-P.; Chen, H.; Wu, Y.-C.; Wang, L.; Pu, X.; Yue, G.-Z.; Zhang, L. Tanshinone IIA Suppresses Ovarian Cancer Growth through Inhibiting Malignant Properties and Angiogenesis. *Ann. Transl. Med.* **2020**, *8*, 1295. [[CrossRef](#)] [[PubMed](#)]
124. Liskova, A.; Koklesova, L.; Samec, M.; Varghese, E.; Abotaleb, M.; Samuel, S.M.; Smejkal, K.; Biringner, K.; Petras, M.; Blahutova, D.; et al. Implications of Flavonoids as Potential Modulators of Cancer Neovascularity. *J. Cancer Res. Clin. Oncol.* **2020**, *146*, 3079–3096. [[CrossRef](#)]
125. Gao, J.; Zhu, H.; Wan, H.; Zou, X.; Ma, X.; Gao, G. Harmine Suppresses the Proliferation and Migration of Human Ovarian Cancer Cells through Inhibiting ERK/CREB Pathway. *Oncol. Rep.* **2017**, *38*, 2927–2934. [[CrossRef](#)]
126. Kim, K.K.; Singh, A.P.; Singh, R.K.; DeMartino, A.; Brard, L.; Vorsa, N.; Lange, T.S.; Moore, R.G. Anti-Angiogenic Activity of Cranberry Proanthocyanidins and Cytotoxic Properties in Ovarian Cancer Cells. *Int. J. Oncol.* **2012**, *40*, 227–235. [[CrossRef](#)]
127. Dias, A.S.; Helguero, L.; Almeida, C.R.; Duarte, I.F. Natural Compounds as Metabolic Modulators of the Tumor Microenvironment. *Molecules* **2021**, *26*, 3494. [[CrossRef](#)]
128. Zhang, W.; Li, S.; Li, C.; Li, T.; Huang, Y. Remodeling Tumor Microenvironment with Natural Products to Overcome Drug Resistance. *Front. Immunol.* **2022**, *13*, 1051998. [[CrossRef](#)] [[PubMed](#)]
129. Kenny, H.A.; Hart, P.C.; Kordylewicz, K.; Lal, M.; Shen, M.; Kara, B.; Chen, Y.-J.; Grassl, N.; Alharbi, Y.; Pattnaik, B.R.; et al. The Natural Product β -Escin Targets Cancer and Stromal Cells of the Tumor Microenvironment to Inhibit Ovarian Cancer Metastasis. *Cancers* **2021**, *13*, 3931. [[CrossRef](#)]

130. Di, W.; Zhang, L.; Yi, H.; Han, X.; Zhang, Y.; Xin, L. Exopolysaccharides Produced by *Lactobacillus* Strains Suppress HT-29 Cell Growth via Induction of G0/G1 Cell Cycle Arrest and Apoptosis. *Oncol. Lett.* **2018**, *16*, 3577–3586. [[CrossRef](#)]
131. Ren, L.; Cao, Q.X.; Zhai, F.R.; Yang, S.Q.; Zhang, H.X. Asiatic Acid Exerts Anticancer Potential in Human Ovarian Cancer Cells via Suppression of PI3K/Akt/MTOR Signalling. *Pharm. Biol.* **2016**, *54*, 2377–2382. [[CrossRef](#)]
132. Yu, S.; Yan, H.; Zhang, L.; Shan, M.; Chen, P.; Ding, A.; Li, S.F.Y. A Review on the Phytochemistry, Pharmacology, and Pharmacokinetics of Amentoflavone, a Naturally-Occurring Biflavonoid. *Molecules* **2017**, *22*, 299. [[CrossRef](#)]
133. Zhang, Y.; Chen, S.; Wei, C.; Rankin, G.O.; Ye, X.; Chen, Y.C. Dietary Compound Proanthocyanidins from Chinese Bayberry (*Myrica Rubra* Sieb. et Zucc.) Leaves Attenuate Chemotherapy-Resistant Ovarian Cancer Stem Cell Traits via Targeting the Wnt/ β -Catenin Signaling Pathway and Inducing G1 Cell Cycle Arrest. *Food Funct.* **2018**, *9*, 525–533. [[CrossRef](#)] [[PubMed](#)]
134. Nordin, N.; Fadaeinasab, M.; Mohan, S.; Hashim, N.M.; Othman, R.; Karimian, H.; Iman, V.; Ramli, N.; Ali, H.M.; Majid, N.A. Pulchrin A, a New Natural Coumarin Derivative of *Encisanthellum Pulchrum*, Induces Apoptosis in Ovarian Cancer Cells via Intrinsic Pathway. *PLoS ONE* **2016**, *11*, e0154023. [[CrossRef](#)] [[PubMed](#)]
135. Kavandi, L.; Lee, L.R.; Bokhari, A.A.; Pirog, J.E.; Jiang, Y.; Ahmad, K.A.; Syed, V. The Chinese Herbs *Scutellaria Baicalensis* and *Fritillaria Cirrhosa* Target NF κ B to Inhibit Proliferation of Ovarian and Endometrial Cancer Cells. *Mol. Carcinog.* **2015**, *54*, 368–378. [[CrossRef](#)] [[PubMed](#)]
136. Jia, S.; Shen, M.; Zhang, F.; Xie, J. Recent Advances in *Momordica Charantia*: Functional Components and Biological Activities. *Int. J. Mol. Sci.* **2017**, *18*, 2555. [[CrossRef](#)] [[PubMed](#)]
137. Chen, H.Y.; Huang, T.C.; Shieh, T.M.; Wu, C.H.; Lin, L.C.; Hsia, S.M. Isoliquiritigenin Induces Autophagy and Inhibits Ovarian Cancer Cell Growth. *Int. J. Mol. Sci.* **2017**, *18*, 2025. [[CrossRef](#)]
138. Zhan, L.; Zhang, Y.; Wang, W.; Song, E.; Fan, Y.; Li, J.; Wei, B. Autophagy as an Emerging Therapy Target for Ovarian Carcinoma. *Oncotarget* **2016**, *7*, 83476–83487. [[CrossRef](#)] [[PubMed](#)]
139. Wang, H.Y.; Peng, Y.; Wang, J.; Gu, A.X.; Li, Q.; Mao, D.W.; Guo, L.Y. Effect of Autophagy on the Resveratrol-Induced Apoptosis of Ovarian Cancer SKOV3 Cells. *J. Cell. Biochem.* **2019**, *120*, 7788–7793. [[CrossRef](#)]
140. Fong, M.Y.; Jin, S.; Rane, M.; Singh, R.K.; Gupta, R.; Kakar, S.S. Withaferin A Synergizes the Therapeutic Effect of Doxorubicin through ROS-Mediated Autophagy in Ovarian Cancer. *PLoS ONE* **2012**, *7*, e42265. [[CrossRef](#)]
141. Che, X.; Yan, H.; Sun, H.; Dongol, S.; Wang, Y.; Lv, Q.; Jiang, J. Grifolin Induces Autophagic Cell Death by Inhibiting the Akt/MTOR/S6K Pathway in Human Ovarian Cancer Cells. *Oncol. Rep.* **2016**, *36*, 1041–1047. [[CrossRef](#)] [[PubMed](#)]
142. Lin, L.; Baehrecke, E.H. Autophagy, Cell Death, and Cancer. *Mol. Cell. Oncol.* **2015**, *2*, e985913. [[CrossRef](#)] [[PubMed](#)]
143. Zhou, J.; Jiang, Y.-Y.; Chen, H.; Wu, Y.-C.; Zhang, L. Tanshinone I Attenuates the Malignant Biological Properties of Ovarian Cancer by Inducing Apoptosis and Autophagy via the Inactivation of PI3K/AKT/MTOR Pathway. *Cell Prolif.* **2020**, *53*, e12739. [[CrossRef](#)] [[PubMed](#)]
144. Gossner, G.; Choi, M.; Tan, L.; Fogoros, S.; Griffith, K.A.; Kuenker, M.; Liu, J.R. Genistein-Induced Apoptosis and Autophagocytosis in Ovarian Cancer Cells. *Gynecol. Oncol.* **2007**, *105*, 23–30. [[CrossRef](#)] [[PubMed](#)]
145. Engelke, L.H.; Hamacher, A.; Proksch, P.; Kassack, M.U. Ellagic Acid and Resveratrol Prevent the Development of Cisplatin Resistance in the Epithelial Ovarian Cancer Cell Line A2780. *J. Cancer* **2016**, *7*, 353–363. [[CrossRef](#)] [[PubMed](#)]
146. Pastorek, M.; Simko, V.; Takacova, M.; Barathova, M.; Bartosova, M.; Hunakova, L.; Sedlakova, O.; Hudecova, S.; Krizanova, O.; Dequiedt, F.; et al. Sulforaphane Reduces Molecular Response to Hypoxia in Ovarian Tumor Cells Independently of Their Resistance to Chemotherapy. *Int. J. Oncol.* **2015**, *47*, 51–60. [[CrossRef](#)] [[PubMed](#)]
147. Kim, Y.; Lee, S.M.; Kim, J.H. Unripe *Rubus Coreanus* Miquel Suppresses Migration and Invasion of Human Prostate Cancer Cells by Reducing Matrix Metalloproteinase Expression. *Biosci. Biotechnol. Biochem.* **2014**, *78*, 1402–1411. [[CrossRef](#)]
148. Kim, M.K.; Choi, H.S.; Cho, S.G.; Shin, Y.C.; Ko, S.G. *Rubus Coreanus* Miquel Extract Causes Apoptosis of Doxorubicin-Resistant NCI/ADR-RES Ovarian Cancer Cells via JNK Phosphorylation. *Mol. Med. Rep.* **2016**, *13*, 4065–4072. [[CrossRef](#)]
149. Uche, F.I.; McCullagh, J.; Claridge, T.W.D.; Richardson, A.; Li, W.-W. Synthesis of (Aminoalkyl)Cycleanine Analogues: Cytotoxicity, Cellular Uptake, and Apoptosis Induction in Ovarian Cancer Cells. *Bioorg. Med. Chem. Lett.* **2018**, *28*, 1652–1656. [[CrossRef](#)]
150. Chen, H.; Landen, C.N.; Li, Y.; Alvarez, R.D.; Tollefsbol, T.O. Epigallocatechin Gallate and Sulforaphane Combination Treatment Induce Apoptosis in Paclitaxel-Resistant Ovarian Cancer Cells through HTERT and Bcl-2 down-Regulation. *Exp. Cell Res.* **2013**, *319*, 697–706. [[CrossRef](#)]
151. Chen, T.; Xu, Y.; Guo, H.; Liu, Y.; Hu, P.; Yang, X.; Li, X.; Ge, S.; Velu, S.E.; Nadkarni, D.H.; et al. Experimental Therapy of Ovarian Cancer with Synthetic Makaluvamine Analog: In Vitro and In Vivo Anticancer Activity and Molecular Mechanisms of Action. *PLoS ONE* **2011**, *6*, e20729. [[CrossRef](#)] [[PubMed](#)]
152. Li, N.; Li, C.; Zhang, J.; Jiang, Q.; Wang, Z.; Nie, S.; Gao, Z.; Li, G.; Fang, H.; Ren, S.; et al. Discovery of Semisynthetic Celastrol Derivatives Exhibiting Potent Anti-Ovarian Cancer Stem Cell Activity and STAT3 Inhibition. *Chem. Biol. Interact.* **2022**, *366*, 110172. [[CrossRef](#)]
153. Beretta, G.L.; Ribauda, G.; Menegazzo, I.; Supino, R.; Capranico, G.; Zunino, F.; Zagotto, G. Synthesis and Evaluation of New Naphthalene and Naphthoquinone Derivatives as Anticancer Agents: Naphthalene and Naphthoquinone Derivatives as Anticancer Agents. *Arch. Pharm. Chem. Life Sci.* **2017**, *350*, e1600286. [[CrossRef](#)]
154. Amrine, C.S.M.; Huntsman, A.C.; Doyle, M.G.; Burdette, J.E.; Pearce, C.J.; Fuchs, J.R.; Oberlies, N.H. Semisynthetic Derivatives of the Verticillin Class of Natural Products through Acylation of the C11 Hydroxy Group. *ACS Med. Chem. Lett.* **2021**, *12*, 625–630. [[CrossRef](#)]

155. Prasad, S.; Aggarwal, B.B. Turmeric, the Golden Spice. In *Herbal Medicine: Biomolecular and Clinical Aspects*, 2nd ed.; CRC Press: Boca Raton, FL, USA, 2011.
156. Zhou, H.; Beevers, C.S.; Huang, S. The Targets of Curcumin. *Curr. Drug Targets* **2012**, *12*, 332–347. [[CrossRef](#)] [[PubMed](#)]
157. Dobbin, Z.C.; Landen, C.N. The Importance of the PI3K/AKT/MTOR Pathway in the Progression of Ovarian Cancer. *Int. J. Mol. Sci.* **2013**, *14*, 8213–8227. [[CrossRef](#)] [[PubMed](#)]
158. Yu, Z.; Wan, Y.; Liu, Y.; Yang, J.; Li, L.; Zhang, W. Curcumin Induced Apoptosis via PI3K/Akt-Signalling Pathways in SKOV3 Cells. *Pharm. Biol.* **2016**, *54*, 2026–2032. [[CrossRef](#)]
159. Watson, J.L.; Greenshields, A.; Hill, R.; Hilchie, A.; Lee, P.W.; Giacomantonio, C.A.; Hoskin, D.W. Curcumin-Induced Apoptosis in Ovarian Carcinoma Cells Is P53-Independent and Involves P38 Mitogen-Activated Protein Kinase Activation and Downregulation of Bcl-2 and Survivin Expression and Akt Signaling. *Mol. Carcinog.* **2010**, *49*, 13–24. [[CrossRef](#)]
160. Bowman, T.; Garcia, R.; Turkson, J.; Jove, R. STATs in Oncogenesis. *Oncogene* **2000**, *19*, 2474–2488. [[CrossRef](#)]
161. Saydmohammed, M.; Joseph, D.; Syed, V. Curcumin Suppresses Constitutive Activation of STAT-3 by up-Regulating Protein Inhibitor of Activated STAT-3 (PIAS-3) in Ovarian and Endometrial Cancer Cells. *J. Cell. Biochem.* **2010**, *110*, 447–456. [[CrossRef](#)]
162. Seo, J.H.; Jeong, K.J.; Oh, W.J.; Sul, H.J.; Sohn, J.S.; Kim, Y.K.; Cho, D.Y.; Kang, J.K.; Park, C.G.; Lee, H.Y. Lysophosphatidic Acid Induces STAT3 Phosphorylation and Ovarian Cancer Cell Motility: Their Inhibition by Curcumin. *Cancer Lett.* **2010**, *288*, 50–56. [[CrossRef](#)] [[PubMed](#)]
163. Kinose, Y.; Sawada, K.; Nakamura, K.; Kimura, T. The Role of MicroRNAs in Ovarian Cancer. *BioMed Res. Int.* **2014**, *2014*, 249393. [[CrossRef](#)] [[PubMed](#)]
164. Du, Z.; Sha, X. Demethoxycurcumin Inhibited Human Epithelia Ovarian Cancer Cells' Growth via up-Regulating MiR-551a. *Tumor Biol.* **2017**, *39*, 1010428317694302. [[CrossRef](#)] [[PubMed](#)]
165. Takei, Y.; Kadomatsu, K.; Muramatsu, T.; Matsuo, S.; Itoh, H.; Nakazawa, K.; Kubota, S. Antisense Oligodeoxynucleotide Targeted to Midkine, a Heparin-Binding Growth Factor, Suppresses Tumorigenicity of Mouse Rectal Carcinoma Cells. *Cancer Res.* **2001**, *61*, 8486–8491. [[PubMed](#)]
166. Zhao, S.F.; Zhang, X.; Zhang, X.J.; Shi, X.Q.; Yu, Z.J.; Kan, Q.C. Induction of MicroRNA-9 Mediates Cytotoxicity of Curcumin against SKOV3 Ovarian Cancer Cells. *Asian Pac. J. Cancer Prev.* **2014**, *15*, 3363–3368. [[CrossRef](#)]
167. Al-Alem, L.; Curry, T.E., Jr. Ovarian Cancer: Involvement of the Matrix Metalloproteinases. *Reproduction* **2015**, *150*, R55. [[CrossRef](#)]
168. Lv, J.; Shao, Q.; Wang, H.; Shi, H.; Wang, T.; Gao, W.; Song, B.; Zheng, G.; Kong, B.; Qu, X. Effects and Mechanisms of Curcumin and Basil Polysaccharide on the Invasion of SKOV3 Cells and Dendritic Cells. *Mol. Med. Rep.* **2013**, *8*, 1580–1586. [[CrossRef](#)]
169. Pei, H.; Yang, Y.; Cui, L.; Yang, J.; Li, X.; Yang, Y.; Duan, H. Bisdemethoxycurcumin Inhibits Ovarian Cancer via Reducing Oxidative Stress Mediated MMPs Expressions. *Sci. Rep.* **2016**, *6*, 28773. [[CrossRef](#)]
170. Slack-Davis, J.K.; Atkins, K.A.; Harrer, C.; Daniel Hershey, E.; Conaway, M. Vascular Cell Adhesion Molecule-1 Is a Regulator of Ovarian Cancer Peritoneal Metastasis. *Cancer Res.* **2009**, *69*, 1469–1476. [[CrossRef](#)]
171. Daleprane, J.B.; Abdalla, D.S. Emerging Roles of Propolis: Antioxidant, Cardioprotective, and Antiangiogenic Actions. *Evid.-Based Complement. Altern. Med.* **2013**, *2013*, 175135. [[CrossRef](#)]
172. Baur, J.A.; Sinclair, D.A. Therapeutic Potential of Resveratrol: The in Vivo Evidence. *Nat. Rev. Drug Discov.* **2006**, *5*, 493–506. [[CrossRef](#)] [[PubMed](#)]
173. Pavan, V.; Mucignat-Caretta, C.; Redaelli, M.; Ribaudo, G.; Zagotto, G. The Old Made New: Natural Compounds against Erectile Dysfunction: Natural Compounds against Erectile Dysfunction. *Arch. Pharm. Chem. Life Sci.* **2015**, *348*, 607–614. [[CrossRef](#)] [[PubMed](#)]
174. Tan, L.; Wang, W.; He, G.; Kuick, R.D.; Gossner, G.; Kueck, A.S.; Wahl, H.; Opipari, A.W.; Liu, J.R. Resveratrol Inhibits Ovarian Tumor Growth in an in Vivo Mouse Model. *Cancer* **2016**, *122*, 722–729. [[CrossRef](#)]
175. Gwak, H.; Kim, S.; Dhanasekaran, D.N.; Song, Y.S. Resveratrol Triggers ER Stress-Mediated Apoptosis by Disrupting N-Linked Glycosylation of Proteins in Ovarian Cancer Cells. *Cancer Lett.* **2016**, *371*, 347–353. [[CrossRef](#)]
176. Majewska, E.; Szeliga, M. AKT/GSK3 β Signaling in Glioblastoma. *Neurochem. Res.* **2017**, *42*, 918–924. [[CrossRef](#)]
177. Tino, A.B.; Chitcholtan, K.; Sykes, P.H.; Garrill, A. Resveratrol and Acetyl-Resveratrol Modulate Activity of VEGF and IL-8 in Ovarian Cancer Cell Aggregates via Attenuation of the NF-KB Protein. *J. Ovarian Res.* **2016**, *9*, 84. [[CrossRef](#)] [[PubMed](#)]
178. Mikula-Pietrasik, J.; Sosińska, P.; Książek, K. Resveratrol Inhibits Ovarian Cancer Cell Adhesion to Peritoneal Mesothelium in Vitro by Modulating the Production of A5 β 1 Integrins and Hyaluronic Acid. *Gynecol. Oncol.* **2014**, *134*, 624–630. [[CrossRef](#)]
179. Park, S.Y.; Jeong, K.J.; Lee, J.; Yoon, D.S.; Choi, W.S.; Kim, Y.K.; Han, J.W.; Kim, Y.M.; Kim, B.K.; Lee, H.Y. Hypoxia Enhances LPA-Induced HIF-1 α and VEGF Expression: Their Inhibition by Resveratrol. *Cancer Lett.* **2007**, *258*, 63–69. [[CrossRef](#)]
180. Sopo, M.; Anttila, M.; Hämäläinen, K.; Kivelä, A.; Ylä-Herttua, S.; Kosma, V.M.; Keski-Nisula, L.; Sallinen, H. Expression Profiles of VEGF-A, VEGF-D and VEGFR1 Are Higher in Distant Metastases than in Matched Primary High Grade Epithelial Ovarian Cancer. *BMC Cancer* **2019**, *19*, 584. [[CrossRef](#)]
181. Nag, S.A.; Qin, J.J.; Wang, W.; Wang, M.H.; Wang, H.; Zhang, R. Ginsenosides as Anticancer Agents: In Vitro and in Vivo Activities, Structure-Activity Relationships, and Molecular Mechanisms of Action. *Front. Pharmacol.* **2012**, *3*, 25. [[CrossRef](#)]
182. Ahuja, A.; Kim, J.H.; Kim, J.-H.; Yi, Y.-S.; Cho, J.Y. Functional Role of Ginseng-Derived Compounds in Cancer. *J. Ginseng Res.* **2018**, *42*, 248–254. [[CrossRef](#)]
183. Li, J.; Liu, T.; Zhao, L.; Chen, W.; Hou, H.; Ye, Z.; Li, X. Ginsenoside 20(S)-Rg3 Inhibits the Warburg Effect through STAT3 Pathways in Ovarian Cancer Cells. *Int. J. Oncol.* **2015**, *46*, 775–781. [[CrossRef](#)]

184. Lu, J.; Wang, L.; Chen, W.; Wang, Y.; Zhen, S.; Chen, H.; Cheng, J.; Zhou, Y.; Li, X.; Zhao, L. MiR-603 Targeted Hexokinase-2 to Inhibit the Malignancy of Ovarian Cancer Cells. *Arch. Biochem. Biophys.* **2019**, *661*, 1–9. [CrossRef]
185. Liu, W.; Zhang, S.-X.; Ai, B.; Pan, H.-F.; Zhang, D.; Jiang, Y.; Hu, L.-H.; Sun, L.-L.; Chen, Z.-S.; Lin, L.-Z. Ginsenoside Rg3 Promotes Cell Growth Through Activation of MTORC1. *Front. Cell Dev. Biol.* **2021**, *9*, 730309. [CrossRef]
186. Li, J.; Xi, W.; Li, X.; Sun, H.; Li, Y. Advances in Inhibition of Protein-Protein Interactions Targeting Hypoxia-Inducible Factor-1 for Cancer Therapy. *Bioorg. Med. Chem.* **2019**, *27*, 1145–1158. [CrossRef]
187. Liu, T.; Zhao, L.; Hou, H.; Ding, L.; Chen, W.; Li, X. Ginsenoside 20(S)-Rg3 Suppresses Ovarian Cancer Migration via Hypoxia-Inducible Factor 1 Alpha and Nuclear Factor-Kappa B Signals. *Tumor Biol.* **2017**, *39*, 1010428317692225. [CrossRef] [PubMed]
188. Liu, D.; Liu, T.; Teng, Y.; Chen, W.; Zhao, L.; Li, X. Ginsenoside Rb1 Inhibits Hypoxia-Induced Epithelial-Mesenchymal Transition in Ovarian Cancer Cells by Regulating MicroRNA-25. *Exp. Ther. Med.* **2017**, *14*, 2895–2902. [CrossRef] [PubMed]
189. Lengyel, E. Ovarian Cancer Development and Metastasis. *Am. J. Pathol.* **2010**, *177*, 1053–1064. [CrossRef]
190. Ribaudo, G.; Oselladore, E.; Ongaro, A.; Zagotto, G.; Memo, M.; Gianoncelli, A. Enhanced G-Quadruplex Selectivity of Flavonoid Glycoside Rutin over Quercetin. *Nat. Prod. Res.* **2020**, *36*, 3469–3473. [CrossRef] [PubMed]
191. Petrescu, I.; Lamotte-Brasseur, J.; Chessa, J.P.; Ntarima, P.; Claeysens, M.; Devreese, B.; Marino, G.; Gerday, C. Xylanase from the Psychrophilic Yeast *Cryptococcus Adeliae*. *Extremophiles* **2000**, *4*, 137–144. [CrossRef]
192. Liu, Y.; Gong, W.; Yang, Z.Y.; Zhou, X.S.; Gong, C.; Zhang, T.R.; Wei, X.; Ma, D.; Ye, F.; Gao, Q.L. Quercetin Induces Protective Autophagy and Apoptosis through ER Stress via the P-STAT3/Bcl-2 Axis in Ovarian Cancer. *Apoptosis* **2017**, *22*, 544–557. [CrossRef]
193. Driak, D.; Dvorska, M.; Bolehovska, P.; Svandova, I.; Novotny, J.; Halaska, M. Bad and Bid—Potential Background Players in Preneoplastic to Neoplastic Shift in Human Endometrium. *Neo* **2014**, *61*, 411–415. [CrossRef] [PubMed]
194. Kemp, K.; Griffiths, J.; Campbell, S.; Lovell, K. An Exploration of the Follow-up up Needs of Patients with Inflammatory Bowel Disease. *J. Crohn's Colitis* **2013**, *7*, e386–e395. [CrossRef] [PubMed]
195. Gao, X.; Wang, B.; Wei, X.; Men, K.; Zheng, F.; Zhou, Y.; Zheng, Y.; Gou, M.; Huang, M.; Guo, G.; et al. Anticancer Effect and Mechanism of Polymer Micelle-Encapsulated Quercetin on Ovarian Cancer. *Nanoscale* **2012**, *4*, 7021–7030. [CrossRef] [PubMed]
196. Gong, C.; Yang, Z.; Zhang, L.; Wang, Y.; Gong, W.; Liu, Y. Quercetin Suppresses DNA Double-Strand Break Repair and Enhances the Radiosensitivity of Human Ovarian Cancer Cells via P53-Dependent Endoplasmic Reticulum Stress Pathway. *OncoTargets Ther.* **2018**, *11*, 17–27. [CrossRef] [PubMed]
197. Yang, Z.; Liu, Y.; Liao, J.; Gong, C.; Sun, C.; Zhou, X.; Wei, X.; Zhang, T.; Gao, Q.; Ma, D.; et al. Quercetin Induces Endoplasmic Reticulum Stress to Enhance CDDP Cytotoxicity in Ovarian Cancer: Involvement of STAT3 Signaling. *FEBS J.* **2015**, *282*, 1111–1125. [CrossRef] [PubMed]
198. Long, Q.; Xie, Y.; Huang, Y.; Wu, Q.; Zhang, H.C.; Xiong, S.; Liu, Y.; Chen, L.; Wei, Y.; Zhao, X.; et al. Induction of Apoptosis and Inhibition of Angiogenesis by PEGylated Liposomal Quercetin in Both Cisplatin-Sensitive and Cisplatin-Resistant Ovarian Cancers. *J. Biomed. Nanotechnol.* **2013**, *9*, 965–975. [CrossRef] [PubMed]
199. Catanzaro, D.; Ragazzi, E.; Vianello, C.; Caparrotta, L.; Montopoli, M. Effect of Quercetin on Cell Cycle and Cyclin Expression in Ovarian Carcinoma and Osteosarcoma Cell Lines. *Nat. Prod. Commun.* **2015**, *10*, 1365–1368. [CrossRef]
200. Rashidi, Z.; Khosravizadeh, Z.; Talebi, A.; Khodamoradi, K.; Ebrahimi, R.; Amidi, F. Overview of Biological Effects of Quercetin on Ovary. *Phytother. Res.* **2021**, *35*, 33–49. [CrossRef]
201. Dhanaraj, T.; Mohan, M.; Arunakaran, J. Quercetin Attenuates Metastatic Ability of Human Metastatic Ovarian Cancer Cells via Modulating Multiple Signaling Molecules Involved in Cell Survival, Proliferation, Migration and Adhesion. *Arch. Biochem. Biophys.* **2021**, *701*, 108795. [CrossRef] [PubMed]
202. Yamauchi, K.; Afroze, S.H.; Mitsunaga, T.; McCormick, T.C.; Kuehl, T.J.; Zawieja, D.C.; Uddin, M.N. 3,4',7-O-Trimethylquercetin Inhibits Invasion and Migration of Ovarian Cancer Cells. *Anticancer Res.* **2017**, *37*, 2823–2829. [CrossRef]
203. Li, N.; Sun, C.; Zhou, B.; Xing, H.; Ma, D.; Chen, G.; Weng, D. Low Concentration of Quercetin Antagonizes the Cytotoxic Effects of Anti-Neoplastic Drugs in Ovarian Cancer. *PLoS ONE* **2014**, *9*, e100314. [CrossRef]
204. Scambia, G.; Ranelletti, F.O.; Benedetti Panici, P.; Bonanno, G.; De Vincenzo, R.; Piantelli, M.; Mancuso, S. Synergistic Antiproliferative Activity of Quercetin and Cisplatin on Ovarian Cancer Cell Growth. *Anti-Cancer Drugs* **1990**, *1*, 45–48. [CrossRef] [PubMed]
205. Tiwari, H.; Karki, N.; Pal, M.; Basak, S.; Verma, R.K.; Bal, R.; Kandpal, N.D.; Bisht, G.; Sahoo, N.G. Functionalized Graphene Oxide as a Nanocarrier for Dual Drug Delivery Applications: The Synergistic Effect of Quercetin and Gefitinib against Ovarian Cancer Cells. *Colloids Surf. B Biointerfaces* **2019**, *178*, 452–459. [CrossRef] [PubMed]
206. Fatease, A.A.; Shah, V.; Nguyen, D.X.; Cote, B.; LeBlanc, N.; Rao, D.A.; Alani, A.W.G. Chemosensitization and Mitigation of Adriamycin-Induced Cardiotoxicity Using Combinational Polymeric Micelles for Co-Delivery of Quercetin/Resveratrol and Resveratrol/Curcumin in Ovarian Cancer. *Nanomed. Nanotechnol. Biol. Med.* **2019**, *19*, 39–48. [CrossRef]
207. Xu, G.; Li, B.; Wang, T.; Wan, J.; Zhang, Y.; Huang, J.; Shen, Y. Enhancing the Anti-Ovarian Cancer Activity of Quercetin Using a Self-Assembling Micelle and Thermosensitive Hydrogel Drug Delivery System. *RSC Adv.* **2018**, *8*, 21229–21242. [CrossRef] [PubMed]
208. Palanisamy, C.P.; Cui, B.; Zhang, H.; Panagal, M.; Paramasivam, S.; Chinnaiyan, U.; Jeyaraman, S.; Murugesan, K.; Rostagno, M.; Sekar, V.; et al. Anti-Ovarian Cancer Potential of Phytocompound and Extract from South African Medicinal Plants and Their Role in the Development of Chemotherapeutic Agents. *Am. J. Cancer Res.* **2021**, *11*, 1828–1844.

209. Löcken, H.; Clamor, C.; Müller, K. Napabucasin and Related Heterocycle-Fused Naphthoquinones as STAT3 Inhibitors with Antiproliferative Activity against Cancer Cells. *J. Nat. Prod.* **2018**, *81*, 1636–1644. [[CrossRef](#)] [[PubMed](#)]
210. Shchekotikhin, A.E.; Nadysev, G.Y.; Tikhomirov, A.S.; Dezhenkova, L.G. Semi-Synthetic Derivatives of Heliomycin with an Antiproliferative Potency. *PRA* **2018**, *13*, 469–472. [[CrossRef](#)]
211. Ferry, D.R.; Smith, A.; Malkhandi, J.; Fyfe, D.W.; deTakats, P.G.; Anderson, D.; Baker, J.; Kerr, D.J. Phase I Clinical Trial of the Flavonoid Quercetin: Pharmacokinetics and Evidence for in Vivo Tyrosine Kinase Inhibition. *Clin. Cancer Res.* **1996**, *2*, 659–668.
212. Mei, J.-Y.; Zhang, M.-J.; Wang, Y.-Y.; Liu, Y.-H. The Positive Clinical Therapeutically Effects of Escin on Advanced Thyroid Cancer. *Cancer Med.* **2017**, *6*, 937–943. [[CrossRef](#)] [[PubMed](#)]
213. Berman, A.Y.; Motechin, R.A.; Wiesenfeld, M.Y.; Holz, M.K. The Therapeutic Potential of Resveratrol: A Review of Clinical Trials. *NPJ Precis. Oncol.* **2017**, *1*, 35. [[CrossRef](#)] [[PubMed](#)]
214. Budisan, L.; Gulei, D.; Zanoaga, O.M.; Irimie, A.I.; Sergiu, C.; Braicu, C.; Gherman, C.D.; Berindan-Neagoe, I. Dietary Intervention by Phytochemicals and Their Role in Modulating Coding and Non-Coding Genes in Cancer. *Int. J. Mol. Sci.* **2017**, *18*, 1178. [[CrossRef](#)] [[PubMed](#)]
215. Yan, Y.B.; Tian, Q.; Zhang, J.F.; Xiang, Y. Antitumor Effects and Molecular Mechanisms of Action of Natural Products in Ovarian Cancer (Review). *Oncol. Lett.* **2020**, *20*, 141. [[CrossRef](#)] [[PubMed](#)]

Disclaimer/Publisher’s Note: The statements, opinions and data contained in all publications are solely those of the individual author(s) and contributor(s) and not of MDPI and/or the editor(s). MDPI and/or the editor(s) disclaim responsibility for any injury to people or property resulting from any ideas, methods, instructions or products referred to in the content.

Article

Two New 4-Hydroxy-2-pyridone Alkaloids with Antimicrobial and Cytotoxic Activities from *Arthrinium* sp. GZWMJZ-606 Endophytic with *Houttuynia cordata* Thunb

Ying Yin ^{1,2,3,†}, Dongyang Wang ^{1,2,†}, Dan Wu ^{1,2}, Wenwen He ^{1,2}, Mingxing Zuo ^{1,2}, Weiming Zhu ^{1,4},
Yanchao Xu ^{1,3,*} and Liping Wang ^{1,2,3,*}

- ¹ State Key Laboratory of Functions and Applications of Medicinal Plants, Guizhou Medical University, Guiyang 550014, China
 - ² Key Laboratory of Chemistry for Natural Products of Guizhou Province, Chinese Academy of Sciences, Guiyang 550014, China
 - ³ School of Pharmaceutical Sciences, Guizhou Medical University, Guiyang 550025, China
 - ⁴ Key Laboratory of Marine Drugs, Ministry of Education of China, School of Medicine and Pharmacy, Ocean University of China, Qingdao 266003, China
- * Correspondence: xuyanchao@gmc.edu.cn (Y.X.); lipingw2006@163.com (L.W.)
† These authors contributed equally to the work.

Abstract: Two new 4-hydroxy-2-pyridone alkaloids furanpyridone A and B (**1** and **2**), along with two known compounds N-hydroxyapiosporamide (**3**) and apiosporamide (**4**) were isolated from the endophytic fungus *Arthrinium* sp. GZWMJZ-606 in *Houttuynia cordata* Thunb. Furanpyridone A and B had unusual 5-(7-oxabicyclo[2.2.1]heptane)-4-hydroxy-2-pyridone skeleton. Their structures including absolute configurations were determined on the basis of spectroscopic analysis, as well as the X-ray diffraction experiment. Compound **1** showed inhibitory activity against ten cancer cell lines (MKN-45, HCT116, K562, A549, DU145, SF126, A-375, 786O, 5637, and PATU8988T) with IC₅₀ values from 4.35 to 9.72 μM. Compounds **1**, **3** and **4** showed moderate inhibitory effects against four Gram-positive strains (*Staphylococcus aureus*, methicillin-resistant *S. aureus*, *Bacillus Subtilis*, *Clostridium perfringens*) and one Gram-negative strain (*Ralstonia solanacarium*) with MIC values from 1.56 to 25 μM. However, compounds **1–4** showed no obvious inhibitory activity against two Gram-negative bacteria (*Escherichia coli* and *Pseudomonas aeruginosa*) and two pathogenic fungi (*Candida albicans* and *Candida glabrata*) at 50 μM. These results show that compounds **1–4** are expected to be developed as lead compounds for antibacterial or anti-tumor drugs.

Keywords: pyridone alkaloids; *Arthrinium* sp.; endophytic fungus; antibacterial; cytotoxicity

Citation: Yin, Y.; Wang, D.; Wu, D.; He, W.; Zuo, M.; Zhu, W.; Xu, Y.; Wang, L. Two New 4-Hydroxy-2-pyridone Alkaloids with Antimicrobial and Cytotoxic Activities from *Arthrinium* sp. GZWMJZ-606 Endophytic with *Houttuynia cordata* Thunb. *Molecules* **2023**, *28*, 2192. <https://doi.org/10.3390/molecules28052192>

Academic Editor: Giovanni Ribaudò

Received: 2 February 2023

Revised: 22 February 2023

Accepted: 22 February 2023

Published: 27 February 2023



Copyright: © 2023 by the authors. Licensee MDPI, Basel, Switzerland. This article is an open access article distributed under the terms and conditions of the Creative Commons Attribution (CC BY) license (<https://creativecommons.org/licenses/by/4.0/>).

1. Introduction

Since ricinin [1] and ilicicolin H [2] were found in the early 1970s, a series of 4-hydroxy-2-pyridinone alkaloids with diverse structures were reported [3–6]. These alkaloids were mainly isolated from plants and fungi and had good biological activity [7]. According to the position and type of substituents, C-3 was often replaced by alkanes (e.g., septoriamycin from *Septoria pistaciarum* [8]) or terpenes (e.g., tenelin from *Beauveria tenella* and *Beauveria bassiana* [9]), and C-5 was often replaced by phenyl (e.g., sambutoxin from *Fusarium sambucinum* [10]) or cyclohexyl (e.g., torrubiellone A-B from *Torrubiella* sp. [11]). There were also a small number of derivatives whose C-6 was replaced by alkanes (e.g., pyridomacrolidin from *Beauveria basiana* [12]). These kind of compounds usually have anti-inflammatory, antibacterial, cytotoxicity, antimalarial, antiviral, insecticidal, antioxidant, anti-fibrosis, neuroprotection, inhibition of protein tyrosine kinase, and so on [13–16], which have attracted widespread attention.

In the past few years, there were some new 4-hydroxy-2-pyridones discovered from fungi, such as (+)-didymellamide B, (±)-didymellamide E, (+)-N-hydroxyapiosporamide,

and didymellamides F–H which were isolated from *Coniochaeta cephalothecoides* [17], and arthopyrones A and B with novel oxabicyclo[3.3.1]-nonane ring which were isolated from *Arthrinium arundinis* ZSDS1-F3 [18]. Three new 4-hydroxy-2-pyridone alkaloids citridones E–G with antibacterial activity were isolated from the endophytic fungus *Penicillium sumatrense* GZWMJZ-313 in our previous studies [19]. In order to obtain more compounds of this type from endophytic fungus, *Arthrinium* sp. GZWMJZ-606 was isolated from *Houttuynia cordata* Thunb. Further chemical investigation of this fungal strain led to the isolation of two new 4-hydroxy-2-pyridone derivatives (**1** and **2**) which we named fuprazone A and B (Figure 1), along with the known *N*-hydroxyapiosporamide (**3**) [18,20] and apiosporamide (**4**) [21]. Compounds **1** and **2** were the first reported compounds with 5-(7-oxabicyclo[2.2.1]heptane)-4-hydroxy-2-pyridone skeleton. Compared with the previously reported 1,2-epoxyhexane [17,21], 2-oxobicyclo[3.3.1]nonane [18] or benzene [22], 7-oxadicyclo[2.2.1]heptane can improve some biological activities [23–25]. Herein, the isolation, structure elucidation, the antimicrobial and cytotoxic activity of these compounds are described.

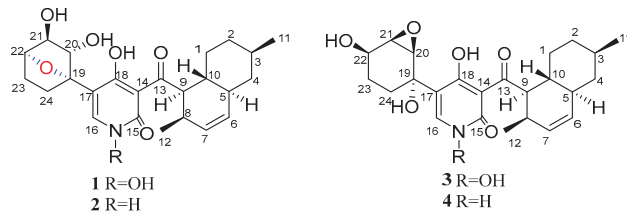


Figure 1. Structures of compounds **1–4**.

2. Results and Discussion

Structure Elucidation

Compound **1** was obtained as a yellow crystal. The molecular formula was deduced as $C_{24}H_{31}NO_7$ based on the HRESIMS ion peak at m/z 468.19861 $[M + Na]^+$ (calcd. for $C_{24}H_{31}NO_7Na = 468.19927$). Its IR (KBr) spectrum exhibited absorptions at 3434 cm^{-1} (hydroxy), 1649 cm^{-1} (carbonyl), and $1605/1552/1446\text{ cm}^{-1}$ (aromatic heterocycle). Compound **1** had the same molecular formula with *N*-hydroxyapiosporamide (**3**) and showed a high degree of similarity in UV absorption. The NMR spectra displayed two methyls, five sp^3 -methylenes, eight sp^3 -methines, three sp^2 -methines, one sp^3 -quaternary carbon, five sp^2 -quaternary carbons (including two carbonyls) (Table 1), which was also similar to those of compound **3**, especially for the important 1H NMR signals, such as two methyl groups at H₃-11 (δ_H 0.94) and H₃-12 (δ_H 0.82), a single special hydrogen signal at H-16 (δ_H 7.93), two olefinic protons at H-6 (δ_H 5.41) and H-7 (δ_H 5.60). The above evidence suggested that compound **1** has a similar skeleton with compound **3**. The 1H - 1H COSY correlations (Figure 2) from H₂-1 (δ_H 0.88 and 1.95) to H-10 (δ_H 1.58), H-3 (δ_H 1.50) to H₃-11, and H-8 (δ_H 2.85) to H-12 proved the existence of a decalin moiety. The relative configurations of this part were confirmed by the NOESY correlations (Figure 2) from H-10 to H₃-11/H₃-12 and H-5 (δ_H 1.83) to H-3/H-9 (δ_H 4.45), and indicated that compound **1** has the same decalin moiety as compound **3**. The 1H - 1H COSY correlations from H-20 (δ_H 3.87) to H₂-24 (δ_H 1.63 and 2.25) and the HMBC correlations (Figure 2) from H-21 (δ_H 4.00) and H₂-23 (δ_H 1.70 and 2.25) to C-19 (δ_C 89.4) confirmed the presence of an oxygenated cyclohexane moiety in compound **1**. However, there was a large chemical shift difference between these two compounds at C-19/20/21/22 (δ_C 89.4, 82.1, 82.9, 78.6 for **1**; 70.4, 60.5, 57.7, 67.2 for **3**). Nevertheless, there is still one degree of unsaturation in the structure **1**, implying an oxygen bridge in this cyclohexane moiety, but the HMBC correlations cannot be used to confirm it. The key HMBC correlations from H-9 to C-13 (δ_C 211.4), H-16 to C-15 (δ_C 159.9)/C-18 (δ_C 173.2)/C-19 indicated that the decalin and hexane moieties substituted at C-13 and C-17 of the 4-hydroxy-2-pyridinone part. The crystal of compound **1** was fortunately acquired in methanol/water (*v/v*, 1:1) solution. The

results of the X-ray (Figure 3) analysis (Flack parameter = -0.15 (11), CCDC: 2218951) confirmed an oxygen bridge between C-19 and C-22 forming the furan ring and led to the final determination of its absolute configuration as 3*R*, 5*S*, 8*R*, 9*R*, 10*R*, 19*S*, 20*S*, 21*S*, 22*S*. This novel 4-hydroxy-2-pyridone was named furanpydone A.

Table 1. ^1H (600 MHz) and ^{13}C (150 MHz) NMR data of 1–4.

Position	1 ^b		2 ^a		3 ^b		4 ^b	
	δ_{C}	δ_{H} (J in Hz)	δ_{C}	δ_{H} (J in Hz)	δ_{C}	δ_{H} (J in Hz)	δ_{C}	δ_{H} (J in Hz)
1	31.0, CH ₂	0.86–0.91, m 1.95, d (11.1)	29.6, CH ₂	0.77–0.85, m 1.83, dd (12.2, 3.0)	31.0, CH ₂	0.87–0.91, m 1.91–1.94, m	31.0, CH ₂	0.86–0.92, m 1.90–1.95, m
2	36.6, CH ₂	0.99–1.11, m 1.74, overlap	35.1, CH ₂	0.92–1.00, m 1.67, d (12.1)	36.6, CH ₂	1.00–1.09, m 1.73–1.77, overlap	36.6, CH ₂	1.00–1.08, m 1.73–1.78, overlap
3	34.4, CH	1.48–1.53, m	32.6, CH	1.43–1.49, overlap 0.72–0.78, overlap	34.3, CH	1.49–1.52, m	34.4, CH	1.48–1.53, m
4	43.2, CH ₂	0.80, t (12.2) 1.72–1.80, overlap	41.4, CH ₂	1.69–1.72, overlap	43.1, CH ₂	0.80, t (12.2) 1.73–1.77, overlap	43.2, CH ₂	0.79, t (12.2) 1.73–1.78, overlap
5	43.2, CH	1.83, “t” like (10.8)	41.4, CH	1.75, “t” like (10.1)	43.3, CH	1.81–1.85, overlap	43.2, CH	1.80–1.86, overlap
6	131.7, CH	5.41, d (9.7)	130.4, CH	5.37, d (9.9)	131.7, CH	5.42, d (9.9)	131.7, CH	5.41, d (9.8)
7	132.6, CH	5.58–5.63, m	131.7, CH	5.56–5.59, m	132.5, CH	5.58–5.62, m	132.6, CH	5.60, ddd (9.8, 4.5, 2.7)
8	32.3, CH	2.83–2.90, m 4.42–4.47, overlap	30.6, CH	2.71–2.76, m 4.33, dd (11.4, 5.7)	32.3, CH	2.82–2.86, m 4.45, dd (11.3, 5.7)	32.4, CH	2.80–2.86, m 4.43, dd (11.4, 5.8)
9	54.5, CH	1.56–1.60, overlap	51.8, CH	1.41–1.49, m	54.5, CH	1.56–1.60, m	54.2, CH	1.54–1.60, m
10	37.5, CH	0.94, d (6.5)	35.8, CH	0.87, d (6.5)	37.6, CH	0.94, d (6.5)	37.6, CH	0.93, d (6.5)
11	22.9, CH ₃	0.82, d (7.0)	22.5, CH ₃	0.74, d (7.3)	23.0, CH ₃	0.83, d (7.3)	22.9, CH ₃	0.83, d (7.2)
12	18.4, CH ₃		17.9, CH ₃		18.4, CH ₃		18.4, CH ₃	
13	211.4, C		209.6, C		211.7, C		212.0, C	
14	108.2, C		106.7, C		108.6, C		108.8, C	
15	159.9, C		161.8, C		159.6, C		163.9, C	
16	139.5, CH	7.93, s	139.1, CH	7.33, d (6.0)	140.0, CH	8.04, s	139.9, CH	7.58, s
17	111.0, C		110.8, C		114.5, C		116.6, C	
18	173.2, C		175.7, C		175.6, C		179.3, C	
19	89.4, C		88.0, C		70.4, C		70.4, C	
20	82.1, CH	3.87, brs	80.5, CH	3.58, dd (6.1, 1.4)	60.5, CH	3.66, d (3.7)	60.5, CH	3.64, “t” like (2.1)
21	82.9, CH	4.00, d (4.3)	81.2, CH	3.78, “t” like (4.7)	57.7, CH	3.43, “t” like (3.3)	57.6, CH	3.42, “t” like (3.3)
22	78.6, CH	4.42–4.47, overlap 1.68–1.73, overlap 2.20–2.27, overlap	76.6, CH	4.30, “t” like (5.1)	67.2, CH	4.12–4.14, m	67.2, CH	4.13, ddd (8.6, 5.7, 2.8)
23	24.1, CH ₂	1.60–1.65, overlap 2.20–2.27, overlap	23.0, CH ₂	1.45–1.54, m 2.02–2.10, overlap	25.7, CH ₂	1.34–1.38, m 1.81–1.85, overlap	25.8, CH ₂	1.32–1.38, m 1.80–1.86, overlap
24	33.1, CH ₂		31.8, CH ₂	1.45–1.49, overlap 2.01–2.08, overlap	31.8, CH ₂	1.70, ddd (13.9, 10.2, 2.8) 2.26, ddd (14.4, 8.4, 2.5)	31.6, CH ₂	1.70, ddd (13.5, 10.4, 2.5) 2.22, dd (13.3, 8.6)
20-OH				4.77, d (6.1)				
21-OH				5.31, d (4.7)				
-NH				11.38, brs				

^a measured in DMSO-*d*₆, ^b measured in methanol-*d*₄ solvent.

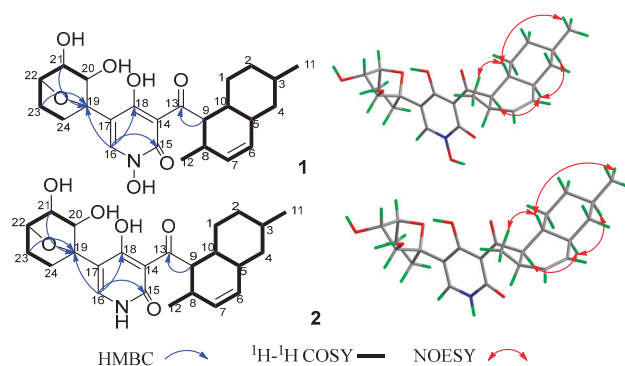


Figure 2. The key 2D NMR correlations of compounds **1** and **2**.

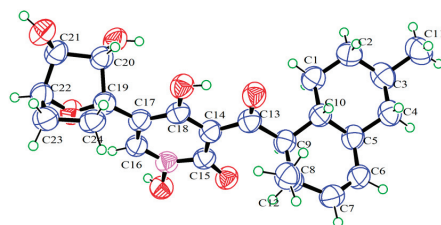


Figure 3. ORTEP drawing of **1**.

Compound **2** was obtained as a yellow powder. The molecular formula was deduced as $C_{24}H_{31}O_6N$ based on the HRESIMS peak at m/z 452.20319 ($[M + Na]^+$, calcd. for 452.20436), which has ten degrees of unsaturation as furanopyridone A (**1**), but one less oxygen atom than it. According to IR (KBr) spectrum data, they seem to have similar functional groups at 3445 cm^{-1} (hydroxy), 1652 cm^{-1} (carbonyl), and $1604/1557/1456\text{ cm}^{-1}$ (aromatic heterocycle). According to 1D NMR and HSQC data, compound **2** displayed two methyl ($\delta_{H/C}$ 0.74/17.9, 0.87/22.5), five sp^3 -methylene ($\delta_{H/C}$ 1.50 and 2.06/23.0; 0.81 and 1.83/29.6; 1.47 and 2.04/31.8; 0.96 and 1.67/35.1; 0.75 and 1.70/41.4), eight sp^3 -methines ($\delta_{H/C}$ 2.74/30.6, 1.46/32.6, 1.45/35.8, 1.75/41.4, 4.33/51.8, 4.30/76.6, 3.58/80.5, 3.78/81.2), three sp^2 -methines ($\delta_{H/C}$ 5.37/130.4, 5.57/131.7, 7.33/139.1), one sp^3 -quaternary carbon (δ_C 88.0), and five sp^2 -quaternary carbons (δ_C 106.7, 110.8, 161.8, 175.7, 209.6), which were extremely similar to compound **1** (Tables 1 and S1) suggested the similar structure of these two compounds. The 1H - 1H COSY correlations (Figure 2) from H₂-1 (δ_H 0.81 and 1.83) to H-10 (δ_H 1.45), H-3 (δ_H 1.46) to H₃-11 (δ_H 0.87), H-8 (δ_H 2.74) to H₃-12 (δ_H 0.74), H-20 (δ_H 3.58) to H₂-24 (δ_H 1.47 and 2.04), the key HMBC correlations (Figure 2) from H-9 (δ_H 4.33) to C-13 (δ_C 209.6), H-16 (δ_H 7.33) to C-15 (δ_C 161.8)/18 (δ_C 175.7)/19 (δ_C 88.0), H-21 (δ_H 3.78) to C-19 further confirmed that compound **2** and **1** have the same skeleton structure. Analysis of the NMR spectral data revealed that the chemical shift of C-15 (δ_C 161.8) moved to a lower field, which was similar to compound **4**, the key 1H - 1H COSY correlation between H-16 and H-NH (δ_H 11.38) confirmed the absence of an N-hydroxy group in **2**. The key NOESY correlations from H-10 to H₃-11/H₃-12, H-5 (δ_H 1.75) to H-3 (δ_H 1.47)/H-9 (δ_H 4.33), as well as the same chemical shift for C-19/20/21/22/23/24 with furanopyridone A (**1**) suggested that these two compounds had the same relative configuration. The similarity of electronic circular dichroism (ECD) curve of compound **2** (213 (−5.83), 228 (−11.74), 265 (+5.40), 310 (+7.09), 341 (−1.63)) to **1** (217 (−2.73), 242 (−3.51), 270 (+2.00), 316 (+2.75), 343 (−0.27)) (Figure 4) along with the similar optical rotation values (**1**: −89.7, **2**: −80.0) indicated the same absolute configuration for **2** and **1**. This novel 4-hydroxy-2-pyridone was named furanopyridone B.

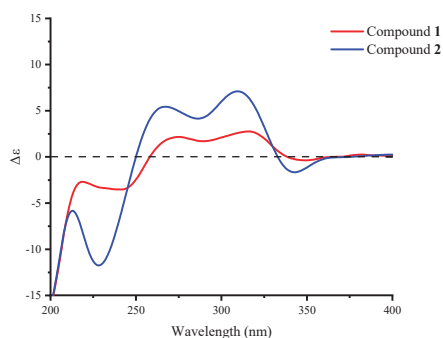


Figure 4. Experimental CD spectra of compounds 1 and 2.

We propose a possible biosynthetic pathway for compounds 1–4. Didymellamide B was the key intermediate in the biosynthesis of these compounds [18]. The intermediates **a** and **b** were obtained by reduction from didymellamide B. Compound 2 was obtained by oxidation, hydration and cyclization reaction from **a**, and compound 1 was synthesized by further oxidation. Compound 4 was obtained by two oxidation reactions from **b**, and compound 3 was synthesized by further oxidation. (Figure 5).

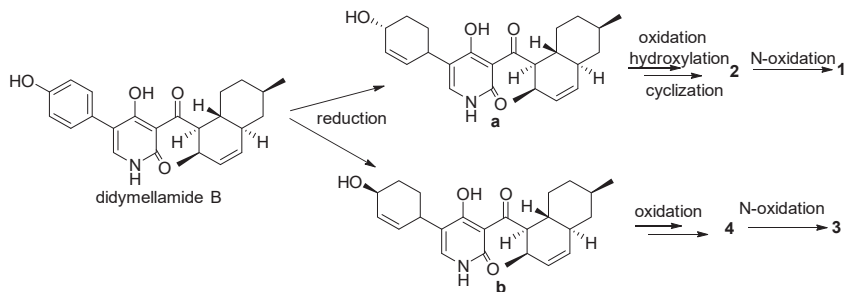


Figure 5. Proposed biosynthetic pathway for compounds 1–4.

Compounds 1–4 were tested for their antimicrobial activities against nine pathogenic microorganisms. As shown in Table 2, compound 4 exhibited broad inhibitory activities against *Staphylococcus aureus*, methicillin-resistant *S. aureus* (MRSA), *Bacillus subtilis*, *Clostridium perfringens*, and *Ralstonia solanacearum* with the MIC values ranging from 1.56 to 6.25 μM . Compounds 1 and 3 showed moderate selective activities against *S. aureus* and MRSA with the MIC values of 12.5–25.0 μM . Compounds 1–4 showed no obvious inhibitory activity against two Gram-negative bacteria (*E. coli* and *P. aeruginosa*) and two pathogenic fungi (*C. albicans* and *C. glabrata*) at 50 μM . According to the results, it seems that the compounds with ternary epoxide showed better antibacterial activity than those with furan ring, but the effect of N-OH needs more research to determine.

The antiproliferative activities against 18 cancer cell lines and one normal cell line were assayed by the CCK-8 method. Compound 1 showed significant cytotoxicity against 10 cancer cell lines, compound 3 showed activities against HCT116 and 786-O cell lines (Table 3). The compounds with furan ring showed better antiproliferative activities than those with ternary epoxide. At the same time, nitrogen hydroxyl is the necessary group for maintaining the inhibitory activity.

Table 2. Antimicrobial activity of 1–4 (MIC, μM), $n = 3$.

Pathogenic Bacteria	1	2	3	4	Positive Drug
<i>E. coli</i> ATCC 11775	>50	>50	>50	>50	0.10 *
<i>P. aeruginosa</i> ATCC 10145	>50	>50	>50	>50	1.56 *
<i>S. aureus</i> ATCC6538	12.5	>50	12.5	6.25	0.20 *
MRSA ATCC 43300	12.5	>50	25.0	6.25	0.38 *
<i>B. subtilis</i> ATCC 6051	>50	>50	>50	1.56	6.25 *
<i>C. perfringens</i> ATCC 13124	>50	>50	>50	3.13	0.047 *
<i>R. solanacarum</i>	>50	>50	>50	6.25	3.12 *
<i>C. albicans</i> ATCC10231	>50	>50	>50	>50	3.13 #
<i>C. glabrata</i> ATCC2001	>50	>50	>50	>50	3.13 #

* the positive drug is ciprofloxacin, # the positive drug is amphotericin B.

Table 3. Cytotoxic activity (μM , $\text{IC}_{50} \pm \text{SD}$), $n = 3$.

Cell Line	1	2	3	4	Dox
A549	6.47 \pm 0.31	>10	>10	>10	0.849 \pm 0.013
MKN-45	5.41 \pm 0.09	>10	>10	>10	0.307 \pm 0.005
HCT116	5.64 \pm 0.05	>10	6.09 \pm 0.02	>10	0.121 \pm 0.005
K562	9.22 \pm 0.93	>10	>10	>10	0.948 \pm 0.058
DU145	9.01 \pm 0.07	>10	>10	>10	0.189 \pm 0.003
SF126	9.72 \pm 0.46	>10	>10	>10	0.164 \pm 0.016
A-375	7.16 \pm 0.17	>10	>10	>10	0.064 \pm 0.003
786-O	5.93 \pm 0.13	>10	9.13 \pm 0.48	>10	0.726 \pm 0.028
PATU8988T	6.46 \pm 0.09	>10	>10	>10	0.167 \pm 0.012
5637	4.35 \pm 0.08	>10	>10	>10	0.185 \pm 0.002
HeLa	>10	>10	>10	>10	0.177 \pm 0.006
TE-1	>10	>10	>10	>10	0.240 \pm 0.030
GBC-SD	>10	>10	>10	>10	0.592 \pm 0.069
MCF-7	>10	>10	>10	>10	0.966 \pm 0.011
HepG2	>10	>10	>10	>10	0.619 \pm 0.054
CAL-62	>10	>10	>10	>10	0.277 \pm 0.019
HOS	>10	>10	>10	>10	0.090 \pm 0.013
A-673	>10	>10	>10	>10	0.380 \pm 0.030
L-02	7.09 \pm 0.10	>10	9.70 \pm 0.06	>10	0.243 \pm 0.005

3. Materials and Methods

3.1. General Experimental Procedures

The NMR spectra were recorded on Bruker Advance NEO 600 spectrometer (Bruker Corporation, Zurich, Switzerland) using TMS as an internal standard. MS analysis were carried out on Agilent 1100 instrument (Agilent Technologies, Santa Clara, CA, USA) and Thermo ultimate 3000/Q EXACTIVE FOCUS mass spectrometers (Thermo Scientific™, Waltham, MA, USA), respectively. Optical rotations were determined on Rudolph Autopol1 automatic polarimeter (Rudolph Research Analytical, Hackettstown, NJ, USA). UV spectra were detected on a Cary 60-UV-Vis spectrometer (Agilent Technologies, Santa Clara, CA, USA). IR spectra were determined on an iCAN 9 infrared spectrophotometer (Tianjin Nengpu Technology Co., Ltd, Tianjin, China) with KBr disks. X-ray data were generated using a Bruker Smart-1000 CCD (Bruker Corporation, Billerica, MA, USA) area detector diffractometer with graphite monochromatic Cu-K α radiation. Column chromatography was performed on silica gel (200–300 mesh; Qingdao Puke Parting Materials Co., Ltd., Qingdao, China), Sephadex LH-20 gel (Amersham Biosciences, Uppsala, Sweden). HPLC separation was performed on HITACHI Primaide with an ODS-A column (YMC-pack ODS-A, 10 \times 250 mm, 5 μm , 4 mL/min). Melting point instrument (SGW X-4).

3.2. Fungal Material

The endophytic fungus *Arthrinium* sp. GZWMJZ-606 was isolated from the leaves of *Houttuynia cordata* Thunb., which was collected from Longli, Guizhou, China. The leaves were treated with 75% alcohol for 30 s, and the residual alcohol was washed with sterile water. Then 1 g of fresh leaves was grinded into a pulp and 10 mL sterile water added. The suspension (100 μ L) was deposited on a rice agar plate, which was prepared from rice powder (10 g), agar (18 g), and 1 L water containing chloramphenicol (0.3%) as a bacterial inhibitor, and incubated at 28 °C for 5 days. Monoclonal was selected and streaked to purity using the same agar medium. This strain was determined as *Arthrinium* sp. by the phylogenetic tree (Figure S1) of the ITS sequence (GenBank No. OP810989). The strain was deposited in our laboratory of Guizhou in 20% glycerol at -80 °C.

3.3. Fermentation and Extraction

The fungal strain GZWMJZ-606 was cultured on PDA at 28 °C for 3 days and then was cut into 100 \times 1000 mL Erlenmeyer flasks, each containing a solid medium prepared from 100 g rice and 110 mL distilled water. These flasks were incubated at room temperature under static conditions for 40 days. The cultures were extracted three times by EtOAc (each 500 mL) and the combined EtOAc solutions were dried in vacuo to yield the extract (480.0 g).

3.4. Isolation and Purification

The EtOAc extract (480.0 g) was fractionated into 19 fractions (Fr.1–Fr.19) by chromatography on a silica gel column using step gradient elution of petroleum ether (PE)-EtOAc (v/v , 100:1–1:1) and CH_2Cl_2 -MeOH (v/v , 20:1–1:1). Fr.17 (9.4 g) was further separated into 15 subfractions (Fr.17.1–Fr.17.15) by Sephadex LH-20 (CH_2Cl_2 -MeOH, v/v , 1:1). Fr.17.11 (207.6 mg) was purified by semipreparative HPLC on an ODS-A column eluting with 60% MeCN- H_2O containing 0.05% trifluoroacetic acid (TFA) to yield compound 1 (35.6 mg, t_R 11.1 min). Fr.17.14 (75.8 mg) was purified by semipreparative HPLC on an ODS-A column (60% MeCN- H_2O containing 0.05% TFA) to yield compound 2 (6.8 mg, t_R 9.3 min). Fr.17.2 (830.5 mg) was further separated into 7 subfractions (Fr.17.2.1–Fr.17.2.7). Compound 4 (12.2 mg, t_R 10.1 min) was obtained from Fr.17.2.1 (57.1 mg) by semipreparative HPLC (55% MeCN- H_2O containing 0.05% TFA). Fr.16 (1.6 g) was further separated into 6 subfractions (Fr.16.1–Fr.16.6), and Fr.16.4 (120.5 mg) was performed on a semipreparative ODS-A column (61% MeCN- H_2O containing 0.05% TFA) to yield compound 3 (38.6 mg, t_R 8.4 min).

3.5. Physical Properties and Spectral Data of 1–4

Compound 1: yellow crystal; m.p. 167.5–168.5 °C; ECD (1.12 mM, MeOH) λ_{max} ($\Delta\epsilon$) 217 (−2.73), 242 (−3.51), 270 (+2.00), 316 (+2.75), 343 (−0.27) nm; $[\alpha]_D^{22}$ −89.7 (c 0.58, MeOH); UV (MeOH) λ_{max} (log ϵ) 281 (0.75), 341 (0.72) nm; IR (KBr) ν_{max} 3434, 2913, 2953, 1649, 1605, 1446 cm^{-1} ; ^1H NMR and ^{13}C NMR data see Tables 1 and S1 and Figures S3–S10; HRESIMS m/z 468.19861 $[\text{M} + \text{Na}]^+$ (Figure S2), molecular formula: $\text{C}_{24}\text{H}_{31}\text{NO}_7$.

X-ray crystallographic analyses of 1: $\text{C}_{24}\text{H}_{31}\text{NO}_7 \cdot \text{CH}_3\text{OH}$, orthorhombic, $M = 477.54$, $a = 7.6539$ (3) Å, $b = 14.5093$ (6) Å, $c = 21.7608$ (11) Å, $\alpha = 90^\circ$, $\beta = 90^\circ$, $\gamma = 90^\circ$, $V = 2416.60$ (18) Å³, $T = 150$ K, space group $P21 21 21$, $Z = 4$, μ (Cu K α) = 0.807 mm^{-1} , 8074 reflections measured, 4534 independent reflections ($R_{\text{int}} = 0.019$). The final R_1 values were 0.0724 ($I > 2\sigma(I)$). The final $wR(F^2)$ values were 0.1921 ($I > 2\sigma(I)$). The final R_1 values were 0.0767 (all data). The final $wR(F^2)$ values were 0.1991 (all data). The goodness of fit on F^2 was 1.022. Flack parameter = -0.15 (11). CCDC: 2218951.

Compound 2: yellow powder; ECD (1.17 mM, MeOH) λ_{max} ($\Delta\epsilon$) 213 (−5.83), 228 (−11.74), 265 (+5.40), 310 (+7.09), 341 (−1.63) $[\alpha]_D^{22}$ −80.0 (c 0.20, MeOH); UV (MeOH) λ_{max} (log ϵ) 235 (1.05), 270 (0.50), 338 (0.74) nm; IR (KBr) ν_{max} 3445, 2909, 1652, 1604, 1456 cm^{-1} ; ^1H NMR and ^{13}C NMR data see Table 1 and Figures S12–S17; HRESIMS m/z 452.20319 $[\text{M} + \text{Na}]^+$ (Figure S11), molecular formula: $\text{C}_{24}\text{H}_{31}\text{NO}_6$.

Compound 3: yellow solid; the molecular formula is $C_{24}H_{31}NO_7$ (m/z 444.1 [$M - H$] $^-$) determined by ESIMS. $[\alpha]_D^{22} - 57.4$ (c 2.3, MeOH); based on 1H NMR and ^{13}C NMR data (Table 1, Figures S18 and S19) proved that compound 3 was N-hydroxyapiosporamide.

Compound 4: faint yellow solid powder; the molecular formula is $C_{24}H_{31}NO_6$ (m/z 452.5 [$M + Na$] $^+$) determined by ESIMS. $[\alpha]_D^{22} - 32.2$ (c 0.87, MeOH); based on 1H NMR and ^{13}C NMR data (Table 1, Figures S20 and S21) proved that compound 4 was apiosporamide.

3.6. Antimicrobial Activities Assay

The isolated compounds were evaluated for antibacterial activity against pathogenic microorganisms including three Gram-negative strains (*Escherichia coli* ATCC11775, *Pseudomonas aeruginosa* ATCC10145, *Ralstonia solanacearum* [26]), and four Gram-positive strains (*Staphylococcus aureus* ATCC6538, methicillin-resistant *S. aureus* ATCC43300 MRSA, *Clostridium perfringens* ATCC13124, and *Bacillus subtilis* ATCC6051), and two pathogenic fungi (*Candida albicans* ATCC10231 and *Candida glabrata* ATCC2001). The tested bacterial suspensions were incubated in Luria–Bertani (LB) medium and fungi in Mueller–Hinton agar (HMA) medium at 28 °C for 12 h and diluted to be 1×10^6 CFU/mL by the same medium. Then, the DMSO solution of each compound was diluted into the corresponding concentration using the LB or MHA medium; 100 μ L solution of compound was added into the first well of a 96-well plate and resulted the initial tested concentration of each compound to be 50 μ mol/L (DMSO < 0.5‰ in each well) and the concentration of each compound to be 25 μ mol/L (DMSO < 0.5‰ in each well) in the second well of a 96-well plate after then following this method in sequence, adding 100 μ L microbial suspension into a 96-well plate. The ciprofloxacin and DMSO were used as the positive and negative controls, respectively. All experiments were repeated three times. MIC values were assessed by whether compounds can inhibit the growth of microorganisms [19].

3.7. Cytotoxic Activity Assay

Cell proliferation was measured with the CCK-8 method. By the dye of WST-8 (2-(2-methoxy-4-nitrophenyl)-3-(4-nitrophenyl)-5-(2,4-disulfophenyl)-2H-tetrazolium, monosodium salt) was reduced by dehydrogenase in cells to form a water-soluble tetrazolium salt product (formazan dye) with orange color. In the measurement, the amount of the formazan dye is proportional to the number of living cells. Finally, the cell viability can be estimated by recording the optical density (OD) of formazan dye at 450 nm using a microplate reader [27].

A cell suspension of 100 μ L was dispensed (adherent cell viewed 5×10^4 /mL and suspension cell viewed 9×10^4 /mL) in 96-well plates. With doxorubicin hydrochloride as positive drug and DMSO as control, plates were pre-cultured for 24 h, followed by treatments with various concentrations of compound (eight concentration gradients were set for each sample for IC_{50} determination and three multiple holes were set for each concentration, $n = 3$). Keep the 96-well plates at 37 °C in an incubator with 5% CO_2 for 72 h. After the aspiration of the old medium, the 10-fold diluted CCK-8 (100 μ L) solution was added to each well of the plate, which was then incubated for another 3 h. An absorbance microplate reader was used to measure the absorbance at 450 nm. The optical density values (OD) of each well represented the survival/proliferation of cells. The toxicity is expressed by cell inhibition. The half inhibitory concentration (IC_{50}) was defined as the concentration causing 50% inhibition, each group of data has 8 concentration gradient responses. The IC_{50} value is calculated by curve fitting using the software GraphPad Prism 8 (version 8.0.2, from GraphPad Software Inc., Boston, MA, USA), the experimental results are expressed in $IC_{50} \pm SD$ [28,29].

$$\text{Cell inhibition rate} = (\text{OD}_{\text{Control}} - \text{OD}_{\text{Drug}}) / (\text{OD}_{\text{Control}} - \text{OD}_{\text{Blank}}) \times 100\%.$$

The tested cell lines: A549: human lung cancer cells; MKN-45: human gastric cancer cells; HCT116: human colon cancer cells; K562: human chronic myeloid leukemia cells; DU145: human prostate cancer cells; SF126: human brain tumor cells; A-375: human malignant melanoma cells; MCF-7: human breast cancer cells; 786-O: human renal clear cell

adenocarcinoma cells; PATU8988T: human pancreatic cancer cells; 5637: human bladder cancer cells; HeLa: human cervical cancer cells; TE-1: human esophageal cancer cells; GBC-SD: human gallbladder cancer cells; HepG2: human hepatoma cells; CAL-62: human thyroid cancer cells; HOS: human osteosarcoma cells; A-673: human rhabdomyosarcoma cells; L-02: human normal liver cells.

4. Conclusions

Two new 4-hydroxy-2-pyridone alkaloids were isolated from an endophytic fungus *Aspergillus* sp. GZWMJZ-606, which was obtained from *Houttuynia cordata* Thunb. Compounds **1** and **2** are the first example of 4-hydroxy-2-pyridone alkaloids possessing novel 7-oxidicyclo[2.2.1]heptane part. Compound **1** exhibited broad-spectrum cytotoxicity against 10 cancer cell lines with the IC₅₀ values of 4.35–9.72 μ M, and showed selective activities against *S. aureus* and MRSA *S. aureus* with MIC values of 12.5 μ M. The discovery of novel 4-hydroxy-2-pyridinone alkaloids can provide a material basis for the discovery of potential drug molecules.

Supplementary Materials: The following supporting information can be downloaded at: <https://www.mdpi.com/article/10.3390/molecules28052192/s1>, ITS1 gene sequences of *Arthrinium* sp. GZWMJZ-606; Figure S1: Species identification of endophytic fungi strain; Table S1: ¹H (600 MHz) and ¹³C (150 MHz) NMR data of compound **1** DMSO-*d*₆; Figure S2: HRESIMS spectrum of **1**; Figure S3: ¹H NMR spectrum (600 MHz, Methanol-*d*₄) of **1**; Figure S4: ¹³C NMR spectrum (150 MHz, Methanol-*d*₄) of **1**; Figure S5: HSQC spectrum (Methanol-*d*₄) of **1**; Figure S6: HMBC spectrum (Methanol-*d*₄) of **1**; Figure S7: ¹H-¹H COSY spectrum (Methanol-*d*₄) of **1**; Figure S8: NOESY spectrum (Methanol-*d*₄) of **1**; Figure S9: ¹H NMR spectrum (600 MHz, DMSO-*d*₆) of **1**; Figure S10: ¹³C NMR spectrum (150 MHz, DMSO-*d*₆) of **1**; Figure S11: HRESIMS spectrum of **2**; Figure S12: ¹H NMR spectrum (600 MHz, DMSO-*d*₆) of **2**; Figure S13: ¹³C NMR spectrum (150 MHz, DMSO-*d*₆) of **2**; Figure S14: HSQC spectrum (DMSO-*d*₆) of **2**; Figure S15: HMBC spectrum (DMSO-*d*₆) of **2**; Figure S16: ¹H-¹H COSY spectrum (DMSO-*d*₆) of **2**; Figure S17: NOESY spectrum (DMSO-*d*₆) of **2**; Figure S18: ¹H NMR spectrum (600 MHz, Methanol-*d*₄) of **3**; Figure S19: ¹³C NMR spectrum (150 MHz, Methanol-*d*₄) of **3**; Figure S20: ¹H NMR spectrum (600 MHz, Methanol-*d*₄) of **4**; Figure S21: ¹³C NMR spectrum (150 MHz, Methanol-*d*₄) of **4**.

Author Contributions: Y.Y. performed the experiments and wrote the original draft; D.W. (Dongyang Wang) analyzed the data and confirmed the structure; D.W. (Dan Wu) and M.Z. performed the biological activity test; W.H. performed the fermentation and extraction; W.Z. helped to modify the manuscript; Y.X. isolated the strain and directed the implementation of the study; L.W. designed the study and revised the manuscript. All authors have read and agreed to the published version of the manuscript.

Funding: This work was financially supported by the National Natural Science Foundation of China, grant numbers 22207020 and U1812403; Guizhou Provincial Science and Technology Projects, grant numbers QKHJC-ZK[2021]ZD017, QKHZC[2022]YB191, QKHJC-ZK [2022]YB392, and QKHZYD[2022]4015; “Light of the West” Talent Cultivation Program of Chinese Academy of Sciences, grant numbers RZ [2022]4 for L. Wang, GMU (J [2020]006, 19NSP078, 20NSP065), and 100 Leading Talents of Guizhou Province for W. Zhu.

Institutional Review Board Statement: Not applicable.

Informed Consent Statement: Not applicable.

Data Availability Statement: Not available.

Conflicts of Interest: The authors declare no conflict of interest.

Sample Availability: Samples of the compounds are available from the authors.

References

1. Tuson, R.V. XII.-Note on an Alkaloid contained in the seeds of the *Ricinus communis*, or Castor-oil Plant. *J. Chem. Soc.* **1864**, *17*, 195–197. [\[CrossRef\]](#)
2. Hayakawa, S.; Minato, H.; Katagori, K. The ilicicolins antibiotics from *Cylindrocladium ilicicola*. *J. Antibiot.* **1971**, *24*, 653–654. [\[CrossRef\]](#) [\[PubMed\]](#)
3. Zhu, M.; Zhang, X.; Feng, H.; Che, Q.; Zhu, T.; Gu, Q.; Li, D. Campyridones A-D, pyridone alkaloids from a mangrove endophytic fungus *Campylocarpon* sp. HDN13-307. *Tetrahedron* **2016**, *72*, 5679–5683. [\[CrossRef\]](#)
4. Zhang, W.Y.; Zhong, Y.; Yu, Y.; Shi, D.F.; Huang, H.Y.; Tang, X.L.; Wang, Y.H.; Chen, G.D.; Zhang, H.P.; Liu, C.L.; et al. 4-Hydroxy Pyridones from Heterologous Expression and Cultivation of the Native Host. *J. Nat. Prod.* **2020**, *83*, 3338–3346. [\[CrossRef\]](#) [\[PubMed\]](#)
5. Li, L.N.; Wang, L.; Cheng, Y.N.; Cao, Z.Q.; Zhang, X.K.; Guo, X.L. Discovery and Characterization of 4-Hydroxy-2-pyridone Derivative Sambutoxin as a Potent and Promising Anticancer Drug Candidate: Activity and Molecular Mechanism. *Mol. Pharm.* **2018**, *15*, 4898–4911. [\[CrossRef\]](#)
6. Tang, Y.; Li, J.; Zhao, S. Progress in the Study of 4-Hydroxy-2-pyridone Natural Alkaloids. *Chin. J. Org. Chem.* **2011**, *31*, 9–21.
7. Sarita, S.; Neelam, Y.; Ravi, K.; Sonu, C.; Vidhi, D.; Pooja, W.; Anil, D. A score years' update in the synthesis and biological evaluation of medicinally important 2-pyridones. *Eur. J. Med. Chem.* **2022**, *232*, 114199.
8. Ando, K.; Suzuki, S.; Saeki, T.; Tamura, G.; Arima, K. Funiculosin, A New Antibiotic. I Isolation, Biological and Chemical Properties. *J. Antibiot.* **1969**, *22*, 189–194. [\[CrossRef\]](#)
9. Wat, C.K.; Mcinnes, A.G.; Smith, D.G.; Wright, J.L.C.; Vining, L.C. The yellow pigments of *Beauveria* species. Structures of tenellin and bassianin. *Can. J. Chem.* **1977**, *55*, 4090–4098. [\[CrossRef\]](#)
10. Kim, J.C.; Lee, Y.W.; Tamura, H.; Yoshizawa, T. Sambutoxin: A new mycotoxin isolated from *Fusarium sambucinum*. *Tetrahedron Lett.* **1995**, *36*, 1047–1050. [\[CrossRef\]](#)
11. Isaka, M.; Chinthanom, P.; Supothina, S.; Tobwor, P.; Hywel-Jones, N.L. Pyridone and Tetramic Acid Alkaloids from the Spider Pathogenic Fungus *Torrubiella* sp. BCC 2165. *J. Nat. Prod.* **2010**, *73*, 2057–2060. [\[CrossRef\]](#)
12. Takahashi, S.; Kakinuma, N.; Uchida, K.; Hashimoto, R.; Yanagisawa, T.; Nakagawa, A. Pyridovericin and pyridomacrolidin: Novel metabolites from entomopathogenic fungi, *Beauveria bassiana*. *J. Antibiot.* **1998**, *51*, 596–598. [\[CrossRef\]](#)
13. Li, M.; Zhang, A.; Qi, X.; Yu, R.; Li, J. A novel inhibitor of PKG1 suppresses the aerobic glycolysis and proliferation of hepatocellular carcinoma. *Biomed. Pharmacother.* **2023**, *158*, 114115. [\[CrossRef\]](#)
14. Zhu, Y.X.; Peng, C.; Ding, W.; Hu, J.F.; Li, J. Chromenopyridin A, a new N-methoxy-1-pyridone alkaloid from the endophytic fungus *Penicillium nothofagi* P-6 isolated from the critically endangered conifer *Abies beshanzuensis*. *Nat. Prod. Res.* **2022**, *36*, 2049–2055. [\[CrossRef\]](#)
15. Chicca, A.; Berg, R.; Jessen, H.J.; Marck, N.; Schmind, F.; Burch, P.; Gertch, J.; Gademann, K. Biological evaluation of pyridone alkaloids on the endocannabinoid system. *Bioorgan. Med. Chem.* **2017**, *25*, 6102–6114. [\[CrossRef\]](#)
16. Huang, B.; Lu, H.; Zhang, Y.; Gan, X.; Wang, X.; Liu, Y.; Luo, X. Bioactive Alkaloids from the Beibu Gulf Coral-associated Fungus *Acremonium sclerotigenum* GXIMD 02501. *Rec. Nat. Prod.* **2023**, *17*, 165–169.
17. Han, J.; Liu, C.; Li, L.; Zhou, H.; Liu, L.; Bao, L.; Chen, Q.; Song, F.; Zhang, L.; Li, E.; et al. Decalin-Containing Tetramic Acids and 4-Hydroxy-2-pyridones with Antimicrobial and Cytotoxic Activity from the Fungus *Coniochaeta cephalothecoides* Collected in Tibetan Plateau (Medog). *J. Org. Chem.* **2017**, *82*, 11474–11486. [\[CrossRef\]](#)
18. Wang, J.; Wei, X.; Qin, X.; Lin, X.; Zhou, X.; Liao, S.; Yang, B.; Liu, J.; Tu, Z.; Liu, Y. Arthryprones A–C, Pyridone Alkaloids from a Sponge-Derived Fungus *Arthrinium arundinis* ZSDS1-F3. *Org. Lett.* **2015**, *17*, 656–659. [\[CrossRef\]](#)
19. Xu, Y.; Wang, L.; Zhu, G.; Zuo, M.; Gong, Q.; He, W.; Li, M.; Yuan, C.; Hao, X.; Zhu, W. New phenylpyridone derivatives from the *Penicillium sumatrense* GZWM]Z-313, a fungal endophyte of *Garcinia multiflora*. *Chin. Chem. Lett.* **2019**, *30*, 431–434. [\[CrossRef\]](#)
20. Williams, D.R.; Kammler, D.C.; Donnell, A.F.; Goundry, W.R.F. Total Synthesis of (+)-Aposporamide: Assignment of Relative and Absolute Configuration. *Angew. Chem. Int. Ed.* **2005**, *44*, 6715–6718. [\[CrossRef\]](#)
21. Bao, J.; Zhai, H.; Zhu, K.; Yu, J.H.; Zhang, Y.; Wang, Y.; Jiang, C.S.; Zhang, X.; Zhang, Y.; Zhang, H. Bioactive Pyridone Alkaloids from a Deep-Sea-Derived Fungus *Arthrinium* sp. UJNMF0008. *Mar. Drugs* **2018**, *16*, 174. [\[CrossRef\]](#) [\[PubMed\]](#)
22. Wang, H.; Umeokoli, B.O.; Eze, P.; Heering, C.; Janiak, C.; Müller, W.E.G.; Orfali, R.S.; Hartmann, R.; Dai, H.; Lin, W.; et al. Secondary metabolites of the lichen-associated fungus *Apiospora montagnei*. *Tetrahedron Lett.* **2017**, *58*, 1702–1705. [\[CrossRef\]](#)
23. Bockstahler, E.R.; Weaver, L.C.; Wright, D.L. 7-Oxabicyclo [2.2.1] heptane-2,3-dicarboximides with anticonvulsant activity. *J. Med. Chem.* **1968**, *11*, 603–606. [\[CrossRef\]](#) [\[PubMed\]](#)
24. Misra, R.N.; Brown, B.R.; Sher, P.M.; Patel, M.M.; Hall, S.E.; Han, W.C.; Barrish, J.C.; Kocy, O.; Harris, D.N.; Goldenberg, H.J.; et al. Interphenylene 7-oxabicyclo [2.2.1] heptane oxazoles. Highly potent, selective, and long-acting thromboxane A2 receptor antagonists. *J. Med. Chem.* **1993**, *36*, 1401–1417. [\[CrossRef\]](#)
25. Walter, W.G. Antitumor Imide Derivatives of 7-Oxabicyclo [2.2.1] heptane-2,3-dimethyl-2,3-dicarboxylic Acid. *J. Pharm. Sci.* **1989**, *78*, 66–67. [\[CrossRef\]](#)
26. Li, Y.; Zeng, Y.; Wang, Z.; Fan, Y.; Yang, X.; Wang, Z.; Yu, S.; Pang, Q.; Cao, A. Deoxymikanolide adversely altered physiology and ultrastructure of *Ralstonia solanacearum*. *Pestic. Biochem. Phys.* **2021**, *174*, 104803. [\[CrossRef\]](#)
27. Dockray, G.J. Cholecystokinins in rat cerebral cortex: Identification, purification and characterization by immunochemical methods. *Brain Res.* **1980**, *188*, 155–165. [\[CrossRef\]](#)

28. Cai, L.; Qin, X.; Xu, Z.; Song, Y.; Jiang, H.; Wu, Y.; Ruan, H.; Chen, J. Comparison of Cytotoxicity Evaluation of Anticancer Drugs between Real-Time Cell Analysis and CCK-8 Method. *ACS Omega* **2019**, *4*, 12036–12042. [[CrossRef](#)]
29. Wufuer, H.; Xu, Y.; Wu, D.; He, W.; Wang, D.; Zhu, W.; Wang, L. Liglaurates A–E, cytotoxic bis (lauric acid-12yl) lignanoates from the rhizomes of *Drynaria roosii* Nakaike. *Phytochemistry* **2022**, *198*, 113143. [[CrossRef](#)]

Disclaimer/Publisher’s Note: The statements, opinions and data contained in all publications are solely those of the individual author(s) and contributor(s) and not of MDPI and/or the editor(s). MDPI and/or the editor(s) disclaim responsibility for any injury to people or property resulting from any ideas, methods, instructions or products referred to in the content.

MDPI
St. Alban-Anlage 66
4052 Basel
Switzerland
www.mdpi.com

Molecules Editorial Office
E-mail: molecules@mdpi.com
www.mdpi.com/journal/molecules



Disclaimer/Publisher's Note: The statements, opinions and data contained in all publications are solely those of the individual author(s) and contributor(s) and not of MDPI and/or the editor(s). MDPI and/or the editor(s) disclaim responsibility for any injury to people or property resulting from any ideas, methods, instructions or products referred to in the content.



Academic Open
Access Publishing

www.mdpi.com

ISBN 978-3-0365-8485-0